The evolution of Maroa Volcanic Centre, Taupo Volcanic Zone, New Zealand

A thesis submitted in fulfilment
of the requirements for the Degree
of
Doctor of Philosophy in Geology
at the
University of Canterbury
by
Graham S. Leonard

University of Canterbury
2003

Frontispiece

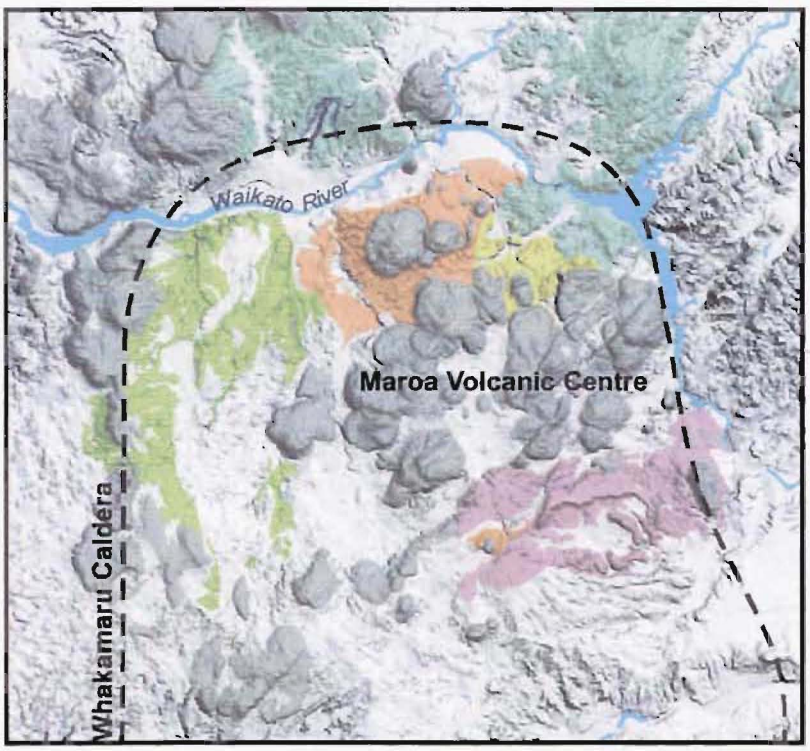

Shaded relief digital elevation model of Maroa illuminated from the northeast, kindly provided by K. Spinks. The Waikato River and the approximate location of Whakamaru caldera are shown for reference. The northern shore of Lake Taupo is a few kilometres south of the area shown. The image measures approximately 30 by 30 kilometres.

Abstract

Maroa Volcanic Centre (Maroa) is located within the older Whakamaru caldera, central Taupo Volcanic Zone, New Zealand. Dome lavas make up the majority of Maroa volume, with the large Maroa West and East Complexes (MWC and MEC, respectively) erupted mostly over a short 29 kyr period starting at 251 ± 17 ka. The five mappable Maroa pyroclastics deposits are discussed in detail. The Korotai (283 ± 11 ka), Atiamuri (229 ±12 ka), and Pukeahua (~ 229 – 196 ka) pyroclastics are all ≤ 1 km^3 and erupted from (a) northern Maroa, (b) a vent below Mandarin Dome and (c) Pukeahua Dome Complex vents, respectively. The Putauaki (272 ± 10 ka) and Orakonui (256 ± 12 ka) pyroclastics total ~ 4 km^3 from a petrologically and geographically very similar central Maroa source. The ~ 220 ka Mokai pyroclastics outcrop partly within Maroa but their source remains unclear, whereas the ~ 240 ka Ohakuri pyroclastics appear to have come from a caldera just north of Maroa. The ages of the Mamaku, Ohakuri and Mokai pyroclastics are equivocal. The Mamaku and Ohakuri pyroclastics appear to be older (~ 240 ka) than the age previously accepted for the Mamaku pyroclastics.

Maroa lavas are all plagioclase-orthopyroxene bearing, commonly with lesser quartz. Hornblende +/- biotite are sometimes present and their presence is correlated with geochemical variation. All Maroa deposits are rhyolites (apart from two high-silica dacite analyses) and are peraluminous and calcic. They all have the trace element signatures of arc-related rocks typical of TVZ deposits. Maroa deposits fall geochemically into three magma types based on Rb and Sr content: M (Rb 80-123 ppm, Sr 65-88 ppm), T (Rb 80-113 ppm, Sr 100-175 ppm) and N (Rb 120-150 ppm, Sr 35-100 ppm). The geochemical distinction of these types is also seen in the concentrations of most other elements. Based on the spatial, chronological and petrological similarities of the MWC/MEC and Pukeahua eastern magma associations (termed (1) and (2)) a further four magma associations are determined ((3) through (6)). These six associations account for almost all Maroa deposits. Two end-member models are proposed for the sources of each of the Maroa magma associations: (a) a single relatively shallow magma source feeding spatially clustered eruptions, and (b) a deeper source feeding multiple shallower offshoots over a wider area. Sources for the Maroa magma associations probably lie on a continuum between these two model end members. The distinction between Maroa and Taupo Volcanic Centres is somewhat arbitrary and is best considered to be the easting directly north of Ben Lomond, north of which most volcanism is older than 100 ka and M and N type, and south of which most volcanism is younger than 100 ka and T type. The remaining boundaries (north to include Ngautuku, west to include Mokauteure and east to include Whakapapa domes) are arbitrary, and include the farthest domes linked closely, spatially and magmatically, to the other Maroa domes.

From 230 to 64 ka there was a hiatus in caldera-forming ignimbrite eruptions. Maroa and the Western Dome Belt (WDB) constitute the largest concentrated volume of eruptions (as relatively gentle lava extrusion) during this period. The rate of Maroa volcanism has decreased exponentially from a maximum prior to 200 ka. In contrast volcanism at Taupo and Okataina has increased from ~ 64 ka to present. The oldest Maroa dome (305 ± 17 ka) constrains the maximum rate of infilling of Whakamaru caldera as 39-17 km^3/kyr. This highlights the extraordinarily fast rate of infilling common at silicic calderas and is in agreement with international case studies, except

where post-collapse structural resurgence has continued for more than 100 kyr. The majority of caldera fill, representing voluminous eruption deposits in the first tens of thousands of years post collapse, is buried and only accessible via drilling. The WDB and Maroa are petrologically distinct from one another in terms of some or all of Rb, Sr, Ba and Zr content, despite eruption over a similar period. Magma sources for Maroa and the WDB may have been partly or wholly derived from the Whakamaru caldera magma system(s), but petrological distinctions among all three mean that Maroa and the WDB cannot be considered as simple magmatic resurgence of the Whakamaru caldera.

Maroa's distinct Thorpe Rd Fault is in fact a fossil feature which hasn't been active in almost 200 kyr. In addition, the graben across Tuahu Dome was likely created by shallow blind diking. Several recent studies across TVZ show structural features with some associated dike intrusion/eruption. Such volcano tectonic interaction is rarely highlighted in TVZ but may be relatively common and lie on a continuum between dike-induced faulting and dikes following structural features. Although rates of volcanism are now low in Maroa magmatic intrusion appears to remain high. This raises the possibility of a causative link between faulting and volcanism in contrast to traditional views of volcanism controlled by rates of magmatic ascent. Probable future eruptions from Maroa are likely to be of similar scale (< 0.1 km^3) and frequency (every ~ 14,000 years) to most of those over the last 100 ka. Several towns lie in a range of zones of Maroa volcanic hazard from total destruction to possible ash fall. However, the probability of a future eruption is only ~ 0.6 % in an 80 year lifetime.

Table of contents

List of figures

List of tables

CHAPTER 1

Introduction

1.1 Overview and Objectives

1.1.1 Overview

Volcanism producing the lava-dome-cluster and associated pyroclastics referred to as Maroa Volcanic Centre (here after referred to as 'Maroa') occurred in the period between formation of the large Whakamaru and Oruanui (Taupo) calderas. Detailed study of the centre allows new interpretations of the evolution of silicic volcanoes in New Zealand and elsewhere in the world.

Maroa is one of the last eruptive centres of significant size within Taupo Volcanic Zone (TVZ) that has not been studied in detail. There has been no comprehensive study of the history and volcanology of Maroa, or its magma system. The relationship of Maroa to the regional stress and fault systems has been hitherto unclear. Because of its proximity to the cities of Tokoroa, Rotorua and Taupo, determining the risk to people and infrastructure from further activity at Maroa is important.

The location of Maroa is illustrated in Figure 1.1. The centre is made up of roughly 60 rhyolite lava domes, at least three pyroclastic density current deposits with volume 1 km^3 or greater and occasionally-preserved airfall deposits. It sits within the northeastern quadrant of the Whakamaru caldera (which is older), and has been postulated to fill a younger smaller caldera. Detailed mapping of the area was conducted during the 1980s by the New Zealand Geological Survey (now the Institute of Geological and Nuclear Sciences), but this has not been published.

From the early 1970s to present, most of Maroa has been covered in pine plantations as part of Carter Holt Harvey's Kinleith Forest. From 2000 to 2002 this forest has been systematically clear-felled in large blocks, allowing unprecedented visibility and access to exposures. It was determined that, in light of how little is known about Maroa, a comprehensive study of the centre could and should now be conducted. Methodology details are given in Appendix 9.

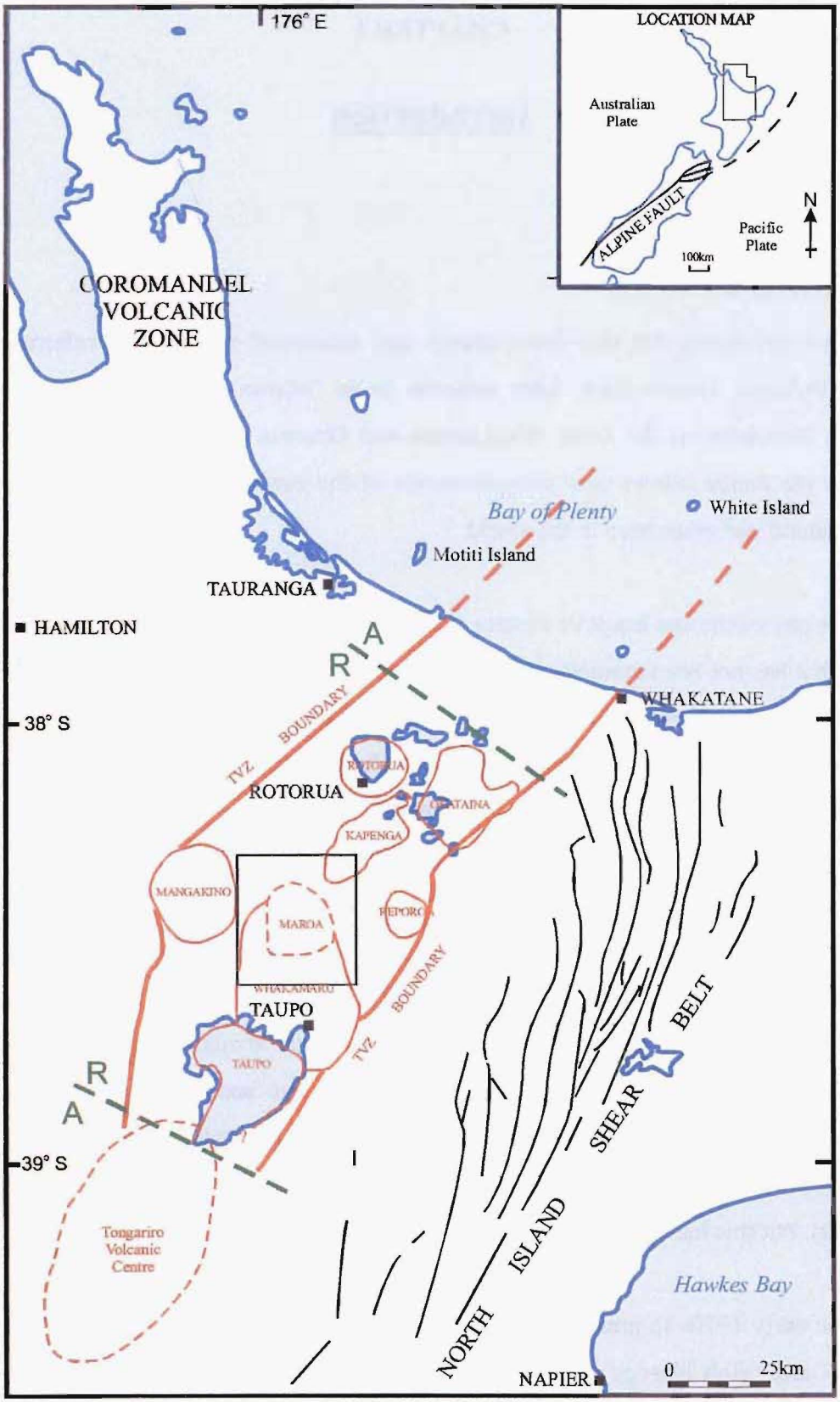

Figure 1.1 The location of the field area (black box) and volcanic (dashed) and caldera (solid) centres within TVZ. Top right inset: position of TVZ in New Zealand. Modified after Wilson et al. (1995). Green lines separate southern andesitic (A), central rhyolitic (R) and northern andesitic (A) sections.

1.1.2 Objectives

The aims of this thesis are to comprehensively (a) document the geology and volcanology of Maroa, (b) model its evolution and role in the history of TVZ and (c) compare its character to that of other silicic systems. To achieve these aims the thesis addresses the following 10 objectives:

1. Map in detail and interpret the geology of Maroa (Chapter 2).
2. Determine the role of regional tectonics in Maroa's evolution (Chapter 5).
3. Determine the geochronology and volumes of a) Maroa and b) related eruptives (Chapter 3).
4. Investigate in detail the geochemistry and petrography of Maroa eruptives, and compare and correlate these between pyroclastics and lavas (Chapter 4).
5. Model the series of events that produced Maroa (Chapters 2 through 5).
6. Petrologically compare Maroa eruptives to those erupted earlier from Whakamaru Caldera and more recently from Taupo Volcanic Centre (here after referred to as 'Taupo') (Chapters 4 and 5).
7. Define some preliminary constraints on the magma system feeding Maroa (Chapters 3, 4 and 5).
8. Place Maroa's history in the context of the evolution of the wider TVZ (Chapter 5).
9. Combine the Maroa data with other examples to facilitate comment on the rates of infilling of caldera structures (Chapter 5).
10. Evaluate the likely characteristics of, and hazard potential to the New Zealand public from, future Maroa eruptions (Chapter 5).

1.2 Location and physiography of the research area

The research area lies from approximately 30 to 50 km north of the northeastern shores of Lake Taupo. It is traversed by a 20 km stretch of State Highway 1 (SH1) from Atiamuri in the north to ~ 15 km north of Wairakei in the southeast. Maroa covers an irregular elliptical area of about 400 km^2 from 2767000 to 2785000 west to east, and from 6287000 to 6311000 south to north (in metres using the N.Z. metric map grid, Fig. 1.2). Field investigation was also extended further south to cover lava domes between Maroa and Taupo, further west to include the Mokai pyroclastics and further north to include lavas and pyroclastics that were erupted coevally with (and in some cases possibly from) Maroa. The surface geology to the east of Maroa consists of sediments, mostly not derived from Maroa, covered by young Taupo-derived pyroclastics and alluvium.

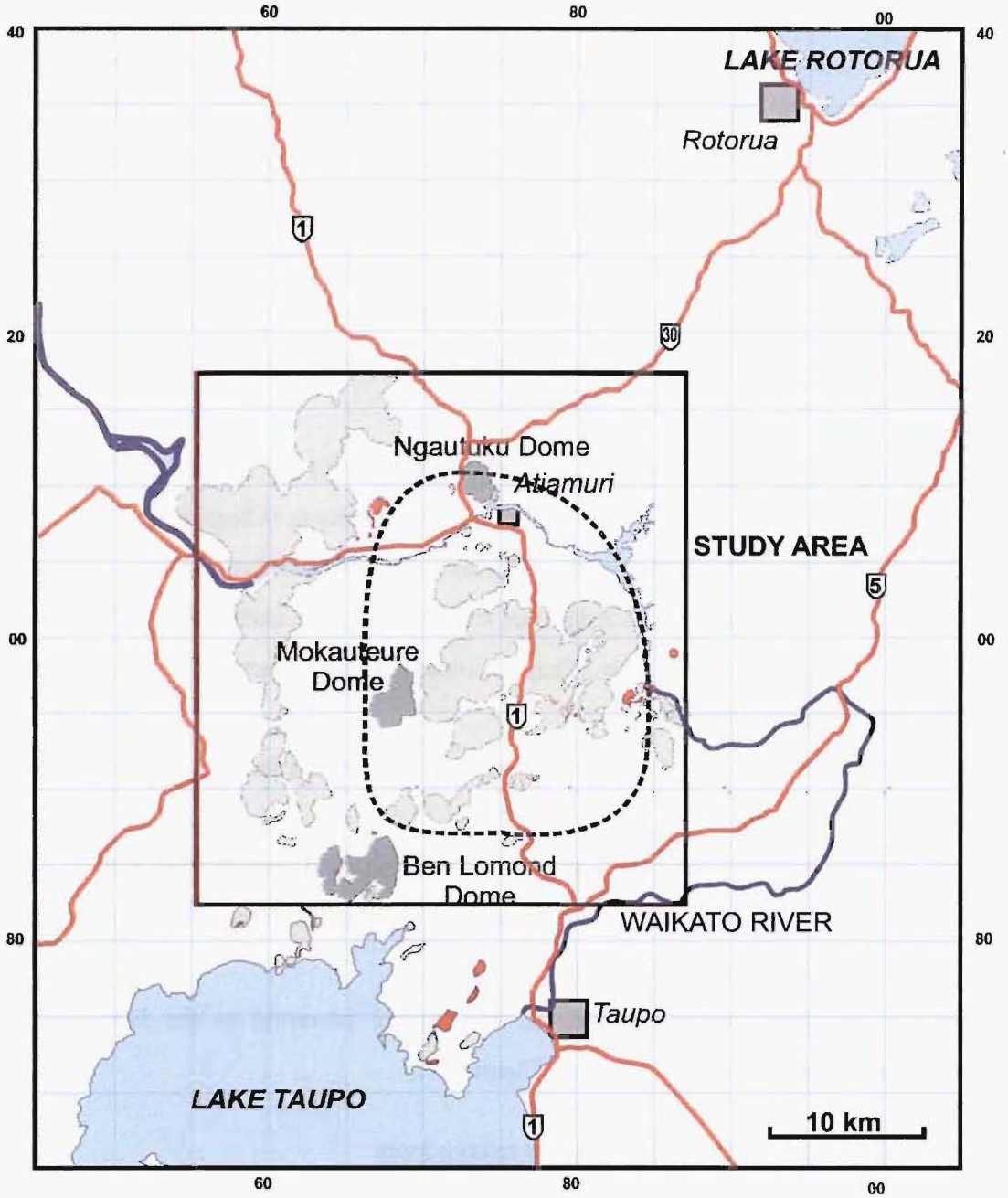

Figure 1.2 Outline of Maroa Volcanic Complex (dashed black line) in relation to Lakes Rotorua and Taupo. Lava domes in the Maroa/Taupo area shown in grey, with domes defining the boundary of Maroa named, and in darker grey. Basalts and key state highways are shown in red. Grid in NZ map grid (labelled in N.Z. metric map grid km on NZ Map Series 260 sheets T16,T17,T18,U16,U17 and U18).

The complex is comprised of hills and ridges (reaching to ~ 500 m above the east- and north-bounding Waikato River) formed by variably coalescing rhyolite lava domes that are flanked by aprons of pyroclastics and alluvium. The valleys are filled, to depths sometimes exceeding 100 m, by ignimbrites from Taupo and lesser volumes of lacustrine and alluvial sediments. In some areas, Maroa-derived ignimbrite plateaus rise up to 100 m above the younger fill.

A drainage network, often deeply incised into sediments and pyroclastics, follows valleys between the domes to reach the Waikato River. The Waikato River forms the eastern and northern boundary of Maroa. It is dammed to form the Atiamuri and Ohakuri lakes in the study area.

1.3 Volcanic nomenclature

Definitions of several key terms are given here. This is critical because these terms are used in the literature with a variety of definitions and those definitions are often ambiguous or only implied.

1.3.1 Block-and-Ash-Flow (BAF) deposit

A BAF is a flow with a specific grainsize characteristic and temperature which can correctly be considered both a debris flow and a pyroclastic density current. It is a hot flow that contains a large fraction of blocks (> 64 mm long) which grade continuously in grainsize to fine ash (Freundt, Wilson and Carey, 2000). It is, therefore, very poorly sorted. It is commonly produced by the collapse of part of a hot growing lava dome. The deposit left by a BAF is termed a 'BAF deposit'.

There is a continuum between the end-member pyroclastic flow deposit 'ignimbrite' and 'BAF deposit', which is expressed well in the deposits of the Pukeahua Fan discussed in Chapter 2. Another pyroclastic density current end-member is a 'surge', but these are not well preserved/exposed at Maroa (other than the Puketarata eruption, Brooker et al., 1993). so the term is not used herein.

1.3.2 Caldera

A caldera is defined as a collapse-induced volcanic depression produced when country rock overlying a magma chamber collapses while, or immediately after, part or all of the volume of the magma chamber is erupted (this is the 'collapse caldera' as defined by Williams, 1941). Calderas can theoretically occur as a simple piston, or more complex piecemeal, trap-door, downsag or funnel collapse (Lipman, 1997). Milner et al. (2002a) noted that Rotorua Caldera in TVZ was a product of a complex combination of these styles, which is probably a result of the transtensional structural setting of TVZ.

1.3.3 Ignimbrite

Ignimbrite is a deposit from a ballistically, or column collapse, driven, concentrated pyroclastic density current (Cas and Wright, 1988). 'Ignimbrite' is not considered here to include the deposits of Block-and-Ash-Flows (BAFs, see below). The term 'ignimbrite' is only used to describe the deposit of a pyroclastic flow. In addition to the use of 'ignimbrite' as a genetic term, New Zealand stratigraphy (e.g. Martin, 1965) uses 'ignimbrite' to as a stratigraphic term. In this thesis the total deposits of an eruption, or group of related eruptions, are referred to by the capitalised name and the suffix 'pyroclastics' (even if previous workers have formally named them with the capitalised suffix 'Ignimbrite'). This separates the descriptive term ignimbrite from possibly confusing use as a formal term for the deposits from an eruption that may include a variety of deposits.

1.3.4 Lava dome

Rhyolite lava is often extruded as lava 'domes'. The following description is modified after Cole (1970) and Richnow (1999)'s descriptions of dome structure. A core of crystalline rhyolite is sometimes surrounded by finely vesicular pumiceous glassy rhyolite (Fig. 1.3). The dome often overlies a basal auto-breccia. The subaerial surfaces are enclosed by a pumiceous carapace breccia. The vesicular zone and carapace vary in thickness and if the carapace is thin enough a quenched obsidian facies forms around the core. Localised hydrothermal alteration is common.

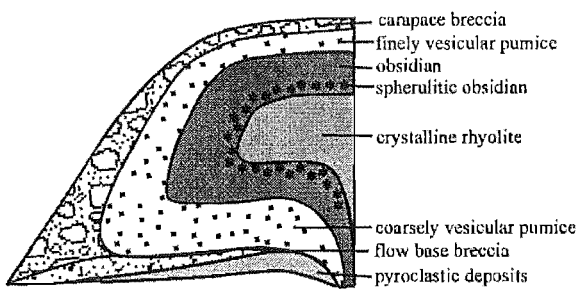

Figure 1.3 Idealised representation of the lithological zonation of a rhyolite dome. Modified after Richnow (1999).

Domes may be completely isolated or within a dome complex. Over 90 % of the volume of Maroa domes coalesce to form dome complexes. Within complexes, separation into named domes is done in this thesis to facilitate discussion and does not necessarily distinguish eruptions. Any one dome is often comprised of a series of lobes.

The summit plateau and any lobes are morphological units that are not distinguished from one another in this thesis, unless there is evidence to suggest temporal or magmatic distinction between them.

1.3.5 Pyroclastics

'Pyroclastics' has the same definition as tephra (below), although pyroclastics may be consolidated whereas tephra is generally not used to describe consolidated deposits in New Zealand. Many authors shorten 'airfall tephra' to 'tephra' so the latter is often colloquially used to refer to an airfall deposit. Any deposit not formally named a tephra by previous worker(s) is referred to as a 'pyroclastics' unit in this thesis to avoid confusion over the meaning of the term 'tephra'.

'Pyroclastics' is used here to refer to the deposits of a specific eruption, or related group of eruptions, including all pyroclastic density current and airfall lithologies. Many of the former have been formally named by previous workers. The word 'ignimbrite' (lowercase) is a genetic term which is reserved in this thesis for the description of a specific unit deposited by a known process (see above). The only instance in which a deposit is referred to here by name as an 'Ignimbrite' (capitalised) is where it has been accepted as a formal stratigraphic name for an ignimbrite-only deposit (with reference given to the defining publication). In contrast the Mamaku pyroclastics have been referred to by most previous workers (most recently Milner et al., 2002b) as the 'Mamaku Ignimbrite', even though they contain multiple ignimbrites and non-ignimbrite pyroclastics.

1.3.6 Tephra

Tephra is any pyroclastic deposit produced by a volcanic eruption. This includes airfall and pyroclastic density current deposits. This is the definition as used by Froggatt and Lowe (1990) and is kept here only because most previous workers in New Zealand have formally used 'Tephra'(capitalised) as a suffix to the names of eruptions producing stratigraphically important airfall deposits. This term is only used in this thesis where other authors have used it to formally name a unit. Otherwise the term pyroclastics is used (see above).

1.4 Previous work and the geological setting

1.4.1 Evolution of understanding of TVZ

Hochstetter et al. (1864) first mapped this area of the North Island and recognised the area as being primarily comprised of volcanic material. More detail was provided by soil mapping, which focussed on young surficial pyroclastics deposits from Okataina (hereafter referred to as 'Okataina') and Taupo volcanic centres (Grange, 1929; Grange, 1931). Grange (1937) defined the term Taupo Volcanic Zone as the broad swath of volcanics from Mt Ruapehu to White Island. As part of a New Zealand Geological Survey mapping campaign at 1:250,000, the Taupo area and the southern half of Maroa were mapped by Grindley (1960) and the Bay of Plenty, Rotorua and the northern half of Maroa by Healy et al. (1964).

Previous work on the area was by Martin (1961) and Healy (1962), who divided the more extensive pyroclastic deposits into named 'ignimbrites'; most of these names are still in use. A review of recent TVZ tephra stratigraphy is provided by Froggatt and Lowe (1990), partly superseded by Wilson (1993) and Jurado-Chichay and Walker (2000). Gamble et al. (1993) discussed the role of minor basalts in TVZ evolution.

TVZ was the focus of a Journal of Volcanology and Geothermal Research special volume (number 68) in 1995. It contained review papers on: geophysical modelling of the sub-surface structure of TVZ by Bibby et al. (1995); the sources and evolution of TVZ magmas by Graham et al. (1995); and the Wilson et al. (1995) review of the volcanic and structural evolution of TVZ. The chronology of eruptions from TVZ has most recently been summarised by Houghton et al. (1995), while a publication in preparation by B. F. Houghton, C. J. N. Wilson and others will provide a new revision of the chronology, volcanology and structure of TVZ. The only comprehensive recent paleomagnetic study of TVZ was conducted by Tanaka et al. (1996). Wilson et al. (1986) defined the location and inferred margins of the Whakamaru caldera.

1.4.2 Defining Maroa

It is important to clarify what is referred to by the term 'Maroa Volcanic Centre'. Healy (1962) drew a dashed line connecting domes north and northeast of Lake Taupo to what is now know as the Western Dome Belt (WDB, see below). Later, Healy (1964) joins this dashed line in an oval through domes to the north, near Rotorua and Okataina,

calling the enclosed area the Mokai Ring Complex and the complex of domes in the centre of the circle Maroa Volcanic Complex. Subsequent work has shown that there is no evidence to justify linking the domes that Healy used to define his ring complex (e.g. Wilson et al., 1986). However, Cole (1990) refers to Maroa as the entire area within Healy's Mokai Ring Complex, including Whakamaru and Kapenga calderas.

The WDB is comprised of the Northwestern Dome Complex (NWDC) and Western Dome Complex (WDC) (Fig 1.4), divided by the Waikato River at the Ongaroto Gorge. The Mokai Ring Complex is considered to be an invalid term and, therefore, Cole's (1990) application of the term Maroa appears to be incorrect. Healy's (1962) original definition of Maroa, as a cluster of rhyolite domes within an area about 16 km in diameter with vents aligned northeast, is preferred and is adopted here. The boundary between Maroa and Taupo is shown in Chapters 3, 4 and 5 to be somewhat arbitrary. The southern boundary of Maroa is here considered to be an east-west line immediately north of Ben Lomond dome, which has been defined by previous workers (esp. Wilson et al., 1986) as the northernmost dome not part of Maroa. The westernmost dome within Maroa is Mokauteure, the northernmost Ngautuku and the eastern boundary is approximately the present location of Waikato River (Fig. 1.2). Maroa domes are described in detail in Chapter 2. The reader is referred to maps in that chapter for the locations of these individual domes.

1.4.3 Previous work on Maroa geology

Some local Maroa geology was summarised in the Atiamuri hydroelectric investigation (Thompson, 1958) and the first mapping of the Maroa area was published around 1960 (see below). Following this mapping, Maroa and the WDB were defined by Healy (1962) (see discussion above). The Whakamaru group pyroclastics were mapped and studied by Martin (1965). The only published detailed mapping of the area is by Lloyd (1972), which covers the eastern half of Maroa, but is primarily a geological and geothermal description of Orakeikorako geothermal area. Brooker et al. (1993) describe and interpret the youngest (Puketarata) eruption from southern Maroa. The most recent work on Maroa, prior to this thesis, was various mapping conducted by the New Zealand Geological Survey which remains largely unpublished (see below).

1.4.4 Mapping of Maroa

Boundaries of previous mapping are shown in Figure 1.4. New Zealand Geological Survey (NZGS) Geological Map of New Zealand sheets combine to form the only published maps of the entire Maroa area. These are: Sheet 5, 1:250,000 Rotorua (Healy et al., 1964); Sheet 8, 1:250,000 Taupo (Grindley, 1960); Sheet N85 1:63,360 Waiotapu (Grindley, 1959); and Sheet N94 1:63,360 Taupo (Grindley, 1961).

In 1966 B. N. Thompson completed a detailed geological map of the Maroa district as a Masters thesis at Auckland University (Thompson, 1966). E. F. Lloyd produced the most detailed published map as part of a bulletin (Lloyd, 1972), but it only covers part of the Maroa area. In the 1970s and 1980s E. F. Lloyd, C.P. Wood, B. F. Houghton and I. A. Nairn, with help from others, worked on and off revising the mapping of Maroa. Results of the detailed mapping from the 1970s have not been published in detail, although a summary was published by Wilson et al. (1986). The Institute of Geological and Nuclear Sciences (IGNS) and E. F. Lloyd have kindly provided drafts of these maps as a resource for the preparation of this thesis. They have been summarised and adapted here with appropriate acknowledgement.

1.4.5 Key theses

This is a summary of relevant pervious graduate theses on the geology of the Whakamaru – Maroa – Taupo area, and their use in this work. Results of these theses are discussed in later chapters. Thompson (1966) produced a detailed morphological map of the Maroa lava domes and described outcrops of many of the pyroclastic deposits. No interpretation of the data was made beyond a brief analysis of the economic potential of the eruptives.

During the 1980s Graeme Corlette started a thesis at Australia National University, Canberra, based on geochemical analyses of eruptive units (mostly lavas) in the Maroa area. Before discontinuing his thesis research, he had completed whole-rock chemical analyses of a partial range of WDB samples, and a few eruptives within Maroa. These analyses have been kindly made available by Professor Ian Smith of the University of Auckland and are used (with acknowledgement) in this thesis where referenced.

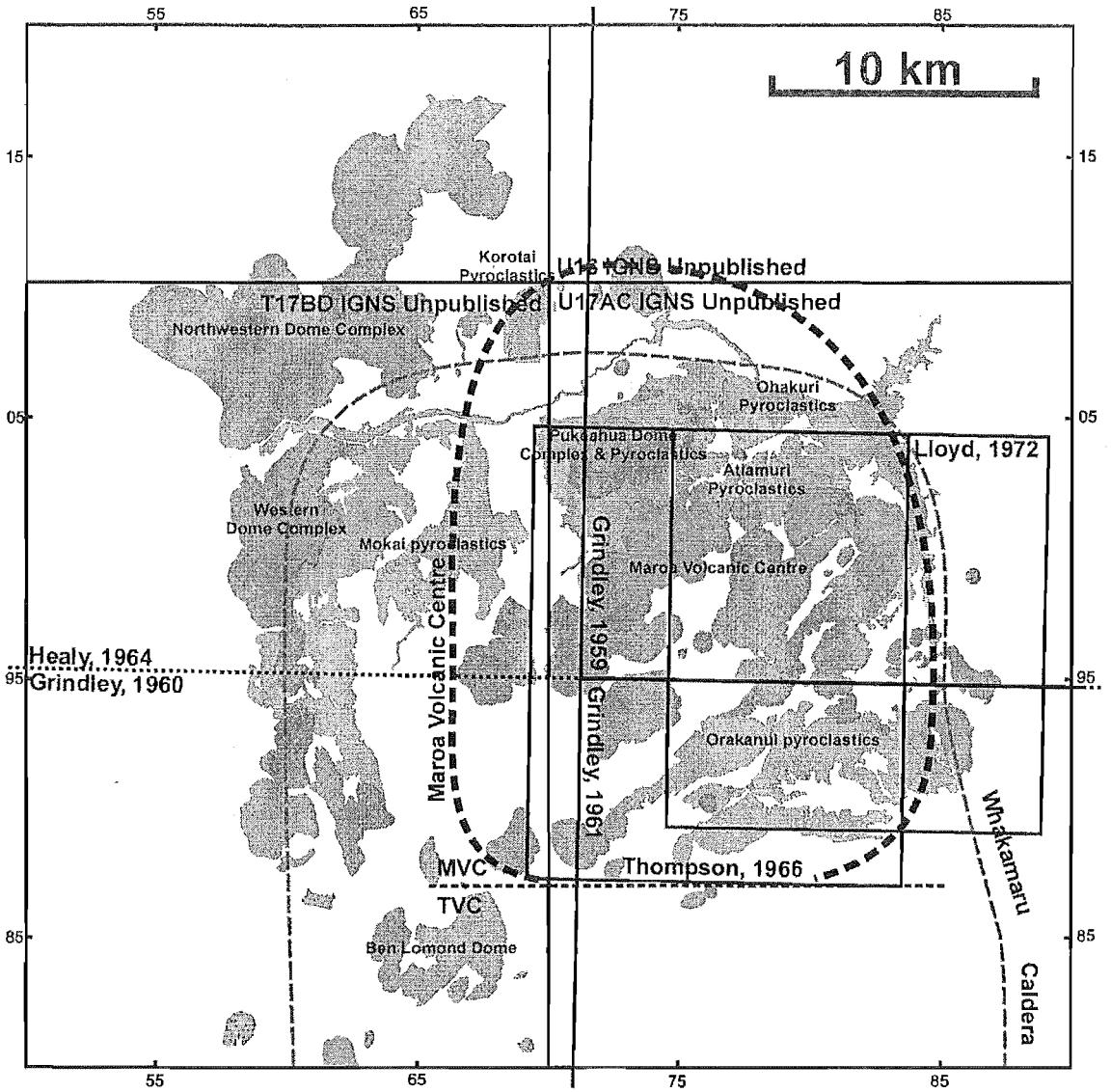

Figure 1.4 Boundaries of previous geological maps in the Maroa area. The boundary between Maroa and Taupo is marked. Map grid numbers as in Figure 1.2.

Brown (1994) studied the geology and geochemistry of the Whakamaru group pyroclastics and the WDB as part of a Ph.D. thesis from the University of Canterbury. He also added data supporting the probable boundary for the Whakamaru caldera defined by Wilson et al. (1986). Subsequently published articles by Brown (Brown et al., 1998; Brown and Fletcher, 1999) addressed magma chamber dynamics of the Whakamaru group pyroclastics.

Sutton (1995) investigated the evolution of the magma system below Taupo for a Ph.D. thesis at the Open University, U.K.. Charlier (2000), also as a doctoral student at the Open University, investigated the long-term dynamics of magma storage and generation below Okataina and Taupo using U-Th isotopes.

Milner (2001) completed a Ph.D. thesis at the University of Canterbury modelling the formation of Rotorua caldera and its eruptives, the Mamaku pyroclastics. He addressed previous inferences that the Mokai pyroclastics, west of Maroa, were a distal correlative of the Mamaku pyroclastics.

Darren M. Gravley is currently completing a Ph.D. thesis at the University of Canterbury on the eruption dynamics and emplacement of the Ohakuri pyroclastics. These deposits overlap into Maroa and were erupted from a source geographically and temporally associated with the Maroa magma system. This thesis is integrated with the research of Gravley, and fieldwork for the two was conducted concurrently. Gravley is also reviewing the geology of parts of the Kinleith Forest area north of Maroa.

1.4.6 Structural and geological setting

TVZ is the surface expression of magmatic activity generated at the convergent boundary of the Pacific (oceanic crust portion) and Australian (continental crust portion) Plates. Off the east coast of the North Island the Pacific Plate is subducting westward below the Australian Plate (Fig. 1.5) at ~ 50 mm/year, around a relative instantaneous pole of rotation at 62°S, 174°E southeast of the North Island (Chase, 1978). The top of the subducting slab is metamorphically dehydrating at ~ 50 to 100 km depth below the central North Island (Fig. 1.6); the resultant fluids produce partial melts in the mantle wedge above, and this melt is driven towards the surface of the continental crust of the Australian Plate as a result of its relative buoyancy.

The bulk of the upper crust in the central North Island is made up of various sedimentary lithologies, most of which is greywacke (Mortimer, 1994). Greywacke comprises the backbone of New Zealand and based on surface outcrop in the central North Island it is likely that only Torlesse and/or Waipapa Terranes (both Permian or younger) are present below TVZ (Bradshaw, 1989). Older basement only appears to be present at this latitude to the west of Taranaki, offshore of the central North Island. Note that in contrast to similar caldera-hosting volcanic fields elsewhere in the world, notably at Yellowstone (USA), there is no evidence for pre-Cambrian-aged basement below TVZ. Rising magma below TVZ probably assimilates some of this sediment and also undergoes fractional crystallisation (Graham et al., 1995). The surface pattern of eruption locations has been modelled in three ways (Fig. 1.7):

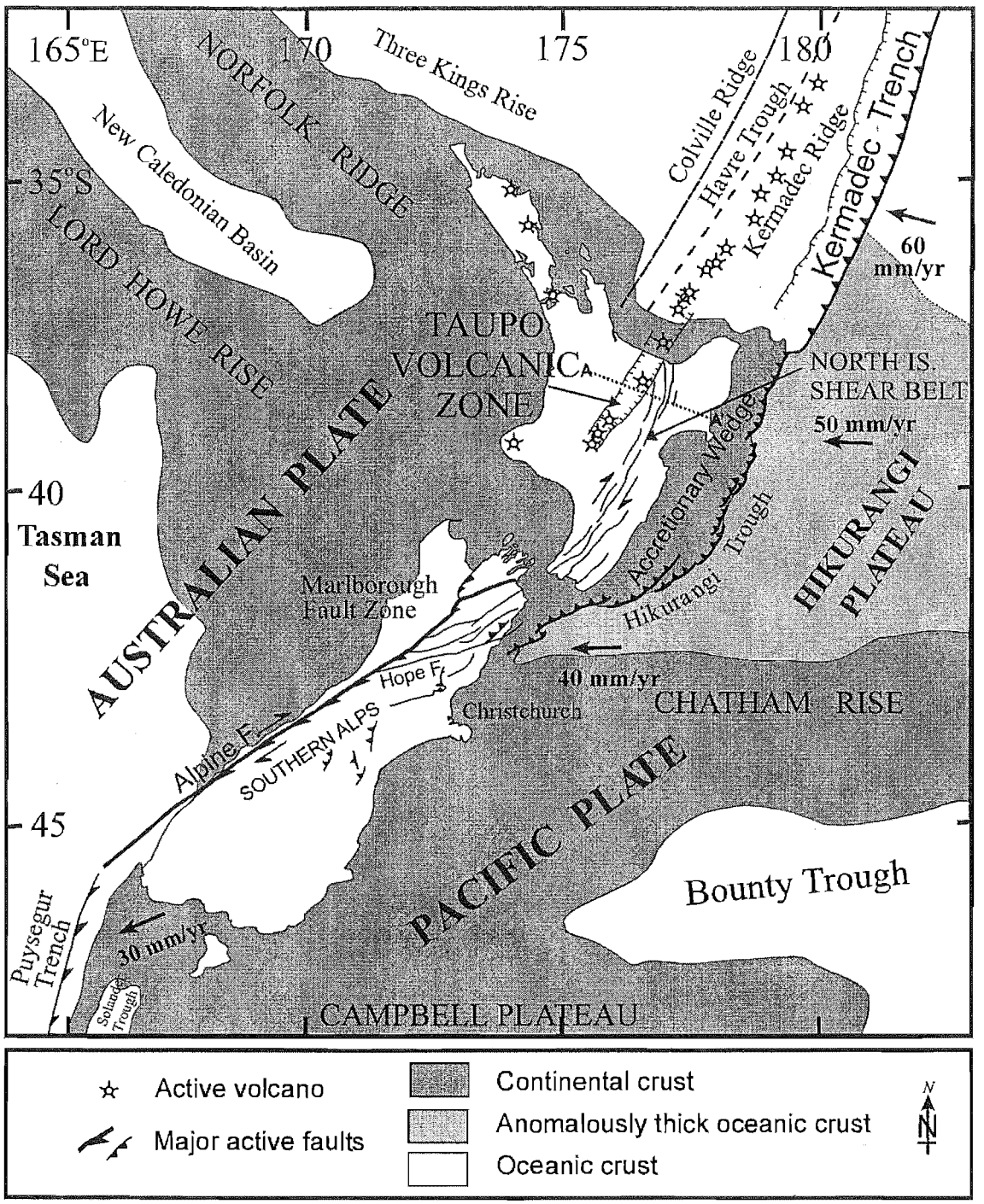

Figure 1.5 Generalised map of New Zealand structural features associated with the obliquely convergent Australia-Pacific plate boundary zone. Grey area within ocean areas represents continental crust. Light grey area indicates anomalously thick oceanic crust. White area (other than New Zealand) indicates oceanic crust. Arrows show motion of Pacific plate relative to the Australian plate. Rates are from Walcott (1987) (F) = fault. Adapted from Pettinga et al. (1998) and Cole (1990). Line A-A' is cross section in Figure 1.6.

(a) Stern and Davey (1987): Present-day volcanism follows the front of a migrating andesitic arc of the Central Volcanic Region (CVR). Prior to 4 Ma, this front was nearly

north trending and in line with the Coromandel Peninsula. Behind this front is a zone of rhyolite volcanism, which Stern and Davey saw as only the more visible, younger expression of volcanism across the more significant wider CVR. Their conclusion that the CVR is the most significant volcanic structure is the result of their focus on seismic data. They modelled low velocity mantle and thin crust across the entire wedge-shaped CVR.

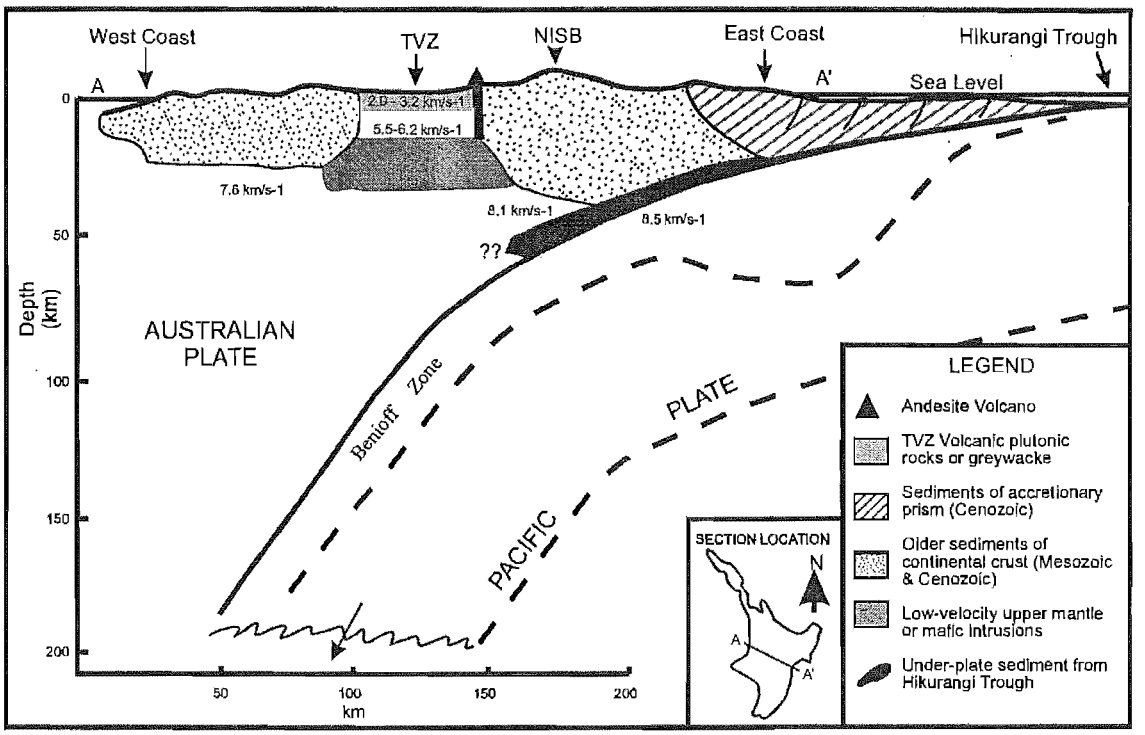

Figure 1.6 Schematic cross-section through the central North Island showing crustal and upper mantle structure as determined from seismology. 'NISB' refers to the location of the North Island Shear Belt. After Cole (1990) and Wilson et al. (1995). Line of section is shown as A-A' in Figure 1.4.

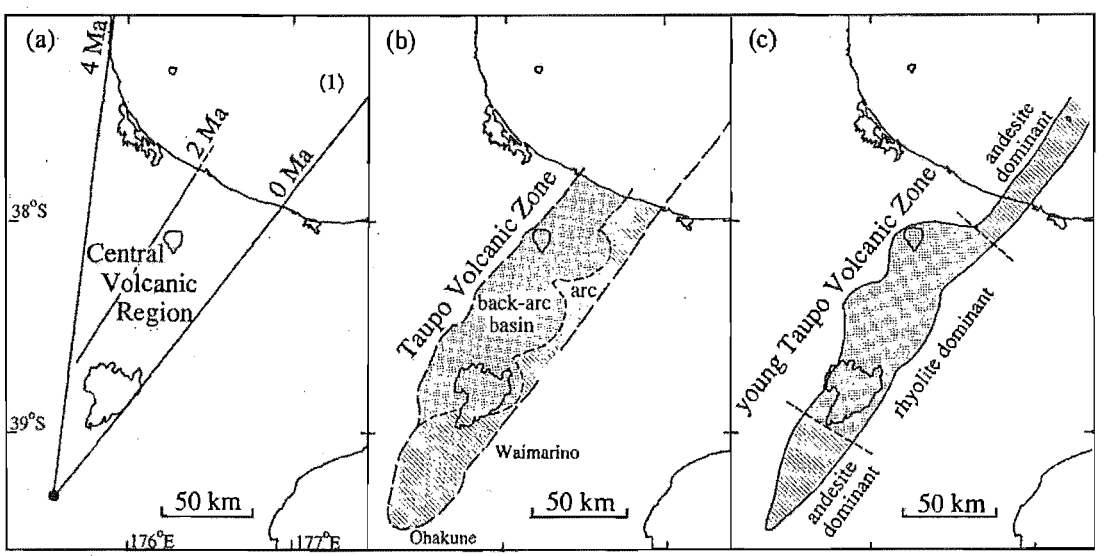

Figure 1.7 Three models of TVZ activity modified from Wilson et al. (1995). See text for details.

(b) (Cole, 1990): Fractionated magma erupts as the line of andesitic cone-building volcanoes stretching from the southwestern end of TVZ to offshore vents in the northeast, and beyond the continental crust, to the chain of islands and submarine vents of the Kermadec Ridge. To the northwest, behind the middle of this arc, is a zone of active rifting. Most magmas reaching the surface within this zone are rhyolites, which form caldera volcanoes, lava domes and associated tephras. The rifting stress is overprinted by shear stress from the oblique component of the plate convergence.

(c) (Wilson et al., 1984): The TVZ is segmented into andesite-dominated northeastern and southwestern sections separated by a central rhyolite dominated section. The central section contains a few dispersed andesite vents that are minor in volume compared to the dominant rhyolite lithology, with which they are closely spatially associated.

The rhyolitic volcanics are broken by many normal, extension-driven faults collectively referred to as the Taupo Fault Belt (Grindley, 1960; Villamor and Berryman, 2001). The tensional stress field, in which the principle regional stress is gravitational, leads to a complex geomorphic relationship between volcanic and tectonic structures. This is discussed in more detail in Section 1.7.

1.4.7 Subsurface geology

TVZ probably lies over a basement partly comprised of greywacke. This has been inferred from a few deep geothermal drill holes striking greywacke (Wilson et al., 1995), a seismic basement of V_p 4.8 – 5.5 km/s at ~ 2.2 km depth (Stern and Davey, 1987), and nearby surface greywacke outcrops outside of TVZ. The greywacke is probably interspersed with an uncertain quantity of young plutonic rocks. Some workers (e.g. Stern and Davey, 1987) have suggested, based on geophysical evidence, that andesite intrusions have entirely replaced any sedimentary basement. Above the basement lies a stack of lavas and tephras erupted from TVZ vents within the region of extension. This suggestion has been supported by geothermal drill holes throughout the Zone.

The base of the crust has been suggested to lie at ~ 15 km depth where rocks change in seismic velocity from V_p 6.1 km/s to 7.4 – 7.5 km/s below (Stern and Davey, 1987). The transition at ~ 15 km is probably complex as there must be a large volume of

intrusives at deep crustal levels to produce (through melting or fractionation) the volumes of rhyolite magma erupted at the surface of TVZ. Hochstein et al. (1993) suggested that the seismic boundary at ~ 15 km may represent the top of these mafic plutonic intrusives and that the boundary between these and true mantle has not yet been resolved.

1.4.8 Distribution of volcanism

Active andesitic volcanism is confined to the northeastern and southwestern ends of the onshore TVZ, with variously aged andesite volcanoes throughout the central section of the zone, where caldera collapse is absent. The area of active rifting is dominated by spatially overlapping calderas that have been active at different times throughout the last 1.6 Ma (Houghton et al., 1995). Surface expression of older calderas is quickly lost through erosion and burial by subsequent eruptions. The distribution of currently discernible calderas and volcanic centres is shown in Figure 1.1. Although these appear to be spatially independent features, if all of the vents from the last 1.6 Ma could be mapped the Zone might well look more like a single complex of overlapping calderas (Wilson et al., 1995). This pattern is repeated at a smaller scale by the multiple collapses distinguished within the Okataina and Taupo caldera complexes (Nairn, 1989).

1.4.9 Chronology

Activity in TVZ is divided into three periods: Old, Young and Modern TVZ (Wilson et al., 1995). **Old TVZ** encompasses all activity between the onset of volcanism at 2 Ma and the eruption of the Whakamaru group pyroclastics from Whakamaru caldera at 320 - 340 ka (Pringle et al., 1992; Houghton et al., 1995). The extent to which eruptives from Old TVZ activity are preserved at the surface roughly decreases with increasing age. Only deposits from some of the largest eruptions during this period are preserved. Some of these (Ongatiti, Ahuroa, Rocky Hill and Marshall pyroclastics) are attributed to Mangakino Volcanic Centre, while others (Tikorangi, Matahana, Rahopaka and Waiotapu pyroclastics) are thought to have come from Kapenga Volcanic Centre (Houghton et al., 1995). The locations of both of these volcanic centres are inferred from the distribution of these deposits and from geophysical data (Rogan, 1982; Wilson et al., 1984).

Young TVZ units were erupted between the Whakamaru group pyroclastics and the present day. There is reasonable preservation of the larger ignimbrites from the caldera

collapses during this period. Some of these units can be clearly traced to a source (e.g. the Mamaku pyroclastics, Milner et al., 2002a). Some of the smaller lavas and tephras are also preserved. The tephras are generally only preserved in small isolated areas.

Modern TVZ activity, from (and including) the caldera-forming Rotoiti eruption at Okataina to the present day, is much better preserved. Tephras from many smaller, non-caldera-forming eruptions are preserved at many locations. Isopach maps for almost all individual plinian eruptions have been constructed and vent sources inferred for most (Froggatt and Lowe, 1990, in their 'Table 1', provide the references for many articles containing isopach maps and inferred vent locations). There have also been two major caldera forming ignimbrite eruptions from Taupo during this period, the Oruanui and Taupo eruptions (discussed below).

It is most likely that activity of the scale and style recorded in modern TVZ has also occurred over much of the total TVZ history, but is poorly represented due to erosion.

1.5 Modern TVZ eruptions and their deposits present in Maroa

Those modern TVZ eruptions that produced deposits still preserved within Maroa are described here. These deposits are important to Chapter 2 interpretations of Maroa activity during Modern TVZ. Rotoehu Ash, from the Rotoiti eruption, in particular mantles many domes, providing a younger age-limit for them. There were at least eight other eruptions and eruptive episodes from Okataina, and one other eruption from Taupo (Froggatt and Lowe, 1990), during this time for which there are no deposits preserved near Maroa. The locations of modern TVZ vents are shown in Figure 1.8, and each eruption important to this work is described below.

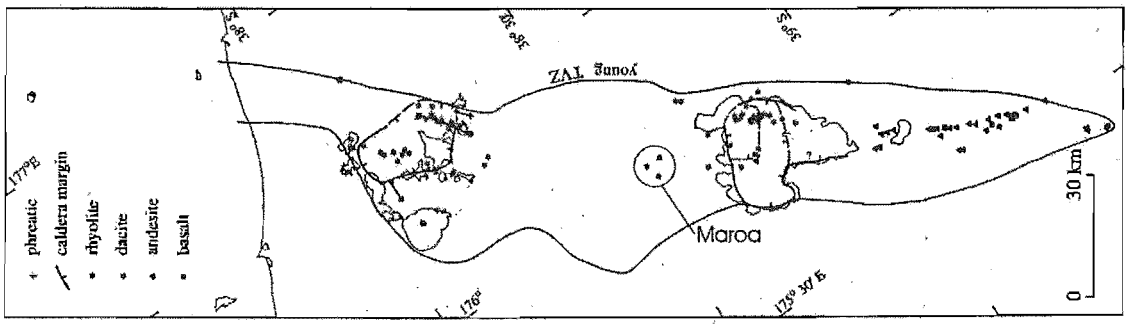

Figure 1.8 A provisional distribution of modern TVZ vent sites (Maroa vent sites are circled) and calderas. Some have been omitted because of a lack of information on the vent position. From Wilson et al. (1995).

1.5.1 26.5 ka Oruanui and 1.8ka AD Taupo eruptions –Taupo Volcanic Centre

The Taupo eruption culminated in the second and most recent caldera collapse event at Taupo (Wilson and Walker, 1985). It evacuated > 35 km^3 of magma and resulted in the collapse of a section of the northeastern portion of the older syn-Oruanui caldera, below Lake Taupo. The eruption culminated in a super-high 'ultraplinian' eruption column and widespread ignimbrite deposit (Walker, 1980; Wilson, 1985). The latter is found throughout Maroa (see Chapter 2). The 26.5 ka Oruanui eruption produced the largest caldera collapse at Taupo. Approximately 530 km^3 of magma was erupted as very widely distributed airfall and pyroclastic density current deposits and intra-caldera tuff (Self, 1983; Wilson, 2001). The pyroclastic density current deposits reached 90 km from source.

Combined ignimbrites and fall deposits from these two eruptions are up to 100 m thick within Maroa. They tend to be preserved within depressions such as stream gullies and valleys and basins between lava domes, where the ignimbrites would have initially ponded to the greatest thickness. Oruanui airfall, and relatively thin ignimbrite, originally covering Maroa lava domes has largely been eroded away. The distribution of Oruanui eruption deposits is shown in Chapter 2.

1.5.2 ~27.3 ka Poihipi Tephra – Taupo Volcanic Centre

Probably erupted from a source immediately east of Taupo township (Sutton et al., 1995), this small volume (1 km^3) airfall deposit is distributed to the north and east from Taupo and reaches Maroa. At its type section (the eastern end of the northern side of a deep road cutting along Poihipi Rd at T17/657890[1]) it is a blue-grey fine to medium massive indurated and cemented ash (Vucetich and Howorth, 1976). The colour, massive appearance, fine grainsize and stratigraphic context are characteristic of this deposit.

1.5.3 ~29 ka Okaia tephra – Taupo Volcanic Centre

The Okaia tephra decreases in thickness to the north, away from a source in northeastern Taupo. The airfall deposit is of moderate size (7 km^3) (Vucetich and Howorth, 1976). The Okaia tephra is a bedded plinian pumice fall deposit, which

[1] Grid references are to the nearest 100 m in the N. Z metric map grid, preceded by the sheet number in the N.Z. Map Series 260, 1:50,000 maps.

commonly sits on a well-developed, cemented paleosol. The ages for Poihipi and Okaia tephras are from Newnham et al. (2003).

1.5.4 c. 40 ka Tahuna Tephra – an eruption in the Maroa area?

The Tahuna airfall deposits in the Maroa area reach 400 mm in thickness (see Chapter 2). A rough plot of the distribution of this deposit shows that it probably thickens in the central TVZ (Fig. 1.9, from Smith and Shane, 2002). Froggatt and Lowe (1990) attributed it to Taupo but it is thicker in the Maroa area than at the northern edge of Lake Taupo (C. J. N. Wilson pers. comm., 2002). It may well have a source in the vicinity of Maroa. It was a relatively small rhyolitic eruption with a minimum magmatic volume of 1 km^3. Without mineral or glass chemistry on Maroa eruptives, or isotopic data on the tephra (neither available at present) any petrological links of the Tahuna Tephra to Maroa cannot be explored.

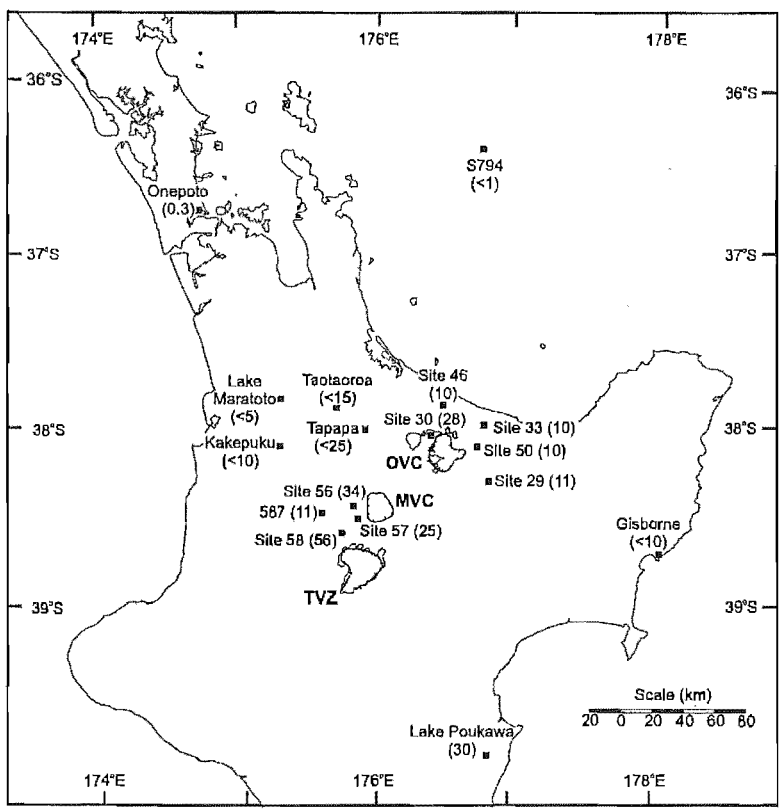

Figure 1.9 A few thicknesses (given in brackets in mm) of the Tahuna Tephra from (Smith and Shane, 2002).

1.5.5 c. 45 ka Tihoi Tephra – Taupo Volcanic Centre

The Tihoi Tephra is a bedded plinian pumice fall deposit, which is 500 mm thick at its type section at T17/575881. It has a lower lithic content, and sometimes better

developed bedding, than Okaia tephra. Distribution suggests a volume > 5 km^3, from a source near the northern shore of Lake Taupo (Vucetich and Howorth, 1976).

1.5.6 50-60 ka Otake Tephra – Taupo Volcanic Cenre

Otake tephra is a small volume (> 2 km^3) deposit distributed north and west of northern Lake Taupo. The source is probably in the northern part of Taupo. The type section, at T17/678866 on the south side of Poihipi Rd, exposes (a) 250 mm yellow brown fine to medium ash as a slippery paleosol, over (b) 770 mm of light yellowish brown thinly bedded fine to medium ash with abundant accretionary lapilli (up to 10 mm) in alternate layers, over (c) 150 mm of grey to pale yellow medium coarse ash with minor lapilli (Vucetich and Howorth, 1976). Numerous accretionary lapilli are the characteristic feature.

1.5.7 50-60 ka Waihora Tephra – Taupo Volcanic Centre

The Waihora Tephra is a small-volume, weakly bedded coarse ash of very limited known extent (Vucetich and Howorth, 1976). It is distributed in the area between Taupo and Maroa around Ben Lomond dome. Only a few exposures are known and its thickness is always less than 200 mm.

1.5.8 62 ka Rotoehu Tephra – Okataina Volcanic Centre

The age of the Rotoehu Tephra is estimated at 62 ± 2 ka from bracketing lavas and deposits dated by K-Ar and Ar-Ar techniques from Mayor Island (Wilson et al., 1992) and modified by new data from M. A. Lanphere at USGS Menlo Park cited in Charlier et al. (2003).

The Rotoiti Tephra consists of the Rotoehu Ash, Rotoiti ignimbrite and Matahi scoria (Nairn, 1972). The Rotoehu Ash, with a bulk volume of at least 50 km^3 (Nairn, 1972), is an important New Zealand marker horizon because it is extremely widely dispersed. It is preserved at several locations around Maroa and it caps most Maroa domes. The usual ferromagnesian mineral assemblage is orthopyroxene (hypersthene), cummingtonite ± hornblende. The presence of cummingtonite is distinctive and unique to this tephra in the Maroa area. Some Rotoehu ash layers stratigraphically above the Rotoiti ignimbrites contain sparse biotite (Nairn, 1972). Outside Okataina, biotite is only found in a few young Maroa lavas (see Chapter 4). The Rotoehu Ash is overlain by Rifle Range Ash from an immediately following, but magmatically independent

eruption (Nairn and Kohn, 1973; Charlier et al., 2003). The Rifle Range Ash contains a ferromagnesian assemblage of orthopyroxene (hypersthene), hornblende and biotite.

1.6 Geological setting: pre-Rotoiti eruptions affecting Maroa

The pre-Rotoiti eruptions listed below have deposited large-scale pyroclastics that are preserved in and around Maroa and are of importance in understanding the evolution of Maroa as described in later Chapters. At least two of these eruptions had vents overlapping with Maroa (see the Ohakuri and Whakamaru eruptions).

1.6.1 ~240 ka Ohakuri pyroclastics

The Ohakuri pyroclastics (Fig. 1.10) is a somewhat ambiguous term within TVZ. They were originally described as the primary lithology in the Ohakuri Group (Grindley, 1959). The definition of the Group included cream to slightly pink or green ignimbrites, sandstones and mudstones. Sedimentary terms were sometimes used partly because early workers didn't recognise airfall and surge deposits interbedded with massive ignimbrites as primary volcanics (Langridge, 1990).

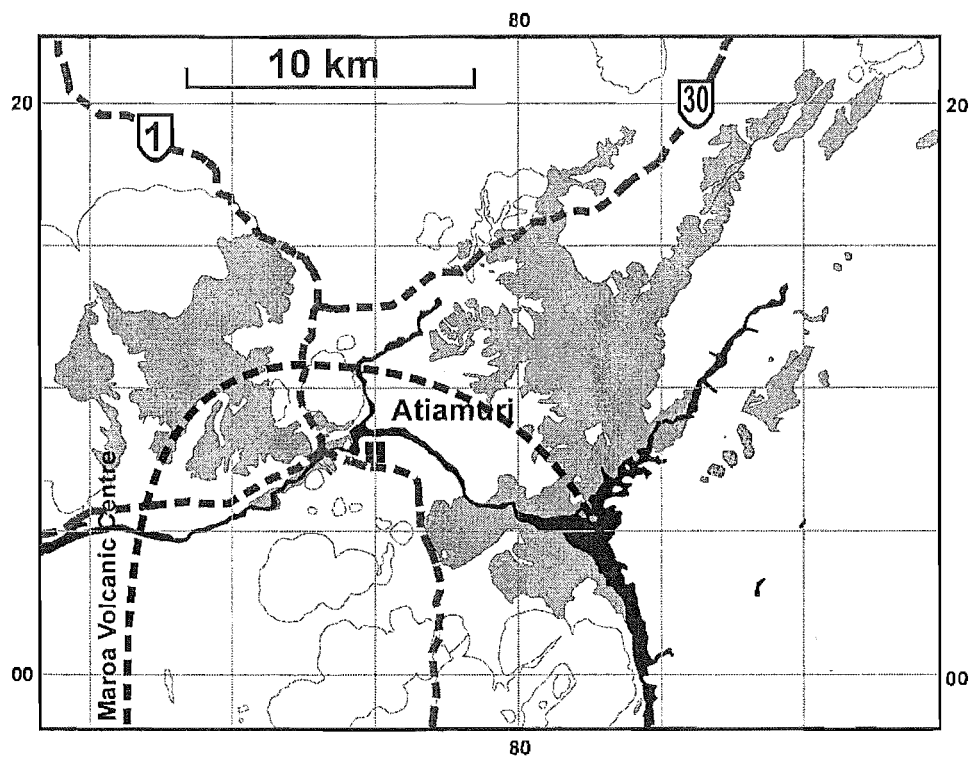

Figure 1.10 Distribution of the Ohakuri pyroclastics (grey). Domes are outlined in black; State highways are dashed. Grid is NZ Map Grid, sheets T16/T17/U16/U17 of series 260. Adapted from unpublished mapping by E.F. Lloyd, C. P. Wood, I. A. Nairn, B. F. Houghton, and others at the Institute of Geological and Nuclear Sciences, and kindly provided for this thesis.

Henneberger and Browne (1988) described the pyroclastic unit "Ohakuri Ignimbrite", and Langridge (1990) commented that the deposits within the Ohakuri group that had previously been interpreted to be sedimentary were probably primary volcanics. Until this time the Ohakuri group had been used as a convenient 'lump term' ascribed to any cream-coloured pyroclastics or sedimentary unit that could not be easily fitted into the existing stratigraphy. Langridge (1990), and work in progress by Darren Gravley, have separated out primary volcanics of the Ohakuri pyroclastics from sedimentary deposits and pyroclastics from eruptions unrelated to them (see Chapter 2 for a summary of Gravley's work to date).

Langridge (1990) considered the "Ohakuri ignimbrite group" to have been erupted from Kapenga Volcanic Centre to the north. However, unpublished New Zealand Geological Survey mapping (E. F. Lloyd, pers comm. 2002), and work in progress by Darren Gravley, suggest a source just north of Maroa.

1.6.2 ~ 240 ka Mamaku pyroclastics

As part of recent Ph.D. research on Rotorua Caldera, David Milner (Milner, 2001) studied the field character and distribution of the Mamaku pyroclastics. He considers them to have been deposited from the eruption that was associated with collapse of Rotorua caldera ~ 240 ka (Milner et al., 2002a, age defined in Chapter 3). Milner et al. (2002b) separate the Mamaku pyroclastics into a basal airfall sequence and a main ignimbrite sequence. The latter is usually massive, from (a) light grey, unconsolidated, pumiceous coarse ash at the base, through (b) dark grey, welded, lenticular material to (c) pink-purple, devitrified, vapour-phase-altered at the top. The Mamaku ignimbrite is distributed radially (apart from a lack of distribution/preservation to the east and southeast) around Rotorua Caldera (Fig. 1.11) and is preserved to within 10 km of Maroa in the south. The Mokai pyroclastics, nestled between Maroa and the WDB, and the Ohakuri pyroclastics were once proposed to be southern correlatives to the Mamaku pyroclastics (Tanaka et al., 1996), however, the correlation between Mamaku deposits and Ohakuri deposits, has recently been disputed (Milner, 2001). The Mokai pyroclastics are discussed in greater detail in Chapter 2.5.2.

1.6.3 ~ 280 ka Pokai pyroclastics

Within the Kinleith Forest, north of Maroa and east of SH1, is an area dominated by pyroclastics with complex and often ambiguous stratigraphic relationships. This area

lies roughly in the rectangle from T16/600400 to T16/700200, and includes the Korotai, Pokai, Chimp, Waimakariri and Ohakuri pyroclastics. Isolated outcrops of older, distinct, Whakamaru (crystal rich and welded), Waiotapu (highly welded) and Rahopaka pyroclastics also occur in this area.

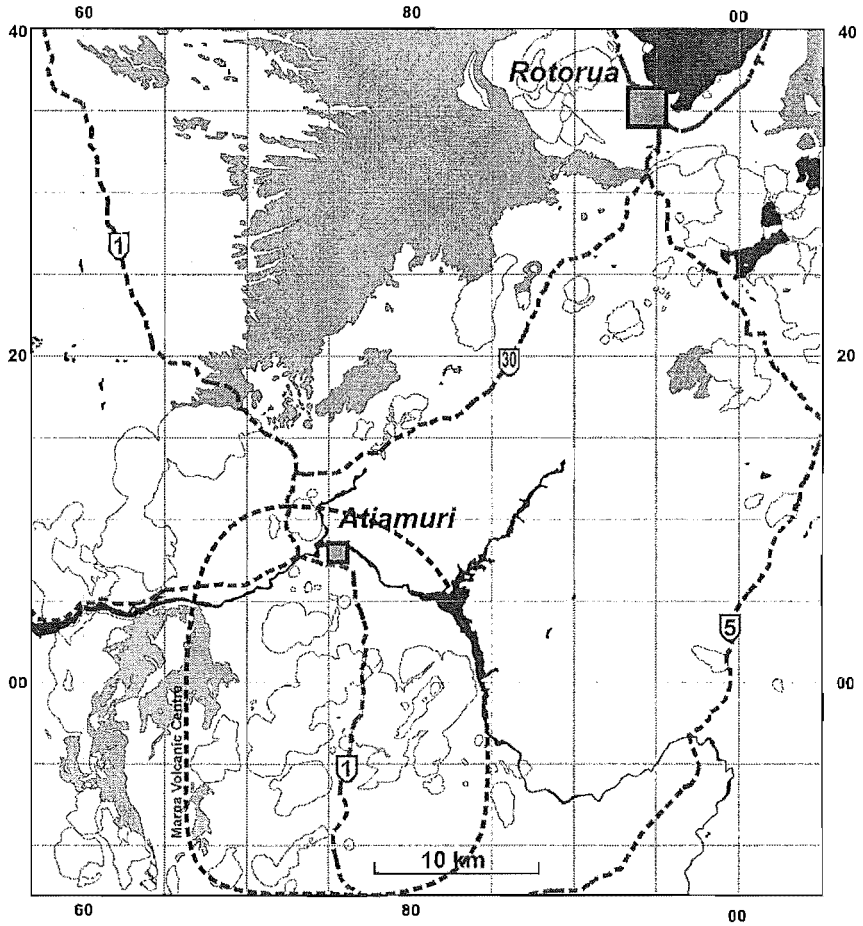

Figure 1.11 Distribution of the Mamaku (grey – outcrop continues north beyond map boundary) and Mokai (light grey) pyroclastics in the area of interest. Lava domes are outlined in black, State highways are dashed. Grid is NZ Map Grid, sheets T16/T17/U16/U17 of series 260. Adapted from unpublished mapping by E.F. Lloyd, I. A. Nairn, B. F. Houghton and others at the Institute of Geological and Nuclear Sciences, and kindly provided for this thesis.

Karhunen (1993) reviewed the distribution of the Pokai and Chimp pyroclastics and investigated their petrology and origin. The Pokai pyroclastics overlap in distribution with the Korotai and Ohakuri pyroclastics which are discussed in later chapters of this thesis. Karhunen (1993) determined that the Pokai and Chimp pyroclastics had come from the east of where they outcrop, probably from Kapenga Volcanic Centre, as previously outlined by Wilson et al. (1984). Their distribution is shown in Figure 1.12.

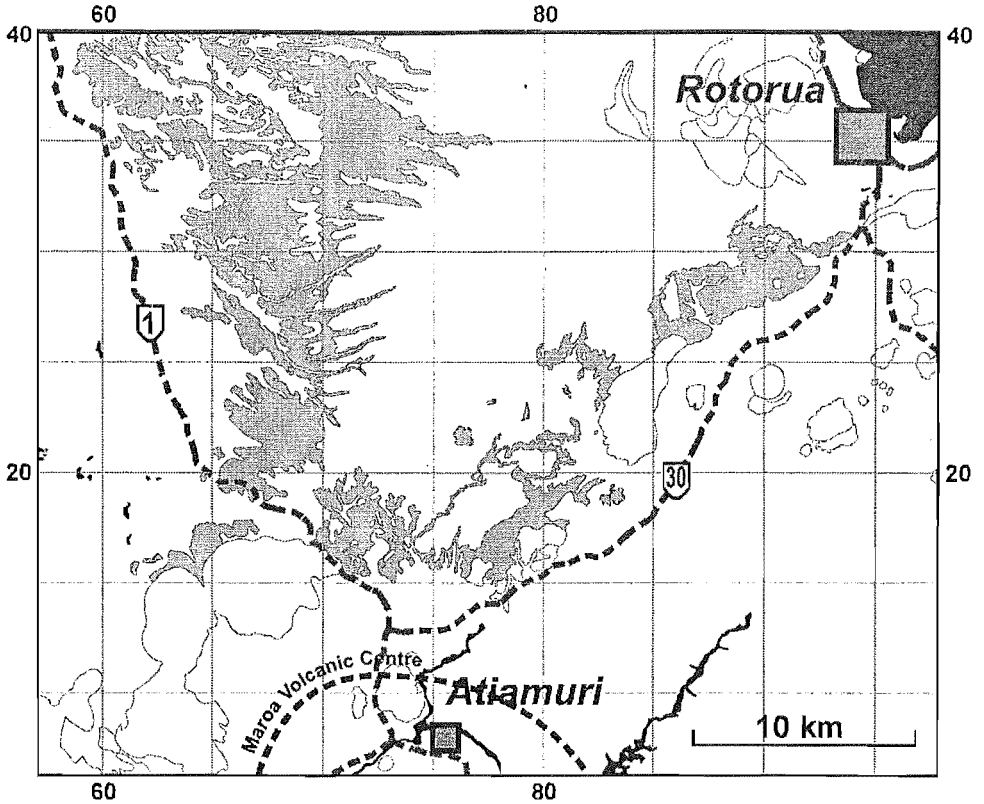

Figure 1.12 Distribution of the Pokai, Chimp and Waimakariri pyroclastics (grey). Domes are outlined in black, State highways are dashed. Grid is NZ Map Grid, sheets T16/T17/U16/U17 of series 260. Adapted from unpublished mapping by E.F. Lloyd, C. P. Wood, I. A. Nairn, B. F. Houghton and others at the Institute of Geological and Nuclear Sciences, and kindly provided for this thesis.

A minimum of 33 km^3 Dense Rock Equivalent (DRE) of magma was deposited as the Pokai pyroclastics, and a further 5 km^3 DRE as the Chimp pyroclastics. Both were preceded by plinian activity. Three pumice types were erupted from either a zoned magma chamber (Karhunen, 1993) or multiple magma bodies. Pumice type 1a is relatively crystal poor, high in silica and low in Sr; Type 1b is relatively crystal poor, low to high in silica and high in Sr; and Type 2 is relatively crystal rich, moderate to low in silica and high in Sr.

Ph.D. research currently being undertaken by Blair Lynch-Bloss at Waikato University is attempting to further constrain field relationships within and surrounding the Pokai pyroclastics. Darren M. Gravley is investigating the field relationship of the Pokai pyroclastics to the Ohakuri pyroclastics as part of his Ph.D. research at the University of Canterbury.

1.6.4 320 – 340 ka Whakamaru eruptions

Overview

The Whakamaru pyroclastics were first described and discussed in detail by Martin (1965) and Briggs (1976a; 1976b). The eruption of the Whakamaru group pyroclastics was the focus of a Ph.D. thesis by Stuart Brown (Brown, 1994). His work built on that of Wilson et al. (1986) who originally defined the group of pyroclastics and a probable location for the source caldera. The description that follows is a revised summary of these two pieces of work. The group comprises the previously mapped Whakamaru, Mananui, Rangataiki, Te Whaiti and Paeroa ignimbrites, which were erupted between 320 and 340 ka (Houghton et al., 1995), from a caldera stretching from the WDB to northern Lake Taupo (Fig. 1.13).

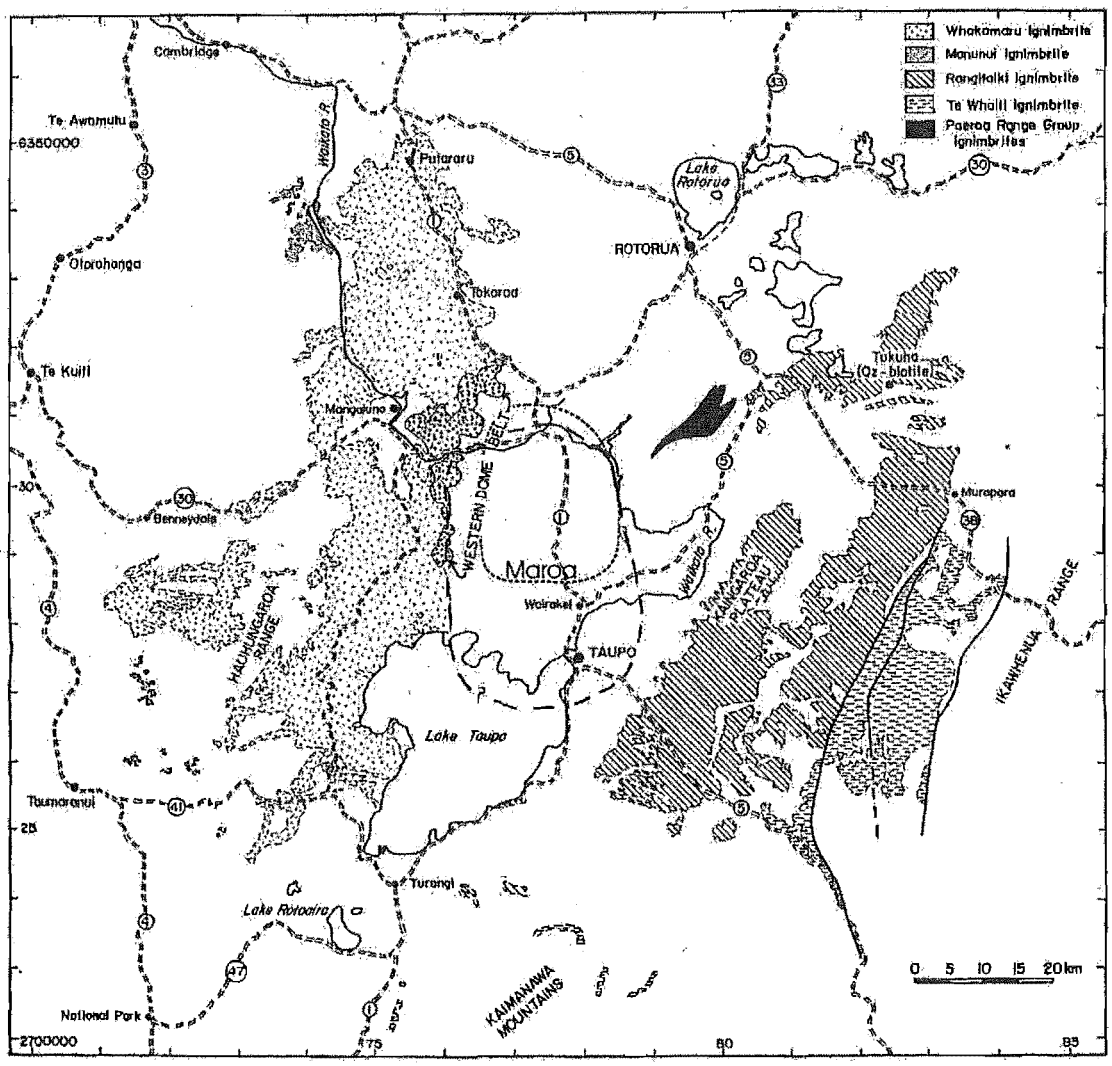

Figure 1.13 Map of proposed Whakamaru caldera (dashed oval) and associated eruptives from Brown (1994).

Deposits

The Whakamaru group pyroclastics outcrop over a total area of 13,000 km^2 (Fig. 1.13). The group consists of the Whakamaru and Manunui ignimbrites outcropping to the west of Whakamaru caldera, and Paeroa Range group, Rangitaiki and Te Whaiti pyroclastics to the east. Manunui ignimbrites may be generally considered equivalent to the Te Whaiti pyroclastics. Similarly, the Whakamaru pyroclastics appears equivalent to the Rangitaiki pyroclastics (Brown et al., 1998).

Within Whakamaru caldera, the Whakamaru group pyroclastics are over-thickened to up to ~ 1 km in some places, based on drill-core (Wilson et al., 1986). The top of the pyroclastics is down-faulted to ~ 700 m below the present-day land surface, as revealed in drill cores at Mokai (Wilson et al., 1986).

Eruptive source

Wilson et al. (1986) delineated Whakamaru caldera (Fig. 1.13) based on drill-hole data, geophysical data and the distribution of the Whakamaru group pyroclastics. Previously, a source in western Lake Taupo had been inferred (Briggs, 1976a). The western boundary of the caldera is the most clearly defined. The position of the WDC (part of the WDB, described below) coincides with down-faulting and over-thickening of the Whakamaru group pyroclastics to the east, making the complex a likely marker for the caldera's western margin. Maroa volcanism, extensional northeast trending faulting, and the emplacement, and possible source caldera, of the Ohakuri pyroclastics overprint the northern margin. The southern margin lies somewhere within the collapse areas of the younger Taupo Volcanic Centre calderas and the eastern margin probably coincides with the north-northwest trending structures parallel to Whakapapataringa dome (Wilson et al., 1986). Multiple vents probably coincided with collapse in different areas at different stages in the eruption from north Taupo to near the Paeroa Fault Scarp (Fig. 1.14) (Brown, 1994).

Eruption dynamics

Eruption dynamics are briefly summarised here as they have implications bearing on the subsurface geology at Maroa, discussed in Chapter 5. There is no evidence of an early plinian phase to the Whakamaru eruption so the initial vent was probably relatively wide and/or gas velocity at the vent was low (Brown et al., 1998). Multiple collapses over a wide area of the central TVZ, heavily controlled by regional faulting, probably

drove the eruption (Brown, 1994). Lithics of what appears to be Whakamaru ignimbrite occur in upper Whakamaru and Rangitaiki ignimbrite units, indicating that the vent area(s) moved, possibly widening, over the course of the eruption (Wilson et al., 1986).

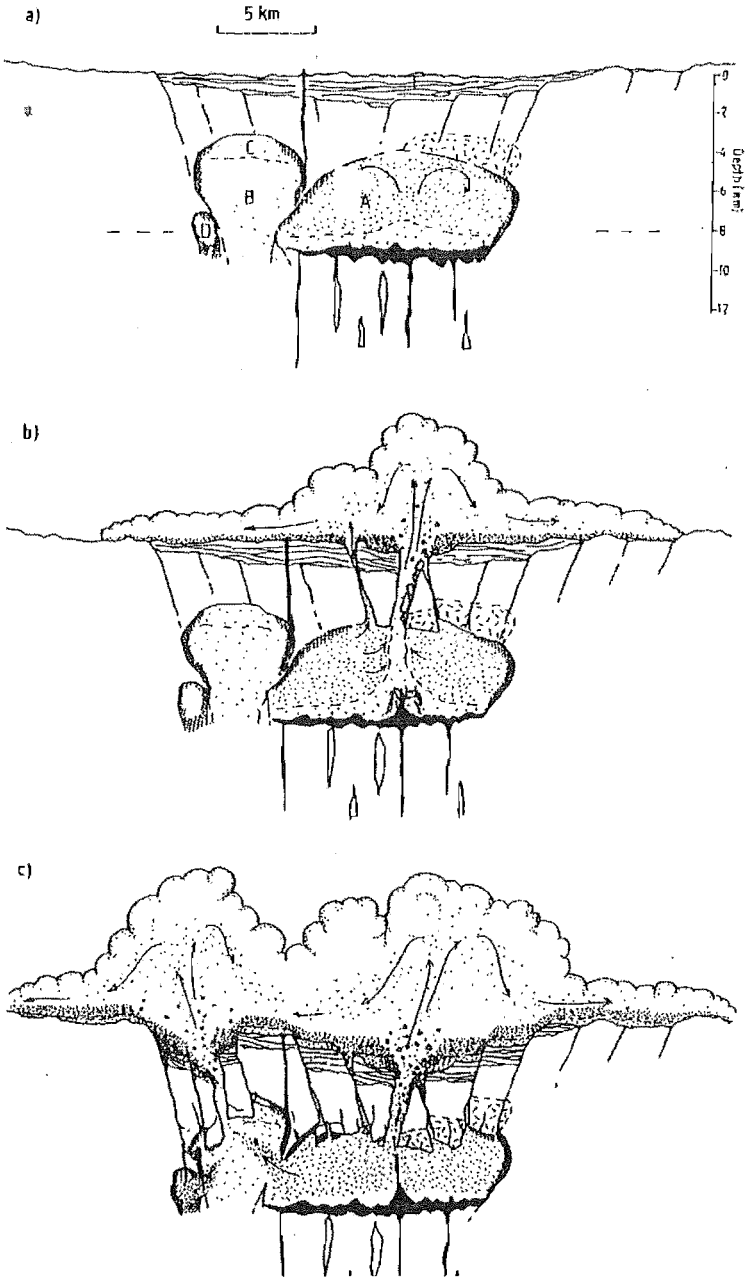

Figure 1.14 Eruption of Whakamaru caldera. (a) Stratified magma chamber prior to eruption, (b) low, fountaining eruptions and then (c) widespread caldera collapse. From Brown (1994).

Magma system

The total erupted volume probably exceeded 1000 km^3 DRE over a period of less than a thousand years. During this period four distinct rhyolite magma types (A to D, Fig. 1.15), and basalt, were erupted. These types are characterised by differences in mineralogy, whole rock chemistry, $P_{(H_2O)}$ and Fe-Ti oxide equilibrium temperatures

(Brown et al., 1998). Type A magma is the most voluminous eruptive. It is low-Si rhyolite, crystal rich, contains phenocrysts of plagioclase, quartz, orthopyroxene, hornblende, biotite and Fe-Ti oxides and has characteristic large resorbed quartz crystals. Type B and C magmas are higher-Si rhyolite and contain smaller phenocrysts of quartz, plagioclase, sanidine, biotite and Fe-Ti oxides. Type D magma contains a similar mineral assemblage to type A but is enriched in plagioclase and biotite and contains more Rb than the other magma types.

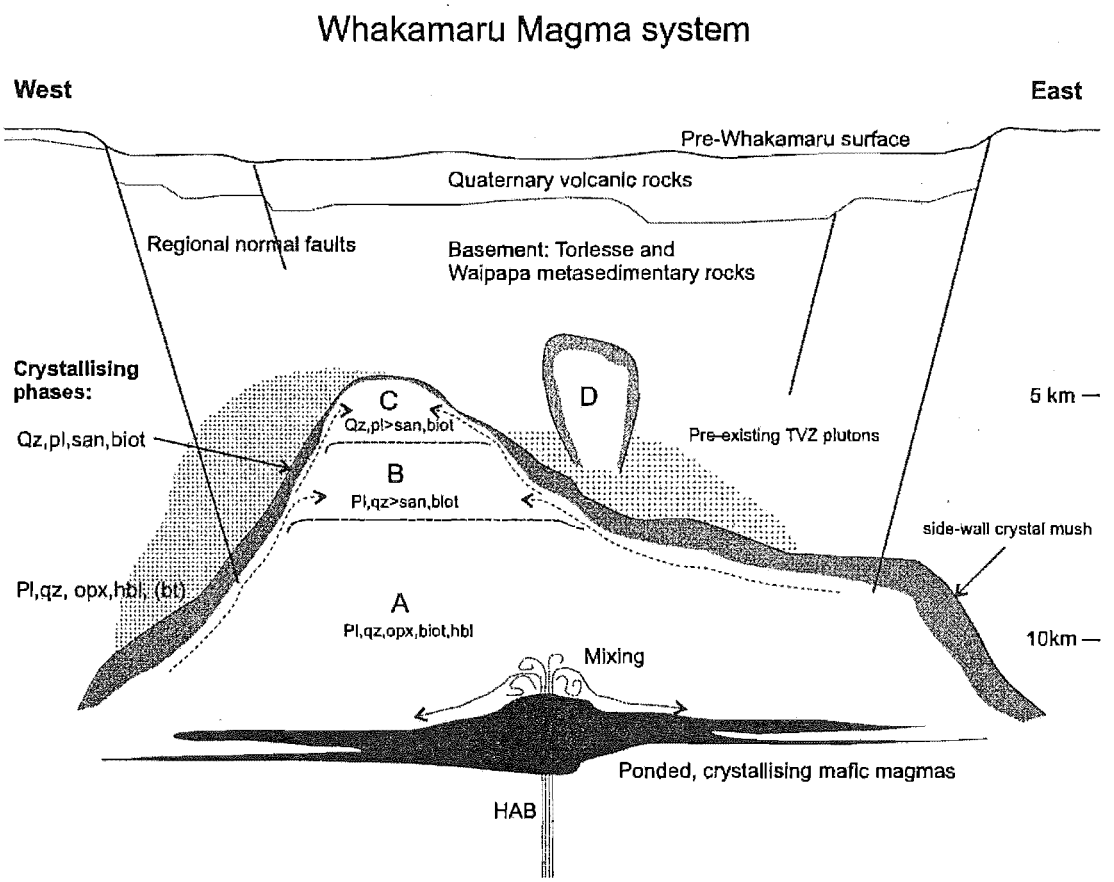

Figure 1.15 Model of the Whakamaru group magma system. From Brown et al. (1998).

Three of the rhyolite magmas (A to C) appear to be related through a two-stage (A fractionates to B, and B to C) crystal fractionation process (Brown et al., 1998). The less-evolved Type A was erupted earlier, with Types B to D, and basalt, introduced later in the eruption. This reverse-zoned eruption sequence requires a more complex withdrawal, and/or magma chamber, configuration than simple top-to-bottom tapping of a zoned magma chamber. A possible model for the magma chamber(s) feeding the Whakamaru eruptions is given in Figure 1.15.

The Western Dome Belt (WDB)

The WDB lavas were originally considered to be part of the (since refuted, see Section 1.4.2) 'Mokai Ring Complex' by Healy (1964). The WDB domes have similar whole rock chemistry to, but different $^{87}Sr/^{86}Sr$ ratios to, those of the Whakamaru group pyroclastics indicating that the domes represent separate younger magmas (Brown, 1994). K-Ar age dates of these domes suggest that they were emplaced over an extended period, apparently > 100 k years, after the Whakamaru eruptions (Houghton et al., 1991).

1.7 Geological setting: Extension and faulting

1.7.1 TVZ extension

As described in Section 1.4.6, TVZ is a product of the oblique convergence of the Australian and Pacific plates. TVZ is under (a) extensional stress from the force of rising partial-melt from below (see Fig. 1.16 for the present day GPS-derived distribution of extension) and (b) shear stress parallel to the plate margin (see Fig. 1.5 for plate movement vectors).

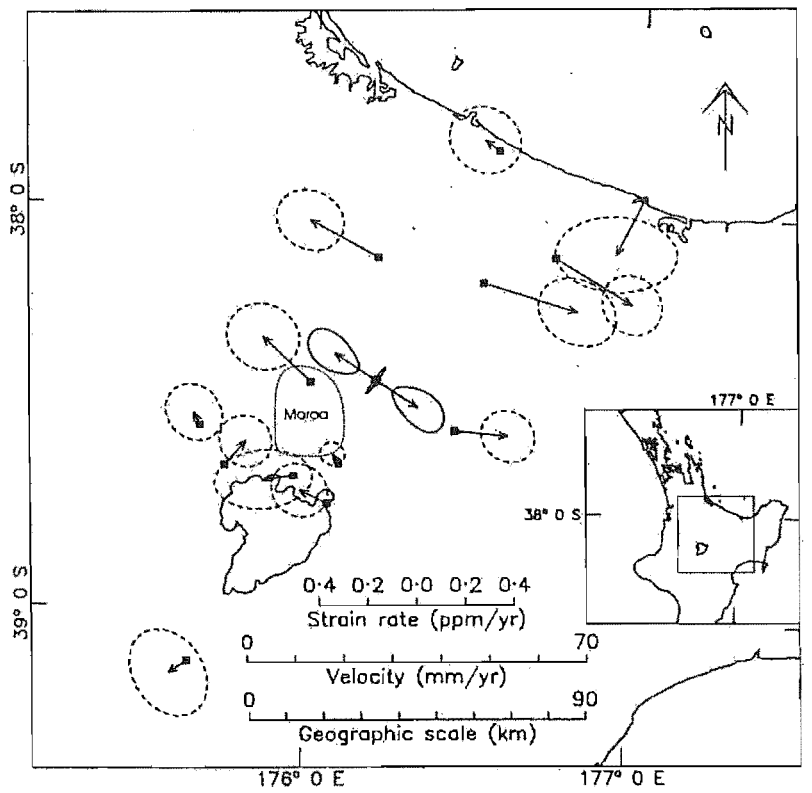

Figure 1.16 Observed displacements (relative to the Australian Plate) for 13 TVZ GPS stations between 1990 and 1991. This is a minimum magnitude principal strain solution. 68 % confidence regions are shown for magnitude and orientation. Applying the network translation, which minimises the sum of squared displacements, derives the displacement solution. From Darby and Meertens (1995).

Figure 1.17 shows a cross section of earthquake locations through the TVZ. Relatively shallow earthquakes (< 25 km) from roughly 170 to 230 km behind the plate boundary coincide with the area of active TVZ volcanism and extension. Webb and Anderson (1998) note that the spatial distribution of these earthquakes is diffuse across the TVZ and not particularly well correlated to the location of surface faulting. As a consequence of the stress field most TVZ faults are normal, parallel to the plate boundary and volcanic arc (Webb and Anderson, 1998). Graben and half-graben formation is ubiquitous. In the onshore TVZ the oblique nature of the plate convergence imparts a dominantly strike slip component to some of these faults (Bibby et al., 1995).

A smaller number of lineaments are perpendicular to these, in an approximately northwest trend (Rowland and Sibson, 2001), although there is a lack of evidence linking these to volcanic activity (Wilson et al., 1986) and they are particularly scarce in the Maroa area. There are also a minor number of approximately north-trending faults in TVZ. These are sub-parallel to the Coromandel Volcanic Zone and the Hauraki Rift (Hochstein and Ballance, 1993), and may be related to one or both of these. In the Maroa area the western and eastern margins of the Whakamaru Caldera, and the Pokuru Fault, follow this north trend.

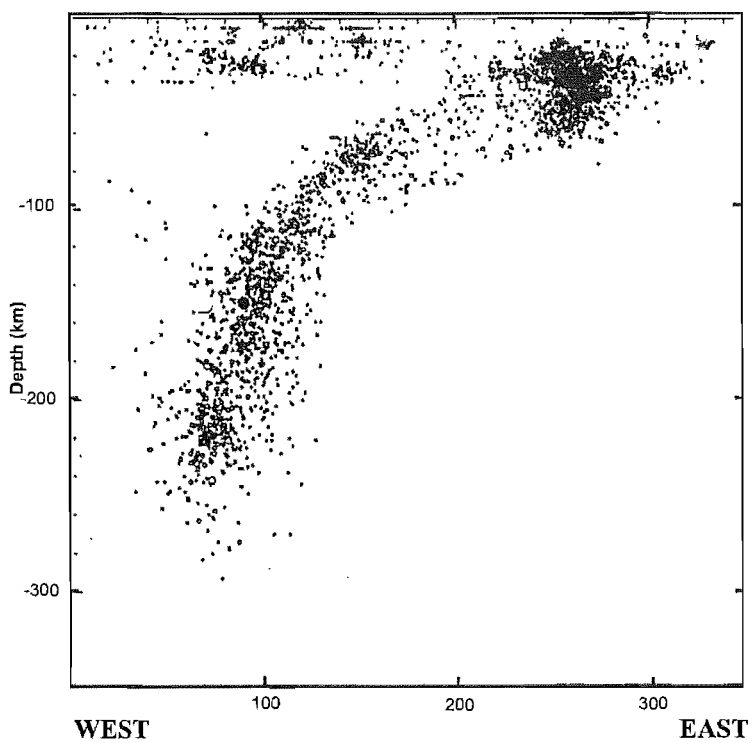

Figure 1.17 A cross section of hypocentres for magnitude 2-5 earthquakes from 1990 to 1994 along a southeast trending line from offshore west to offshore east of the North Island, approximately under Tongariro Volcanic Centre. From Webb and Anderson (1998).

Marine seismic reflection profiles show normal faults projecting 2 to 3 kilometres below the sea floor, to the base of the sedimentary fill, in offshore TVZ (Bibby et al., 1995; Davey et al., 1995). There are no deep seismic profiles available for the onshore TVZ but gravity and seismic inversion modelling suggests that low-density pyroclastics dominate fill to a depth of ~ 2.5 km, similar to the offshore setting (Bibby et al., 1995; Stagpoole, 2000; Sherburn et al., 2003). Many onshore normal faults probably also propagate to ~ 2.5 km, as they are in a similar tectonic and lithological setting to those offshore (Bibby et al., 1995).

1.7.2 Central TVZ faulting

The maximum rates of extension across TVZ coincide with the central rhyolite-dominated section from Taupo in the southwest through Okataina in the northeast (Wilson et al., 1986). The bulk of rhyolite erupted in this zone is emplaced as ignimbrite-dominated pyroclastics from caldera forming eruptions. Regional stresses, and especially the location of pre-existing defects (mostly faults), have a significant influence on the style of caldera volcanism (e.g. see review in Milner, 2001). The classical piston-shaped caldera model gives way to a variety of styles of collapse (see Section 1.3.2) depending on the complex local stress regime.

In the central TVZ, magmatically driven fault events have a very different character to extension-driven faults. Caldera-bounding faults undergo hundreds of metres of displacement during a single collapse event (Spray, 1997). The orientation of caldera-bounding faults in TVZ appears to, in many cases, have no relationship to the regional stress field.

In contrast to caldera faults, most extension-driven faults undergo a displacement of the order of a metre per event, and strike parallel to the TVZ long axis (Rowland and Sibson, 2001). Villamor and Berryman (2001) have determined the extension rate from 64 to 10 ka in the Ngakuru-Waikite depression to be 1.9 ± 0.7 mm/yr in the near surface and 6.4 ± 2.8 mm/yr at seismogenic depths of 6 to 10 km. They calculate this from a model using a range of geometries of normal faults in the area, and a total vertical displacement rate of 7.2 ± 0.4 mm/yr across eight faults and fault zones. There is little data for the rate of extension across Maroa. Previous workers have estimated TVZ extension in general at rates from 3 to 8 mm/yr (Darby and Meertens, 1995; Villamor and Berryman, 2001).

Segmentation in the amounts and rates of faulting along central TVZ has been identified by several worker (e.g. Rowland and Sibson, 2001; Villamor and Berryman, 2001). A segment boundary is often identified at the northeastern edge of Maroa, between a relatively tectonically quiet segment in the Whakamaru/Maroa area and a highly active segment in the Paeroa fault zone, Ngakuru Graben and Guthries Graben areas. It has been suggested by Rowland and Sibson (2001), J. Rowland (pers comm., 2003), P. Villamor (pers comm., 2003), K. Berryman (pers comm., 2003) and others that segment boundaries may represent (a) deep northwest trending structures/faults, (b) transfer zones between relatively homogeneous structural domains, akin to those seen in rift systems or (c) changes in the seismogenic thickness of the TVZ. Little evidence has been seen so far that supports any or all of these options.

1.8 Geophysical characteristics of Maroa

Available geophysical data across Maroa is restricted to the relatively large-scale airborne gravity, aeromagnetic and Schlumberger apparent resistivity data.

1.8.1 Gravity and aeromagnetics

Anomalies in gravity and magnetic data have been correlated to several TVZ calderas. Figure 1.18 gives a residual gravity anomaly map for the central TVZ. Okataina, Rotorua, Reporoa and Taupo Volcanic Centres all contain gravity lows that have been used to delineate caldera boundaries. The Guthrie Graben has been suggested to overly Kapenga Caldera because it correlates well to a negative gravity anomaly.

Aeromagnetic anomalies are also seen at most TVZ volcanic centres and a particularly strong anomaly below Maroa has been used, along with gravity data, as evidence for the existence of a Maroa caldera. Figure 1.19 presents a residual magnetic anomaly map of the TVZ.

Maroa overlies one of the two foci of maximum gravity low within Whakamaru Caldera (Fig. 1.18). This low dominates the northern end of the caldera, whereas the other low is in the central western half of the caldera. There is a gravity-low embayment projecting from Maroa into the Whangapoa Basin. Maroa overlies one of the strongest regional/deep magnetic anomalies in TVZ (delineated by higher-altitude aeromagnetic data, Fig. 1.19 (b), Soengkono, 1995). Another deep/regional aeromagnetic anomaly,

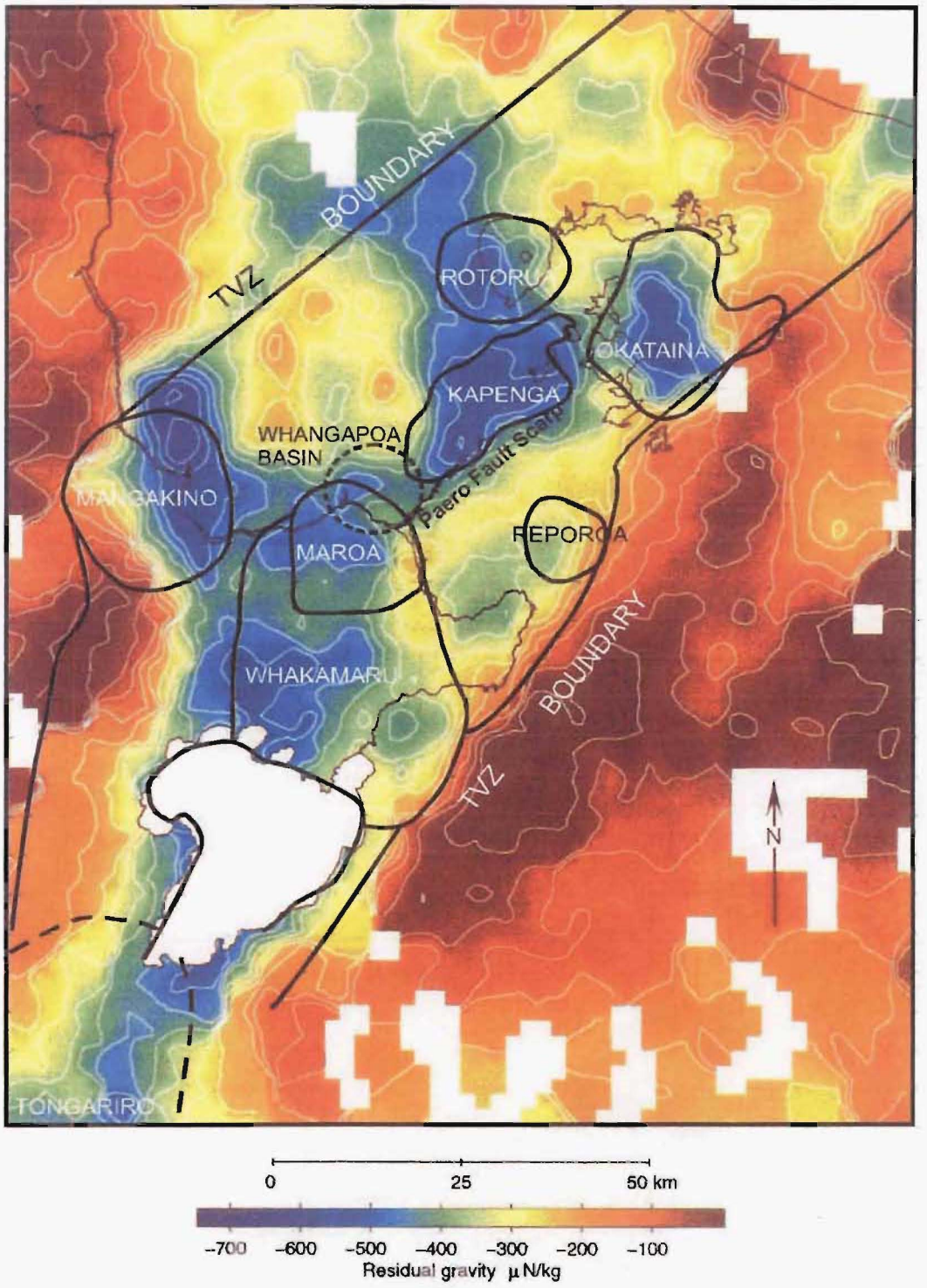

Figure 1.18 Residual gravity anomaly map of the TVZ from Bibby et al. (1995), overlain by the locations of TVZ volcanic centres from Houghton et al. (1995). The strongest gravity low below Whakamaru caldera is in the central western portion. The approximate boundary of Whangapoa basin is dashed. Note that Rotorua, Mangakino and Whakamaru volcanic centres are partly offset from their gravity lows because they are also defined by the distribution of associated deposits.

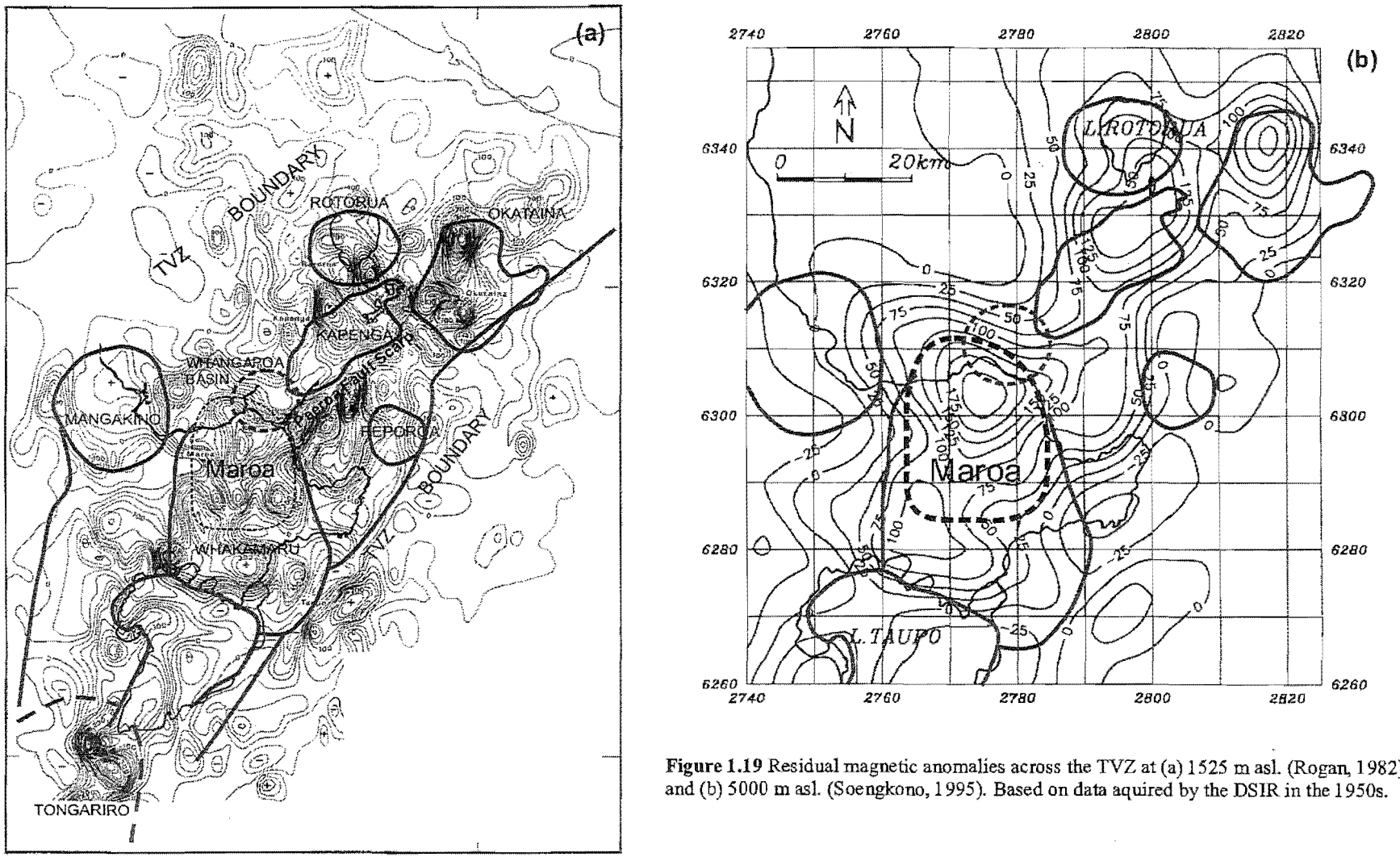

Figure 1.19 Residual magnetic anomalies across the TVZ at (a) 1525 m asl. (Rogan, 1982) and (b) 5000 m asl. (Soengkono, 1995). Based on data aquired by the DSIR in the 1950s.

but not as strong, is seen in the southwestern part of Whakamaru Caldera and under Rotorua and Okataina. These anomalies are also seen at more shallow levels in 1525 m asl. aeromagnetic surveys (Fig. 1.19(a)), but a number of separate smaller dipole features can be seen within each of the larger anomalies (Rogan, 1982). In the 1525 m asl. aeromagnetic data, an aeromagnetic dipole feature below Maroa is distinct from two below the Paeroa Fault scarp to the northeast, which show even stronger anomalies than in Maroa.

1.8.2 Resistivity

Apparent resistivity maps (Fig. 1.20) are generally dominated by very low resistivity at geothermal areas, and very high resistivity in areas where there is down-going cold groundwater (Bibby et al., 1995). In Maroa low resistivity is seen at Mokai, Ohakuri and Orakeikorako geothermal areas, and high resistivity across the western part of the complex. This central, western part of Maroa contains the older (mostly > 200 ka from my new age data, Chapter 3) major MWC and MEC dome complexes. The lack of evidence for current or relict geothermal activity here suggests that volcanic activity was indeed early in western Maroa and this area has been high ground ever since, corroborating the new age data presented in Chapter 3.

Mokai geothermal area is tapped as a commercial geothermal power source and Orakeikorako is preserved as a geothermal tourist attraction with sinter terraces and hot springs. Ohakuri has little modern surface expression as a geothermal system and low resistivity there reflects alteration from previously high-intensity hydrothermal activity. The implications for the evolution of Maroa from this evidence for high geothermal heat flow are discussed further in Sections 5.2.7 and 5.4.5.

Orakeikorako is the only geothermal field of these three that coincides with active faulting. It lies at the transition of the Whangamata Fault (one of the few 'active' faults in Maroa, Section 5.4.4) into the Paeroa Fault Zone. This fault is probably providing a preferred pathway for the ascent of geothermal fluids at Orakeikorako.

In contrast, the Mokai geothermal system lies in an area apparently free of active fault traces, between the WDC and the western edge of Maroa. The Ohakuri geothermal system is partly in line with Ngakuru Graben active faults to the northeast, across Lake Ohakuri. The only visible faults within Maroa in the Ohakuri fossil geothermal area are

likely not 'active' (no Holocene displacement) and southeast of the region of low resistivity. These are discussed further in Section 5.4.2.

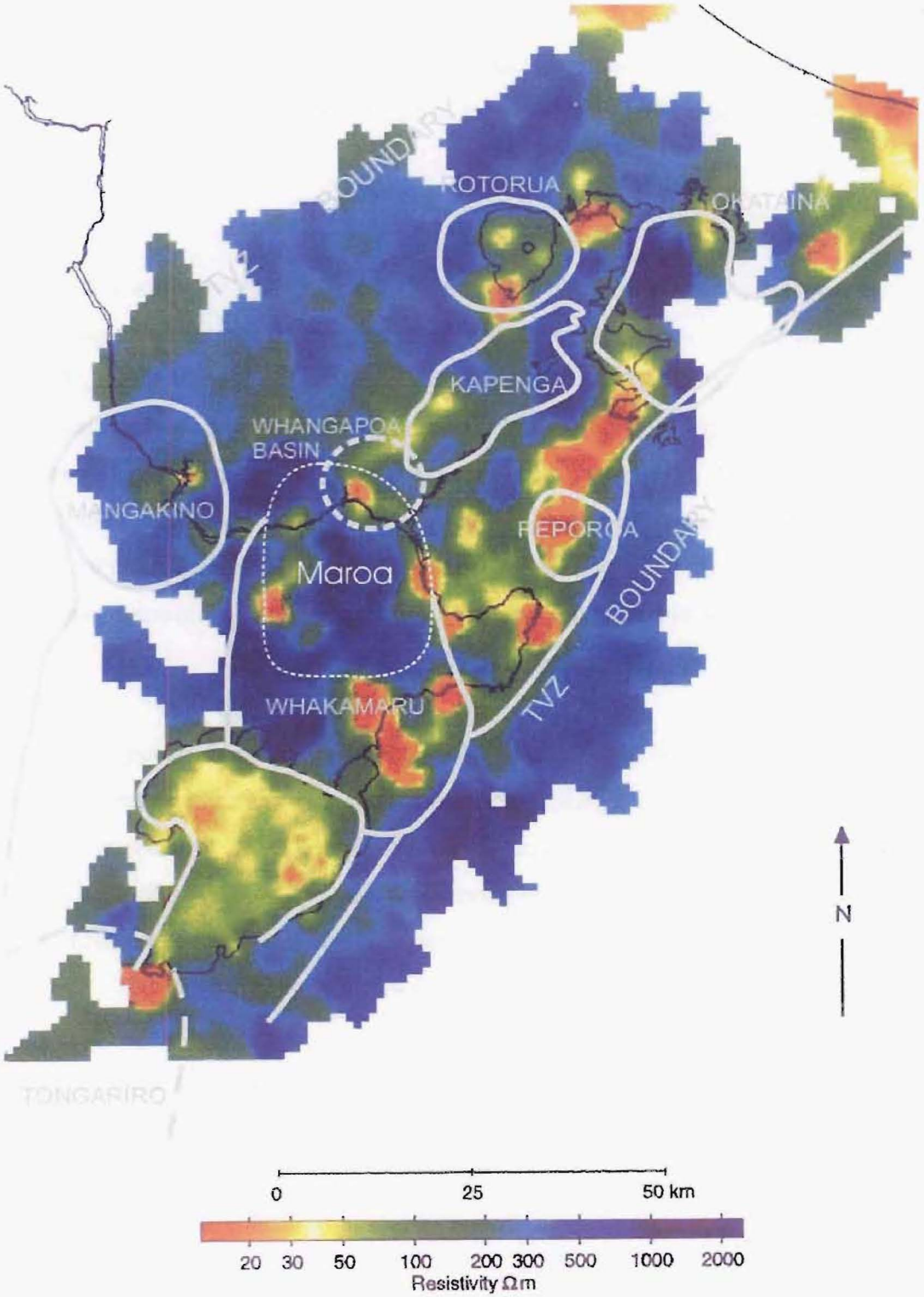

Figure 1.20 Regional map of Schlumberger apparent resistivity (with electrode spacing of 500 m) across central TVZ. From Bibby et al. (1995).

CHAPTER 2

Surface Geology of Maroa Volcanic Centre

2.1 Introduction

This chapter presents results of mapping the Maroa Volcanic Centre, and describes and interprets the volcanology of Maroa deposits. Map 1 (back pocket) is a revised summary of the work by NZGS staff, especially E. F. Lloyd, detailed in Section 1.4.4. Detailed descriptions of major Maroa pyroclastic units are given to provide a framework for Maroa structure and subsurface geology data in subsequent chapters. The maps presented combine previous geological maps (Chapter 1), together with the revisions based on my thesis research. The main focus of this study is the overall evolution of Maroa. Therefore, the physical volcanology of individual Maroa eruptive units is fully discussed in this chapter.

2.2 Maroa lava domes

There is at least 20 km^3 of lava represented by surface exposures in Maroa (this is quantified further in Chapter 3). The distribution of Maroa rhyolite lava domes is shown in Figure 2.1 and selected aerial views are shown in Figure 2.2(a) and (b). The lavas are inferred to have been emplaced in a similar fashion to the processes described by Cole (1970) and Richnow (1999) for the Kaharoa eruption-related domes on Mt Tarawera. On eruption, domes form with steep margins, relatively flat tops with 'spines', all surrounded by an apron of talus derived from disintegration of the expanding dome. This may be superimposed on a fan of tephra formed around the vent during preceding pyroclastic eruptions. At Maroa these features have been subsequently variably eroded and/or buried over time. Maroa rhyolite lavas have a variety of characters from aphyric glassy obsidian at Ben Lomond dome (Fig. 2.2(c)), to devitrified, weathered, flow-banded porphyritic lava (e.g. Hauwai dome Fig. 2.2(d)).

Faults displacing domes are given specific mention only where relevant to discussion of Maroa evolution. Significant faults and lineaments are mapped in Chapter 5. Thompson (1966) has mapped and described the morphology of most Maroa dome lobes, talus, and cross-cutting lineaments in great detail.

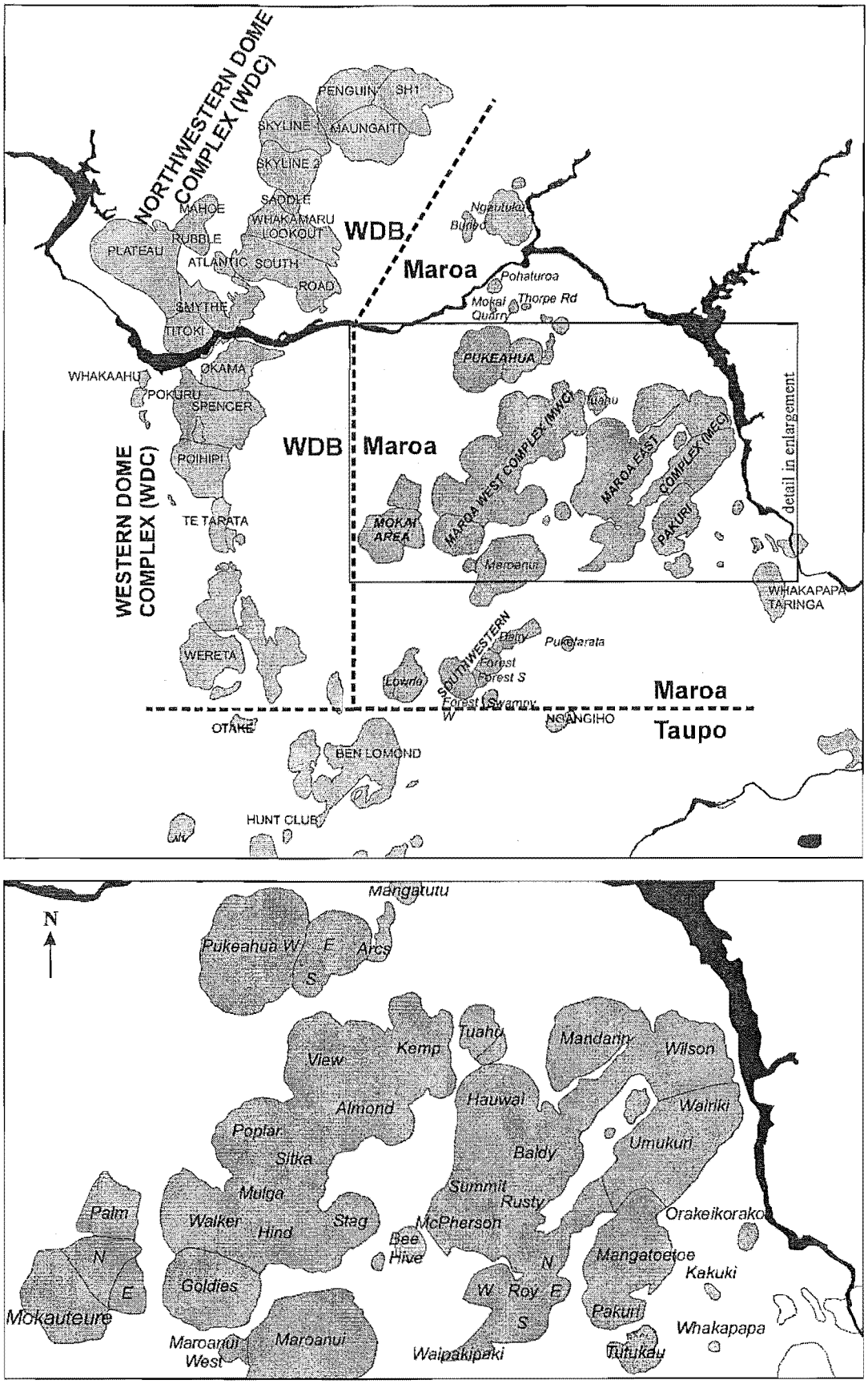

Figure 2.1 Map of domes in the Maroa area, showing informal labels adopted for this thesis. Light grey is non-Maroa domes with their names in capitals. Names of Maroa domes are italicised in lower case. Maroa dome complex names are italicised in capitals. The upper map shows the locations of major dome complexes and the boundaries of Maroa. The lower enlargement shows the names of Maroa domes in the Maroa West and East complexes and adjacent areas.

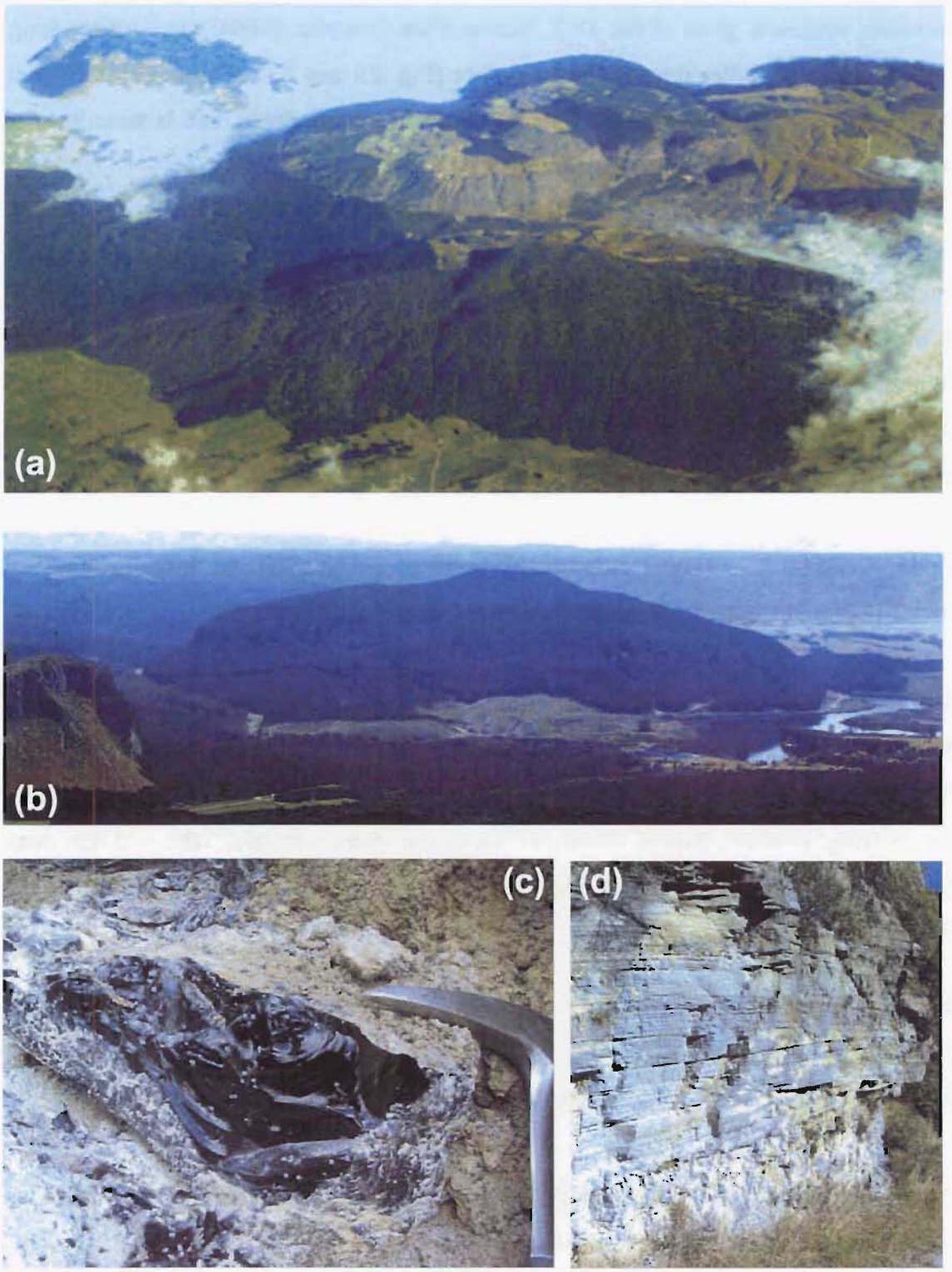

Figure 2.2 (a) aerial photo, looking northwest across Maroanui dome (foreground) and part of MWC (behind), (b) looking north at Pohaturoa (left) and Ngautuku (right) domes, with Lake Atiamuri between, (c) Ben Lomond dome obsidian akt M325 (technically part of TVC, but the freshest obsidian in the area) and (d) weathered flow-banded lava of Hauwai dome at M193 (outcrop is three metres high).

2.2.1 Major dome lineaments

The two largest dome complexes are elongated northeast-southwest, parallel to the dominant structural grain of the TVZ. Maroa West Complex (MWC) is ~ 10 km long, stretching from Goldies through Tuahu domes (Fig. 2.1 and 2.2). Maroa East Complex (MEC) is ~ 7 km long, from McPherson through Mandarin dome, and is taken here to include Umukuri and Wairiki domes (Fig. 2.1).

2.2.2 Other dome complexes

Pukeahua dome complex (Fig. 2.1) consists of Pukeahua-west, -east and –south domes, in order of decreasing volume. A fan of pyroclastics (> 0.5 km^3) surrounds them. The summit of Pukeahua West dome is the second highest in Maroa and provides a good vantage for viewing the northern part of the centre. North of Pukeahua, Ngautuku dome complex consists of two coalescing domes.

Pakuri dome complex (Fig. 2.1) is situated in the southeast of Maroa. It is distinguished from MEC on the basis of petrological data (presented in Chapter 4).

Mokai and Maroanui dome complexes are located in the southwest of Maroa. Mokai dome complex is comprised of Mokauteure, Mokauteure North and Palm domes. The summit of Maroanui dome is the highest point in Maroa and provides a good vantage for viewing southern Maroa. South of Maroanui dome complex, the ~ 5 km long Southern dome complex extends from Forest West through Dairy dome, parallel to the trace of the Whangamata Fault.

2.2.3 Isolated domes

The lavas of isolated domes are not sub-aerially connected to any other domes. Each dome has a single summit point or plateau. Their distribution is shown in Figure 2.1.

Buried dome, to the west of Ngautuku dome complex, is mostly eroded, and/or buried by younger pyroclastics and sediments.

There are several isolated domes north and northeast of Pukeahua dome. Pohaturoa dome forms an unusually steep-sided spine beside the Waikato River. Aggregate for forest roads is extracted at Mokai Quarry from a buried, silicified dome. There are two

mostly eroded and/or buried domes on Thorpe Road (Thorpe One and Two). Also near Thorpe Rd, Mangatutu dome has a steep rounded morphology, and is visible from State Highway 1.

Between MWC and MEC lies Beehive dome. This may be connected at a shallow depth below the surrounding pyroclastics to MEC. Stag dome appears connected to MWC, but is off of the main lineament and could be considered an independent dome. The relationship of these domes to the Maroa West and East complexes is discussed in Chapter 5.

There are several isolated domes in the southeast of Maroa. These are Orakeikorako, Kakuki, Whakapapataringa, Tutukau and mostly-buried domes east of the Waikato River. Whakapapataringa is substantially larger than the others and the high summit provides a good vantage for viewing the southeast Maroa area. Waipakipaki dome touches the south end of MEC, but is petrologically distinct from it (Chapter 4), and underlies the Putauaki pyroclastics at locality M34 (U17/760933).

In the south of Maroa, Lowrie and Swampy domes surround the Southern dome complex. Puketarata dome has been erupted during Modern TVZ activity. There are numerous additional domes between Maroa and Taupo that have been partly buried (especially by the 26.5 ka Oruanui ignimbrite) and which overlap in time with activity at Maroa (Ewart, 1967; Ewart, 1968; Sutton, 1995; Sutton et al., 1995).

2.3 Maroa Pyroclastics

2.3.1 Overview of local pyroclastic deposits

Definition

Defining characteristics of major Maroa-related pyroclastics are summarised in Table 2.1, and the Pukeahua, Atiamuri, Orakonui and Korotai pyroclastics are described in detail below. The description of Mokai and Mamaku pyroclastics is summarised from other workers (see later sections, with new data added to Mokai); Mamaku pyroclastics and Whakamaru group are also introduced as part of the regional geology in Chapter 1.

Name of deposit		Defining characteristics
Pukeahua pyroclastics	**Source**	Below Pukeahua dome complex
	Notes	Lobes of massive BAF deposits and ignimbrite with occasional airfall layers. Includes the Manawa ignimbrite.
	Matrix	Cream to white colour (occasionally pink to orange)
	Juvenile clasts	BAF: Angular low to moderately vesicular rhyolite lava Ignimbrite: Moderately to highly vesicular rhyolite pumice.
	Lithics	Ignimbrite only: Fresh obsidian and dense porphyritic rhyolite lava
Atiamuri pyroclastics	**Source**	Mandarin dome vent, MEC
(where non-welded)	**Matrix**	Orange to pink (occasionally cream),
	Juvenile clasts	Pink to orange (occasionally cream) Moderately vesicular, fresh, hard angular pumice.
	Lithics	Variable fine to coarse fresh obsidian and minor devitrified rhyolite lava.
Putauaki pyroclastics	**Source**	Central Maroa
	General	Massive vapour-phase-altered
	Matrix	Tan to pink or brown, soft.
	Juvenile clasts	Pinky purple and powdery.
	Lithics	5 to 40 vol.% usually up to 100 mm.
Tram Road	**Source**	Tutukau/Tram Rd area
pyroclastics	**General**	Small (< 0.1 km^3), locally derived and massive
	Matrix	Cream
	Juvenile clasts	Grey and fresh.
	Lithics	10 vol.% usually up to 10 mm.
Orakonui pyroclastics	**Source**	Central Maroa
	General	Massive
	Matrix	(a) Cream to light grey, firm (outcrops often case hardened).
	Juvenile clasts	(a) Orange to grey and fresh to devitrified and soft.
	Lithics	(a) up to 5 vol.% devitrified rhyolite lava usually up to 10 mm.
Korotai pyroclastics	**Source**	Local, possibly under Buried dome.
	General	(a) Massive unwelded and (b) strongly-welded to well-lithified.
	Matrix	(a) Grey, tan or orange, soft to hard (b) dark grey and recrystallised.
	Juvenile clasts	(a) Cream, orange or grey and fresh, (b) lenticular pumice to obsidian fiamme.
	Lithics	5 to 40 vol.% angular black dense to vesicular obsidian
Puketarata Tuff	**Source**	Vent below Puketarata dome
	General	Finely to moderately layered surge and airfall deposits
	Matrix	Grey, fine ash.
	Juvenile clasts	Cream moderately vesicular pumice, containing biotite.
	Lithics	5 to 10 vol.%

Table 2.1 Summary of defining characteristics of Maroa pyroclastic deposits.

Distribution

The distribution of Maroa pyroclastics (and significant regional pyroclastics) is shown in Figure 2.3. Only ignimbrites and BAF deposits are thick and widespread enough to form mappable units. Maroa-derived airfall pyroclastics are preserved at isolated localities. Pyroclastics have been separated into the units used here based on field character and petrological data. Lloyd (1972) provides a summary of the basis on which deposits with these names have previously been distinguished. Some revisions are made to Maroa pyroclastic nomenclature in this thesis where noted.

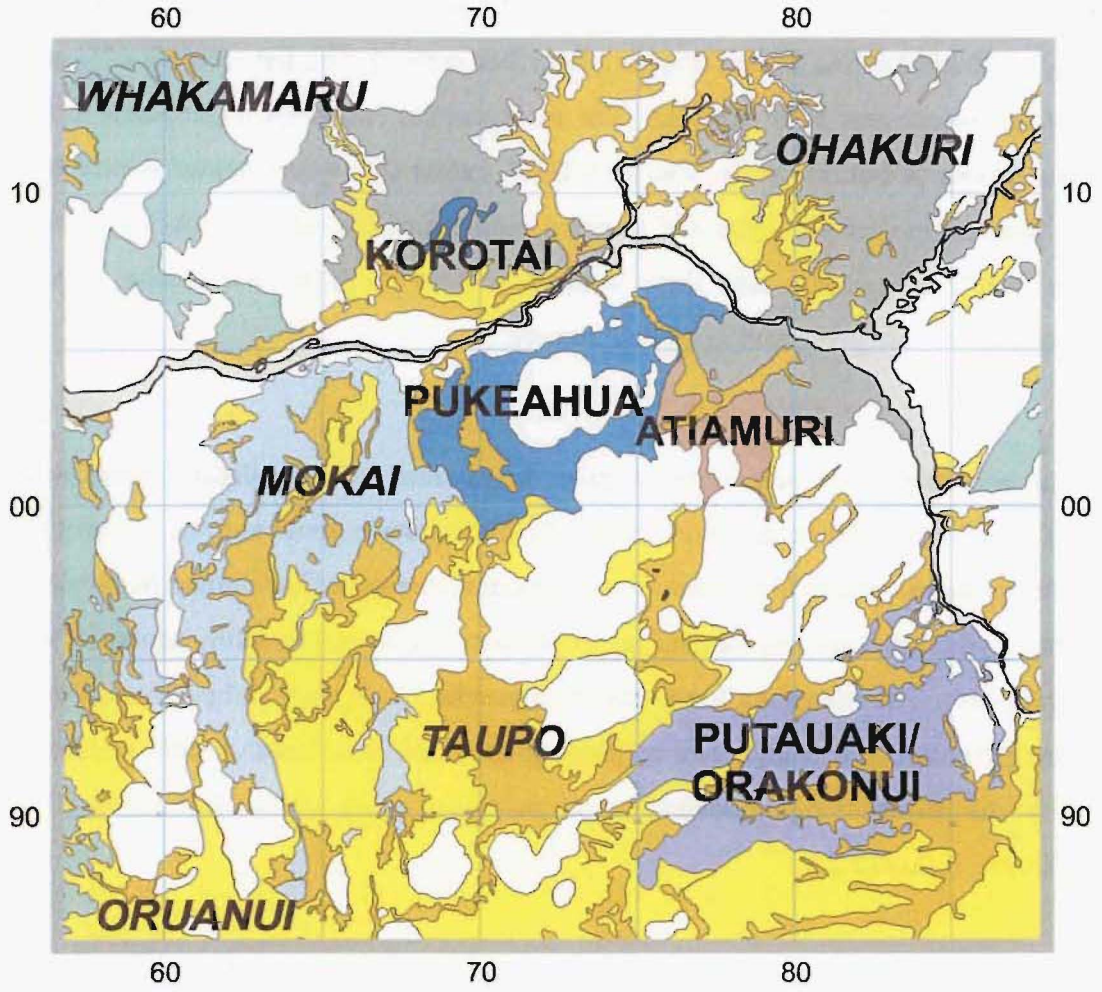

Figure 2.3 Distribution of pyroclastics discussed in this chapter. Adapted from unpublished mapping by E.F. Lloyd, C. P. Wood, I. A. Nairn, B. F. Houghton, C. J. N. Wilson and others at the Institute of Geological and Nuclear sciences and kindly provided for this thesis. Maroa pyroclastics are labelled in capitals: Putauaki/Orakonui are purple, Pukeahua is mid-blue, Korotai is dark blue, Atiamuri is pink. Non-Maroa pyroclastics in the Maroa area are labelled in italicised capitals: Ohakuri is mid-grey, Whakamaru is green, Mokai is light blue, Oruanui is yellow and Taupo is orange. The Waikato river lakes are light grey. Grid spacing is 5 km on the NZ map grid.

2.3.2 Pukeahua pyroclastics

Type locality

M64 (U17/722016); cutting on south side of Tatua Rd, defined by Lloyd (1972). This outcrop exposes a lower BAF unit and upper ignimbrite unit, with an airfall deposit dividing them.

Source and distribution

The Pukeahua pyroclastics form a relatively steeply inclined (average ~ 6°) apron surrounding the Pukeahua dome complex (described earlier). The fan consists of layered lobes of ignimbrite and BAF deposits. The emplacement mode for a particular unit is not always clear at outcrop scale. The term BAF, rather than concentrated debris flow, is used because gas escape pipes and thermal colouration are seen in BAF deposits at location M132 suggesting that they were deposited at high temperature. Airfall pyroclastic layers are preserved in some outcrops.

Pukeahua pyroclastics fan and dome complex are divided into two distinct parts on the basis of petrological characters (see Chapter 4). The western dome and the western half of the fan appear to post-date the rest of the Pukeahua deposits. The contact between the Pukeahua pyroclastics eastern fan and upper western fan is seen at M63, separated by a thin airfall unit. The Pukeahua lower eastern pyroclastics appear to dip down over the Atiamuri pyroclastics in analysis of air photographs, but the contact is not exposed. A model for this sequence of emplacement, and processes acting within both halves of the fan, is shown in Figure 2.4.

The characteristics distinguishing end-member ignimbrites compared to end-member BAF deposits in the Pukeahua pyroclastics fan are as follows (refer to Fig. 2.5 for graphic logs):

(1) Ignimbrite units have a visually-distinct bimodal grainsize distribution, with concentration into matrix and clast modes, where BAF deposits do not show such a feature;

(2) Ignimbrites show a more varied clast componentry, with separate pumice and dense lava lithic populations distinguishable from each other;

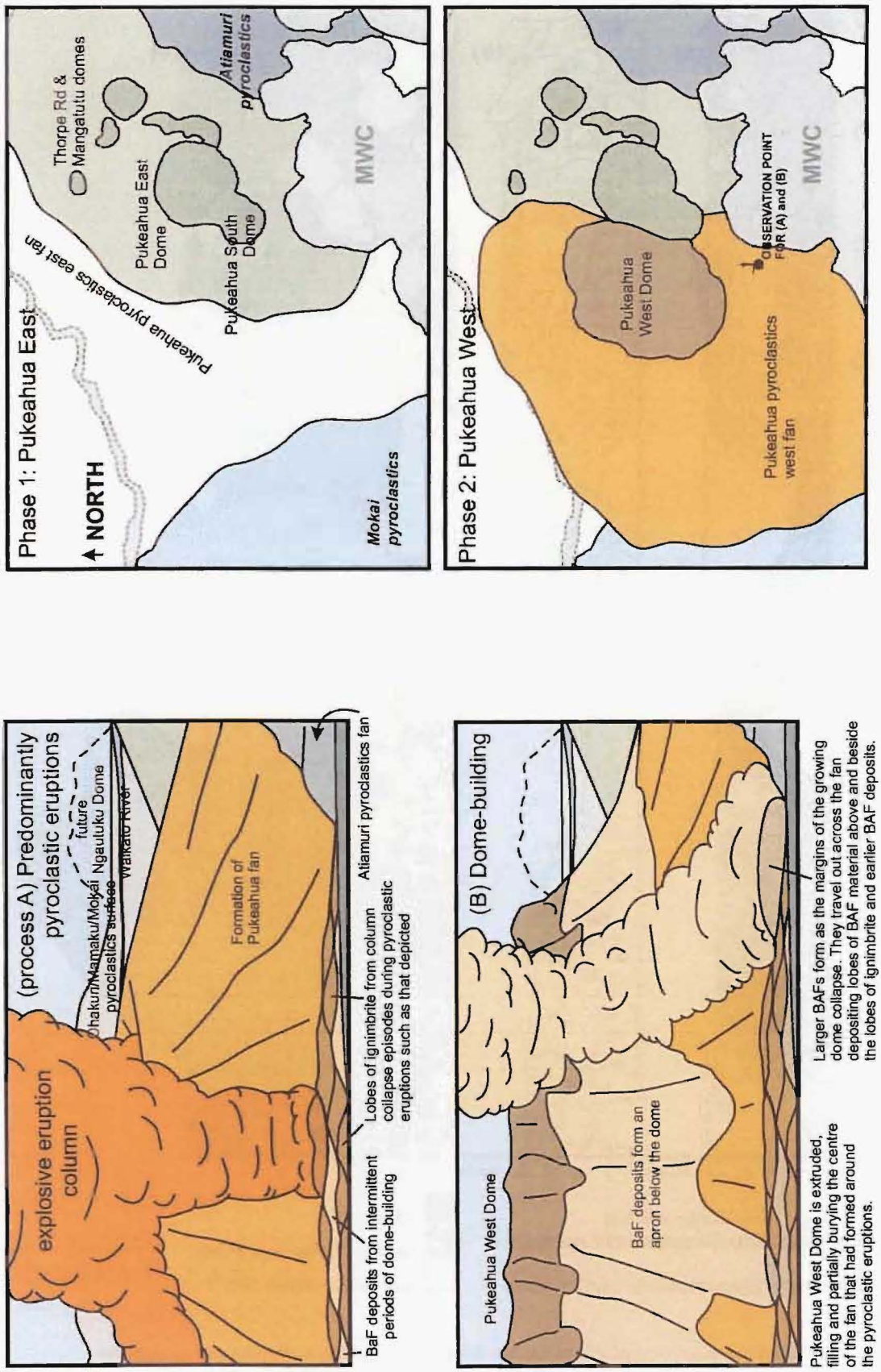

Figure 2.4 A cartoon model of the two processes (A and B) producing the Pukeahua pyroclastics fan, and the two phases (1 and 2) of activity. Eruption graded back and forth between the two process end members within both phases of activity.

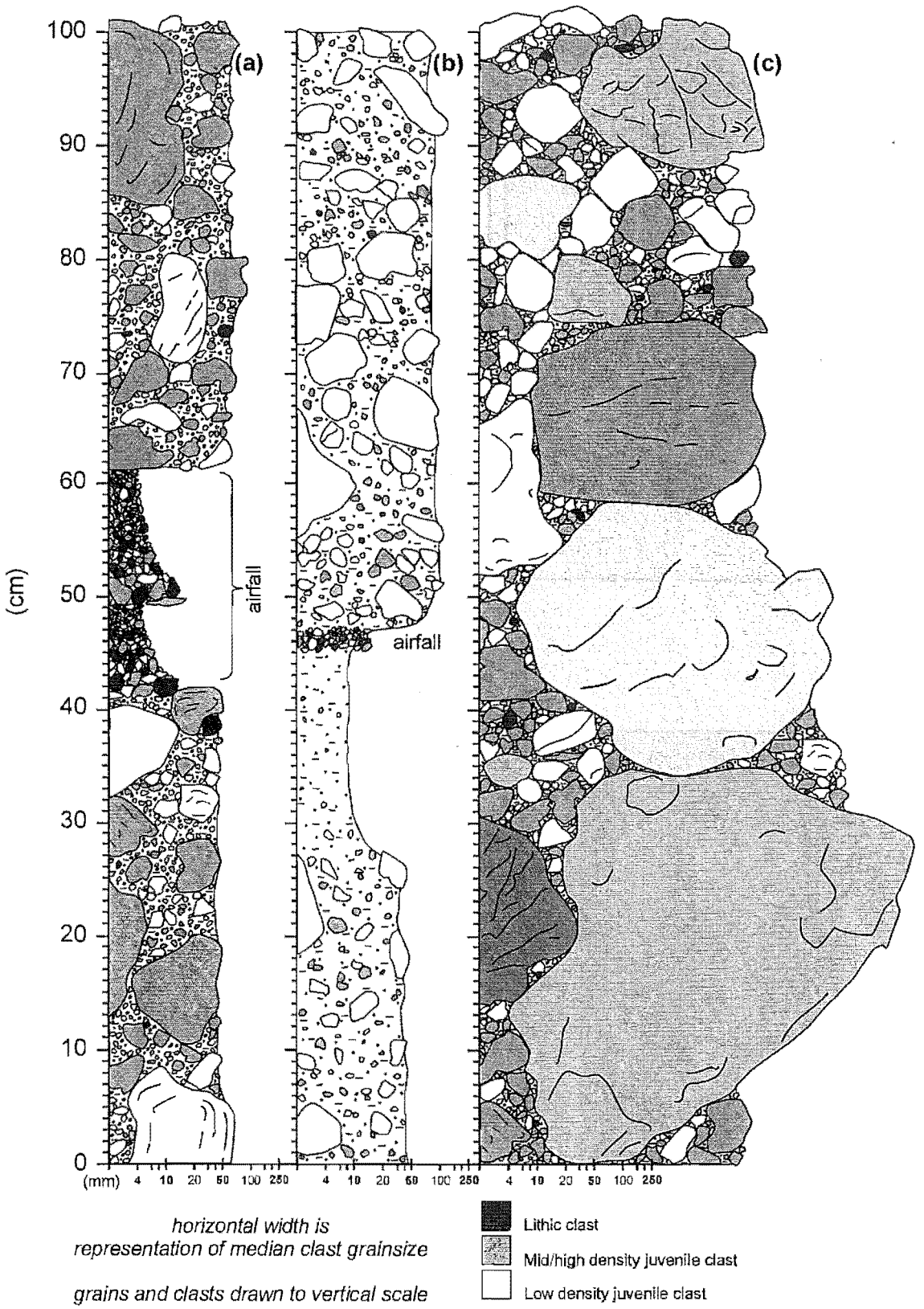

Figure 2.5 Logs, of typical Pukeahua fan (a) and (c) BAF deposits, and (b) ignimbrite. (a) and (b) contain airfall layers (labelled). From left to right:
(a) M64 (U17/722016) - Pukeahua pyroclastics type section, massive BAF deposits with airfall units
(b) M63 (U17/728021) - Pukeahua pyroclastics, massive ignmbrite with airfall unit
(c) M476 (U17/711017) - Pukeahua pyroclastics, massive clast-supported BAF depositg

(3) In thin section juvenile clasts in ignimbrites are less dense (pumice) while in BAF deposits they often range from pumice to slightly vesicular dome material (dense lava); and

(4) Under binocular microscope ignimbrites contain a relatively high crystal content in their matrix, compared to pumices, inferred to be a result of fine ash preferentially being winnowed out during transport.

Deposits within the Pukeahua pyroclastics fan range between the ignimbrite and BAF deposit end members described above. Pukeahua fan deposits usually only crop out within 2 km of the dome complex and almost all lithics within Pukeahua pyroclastics are derived from Pukeahua lava and the fan itself.

Pukeahua ignimbrites

General: Massive. Occasionally stratified into up to 500 mm thick beds, slightly richer in pumice, or graded across outcrop. **Matrix:** Cream to white (sometimes pinky orange), soft to slightly firm, poorly sorted, fine to medium ash, 5 to 20 vol.% felsic subhedral crystals. **Juvenile clasts:** 20 to 40 vol.%, usually up to 300 mm, occasionally up to 500 mm, cream, poorly sorted, sub-rounded, moderately vesicular (often with open vesicles up to 10 mm wide) fresh rhyolite pumice. See thin section description M64c for representative petrography. **Lithics:** up to 1 vol.%, dark grey to black, fine lapilli, angular obsidian.

Pukeahua BAF deposits

General: Massive, clast supported in places, not possible to determine which clasts are directly from deposit-forming dome collapse or lithics from reworked older material. **Matrix:** Cream to white (sometimes pinky orange), soft to slightly firm, usually free-draining and dry, poorly sorted; complete range of grains from fine ash to blocks up to 300 mm, **Clasts (grade from juvenile to lithics):** 30 to 50 vol.% (some clast-supported up to 60 vol.%), usually up to 200 mm, sometimes up to 600 mm, cream, poorly sorted, angular, slightly to moderately vesicular pumices (occasionally low density, with up to 5 mm diameter vesicles), sometimes flow-banded, rhyolite lava. Clasts vary from fresh, to devitrified (must be lithics, occasionally silicified) and grey. See thin section description M63c for representative petrography.

Pukeahua airfall pyroclastics

General: Fines poor, normally graded and moderately sorted. Usually free-draining and dry, but finer deposits act as aquitards holding groundwater and saturating them. **Juvenile clasts:** 70 to 90 vol.%, Cream colour, moderate vesicularity, usually fine up to 40 mm lapilli (some airfall layers are fine ash), sub-angular pumice. **Lithics:** 10 to 30 vol.%, fine lapilli to 25 mm lapilli, black to grey, normally graded along with pumice clasts, variably hydrated, fractured, angular obsidian.

2.3.3 Atiamuri pyroclastics

Type locality

M12 (U17/772035); west side of SH1 road cutting. Cutting at base exposes airfall layers probably near the base of the pyroclastics; top of cutting reaches the welded zone at or near the top of the pyroclastics. Previous type section, defined by Lloyd (1972) as the bluffs around M430 (U17/773043), is mostly in the welded zone and does not expose airfall units. The M12 type location has been created by road realignment since 1972 and I propose it here as a new type section.

Source and distribution

Atiamuri pyroclastics consist of ignimbrite flow units interspersed with airfall layers; most of the latter occur towards the base. The former are generally fresh, orange to pink, containing angular, moderate-density pumice clasts, are moderately crystal-bearing with felsic phenocrysts up to 4 mm and often contain abundant fresh obsidian lithics. At some localities obsidian constitutes up to 30 vol.% of the ignimbrite (Fig. 2.6(a)).

The relatively low volume (> 1 km^3) Atiamuri pyroclastics occupy a small area (ca. 10 km^2) in central Maroa. They probably formed as a constructional fan from column collapse events during a phase of pyroclastic activity that preceded or accompanied dome-building eruptions. The Atiamuri pyroclastics appear to lap onto Ohakuri pyroclastics along their northeastern margin, with a cap of the former sitting atop a hill of the latter around U17/773042. However, the contact between the two deposits is not exposed. The Atiamuri pyroclastics are in direct contact with Mandarin dome in MEC. Mandarin dome has similar petrography to the Atiamuri pyroclastics and is approximately the same age as the pyroclastics (see Chapter 3); it is assumed to occupy the source vent. The dome was probably erupted after the ignimbrite had cooled because

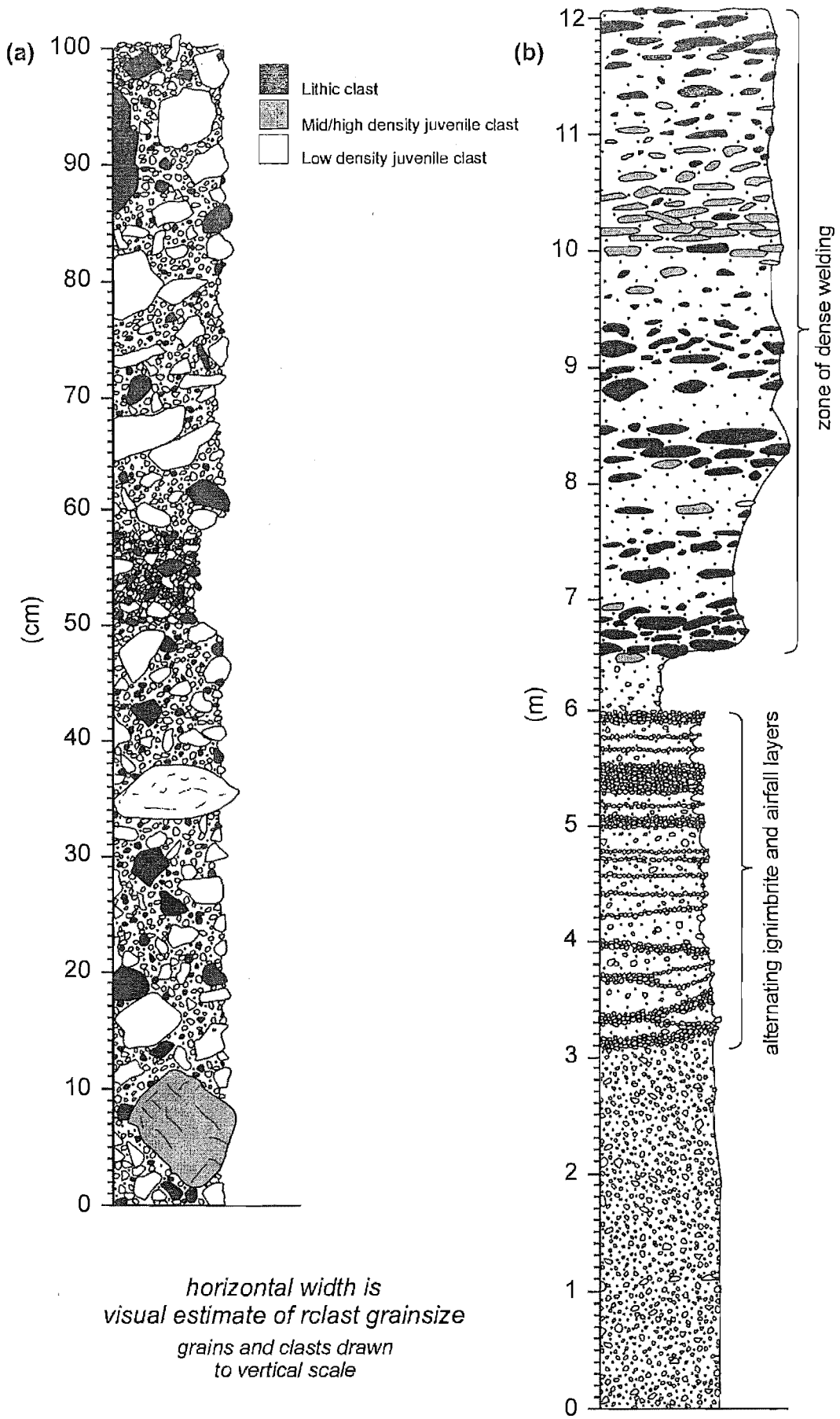

Figure 2.6 Log of (a) M270 (U17/776023) lithic-rich Atiamuri pyroclastics: massive ignimbrite with airfall unit; and (b) M339 (U17/798024) Atiamuri pyroclastics: ignimbrite, airfall and lenticulite.

a highly-welded zone (at location M339, Fig. 2.6(b)) in the ignimbrite is preserved right up to the topographic margin of the dome. A moat of unwelded ignimbrite (which would be expected to have preferentially eroded) would be expected if the ignimbrite had been deposited and chilled against a pre-existing dome.

A map of maximum pumice and maximum lithic distributions for the Atiamuri pyroclastics shows little clear pattern that can be contoured (Fig. 2.7). Generally pumice and lithic clasts are larger in the centre of the area of outcrop, compared to the margins. Because marker horizons could not be found at most outcrops, data are probably not from a consistent stratigraphic level within the pyroclastics. Data was collected ~ 10 m below the welded zone where present.

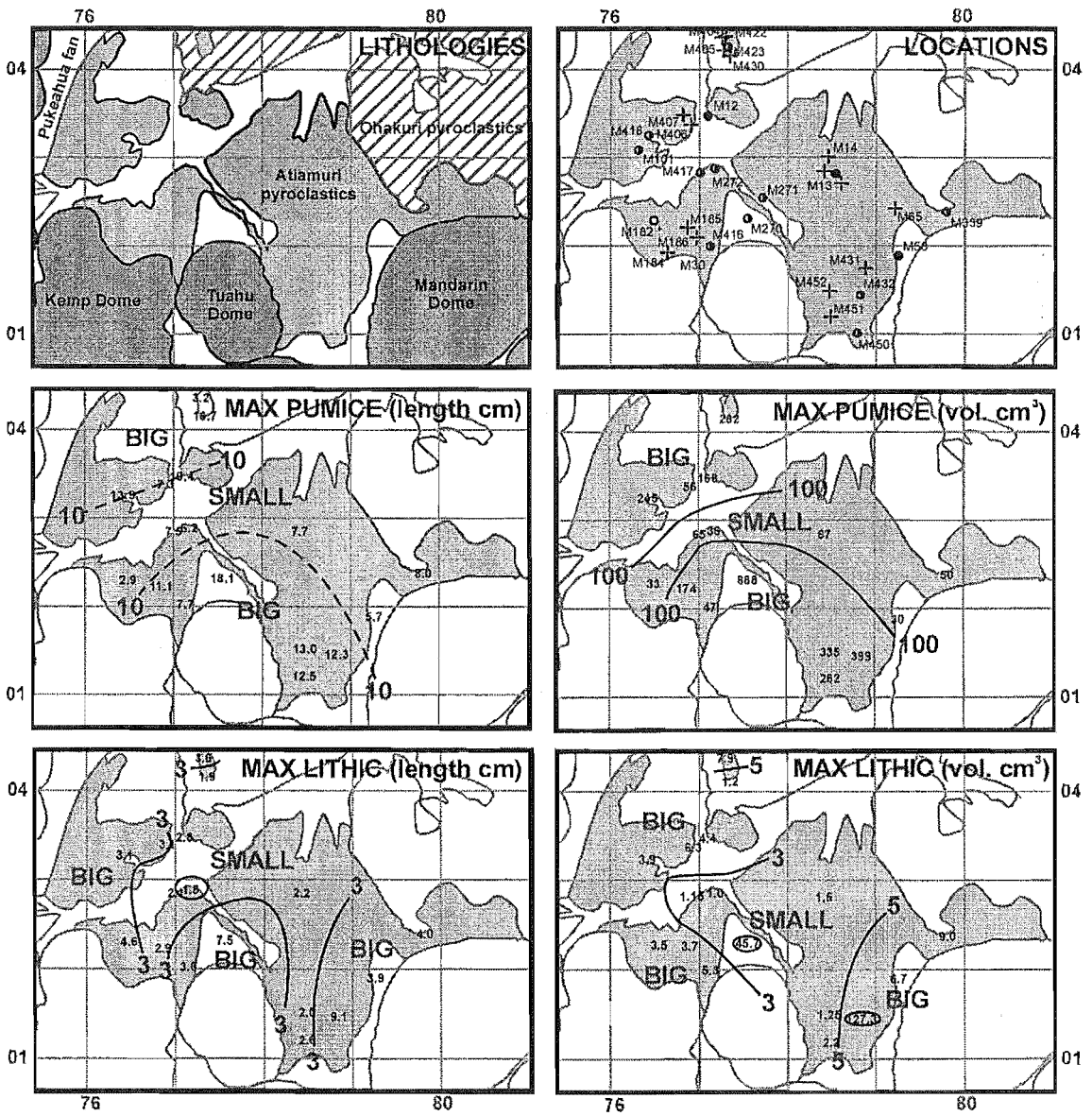

Figure 2.7 Maximum pumice and lithic distributions for the massive ignimbrite facies in the Atiamuri pyroclastics.

Exposure at location M272 (U17/772028, see Fig. 2.8) extends from massive ignimbrite down into multiple layers of airfall tephra with intervening paleosols. The base of the Atiamuri pyroclastics is considered to be the top contact of the uppermost of these paleosols. The fact that there is a sequence of distinct paleosols up to 200 mm thick below the Atiamuri pyroclastics indicates substantial periods of soil formation, likely thousands of years at least, between the deposition of the lowest airfall unit and the onset of the Atiamuri eruption. The thickness of these soils, and the airfall units that they contain, suggests small eruption events were continuing at frequent intervals between larger eruptions during this time period.

The base of the Atiamuri pyroclastics at M272 is considered to be at 118 mm in the log in Figure 2.8. A subsequent sequence of silty airfall units containing abundant accretionary lapilli are interpreted to suggest water ingress occurred into the eruption column. A sequence of coarse-ash to fine-lapilli airfall was then deposited before the emplacement of the ignimbrite.

Airfall sequences at other outcrops of Atiamuri pyroclastics are thinner (usually < 50 mm), isolated and are thus probably deposits from local smaller discrete airfall events between the emplacement of the main ignimbrite sheets.

Figure 2.9 gives a schematic summary of the sequence of the Atiamuri pyroclastics. At many other outcrops poorly stratified ignimbrite dominates with lenses of lithic-rich ignimbrite (e.g. M270, Fig. 2.6(a)) and/or airfall layers (multiple at M12) sometimes present. The well-lithified to slightly welded section (with an inferred near-vent highly-welded facies at M339) lies near the top of the sequence and appears to grade back up into a thin-non-welded zone above (visible at M182, but usually eroded).

The lithology in lithic-rich layers is obsidian, the petrology of which is similar to that of Mandarin dome and is consistent with a magma source that is in common with juvenile pumice clasts (see Chapter 4). These lithics are considered to have been produced by fragmentation of dome material which was extruded in between periods of pyroclastic eruption, and which was subsequently buried below Mandarin dome. Further detailed study will be needed to determine the number of airfall and dome-fragmenting events within the Atiamuri pyroclastics. It is not clear if sufficient outcrop exists for such a study to determine a continuous stratigraphy.

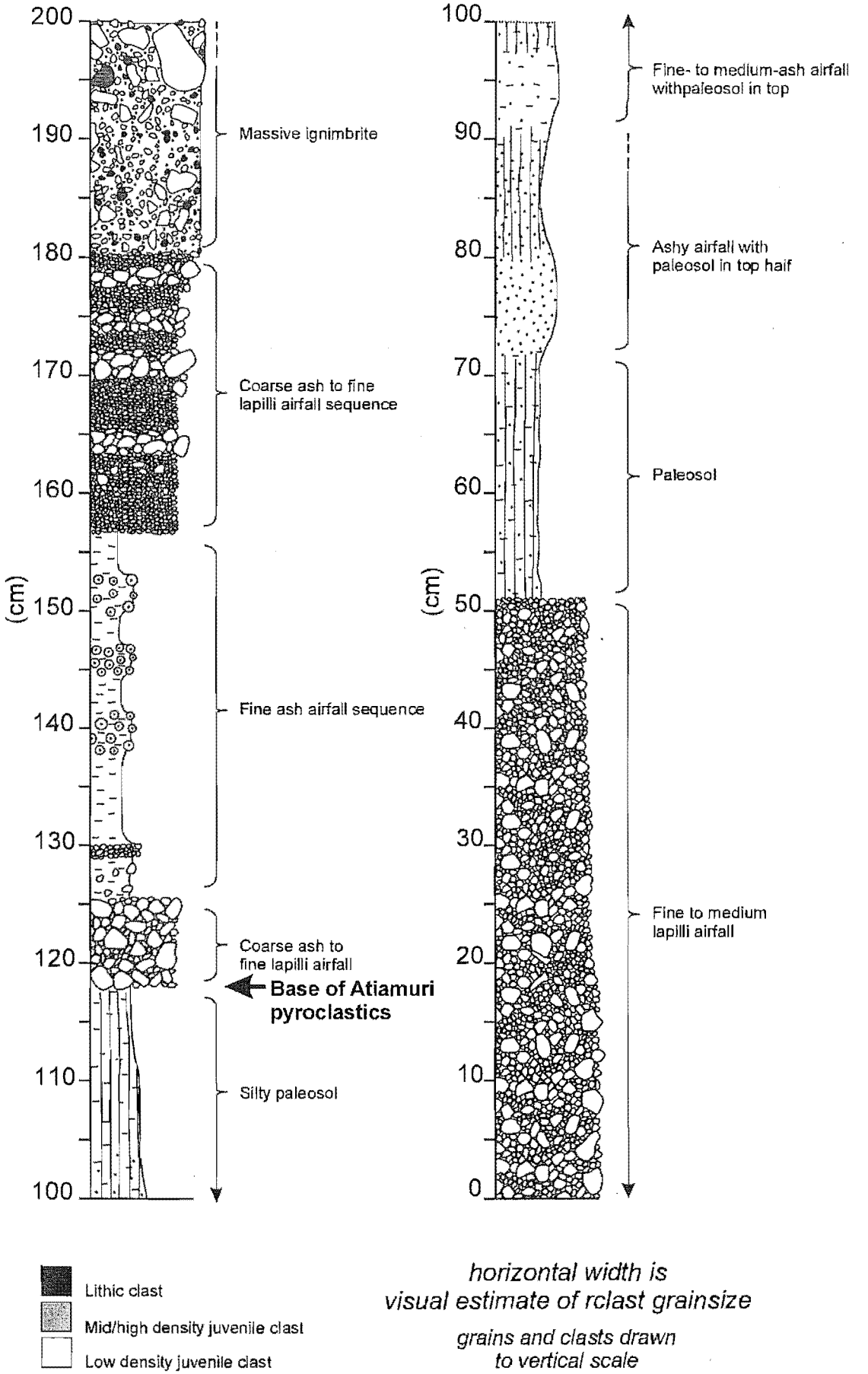

Figure 2.8 Log of base of Atiamuri pyroclastics, including airfall sequence, at M272 (U17/772028) in cutting in Sh1. Upper 100 cm on left.

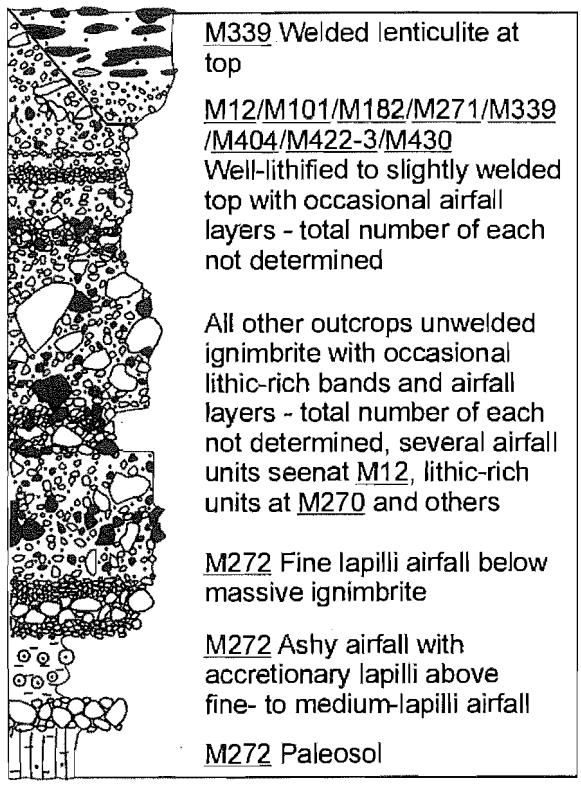

Figure 2.9 Diagrammatic summary of the Atiamuri pyroclastics sequence.

Along many gullies in the Atiamuri pyroclastics (e.g. M12 area) the well-lithified to slightly welded top is bluff-forming and erosion resistant, and forming a plateau surface above (Fig. 2.10(a) and (c)). At M339 this top is highly-welded with glassy fiamme that appear to be abundant blobs of dense juvenile material probably with the addition of some collapsed pumices (Fig. 2.10(b) and (e)). The unwelded character of the bulk of the Atiamuri pyroclastics is seen at the basal section at M272 (Fig. 2.10(d)).

Atiamuri ignimbrites

General: Usually massive with stratification into coarse (200 to 500 mm thick) lithic and pumice concentration bands at some locations. **Matrix:** Orange to pink (occasionally cream to white), soft in main body to hard at top (well-lithified/slightly welded – one layer highly welded at M339), moderately sorted, fine to coarse ash, 20 vol.% subhedral felsic crystals. **Juvenile clasts:** 10 vol.% cream to pink and orange, poorly sorted, up to 250 mm max, up to 100 mm usually, sub-angular, fresh, hard, moderately vesicular pumice. Pumice collapsed to dark grey glassy fiamme at M339 - see thin section description M339a for representative pumice petrography. Abundant fiamme of dense juvenile material up to 300 mm long in the welded zone at M339 **Ash-**

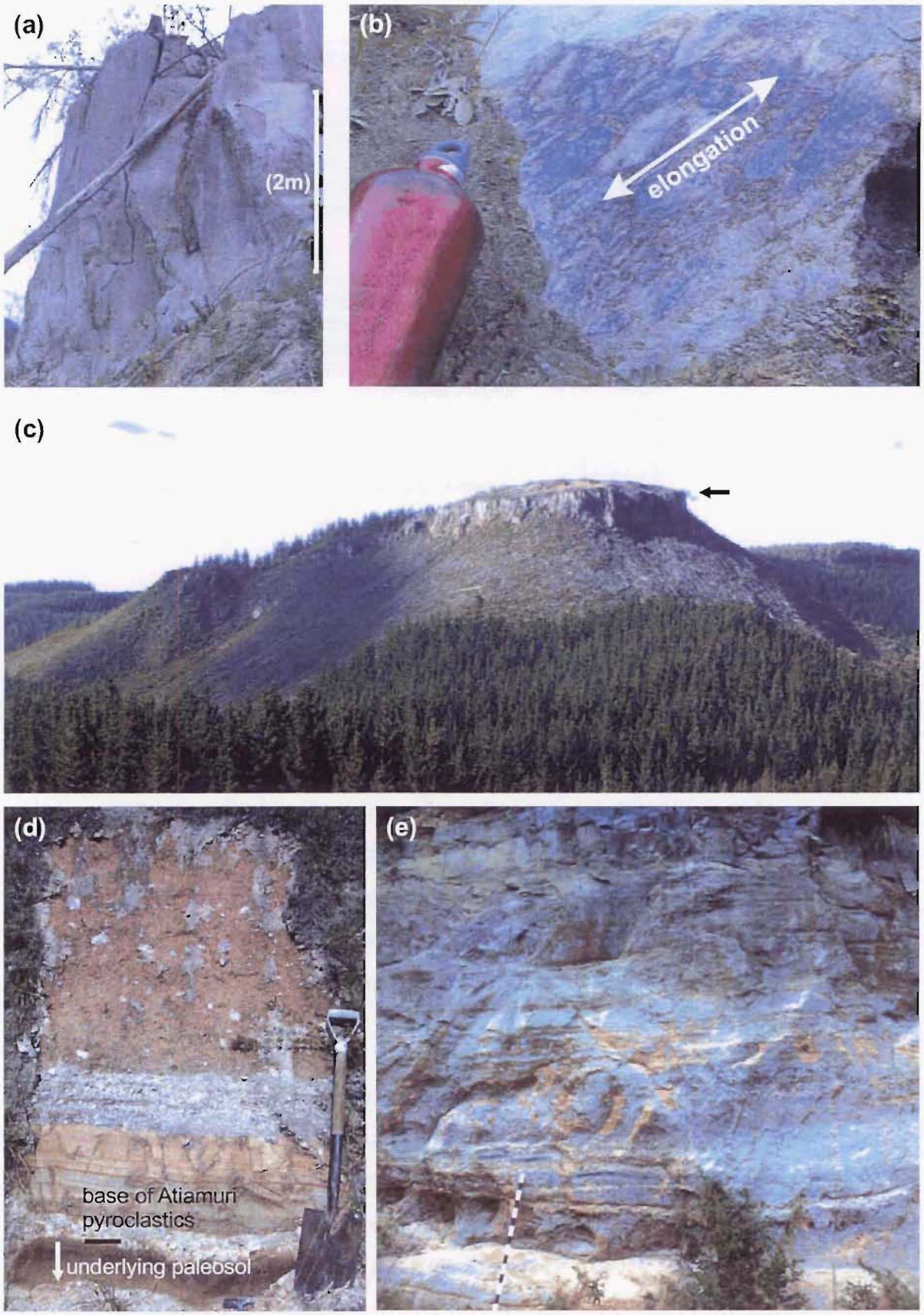

Figure 2.10 Images of (a) Atiamuri bluffs at M430 (U17/773042), (b) Atiamuri highly welded ignimbrite (M339, U17/798024), (c) Atiamuri bluffs plateau - location M430 (arrow) at right, (d) base of Atiamuri at M272 (U17/772028) and (e) unwelded Atiamuri ignimbrite and airfall (below) and highly welded ignimbrite (above) at M339 (scale is white/black alternating every 10 cm).

sized lithics: 5 to 10 vol.%, fine ash, angular, dark grey devitrified lava and obsidian. **Lapilli and larger sized lithics:** usually up to 5 vol.%, but up to 30 vol.% in concentration layers at some outcrops. ***Obsidian:*** Black obsidian lithics, angular, usually up to 30 mm (up to 150 mm at some outcrops) ***Devitrified lava:*** Devitrified grey rhyolite lava, sub-angular, usually up to 30 mm (up to 150 mm at some outcrops). ***Ignimbrite:*** Occasional angular lithics of ignimbrite, pink to orange, up to 40 mm. Contain clasts of pumice and lithic material similar to those within the main Atiamuri ignimbrites. These are likely to be recycled fragments of earlier-erupted Atiamuri ignimbrites.

Atiamuri airfall

General: 10 to 500 mm thick, fines poor, normally graded, well sorted, vary from fine ash to fine lapilli. Sometimes form multiple layers of distinct grainsize ranges (esp. at location M272). **Juvenile clasts:** ~ 80 vol.%, white to orange colour, moderate vesicularity, usually occupy a narrower grainsize range within fine ash up to 30 mm lapilli, fresh, angular pumice. **Lithics:** ~ 20 vol.%, fine lapilli to 20 mm lapilli, black to grey, normally graded along with pumice clasts, variably hydrated, fractured, angular obsidian.

2.3.4 Orakonui, Putauaki and Tram Rd pyroclastics

Type localities

Orakonui pyroclastics: M47 (U17/832925). A cutting on the south side of Whakapapa Rd exposes firm massive ignimbrite where pumice clasts are fresh and componentries are easily discernible. Lloyd (unpublished Geological Survey notes provided by GNS) defined a type section at U17/830930 (retained as the formal type section here), but noted that this was impossible to reach due to Ongaonga stands. Thompson (1966) suggested the bluffs at U17/808935 as a more-easily accessed alternative type section. Unlike Lloyd's type section, these bluffs are case hardened, masking a lot of internal structure. Both previous locations have been suggested to display multiple flow units, but this has not been verified in this project. Until access is restored to the formal type section the reader is referred to location M47 as the most easily accessible section of fresh Orakonui ignimbrite.

Putauaki pyroclastics: M33 (U17/753923). Weathered outcrops in a grassy slope off of the west side of an airstrip (Lloyd, 1972). This location displays the largest and most abundant lithic clasts.

Tram Rd pyroclastics:

Around its type section at M274 (U17/783909), an outcrop of a locally distributed pyroclastic deposit, referred to here at the Tram Rd pyroclastics, is seen below the Orakonui pyroclastics and is inferred to overlie the Putauaki pyroclastics. Lithics within it reach almost twice the length and ~ 6 times the volume as those in the Orakonui pyroclastics, shown below. They are geochemically distinct from the Orakonui and Putauaki pyroclastics (discussed further in Chapter 4).

Source and Distribution

The Orakonui pyroclastics initially included deposits west of Tram Rd (Lloyd, 1972). However, Houghton et al. (1995) listed these as the Putauaki Ignimbrite based on the unpublished field evidence of Lloyd. New data presented in Chapter 4 suggests that they are petrologically similar, and there may simply be a time-break in between eruptions from the same magma system. Although their field characters are markedly different (Putauaki pyroclastics are pervasively vapour-phase-altered, whereas Orakonui pyroclastics are not) the componentry of the two units is very similar (Fig. 2.11). The field contact between them has unfortunately not been observed and at least at its type locality the Tram Road Pyroclastics lie between these two eruptive units; therefore, the Orakonui and Putauaki pyroclastics are treated as separate units for the purposes of this thesis.

The Orakonui and Putauaki pyroclastics form a low-angle surface dipping towards the southeast, away from central Maroa. A diagrammatic representation of this relationship is shown in Figure 2.12. The Putauaki pyroclastics are older than the Orakonui pyroclastics and underlie them. The two deposits appear to lie next to one another because of (a) the truncation of the west side of the fan by the Whangamata Fault, (b) the dip of the fan and (c) down-dip erosion of the Orakonui scarp.

Lithics within the Putauaki pyroclastics reach 0.5 m in size and 40 vol.% at M33 but are 5 to 10 vol.% and up to 10 mm elsewhere. Lithic sizes within the Orakonui pyroclastics were determined at multiple locations south of Tutukau Rd. All determinations were ~

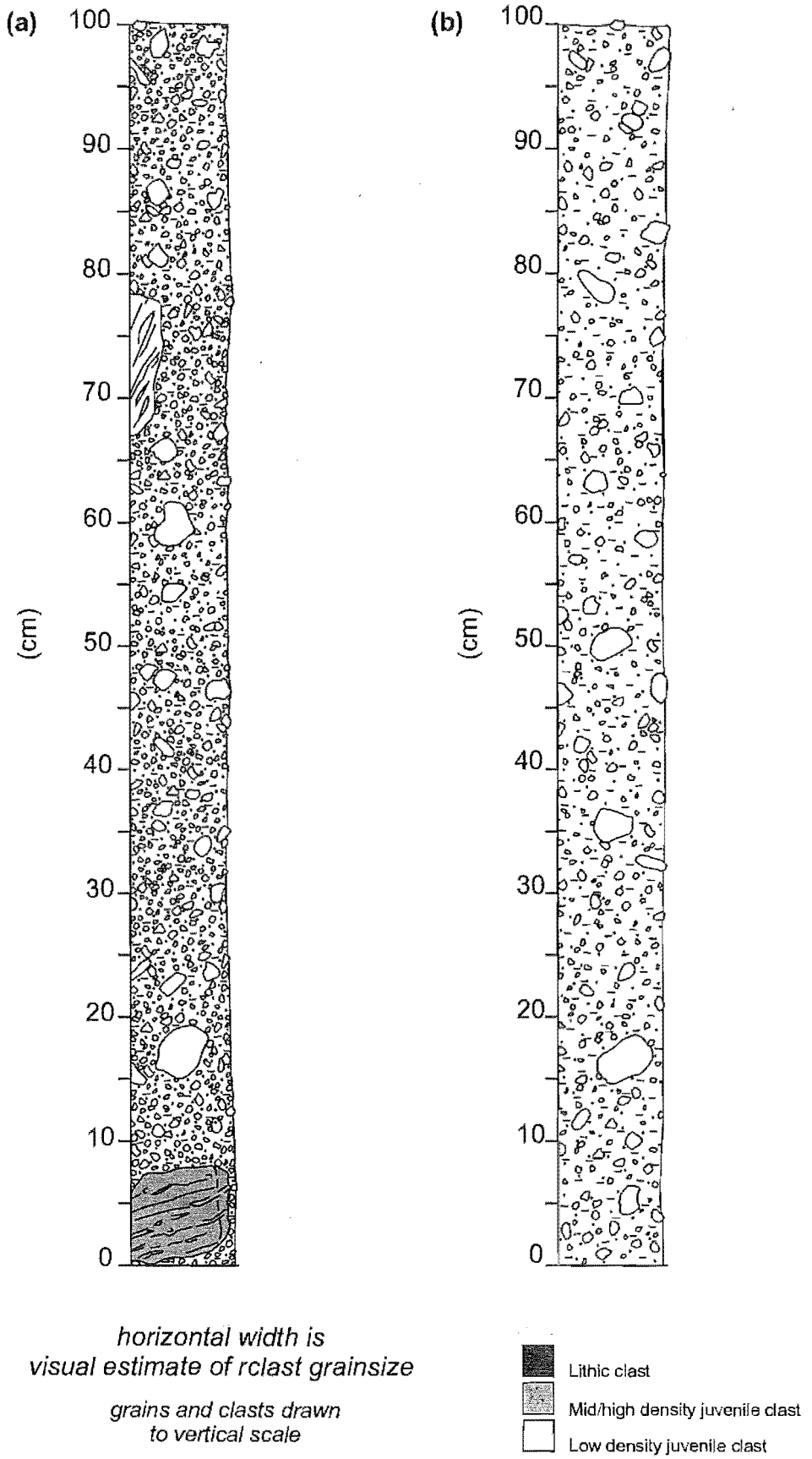

Figure 2.11 Graphic log of Orakonui pyroclastics (a) M46 (U17/482930) Orakonui member and (b) M47 (U17/832925) Putauaki member

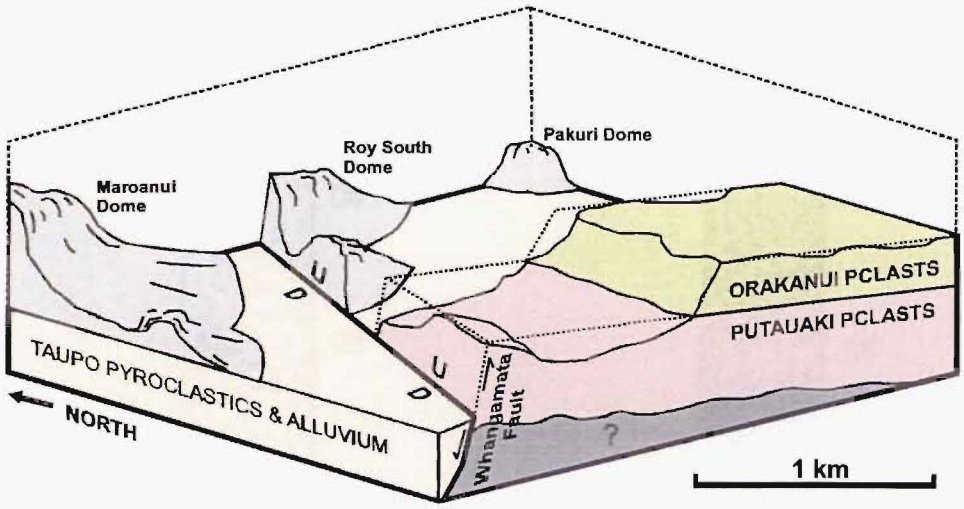

Figure 2.12 A block diagram showing the field relationship of the Orakonui and Putauaki pyroclastics relative to Maroa.

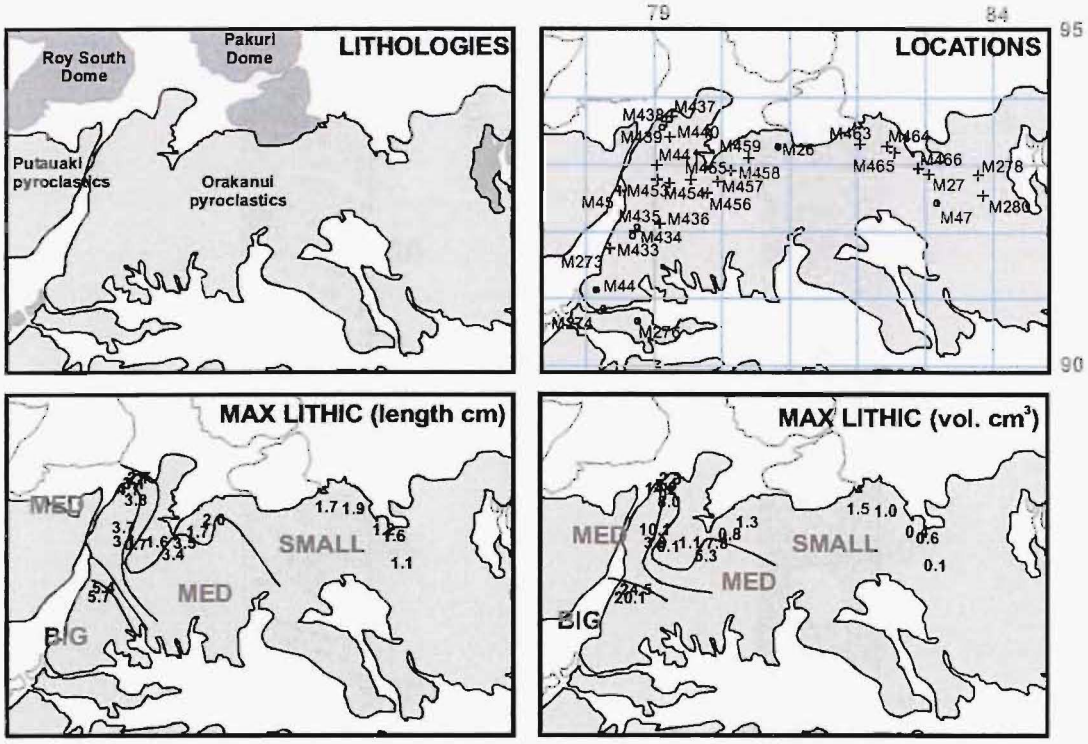

Figure 2.13 Lithic size distribution in the Orakonui pyroclastics.

10 m below the top of the bluffs. The distribution is shown in Figure 2.13. Both maximum length and volume show an increase to the southwest.

Lithic size distributions in both the Orakonui and Putauaki pyroclastics decrease to the east, in the direction of dip. These deposits, therefore, probably formed from a source to the west of their outcrop within central Maroa, but close to locality M33.

Orakonui pyroclastics

General: Usually massive with slight lithic and pumice concentration bands at some locations. Weathered exposures usually case hardened. **Matrix:** Cream to light grey, soft to firm, moderately sorted, very fine to medium ash, mostly fine ash. Medium ash is mostly subhedral felsic crystals (plagioclase with minor quartz) which constitute ~ 20 vol.% of the rock. **Juvenile clasts:** 15 vol.% orange (some streaked light and dark grey), poorly sorted, large- to very fine-lapilli, sub-angular, hard and fresh to devitrified and soft, moderately to highly vesicular pumice. **Lithics:** ~ 5 vol.% medium ash to lapilli, usually up to 10 mm, mostly devitrified, dark grey, angular to sub-angular lava and up to 1 % angular black obsidian.

Putauaki pyroclastics

General: Massive and vapour-phase-altered. Case hardened in weathered outcrops. **Matrix:** Tan to pink or brown, soft, well sorted, very fine ash (original grainsize distribution masked by vapour-phase-alteration and weathering). Crystals may have been 10 to 20 vol.% of rock but have weathered to clay. Brown spots throughout juvenile clasts and matrix may be weathered ferromagnesian crystals. **Juvenile clasts:** Probably originally pumice ~ 10 vol.%, usually up to 30 mm, pinky purply tan, well sorted, rounded, soft and powdery, devitrified, weathered and vapour-phase-altered, vesicularity masked by alteration. ~ 10 vol.% grey remnants of euhedral, probably felsic, phenocrysts. **Lithics:** Vary between 5 and 40 vol.% of deposit, usually up to 15 vol.% and up to 100 mm at M33, and up to 10 vol.% and up to 10 mm elsewhere. Lloyd (1972) observed up to 500 mm lithics at M33. Angular to sub-angular lava, ~ 20 vol.% phenocrysts still visible in all lithics. Some weathered to grey clay. Some dark grey and highly devitrified. A few pink ignimbrite lithics probably derived from the same unit. A few are speckled dark grey and cream and may have been obsidian.

2.3.5 Korotai pyroclastics

Type locality

Type location M2 (T17/688084). Bluffs of two zones of highly welded Korotai ignimbrite with unwelded ignimbrite below and between them, to the east above Korotai Rd. Suggested by E. F. Lloyd (pers. comm., 2001).

Overview of deposits

The Korotai pyroclastics out crop over an area of ~ 3 km^2 and have a preserved volume < 1 km^3. The pyroclastics are primarily composed of massive unwelded ignimbrite with at least two horizons > 5 m thick, each of highly welded ignimbrite. The horizons form bluffs along the hill slopes east of Korotai Rd and are separated about 10 m vertically by unwelded ignimbrite that is often covered by slope alluvium. At some outcrops, lithics grade in character from obsidian to pumiceous lava. There is little petrological difference (discussed in Chapter 4) between apparently-juvenile clasts and obsidian lithics. Both are interpreted to be from the same magma and eruption. The dome(s) that the lithics have been derived from were likely produced by earlier phase(s) of the eruption that later blasted it/them apart. A diagram of the outcrop, field relationships, stratigraphy and character of the Korotai pyroclastics is shown in Figure 2.14. The

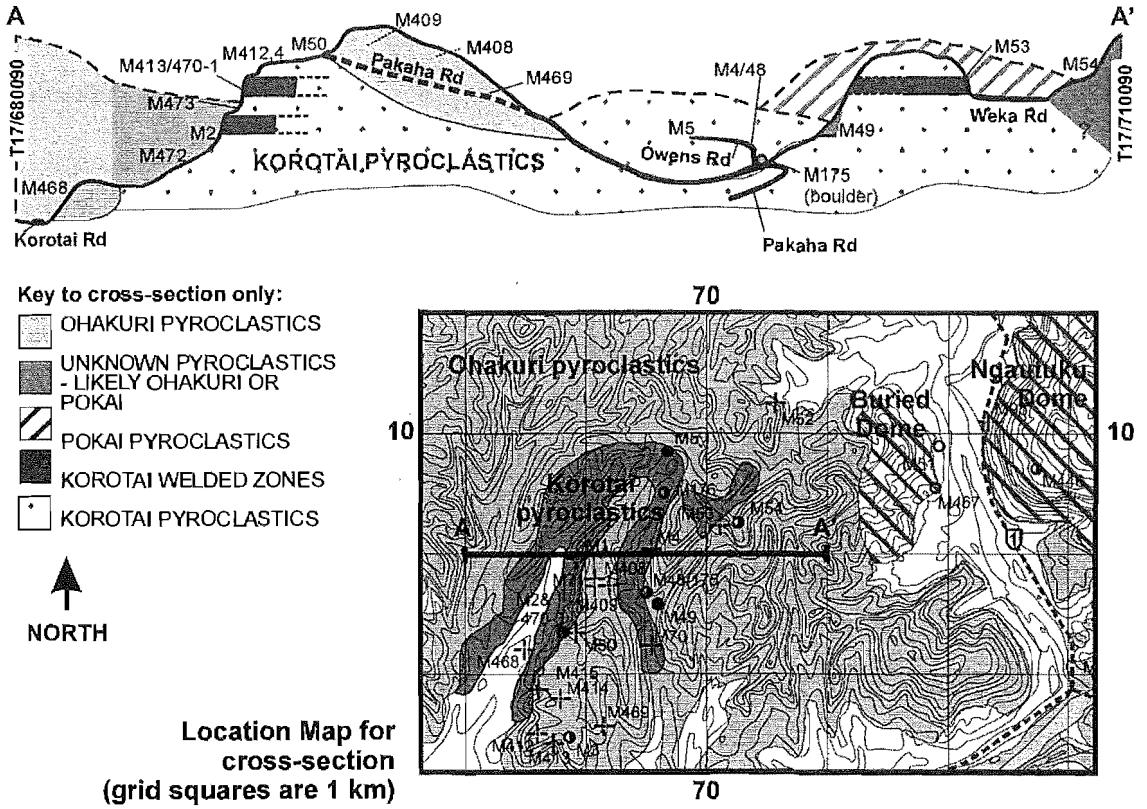

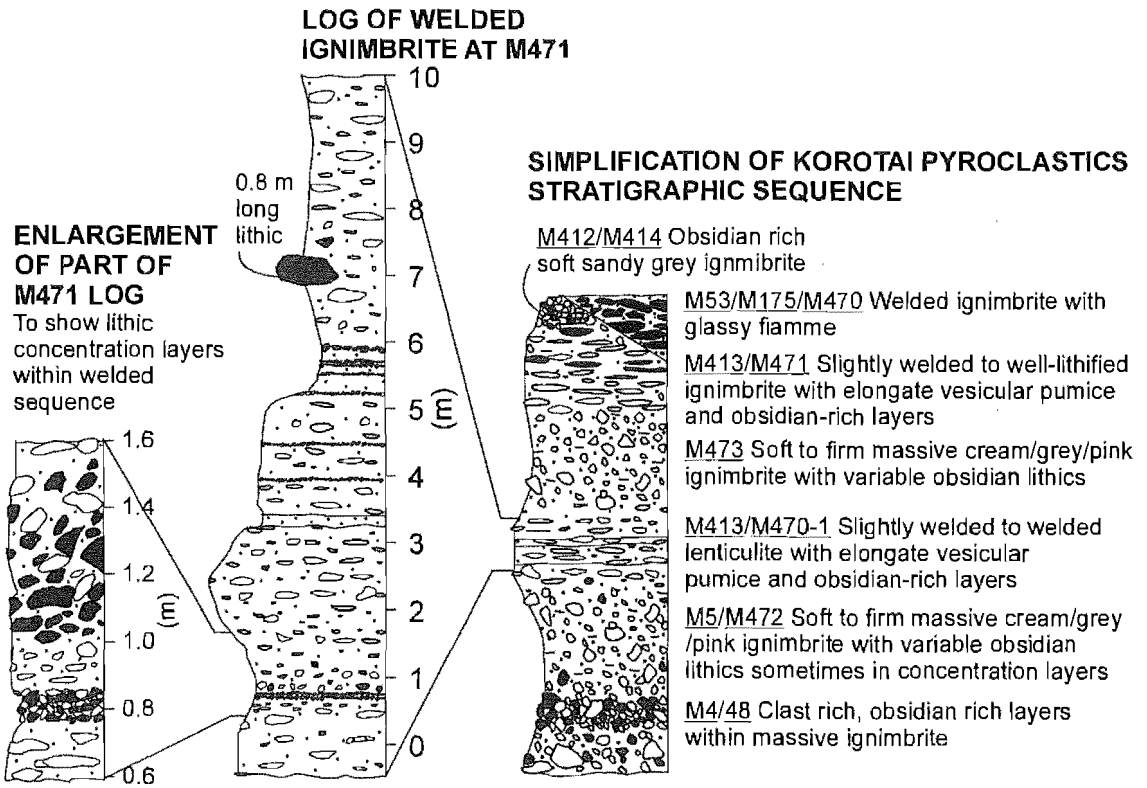

Figure 2.14 Diagrammatic cross-section, location map and stratigraphic sequence for the Korotai pyroclastics.

glassy-fiamme-bearing highly-welded layer at Weka Rd, and the soft obsidian-rich ignimbrite at M414, represent the two end-members of Korotai pyroclastics character (Fig. 2.15 (a) and (b) respectively).

Korotai unwelded ignimbrite

General: Massive, some well-lithified outcrops grade into highly-welded. Vesicularity and colour of juvenile clasts overlap with those of lithics. **Matrix:** Grey or tan to orange, soft to hard and well-lithified, usually firm, moderately sorted, very fine to fine ash, 10 to 15 vol.% felsic crystal, up to 5 vol.% angular obsidian ash-sized lithics at some outcrops. **Juvenile clasts:** 20 to 30 vol.%, usually up to 100 mm, orange, sometimes with grey core, some grey to dark grey, fresh and hard, well sorted, sub-rounded, often in concentration layers, slightly to highly vesicular, up to 5 vol.% felsic phenocrysts. **Lithics:** Vary from 5 to 40 vol.% of deposit, usually up to 20 vol.%, up to 130 mm, usually angular black obsidian variably dense to vesicular and hydrated, up to 5 vol.% dark grey partly devitrified lava at some outcrops.

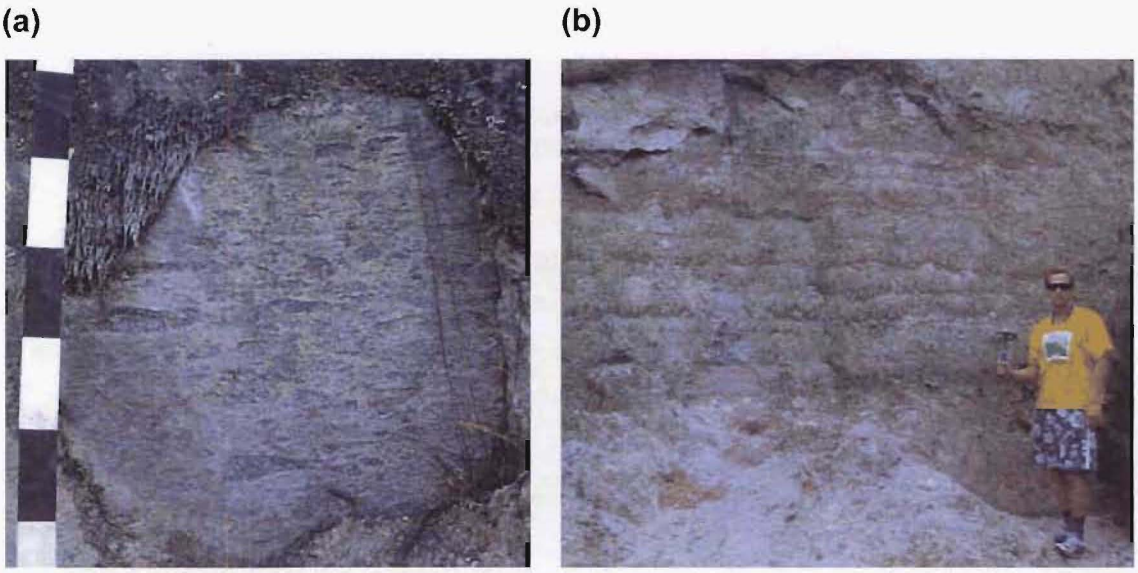

Figure 2.15 (a) Highly welded zone of Korotai pyroclastics, with glassy fiamme, at Weka Rd and (b) non-welded, obsidian-rich Korotai ignimbrite at M414.

Korotai welded ignimbrite

General: Massive and highly-welded with fiamme, some outcrops grade into moderately welded ignimbrite with elongated pumices. **Matrix:** Dark grey, recrystallised and strongly welded; individual grains are no longer discernible. **Pumiceous juvenile clasts:** 20 to 30 vol.%. In the least welded cases pumices are similar to those in well-lithified ignimbrite outcrops and vesicular but are lenticular with

parallel elongate vesicles. At most outcrops pumices have collapsed to black obsidian fiamme. At least some of these clasts were probably fluidal dense juvenile material in the first instance, but it is difficult to distinguish these from collapsed pumiceous material. Fiamme are fresh, rounded, with high aspect ratio, well sorted, often in concentration layers, sometimes slightly vesicular. **Dense juvenile clasts:** Vary 5 to 40 vol.% of deposit, usually up to 20 vol.%, up to 130 mm, usually angular black obsidian variably dense to vesicular and hydrated, up to 5 vol.% dark grey partly devitrified lava at some outcrops. The latter may be lithic lava from non-juvenile sources. Often elongate parallel to fiamme and in some cases the only distinction between obsidian lithics and fiamme is the angular morphology of the lithics.

2.3.6 Maroa derived airfall sequences

Maroa-derived airfall pyroclastics

Airfall deposits at a handful of other locations (M7, M12, M42, M63, M148, M258, M272, and M339) in Maroa cannot be correlated to other outcrops and are probably deposits of local pyroclastic eruptions related to nearby dome-forming eruptions. Airfall deposits/layers are typically variably finely layered, sometimes normally graded, moderately to well sorted, lapilli-sized cream pumice, accompanied by 5 to 10 vol.% fine lapilli-grade, angular, grey, devitrified rhyolite lava and obsidian lithics.

The airfall sequence at M258 (Fig. 2.16) shows a typical outcrop of these airfall deposits, sandwiched between locally-derived BAF deposits. This sequence of units has not been observed in outcrop anywhere else and is considered to have a very limited preservation. This may represent a very limited initial distribution, and/or substantial post-depositional erosion.

New3 airfall ~ 45 ka, of unknown origin

A unit of sticky, clay-rich material is found within the Maroa area, stratigraphically between the Tihoi and Tahuna Tephras. It thins rapidly away from a maximum thickness near Orakeikorako (~ 600 mm thick in the Te Kopia Rd section, see Section 2.6.1). At Te Kopia Rd it contains three horizons of pumice clasts and the maximum grainsize and thickness of these horizons is in the vicinity of Mokauteure dome. The sticky clay material may be the result of a local hydrothermal eruption in the

Orakeikorako area that has trapped airfall from an event sourced in the Mokauteure dome area. The source of the airfall material is discussed further in Chapters 4 and 5.

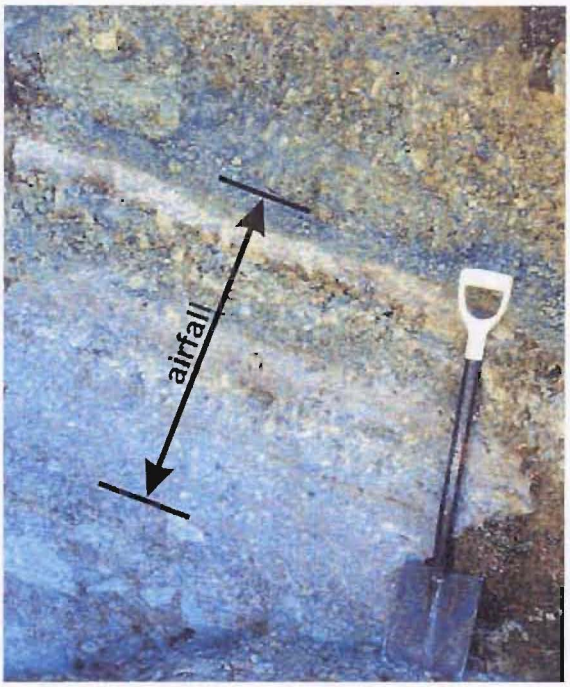

Figure 2.16 Photo of locally distributed Maroa airfall deposits sandwiched between two BAF deposits at M258 (U17/785965).

2.3.7 Puketarata pyroclastics

The Puketarata tuff ring and dome are the products of the youngest eruption from Maroa (~ 16.7 ka) based on the bracketing ages of the Rotorua and Rerewhakaaitu eruptions from Okataina (Newnham et al., 2003). A model of the eruption by Brooker et al. (1993) is shown in Figure 2.17. A mostly-degassed body of magma sometimes interacted with shallow groundwater to produce surge deposits which, together with dominantly fall deposits, formed a small tuff ring. As the supply of water diminished, and effusion rates decreased, a lava dome formed in the centre of the ring. A pyroclastic deposit, comprised of varied airfall and surge lithologies from multiple stages in the eruption, is up to 500 mm thick and well preserved within a couple of km of the vent and at many locations throughout Maroa.

This eruption was probably of a similar scale to those producing many other isolated domes in Maroa. Therefore, they could also be expected to have been surrounded by tuff rings at an early stage. Erosion has probably removed traces of most associated pyroclastic deposits, including tuff rings, from the vicinity of any small domes

substantially older than Puketarata; tuff rings around the vents for larger domes may have been buried by the domes themselves.

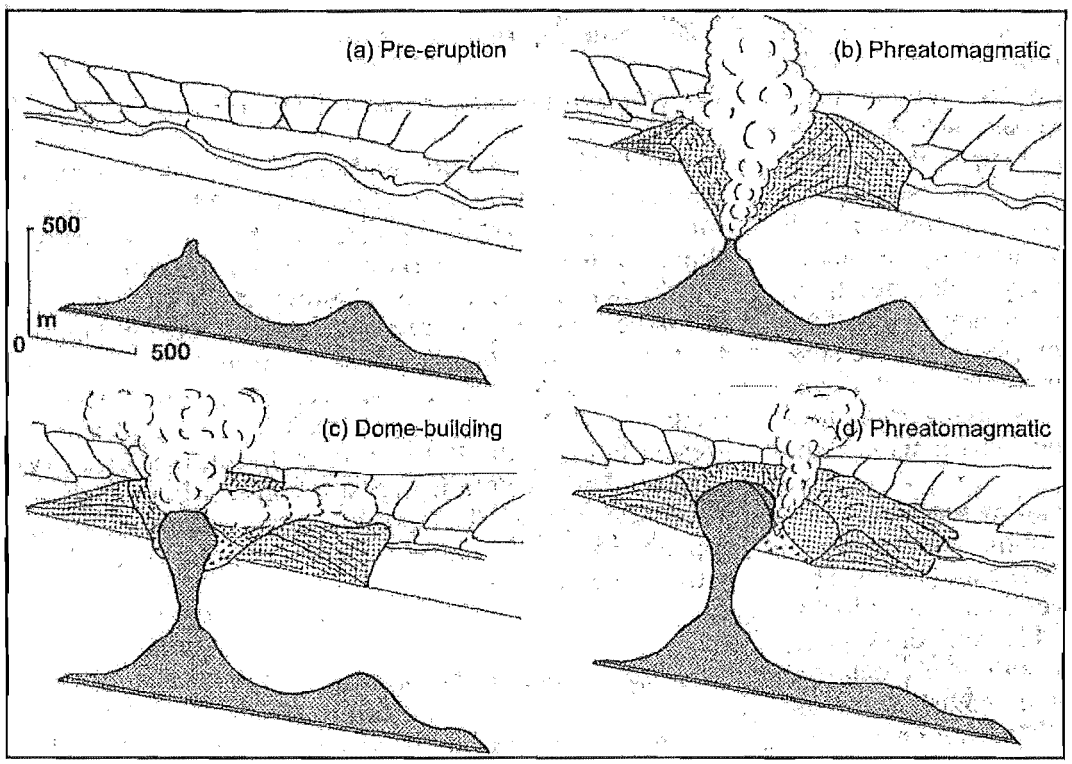

Figure 2.17 Evolution of the Puketarata lava dome and tuff ring from Brooker et al. (1993).

2.4 Basalt and 'andesite'

2.4.1 Introduction

Basalt makes up less than 1 % of the volume of TVZ volcanics. It occurs as small scoria cones and/or lava flows, sometimes with phreatomagmatic deposits. Figure 2.18 shows the distribution of basalt outcrops in the Maroa area. The 5 basaltic deposits found around Maroa are briefly summarised below.

Andesites are found as lavas and scoriaceous airfall deposits forming discrete monogenetic cones and stratovolcanoes along the margins of the active-TVZ, but Parekauau 'andesite' had been considered the only known andesite associated with Maroa. It has been analysed by XRF here and is geochemically a dacite (see Chapter 4). Basalt and andesite do not appear to play an important role in the evolution of Maroa and are, therefore, only described for the sake of completeness in this thesis. Descriptions are modified after unpublished notes of E. F. Lloyd c. 1990, kindly provided by the Institute of Geological and Nuclear Sciences and E. F. Lloyd (pers. comm., 2003).

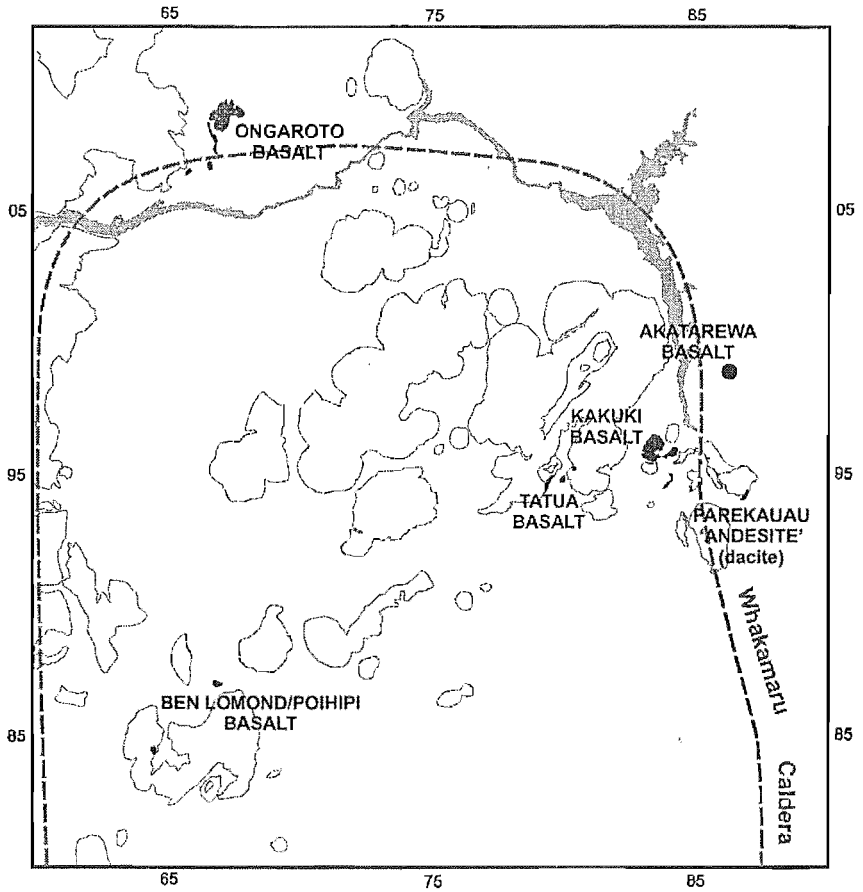

Figure 2.18 Map of basalts and andesites in the Maroa area. Grid is New Zealand Map Grid (km).

2.4.2 Akatarewa basalt

This deposit forms strombolian scoria beds > 2 m in thickness at U17/863001 and U17/865001 (E. F. Lloyd's proposed type section) in Akatarewa stream. It comprises > 1 m thick interbedded phreatomagmatic and scoria deposits in the Te Kopia Rd regional tephra sequence at M43 (U17/861989) described above. Akatarewa basalt was previously included with Tatua Basalt (Lloyd, 1972).

2.4.3 Kakuki basalt

This is a low cone of alternating strombolian and phreatomagmatic deposits near Orakeikorako. A good exposure of this finely-layered sequence is the type section (Fig. 2.19) at M291 (U17/833964), which is a cutting in the northwest side of Orakeikorako Rd. Near the centre of the cone > 40 m of coarsely layered scoria and ash, with variable coarse lapilli sized, smooth, dense, round lava bombs, is exposed in gully sides at U17/832959. Lava exposed further down the gully at U17/832959 is probably part of a feeder dike. The total area of the cone is > 0.5 km^2.

Figure 2.19 Photo of Kakuki basalt stratigraphy at M291 type section.

2.4.4 Tatua basalt

This deposit comprises an outcrop of bedded scoria on the cutting of a farm track on the side of Pakuri rhyolite dome near M304 (U17/803954) and layered lava flows at M303 (U17/795974). The scarp exposing M303 is the preferred type section. E. F. Lloyd proposed that the low hill at U17/799948 is also a poorly exposed scoria cone of Tatua basalt, but no exposure can now be found. The deposit on Pakuri dome appears to have been the product of low strombolian fountaining from a vent fed through the older dome.

2.4.5 Poihipi/Ben Lomond basalt

This is a small cone of bedded basalt scoria that is variably welded. It contains fluidal lava bombs and all components contain abundant rhyolite lava lithics. The type locality is defined at T17/668870 in a quarry on Poihipi Rd, where a section of the northwest dipping flank of the cone is exposed. The only other exposure is a small cutting (T17/667871) along Poihipi Rd.

2.4.6 Ongaroto basalt

This deposit forms up to 4 aa lava flows up to 17 m thick in total at the type locality T17/667078, a waterfall in Opareiti Stream. More readily accessible, Watts Quarry at

M112 (T17/089669) has exposed a 5.5 m thick layer of Ongaroto basalt lava, now extracted for roading aggregate.

2.4.7 Parekauau 'Andesite' (Dacite)

Parekauau 'andesite' is probably a dike (Lloyd, 1972), up to 500 m long, cutting southwest across the Waikato River to an outcrop in Tutukau Rd at M279 (the type section, U17/868941). At this outcrop it is dark grey highly fractured lava. It is geochemically a dacite (see Chapter 4).

2.5 Key regional deposits

This section provides details of the Ohakuri and Mokai pyroclastics, and also briefly summarises the deposits east of the Waikato River. The Ohakuri and Mokai pyroclastics are introduced in Section 1.6 along with the Whakamaru group, Mamaku and Pokai pyroclastics as part of the geological setting; this section serves to provide more detail on the former two because, although they appear to have origins outside of the centre, they both outcrop significantly within Maroa. Most of the deposits east of the Waikato River are in very close proximity to Maroa, but do not appear to have much significance to its evolution.

2.5.1 Ohakuri pyroclastics

Darren Gravley, as part of a Ph.D. at the University of Canterbury, is conducting field research on the Ohakuri pyroclastics concurrently with this thesis project.

Description

The matrix of the Ohakuri pyroclastics is white to cream, clayey to silty sand, firm to hard (the latter usually due to case hardening). There are three distinct facies. The majority of the volume is dominated by a massive non-bedded ignimbrite facies and a bedded, often cross-bedded, often graded, surge deposit facies. The surge deposit facies varies between ignimbrite and airfall end members probably depending on rate, style and energy of eruption. A third, minor, airfall facies comprises jigsaw fit, often normally graded, fines-poor, well sorted angular pumice. In some cases two or even all three facies alternate in varying thicknesses within a single exposure, while in others a single ignimbrite or surge facies comprises an entire exposure or area of exposure (D. M. Gravley, pers. comm. 2003).

Pumice within all facies varies from < 1 to 30 vol.% of the deposit and is generally of low density (D. M. Gravley, pers. comm. 2003). Hand specimen pumice clasts are moderately to highly vesicular. Lithics are almost all dark grey, devitrified, angular rhyolite lava. Occasional ignimbrite lithics are usually up to 20 mm and difficult to determine provenance for.

Origin

The pyroclastics have a partly radial distribution around a depression just north of Maroa, suggesting that the source caldera is probably in that area. There is a lack of distribution across Maroa to the south and southwest as this would have been high ground at the time of eruption (see geochronology in Chapter 3). Massive Ohakuri-style ignimbrite is over-thickened to > 600 m within the basin (based on drill hole logs near Atiamuri from confidential Crown Minerals reports), consistent with it being an intra-caldera deposit. The southern boundary of this basin could overlap with present Maroa deposits such as the Pukeahua dome complex and surrounding isolated domes, as these all appear younger (Chapter 3).

2.5.2 Mokai pyroclastics

Type Section

Healy et al. (1964) defined a type section at T17/677035 along the Pokuru Fault. However the type section preferred here was defined by Milner (2001) and is along the face of the Okama Stream gorge where it opens out to the Waikato River, at T17/634040–634037–640034. Massive ignimbrite is broken by two fine-ash rich layers here. Figure 2.20 gives a log of typical Mokai pyroclastics and the stratigraphy at the type section. Healy et al.'s type section does not include exposure of the fine-ash rich layers.

Previous Work

E. F. Lloyd mapped ignimbrite between Maroa and the Western Dome Belt as Mokai ignimbrite (E. F. Lloyd, pers. comm. 2003). Other workers have suggested that the Mokai is a distal facies of the Mamaku pyroclastics (e.g. McWilliams, 2001; Tanaka et al., 1996). There is no meaningful variation in size or concentration at any outcrop visited during this research (locations on Map 1, back pocket), including those along Pokuru Fault, on the edge of Maroa. Some increase in lithic size and content nearer

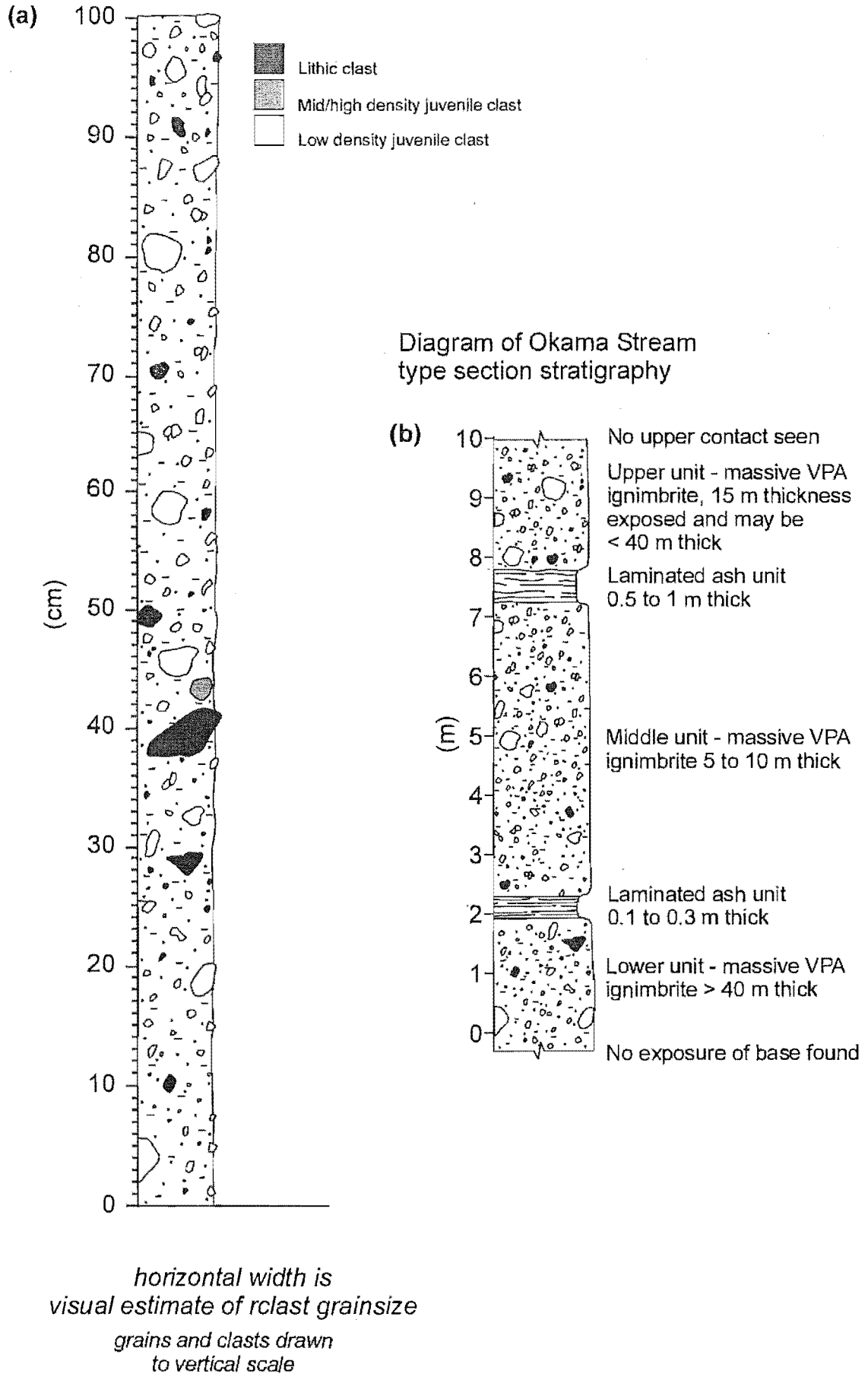

Figure 2.20 (a) Log of typical massive Mokai pyroclastics ignimbrite at M421 (T17/664000) fits into the top section of (b) a diagram of the sequence at Okama Stream (~ T17/637035)

Maroa would be expected if that were the source. The petrology and vapour-phase-altered character of Mokai ignimbrite are as similar to the Putauaki pyroclastics as they are to the Mamaku pyroclastics. Prior to this project, the main evidence for or against a link to any source, or correlation to other deposits, had been given by Tanaka et al. (1996) who suggest a correlation to the Mamaku pyroclastics based on the similar unusual paleomagnetic orientation of both (discussed further in Section 3.5.2). No new evidence has been revealed in the research conducted during this thesis. This deposit remains something of an enigma.

Description

General: Massive, with two laminated fines-rich layers < 1 m thick, see only at type section **Matrix:** Grey to orange-grey, soft to hard and well-lithified, usually firm, poorly sorted, fine to medium ash with coarse-ash sized grains of pumice, 25 to 30 vol.% felsic crystals, < 5 vol.% Fe/Mg crystals. **Juvenile clasts:** 20 to 30 vol.%, usually up to 100 mm, creamy white to orange, fresh and hard to vapour-phase-altered and powdery, well sorted, sub-rounded, moderately vesicular. **Lithics:** Trace to 5 vol.% of deposit, usually 2 to 3 vol.%, up to 130 mm, angular, (a) black to devitrified grey obsidian and (b) cream to grey, sugary, fresh to silicified lava.

2.5.3 Deposits east of the Waikato River

The area to the east of Maroa, across Lake Okahuri, is dominated by four deposits. In the northwest of this area, beyond the Paeroa fault scarp, the landscape is dominated by Ohakuri pyroclastics. The deposits that make up the Paeroa fault scarp are primarily Whakamaru group pyroclastics. Close to Maroa they are covered by Kaingaroa pyroclastics from Reporoa caldera (Beresford et al., 2000). Fluvial and lacustrine sediments, which are not differentiated here, form a block that extends further southeast of the Kaingaroa pyroclastics to about parallel with the southern end of Maroa. To the south of this most material is covered by thick Oruanui and Taupo pyroclastics.

2.6 Younger overlying deposits

These deposits are found throughout Maroa and mantle most of the older Maroa-derived units. This is a brief summary of the key aspects of (a) regional airfall deposits (b) the Oruanui Formation, (c) the post-Oruanui sedimentary deposits Mokai Sand and Hinuera Formation, and (d) Taupo Formation.

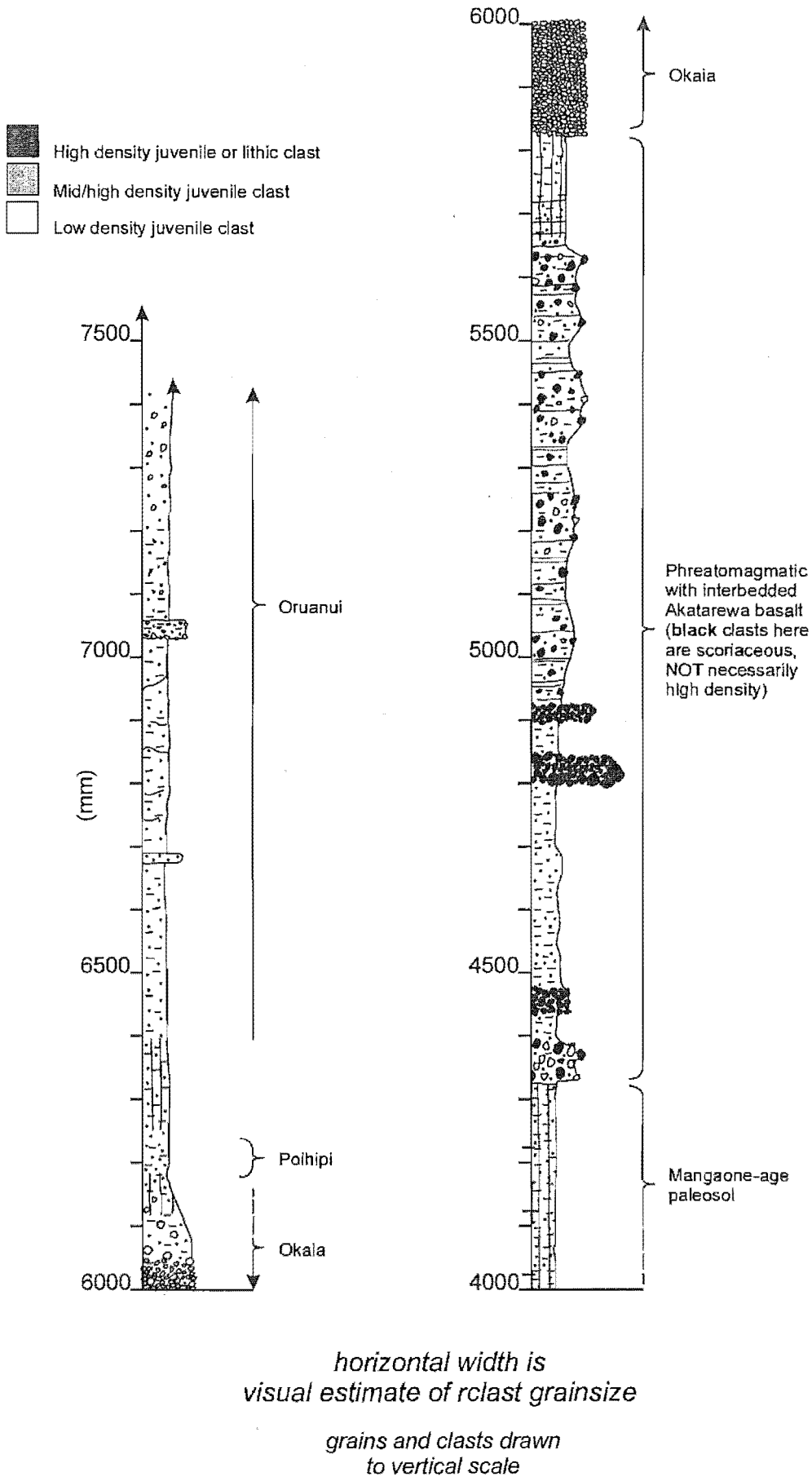

Figure 2.21 Log of regional airfall sequence, representative of those present around MVC, at M43 (U17/861989) in Te Kopia Rd. (Part 1 of 2 - continued in Figure 2.22)

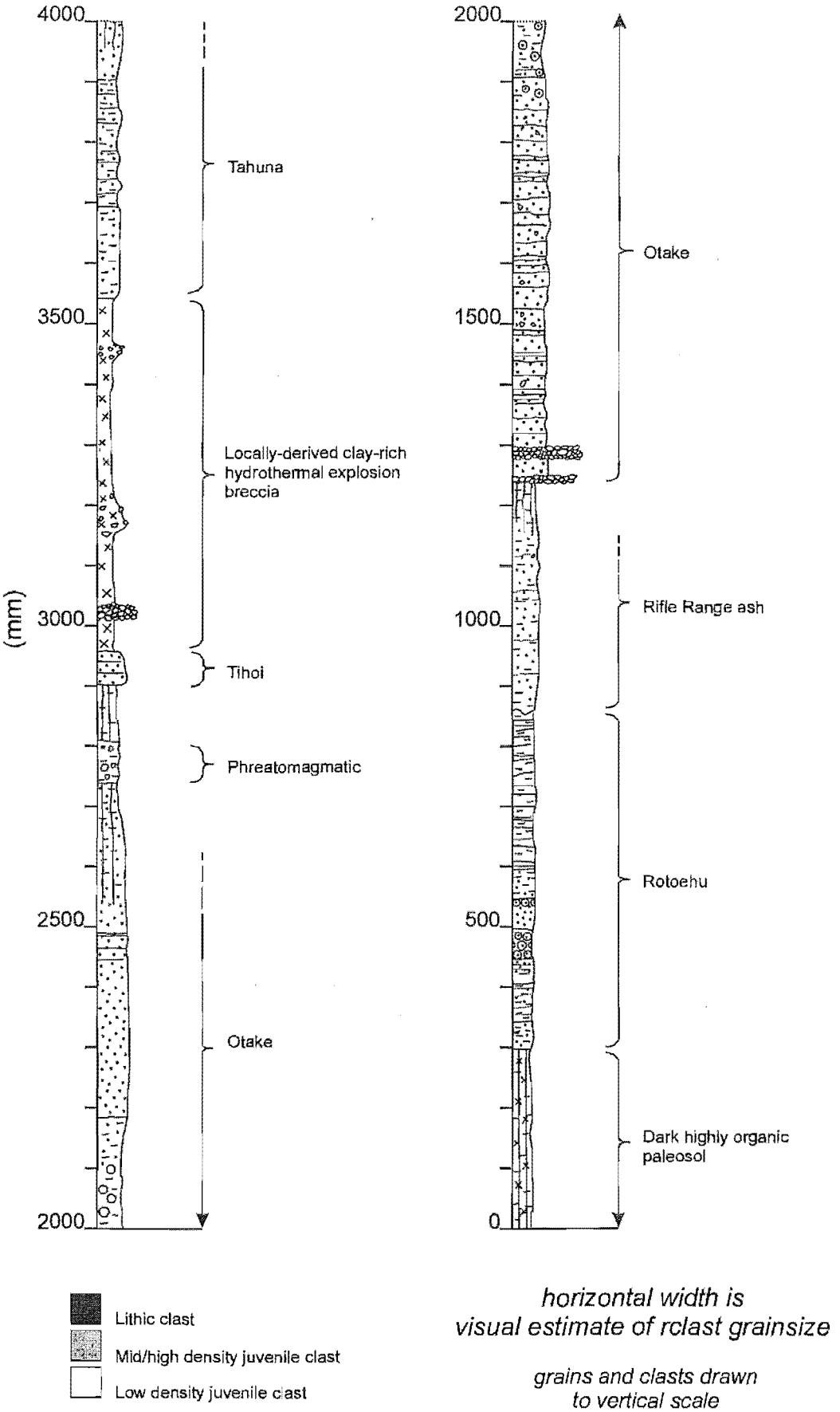

Figure 2.22 Log of regional airfall sequence, representative of those present around MVC, at M43 (U17/861989) in Te Kopia Rd. (Part 2 of 2 - continued from Figure 2.21)

2.6.1 Regional airfall deposits within Maroa

Airfall pyroclastics from some Taupo and Okataina modern-TVZ eruptions are preserved in and around Maroa. The most complete section is found in on Te Kopia Road at location M43 (U17/86119885). It exposes a sequence from a thick pre-Rotoehu paleosol to the Taupo ignimbrite. There are three units in this section (Figures 2.21 and 2.22 give a graphic log) of importance in this study: (1) scoriaceous airfall of the Akatarewa basalt (described above in Section 2.4.2), (2) the Tahuna Tephra (discussed in Section 1.5.4) and (3) the New3 tephra (discussed below).

2.6.2 Oruanui Formation

The eruption has been divided by Wilson (2001) into 10 phases each based on mappable fall units. Pyroclastic density current deposits are found interbedded with airfall units throughout the sequence. Oruanui pyroclastic density current deposits range from thin veneers to > 200 m thick near vent.

The bulk of Oruanui Formation deposits within Maroa are ignimbrite. Oruanui ignimbrite matrix is buff-coloured, soft to firm, moderately sorted, fine ash with sparse to 10 vol.% 'silky', fibrous, fresh, hard, low density pumice. Its fresh, unaltered, uniform matrix and pumice make it easily discernable from Maroa deposits.

2.6.3 Mokai Sand and Hinuera Formation

After the cessation of eruptive activity from Oruanui vents a large part of the central North Island was left blanketed by a barren sheet of Oruanui pyroclastics. Wind action across this plain has extensively reworked, transported and redeposited this material (referred to as Mokai Sand where pure and fresh), often weathered as thick loess around Maroa. Damming of the Waikato and tributary river systems by Oruanui pyroclastics produced temporary lakes, and subsequent floods when dams were breached. Fluvial sediments along the Waikato River are collectively referred to as Hinuera Formation (Healy, 1946; Schofield, 1965), and in the Maroa area most of this is contemporaneous with the wind-blown material described above.

2.6.4 Taupo Formation

The 1.8 ka Taupo eruption from Taupo involved several pyroclastic phases. These culminated in a very widespread (~ 80 km from source) ignimbrite (Wilson and Walker,

1985). The Taupo ignimbrite, emplaced in a single flow event (Wilson, 1985), can be divided into two layers, both of which show great lateral variations. The deposit can be clearly distinguished in the field around Maroa as it is always the uppermost unit below the present-day soil horizon. It is white to light-cream and contains low-density pumice with tubular expanded vesicles often up to 10 mm wide. These pumices are fibrous, fresh and strong, and sometimes form concentration zones that approach a clast-supported nature.

2.7 Drainage, lakes and floods

The drainage network around Maroa is shown in Figure 2.23. Lacustrine deposits show the existence of paleo-lakes at times during the formation of Maroa. These probably formed after lavas and pyroclastics from that eruption dammed valley(s). The Whangapoa basin, Ngaukuru Graben and probably the Guthrie Graben have all had paleo-lakes present in them at times before and after the emplacement of Ohakuri and Mamaku pyroclastics (discussed further in Section 5.2.2). This is indicated by the presence of lacustrine beds around these basins at relatively high elevation overlying the pyroclastics (D. M. Gravley, pers. comm. 2002). Significant flood deposits of the Hinuera Formation, including large boulders up to 10 m wide in the Waikato valley around Atiamuri, are probably remnants of floods following breaches of lake(s) dammed by the Oruanui eruption (Thompson, 1958; Manville and Wilson, 2003).

2.8 Reconstructing the typical Maroa eruption sequence

If the Puketarata and Pukeahua eruptions are representative of activity from the centre, then eruptions have been generally small sub-plinian to plinian silicic events (see descriptions and distributions of airfall deposits in Sections 2.3.2, 2.3.6 and 2.3.7) culminating in the formation of lava domes. Such relatively low explosivity is supported by the paucity of Maroa-derived pyroclastic units (both pyroclastic density current and airfall deposits) found relative to the number of dome extrusions. This is common within and around the margins of caldera volcanoes worldwide (e.g. Long Valley and Yellowstone Calderas, Bailey, 1989; Christiansen, 2001). In New Zealand this is most prominent at Okataina where most Holocene eruptions have followed this pattern, but where pyroclastics constitute a greater volume relative to lavas (Nairn, 1989).

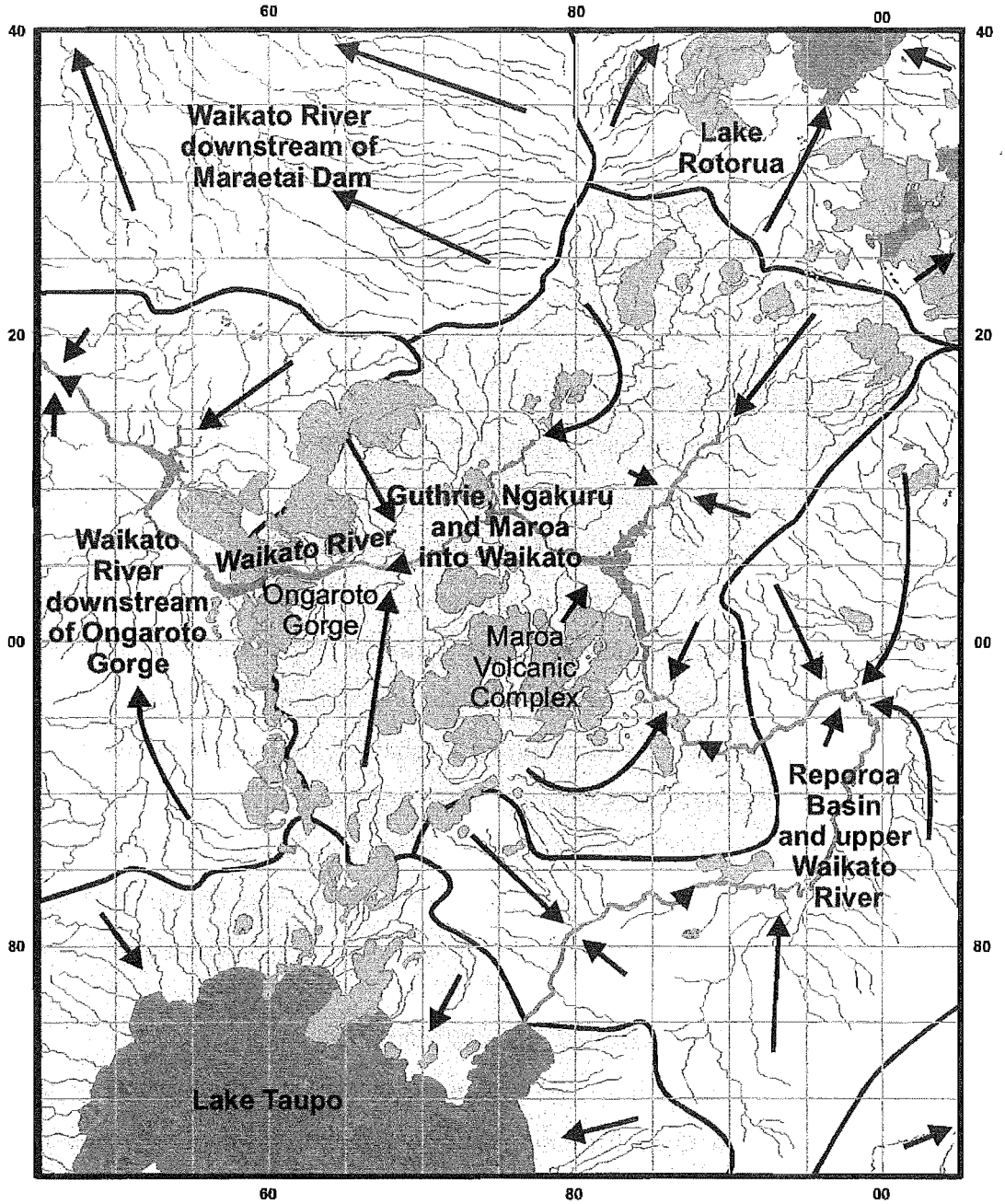

Figure 2.23 Map of the drainage network and catchments around Maroa. Rhyolite lavas are detailed in mid grey for reference, Lakes in darker grey.

In the Puketarata and Pukeahua eruptions, initial vent opening appears to have been associated with a pyroclastic eruption column. A pyroclastic apron forms around the vent and the shape and diameter of this is controlled by eruption style, volume, energy and wind direction. In the case of the Puketarata eruption (Section 2.3.7, Fig. 2.17) the tuff ring is composed mostly of surge deposits, whereas most Maroa tuff rings appear to have been formed from airfall (e.g. M258) and lower-energy pyroclastic density current deposits (e.g. M59 is a small BAF deposit from Mandarin dome). The best example of

this is the fan of Pukeahua pyroclastics surrounding Pukeahua dome complex (Section 2.3.2, Fig. 2.5).

As rhyolite eruptions progress, effusion rates eventually decrease, the magma often becomes more degassed, and pyroclastic activity decreases. At this point a lava dome often grows in the vent (e.g. Pukeahua dome complex, Mandarin dome and Puketarata dome). Partial cooling of the dome, and varying effusion rates, result in multiple spines and lobes. Multiple vents, often along a lineament, or a fissure vent, may produce dome complexes. The margin of the expanding dome crumbles and collapses under gravity to produce BAFs.

Erosion quickly removes much of the pyroclastic material meaning that only a few of the larger ignimbrites and BAF deposits, are preserved. Lava domes are more resistant and are preserved from many small eruptions for which there is no pyroclastic material remaining.

CHAPTER 3

Geochronology and volume estimates

3.1 Introduction

The mapping completed by previous workers provides a useful, accurate basis for the presentation and discussion of surface geology in the previous chapter. In contrast, the chronology for Maroa eruptions was largely unknown (previously published ages are summarised here, with acknowledgement) and there has been little work on petrology and geochemistry of Maroa deposits. To address these aspects a comprehensive geochronology-geochemistry sampling program was undertaken. The geochronology and volumes of Maroa-related deposits are presented in this chapter and the petrology is presented in Chapter 4.

Twenty four samples were dated using the Ar-Ar facility at the U.S. Geological Survey facility in Menlo Park, California. Analyses were carried out in cooperation with Drs. M. A. Lanphere and A. Calvert at that laboratory. Quantification of volumes of Maroa deposits is also detailed in this chapter to allow estimates of the rates of volcanic activity and Whakamaru caldera infilling to be made. All age errors presented in this chapter are 1 standard deviation, unless otherwise stated.

3.2 Sampling and sample quality for geochronology-geochemistry

3.2.1 Aims and design of sampling program

The collection program for this thesis aimed to provide the best samples from as many accessible deposits as possible. From the total set, selected samples were chosen to produce detailed geochronological and petrological data sets. The data could then be used to: (a) interpret the chronology of, and compare compositions between, Maroa deposits; (b) model the dynamics of the magma system(s) below Maroa; and (c) compare Maroa magmas to others in TVZ, specifically those from Taupo to the south.

Samples were collected from every definable eruptive unit cropping out within the centre (see Map 1, back pocket, for sample locations). The program aimed to maximise spatial coverage. Lava domes were distinguished on the basis of geomorphology and,

where physically possible, at least two spatially separate samples were taken from each dome to check for petrological homogeneity. Ignimbrite, BAF deposits and airfall deposit sequences were sampled from each visibly distinct eruptive unit where clast size was large enough for analysis of juvenile clasts. Some lithic clasts were analysed where correlating the origin of lithic material was deemed important. Access limitations (including forest cover, steep terrain, lack of outcrop and burial by relatively young deposits) forced less-than-ideal sampling of some areas.

3.2.2 Post-emplacement weathering effects on data quality

Some samples, particularly those from lava domes, tended to be weathered. To indicate the extent of weathering all samples were graded on amount and type of weathering using a scale from 1 (best) to 5 (worst) (see Table 3.1, note that codes 1 and 2 are often of comparable freshness). Quality code 4 is reserved for samples where spherulites are visibly weathering out in hand specimen; quality codes 2 and 3 may have un-weathered spherulites present in their groundmass. The symbol used for each sample on Map 1 (back pocket) corresponds to the quality code assigned to it. To assess the effect of sample quality on geochemistry, multiple samples were taken from some locations where the same unit showed variable alteration (See Section 4.3 for detailed statistical analysis of the geochemistry of the different qualities of sample). This process showed that there was generally little effect, if any, of sample quality on the geochemical data for the parameters measured here. Sutton (1995) noted a similar lack of chemical variability in glassy versus devitrified lavas of Taupo.

Quality code	Definition
1	Minerals and groundmass appear fresh
2	Minerals appear fresh, groundmass slightly devitrified, or slightly weathered
3	Felsic minerals appear fresh, mafic minerals and/or groundmass weathered
4	Mineral alteration possible, groundmass spherulites weathering out
5	Minerals and groundmass weathered

Table 3.1 Sample quality codes applied to hand specimens prior to petrographic analysis and used in text and Map 1 (back pocket).

To minimise the effects of post-emplacement alteration on geochronology data, only samples of quality code 3 (felsic minerals appear fresh in hand specimen) or better were used. This was a first step in making sure that the plagioclase on which all age-determinations were made was fresh and would therefore produce the most accurate and

reliable data. Further control on the quality of geochronology samples is described in Section 3.4.2.

3.3 Geochronology Data

3.3.1 Summary of previously published geochronology data

The pre-existing age data for the post-Whakamaru eruption sequences were sporadic and some of the ages presented are reassessed in this thesis. Data fall into four suites: (1) whole-rock K-Ar ages on lavas (Stipp, 1968; Houghton et al., 1991; Table 3.2); (2) fission-track ages on lavas (Kohn, 1973; Table 3.2); (3) fission-track ages on pyroclastic deposits (Kohn, 1973); and (4) Ar-Ar ages on feldspar phenocrysts (Houghton et al., 1995). Additional multiple age data for the Maroa area have been made available by B. F. Houghton, and are currently being published in conjunction with the new data in this thesis (Leonard et al., in prep).

No.	Age, ka	Grid reference	Eruptive Grouping	Ref.	Notes
1	219±10	T17/585034	WDB	1	Age is consistent with geological information
2	141±15	T17/639083	WDB	2	Age is consistent with geological information
3	187±14	T17/598077	WDB	2	Age is consistent with geological information
4	251±10	T17/620141	WDB	2	Age is consistent with geological information
5	287±13	T17/586073	WDB	2	Age is inconsistent with geological information
6	293±9	T17/594021	WDB	2	Same sample as 9 (weighted mean of 6 and 9 is 306 ± 12 ka)
7	301±7	T17/642086	WDB	2	Age is inconsistent with geological information
8	313±10	T17/580084	WDB	2	Age is inconsistent with geological information
9	342±15	T17/594021	WDB	2	Same sample as 6; both ages are inconsistent with geological information
10	397±16	T17/656086	WDB	2	Age is inconsistent with geological information
11	105±9	T17/663824	NT	2	Age is consistent with geological information
12	120±20	N/A (Ben Lomond)	NT	3	Fission track age, same lava dome as No. 11

Table 3.2 Summary of previously published age data on lavas associated with Maroa (errors are 1 s.d.). See Figure 3.1 (coded in blue) and original references for sample locations, and details of analytical techniques. References are: (1) Stipp (1968); (2) Houghton et al. (1991); (3) Kohn (1973); WDB denotes Western Dome Belt (Wilson et al., 1986); NT = northern Taupo domes (i.e. between Lake Taupo and the southern boundary of Maroa Volcanic Centre).

Of the ages presented in Table 3.2, those that are now considered unreliable (after discussions with C. J. N. Wilson and B. F. Houghton, 2002) on the basis of field relationships are those (a) that pre-date the range of Ar-Ar ages on pyroclastic deposits associated with the formation of Whakamaru caldera (for which field evidence implies an earlier age than these lavas), and (b) where disparate ages are presented on a single lava. In particular, a dome that yields an age of 251±10 ka at T17/620141 is faulted on its southeast margin and the Ohakuri pyroclastics (here dated at ~240 ka, see below) appears to be banked against, and hence post-date, this fault. Thus age determinations from domes to the southwest of that area (which are not displaced by, and thus post-date, the faulting) that yield values of >~250 ka are considered suspect.

Pringle et al. (1992) and Tanaka et al. (1996) have published Ar-Ar ages for the Whakamaru group ignimbrites and Mamaku pyroclastics, respectively. The former are included in Houghton et al.'s (1995) 340-320 ka age-range for the Whakamaru group pyroclastics, which is assumed accurate here. The age of the Mamaku pyroclastics is discussed later in this chapter.

3.3.2 Introduction to new geochronology data

Geochronology samples were selected from a larger suite of petrologic samples based on stratigraphic importance. Plagioclase was chosen for analysis because it yields the most reliable data on young lavas and pyroclastic rocks that lack sanidine (as is typical in TVZ rhyolites). Only plagioclase crystals that appeared uniformly unaltered and euhedral were used and, within pyroclastic units, care was taken to separate only crystals from pumice to minimize the potential for xenocrystic contamination. The process of sample preparation and laboratory experimentation is detailed in Appendix 2.

3.3.3 Presenting new data

Table 3.3 presents details of the new ages determined here. Weighted Plateau Mean Ages (WPMA) are calculated assuming that all of the non-radiogenic ^{40}Ar in the sample is derived from the atmosphere. This assumption is supported by the fact that isochrons for all experiments have an initial $^{40}Ar/^{36}Ar$ within 2 s.d. of that found in the atmosphere (295.5). Most are within 1 s.d.. Non-radiogenic ^{40}Ar within the sample is subtracted at a rate of 295.5 multiplied by the amount of ^{36}Ar within the sample. A York fit (York, 1969) to the ^{36}Ar-normalised ^{39}Ar vs. ^{40}Ar (normal) isochron was used to determine initial $^{40}Ar/^{36}Ar$. Mean Standard Weighted Deviation (MSWD) gives an indication of

the variability in calculated ages across all heating steps, weighted according to the amount of ^{39}Ar released in each step; from 0.5 to 2.5 is preferable and 1 is ideal, as a general rule.

Unit	Samp. Code	Grid Reference	K/Ca	% Ar in Plateau	MSWD	WPMA (ka)	Isochr. Age (ka)	Initial $^{40}Ar/^{36}Ar$
Isolated domes								
Orakeikorako	M301	U17/838967	0.1362	76%	10.7	**80 ± 7**	122 ± 13	287.5 ± 20.3
Mokauteure	M243	T17/679944	0.1419	78%	1.80	**86 ± 12**	90 ± 19	295.2 ± 2.5
Forest South	M321	U17/722887	0.1379	73%	1.50	**114 ± 11**	67 ± 34	300.9 ± 5.2
Maroanui E	M223	U17/729945	0.1956	59%	1.50	**143 ± 10**	158 ± 48	293.5 ± 3
Pakuri	M304	U17/803951	0.1701	69%	4.50	**152 ± 12**	67 ± 51	299.5 ± 10.8
Pukeahua West	M111	U17/717023	0.1591	47%	0.63	**202 ± 7**	215 ± 51	293.7 ± 7.2
Dome complexes								
MEC (Umukuri)	M460	U17/821992	0.1238	65%	0.47	**189 ± 8**	209 ± 57	289.1 ± 10.5
MEC (Baldy)	M352	U17/788988	0.1167	100%	1.03	**223 ± 7**	215 ± 14	297.5 ± 3.3
MEC (Wairiki)	M211	U17/833009	0.1615	57%	1.12	**235 ± 10**	249 ± 31	291.9 ± 8.4
MEC (Mandarin)	M344	U17/807000	0.1349	88%	0.53	**242 ± 9**	239 ± 13	294.5 ± 2.7
MEC (McPherson)	M260	U17/780962	0.3106	80%	0.93	**251 ± 17**	267 ± 25	294.4 ± 1
MWC (Poplar)	M145	U17/728989	0.1285	61%	0.30	**222 ± 11**	228 ± 15	293.5 ± 0.8
MWC (Kemp)	M188	U17/771003	0.1343	76%	9.40	**230 ± 12**	149 ± 18	300.7 ± 5.7
MWC (Goldies)	M247	U17/701949	0.1743	56%	0.93	**305 ± 17**	342 ± 39	292.2 ± 2.2
Pyroclastics								
Pukeahua west fan	M63	U17/728021	0.1854	91%	2.10	**196 ± 8**	181 ± 44	299.8 ± 24.9
Atiamuri pyroclastics	M12	U17/772035	0.1051	60%	1.09	**229 ± 12**	199 ± 30	297.9 ± 2.5
Ohakuri pyroclastics*	D64	U16/852127	0.1481	94%	0.69	**244 ± 10**	286 ± 33	265.8 ± 18.9
Ohakuri pyroclastics*	OH3	T16/694182	0.1288	99%	2.5	**259 ± 9**	277 ± 14	288.4 ± 11.1
Ohakuri pyroclastics*	D40	U16/807157	0.1414	96%	0.64	**272 ± 16**	231 ± 46	306.1 ± 18
Mamaku pyroclastics*	MK	U16/740340	0.0857	83%	0.70	**240 ± 11**	246 ± 24	293.9 ± 3.4
Orakonui	M47	U17/832925	0.0843	63%	1.50	**256 ± 12**	246 ± 32	297.3 ± 13.6
Putauaki	M46	U17/782930	0.0982	92%	1.40	**272 ± 10**	255 ± 19	298.9 ± 5.1
Korotai	M470	T17/688084	0.0886	68%	1.05	**283 ± 12**	282 ± 28	296.5 ± 5.2
Pokai	PK	T16/682268	0.0889	100%	1.90	**275 ± 10**	261 ± 19	297.5 ± 7.9

Table 3.3 New geochronology data presented in this paper. * Refer to Section 3.5.2 for detailed discussion of these ages. Errors are 1 s.d.. The Weighted Mean Plateau Age (WPMA) is considered in text to be the best representation of the true age of the deposit and is shown in bold for each sample.

3.3.4 Summary and distribution of all available geochronology data

Table 3.4 summarises age data relevant to this study. It is a composite of previously published results (Table 3.2) and new data (Table 3.3).

The ages from Table 3.4 for Maroa and related deposits are shown (a) labelled on a map of Maroa in Figure 3.1 and (b) coloured according to their absolute age in Figure 3.2. Colours follow a spectrum from purple (340-320 ka) through dark blue (320 to 260 ka), light blue (260 to 220 ka), green (220 to 190 ka), yellow (190 to 100 ka) to orange (100 ka to present). The undated domes within MWC/MEC are assumed to lie within the

same 260 to 220 ka age range as the dated domes, on the basis of their similar respective chemistries, morphological development and degrees of dissection.

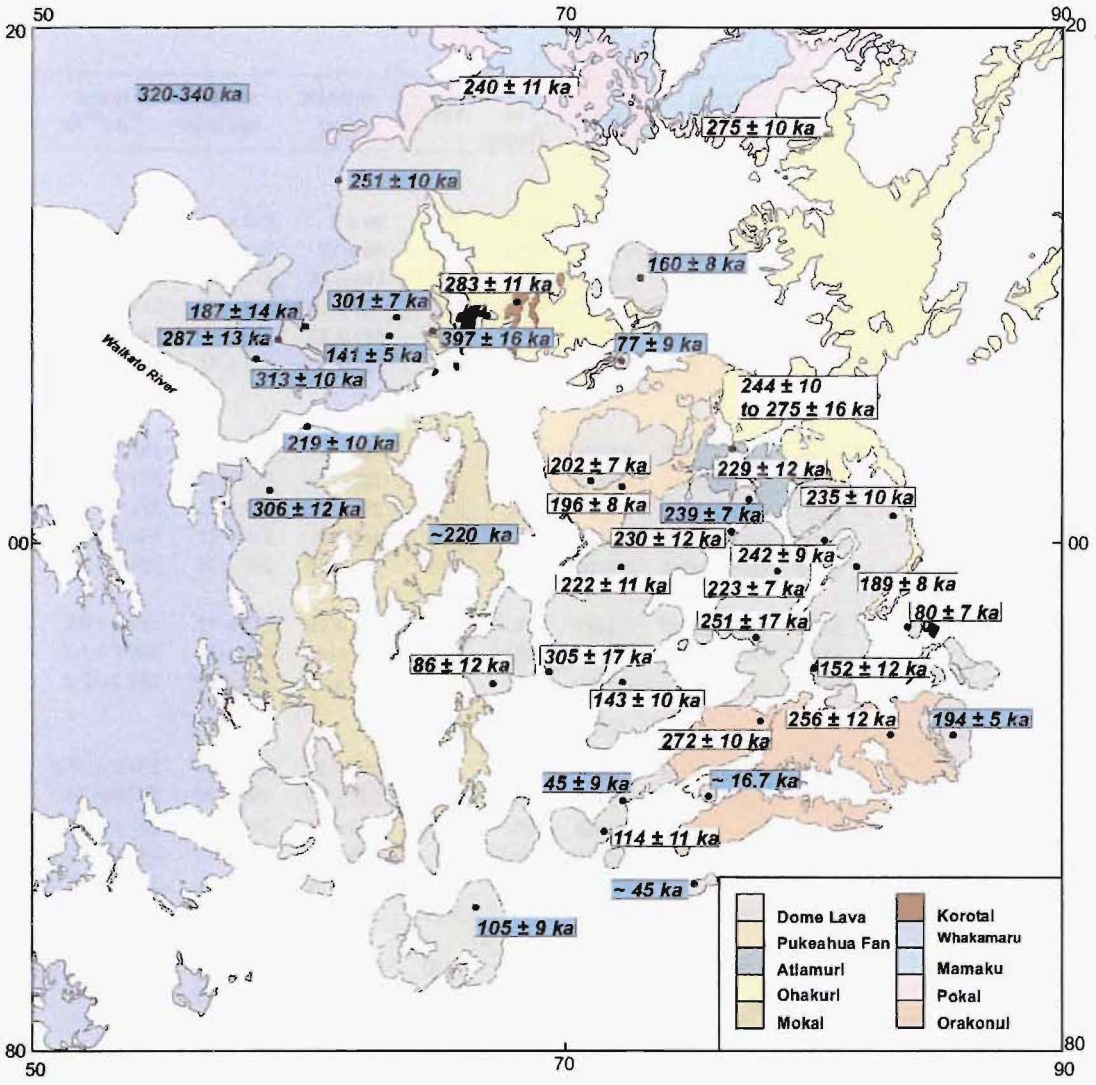

Figure 3.1 Distribution of age data on map of Maroa. Existing published ages are presented in blue. Grid in New Zealand map grid coordinates.

3.4 Analysis of geochronology data quality

3.4.1 Comments on conducting Ar-Ar geochronology on young, low-K samples

The amount of Ar in a mineral depends on the concentration of K in that mineral, as the former substitutes in trace abundances for the latter. TVZ rhyolites are inherently relatively low in K; this is reflected in the fact that crystallisation of K-feldspar as phenocrysts is rare. K-feldspars have not been found as a phenocrystic phase in any Maroa rhyolites.

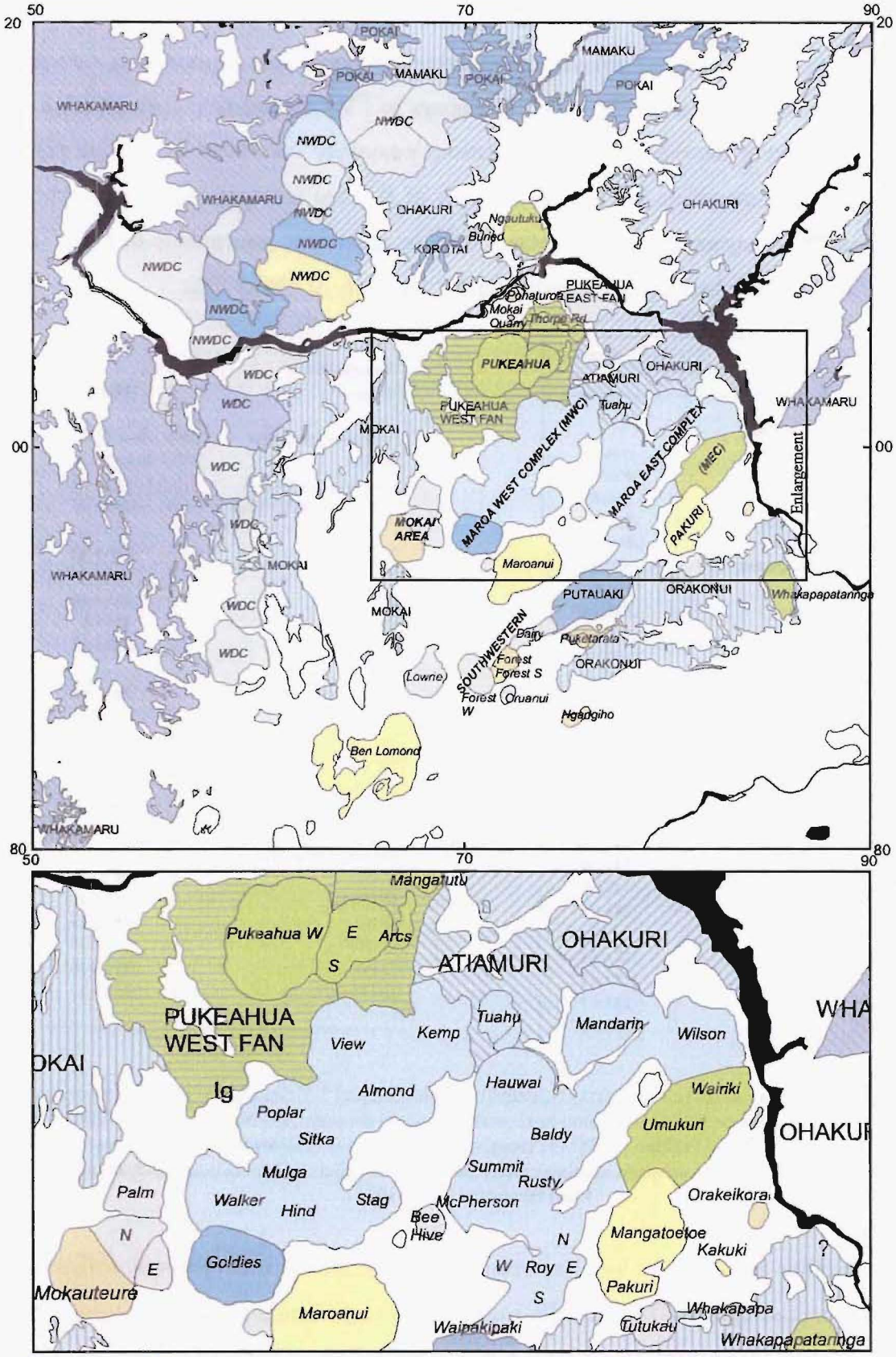

Figure 3.2 Map of age groupings for MVC related deposits. Hatched units are pyroclastics with their names in capitals. Names of domes are italicised in lower case. Dome complex names are italicised in capitals. Inset (MWC/MEC domes) is enlarged below.

In Ar-Ar dating the sample is irradiated, causing a portion of the ^{40}K in it to be converted to ^{40}Ar. The exact amount converted is monitored, and expressed as a *J* value (see Appendix 2). Because ^{40}K naturally decays to ^{39}Ar the relative concentration of ^{39}Ar to ^{40}Ar in a sample is, after irradiation, positively correlated to its age (after correcting for atmosphere-derived abundances of the two isotopes, described earlier). Therefore, in young samples the abundance of ^{39}Ar, relative to atmosphere-derived ^{39}Ar, is very low as there has been very little time for the decay of ^{40}K to ^{39}Ar.

Unit	Source	WPMA (ka)
Independent domes		
Puketarata dome	3	~16.7
Dairy dome	1	**45 ± 9**
Pohaturoa dome	1	**77 ± 9**
Orakeikorako dome	1	**80 ± 7**
Mokauteure dome	1	**86 ± 12**
11 Ben Lomond dome	1	**105 ± 9**
Forest South dome	1	**114 ± 11**
Maroanui dome	1	**143 ± 10**
Pakuri dome	1	**152 ± 12**
Ngautuku	1	**160 ± 8**
Whakapapataringa dome	1	**194 ± 5**
Pukeahua western fan	1	**196 ± 8**
Pukeahua West dome	1	**202 ± 7**
Horohoro dome	2	**222 ± 10**
Dome complexes		
MEC	1	**189 ± 8**
MEC	1	**223 ± 7**
MEC	1	**235 ± 10**
MEC	1	**242 ± 9**
MEC	1	**251 ± 17**
MWC	1	**222 ± 11**
MWC	1	**230 ± 12**
Tuahu dome	1	**239 ± 7**
MWC	1	**305 ± 17**
Pyroclastics		
Atiamuri	1	**229 ± 12**
Ohakuri pyroclastics	230 ± 10 to 272 ± 16	
Mokai	210 ± 20 to 224 ± 14	
Mamaku pyroclastics	216 ± 8 to 240 ± 11	
ALL ASSUMED TO BE:	1	**240 ± 10**
Orakonui	1	**256 ± 12**
Putauaki	1	**272 ± 10**
Pokai	1	**275 ± 10**
Korotai	1	**254 ± 5**
Korotai	1	**283 ± 11**
Whakamaru	6	**320 ± 20**
Te Kopia	2	**340 ± 4**
Te Weta	7	**320 ± 40**
Paeroa	7	**330 ± 10**
Mananui	7	**320 ± 20**
Te Whaiti	7	**340 ± 10**
Western Dome Belt		
2 (4)	4	**141 ± 5**
NEW (1)	2	**179 ± 11**
3 (6)	4	**187 ± 14**
1 NEW	5	**219 ± 10**
4 (69)	4	**251 ± 10**
NEW (87)	2	**257 ± 11**

Table 3.4 Summary of all relevant data presented in Tables 3.2 and 3.3. Sources: (1) New data presented in Leonard et al. (in prep), (2) Houghton et al. with (location) (in prep), (3) Newnham et al. (2003), (4) Houghton et al. (1991) (5) Stipp (1968) (6) Houghton et al. (1995) (7) Brown (1994). Numbers for Ben Lomond and Western Dome Belt are those from Table 3.2. Numbers in brackets are sample numbers from Houghton et al. (1991).

TVZ rhyolites are young, as well as being low-K. Therefore, it is relatively difficult to measure precise ages for TVZ rhyolites using Ar-Ar techniques. To achieve meaningful results: (a) large samples, (b) careful sample preparation and purification, (c) careful and precise heating and Ar extraction and (d) very precise and stable Ar mass-spectrometry (with excellent control and quantification of errors) are all required. The Menlo Park laboratory was chosen because compared to other laboratories around the

world it uses very suitable methods, standards and equipment (see Appendix 2), and has previous experience on low-K TVZ rhyolites (e.g. Pringle et al., 1992; Houghton et al., 1995). Plagioclase separates were used here because they contained the highest K (and therefore Ar) content of any fraction of the deposits.

3.4.2 Analysis of geochronology data quality

Two batches of plagioclase separates were analysed (batch 1 samples: D40, D64, M12, M46, M47, M63, M188, M211, M223, M247, M260, M304, M321 and M344; batch 2 samples: M111, M145, M243, M301, M352, M460, M470, MK, OH3 and PK) and the second batch were more highly purified than the first. Sample M63 was included in batch one and M111 in batch two because these samples are from two deposits that appear to be the same age based on stratigraphy and chemistry. The ages determined for these two samples (196 ± 8 ka and 202 ± 7, respectively) were within 1 s.d. of each other, showing continuity between the two batches (Fig. 3.3). The removal of quartz, and use of an ultrasonic probe[1] to remove glass, for batch two was detectable in results. Low temperature steps (usually 600 to 700 ° C) showed an order of magnitude drop in atmosphere-derived argon content with the extra cleanup. There was little change in the results at higher temperatures.

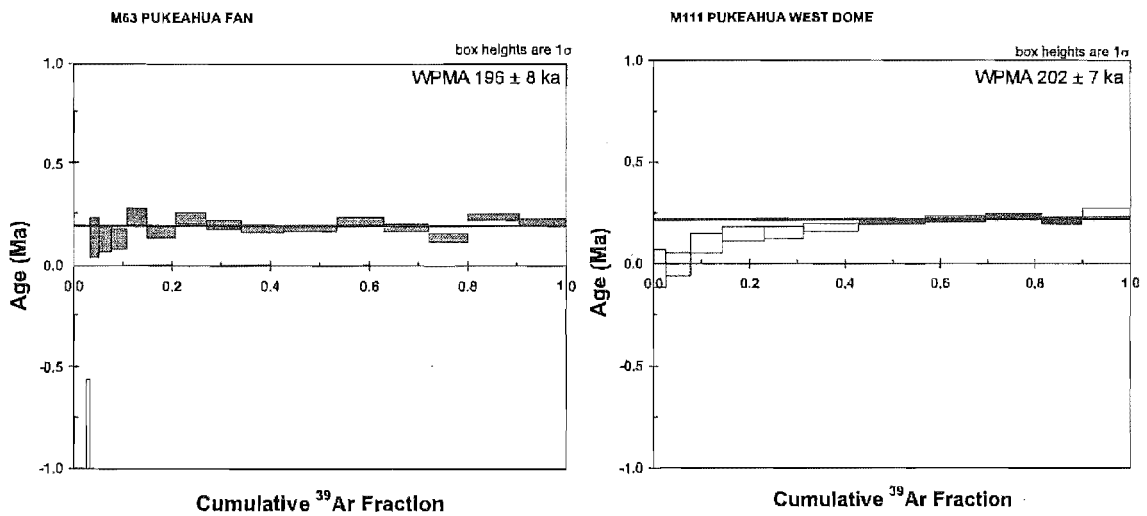

Figure 3.3 Plateau diagrams for Pukeahua western pyroclastics fan (M63) and Pukeahua West dome (M111).

The WPMA for sample M111 was based on 47 % ^{39}Ar – the only sample not to reach the 50 % total ^{39}Ar criterion for a plateau (see Appendix 2). The steps that were

[1] An ultrasonic probe is inserted into a beaker of water, which also contains the sample. This produces high-frequency vibration of the sample that is much more intense than when using an ultrasonic bath.

included produced a plateau (Fig. 3.3) with a relatively consistent age, within a spectrum that otherwise steadily rose in age with each successive temperature step. The M111 age (202 ± 7 ka) is also within 1 s.d. of that determined for M63 (196 ± 8 ka), which was calculated based on 91 % ^{39}Ar. Note that although the young ages calculated from sample M111's lower temperature steps are probably due to higher atmospheric Ar content at these temperatures, the absolute amount of atmospheric Ar in this sample (from batch 2) is still greatly reduced compared to batch 1 samples.

Apparent precision in all experiments is relatively high considering the low-potassium nature of these samples. Analytical error (1 s.d.) is below 17 ka for all samples, and below 10 ka for 11 of the samples.

There is reasonable agreement between ages presented here and those determined by other workers. The Mamaku pyroclastics age we present is within 1 s.d. of one other result (Houghton et al., in prep) and 2 s.d. of other published results for the Mamaku (Houghton et al., 1995; Tanaka et al., 1996). As discussed earlier, isochron-calculated initial ^{40}Ar/^{36}Ar ratios for all samples are not statistically different to that of the atmosphere. Based on these indicators there is no evidence that my samples have been contaminated by argon derived from sources other than the atmosphere.

WPMA values are preferred as the truest estimation of absolute age, compared to isochron ages. This is because WPMA values are calculated assuming all excess argon in the samples is derived from atmosphere. The assumption is supported by the fact that all but three samples have WPMA within 1 s.d. of their isochron age. WPMA for samples M301 and M304 are within 2 s.d. of their isochron age while for sample M188 it is not. All three samples with WPMA not within one s.d. of their isochron age also have the highest MSWD values, suggesting that there is relatively high variability in the ages from individual temperature steps (seen in the plateau diagrams in Appendices M188, M301 and M304). Despite this, the WPMA of these three samples are still consistent with their places in the evolution of Maroa, based on field evidence.

3.5 Discussion of geochronology results

3.5.1 Whakamaru caldera collapse (320-340 ka)

Whakamaru caldera has been proposed as the source for the 320 - 340 ka Whakamaru group ignimbrites (Section 1.6.4; Wilson et al., 1986). Maroa deposits, and WDB lavas, produce Ar-Ar ages postdating the collapse of Whakamaru caldera (Table 3.3). The top of the ignimbrites correlated with the Whakamaru group lies at a depth of up to 1300 m below the present day surface within the caldera (from drill core, Wilson et al., 1986) whereas the inferred correlative ignimbrites lie at the surface in many locations outside the caldera margins. The depth to the top of the group below Maroa is probably the product of caldera collapse (but not Maroa-related colapse) and further down-faulting from continued extension during the young-TVZ period (see Chapter 2). The depression has been infilled by a mixture of rhyolite lava, pyroclastics and volcaniclastics (seen in confidential NZ Geological Survey unpublished Mokai Geothermal Field drill core logs).

The loci of WDC and NWDC lava vents closely follow the postulated northwestern edge of the Whakamaru caldera (Wilson et al., 1986). Ages for these domes range from ~ 141 to 251 ka (ignoring ages considered inconsistent with stratigraphy, discussed earlier). Activity along this margin of the caldera appears to have been long-lived, with the last dome extrusion occurring nearly 190 ka after the Whakamaru eruption.

3.5.2 Regional ignimbrite eruptions 320 to 220 ka

Four substantial eruptions produced ignimbrites (the Pokai, Mamaku, Mokai and Ohakuri pyroclastics), from sources mostly north of Maroa, between 320 and 220 ka. This period of ignimbrite-forming activity coincides with the most voluminous phase of dome-growth at Maroa represented by domes at the present surface (see below). The Pokai eruption is relatively old (275 ± 10 ka, stratigraphically below the Korotai pyroclastics) compared to most of Maroa, and the Pokai pyroclastics source is inferred to be several tens of km to the north of Maroa (Karhunen, 1993) – thus the Pokai pyroclastics are both temporally and spatially distinct from the evolution of Maroa.

The Mamaku, Ohakuri and Mokai pyroclastics

Determining the age of the Mamaku and Ohakuri pyroclastics has been somewhat problematic. The three experiments to determine the age of the Ohakuri pyroclastics

conducted here gave ages of 244 ± 10 to 272 ± 16 ka and are summarised in Table 3.5. Ages for samples D40 and D64 have the highest analytical error and a low initial $^{40}Ar/^{36}Ar$, respectively. OH3 (259 ± 9 ka) has the lowest analytical error and an initial $^{40}Ar/^{36}Ar$ close to that of atmosphere. Stratigraphic work by Gravley (2004) shows that the Ohakuri lie above the Mamaku pyroclastics, but have a negligible time break between them.

The presence of Ohakuri deposits within Maroa, and a possible source just to the north discussed in Chapter 2, makes the age of this deposit important in understanding the evolution of Maroa. Similarly, the proximity of Mokai pyroclastics to Maroa, and the fact that its source remains unknown make its age important to this study.

Possible deposits of the Mamaku pyroclastics from Rotorua Caldera (Milner, 2001) have been dated (Table 3.5) at 216 ± 8 (Houghton et al., 1995; Tanaka et al., 1996) to 240 ± 11 ka (this study). The deposits that Tanaka et al. (1996) sampled had the same paleomagnetic equatorial Atlantic north pole as the Pringle Falls Excursion dated at ~ 223 ka (McWilliams, 2001) (equivocal age, discussed below). The Mokai pyroclastics (dated at 220 ka by Houghton et al., 1995) also have this unusual paleomagnetic orientation (Tanaka et al., 1996).

Unit	Samp. Code	Grid Reference	K/Ca	% Ar in Plateau	MSWD	WPMA (ka)	Isochr. Age (ka)	Initial $^{40}Ar/^{36}Ar$
Mokai (2)	263					**210 ± 20**		
Mokai (3)	263					**212 ± 6**		
Mokai (3)	429					**224 ± 14**		
Ohakuri pyroclastics (2)	MP25					**230 ± 10**		
Ohakuri pyroclastics (1)	D40	U16/807157	0.1414	96%	0.64	**272 ± 16**	231 ± 46	306.1 ± 18
Ohakuri pyroclastics (1)	D64	U16/852127	0.1481	94%	0.69	**244 ± 10**	286 ± 33	265.8 ± 18.9
Ohakuri pyroclastics (1)	OH3	T16/694182	0.1288	99%	2.50	**259 ± 9**	277 ± 14	288.4 ± 11.1
Mamaku pyroclastics (3)	MP27				1.09	**216 ± 8**	216 ± 11	314 ± 5
Mamaku pyroclastics (3)	MP25				1.07	**224 ± 6**	224 ± 13	295 ± 3
Mamaku pyroclastics (2)	MP27					**230 ± 10**		
Mamaku pyroclastics (4)	MP27					**237 ± 8**		
Mamaku pyroclastics (1)	MK	U16/740340	0.0857	83%	0.70	**240 ± 11**	246 ± 24	293.9 ± 3.4

Table 3.5 Age determinations on the Mokai, Ohakuri and Mamaku pyroclastics. (Sources): (1) New data presented in this paper, (2) Houghton et al., (in prep) (3) Tanaka et al. (1996) and (4) McWilliams (2001). Errors are 1 s.d..

The 223 ± 6 ka age for the Pringle Falls excursion proposed by McWilliams (2001) is based on the summary of two ages of 'Mamaku Ignimbrite' and the age of the Mokai pyroclastics. Herrero-Bervera et al. (1994) date the Pringle Falls D Ash (by the Ar-Ar method), at the type section for the magnetic excursion, as 218 ± 10 ka. Figure 3.4(a) presents the plateau diagram for the new age of the Mamaku pyroclastics determined here, compared to McWilliams's (2001) presentation of Herrero-Bervera et al.'s (1994) Pringle Falls D Ash age (Fig. 3.4(b)) and his composite 'Mamaku Ignimbrite' age (Fig. 3.4(c)).

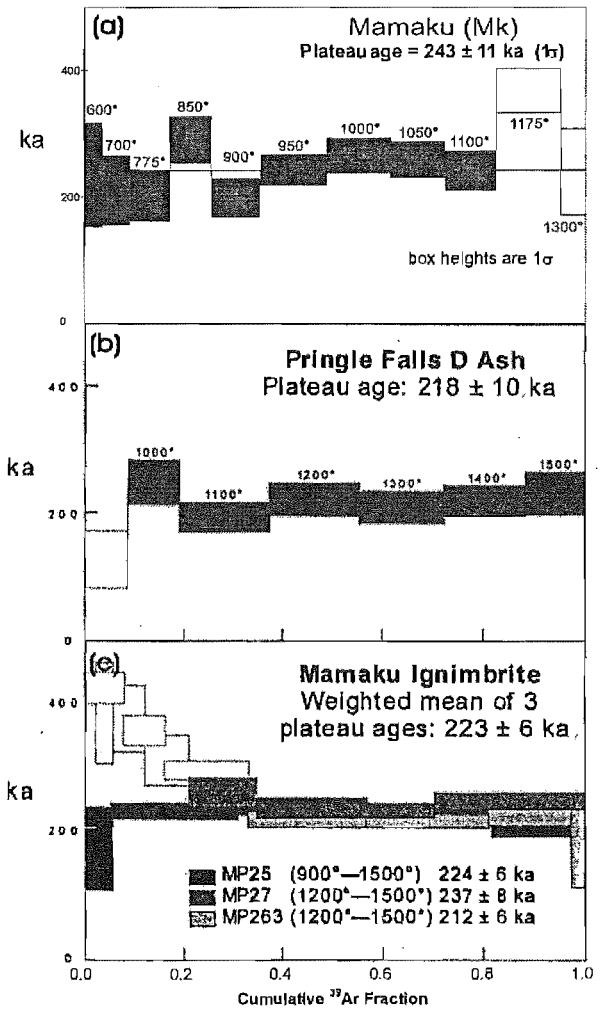

Figure 3.4 $^{40}Ar/^{39}Ar$ age plateau diagrams for (a) The Mamaku pyroclastics (new age, this study), compared to (b) Pringle Falls D Ash from Herrero-Bervera et al. (1994) and (c) 'Mamaku Ignimbrite' from McWilliams (2001). Black/grey steps are those used in the age.

McWilliams (2001) derived the 223 ± 6 ka age for the Mamaku pyroclastics by weighted-averaging ages for samples MP25 (224 ± 6 ka, Mamaku pyroclastics from Rauna Rd, U16/738171) and MP27 (237 ± 8 ka, Mamaku pyroclastics from Pukerimu

Rd, U16/786205), and Mokai pyroclastics MP263 (212 ± 6 ka) (Fig 3.4(c)). There are two possible problems with this approach:

(1) The same MP27 sample was reported by Tanaka et al. (1996) as being 216 ± 8 ka using the same Stanford laboratory and 230 ± 10 ka using the Menlo Park laboratory. (Houghton et al., in prep) The fact that the three ages for MP27 range from 216 ± 8 to 237 ± 8 suggests that there is a larger error in the age determined for this sample than is being reported for each experiment.

(2) This study (Chapter 2) and Milner (2001) have indicated that there is no conclusive field, volcanological or petrological (Chapter 4) evidence for or against the Mokai being correlated to the Mamaku pyroclastics. One of the two main lines of evidence used by previous workers (e.g. Tanaka et al., 1996) to link the two deposits is their similar unusual paleomagnetic orientation. The other is the fact that they share a statistically-similar age. The Mokai pyroclastics age cannot, therefore, now be used in isolation to help define the age of the Mamaku pyroclastics.

This leaves the age MP25 (224 ± 6 ka) as the sole 'reliable' age used by McWilliams (2001) for the Mamaku pyroclastics. Variability in the ages determined for MP27 for the same deposit, which is well beyond the reported error range, brings into question this 6 ka (1 s.d.) error reported for MP25 by Tanaka et al. (1996) and McWilliams (2001). The errors on individual temperature steps of plagioclase ages reported by the Stanford laboratory for TVZ samples appear generally low compared to all of those reported from the Menlo Park laboratory. The Stanford step errors are usually about two thirds of the range of the Menlo Park errors (Fig. 3.4(c) compared to Fig. 3.4(a) and Appendix 2). The Herrero-Bervera et al. (1994) plagioclase age for the Pringle Falls D Ash (Fig. 3.4(b)) presented by McWilliams himself has larger temperature step error ranges similar to those of the Menlo Park data.

In summary, McWilliams's (2001) 'Mamaku Ignimbrite' (and thus Pringle Falls excursion) age (223 ± 6 ka) may be based on a circular argument and on ages with possibly artificially low errors. The 240 ± 11 ka age for the Mamaku pyroclastics determined here appears to be the more reliable age on two grounds:

(a) Ages for the Ohakuri pyroclastics are significantly older than 220 ka, where field evidence implies these should have virtually the same age as the Mamaku.

(b) The age for the stratigraphically younger Atiamuri pyroclastics is 229 ± 12 ka.

Discrepancies among the ages determined for the Mamaku pyroclastics may be explained in one or more of the following ways:

(1) The 'Mamaku Ignimbrite'-based age given to the Pringle Falls Excursion is erroneous (as discussed above) and, therefore, Houghton et al.'s (1995) Mamaku age is also inaccurate.

(2) The Mamaku eruption occurred during another magnetic excursion similar to the Pringle Falls event, but which occurred at an older time (~ 240 ka), and Houghton et al.'s (1995) Mamaku age is also inaccurate.

(3) Some or all of the deposits sampled by other workers as the Mamaku pyroclastics are not actually part of the Mamaku pyroclastics.

The Mamaku, Mokai and Pringle Falls D Ash ages mentioned above used to determine the age of the Pringle Falls paleomagnetic excursion were all determined by the Stanford laboratory before 1994. Prior to about 1994 that laboratory was not conducting mass discrimination corrections on ages determined from individual heating steps (A. Calvert, pers comm., 2003). This correction factor represents the difference between the actual $^{40}Ar/^{36}Ar$ ratio in air and that determined by the mass spectrometer. It is conducted by allowing a precise amount of air of known $^{40}Ar/^{36}Ar$ ratio (an 'air shot') into the mass spectrometer and calculating the ratio (correction factor) to the $^{40}Ar/^{36}Ar$ analysed by the machine. The omission of this correction shifts the ages determined here to ~ 10 kyr younger, and may mean the pre-1994 Stanford calculated ages are younger than the 'actual sample age' by a similar magnitude (without Stanford having run the 'air shot' calibration around the time of their experiments the exact magnitude of the shift such a correction would have made in their results is unknown). An error for this factor is also added to the error of each age step, possibly explaining the relatively small errors of the Stanford ages compared to those determined here.

Variation in the ages determined for the Ohakuri pyroclastics (244 ± 10, 259 ± 9 and 272 ± 16 ka), and the analytical reliability of those ages, may have been influenced by external factors such as inherited Ar, which can arise in a variety of ways. This would imply incomplete Ar degassing in some or all of the Ohakuri magma.

The Mamaku age data presented here appears to be relatively accurate and precise, based on agreement of plateau age with isochron age, MSWD, ^{39}Ar % used in the plateau and agreement of $^{40}Ar/^{36}Ar$ axis intercept on reverse isochron with that of air (Section 3.4.2). The Mamaku and Ohakuri pyroclastics do appear to be distinctly older than the accepted ~ 220 ka age. Further investigation of the paleomagnetic record from 300 to 220 ka, and possibly further dating, are needed to clarify this issue. A paleomagnetic orientation on the Ohakuri pyroclastics also needs to be determined.

In summary, an age of ~ 240 ka is used for the Mamaku and Ohakuri pyroclastics for the purposes of this thesis. This has been selected because it (a) is the age determined here for the Mamaku pyroclastics (justified above), (b) falls within 1 standard deviation of the youngest Ohakuri age presented here and (c) is older than the Atiamuri pyroclastics (229 ± 12 ka), which are determined to be stratigraphically younger in Chapter 2. The Mokai pyroclastics are still considered to have been erupted ~ 220 ka because I have no age evidence to the contrary, but the coincidence in paleomagnetic pole directions with the Mamaku requires explanation if the two units are inferred to be of different ages.

3.5.3 Maroa ignimbrite eruptions 320 to 220 ka

The Korotai pyroclastics (283 ± 11 ka, but stratigraphically above the 275 ± 10 ka Pokai pyroclastics) were erupted from a source in northern Maroa. The Korotai eruption occurred before the main period of Maroa activity, and have the second oldest age of any Maroa deposit analysed.

In the south of Maroa the Orakonui pyroclastics consist of the Orakonui member (~ 256 ± 12 ka), which overlies the Putauaki member (~ 272 ± 10 ka). Although these two ages are within 2 s.d. of each other, field relationships are consistent with the sequence of determined ages. The Putauaki member ignimbrite appears to be more altered and underlies the Orakonui member. The ages of both are older than all surface-expressed domes in Maroa, apart from Goldies dome (305 ± 17 ka) in the MWC. The age for the Orakonui member is only slightly older than that for SE Mandarin dome (242 ± 9 ka) and Roy/McPherson dome (251 ± 17 ka) in the MEC.

The relatively low volume (> 1 km^3) Atiamuri pyroclastics (229 ± 12 ka) occupy a small area (ca. 10 km^2) in central Maroa. They are dominated by ignimbrites that

probably formed as a local constructional fan during a Maroa dome-building eruption. The ignimbrites are in direct contact with a MEC dome dated at 242 ± 9 ka. These two ages are almost within 1 s.d. of each other and based on petrology presented in Chapter 4 the dome may be the same age as the Atiamuri pyroclastics. As mentioned in Section 2.3.3 the dome was probably erupted during and/or after the pyroclastic Atiamuri eruption.

3.5.4 Major Maroa dome-building 260 to 220 ka

Apart from one analysis in each case, domes from the two largest dome complexes (MWC and MEC) are dated from ~ 251 to 222 ka (Fig. 3.2). The outlier age in MWC is Goldies dome, at the southwestern end. This is the oldest within Maroa and only shortly postdates the Whakamaru eruption. This suggests a very short time period for 700-1300 m of caldera infilling between the dome and the top of the intra-caldera Whakamaru group pyroclastics (discussed further in Section 5.5). The relatively young Umukuri dome is the outlier in MEC, which is dated at ~ 189 ka. Tuahu dome has previously been dated at 239 ± 7 ka by B. F. Houghton (pers comm., 2002), and appears to simply be a northeastern-most lava of the MWC.

The western half of the Pukeahua fan (196 ± 8 ka) surrounding Pukeahua West dome (202 ± 7 ka) was probably a constructional fan formed while the dome was being extruded. The eastern half of Pukeahua fan appears to underlie the western half at locality M64 (see Section 2.3.2). Pukeahua East and South domes are petrologically associated with the eastern half of the Pukeahua pyroclastics fan and, therefore, also predate Pukeahua West dome. The eastern half of the Pukeahua pyroclastics fan appears to dip under the Atiamuri pyroclastics, so its age (and that of Pukeahua East and South domes) is constrained as ~ 229 to 196 ka, between the Atiamuri and Pukeahua western pyroclastics.

3.5.5 Discrete large dome extrusions 220 to 160 ka

There are five dome complexes of smaller volumes than MWC/MEC, and which were erupted later, two before 160 ka and three after. Whakapapataringa dome is an elongated complex (194 ± 5 ka, B. F. Houghton, pers comm., 2002), which somewhat arbitrarily has been placed just outside of the southeastern boundary of Maroa. Ngautuku dome complex (160 ± 8 ka, B. F. Houghton, pers comm., 2002) marks the northern boundary of Maroa, extending into the Whangapoa Basin.

3.5.6 Dome extrusion migrating south 160 ka to present

Ngautuku dome complex is the most recent dome complex extruded in the northern half of Maroa. From 160 to 100 ka Maroa-area eruptions occurred in the south of Maroa, and between Maroa and Taupo. Pakuri, Maroanui and Acacia are the only post-160 ka Maroa dome complexes. Pakuri dome complex (~ 152 ka) overlaps onto MEC, but is significantly younger. Maroanui dome complex (~ 143 ka), in central Maroa, has the highest summit elevation in Maroa. Ben Lomond dome complex, the northernmost dome of Taupo, is dated at 105 ± 9 ka (Houghton et al., 1991).

Southern dome complex Lavas along the southwestern end of the Whangamata Fault are dated at 114 ± 11 and 45 ± 9 ka (the latter from B. F. Houghton, pers comm., 2002), and thus are younger than most other Maroa surface extrusions. Ngangiho dome (~ 45 ka) and Puketarata dome (~ 16.7 ka) have been erupted to the south of Maroa (ages from stratigraphic relations, Chapter 2). Mokauteure dome (86 ± 12 ka) is part of a dome complex that is the westernmost vent location in Maroa. Orakeikorako dome (80 ka) and Pohaturoa dome (77 ka) are relatively small extrusions north and east, respectively, of the bulk of Maroa lavas.

3.6 Volume estimates and rates of volcanism

The new age control in the Maroa area provided by this thesis can be used to calculate new estimates of the rates of volcanism in the area. This section provides estimates of the volume of Maroa-related deposits. In Section 3.7 these volumes are combined with the geochronology data above to produce rate estimates.

3.6.1 Approximating natural objects with simple geometric figures

Maroa lava domes, and deposits within Whakamaru caldera, are simplified here as geometric figures with calculable volumes. Whakamaru caldera-fill polyhedrons are approximated as horizontal polygons extended to a depth equal to the average thickness of that specific fill (Fig. 3.5). The areas of the horizontal polygons are calculated as the sum of the areas of a series of constituent triangles and squares.

Lava domes are approximated by more complex curvilinear figures designed to accommodate the variety of dome morphologies present at Maroa. To illustrate this variation Figure 3.6 shows topographic cross sections of three Maroa domes selected because they have distinct morphologies from one another.

The model dome used here is based on a 5 point cross section across the dome. Point 1 is the start point; point two is half way (horizontally) from point 1 to the highest point on the dome; point 3 is the highest point on the dome; point 4 is half way (horizontally) from point 3 to the end of the dome; and Point 5 is the end of the dome. The horizontal distance from point 1 to each of the other points, and the elevation at each of the points, were measured for all domes in Maroa.

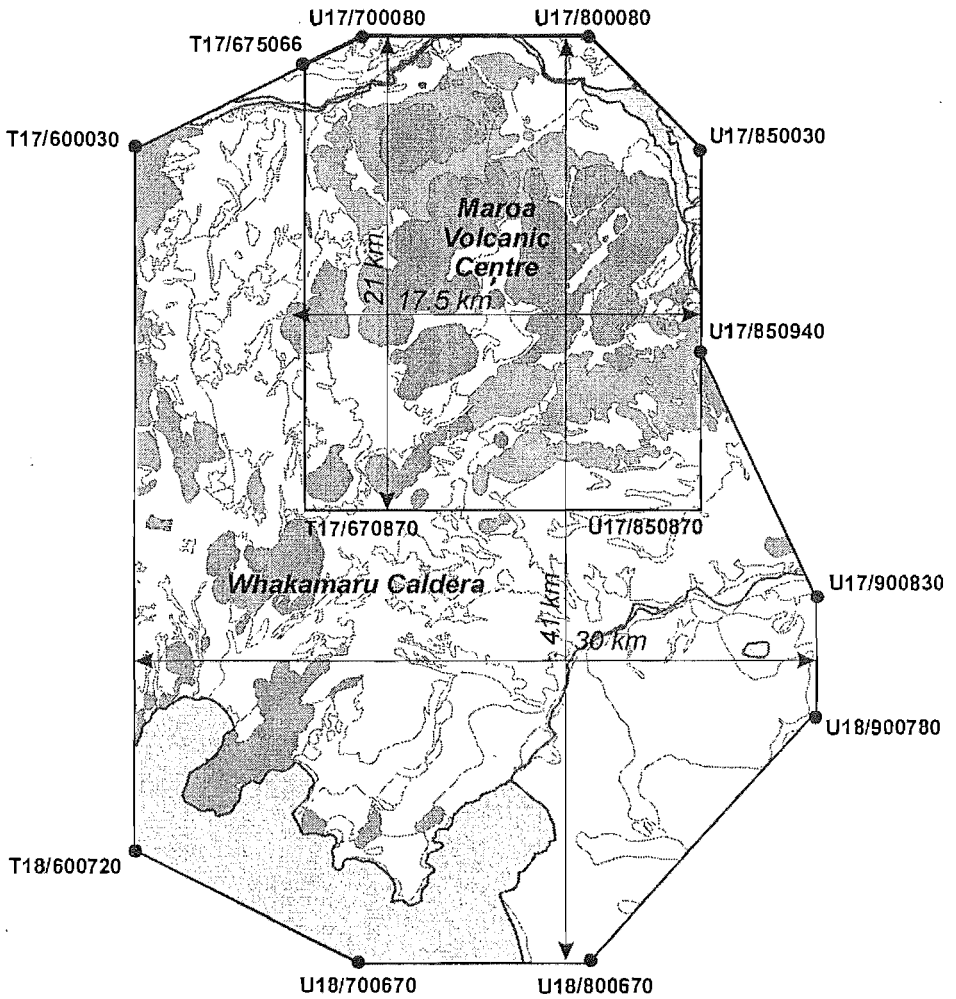

Figure 3.5 polygons used to approximate the volume of Whakamaru caldera and Maroa.

The total volume is calculated by adding the volumes for the following elements (Fig. 3.7). Figures A through D approximate the volume of the dome exposed above the surrounding surface. Elements E and F add the volume between the exposed dome and 300 m asl. elevation:

A Half a truncated cone with centre at point 3, radius to point 1, truncated along radius to point 2 and truncated height the difference from point 1 to 2.

B Half a cone with centre at point 3, radius to point 2 and height the difference from point 2 to 3.

C Half an ellipsoidal cone with centre at point 3, radii to points 2 and 4 and height the difference from point 4 to 3.

D Half a truncated ellipsoidal cone with centre at point 3, radii to points 1 and 5, truncated along radii to points 2 and 4 and truncated height the difference from point 5 to 4.

E Half an ellipsoidal cylinder with centre at point 3, radii to points 1 and 5 and height the difference between point 5 and base Maroa elevation.

F Half a cylinder with centre at point 3, radius to point 1 and height the difference between the elevation of point 1 and the base elevation for exposed Maroa domes (set at 300 m asl.).

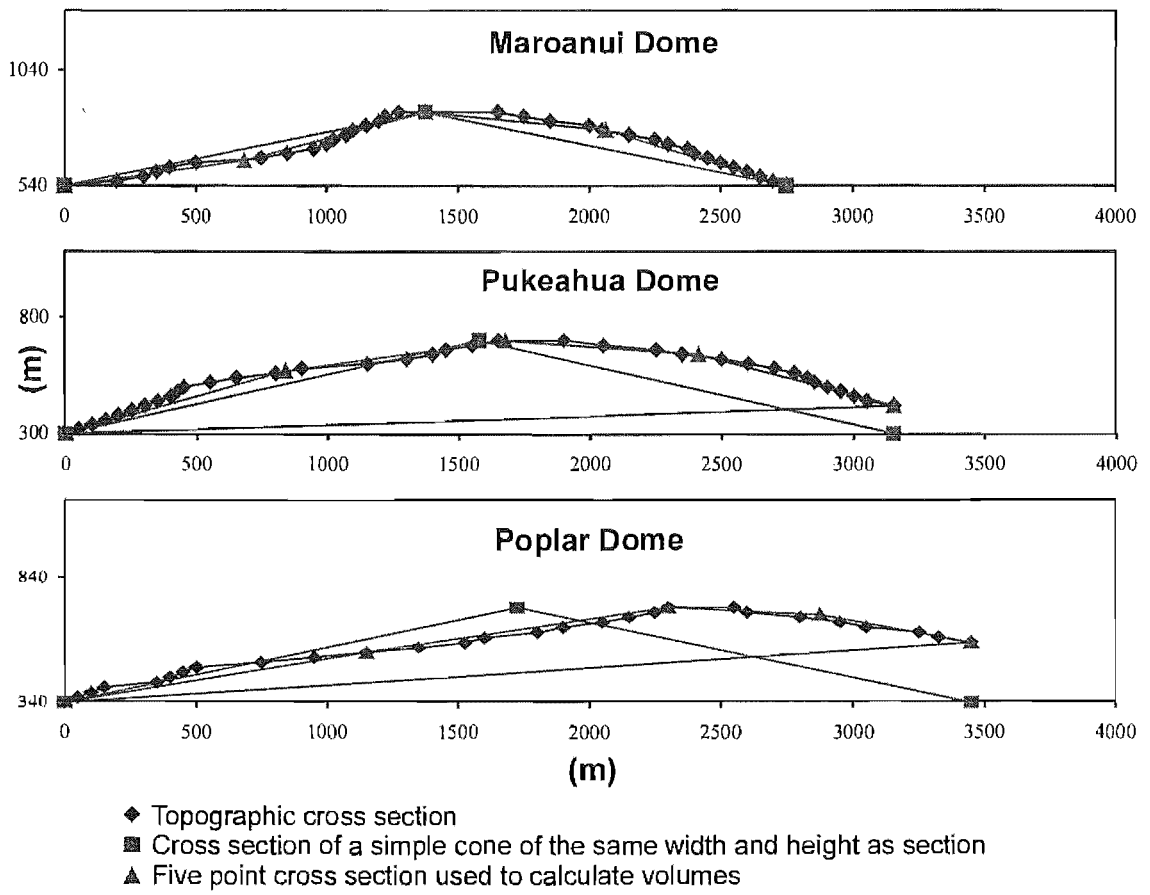

Figure 3.6 Topographic cross sections of three different domes.

Point 1 must be the same elevation or lower than point 5; i.e. the cross section must run from lower to higher end point. Splitting the cones into halves (A and B vs. ellipsoidal C and D) allows for a dome with an off-centre maximum height (point 3). Adding the base half ellipsoidal cylinder (E) approximately projects the volume of the uphill half (C and D) down to the base Maroa surface elevation. Adding the half cylinder (F) projects the volume of the downhill half (A and B) down to the base Maroa surface elevation.

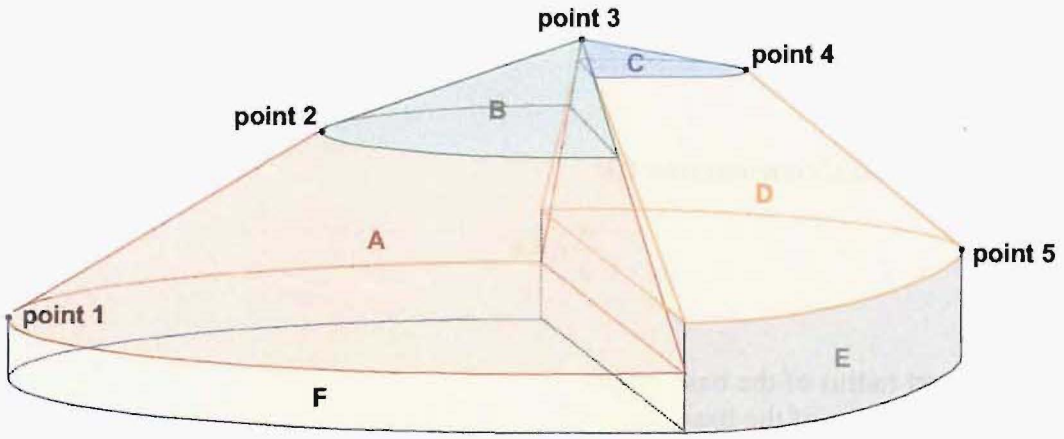

Figure 3.7 Geometry of model dome polyconics

The equations used to calculate volumes of the different sections of the complex geometric model (as shown in Fig. 3.7) are:

Volume of a truncated cone (section A):

$$\frac{\pi}{3}\left[r_b^2 h - r_u^2 (h - h_l)\right]$$

Where:

r_b = radius of the base circle
r_u = radius of the upper (truncating) circle
h = height of the full cone
h_l = height of the lower (truncated) cone section

Volume of a truncated ellipsoidal cone (section D):

$$\frac{\pi}{3}\left[r_{b1} r_{b2} h - r_{u1} r_{u2} (h - h_l)\right]$$

Where:

r_{b1} = short radius of the base ellipse
r_{b2} = long radius of the base ellipse

r_{u1} = short radius of the upper (truncating) ellipse
r_{u2} = long radius of the upper (truncating) ellipse
h = height of the full ellipsoidal cone
h_l = height of the lower (truncated) ellipsoidal cone section

Volume of a cone (section B):

$$\frac{\pi}{3} r^2 h$$

Where:

r = radius
h = height

Volume of a ellipsoidal cone (section C):

$$\frac{\pi}{3} r_1 r_2 h$$

Where:

r_1 = short radius of the base ellipse
r_2 = long radius of the base ellipse
h = height of the ellipsoidal cone

Volume of an ellipsoidal cylinder (section E):

$$\pi r_1 r_2 h$$

Where:

r_1 = short radius
r_2 = long radius
h = height

Volume of a cylinder (section F):

$$\pi r^2 h$$

Where:

r = radius
h = height

3.6.2 Calculated volumes and previously published volumes

The collapse of Whakamaru caldera lowered the intra-caldera area by at least 400 m (the thickness of intra-caldera Whakamaru group ignimbrites). For the purposes of this thesis the area of Whakamaru caldera collapse is ca. 1012 km^2, based on the polygons given in Figure 3.5. Mokai drill hole data show the top of the Whakamaru group within the caldera to be between 400 and 800 m below sea level. A 300 m asl. reference elevation is used as it conveniently represents the lowest exposed Maroa lava and the

lowest area within Whakamaru caldera. The surface elevation below the 305 ka Goldies dome is ~ 400 m asl., which is even higher than the 300 m asl. base elevation. This provides a minimum age for the 300 m asl. surface. Prior to 305 ka there must, therefore, have been infilling of pyroclastics, lavas and sediments 700 to 1100 m thick between the 300 m asl. reference elevation and the Whakamaru group intra-caldera ignimbrites.

Table 3.7 gives the volumes of Maroa domes calculated using the models described above, projected to the 300 m asl. base elevation. Table 3.8 presents the volumes calculated for key Maroa deposits and groups of domes from Table 3.7. It also summarises key volumes for Maroa-related deposits published by other workers. Volumes are all expressed in terms of their thickness relative to the 300 m asl. reference elevation, and the sum of the volumes represents the entire Whakamaru caldera fill.

Dome	(km^3)	Dome	(km^3)	Dome	(km^3)	Dome	(km^3)
Maroanui	2.11	Poplar-Sitka	2.87				
Maroanui South	0.27	Goldies	2.39	Mangatoetoe	0.80		
Maroanui W	0.04	Walker	2.52	Pakuri	0.25		
Maroanui total	**2.42**	Mulga-Hind	1.61	**Pakuri total**	**1.05**	Orakeikorako	0.02
		Stag	1.41			Kakuku	0.02
Mokauteure	1.65	View-Almond	2.31			Waipakipaki	0.08
Palm	0.16	Kemp	1.01	Roy S	0.61	Whakapapa	0.01
Acacia total	**1.81**	**MWC total**	**14.12**	Roy W	0.26	Whakapapataringa	0.61
				Roy N & E	1.16	Puketarata	0.13
Ngautuku N	0.58	Tuahu	**0.26**	Rusty/McPherson	1.74	Nangiho	0.22
Ngautuku S	0.14			Summit/Baldy	3.07	Tutukau	0.01
Ngautuku total	**0.72**	Swampy	0.35	Hauwai	0.91	Mangatutu dome	0.06
		Forest W	0.86	Mandarin	1.65	Pohaturoa	0.02
Pukeahua	1.73	Forest S	0.01	Wilson/Wairiki	1.77	**Misc. total**	**1.18**
Pukeahu East	0.71	Forest	0.03	Umukuri	1.38		
Pukeahua South	0.14	Dairy	0.17	**MEC total**	**12.55**		
Pukeahua total	**2.58**	**Southern total**	**1.42**			**TOTAL**	**38.11**

Table 3.7 Volumes for Maroa domes calculated using the model polyheconics in Section 3.6.1 and projected to a base elevation of 300 m.

Figure 3.8 shows the distribution of the deposits across the 1 km gridded Whakamaru caldera. Average elevation for each square was visually estimated from 20 m interval elevation contours on 1:50,000 topographic map sheets. For each square the thickness of cover deposits (if any) was subtracted out and then thickness of fill down to the 300 m base elevation (if surface elevation is above 300 m), and down to top of intra-caldera Whakamaru group pyroclastics, was calculated. Deposit areas were then multiplied by appropriate thicknesses to give volumes.

	Deposit within Whakamaru caldera	Data Source	area (km^2)	in situ volume (km^3)	Bulk D (g/cm^3)	Lithic content	DRE (@2.3D) (km^3)
Non-Maroa material < 305 ka (> 300 m asl.)	WDC within Whakamaru caldera	1	34	8	2.3	-	8
	Mokai pyroclastics outside of Maroa	1/3	108	18	1.1	0.03	9
	Whakapapataringa dome	1	2	1	2.3	-	1
	Taupo - Ben Lomond dome	1	17	5	2.3	-	5
	Taupo – Ngangiho dome	1	1	0	2.3	-	0
	Taupo - Whakaroa dome	1	20	5	2.3	-	5
	Taupo - Tauhara dome	1	15	7	2.3	-	7
	Other lavas (mostly Taupo domes)	1	9	3	2.3	-	3
	Other non-Maroa fill (mostly Taupo)	1	424	60	1.5	*	39
	Fill underlying the above non-Maroa material (i.e. > 305 ka)	1		462 to 701	1.5	*	297 to 471
	NON-Maroa TOTAL		630	549 to 808			374 to 548
Maroa material < 305 ka (> 300 m asl.)	MWC (above 300 m)	1	30	14	2.3	-	14
	MEC (above 300 m)	1	38	13	2.3	-	13
	Pukeahua domes (above 300 m)	1	10	3	2.3	-	3
	Other Maroa lavas (above 300 m)	1	34	8	2.3	-	8
	Mokai pyroclastics within Maroa	1/3	27	5	1.1	0.03	2
	Pukeahua fan (base elevation < 300 m)	1	32	2	1.3	0.15	1
	Atiamuri (base elevation < 340 m)	1	10	1	1.3	0.15	>1
	Putauaki (base elevation < 460 m)	1	8	2	1.2	0.10	1
	Orakonui + Putauaki (base elevation < 460 m)	1	40	5	1.2	0.05	3
	Korotai pyroclastics	1	3	1	1.3	0.15	<1
	Ohakuri in Maroa	1	41	10	1.2	0.05	5
	Other Maroa fill	1	115	20	1.5	*	13
	Fill underlying the above Maroa deposits (i.e. > 305 ka)	1		233 to 364	1.5	*	156 to 244
	Maroa TOTAL		385	316 to 447			220 to 308
	TOTAL ABOVE WHAKAMARU GROUP INTRA-CALDERA (sum of totals above)	-	1015	865 to 1255			594 to 856
	WHAKAMARU GROUP INTRA-CALDERA PYROCLASTICS	5	1015	505	2.0	0.05**	439
	For Comparison:						
	Taupo ignimbrite	6	20000				30
	Oruanui intra-caldera	2	280				230
	Oruanui downsag	2	600				-
	Oruanui outflow	2	12000				320
	Ohakuri intra-caldera (1 km thick)	7	1-200	70-140	1.7	0.03	52-104
	Ohakuri total outflow (~ 200 m thick)	7	500	40	1.1	0.03	19
	Mamaku pyroclastics outflow	3	3100-3900	225-283			96-121
	Mamaku pyroclastics intra-caldera	3	1122	114			48.7
	Pokai pyroclastics	4	1200+	40			33

Table 3.8 Approximate areas and volumes for Taupo-Maroa related deposits. Sources: (1) this study, (2) Wilson (2001), (3) Milner (2001), (4) Karhunen (1993), (5) Brown et al. (1998), (6) Wilson (1985), (7) Gravley (2003).* Undifferentiated fill of 1.5D = 70 vol.% 1.1D pyroclastics/fill (containing 10 vol.% 2.3D lithics) and 30 vol.% 2.3D lava. Bulk densities for pyroclastics units are based on 1.1D for outflow ignimbrite and 1.7 for intra-caldera ignimbrite, with 2.3D lithic content. ** Approximate value based on low lithic content in all Whakamaru group pyroclastic from Brown (1994). DRE is Dense Rock Equivalent. D = Density in g/cm^3.

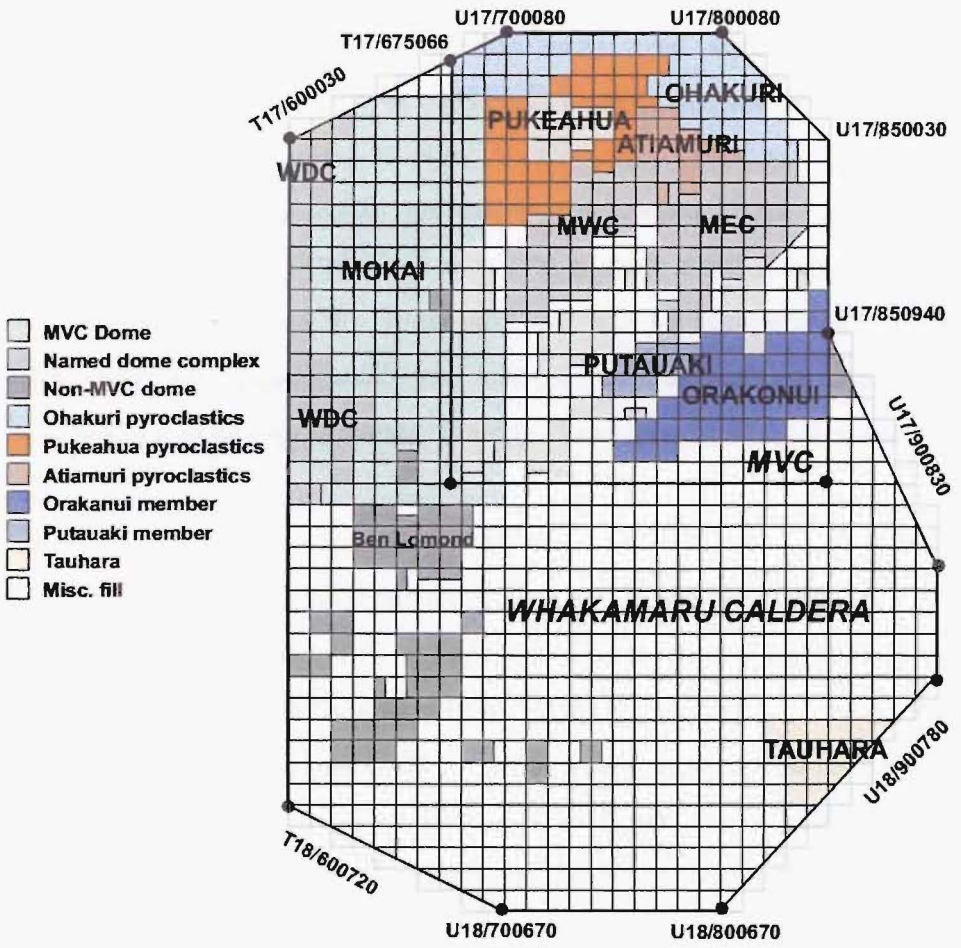

Figure 3.8 Distribution of deposits within Whakamaru caldera, simplified to 1 km grid squares (and half squares where needed) to facilitate caldera volume calculations.

Dense Rock Equivalent (DRE) volumes in Table 3.8 have an assumed density of 2.3 g/cm^3. All densities (D) given in this thesis are in g/cm^3. Calculations for DRE are made at Whakamaru intra-caldera ignimbrite density 2.0 (based on average of densities in Wairakei Geothermal Area drill core from Whiteford and Lumb, 1975), with lithics of 5 vol.% from Brown (1994), with density 2.3. Lavas are considered to be dense rock at density 2.3. Specific pyroclastic deposits are considered to have density 1.1 with stated lithic content at density 2.3. Caldera fill is assumed to be 70 vol.% sediment/pyroclastics with density 1.1 with lithics of 10 vol.% (density 2.3) and 30 vol.% lava with density 2.3. All of these assumed densities are based on Wilson (2001), who in turn based them on the deposits of the Oruanui eruption.

Maroa surface deposits: Pyroclastic units, domes and mixed fill

The boundaries of Maroa have been defined (Section 1.4.2) as the section of Whakamaru caldera within the points T17/675080 in the northwest, and U17/850870 in the southeast. MWC and MEC make up the bulk of Maroa lavas, 14.1 and 12.6 km^3 (areas of 30 and 38 km^2), respectively. Pukeahua dome complex is the next largest single lava body, which has a volume of 2.6 km^3 (10 km^2). The remaining lavas total 8.8 km^3 (34 km^2), of which 2.4 km^3 are Maroanui, 1.8 km^3 are Acacia, 0.7 km^3 are Ngautuku, 1.4 km^3 are Southern and 1.1 km^3 are Pakuri dome complexes. Combined Maroa lavas cover ~ 111 km^2 and total ~ 38 km^3 (when projected to a common base at 300 m asl.).

The Pukeahua pyroclastics fan (32 km^2, a truncated, hollow cone 150 m high at its highest point) and Atiamuri pyroclastics (10 km^2, ~ 100 m thick) each total less than 1 km^3 (all pyroclastics are discussed as DRE in this section). The Orakonui and Putauaki members of the Orakonui pyroclastics (48 km^2, Putauaki member 118 ± 20 m thick, Orakonui member 126 ± 20 m thick) together total > 4 km^3. Part (~ 2 km^3) of the Mokai pyroclastics (134 km^2, ~ 181 m thick) lie within the boundaries of Maroa. Ohakuri pyroclastics cover 41 km^2 of Maroa and using a somewhat arbitrary thickness of 250 m (to accommodate outflows of ~ 100 m thick and intra-caldera material > 600 m thick) the volume is probably ~ 5 km^3. These named surface pyroclastic deposits cover a total area of 157 km^2 within Maroa.

Maroa miscellaneous fill: Mixed sediments, pyroclastics and lava

Miscellaneous fill within Whakamaru caldera is considered to consist of 70 vol.% sediments and pyroclastics, and 30 vol.% rhyolite lava. This is based on confidential drill core logs held by Crown Minerals for the Mokai Geothermal Field (kindly provided to the author) which allow estimation of the relative proportions of sediments/pyroclastics and lavas.

The remaining area of Maroa (~ 115 km^2) is covered by miscellaneous fill reaching the surface. About 13 km^3 of this lies above 300 m asl. and is thus considered younger than 305 ka. All fill below 300 m asl., beneath surface fill and lava domes, is considered to be older than 305 ka (an assumption discussed in Section 5.5.2). All fill below the base of the named Maroa surface pyroclastics deposits (a different elevation for each deposit)

is also calculated as > 305 ka. The total volume of fill > 305 ka is 156 to 244 km^3, depending on whether the base of caldera fill is at -800 or -400 m asl.

Non-Maroa surface deposits: Mixed fill, Mokai pyroclastics, dome lavas and Tauhara

The WDC (34 km^2 within Whakamaru caldera) has a volume of ~ 8 km^3 (Brown, 1994). Ben Lomond (17 km^2) has a volume of 5 km^3, Ngangiho (1 km^2) a volume of up to 1 km^3, Whakapapataringa (2 km^2) a volume of 1 km^3 and Whakaroa dome (20 km^2) a volume of 5 km^3. Other surface lavas in Whakamaru caldera (other than those named here, or within Maroa) cover 9 km^2 and total 3 km^3. Tauhara, behind Taupo City, covers 15 km^2 and has a volume of 7 km^3. All of these lava volumes are projected down to 300 m asl. except for WDC, where Brown (1994) made his volume estimates relative to the ground surface. Mokai pyroclastics outside of Maroa cover 108 km^2 and have a volume of 9 km^3. All of these surface deposits have a total area of 205 km^2. The remaining non-Maroa surface area (~ 424 km^2) is miscellaneous fill reaching the surface and has a < 305 ka volume of ~ 39 km^3 above 300 m asl..

Non-Maroa fill: mixed sediments, pyroclastics and lava

The fill underlying these 630 km^2 of non-Maroa deposits is considered to be the same > 305 ka misc. fill as that described below Maroa. It totals 300 - 470 km^3.

Summary of Maroa areas and volumes compared to all of the Whakamaru caldera fill

The following figures are summarised from Table 3.8 and are rounded to the nearest 10 units of area and volume. Whakamaru caldera covers 1020 km^2. The intra-caldera Whakamaru group pyroclastics total 440 km^3. Material overlying these intra-caldera ignimbrites total 600 - 860 km^3. This is broken down as follows:

The total area covered by Maroa is 390 km^2, which equals a volume of 220 - 310 km^3 above the intra-caldera Whakamaru group ignimbrites. This is comprised of (a) lavas, pyroclastics and miscellaneous fill < 305 ka totalling 60 km^3 and (b) > 305 ka mixed fill underlying (a) which totals 160 – 250 km^3.

Outside of Maroa, but still within Whakamaru caldera: (a) < 305 ka surface lavas, Mokai pyroclastics and mixed fill total 630 km^2 and 80 km^3; (b) > 305 ka mixed fill underlying (a) totals 300 - 470 km^3.

3.7 Rates and timing of volcanism around Maroa

Figure 3.9 presents a plot of volume vs. age for deposits within Maroa, as presented in the section above. These are placed in the context of the wider Maroa-related area in Figure 3.10. Volumes for deposits that project down to the top of the intra-caldera

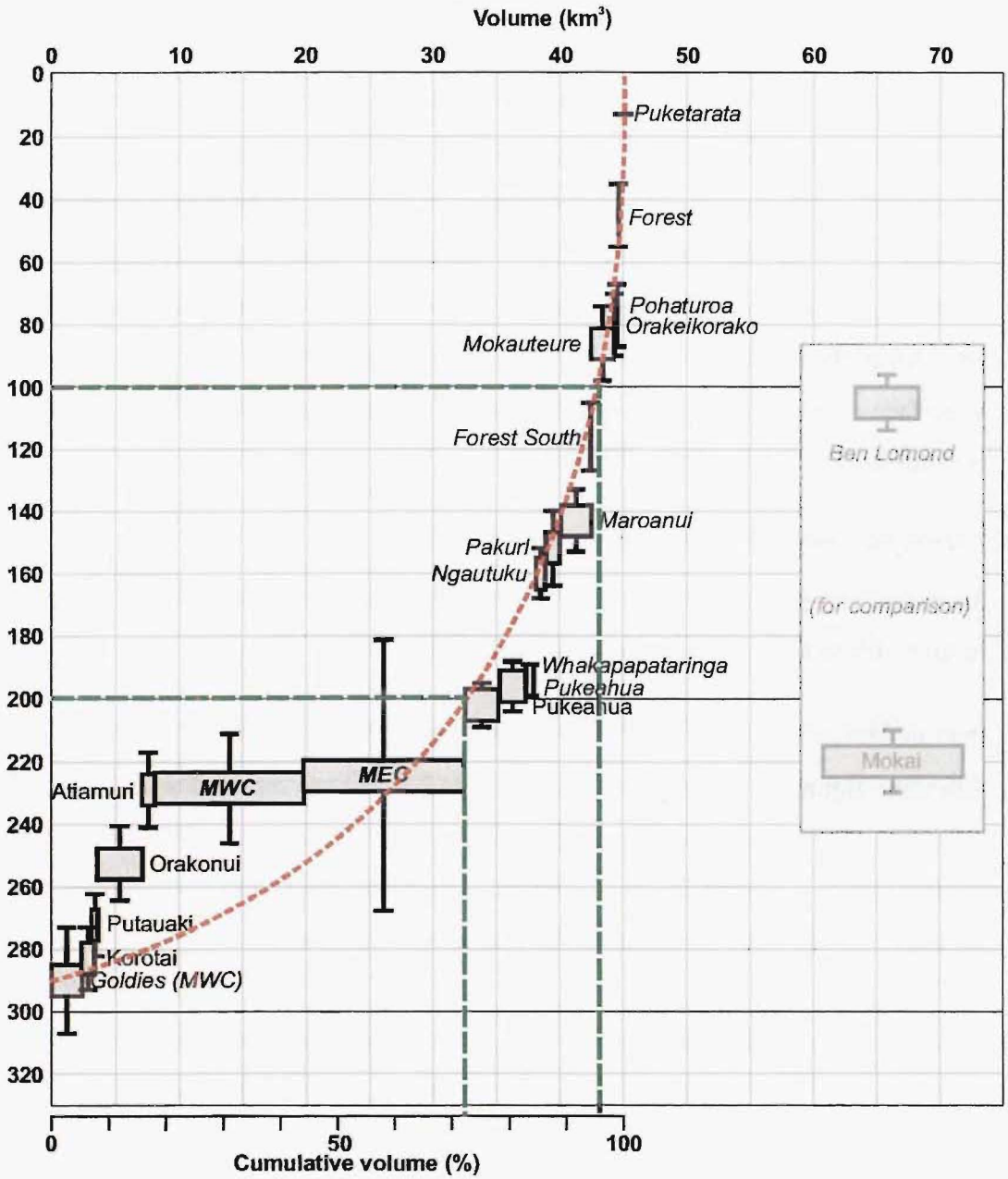

Figure 3.9 Plot of Ar-Ar age vs. cumulative DRE volume (as determined in Chapter 4) for MVC deposits only. Dome lavas are italicised, pyroclastics are not. Mokai and Korotai pyroclastics are shown for comparison, in grey. Sources of ages are detailed in text. Note that a line at 200 ka age intersects the line of best fit at 75 % cumulative. Note that there was an aditional 13 km3 of misc. fill material deposited within MVC post 305 ka, it is assumed to have been emplaced with the same volume time relationship as those deposits presented here.

Whakamaru group pyroclastics are averages of the minimum and maximum estimates made in the previous section.

There has been an exponential decrease in the rate of volcanism at Maroa from 300 ka to the last 20 kyrs (Fig. 3.9). Seventy five percent of the volume was erupted prior to 200 ka (ca. 33 km^3, or 0.33 km^3/kyr). This is composed of the Orakonui, Putauaki, Atiamuri and Pukeahua pyroclastics and MWC and MEC domes. Ninety seven percent of Maroa volume had been erupted by 100 ka (from 200 to 100 ka this is 12 km^3, or 0.12 km^3/kyr), with only Mokauteure, Orakeikorako, Pohaturoa, Forest and Puketarata domes erupted after this time.

Seven of the nine ages from the two major complexes fall between 222 and 251 ka. Assuming that most domes in MEC/MWC fall within this age range, a significant proportion of lava from Maroa (up to 24.7 km^3, ~ 65 vol.% of Maroa lava) was erupted during this period of only 29 ka (a rate of 0.85 km^3/kyr).

In the Whakamaru caldera overall, 95 vol.% of the caldera fill was deposited prior to 200 ka. This is 690 km^3, or 5.8 km^3/kyr since 315 ka, which is almost two orders of magnitude greater than the highest rate after 200 ka (0.12 km^3/kyr in Maroa from 200 to 100 ka). This includes most of the Western Dome Belt, all of the undifferentiated fill below 300 m asl., almost all of the fill above this elevation too and the Maroa pre-200 ka deposits described above.

Eruption of the WDB along the northwestern margin of the caldera continued from < 251 to 141 ka (~ 30 km^3 over 110 kyr). This is a rate of < 0.27 km^3/kyr. Additional pyroclastics from these eruptions may also have contributed some volume to Whakamaru caldera fill.

Discrete small-volume eruptions have migrated south in the Maroa area over the last 100 ka. Activity has also increased at Okataina. Nearly all modern-TVZ volume has come from eruptions in the Taupo and Okataina Volcanic Centres.

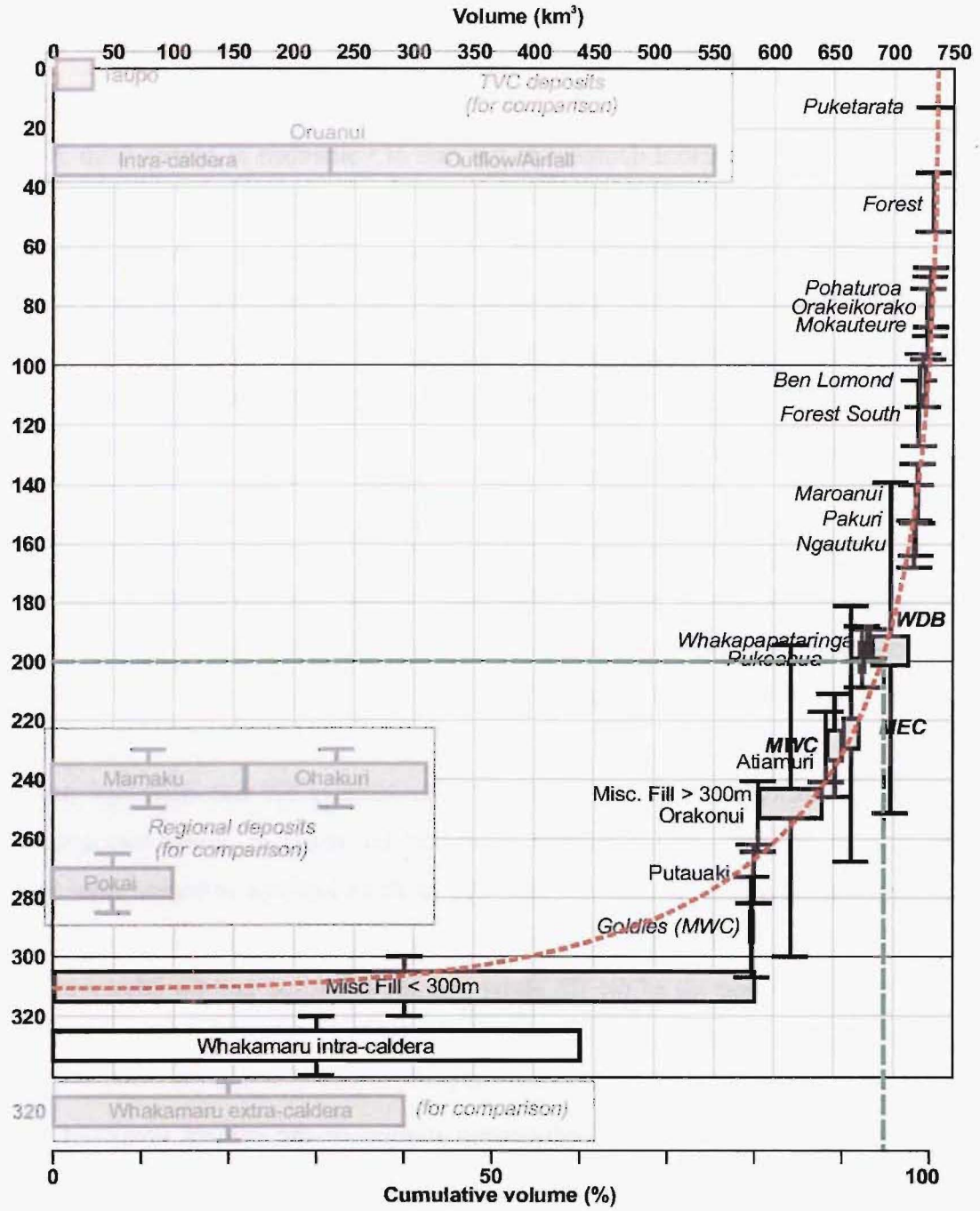

Figure 3.10 Plot of Ar-Ar age vs. cumulative DRE volume (as determined in Chapter 3) for deposits filling Whakamaru caldera. Dome lavas are italicised, pyroclastics are not. Ages and volumes for regional and TVC caldera-forming deposits are shown for comparison, in grey. Sources of ages are detailed in text. Note that a line at 200 ka age intersects the line of best fit at 95 % cumulative.

CHAPTER 4

Petrology

4.1 Introduction

A core objective of this thesis is investigating the petrology of Maroa volcanics. This chapter presents the petrography and geochemistry of new samples collected and analysed as part of this study. Data on the petrography and petrology of other eruptives in and around Maroa from other workers are also summarised here, to allow comparison with Maroa eruptives. The data in Chapters 2 and 3 have been combined with data presented in this chapter to form the basis for discussion of the evolution of Maroa in Chapter 5.

4.2 Rhyolite petrography

4.2.1 Introduction to petrography

Petrographic analysis of 166 samples was conducted on thin sections using a transmitted light polarising microscope. Crystals, vesicularity, glass character and groundmass mineralogy were all described and interpreted. The results of Maroa analyses are summarised here from the data presented in Appendix 3.

In thin section, percentages of each fraction (minerals, groundmass, spherulites and vesicles) have been visually estimated using a comparison chart. Brown (1994) noted that point counting has a particularly high uncertainty in rocks with low crystal contents (true of most Maroa-area eruptives). This is because of the high likelihood of the technique missing many smaller crystals and thus under-representing the overall volume of mineral phases in the rock. Previous use of comparison charts by the writer has also been shown to be sufficiently quantitative for initial statistical comparison of proportions (Leonard, 1999). The best results are likely to be produced when estimates are made by only one worker over a short time period, as was done for this thesis. Table 4.1 shows that these comparison-chart-based estimates of crystal content compare well to point counting from Ewart (1968) for three Maroa eruptives chosen at random. Differences between values from the two methods of estimation are comparable to the variation between thin sections within each deposit (Appendix 3).

No. of samples	Unit	Pl %	Max Pl size (mm)	Qtz %	Max Qtz size (mm)	Amph %	Max Amph size (mm)	Opx %	Max Opx size (mm)	Biot %	Max Biot size (mm)	Opq %	Max Opq size (mm)	Gmass %	Gm sph %	Max shp size (mm)	Vesic %	Max vesic size (mm)
25	MEC (mean)	**9.5**	2.8	**1.1**	1.1	**0.1**	0.1	**0.2**	1.0			**0.3**	0.5	**89**	**49**	1.1	**10**	1
	P29658 (Ewart)	***6.7***		***0.9***				***0.3***				***0.3***		***92***	*46*		***0***	
2	Pukeahua East	**19.1**	3.1	**6.2**	2.2	**0.6**	1.4	**0.8**	1.2			**0.3**	0.4	**73**	3	0.6	**11**	<1
	P29570 recalc (Ewart)	***15.9***		***4.9***		***0.3***		***0.7***				***0.3***		***78***	*1*		***15***	
1	Orakeikorako	**21.3**	2.5	**6.7**	3.0	**1.3**	4.1	**0.1**	0.6	0.1	0.5	**0.1**	0.3	**70**			**25**	1
	P25223 recalc (Ewart)	***18.1***		***2.9***		***1.1***		***0.1***		*0.5*		***0.4***		***77***			***21***	

Table 4.1 Three point-counted estimates of Maroa domes petrography (P25223, P29570 and P29658) from Ewart (1968; italicised), compared to comparison-chart-based estimates from this study for the same lavas, based on an average of 25 samples from MEC, 2 samples from Pukeahua and a single sample from Orakeikorako dome, respectively. Percentages of crystals are calculated on a vesicle-free basis. Abbreviations used in tables are: (Pl) plagioclase feldspar, (Qtz) quartz, (Amph) amphibole - hornblende, (Opx) orthopyroxene, (Biot) biotite, (Opq) opaque minerals - mostly Fe/Ti oxides, (Gmass) groundmass, (Sph) spherulites and (Vesic) vesicles. Underlined percentages indicate that that constituent was not present in all thin sections. Averaged percentages are given in bold. Where data is not present for a given mineral that sample/deposit does not contain this mineral.

Percentages shown in the summary tables in this chapter are averages of all thin sections for that deposit, calculated vesicle free. Underlined average percentages indicate that some thin sections within the averaged deposit did not contain this component (thin sections where that component was absent were still included when calculating the average). Crystal lengths are given in mm as the dimension of the longest axis and those quoted here are the maximum visible in any thin section. Phenocrysts are considered to be all juvenile crystals larger than 0.05 mm in maximum dimension; all smaller crystals are counted as groundmass. Maximum vesicle size (short axis) in summary tables is rounded to the nearest mm.

4.2.2 Crystal content and plagioclase/quartz ratios

Figure 4.1 presents a summary of the crystal contents and plagioclase/quartz ratios of key groups of Maroa eruptives. In addition, the data are coloured according to diagnostic ferromagnesian minerals present. These data are discussed in the following sections.

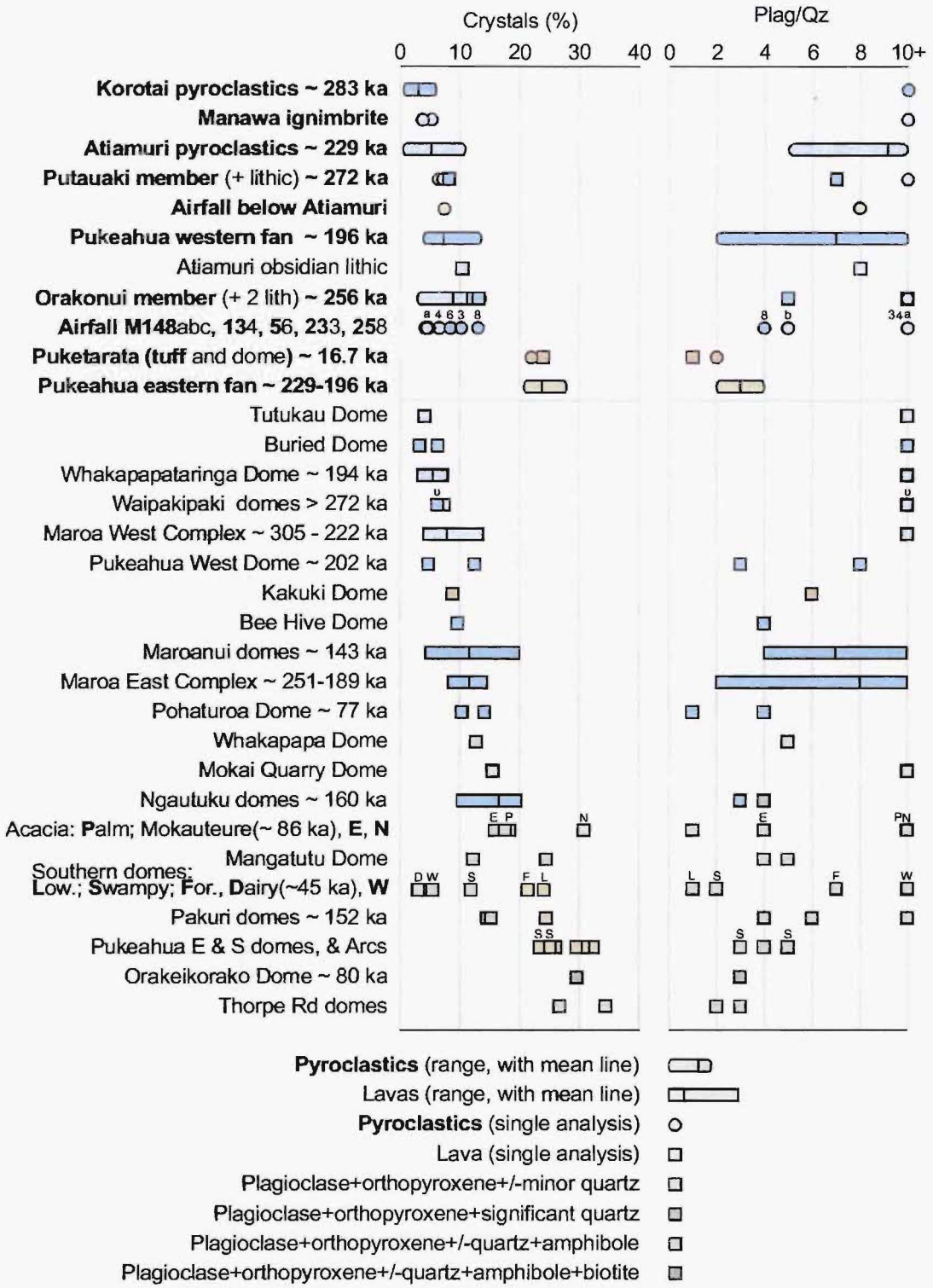

Figure 4.1 Distribution of (a) crystal content (vesicle-free vol.%) and (b) plagioclase/quartz (vol. ratio) for pumice from significant groups of MVC deposits. Symbol shape represents pyroclastics vs. lavas and colour represents key mineralogical fingerprint. Highlighted letter/number corresponds to label on symbol. Manawa ignimbrite lies within the Pukeahua pyroclastics..

4.2.3 Lava domes

All Maroa lavas (apart from two obsidian samples, mentioned below) are porphyritic and hypocrystalline. Crystal contents range from nearly aphyric (1 %) to around 35 %, and vesicularity ranges from zero to 30 vol.%. Microlites (<< 0.05 mm crystals in glassy groundmass, usually with aspect ratios >> 10:1) are minor and dispersed.

Plagioclase is pervasively normal, reverse and oscillatory zoned, usually has glass inclusions, is rounded and is sometimes embayed. It is often fractured with patchy extinction interpreted to reflect strain produced by shearing during extrusion. Plagioclase occasionally contains sieved zones and is usually clumped, often with quartz and other minerals, into glomeroporphyritic aggregates. Quartz is usually subhedral to anhedral and embayed.

Amphibole, biotite and orthopyroxene are usually sub- to euhedral and crystals of these minerals do not often show signs of resorption or alteration. This suggests that they were in thermal equilibrium with the melt. Opaque material appears by reflected light microscopy to be mostly magnetite with minor titanite.

North Maroa

No. of samples	Unit	Pl %	Max Pl size (mm)	Qtz %	Max Qtz size (mm)	Amph %	Max Amph size (mm)	Opx %	Max Opx size (mm)	Biot %	Max Biot size (mm)	Opq %	Max Opq size (mm)	Gmass %	Gm sph %	Max shp size (mm)	Vesic %	Max vesic size (mm)
4	Ngautuku	12.5	2.5	3.7	1.4			0.3	1.1			0.1	0.3	83	50	0.7	7	<1
2	Buried	4.7	2.3	0.1	0.5			0.1	1.4			0.1	0.3	95			3	<1
2	Pohaturoa	8.1	3.4	4.0	1.8			0.1	1			0.1	0.7	88	85	0.3	1	<1
1	Mokai Quarry	14.4	2.7					1.0	1.8			0.1	0.3	84	20	0.3	3	<1

Table 4.2 Petrography of selected domes to the north of Maroa. Percentages of crystals are calculated on a vesicle-free basis. Details as for Table 4.1.

The Ngautuku dome complex samples (Table 4.2) contain plagioclase, quartz, orthopyroxene and trace opaques, have relatively low vesicularity and variable devitrification to spherulites. Buried dome to the west has the same mineralogy but has lower crystal content. Outcrops of Buried dome have lower vesicularity, and are not spherulitic. This dome is highly fractured and generally more weathered in outcrop than

the other Maroa domes. Pohaturoa dome (Table 4.2), just south of the Waikato River, contains plagioclase, quartz, orthopyroxene and trace opaques. It is highly devitrified to spherulites and slightly silicified (it is extremely hard, consistent with minor silica re-crystallisation after emplacement) with very low vesicularity. The largely-buried lava at Mokai Quarry is similarly devitrified and slightly silicified, but has much higher plagioclase content and contains no quartz. It is less spherulitic.

Pukeahua area

No. of samples	Unit	Pl %	Max Pl size (mm)	Qtz %	Max Qtz size (mm)	Amph %	Max Amph size (mm)	Opx %	Max Opx size (mm)	Biot %	Max Biot size (mm)	Opq %	Max Opq size (mm)	Gmass %	Gm sph %	Max shp size (mm)	Vesic %	Max vesic size (mm)
2	**Pukeahua West**	**6.3**	3.5	**1.9**	1.5			**0.1**	0.8			**0.3**	0.5	**91**	**50**	0.2	**5**	<1
2	**Pukeahua South**	**20.0**	4.8	**5.2**	2.9	**1.3**	2.4	**0.6**	1.9			**0.1**	0.4	**73**			**23**	**1**
2	**Pukeahua East**	**19.1**	3.1	**6.2**	2.2	**0.6**	1.4	**0.8**	1.2			**0.3**	0.4	**73**	**3**	0.6	**11**	<1
2	**Pukeahua E Arcs**	**22.1**	4.1	**6.3**	2.4	**0.5**	1.6	**0.1**	0.8			**0.1**	0.3	**71**	**95**	0.5	**5**	1.5
2	**Mangatutu**	**13.9**	3.5	**3.6**	1.9	**0.3**	1.3	**0.5**	0.9			**0.1**	0.3	**82**	**8**	0.1	**23**	**1**
1	**Thorpe 1**	**18.1**	2.5	**7.2**	1.7	**1.2**	3	**0.1**	1.2			**0.1**	0.3	**73**			**17**	<1
1	**Thorpe 2**	**18.8**	3.8	**12.5**	2.3	**1.3**	1.3	**1.3**	0.5			**0.6**	0.4	**65**			**20**	**1**

Table 4.3 Petrography of domes in the Pukeahua area. Percentages of crystals are calculated on a vesicle-free basis. Details as for Table 4.1.

Pukeahua West dome (Table 4.3) contains plagioclase, quartz, orthopyroxene and minor opaques as phenocrysts (Fig. 4.2(a)). Pukeahua East and South domes have the same mineral assemblage as Pukeahua West dome, but with the addition of amphibole (Fig. 4.2(b)). The East and South domes are also significantly more crystal-rich. Variations in devitrification and vesicularity amongst the Pukeahua dome samples show no consistent pattern.

The sample from the two partly buried domes on Thorpe Rd (Thorpe 1 and 2 domes, Table 4.3), and the lava arcs (marked on Fig. 2.1) east of the Pukeahua domes, all have the same high crystal content and mineralogy as Pukeahua East and South domes. Mangatutu dome, which lies northeast of these domes, also has the same amphibole-bearing mineral assemblage as the Arcs, but lower crystal content.

(a) Pukeahua West Dome

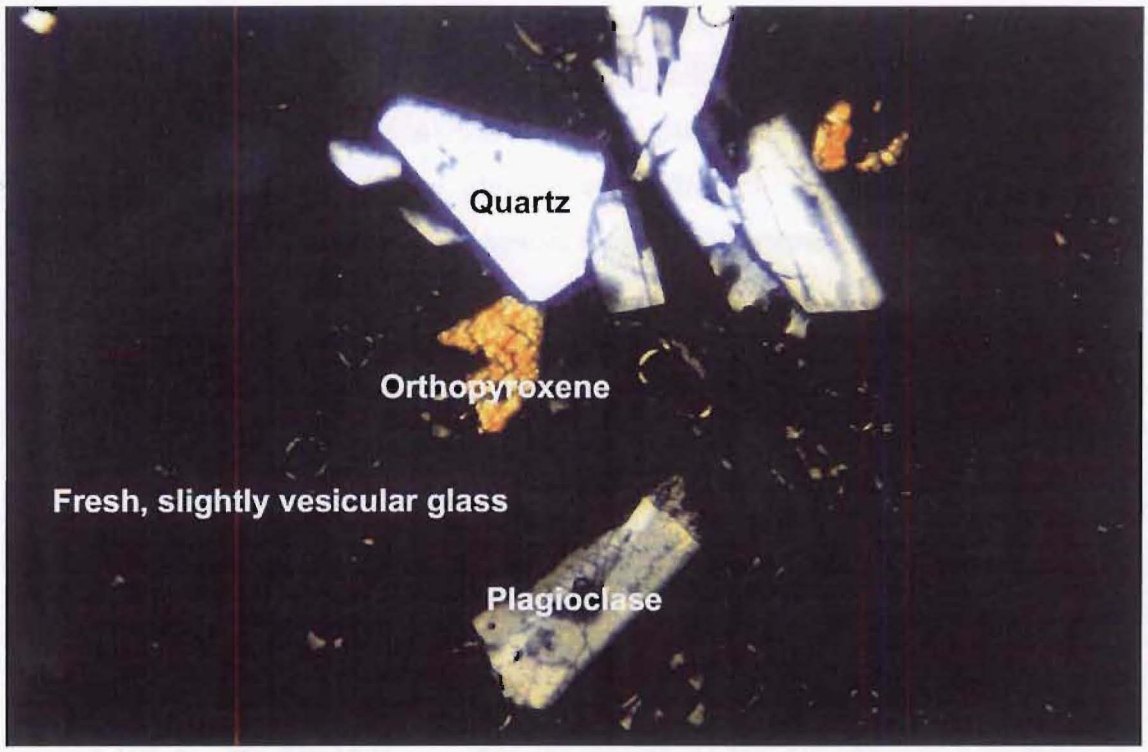

(b) Pukeahua East Dome

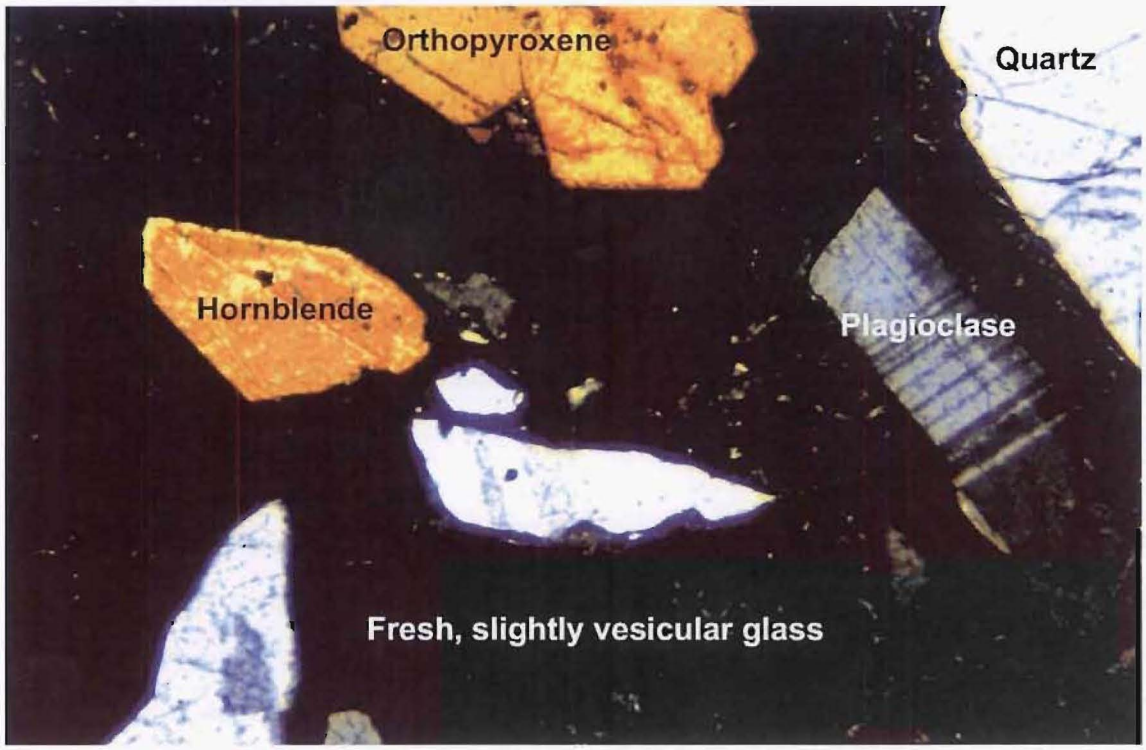

Figure 4.2 Rhyolite lava from Pukeahua (a) West and (b) East domes in thin section. Both domes contain plagioclase, orthopyroxene, quartz and opaque minerals, but note that only Pukeahua East Dome contains hornblende. Pukeahua West also has a notably lower crystal content (mean 9 % vesicle free), and larger quartz and orthopyroxene crystals, than Pukeahua East Dome (mean 27 % vesicle-free). Thin sections are each shown in cross-polarised light and measure 2.6 mm wide.

Major complexes of coalescing domes

The MWC, Tuahu dome and the MEC all contain phenocrysts of plagioclase, quartz, orthopyroxene and minor opaques (Table 4.4). Tuahu dome and the MWC contain only traces of quartz in some thin sections, whereas the MEC contains 1.1 % quartz on average which is present in most thin sections.

No. of samples	Unit	Pl %	Max Pl size (mm)	Qtz %	Max Qtz size (mm)	Amph %	Max Amph size (mm)	Opx %	Max Opx size (mm)	Biot %	Max Biot size (mm)	Opq %	Max Opq size (mm)	Gmass %	Gm sph %	Max shp size (mm)	Vesic %	Max vesic size (mm)
17	MWC (mean)	7.2	2.8	0.1	0.2			0.2	1.1			0.3	0.4	92	19	0.5	9	<1
	MWC (min)	3.0	2.0	0.0				0.0				0.0		86	0		0	
	MWC (max)	13.3	4.1	0.5	0.7			0.7	2.1			1.0	1.2	96	80	2.2	25	1
3	Tuahu	8.2	3	0.1	0.4			0.2	0.9			0.1	0.3	91	18	0.2	4	<1
25	MEC (mean)	9.5	2.8	1.1	1.1	0.1	0.1	0.2	1.0			0.3	0.5	89	49	1.1	10	1
	MEC (min)	4.4	1.6	0.0		0.0		0.0				0.1	0.2	83	0		0	
	MEC (max)	14.3	4.0	3.0	1.8	0.1	.04	0.7	1.5			1.1	1.0	95	100	4.3	50	2.5

Table 4.4 Petrography of domes that comprise MWC and MEC. Percentages of crystals are calculated on a vesicle-free basis. Details as for Table 4.1.

Exposed outcrops of MWC and MEC domes consistently contain relatively low average vesicularities and moderate to low average crystal contents (Fig. 4.1). The MEC lavas have notably higher average spherulite size and content than the MWC lavas and Tuahu dome. An overall lower quality grade (for analytical purposes) is found for the samples from the more spherulitic domes (Appendix 3). Within the MWC, the domes making up the southwestern third of the complex, and also View dome, display relatively higher alteration/weathering compared to the rest of the domes in the complex.

Central and southern Maroa isolated domes

Acacia dome complex domes (Mokauteure, Mokauteure North, Mokauteure East and Palm domes) all contain moderate amounts of plagioclase, orthopyroxene and amphibole +/- quartz, relative to Maroa in general (Table 4.5). Mokauteure and Mokauteure East domes contain amphibole, while Mokauteure North and Palm domes do not. Palm and Mokauteure North domes have an average vesicle content of 38 % which is relatively high for Maroa dome lava samples and suggests the exposed areas which were sampled represent an outer vesiculated facies that has been eroded off most other domes.

The Southern dome complex (Dairy, Forest and Forest West domes along the Whangamata Fault scarp, southwest of the Putauaki pyroclastics) and nearby Lowrie and Swampy domes, have crystal contents from 3 to 24 % (Fig. 4.1, Table 4.5). They contain plagioclase and orthopyroxene +/- quartz and all but Dairy dome samples contain amphibole.

No. of samples	Unit	Pl %	Max Pl size (mm)	Qtz %	Max Qtz size (mm)	Amph %	Max Amph size (mm)	Opx %	Max Opx size (mm)	Biot %	Max Biot size (mm)	Opq %	Max Opq size (mm)	Gmass %	Gm sph %	Max shp size (mm)	Vesic %	Max vesic size (mm)
2	Waipakipaki	6.4	1.9	0.3	0.3			0.1	0.7			0.1	0.3	93	0	1.2	7	<1
1	Tutukau	4.0	2.1					0.1	1.1			0.1	0.2	96	35	2.1		
1	Bee Hive	7.4	3.4	2.1	1			0.1	1.3			0.1	0.2	90			5	<1
3	Maroanui	12.2	2.7	2.1	1.5			0.4	0.6			0.4	0.4	85	33	0.5	6	<1
2	Maroanui West	6.1	2.8	0.1	0.5			0.3	1.2			0.1	0.4	93	45	2.0	8	<1
3	Whakapapataringa	5.2	2.5	0.1	0.2			0.1	0.5			0.3	0.4	94	34	1	13	2
4	Pakuri	14.2	2.9	2.3	1.7	0.6	1.1	0.8	1.4			0.3	0.4	82	10	0.4	6	<1
1	Whakapapa	9.2	1.7	2.0	0.8	0.5	0.6	1.0	0.9					87	80	0.6	2	1
1	Dairy	2.9	1.0					0.1	0.4			0.1	0.2	97			30	1
1	Forest	16.3	3.3	2.5	2.1	1.3	1.0	1.3	1.2			0.1	0.3	79			20	1
1	Forest West	5.2	1.5			0.1	0.3	0.1	0.3			0.1	0.4	95	10	0.3	3	<1
1	Lowrie	12.0	2.7	10.7	2.2	0.7	0.8	0.7	0.7			0.1	0.3	76	10	0.4	25	1
1	Swampy	7.4	2.2	4.2	1.5	0.1	2.1	0.1	1.4			0.1	0.6	88			5	<1
2	Palm & Mk.teure N	22.6	3.5					1.3	1.8			0.7	0.4	75			38	<1
2	Mokauteure & E	10.5	1.8	5.1	2.1	0.6	1.3	0.4	1.4			0.1	0.3	83			18	1
1	Kakuki	21.3	5.3	3.8	4.2	0.6	0.5	0.6	0.5	1.3	1.3	0.1	0.4	74			20	1
1	Orakeikorako	21.3	2.5	6.7	3.0	1.3	4.1	0.1	0.6	0.1	0.5	0.1	0.3	70			25	1
1	Puketarata	11.3	3.0	12.5	3.9	0.1	0.8			2.5	1.7	0.1	0.3	76			20	1

Table 4.5 Petrography of smaller Maroa domes. Percentages of crystals are calculated on a vesicle-free basis. Details as for Table 4.1.

In the southeast of Maroa, Pakuri dome complex, Whakapapa dome and Orakeikorako dome all bear amphibole and contain more than 9 % plagioclase (Table 4.5). In contrast Whakapapataringa dome contains only 5 % plagioclase and no amphibole. Orakeikorako dome also bears 1 % biotite and relatively abundant plagioclase (21 %). These differences in plagioclase content are reflected in the plagioclase/quartz ratios in Figure 4.1.

Orakeikorako, Kakuki and Puketarata domes are the only Maroa lavas analysed that contain biotite (Fig. 4.3, Tables 4.1 and 4.5). They contain more than 20 % vesicles which is more than twice that in most other small dome lavas. This suggests that the zone being sampled on these three domes is further towards the exterior of the dome compared to the other samples. These three domes, along with the Acacia dome complex, are the only isolated domes that do not contain spherulites. This is also in agreement with the sample coming from an outer dome facies.

Waipakipaki and Tutukau domes have relatively low crystal contents (< 7 %), bearing plagioclase, orthopyroxene and opaques +/- quartz (Fig. 4.1, Table 4.5). Bee Hive and Maroanui dome complex domes have the same mineralogies but with slightly higher crystal contents (10 and 12 %, respectively). None of these domes contain amphibole or biotite.

4.2.4 Pyroclastics

This is a summary of the results of thin section analysis of juvenile clasts (mostly pumice) from Maroa pyroclastics, the overall characteristics of which were described in Chapter 2. All of the juvenile clasts are porphyritic and hypocrystalline. Crystal contents range from ~ 1 % to 28 %, and vesicularity ranges up to 60 vol.%. Microlites (as defined for lavas) are minor and dispersed.

The characteristics of phenocryst minerals are similar to those described above for Maroa lavas. Crystals within vesicular juvenile clasts, particularly the larger plagioclase and quartz ones, are sometimes broken into many dispersed fragments consistent with pyroclastic fragmentation (cf. some crystals that are coarsely fractured but still relatively intact in Maroa lavas).

(a) Orakeikorako Dome

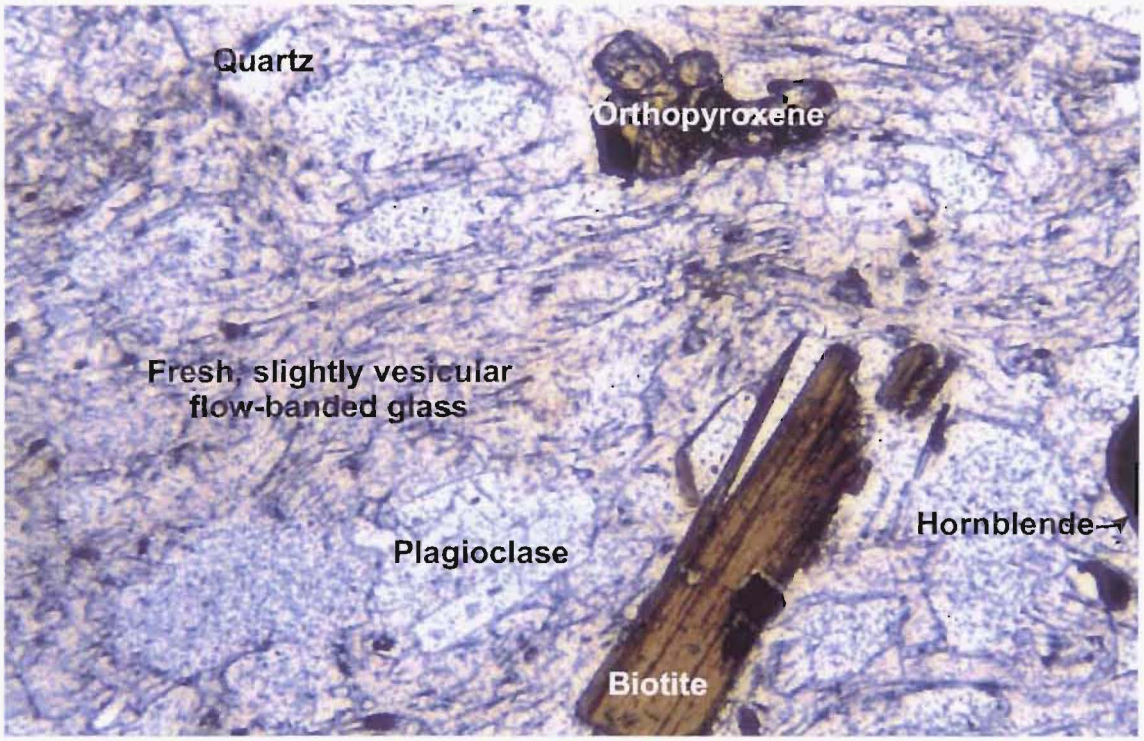

(b) Puketarata Dome

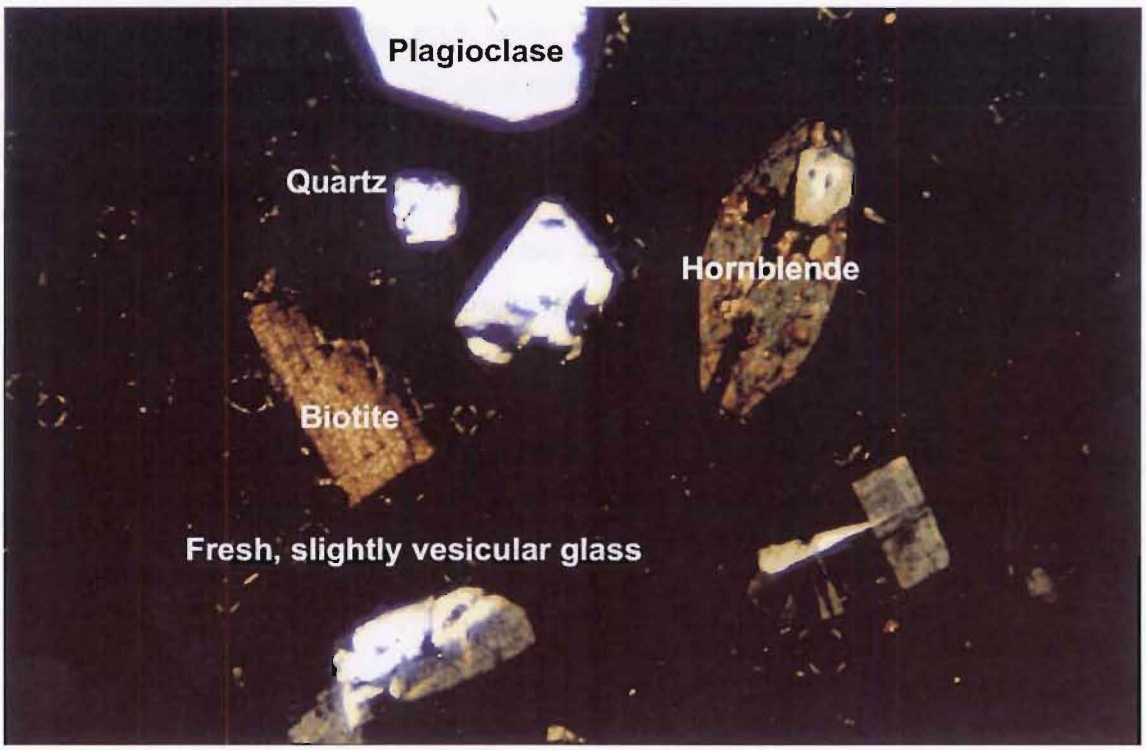

Figure 4.3 Rhyolite lava from (a) Orakeikorako and (b) Puketarata domes in thin section. Both domes contain plagioclase, quartz, biotite and opaque minerals, but note that only Orakeikorako Dome contains orthopyroxene. Together with Kakuki Dome these are the only biotite-bearing Maroa eruptives. Both domes have similar moderate to high crystal contents (Orakeikorako mean 30 % and Puketarata mean 24 %, both vesicle-free). Thin section (a) is shown in plane-polarised light and (b) in cross-polarised light; both measure 2.6 mm wide.

No. of samples	Unit	Pl %	Max Pl size (mm)	Qtz %	Max Qtz size (mm)	Amph %	Max Amph size (mm)	Opx %	Max Opx size (mm)	Biot %	Max Biot size (mm)	Opq %	Max Opq size (mm)	Gmass %	Gm sph %	Max shp size (mm)	Vesic %	Max vesic size (mm)
1	Pre-Atiamuri airfall	5.7	0.2	0.7	1.3	0.1	0.4	0.7	1.0			0.1	0.3	93			30	3
15	Atiamuri pyroclastics	5.0	2.2	0.2	0.3			0.3	0.8			0.1	0.2	94			28	1
1	Atiamuri lithic obsid	6.7	2.3	1.3	1.3			0.1	0.9			0.6	0.5	92			25	1
5	Korotai pyroclastics	2.7	1.6	0.1	0.2	0.1	0.2	0.3	0.4			0.2	0.3	97			19	1
1	Puketarata Tuff	13.3	2.0	8.3	1.8	0.2	1.3			3.3	1.3	0.2	0.2	78			40	2

Table 4.6 Petrography of juvenile clasts from the Atiamuri and Korotai pyroclastics. Percentages of crystals are calculated on a vesicle-free basis. Details as for Table 4.1.

The Atiamuri pyroclastics lie over a sequence of paleosols and airfall units at M272. The lowest exposed airfall unit has a low crystal content (7 %) including plagioclase, quartz, orthopyroxene, amphibole and opaques (Table 4.6).

The Atiamuri pyroclastics themselves (including pumice, denser juvenile clasts, and glassy fiamme) have a low average crystal content of 5 % (individual clasts range from 1 to 11 %, but most contain from 3 to 8 % crystals). They all contain plagioclase and usually orthopyroxene and opaques with occasional trace quartz. None contain amphibole. The fiamme at M339 are fractured fresh obsidian that is virtually aphyric (99 % glass). Sample M13 contains patches of darker glass.

Juvenile clasts in the Korotai pyroclastics all have low crystal contents (obsidian with 1 % crystals, to fiamme with 6 % crystals, Fig. 4.1) and contain plagioclase and minor orthopyroxene and opaques (Table 4.6). Some contain quartz, and fiamme from M53 contain trace amphibole. Juvenile pumice clasts grade in density to obsidian clasts at many outcrops. M176a (pumice) and M176(b) obsidian are mineralogically the same but they contain 3 and 1 % crystals, respectively. Fiamme at M53 are mineralogically the same as pumice and obsidian clasts at other locations. The petrographic difference between the two is that groundmass glass has compacted to dense obsidian which is free of vesicles (Fig. 4.4).

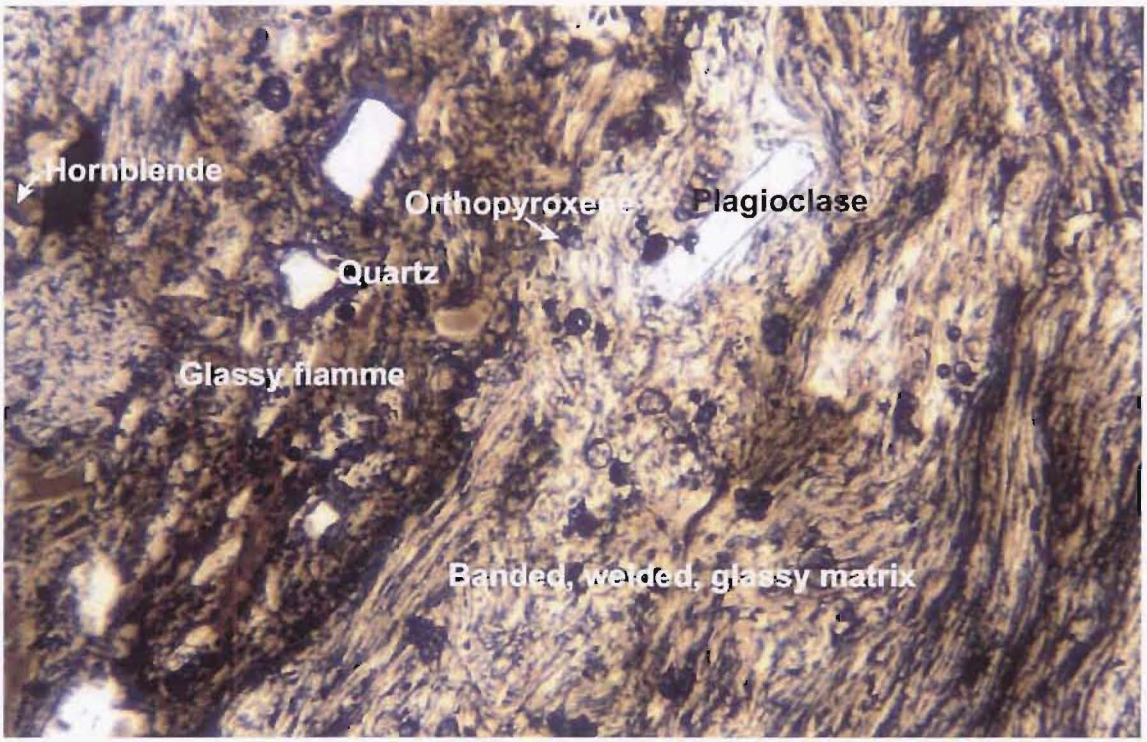

Figure 4.4 Highly welded ignimbrite horizon within the Korotai pyroclastics. Note the presence of plagioclase, quartz, orthopyroxene, hornblende and opaque minerals. The matrix in the highly welded zone is finely banded and glassy with highly elongate glassy fiamme (darker in colour). Pumices in the Korotai pyroclastics generally have a low (mean 3 %, vesicle-free) crystal content. The thin section is shown in plane-polarised light and measure 2.6 mm wide.

Putauaki, Orakonui and Tram Road pyroclastics

No. of samples	Unit	Pl %	Max Pl size (mm)	Qtz %	Max Qtz size (mm)	Amph %	Max Amph size (mm)	Opx %	Max Opx size (mm)	Biot %	Max Biot size (mm)	Opq %	Max Opq size (mm)	Gmass %	Gm sph %	Max shp size (mm)	Vesic %	Max vesic size (mm)
1	**Tram Rd Pclast lg lith**	**12.9**	2.7	**0.1**	0.1	**0.1**	0.5	**1.1**	1.2			**0.1**	0.5	**86**			**7**	1
1	**Tram Rd pyroclastics**	**2.7**	1.7					**0.1**	0.9			**0.1**	0.2	**97**			**25**	1
2	**Orakonui lava lithics**	**10.8**	2.6	**1.1**	1.3			**0.5**	1.0			**0.3**	0.5	**87**	**40**	1.8	**3**	1
2	**Orakonui pclasts**	**11.6**	2.8	**0.3**	0.6			**0.1**	0.9			**0.1**	0.3	**88**			**20**	<1
1	**Putauaki lava lithic**	**7.0**	3.9	**1.0**	1.8			**0.1**	0.8			**0.1**	0.3	**92**	**60**	0.8		
2	**Putauaki pclasts**	**6.7**	1.8					**0.1**	0.7			**0.1**	0.2	**93**			**10**	2

Table 4.7 Petrography of clasts from the Orakonui and Putauaki pyroclastics. Percentages of crystals are calculated on a vesicle-free basis. Details as for Table 4.1.

Both the Orakonui and Putauaki pyroclastics have moderate to low crystal contents (Orakonui pyroclastics 3 to 14 %, Putauaki pyroclastics 7 %, Fig. 4.1). The assemblages are dominated by plagioclase with minor orthopyroxene, +/- quartz in the Orakonui pyroclastics (Fig. 4.5, Table 4.7). In contrast, a pumice sample (M044) from the Tram

(a) Orakonui pyroclastics ignimbrite pumice

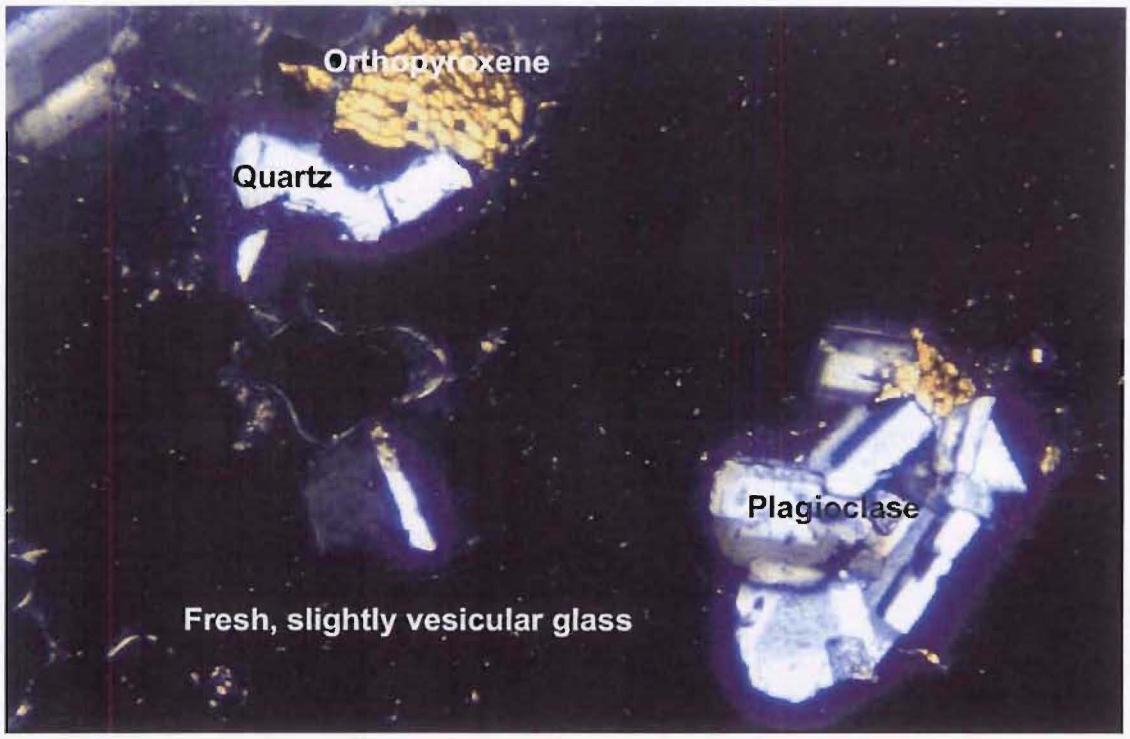

(b) Putauaki pyroclastics ignimbrite pumice

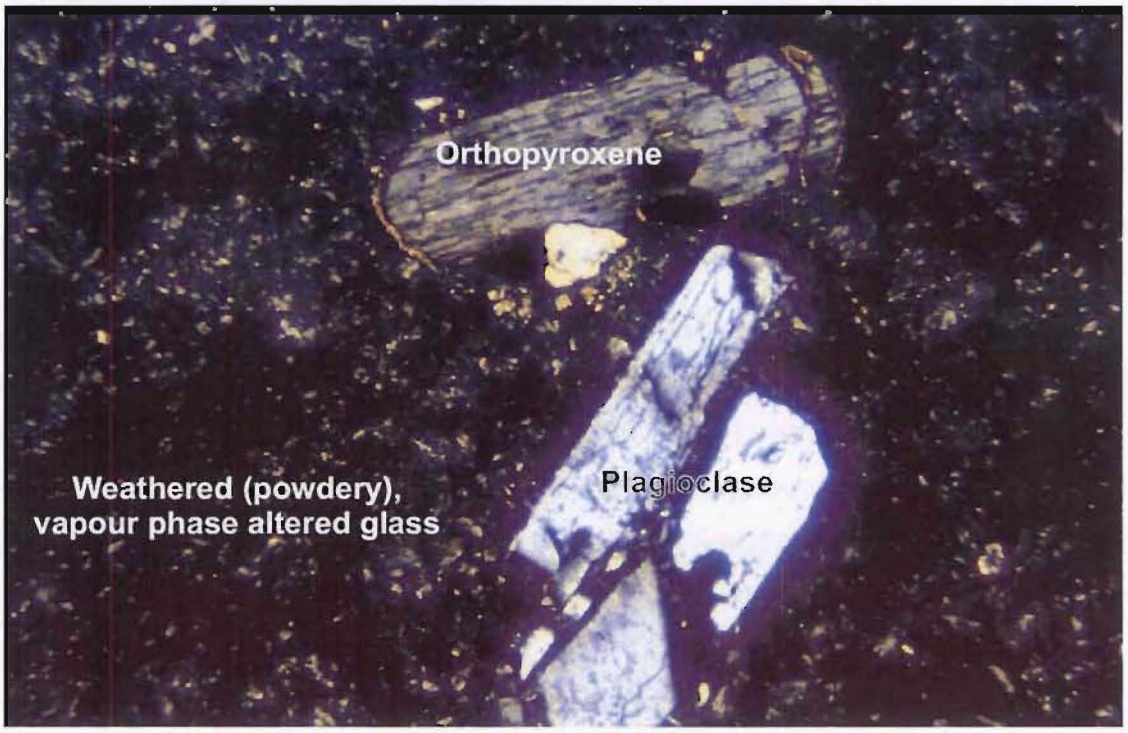

Figure 4.5 Pumice from ignimbrite of the (a) Orakonui and (b) Putauaki pyroclastics in thin section. Both contain plagioclase, orthopyroxene and opaque minerals, but note that only Orakonui pumice contains quartz. Orakonui pumice groundmass is reasonably fresh, slightly vesicular glass, whereas Putauaki pumice groundmass glass is vapour phase altered and weathered to a powder. As a result of the weathering any structure or vesicularity cannot be discerned in Putauaki pumice groundmass. Both pumices have similar moderate to low crystal contents (Orakonui mean 12 % and Putauaki mean 7 %, both vesicle-free). Both thin sections are shown in cross-polarised light and both measure 2.6 mm wide.

Road pyroclastics (which lie stratigraphically between the Orakonui and Putauaki pyroclastics) contains a trace amount of amphibole and also relatively fine-grained aggregates of plagioclase and orthopyroxene crystals. This sample also appears to have slightly darker streaks in hand specimen.

An ignimbrite lithic in the Orakonui pyroclastics has a similar petrological and hand specimen character to both the Putauaki and Orakonui pyroclastics. Rhyolite lava lithics in both eruptives also have a similar mineralogical character to their hosts.

Pukeahua pyroclastics

No. of samples	Unit	Pl %	Max Pl size (mm)	Qtz %	Max Qtz size (mm)	Amph %	Max Amph size (mm)	Opx %	Max Opx size (mm)	Biot %	Max Biot size (mm)	Opq %	Max Opq size (mm)	Gmass %	Gm sph %	Max shp size (mm)	Vesic %	Max vesic size (mm)
1	Pukeahua lg N	8.8	2.4	1.3	1.7			0.1	0.8			0.6	0.5	89	80	0.4	20	2
3	Pukeahua NW fan	6.0	2.4	2.1	1.5			0.1	1.0			0.1	0.3	92			12	1
5	Pukeahua SW fan	5.5	1.7	0.4	0.6			0.2	0.8			0.1	0.3	94			26	1
2	Manawa lg	4.3	2.4					0.1	0.8			0.1	0.3	95			28	
3	Pukeahua NE fan	16.9	2.8	6.7	2.3	0.6	2.9	0.5	1.4			0.3	0.3	75			16	1
1	Puk SE fan (seen in outcrop under SW)	15.3	4	4.7	6	0.1	1.5	0.1	1			0.6	2	79	40	1	15	4
1	Pukeahua SE fan	17.8	2.1	4.4	2.1	0.6	0.8	0.6	0.7			0.1	0.3	77	1	0.2	10	<1

Table 4.8 Petrography of clasts from the Pukeahua pyroclastics. Percentages of crystals are calculated on a vesicle-free basis. Details as for Table 4.1.

Juvenile clasts from deposits in the northwestern and southwestern quadrants of the Pukeahua pyroclastics fan contain plagioclase, orthopyroxene and opaques, +/- quartz in the SW fan (Table 4.8). The western half of the fan does not contain amphibole and has a moderate to low crystal content (average 6 %). Manawa ignimbrite, within the gorge of Manawa Stream in the southern part of Pukeahua SW fan, has similar petrography to that of the bulk of the fan.

Juvenile clasts from the northeastern and southeastern quadrants of the Pukeahua pyroclastics fan also contain plagioclase and orthopyroxene, but contain much more abundant quartz and, more significantly, amphibole than the western half. The eastern half of the fan has significantly higher crystal content (average 21 to 25 %) than the western half (Fig. 4.1).

Pumice clasts from an ignimbrite (M80, U17/733052) in the centre of the north side of the Pukeahua fan have an amphibole-free petrography similar to that of the western half of the fan, and to the Atiamuri pyroclastics. However, the field character of this ignimbrite is more akin to the Atiamuri pyroclastics than to those of the Pukeahua fan (pink with a more densely consolidated matrix than most Pukeahua material).

Location M63 on the boundary of the southwestern and southeastern fans is an outcrop of two ignimbrite units separated by a fines-poor, possibly airfall, layer. The lower unit contains amphibole, while the upper unit does not. Based on the presence of hornblende in the lower ignimbrite this may be the contact between the two halves of the fan. The lower layer is likely to be part of the eastern fan while the upper layer is part of the western fan.

Airfall deposits

No. of samples	Unit	Pl %	Max Pl size (mm)	Qtz %	Max Qtz size (mm)	Amph %	Max Amph size (mm)	Opx %	Max Opx size (mm)	Biot %	Max Biot size (mm)	Opq %	Max Opq size (mm)	Gmass %	Gm sph %	Max shp size (mm)	Vesic %	Max vesic size (mm)
1	M56 airfall	7.8	1.8	0.6	0.9			0.1	1.5			0.1	0.3	91			10	1
1	M134 airfall	8.2	2.3					0.1	1			0.1	0.2	92			15	1
1	M148 airfall lower	4.7	2.5					0.1	1.3			0.1	0.2	95			15	1
1	M148 airfall upper	4.0	2.1					0.1	0.4			0.1	0.2	96			25	2
1	M148 airfall obsidian	6.2	2.3			0.2	0.4	0.2	0.4			0.2	0.2	93			35	<1
1	M233 airfall	8.3	2.6	1.7	1			0.2	0.8			0.2	0.3	90			40	2
1	M258 airfall	10.0	2.8	2.9	1.5			0.1	0.7			0.1	0.4	87			30	<1

Table 4.9 Petrography of clasts from airfall units. Percentages of crystals are calculated on a vesicle-free basis. Details as for Table 4.1.

Locally-derived airfall deposits in the Maroa area all have moderate to low crystal contents (4 to 13 %, Fig. 4.1). Pumice clasts from airfall units at location M148 at the south end of the Pukeahua fan, and from M134 further north, contain plagioclase, orthopyroxene and opaques (Table 4.9). An obsidian clast within the M148 airfall units has the same petrography as the pumices but also contains traces of amphibole. Reworked airfall units on Ohakuri Rd, south of Goldies dome and atop Roy North dome have the same basic petrography as the three pumices above, but also contain some quartz. Airfall pumice clasts are all vitric, with no spherulites visible, and have varied

vesicularity (10 to 40 % vesicle space, Table 4.9). The Ohakuri Rd airfall is relatively dense-pumice-rich, as is the lowest unit at M148.

4.2.5 Summary of petrography of other key eruptives

Post-Oruanui Taupo eruptions

Following is a summary of petrographic data for post-Oruanui eruptions from Taupo, including the Taupo eruption, from Sutton et al. (2000). Juvenile rhyolite pumices are all low in crystal content (2 to 5 %). All contain plagioclase, orthopyroxene, magnetite and ilmenite, in order of decreasing abundance. Augite occurs in significant abundance in the four eruptions from 11800 to 9950 years B.P. and apatite and zircon are ubiquitous in trace amounts. Some authors (e.g. Ewart, 1963) report rare traces of quartz. Trace amphibole is found in eruptions at 11800 and 3550 years B.P..

Oruanui pyroclastics

Oruanui petrography is summarised from Sutton (1995). Pumices contain ~ 4 to 13 % crystals and there is a slight decrease in phenocrysts with increase in SiO_2. The mineral assemblage is plagioclase, orthopyroxene, magnetite, ilmenite, quartz and sometimes hornblende. Trace clinopyroxene and biotite are seen in a few samples. Apatite and zircon are present as accessory minerals in all samples. The plagioclase/quartz ratio is generally around 3:1.

Mamaku pyroclastics

Milner et al. (2002b), also defined three types of pumice based on chemistry. The petrographic descriptions of each of these types are summarised here. Type 1 contains 6 to 7 % crystals and < 60 % vesicle space. Plagioclase (4-5 %), quartz (1-2 %), orthopyroxene (0.5 %) and opaques (0.5 %) are ubiquitous. Trace augite and amphibole sometimes occur. Type 2 contains 5 to 7 % crystals and 30 to 60 % vesicle space. Plagioclase (4 %), quartz (1- 2 %), orthopyroxene (0.5 %) and opaques (0.5 %) are ubiquitous. Trace augite sometimes occurs. Type 3 contains 4 to 5 % crystals and < 60 % vesicle space. Plagioclase (4 %), orthopyroxene (1 %) and opaques (0.5 %) are ubiquitous. Quartz (0.5 %), trace augite and trace amphibole sometimes occur.

Ohakuri pyroclastics

This is a summary of petrographic analyses for the Ohakuri pyroclastics conducted by Gravley (2003). The juvenile pumice crystal assemblage is generally plagioclase,

quartz, orthopyroxene and opaques, in decreasing order of abundance. He has identified three pumice types based on geochemistry. Types 1 and 2 are petrologically distinguished from Type 3 by variations in their total crystal content, ratio of plagioclase to quartz crystals and to a lesser extent mineral assemblage.

In general Type 1 and 2 pumices are very crystal-poor (0 to 5 %), whereas Type 3 is relatively crystal-rich (10 to 15 %). The Type 3 pumices have very high plagioclase to quartz ratios and large abundant crystals of orthopyroxene. They also contain minor amphibole and rare biotite. Type 1 pumice has little or no orthopyroxene and a much lower plagioclase to quartz ratio. Some Type 2 pumices have crystal contents 5 to 10 %, and a higher ratio of plagioclase to quartz than the rest of Types 1 and 2, but not as high as Type 3.

D. M. Gravley is currently investigating whether the Ohakuri and Mamaku magma systems were linked in any way (because they are spatially, temporally and geochemically closely related). Geochemically Ohakuri type 2 correlates to Mamaku types 2 and 3, and type 1 of both pyroclastics are very similar. Ohakuri type 3 geochemistry does not correlate to any found in Mamaku pyroclastics. Petrographically Mamaku types 2 and 3 are also very similar to Ohakuri type 2, but the types 1 differ from each other in crystal content, plagioclase/quartz and orthopyroxene abundance.

Mokai pyroclastics

Milner (2001) described the petrography of juvenile clasts in the lower and upper ignimbrites of the Mokai pyroclastics. His findings are summarised here. Mafic blebs are found in all deposits, at all outcrops and stratigraphic levels. Blebs are grey but contain white bands, which Milner suggests indicate that the blebs are the product of magma mingling. Blebs are porphyritic, containing 20 to 25 % crystals in a very fine holocrystalline groundmass. Crystals in these blebs are plagioclase (~ 15 %), orthopyroxene (3.5 %), opaques (2 %), olivine (1 to 2 %) and amphibole (1 %).

The lower ignimbrite unit contains orange, weathered, fibrous pumices with 30 to 40 % vesicle space and 5 to 10 % crystals. The crystals are plagioclase (5 %), orthopyroxene (1 %), clinopyroxene (0.5 %) and opaques (1 %). Quartz is minor (< 1 %).

Pumices from the upper ignimbrite unit are devitrified and moderately to strongly vapour-phase-altered, which partly masks the original character of the clasts. These pumices contain 5 to 10 % preserved crystals which are mostly plagioclase and quartz. Mafic minerals have mostly been destroyed by vapour-phase-alteration and are now only represented by brown spots in the groundmass. Consequently, they are not included in this estimate of crystal content.

Pokai pyroclastics

Pokai juvenile pumice petrography is summarised here from Karhunen (1993). She divides pumices into two types (A and B) based on crystal content. Crystal-poor type A pumices have 2.2 % mean crystal content, whereas type B pumices have 8 % crystal content. Micro-xenoliths of devitrified rhyolite occur rarely. Ignimbrite pumices are best preserved at base and top, and are glassy with nearly spherical vesicles. Vesicularity varies from < 60 % in non-welded to < 10 % in welded ignimbrite. Slightly flattened pumices have ellipsoidal vesicles and in highly flattened pumices the vesicles have collapsed.

Plagioclase makes up 1.6 to 7.6 %, orthopyroxene trace to 0.7 % and opaques trace to 0.6 %. Quartz occurs as trace to 1.3 % of crystals in half of the samples. There are also trace amounts of zircon, titanite and apatite present in some samples. Occasional < 0.8 mm grains of black amphibole and brownish green clinopyroxene also occur. Type B pumices have slightly higher (0.1 to 1.2 %) mafic crystal contents than Type A pumices (trace to 0.8 %).

Western Dome Belt

The following is a summary from Ewart (1967; 1968) and Brown (1994). WDB domes are generally crystal-poor (< 8 %) and contain plagioclase and lesser orthopyroxene. NWDC lavas are less crystalline, with lower plagioclase/quartz ratios, than the WDC lavas. NWDC crystal contents are usually < 3 %, but a few northern domes are a little more crystal-rich; Penguin dome contains 4 to 6 % crystals, and SH1 dome 6 to 7 % crystals. All NWDC domes, other than South dome, and the WDC domes Pokuru, Spencer and Okama, also contain amphibole. The northern NWDC domes Penguin, Maungaiti and Skyline 2 also contain biotite.

Whakamaru group pyroclastics

All of the pyroclastic deposits that make up the Whakamaru group have generally high crystal contents. They contain plagioclase, quartz, orthopyroxene, sanidine, opaques, biotite and amphibole in order of decreasing abundance (Ewart, 1965; Martin, 1965; Briggs, 1976b).

Variations in the crystal contents of Whakamaru group ignimbrites are summarised from Brown et al. (1998). To the west of Whakamaru caldera total whole-rock crystal content increases from 10 % at the base of the lower Mananui ignimbrite to 35 % by the top of Unit A in the upper Whakamaru ignimbrite. It is consistently high, around 35 %, throughout the remaining units B to F. The increase in crystal content correlates to an increase in the ratio of quartz to plagioclase (although plagioclase remains dominant throughout), and an increase in modal biotite and amphibole. Sanidine is only present in the upper units C to F. These vertical variations are also seen through the lower Te Whaiti and upper Rangitaiki ignimbrites of the group (eastern correlatives of the Mananui and upper Whakamaru ignimbrites, respectively, Brown et al., 1998).

4.2.6 Deposit correlation

To allow easy comparison of the mineralogy of Maroa eruptives, Table 4.10 provides a summary from the petrographic descriptions, and summaries from other workers, above. Figure 4.6 presents the distribution of these key mineralogies in the Maroa area.

Whakamaru group pyroclastics are the only Maroa-area eruptives that are sanidine-bearing. They are also one of only a few eruptives which contain biotite (although this group is almost as voluminous as all of the remaining eruptives combined); Orakeikorako and Kakuki domes and the Puketarata dome and tuff ring are the only other biotite-bearing eruptives. The only Maroa eruptives in which biotite is present are relatively young (16.7 to 80 ka, Chapter 3) and this is discussed in the wider context in Chapter 5. Biotite is also present in traces in pumices at a few Ohakuri pyroclastics outcrops. The bulk of the Maroa-area eruptives are either (a) plagioclase-orthopyroxene, (b) plagioclase-orthopyroxene-quartz or (c) plagioclase-orthopyroxene-amphibole(+/-quartz) bearing. The distinction between amphibole-bearing and amphibole-free is probably the most significant aspect of Maroa petrography and is discussed further in Chapter 5.

Characteristic	Lavas	Pyroclastics
Plagioclase and orthopyroxene (+/- rare quartz) only	MWC, Mokai Quarry, Tuahu, Waipakipaki, Tutukau, Whakapapataringa	Pukeahua northwest fan, Atiamuri, M148 & M134 airfall
	Majority of post-Oruanui Taupo magmas Half of Pokai pyroclastics Some WDB domes	
Plagioclase and orthopyroxene, with quartz common	MEC, Ngautuku, Buried, Pohaturoa, Bee Hive, Maroanui	Pukeahua southwest fan, Orakonui (one trace amphibole), Putauaki, Orakonui & Putauaki lithics, M56, M233 & M258 airfall
	Half of Pokai pyroclastics Ohakuri pyroclastics Most Mamaku pyroclastics	
Plagioclase, orthopyroxene (+/- quartz) + amphibole	Pukeahua East & South, Pukeahua East Arc, Mangatutu, Thorpe, Pakuri, Whakapapa, Acacia complex, Southwestern domes	Pukeahua eastern fan, Korotai, Airfall under Atiamuri, M148 obsidian
	Traces in 11800 and 3550 y.B.P. Taupo eruptions Oruanui pyroclastics Some Mamaku pyroclastics Occasional in Pokai pyroclastics Majority of WDB domes	
Plagioclase, orthopyroxene (+/- quartz) + amphibole & biotite	Orakeikorako, Kakuki, Puketarata	Puketarata
	Rare in Ohakuri pyroclastics Some Whakamaru group pyroclastics A few WDB domes	
Plagioclase, orthopyroxene (+/- quartz) + sanidine, amphibole & biotite	Some Whakamaru group pyroclastics	
Plagioclase, orthopyroxene (+/- quartz, amphibole) +clinopyroxene	four Post-Oruanui Taupo magmas Mokai pyroclastics Some Mamaku pyroclastics Occasional in Pokai pyroclastics	

Table 4.10 Summary of Maroa area deposit mineralogy.

4.3 Whole rock geochemistry - sample quality

Whole rock geochemical data was obtained using XRF and TIMS techniques as described in Appendices 4.1 and 5.1, respectively. The sample quality codes (reflecting the degree of weathering of samples), as described in Chapter 3, are compared to the samples' geochemistry here. All of the Maroa geochemical data can be found in Appendices 4.2 and 5.2. All analyses are recalculated on a volatile-free basis.

There is, at most, only a slightly elevated Na_2O content in samples of lower quality (Fig. 4.7(c)). There is also a very slight increase in the concentration of K_2O in samples with lower sample quality (Fig. 4.7(a)). Samples M078a and M078b, which are from

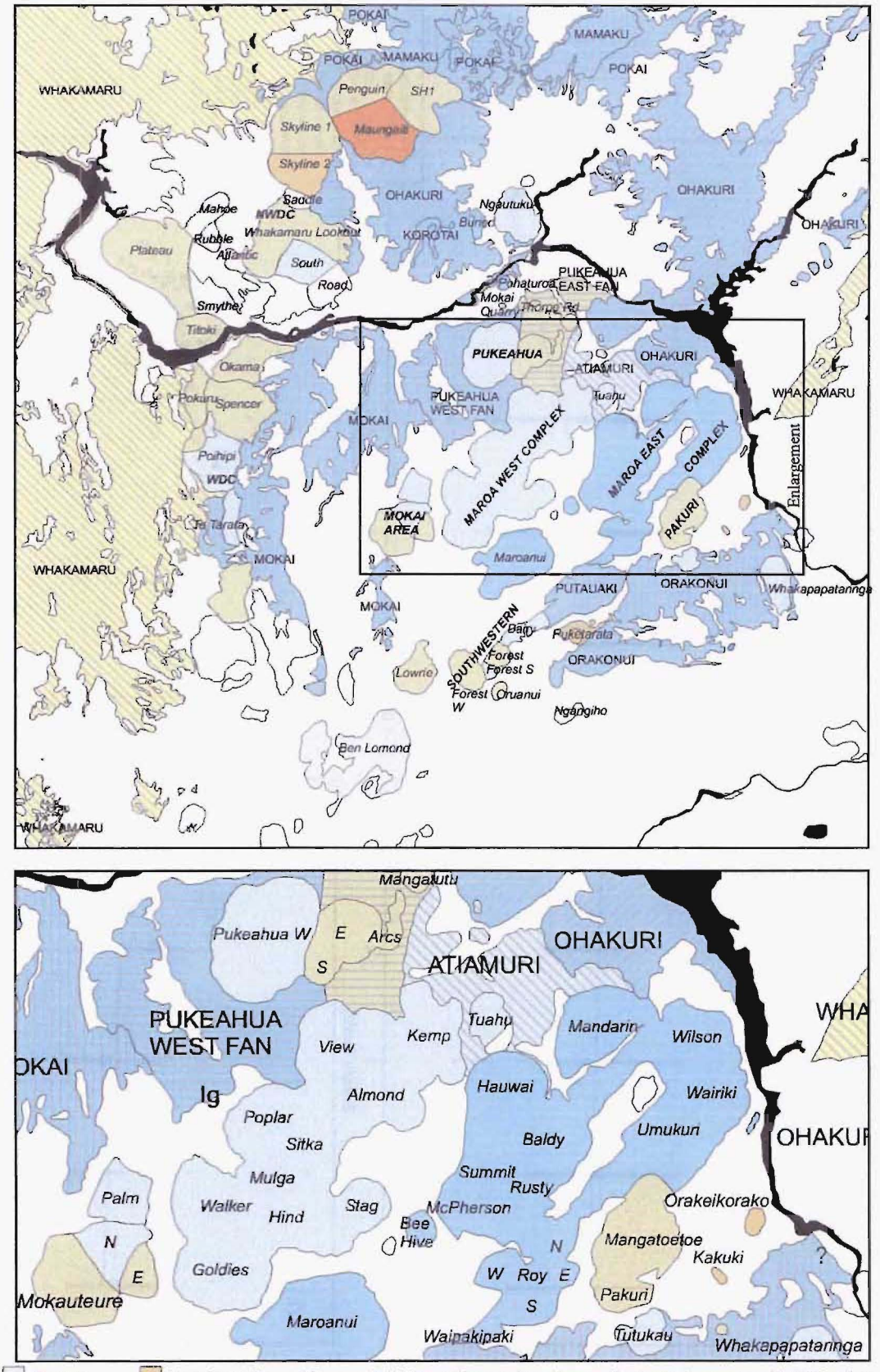

Figure 4.6 Map of key mineralogy of selected groups of MVC related deposits. Hatching distinguishes pyroclastics, with their names in capitals. Names of domes are italicised in lower case. Dome complex names are italicised in capitals. Inset (MWC/MEC domes) is enlarged below.

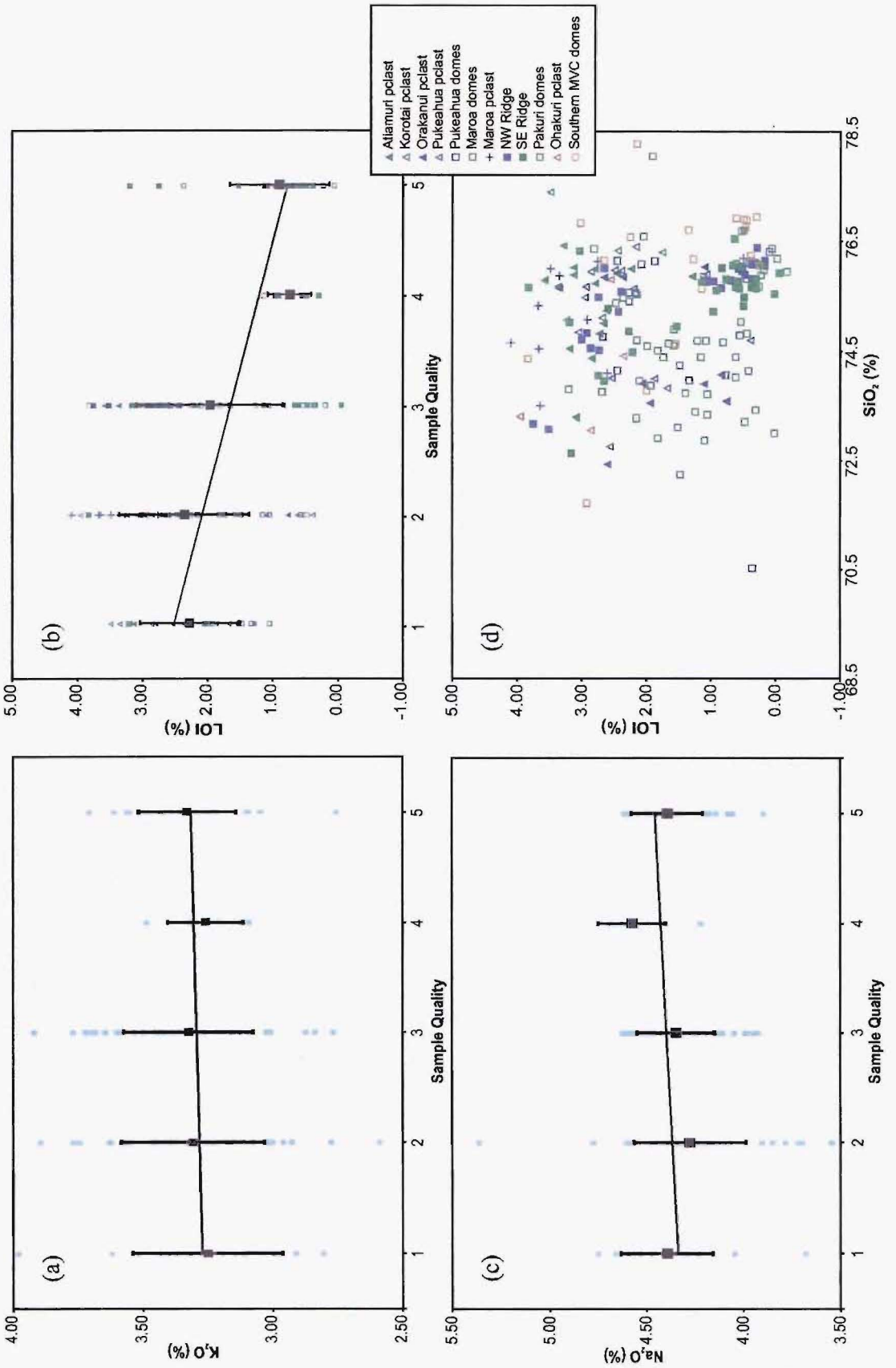

Figure 4.7(a), (b) and (c) K_2O, LOI and Na_2O, respectively, plotted against sample quality. (d) LOI plotted against SiO_2(water-free). Black squares in (a) through (c) are average values, error bars are 1 s.d.. LOI is Loss on Ignition. Sample quality code corresponds to increased degree of weathering (see text).

(a) Ngautuku Dome (M078a) - less weathered (grade 3)

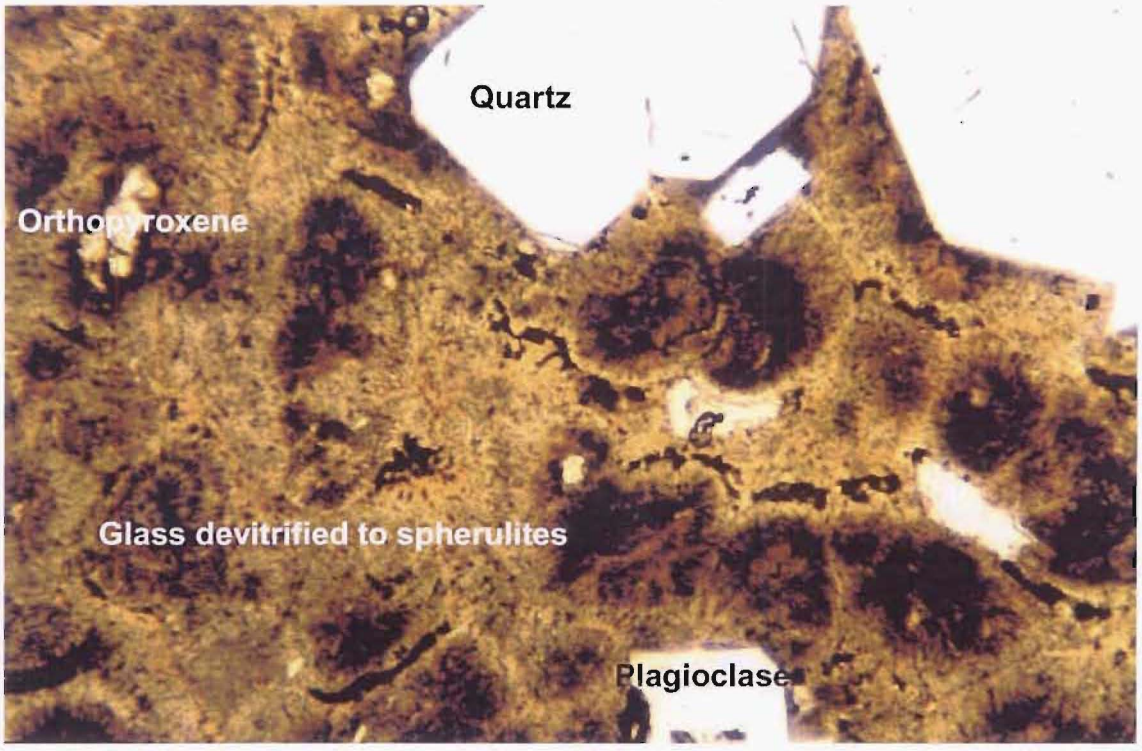

(b) Ngautuku Dome (M078b) - more weathered (grade 5)

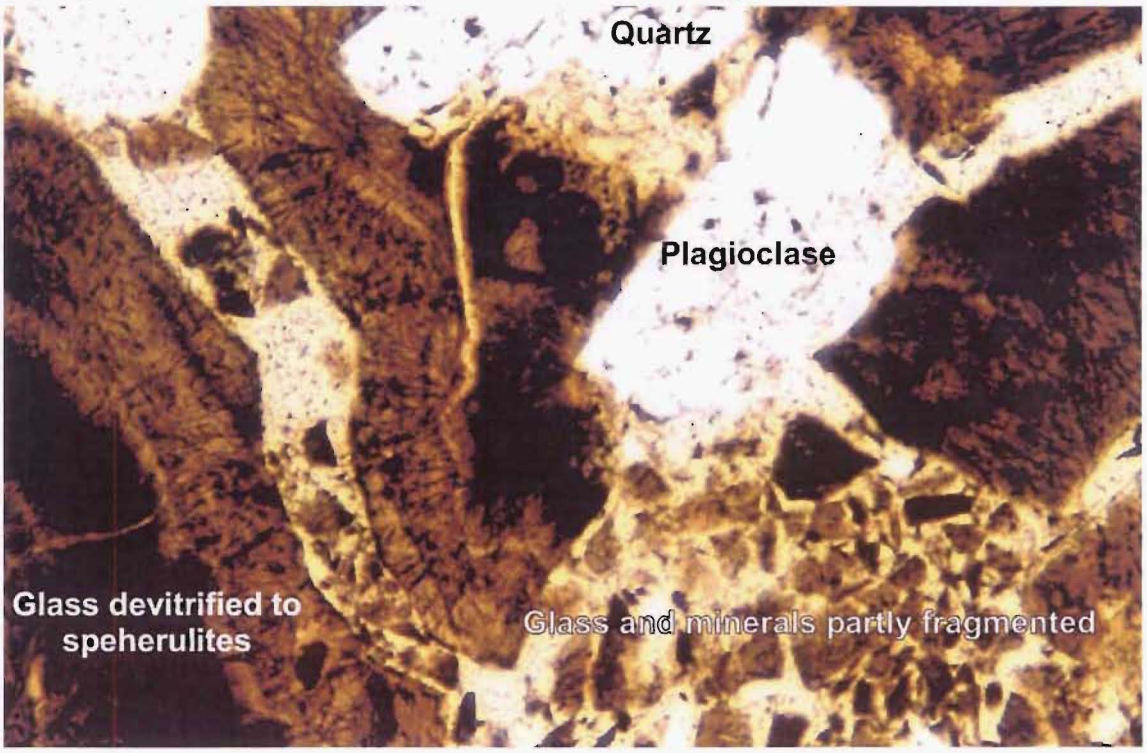

Figure 4.8 Rhyolite lava in thin section from Ngautuku Dome at location M078: (a) less weathered sample M078a (weathering grade 3) and (b) more weathered sample M078b (weathering grade 5). Ngautuku Dome contains plagioclase, quartz, orthopyroxene and opaque minerals. Note that in (b) the groundmass is partly fragmented due to weathering, but this has little or no effect on the results of chemical analysis (see text). Thin sections are both shown in plane-polarised light and both measure 2.6 mm wide.

within 10 m of each other on Ngautuku (western) dome, show grade 3 and 5 weathering, respectively (Fig. 4.8). The more highly weathered M078b had the higher K_2O content (3.44 vs. 3.37 %). For both Na_2O and K_2O, however, the slight positive correlation (a rise of < 0.1 % from quality code 1 to 5) to decreasing sample quality is dwarfed by the range of concentrations (> 0.5 %) of both oxides within each quality code. Note that analytical random error (precision) for the XRF used is only ~ 0.01 wt.% for each of these oxides at these concentrations, and is thus ignored in discussion here.

Figure 4.7(b) shows Loss on Ignition (LOI) plotted against sample quality for all samples analysed. There is a moderate negative correlation of LOI to decreasing sample quality. LOI is the result of a decrease in weight of the sample at the time of fusion, balanced against any addition due to oxidation of Fe (minimal in most of these rhyolitic samples). It may be due to water loss or fusion of some of the sample at ignition[1]. Fresh glass and igneous minerals will not combust, but some weathered material will. The lower LOI for lower quality samples here is probably because sample qualities 4 and 5 represent spherulitic and more weathered rhyolite. Samples given these codes are predominantly dense lava, as pumiceous material would have generally disintegrated and eroded away before reaching these levels of weathering. By contrast quality codes 1 to 3 are applied to samples with a much higher proportion of pumiceous material. Pumiceous samples usually contain more water bound within their glass and the loss of this water is probably what is elevating the LOI for samples of quality 1 to 3 relative to 4 and 5. There is no clear correlation of SiO_2 content to LOI (Figure 4.7 (d)).

In summary: (a) the effect of sample quality on the concentration of the mobile elements K and Na appears to be negligible and (b) LOI shows a moderate negative correlation to sample quality and no correlation to SiO_2 content. Therefore, samples of lower quality are inferred to have had, at most, only slight weathering-induced alteration of the concentration of any element analysed.

[1] 'Ignition' refers to the melting of the fluxed sample at 1050 °C, in preparation for XRF analysis.

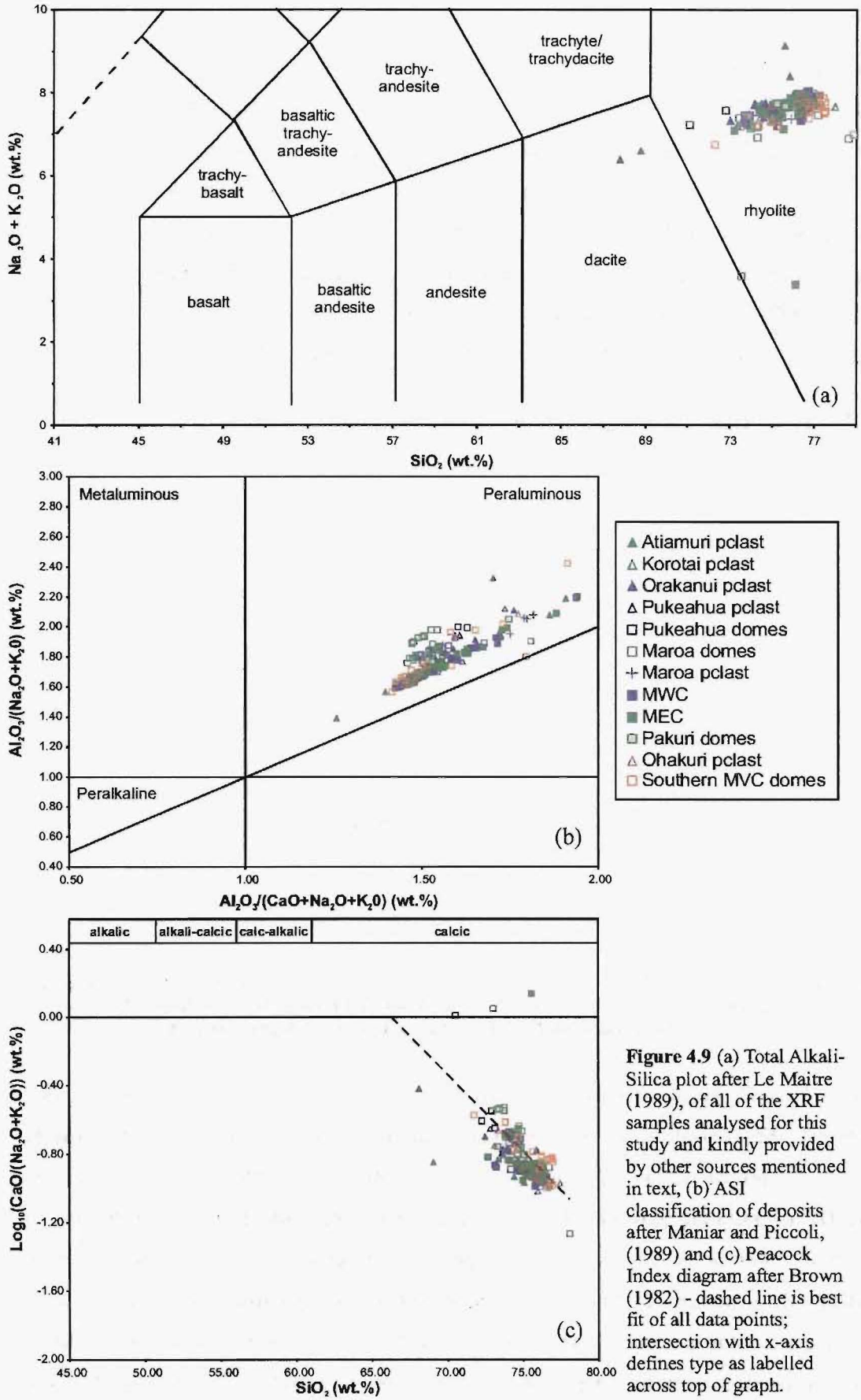

Figure 4.9 (a) Total Alkali-Silica plot after Le Maitre (1989), of all of the XRF samples analysed for this study and kindly provided by other sources mentioned in text, (b) ASI classification of deposits after Maniar and Piccoli, (1989) and (c) Peacock Index diagram after Brown (1982) - dashed line is best fit of all data points; intersection with x-axis defines type as labelled across top of graph.

4.4 Whole rock geochemistry - classification of samples

Nearly all dome lavas and pyroclastics are rhyolites, as classified using the Total-Alkali vs. Silica (TAS) system of Le Maitre et al. (1989) (Fig. 4.9(a)). Two samples are classified as dacites, although they are towards the high-SiO_2 end of this field. These are juvenile clasts from the Atiamuri pyroclastics (M13) and the Tram Rd pyroclastics pyroclastics (M44). For comparison to rhyolite systems elsewhere in the world, all Maroa eruptives are classified as peraluminous following the Aluminium Saturation Index (ASI) classification diagram of Maniar and Piccoli (1989) (Fig. 4.9(b)), and as calcic using the Peacock Index diagram (Brown, 1982) (Fig. 4.9(c)).

4.5 Magma types T, M and N defined on Rb-Sr plots

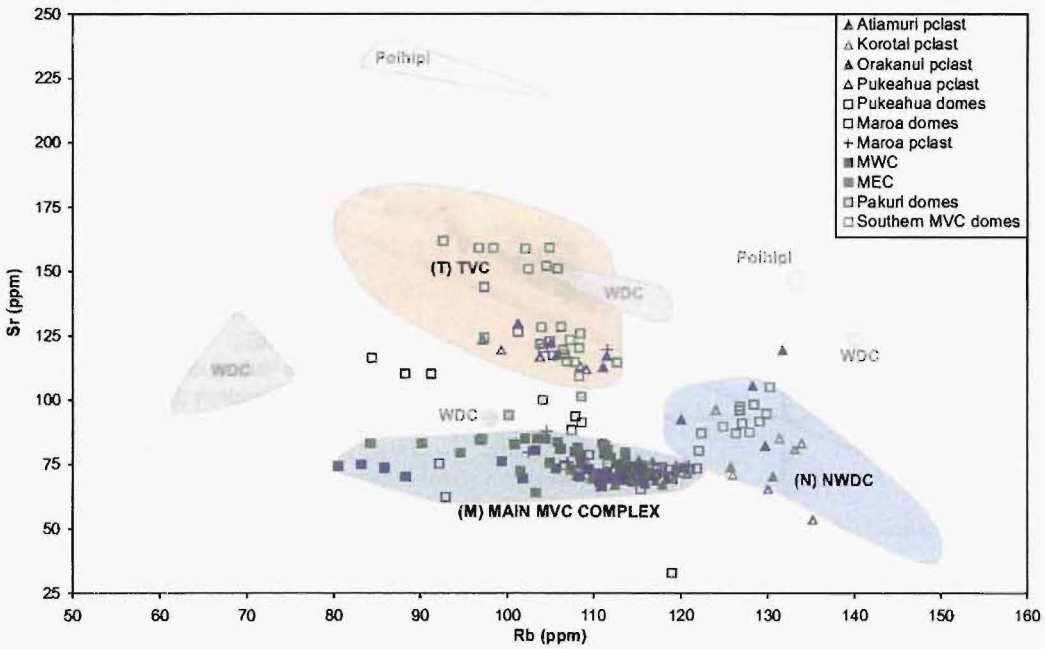

Figure 4.10 Magma types defined on a plot of Rb-Sr concentrations for key Maroa-related eruptives. **T-type (Taupo 100-27 ka eruptives), M-type (MWC/MEC) and N-type (NWDC) fields are shown and formally defined based on these elements (see text).**

Before describing the variation of other oxides and elements it is important to first introduce the concept of Maroa magma types defined by Rb-Sr variation. The following sections demonstrate that the fields for Taupo (100-27 ka eruptives), MWC/MEC and NWDC magmas are most clearly distinguished from one another in terms of Rb and Sr content. Plotting Sr concentration against Rb concentration (Fig. 4.10) also most effectively distinguishes among the remaining Maroa eruptives. Most of the non-MWC/MEC Maroa analyses clearly show affinities for one of the Taupo, MWC/MEC and NWDC fields on the Rb-Sr plot. The only eruptives omitted from the definition of

these fields are Ben Lomond dome (older than 100 ka) and Poihipi (highly variable chemistry) from Taupo, Penguin dome from NWDC, and all WDC domes (WDC domes plot at varied locations across all three fields and outside of them, Fig. 4.10).

For the purposes of this thesis **'T' (Taupo 100ka-27 ka eruptives), 'M' (MWC/MEC) and 'N' (NWDC) type magmas are defined according to the Rb-Sr plot.** Note though, that the terms T-, M- and N-type magmas refer to a similarity to Taupo (100-27 ka eruptives), MWC/MEC and NWDC magmas, respectively, on the Rb-Sr plot ONLY. There is varied correlation of Maroa eruptives to Taupo and NWDC fields based on other elements, and this is described in the following sections.

4.6 Whole rock geochemistry - rhyolite major-oxide variations

Figure 4.11 gives a summary of the major oxide contents of key groups of Maroa-related eruptives. Most of the WDB major oxide and trace element analyses presented here have kindly been provided by S. J. A. Brown, mostly from his thesis (Brown, 1994). Some analyses of WDB and a few Maroa eruptives, conducted by G. Corlette, were kindly provided by I. E. M. Smith (University of Auckland) and are shown in Appendix 4. Analyses of Taupo-related eruptives were kindly provided by A. Sutton, mostly from his thesis (Sutton, 1995). Data from all sources has been recalculated to volatile-free. Harker variation diagrams of major oxides plotted against SiO_2 concentrations are shown in Figure 4.12. Fields for the chemistry of (1) 100-27 ka Taupo eruptives (all post-100 ka eruptives fall within this field apart from a few 26.5 ka Oruanui eruption analyses, which have greater elemental variation; thus the 27 ka cut-off), (2) MWC/MEC domes and (3) NWDC domes are shown in Figure 4.12. These allow comparison to the magma types defined above using Rb-Sr distribution of these three fields in Section 4.5. WDC fields are not plotted because their data points are widely scattered across all three fields on each element plot.

A description of the variation of major oxide chemistry follows. Concentrations are described relative to the range of concentrations in Maroa lavas as shown in Figure 4.11, and relative to SiO_2 content as shown in Figure 4.12, all in weight percent. For most units at least two data values have been determined and are presented. In the case of dome complexes single analyses are presented for each dome, unless significant variation from the field for the whole complex is seen, and then additional analyses

have been added. Only one analysis each is deemed representative for each Maroa airfall unit because they all fall within a relatively narrow field.

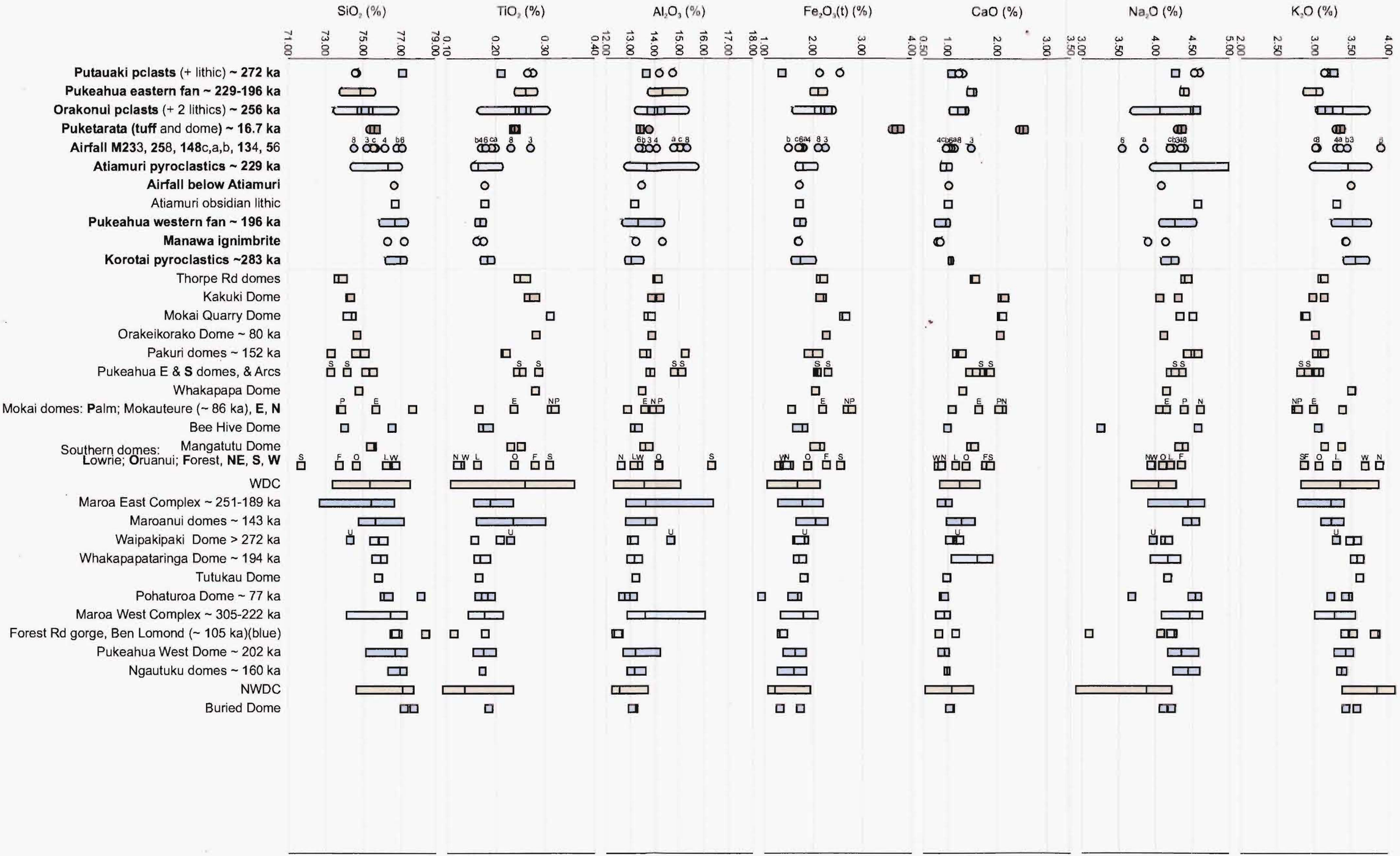

Figure 4.11 Distribution of (a) SiO_2 (b) TiO_2 (c) Al_2O_3 (d) $Fe_2O_3(t)$ (e) CaO (f) Na_2O (g) K_2O for significant groups of MVC-related deposits.Symbol shape represents pyroclastics vs. lavas and colour represents key mineralogical fingerprint. Highlighted letter/number corresponds to label on symbol. Manawa ignimbrite lies within the Pukeahua pyroclastics.

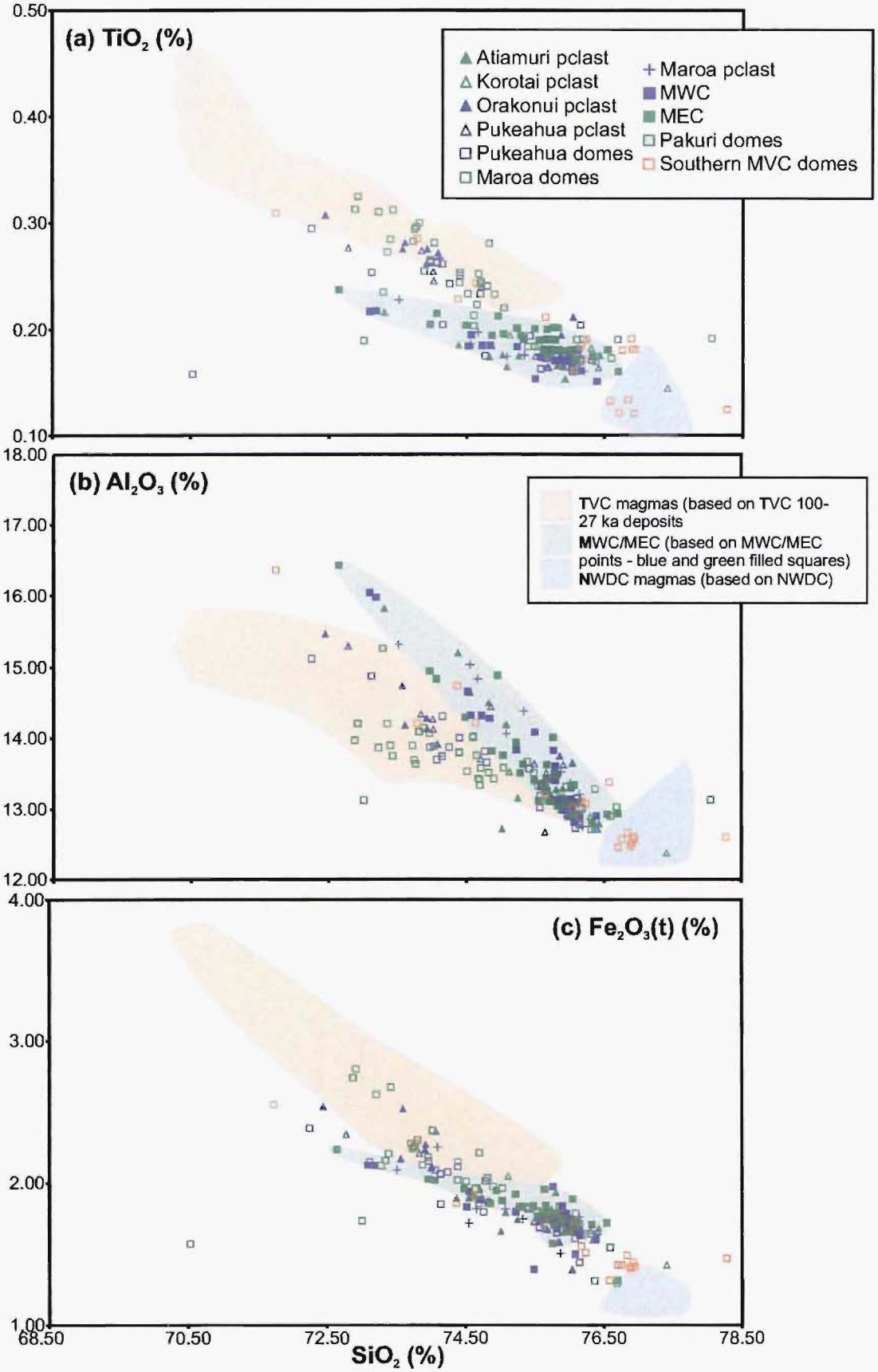

Figure 4.12 (part 1 of 2) (a) to (c): TiO_2, Al_2O_3 and $Fe_2O_3(t)$, respectively, plotted against silica content. Fields for magma types T (TVC 100-27 ka eruptives), M (MWC/MEC points - blue and green filled squares) and N (NWDC magmas, two low- SiO_2 outliers omitted) are shown in orange, green and blue, respectively, and are defined from Rb-Sr plots (Fig. 4.10, above).

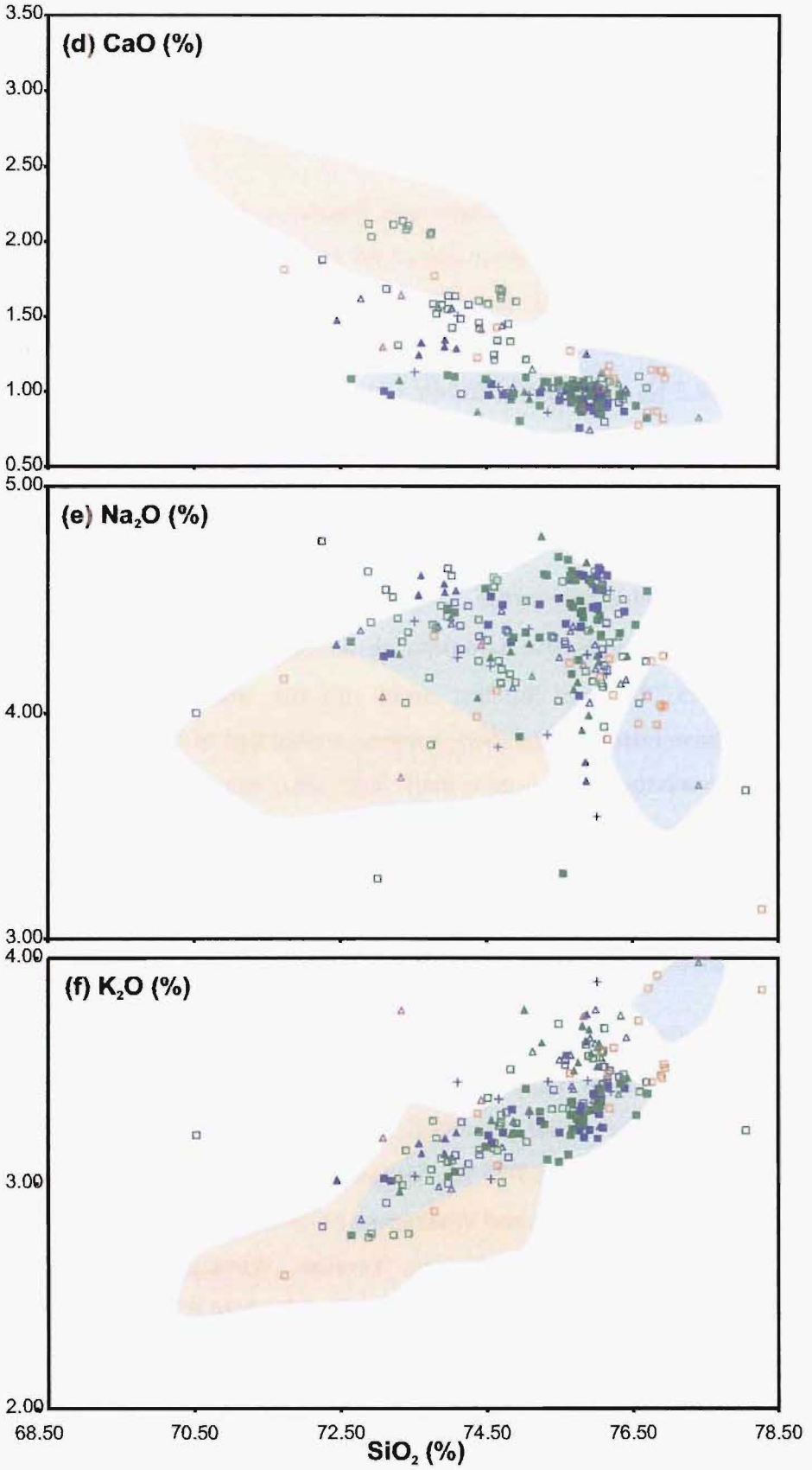

Figure 4.12 (part 2 of 2) (d) to (f): CaO, Na_2O_3, and K_2O, respectively, plotted against silica content.

4.6.1 SiO_2 variation

North Maroa and the Pukeahua area

SiO_2 concentrations (75.4-76.4 %) of Ngautuku and Pohaturoa domes are similar to those of the Korotai pyroclastics. The eastern half of the Pukeahua pyroclastics fan has a lower SiO_2 content (72.7-74.7 %) than the western half (74.9-76.4 %). This corresponds to a higher SiO_2 content in Pukeahua West dome (74.7-76.3 %) than in Pukeahua East (74.0-74.2 %) and South (72.2-73.1 %) domes. The lava arcs east of Pukeahua (74.4-74.8 %) have SiO_2 contents intermediate between Pukeahua West and East domes. Manawa ignimbrite (within the Pukeahua pyroclastics western fan) has a high SiO_2 concentration (75.3-76.1 %) similar to that of Pukeahua West dome.

Atiamuri, Korotai and Orakonui pyroclastics

All of (a) the Atiamuri pyroclastics (74.4-76.0 %), (b) an obsidian lithic from within Atiamuri ignimbrite (75.7 %), and (c) the airfall directly below the Atiamuri pyroclastics (75.7 %) have relatively high SiO_2 contents around that of Pukeahua West dome. The Korotai pyroclastics have a particularly high SiO_2 content (75.1-76.3 %), comparable to this of Buried dome (76.1-76.7 %). Airfall deposits have a range of moderate to high SiO_2 contents (73.5-76.0 %). Both the Putauaki and Orakonui pyroclastics have similar moderate levels of SiO_2 (72.4-73.9 %). The Tram Rd pyroclastics have a relatively high SiO_2 content (75.9 %).

Domes in central and southern Maroa

Palm, Mokauteure North, Mokai Quarry, Kakuki, Orakeikorako, Thorpe Rd and Maroanui West domes all have relatively low SiO_2 contents (72.9-74.0 %). Bee Hive (73-75.5 %), Pakuri dome complex (73.3-75 %), Mokauteure East (74.7 %), Mangatutu (74.4-74.5 %), Puketarata (74.7-74.9 %) and Whakapapa (74.8%) domes have moderate SiO_2 contents. Waipakipaki, Maroanui complex, Tutukau, Whakapapataringa and Mokauteure domes have relatively high SiO_2 contents (74.4-76.6 %, almost all > 75.0 %). MWC (73.1-76.2 %) and MEC (72.6-76.7 %) domes have a wide range of SiO_2 concentrations, though the range and average SiO_2 concentrations of the MWC are both a little higher than those of the MEC.

Forest West and Dairy domes in the Southern dome complex, and Ben Lomond (at the northern end of Taupo) and Lowrie domes, all contain relatively high amounts of SiO_2 (76.2-78.3 %). Forest South dome contains the lowest SiO_2 concentration (71.7 %) of all Maroa units and Forest (73.8 %) and Swampy (74.6 %) domes have moderate SiO_2 concentrations.

Western Dome Belt

WDC SiO_2 concentrations (73.4-75.7 %) are generally lower than those of the NWDC. All but two analyses of NWDC lavas contain 76.5-77.7 % SiO_2. One sample each from two separate NWDC domes contain less SiO_2 (72.9 and 74.7 %), similar to WDC lavas. One WDC dome, and two NWDC domes at Tar Hill on State Highway 1, are intermediate between the NWDC and WDC SiO_2 contents (75.7 to 76.3 %). One WDC dome has relatively high SiO_2 similar to NWDC lavas (77.5 %).

4.6.2 TiO_2, Al_2O_3 and $Fe_2O_3(t)$ variation

Generally TiO_2, Al_2O_3 and $Fe_2O_3(t)$[2] concentrations are higher in Maroa samples with lower SiO_2 concentrations (Fig. 4.12), because the former are all oxides compatible with the minerals crystallising (see earlier sections of this chapter). The relationships between eruptives seen in SiO_2 concentrations are, in most cases, also true for these oxides, but inversely so (i.e. Pukeahua West dome and the western Pukeahua pyroclastics fan both contain high SiO_2 but low TiO_2, Al_2O_3 and Fe_2O_3 (Fig. 4.11).

For these oxides the only marked variation from the relationships described for SiO_2 is in the $Fe_2O_3(t)$ concentrations within Mokauteure North, Palm, Mokai Quarry, Puketarata and a few MEC domes. In all of these samples $Fe_2O_3(t)$ content is relatively high even though these eruptives contain moderate levels of the other oxides (Fig. 4.11). $Fe_2O_3(t)$ contents in Puketarata dome and pyroclastics are especially high, and these are the two Maroa eruptives with the highest biotite content (a variably ferrous mineral).

4.6.3 CaO, Na_2O and K_2O variation

CaO and Na_2O are compatible oxides in Maroa magmas; the concentration of these oxides is generally lower in eruptives with higher SiO_2 contents (Fig. 4.12). However, there is much more overlap in CaO and Na_2O concentration across different Maroa

[2] $Fe_2O_3(t)$ is the total iron oxide in the sample (Fe_2O_3 and FeO), recalculated as Fe_2O_3.

eruptives compared to concentrations of SiO_2, TiO_2, Al_2O_3 and Fe_2O_3(t). This suggests a lesser amount of fractionation of CaO and N_2O relative to these other oxides. K_2O is higher in Maroa eruptives that have higher SiO_2 contents, corroborating petrographic analyses (presented earlier) which show biotite and/or sanidine (minerals with a high partition coefficient for potassium) are generally absent, and potassium is incompatible, in Maroa magmas.

There is a wider range of Na_2O and K_2O concentrations within individual eruptives than the range for other oxides in Maroa eruptives. This gives the distribution pattern of these two oxides in Figure 4.11 a noisier appearance. Samples from Orakonui and some airfall pyroclastics, and from Bee Hive, Ben Lomond (Taupo) and some NWDC domes, have anomalously low Na_2O contents. This variation in K_2O and especially Na_2O concentrations probably relates to a little post-emplacement mobility of these oxides (although it has been demonstrated in Section 4.3 that this mobility is still relatively low overall). Potassium and sodium are relatively easily transported in aqueous solution and may have been slightly altered by meteoric fluid interaction. In most samples unexplained scatter appears to be slight and mostly confined to these two oxides.

4.6.4 Major oxide based fields

This section refers to plots of major oxides against SiO_2 concentration in Figure 4.12. (1) Maroa MWC/MEC, (2) NWDC and (3) Taupo compositional fields are also shown on these diagrams. In terms Rb and Sr content nearly all Maroa eruptives are each demonstrated to have particular similarities to one of these three groups in Section 4.7.6. Atiamuri, Korotai and Maroa airfall pyroclastics mostly lie within the MWC/MEC field for all major oxide plots. On the SiO_2-CaO plot, Orakonui pyroclastics, Pakuri domes and a few other Maroa domes lie at intermediate positions between the Taupo and MWC/MEC fields. Mokai pyroclastics lie within the Taupo field on the SiO_2-TiO_2 plot, but at a distinct low-SiO_2 location outside of all fields on the other plots. Some Pukeahua deposit analyses lie within or near the Taupo field on all of the plots in Figure 4.12. The nature of these relationships is made clearer in trace element plots in Section 4.7.2. Southern Maroa domes, spatially intermediate between Maroa and Taupo, lie across the MWC/MEC and/or NWDC fields in most Figure 4.12 plots.

4.7 Whole rock geochemistry - rhyolite trace elements

Figure 4.13 gives a summary of the trace element contents of key groups of Maroa-related eruptives. Eruptives are separated into lavas and pyroclastics and within these two groups sorted by SiO_2 as a proxy for their level of fractionation. Variation diagrams of rhyolite Zr, Ba, Rb and Sr concentrations plotted against SiO_2 are shown in Figure 4.14. Concentrations of all of the remaining trace elements analysed by XRF (see Appendix 4.2) did not have enough variation to allow meaningful interpretation. Taupo (100-27 ka eruptives), MWC/MEC and NWDC fields are shown for comparison on these diagrams. WDC lavas are not shown because they are scattered across all three fields.

4.7.1 Rb/Sr variation

The Rb/Sr ratios for the key Maroa-related eruptives are plotted against SiO_2 concentration in Figure 4.15. The fields for Taupo (100-27 ka eruptives), MWC/MEC and NWDC are clearly separate from one another on this plot. In contrast, when SiO_2 is plotted against Rb or Sr concentration separately (Fig. 4.14), there is a degree of overlap between these magmas.

The distribution of Rb/Sr ratios across the eruptives shows moderate positive correlation with SiO_2 in most cases (Fig. 4.15). However, some domes (MWC, MEC, Pukeahua East, Pakuri, Mangatutu, and Bee Hive) have Rb/Sr ratios that are not as well correlated with their SiO_2 content (Fig. 4.13), relative to the other Maroa eruptives. Also, the eruptives with the lowest three (Putauaki pyroclastics, Thorpe Rd and Kakuki domes), and highest five (Korotai pyroclastics, Pukeahua West, Ngautuku, NWDC and Buried domes), SiO_2 contents don't have quite as low and high Rb/Sr ratios, respectively, as would be expected from the trend in the right hand column of Figure 4.13. Rb and Sr are partitioned differently in multiple magma batches due to the unique fractionation environment of each part of the system. This indicates Maroa eruptives are not produced from a single fractionating magma body.

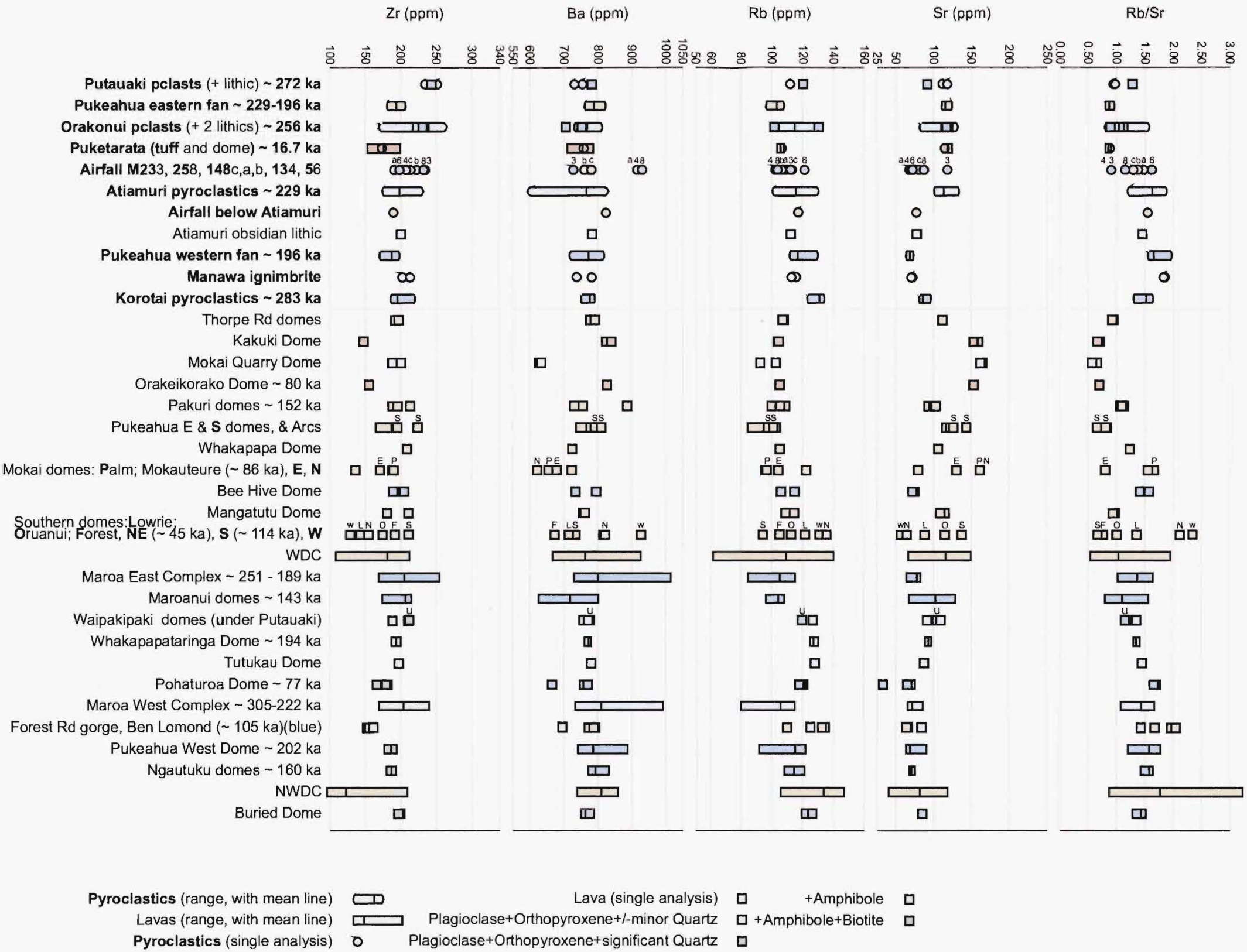

Figure 4.13 Distribution of (a) Zr (b) Ba (c) Rb (d) Sr and (e) Rb/Sr ratios for significant groups of MVC-related deposits.Symbol shape represents pyroclastics vs. lavas and colour represents key mineralogical fingerprint. Highlighted letter/number corresponds to label on symbol. Manawa ignimbrite lies within the Pukeahua pyroclastics.

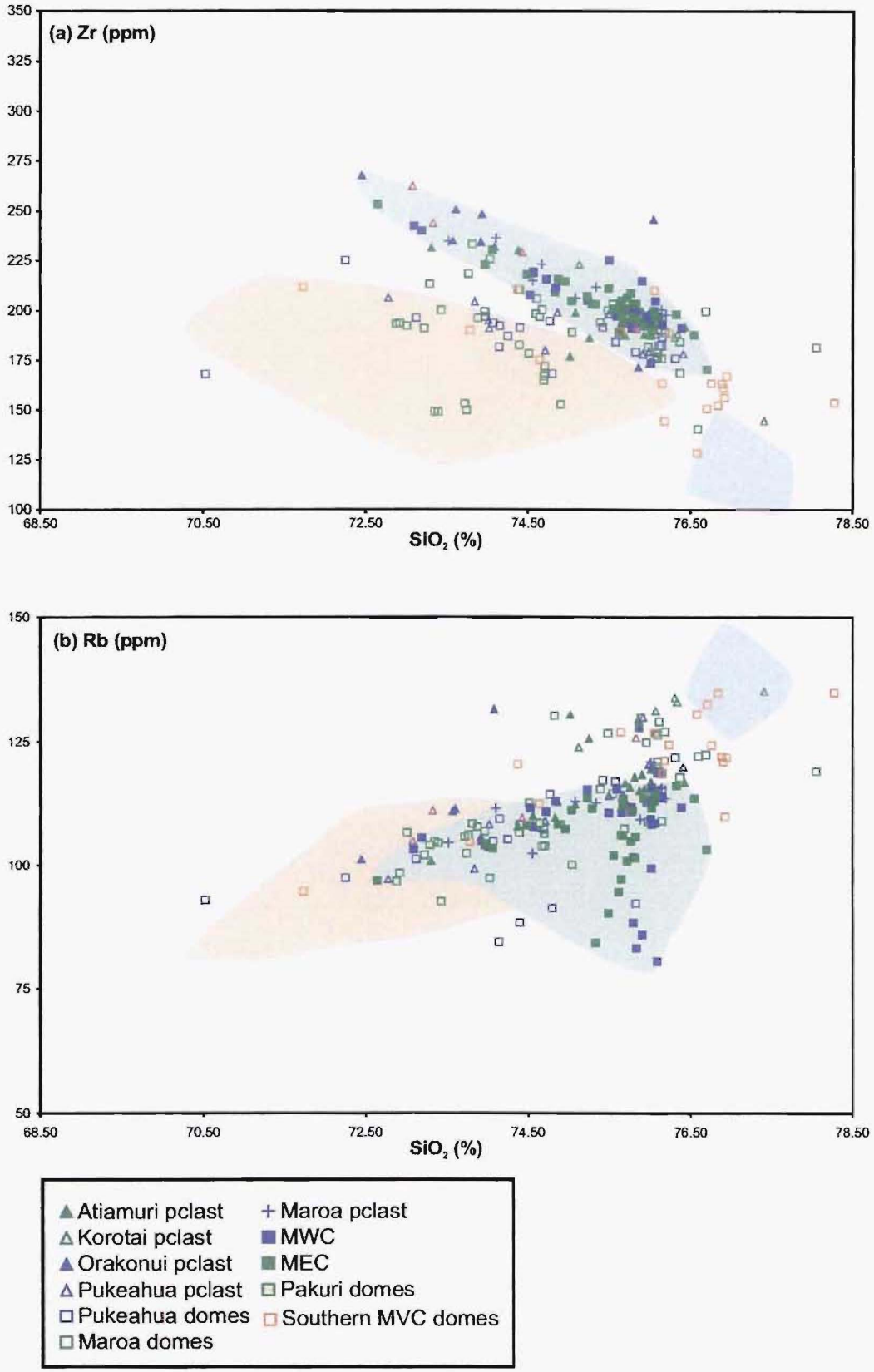

Figure 4.14 (part 1 of 2) (a) and (b): Zr and Rb, respectively, plotted against silica content. Fields for magma types T (TVC 100-27 ka eruptives), M (MWC/MEC points - blue and green filled squares) and N (NWDC magmas, two outliers omitted) are shown in orange, green and blue, respectively, and are defined from Rb-Sr plots (Fig. 4.10, above).

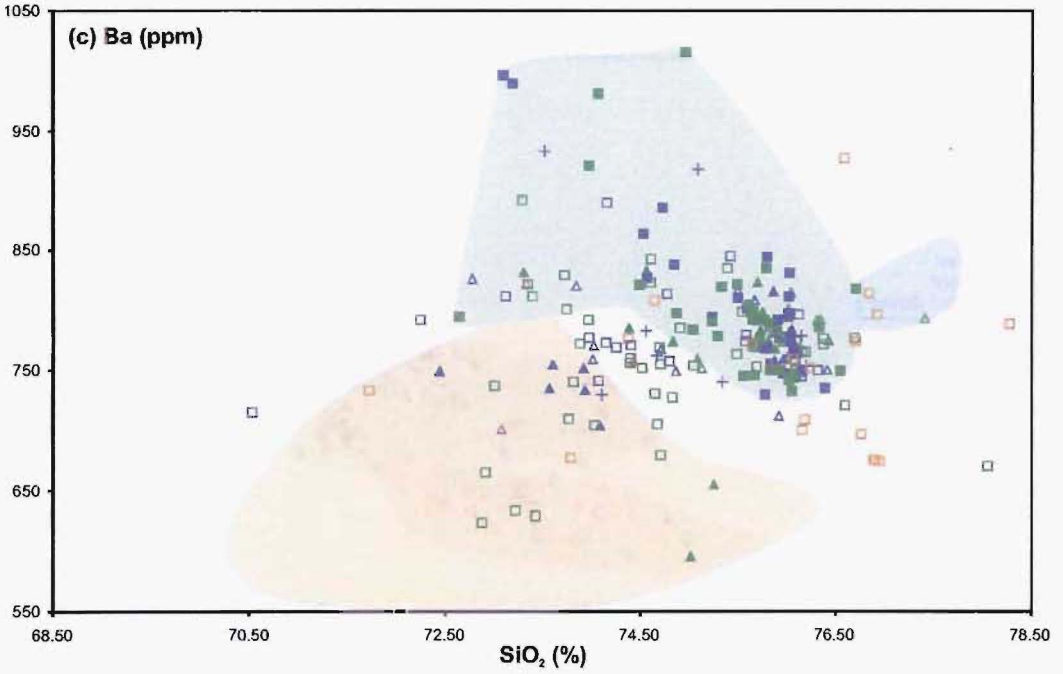

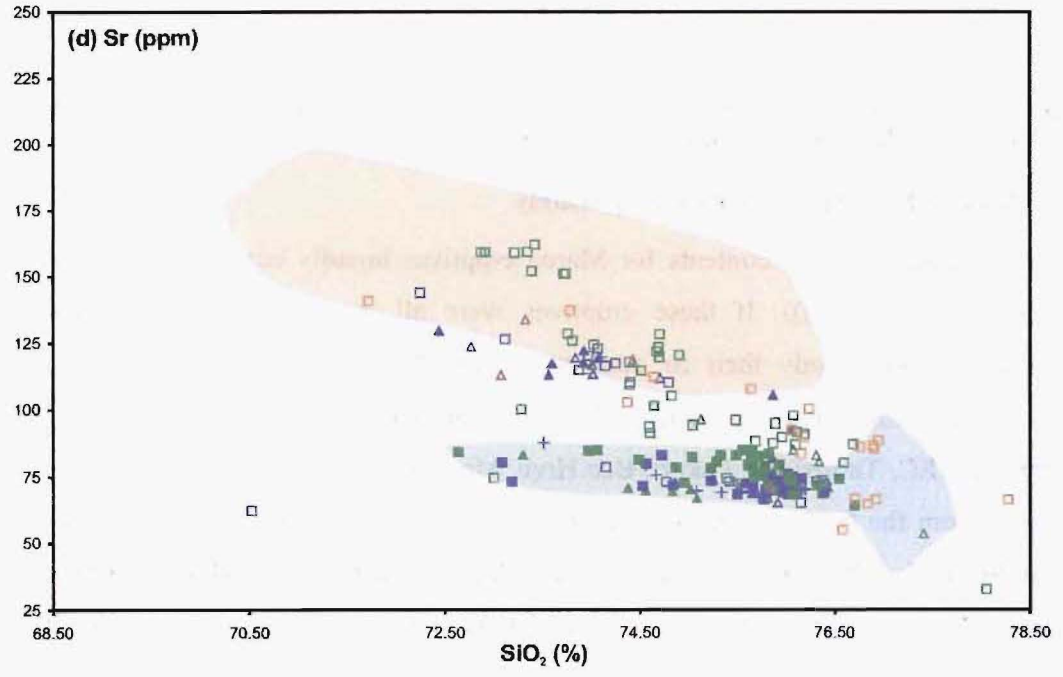

Figure 4.14 (part 2 of 2) (c) and (d): Ba and Sr, respectively, plotted against silica content.

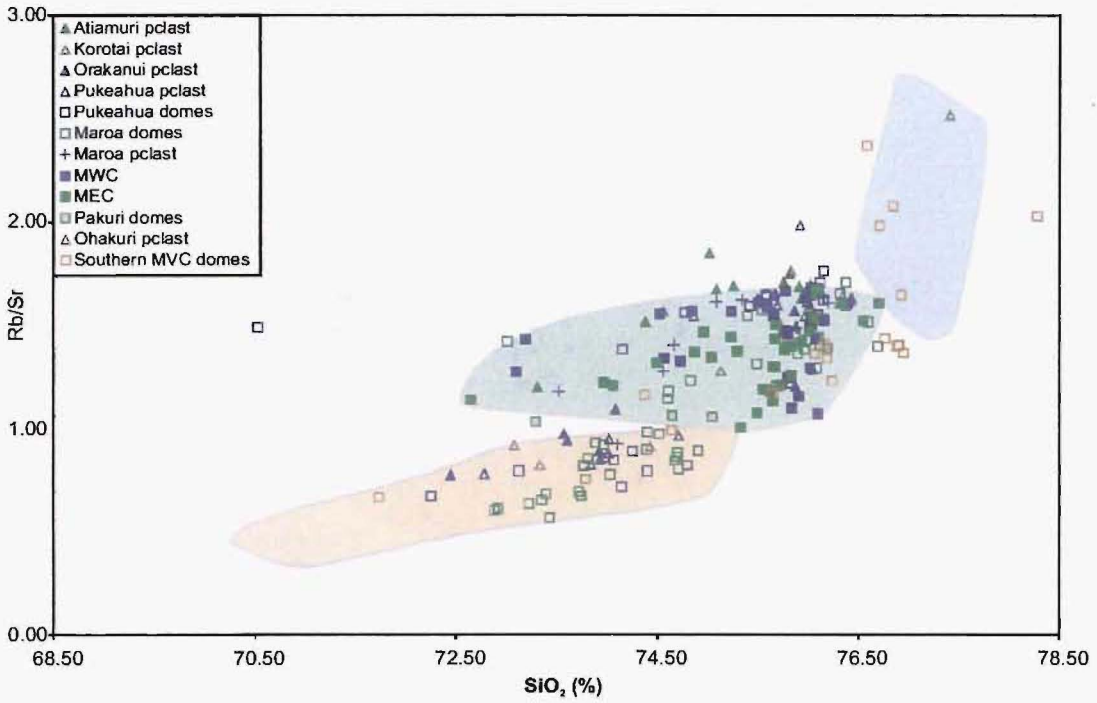

Figure 4.15 SiO_2 concentration plotted against Rb/Sr ratio for key Maroa-related eruptives. Fields for Taupo 100-27 ka, MWC/MEC and NWDC are shown in orange, green and blue respectively.

4.7.2 Rb and Sr variation treated separately

The distribution of the Sr contents for Maroa eruptives broadly correlates negatively with SiO_2 (Fig. 4.14(d)). If these eruptives were all from a single plagioclase-fractionated magma body their Sr contents should decrease in the same order of eruptives as defined by increasing SiO_2. Korotai and Putauaki pyroclastics and Puketarata, MEC, Thorpe Rd, Pakuri, Bee Hive, Mangatutu, NWDC and Buried domes all depart from the Sr concentration that would be expected if such a simple system existed. Similarly, Orakonui pyroclastics and Kakuki, Pukeahua East, MWC and MEC, Maoranui, Pohaturoa, Pukeahua West and Ngautuku domes all depart from the Rb content one would expect (Fig. 4.14(b)).

4.7.3 Zr and Ba variation

Barium concentration variation across all eruptives does not correspond to any regular variation in SiO_2 content (Fig. 4.14(c)). Zr concentration corresponds negatively to SiO_2 content broadly across all Maroa eruptives (Fig. 4.14(a)), and across the field for Taupo magmas. Zr would be expected to fractionate into zircon phenocrysts, so there is probably some zircon fractionation occurring in both Maroa and Taupo magmas. The

concentrations of both of these elements within each deposit generally overlap with one another more than Rb and Sr concentrations do (Figs. 4.10 and 4.16).

Zr concentrations are relatively low in NWDC samples and to a lesser extent in (a) the domes along the southwestern end of Whangamata Fault, (b) Ben Lomond (Taupo), Mokauteure, Orakeikorako, Kakuki domes and (c) Puketarata dome and pyroclastics. Zr concentrations are relatively high in Putauaki pyroclastics. Ba is relatively high in airfall pyroclastics at M134 and M258 and in Pakuri, Forest West, three MEC and two MWC domes. Ba is relatively low in Mokai Quarry, Acacia complex and Dairy domes.

Figure 4.16 shows Ba content plotted against Zr content for Maroa eruptives. 100-27 ka Taupo, NWDC and MWC/MEC fields are clearly distinguished on this diagram. Note that only one Maroa deposit has chemistry lying within the NWDC field, and some Southern dome complex domes have chemistry lying within the MWC/MEC field. This is in contrast to some correlations on the Sr vs. Rb plot described in Section 4.7.6 below and is used to show distinction between Maroa magmas and NWDC magmas in discussion in Section 5.3.6.

4.7.4 Normalised multi-element variation

Figure 4.17 shows a MORB-normalised[3] 'spider diagram' (or normalised multi-element variation diagram, as plotted by Pearce, 1983, and others) of average trace element abundances for key Maroa-related eruptives. Except for P_2O_5 concentration, all of the eruptives plotted have trace element contents very similar to one another, relative to MORB. P_2O_5 scatter is probably due to (a) the low normalising value for this oxide (0.12 %) compared to (b) the low content of this oxide in Maroa-related eruptives (most < 0.1 %), close to the detection limit of XRF (data precision of 0.01 %). Thus slight overall variation in P_2O_5, within he precision range of the XRF, produces a relatively large variation in the normalised value. The samples are LILE enriched and HFSE depleted, relative to MORB, which is a signature of arc-related rocks and is typical of TVZ eruptives (Graham et al., 1995). There is a negative Nb anomaly that is common in subduction related magmas (Weaver and Tarney, 1984).

---

[3] Mid-Ocean Ridge Basalt (MORB) normalisation highlights discrepancies in the concentrations of each element plotted compared to MORB. MORB is used as an analogy for the basalt from which these eruptives have evolved.

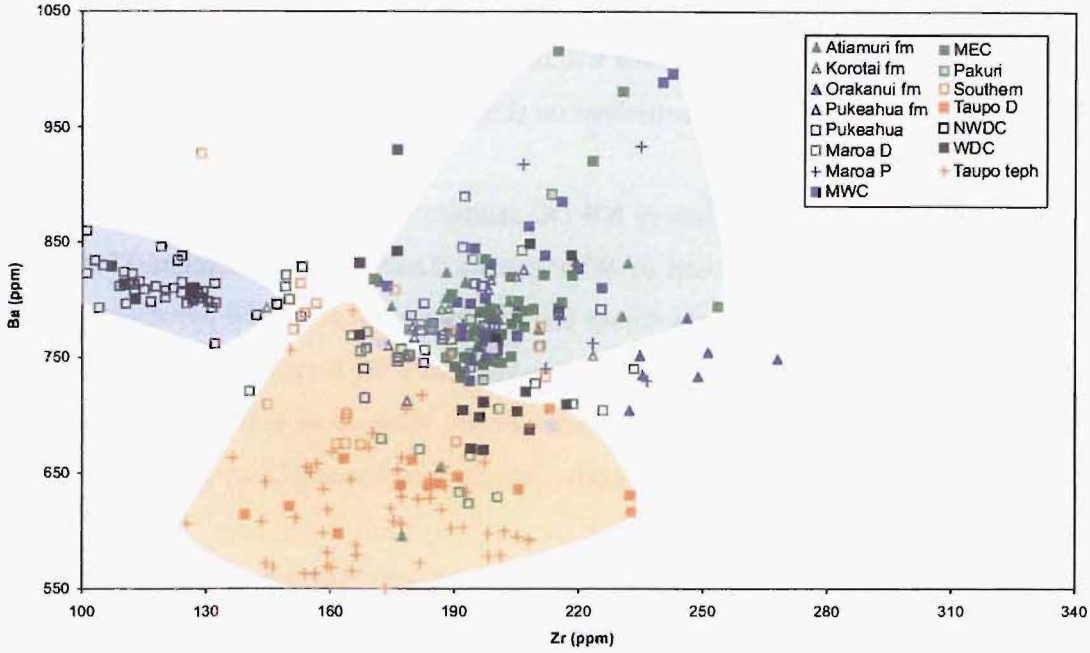

Figure 4.16 Ba content plotted against Zr content for Maroa, NWDC and some Taupo eruptives. Fields for Taupo 100-27 ka, MWC/MEC and NWDC are shown in orange, green and blue respectively.

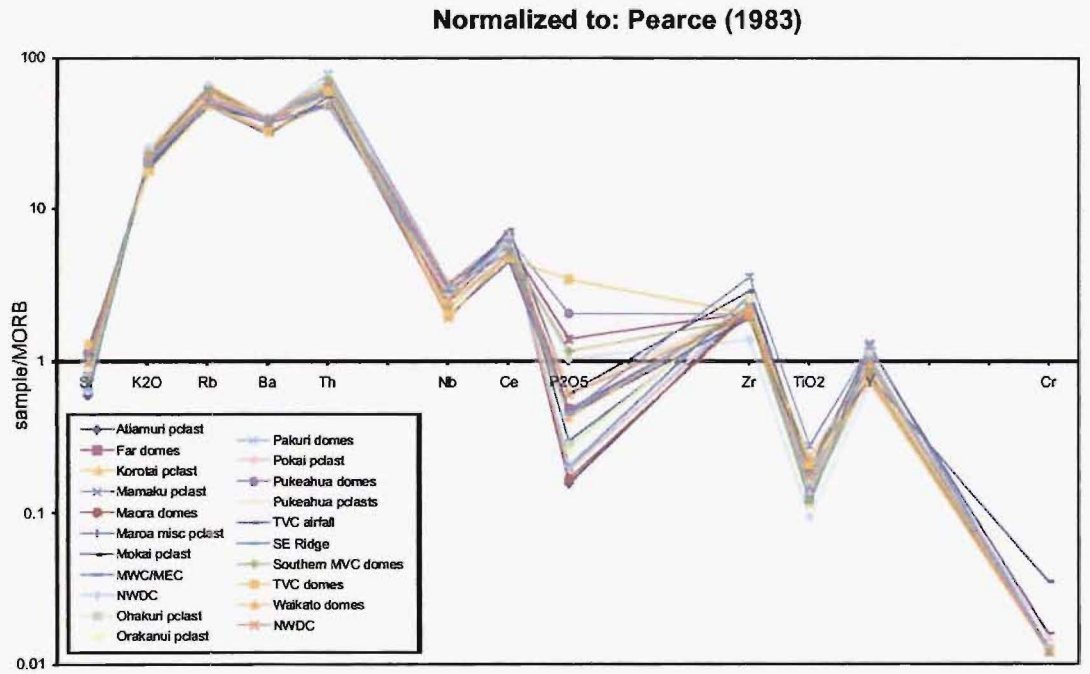

Figure 4.17 Spider diagrams of average trace element concentrations normalised to MORB concentrations from Pearce (1983). Taupo and Waikato river dome values from Sutton (1995) and A. Sutton (pers comm., 2003), and NWDC/WDC values from Brown (1994).

4.7.5 Trace element based groupings

This section refers to trace element variation plots in Figure 4.14. Maroa domes that are not part of MEC or MWC plot across all three fields for Zr, Ba, Rb and Sr concentrations. Maroa airfall pyroclastics plot almost entirely within the MWC/MEC field. The Atiamuri and Korotai pyroclastics plot mostly within the MWC/MEC field. The same is true of Zr, Ba and Rb for Orakonui pyroclastics, but some Orakonui Sr concentrations are closer to those of the Taupo field. Pukeahua dome and pyroclastics points are divided between Taupo and MWC/MEC fields for all four trace elements. Pakuri dome complex points plot between Taupo and MWC/MEC fields. Mokai pyroclastics tend to plot just outside of the low SiO_2 end of the Taupo field.

4.7.6 Magma types T, M and N applied to individual eruptives

Spatial distribution of magma types

Figure 4.18 (a) to (d) presents plots of Rb versus Sr concentration, which show the Maroa-area eruptives in greater detail than Figure 4.10. The three magma type fields are colour coded on Figures 4.10 and 4.18 and these colours are applied to Maroa-area eruptives in Figure 4.19. Low-Sr T-type magmas are orange, M-type are green and N-type are blue. Where the Rb and/or Sr concentration of a deposit is outside of the three main types an additional colour is used. These are (a) light yellow for high-Sr T-type, (b) light blue for low- and high-Sr outliers to N-type, (c) yellow-green for intermediate between T- and M-type and (d) blue-green between M- and N-type magmas.

MWC/MEC

MWC and MEC domes (Fig 4.18(a)) both contain a consistent, relatively low, concentration of Sr from 60 to 85 ppm and a range of Rb contents from 80 to 120 ppm. MEC has lavas plotting across this entire range of Rb concentrations, whereas the area around eastern Goldies dome is the only section of MWC that contains < 100 ppm Rb. The remaining MEC lavas all contain from 100 to 120 ppm Rb. Together MWC and MEC analyses define the M-type magma field (apart from one Pukeahua analysis, discussed later, which defines a section of the low-Sr end of the field).The Pakuri dome complex contains 90 to 100 ppm Sr and 100 to 110 ppm Rb (Fig 4.18(a)). It is one of the few eruptives with a composition intermediate between magma types T and M.

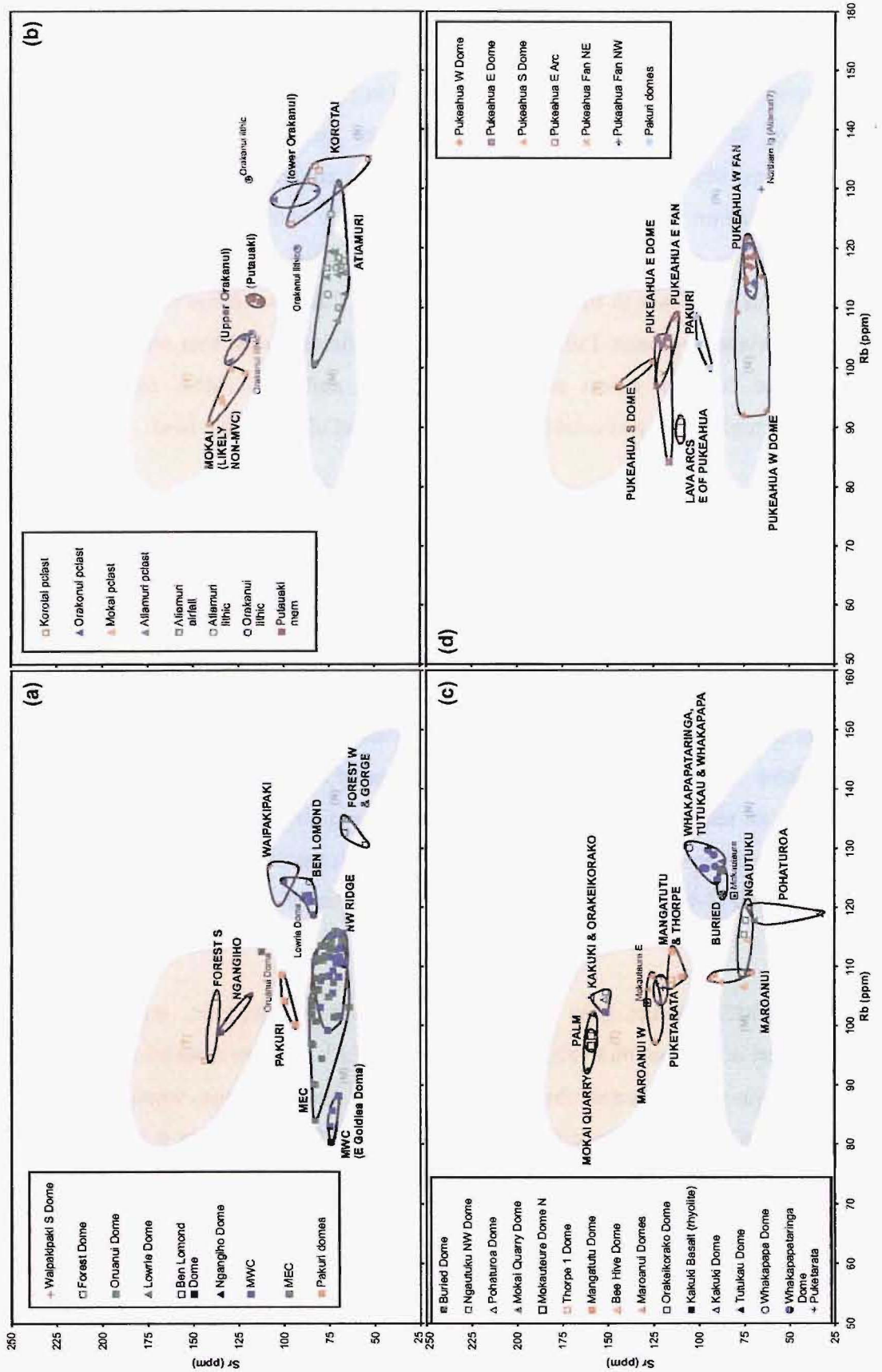

Figure 4.18 (a) to (d): Rb-Sr concentration plots for a variety of MVC deposits (labelled). Fields as for Figure 4.10.

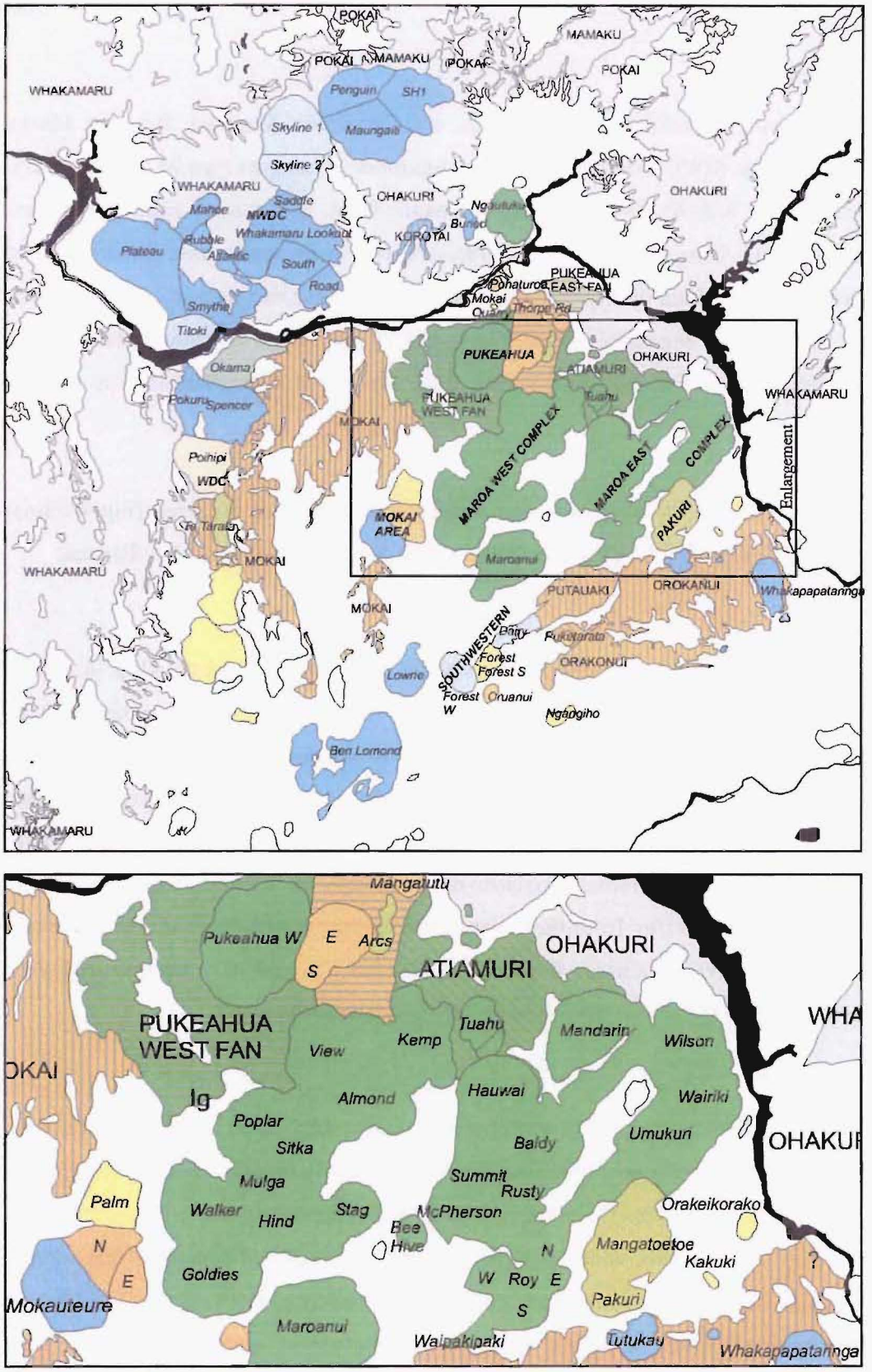

Figure 4.19 Map of Rb-Sr-based magma types for MVC related deposits. Hatched units are pyroclastics with their names in capitals. Names of domes are italicised in lower case. Dome complex names are italicised in capitals. Inset (MWC/MEC domes) is enlarged below.

Other Maroa domes

Maroanui and Ngautuku dome complexes, and Pohaturoa dome are the only Maroa lavas, other than MWC/MEC, that have a composition of magma type M (Fig. 4.18(c)). Mokai Quarry, Kakuki, Orakeikorako, Maroanui West, Mokauteure East, Puketarata, Mangatutu and Thorpe domes (Fig. 4.18(c)) have tightly constrained Rb-Sr content fields that are all within the type T field. Only three of these eruptives overlap with each other. Three of the Maroanui analyses have a few ppm higher Sr content than the M-type field, but they are still much closer in Sr content to this group than to magma type T.

Buried, Mōkauteure, Whakapapataringa, Whakapapa and Tutukau domes (Fig. 4.18(c)) all lie within the field of magma type N and could be used to define its low-Rb end.

Maroa Pyroclastics

Maroa pyroclastic deposits mostly fall into magma types T and N (Fig. 4.18(b)). Orakonui and Putauaki pyroclastics form tightly-defined groups within the field of magma type T. Korotai and Tram Rd pyroclastics lie within magma type N field. Rb-Sr concentrations for three lava lithic samples from the Orakonui pyroclastics are shown on Figure 4.18(b). Two of the three plot well away from Orakonui and Putauaki pyroclastics groups. Of Maroa pyroclastic deposits, only the Atiamuri pyroclastics have Rb-Sr concentrations (for 16 of the 18 analyses) within magma type M. One Atiamuri pyroclastics (a juvenile pumice from massive Atiamuri ignimbrite), and one Atiamuri lava lithic, analysis each lie within the low-Rb end of magma type N.

Pukeahua area

The Pukeahua domes, and the pyroclastics fan surrounding them, can be divided into western and eastern sections. Pukeahua West dome (Fig. 4.18(d)) contains 55 to 75 ppm Sr and 90 to 125 ppm Rb. The western Pukeahua fan deposits contain 70 to 75 ppm Sr and 110 to 125 ppm Rb, which is within the field defined for Pukeahua West dome. Pukeahua East and South domes have Sr concentrations from 115 to 125 and 125 to 145 ppm, respectively (Fig. 4.18(d)). These concentrations are significantly higher than those of the dome and fan to the west. Pukeahua East and South domes have Rb concentrations of 85 to 105 and 95 to 105 ppm, respectively. Deposits of the eastern

half of the Pukeahua fan contain Rb-Sr concentrations closely overlapping those of the East dome.

4.7.7 Maroa magma-type volumes

Table 4.4 presents the erupted volumes and production rates for magmas of each of the magma types. M-type makes up the largest volume (~ 31 km^3), N-type compose the next largest volume (< 15 km^3) and the T-type eruptives total the smallest volume (~ 3 km^3). This is in stark contrast to Taupo, where most eruptions are T-type; the largely-T-type Oruanui magma alone was > 500 km^3.

Type	Age range of eruptions	Duration of activity	Volume erupted	Production rate
M	~ 305 – 77 ka	~ 228 kyr	31 km^3	0.14 km^3/kyr
N	~ 283 – 45 ka	238 ka	< 15 km^3	0.06 km^3/kyr
T	~ 272 – 16.7 ka	~ 255 kyr	3 km^3	0.01 km^3/kyr

Table 4.4 Duration of activity, volume erupted and derived production rate for each of the Maroa magma types. Magma type is defined by Rb-Sr fields for (T)VC 100-27 ka eruptions, (M)WC/MEC eruptions and (N)WDC eruptions.

4.7.8 $^{87}Sr/^{86}Sr$ of selected eruptives

Sr isotope abundances for 19 whole-rock samples were kindly determined by TIMS mass spectrometry at Arthur Holmes Isotope Geology Laboratory, University of Durham, UK, by B. Charlier. Refer to Appendix 5.1 for details of the methodology, and Appendix 5.2 for the raw data.

Figure 4.20 shows the new $^{87}Sr/^{86}Sr$ data plotted against Rb/Sr, along with data for other key eruptives (referenced in the caption). Data fall into three clear $^{87}Sr/^{86}Sr$ groups: (low-$^{87}Sr/^{86}Sr$) from ~ 0.7052 to 0.7053, (moderate-) from ~ 0.7055 to 0.7056 and (high-$^{87}Sr/^{86}Sr$) from ~ 0.7058 to 0.7059. Note that the total range of values is significantly smaller than that recorded at Taupo Volcanic Centre (Sutton et al., 1995) or in the TVZ as a whole (Ewart and Stipp, 1968; Graham et al., 1995). Variation within these groups is mostly in terms of Rb/Sr ratio. The Puketarata sample has $^{87}Sr/^{86}Sr = 0.705039$, distinctly below the low-$^{87}Sr/^{86}Sr$ group. The low-$^{87}Sr/^{86}Sr$ group includes Pukeahua East and MEC magmas (both Maroa), the Mamaku, Ohakuri and Mokai pyroclastics, Ngangiho dome (Taupo) and some WDB lavas. The moderate-$^{87}Sr/^{86}Sr$ group includes the remaining WDB lavas, and New3 airfall and Palm dome

from Maroa. The high-$^{87}Sr/^{86}Sr$ group includes Whakapapataringa dome and the Korotai pyroclastics from Maroa, and the Pokai pyroclastics.

Figure 4.21 shows $^{87}Sr/^{86}Sr$ vs. Rb/Sr for the same analyses as in Figure 4.20, plotted over fields for other selected eruptives (referenced in caption). All data clearly lie at higher $^{87}Sr/^{86}Sr$ than Kakuki basalt (considered the least contaminated basalt erupted in Taupo (Gamble et al., 1993), and much lower $^{87}Sr/^{86}Sr$ than approximate values for Torlesse Greywacke assumed to underlie TVZ (Chapter 1). The Rangitaiki pyroclastics span a range of $^{87}Sr/^{86}Sr$ from low amounts around that of a diorite lithic in the Atiamuri pyroclastics, to low-$^{87}Sr/^{86}Sr$ group; Pre-Oruanui Taupo eruptives and the Whakamaru group pyroclastics span low-moderate $^{87}Sr/^{86}Sr$ groups; the Oruanui and Kaingaroa pyroclastics span moderate-high $^{87}Sr/^{86}Sr$ groups; and post-Oruanui Taupo eruptives lie at distinctly higher $^{87}Sr/^{86}Sr$ than the three groups defined above.

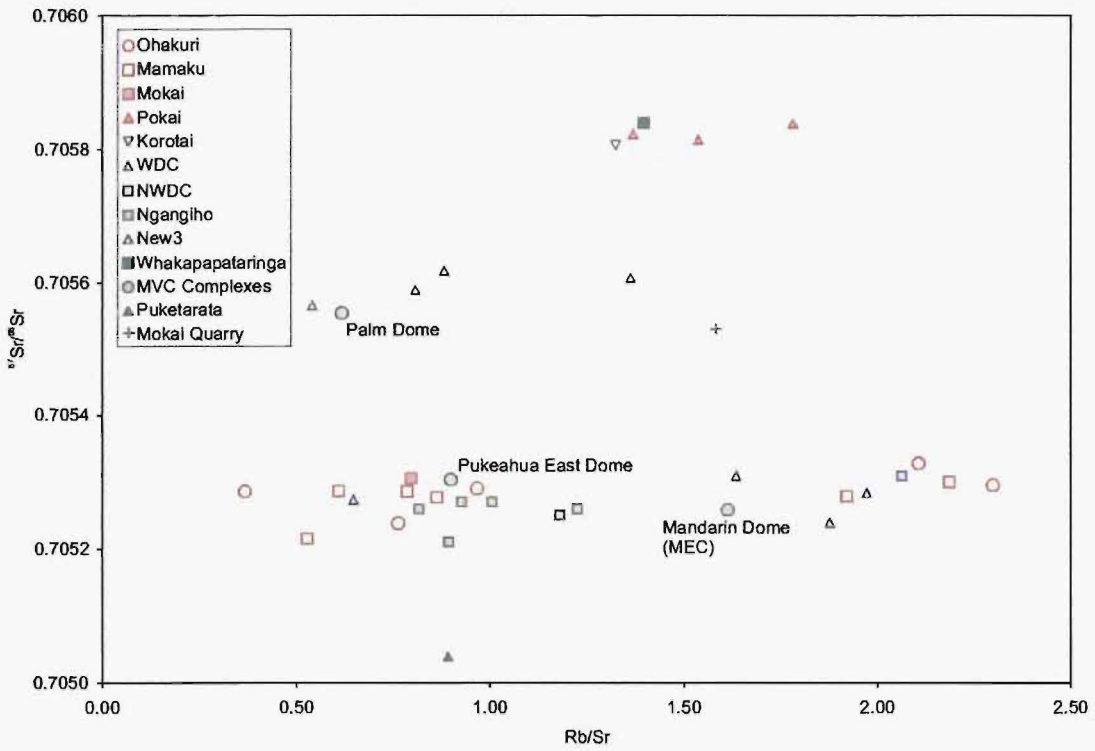

Figure 4.20 $^{87}Sr/^{86}Sr$ plotted against Rb/Sr. Coloured data points are from this study, with the exception of Ngangiho from Sutton (1995), New3 from A. Sutton (written comm., 2003), Whakapapataringa from Brown et al. (1998) and Puketarata and Mokai Quarry (mislabelled Pukeahua in the original paper) from McCulloch et al. (1994).

4.7.9 Comparison of mineralogy with Maroa geochemistry

The mineralogy of Maroa eruptives correlates reasonably well to their geochemistry. Figure 4.22 is a plot of the Rb-Sr concentrations of Maroa eruptives colour coded by

key mineralogy. Samples which contain plagioclase-orthopyroxene+quartz are distributed relatively evenly across the three magma types. The majority of samples containing only plagioclase-orthopyroxene (no quartz) are M- and N-type magmas. Mokai Quarry dome is the only one of this mineralogy that is derived from a T-type magma. Most of the amphibole-bearing eruptives are T-type magmas, but there is no consistent grouping of those which are not. All of the biotite- and cpx-bearing magmas are T-type.

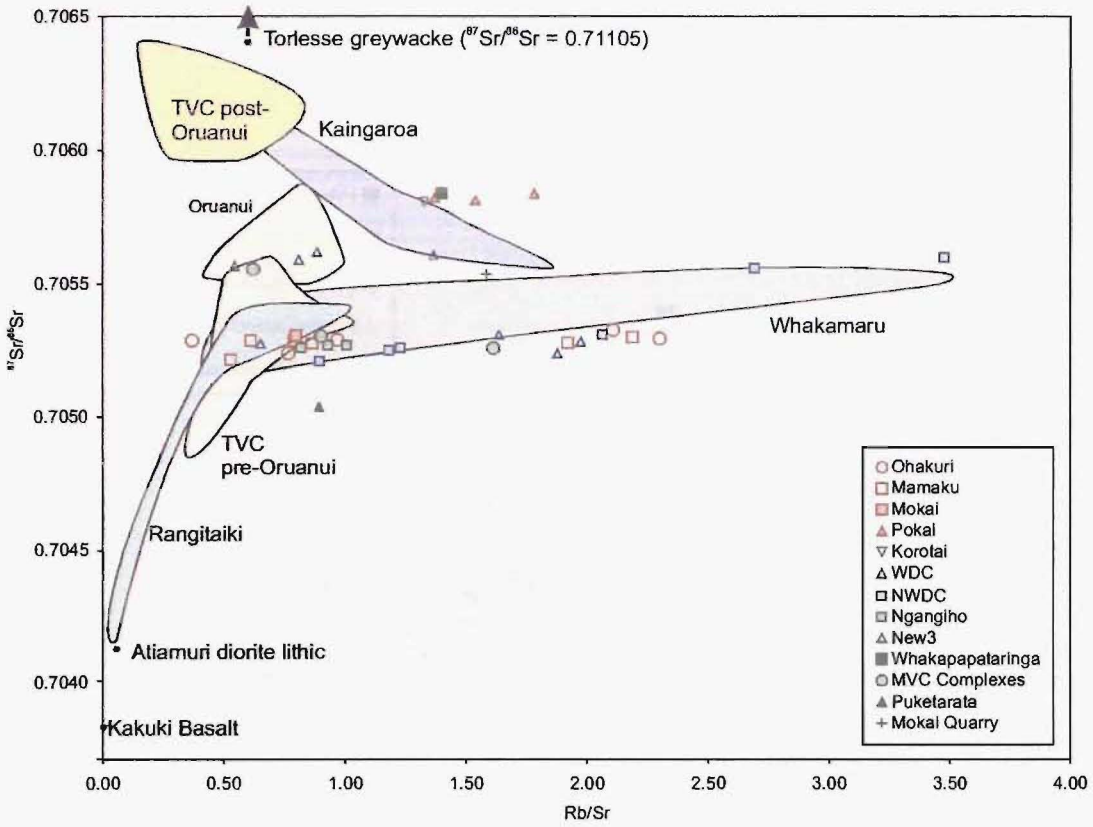

Figure 4.21 $^{87}Sr/^{86}Sr$ plotted against Rb/Sr with fields for other selected eruptives. Coloured data points are from this study, with the exception of Kakuki basalt from Gamble et al. (1993), Torlesse Greywacke from average of borehole samples of Browne et al. (1992) in Sutton (1995), Ngangiho from Sutton (1995), New3 from A. Sutton (written comm., 2003), Whakapapataringa from Brown et al. (1998) and Puketarata and Mokai Quarry (mislabelled Pukeahua in the original paper) from McCulloch et al. (1994). Coloured areas are fields for: Kaingaroa Ignimbrite from Beresford (1997); WDC, NWDC, Atiamuri lithic, and Whakamaru and Rangitaiki Ignimbrite from Brown et al. (1998); Taupo (including Oruanui) from Sutton (1995).

Three features of the major element variations appear to correlate to mineralogy: (1) K appears to be an incompatible element in Maroa eruptives, consistent with a lack of alkali feldspar phenocrysts; (2) high Fe in Puketarata eruptives may be correlated to particularly abundant biotite in these eruptives; and (3) dacite samples are petrographically distinguishable from rhyolite samples in the same deposit. Dacite

sample M13 has darker brown glass patches. Dacite sample M44 is the only Orakonui juvenile clast to contain hornblende, contains fine-grained (lithic?) aggregates and appears to have darker streaks in hand specimen.

4.7.10 Summary of Maroa Petrology compared to chronology and volumes

Figure 4.23 presents a graph summarising key volume, age, geochemical and mineralogical data for each Maroa deposit/group of eruptives, and the Whakamaru group pyroclastics and WDB for comparison. A synthesis of this data is used to produce a model history for Maroa at the start of the following Discussion chapter. The discussion then leads from that model.

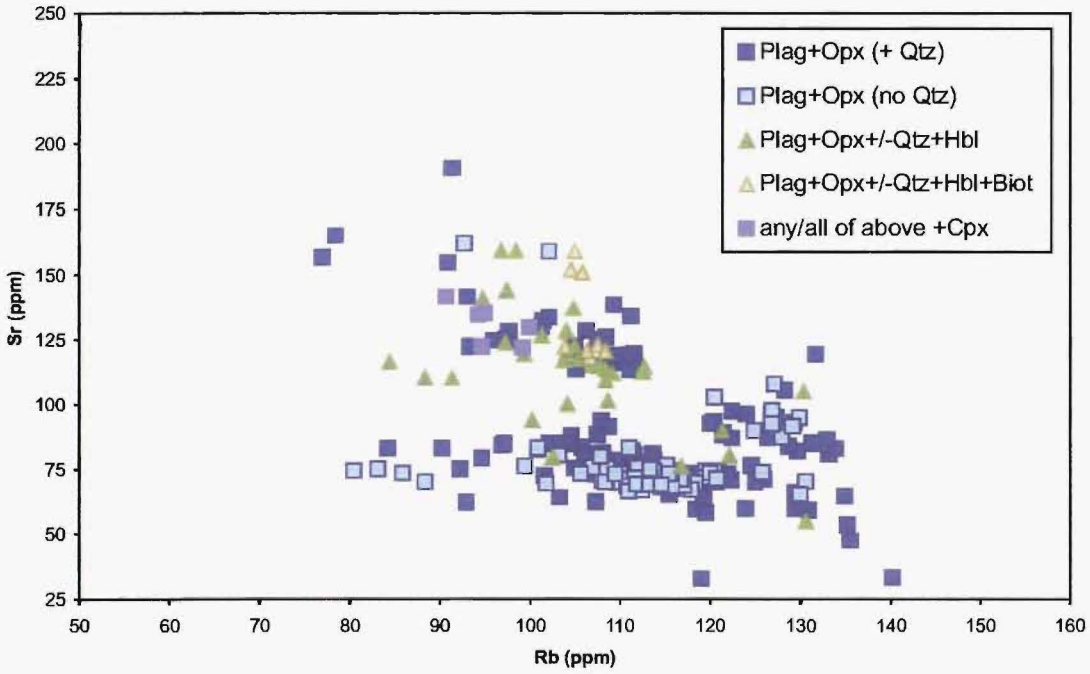

Figure 4.22 Plot of Rb-Sr concentrations for Maroa-related eruptives, colour coded according to ferromagnesian mineralogy. All samples contain at least plagioclase (Plag) and orthopyroxene (Opx). Other minerals are abbreviated as: quartz (Qtz), hornblende (Hbl), biotite (Biot) and clinopyroxene (Cpx).

4.7.11 Maroa in the context of central TVZ compositions

Maroa magma type fields are plotted against Whakamaru, Mamaku, Ohakuri, Pokai, Mokai and Kaingaroa pyroclastics fields in Figure 4.24. Brown et al. classified the Whakamaru magma types based on SiO_2 vs. Rb/Sr and Zr vs. Sr. The Whakamaru compositions cover the widest range of Rb concentrations, encompassing the ranges of all of the other eruptives and more. Ohakuri samples cover a range of Sr concentrations larger than the remaining eruptives combined. Pokai and Mamaku samples fall into

three groups each that cover the whole range of Maroa magma types. Kaingaroa analyses cover a relatively narrow range across T- and N-type fields.

Note that all of the Maroa eruptives combined (T, M and N fields in Fig 4.24) still have a relatively narrow range in compositions when compared to TVZ pyroclastics of similar or greater volume. It is also interesting to note that several discrete magma types exist within many of the TVZ caldera-forming pyroclastic deposits shown in Fig 4.24. This is discussed further in Section 5.3.6.

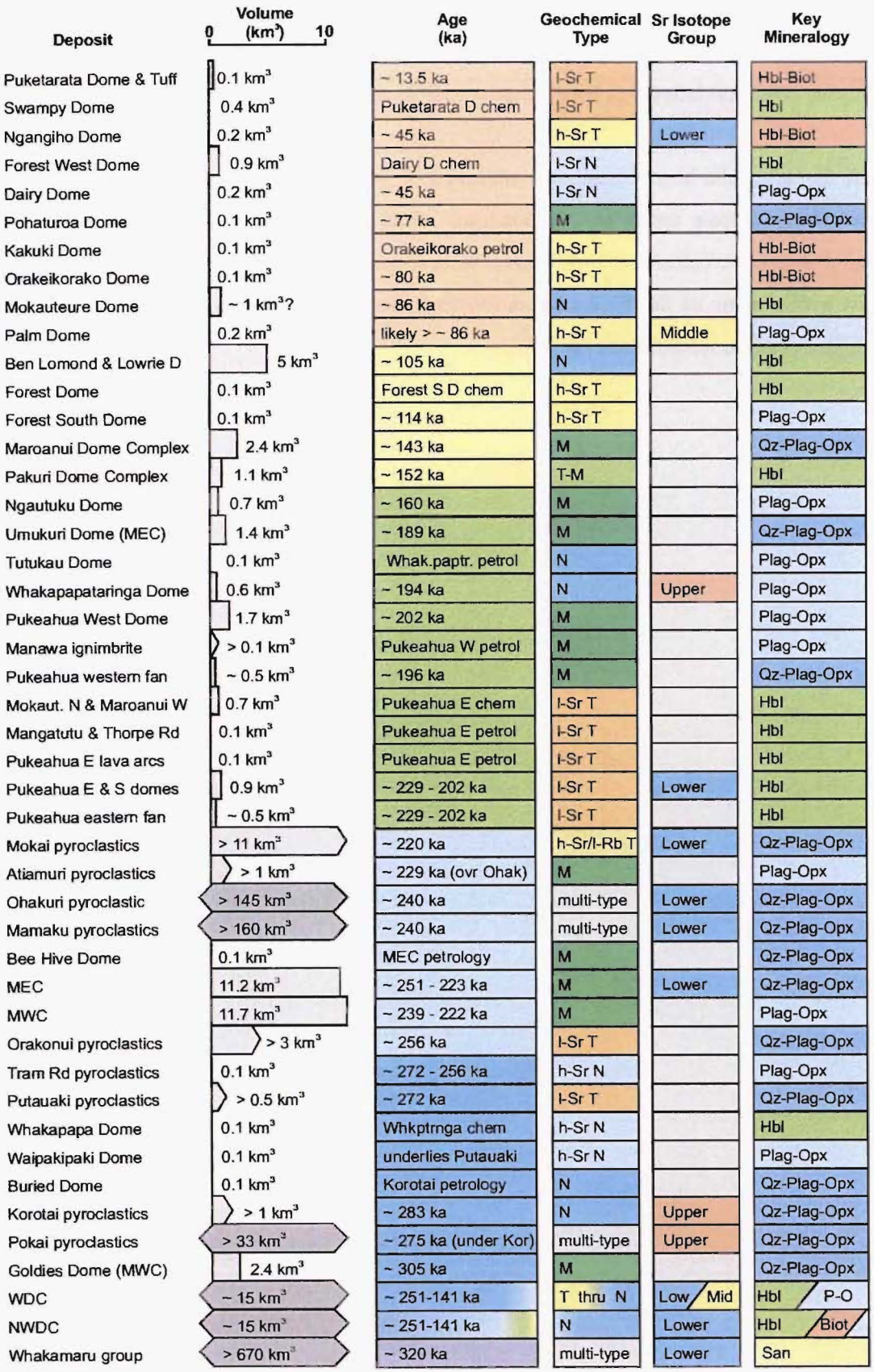

Figure 4.23 Summary of the DRE volume, age and/or stratigraphic position, Rb-Sr-based geochemical type, Sr-isotope-based group and key mineralogy of MVC-related deposits. Coloured after Figures 3.2, 3.9, 4.6, 4.10 and 4.18.

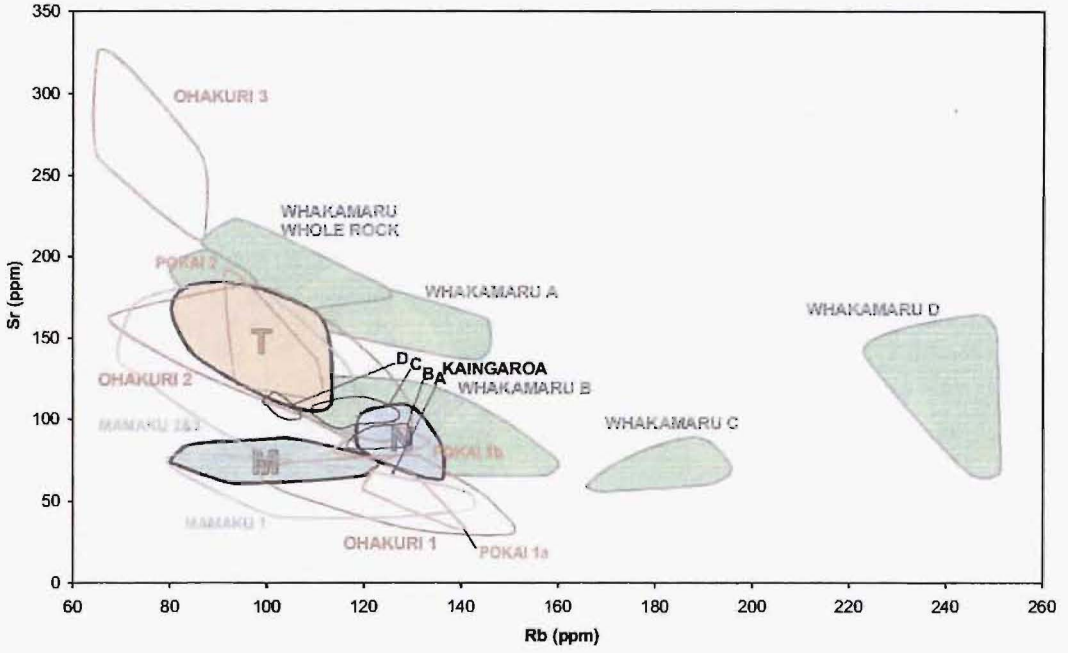

Figure 4.24 Maroa magma types (labelled T, M and N) compared to Whakamaru (green), Mamaku (grey), Ohakuri (brown), Pokai (orange), and Kaingaroa pyroclastics fields on a Rb-Sr concentration plot. Fields from data presented in Brown et al. (1998), Milner (2001), Gravley (2004), Karhunen (1993) and Beresford et al. (2000)

4.8 Maroa Basalts and Parekauau dacite

4.8.1 Basalt petrology

A summary of the petrography of Maroa mafic samples is given in Table 4.11. All of the Maroa basalts are porphyritic with intergranular, hyalopilitic groundmass texture (pyroxene and Fe-Ti oxides in a plagioclase dominated groundmass where crystals are more voluminous than glass) (Fig. 4.25). A plot of Maroa mafic samples in a Total-Alkali-Silica (TAS) classification diagram is given in Figure 4.26. Selected plots of major oxide and trace element contents are shown in Figure 4.27.

An increasing linear trend in Ba content (when plotted against SiO_2) may correlate to variation in crustal interaction, as Ba content is much higher in local sediments than in the more primitive TVZ basalts (e.g. Kakuki basalt) (Briggs et al., 1993). Olivine fractionation would produce a negative trend against silica in Cr and Ni concentrations. Such trends are present in Figure 4.27 but they have only a gentle slope suggesting Olivine fractionation is only slightly varied across these basalts. Particularly high Cr, Ni and Ba in Ongaroto basalt corresponds to the relatively high Olivine content in this basalt.

(a) Tatua Basalt

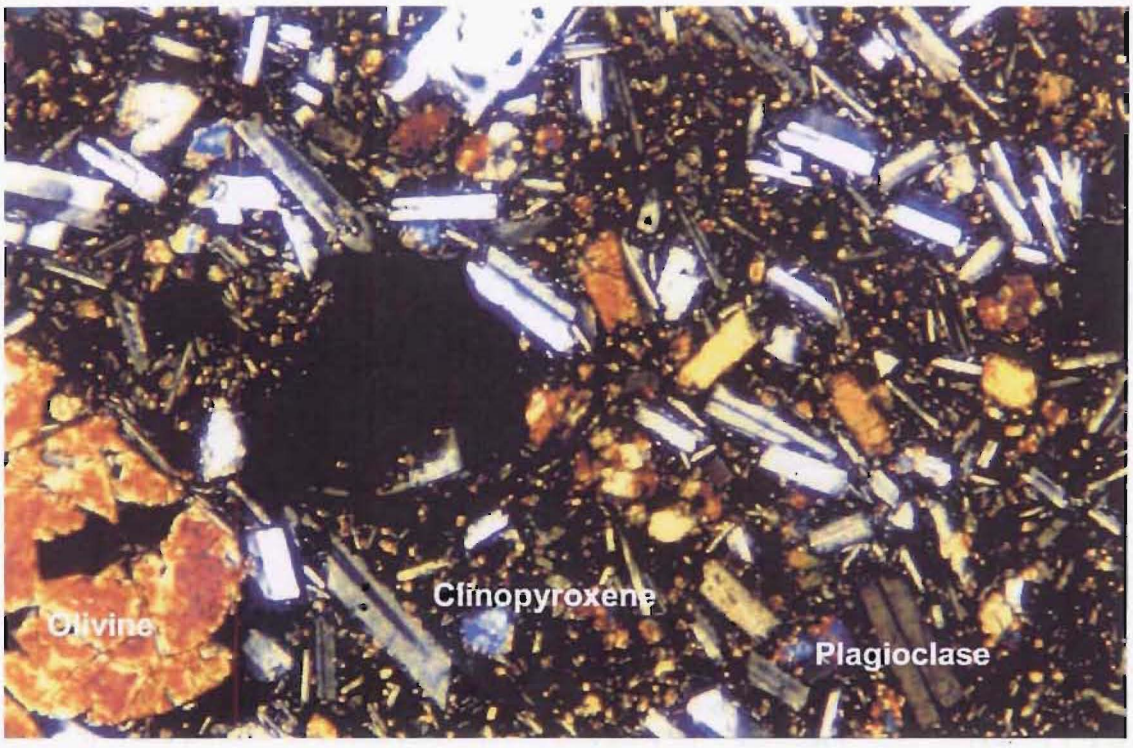

(b) Akatarewa Basalt

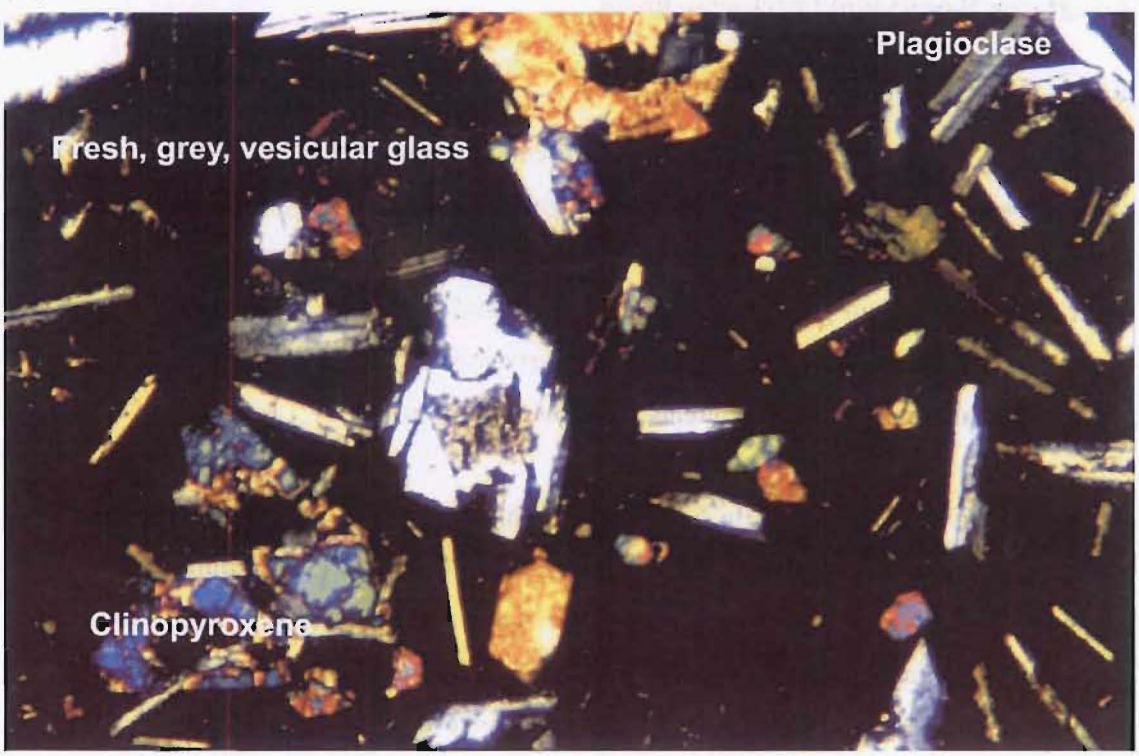

Figure 4.25 Basalt in thin section from (a) Tatua lava flow and (b) Akatarewa scoria airfall in Te Kopia Rd section (U17/861989).Both contain plagioclase, clinopyroxene and opaque minerals, but Tatua Basalt also contains olivine. Note that Tatua basalt groundmass is dominated by fine grains of the same minerals that make up the phenocrysts, with subordinant grey glass, whereas Akatarewa basalt is mostly grey glass with occasional fine crystals. Thin sections are both shown in cross-polarised light and both measure 2.6 mm wide.

The Kakuki and Akatarewa basalts have very similar geochemistry (Figure 4.27). Tatua basalt has similar chemistry to these two, except for significantly higher $Fe_2O_3(t)$ and Zn concentrations. Poihipi basalt contains similar abundances of all elements to Tatua basalt, other than relatively high concentrations of TiO_2, P_2O_5 and Zr. Ongaroto basalt contains lower Al_2O_3, CaO and Sr, and higher P_2O_5 Cr, Ni and Ba, than Kakuki and Akatarewa.

Sample	Pl %	Max Pl size (mm)	Ol %	Max Ol size (mm)	Cpx %	Max Cpx size (mm)	Opq %	Max Opq size (mm)	Gmass %	Max gmass size (mm)	Gmass Gl %	Gmass Pl %	Gmass Cpx/Ol %	Gmass Opq %	Vesic %	Max Vesic size (mm)
Akatarewa basalt	25	1.3			10	0.5			65	.03		50	20	30		
Ongaroto basalt			2.1	0.9	3.3	1.4			95	0.6	3	70	20	7	7	1.5
Kakuki basalt	15	1.4	2.9	0.2	2.5	0.3			79	0.1		40	30	30	7	0.4
Tatua basalt	27	1.8	2.1	0.2	6.1	1.4			65	0.1		30	20	50	15	1.8
Poihipi basalt	3	1.8			0.8	0.4			96	0.2		40	10	40	35	1.8
Parekauau dacite	11	3.3			5.3	1.0	1.1	0.4	83	0.2	5	80	10	10	5	3

Table 4.11 Summary of Maroa-area basalts and Parekauau dacite petrography. Details as for Table 4.1.

Although each Maroa-area basalt has at least one or two element concentrations in common with each other basalt, only Kakuki and Akatarewa basalts have consistently similar chemistry. These two are, therefore, the only basalts that are plausibly from the same 'source' (a common chamber or location of partial melting etc.), based on geochemistry. This suggests a relatively young age for Kakuki basalt similar to the Akatarewa basalt (between ~ 29 and 40 ka, Section 1.5). This is also consistent with the 80 ± 7 ka age of Orakeikorako dome (Chapter 3), which lies on the same paleo-surface as Kakuki basalt. All of the basalts contain clinopyroxene but only Kakuki, Akatarewa and Tatua basalts contain abundant plagioclase. Tatua basalt may, therefore be from a magma that is closely related to the other two. Poihipi and Akatarewa basalts do not appear to contain olivine in samples analysed for this study.

Ongaroto and Poihipi basalts are crystal-poor. Ongaroto basalt contains no plagioclase at all. These two basalts have geochemistry distinct to one another, and compared to all of the other Maroa-area basalts. They are, therefore, likely to represent relatively unique magma sources.

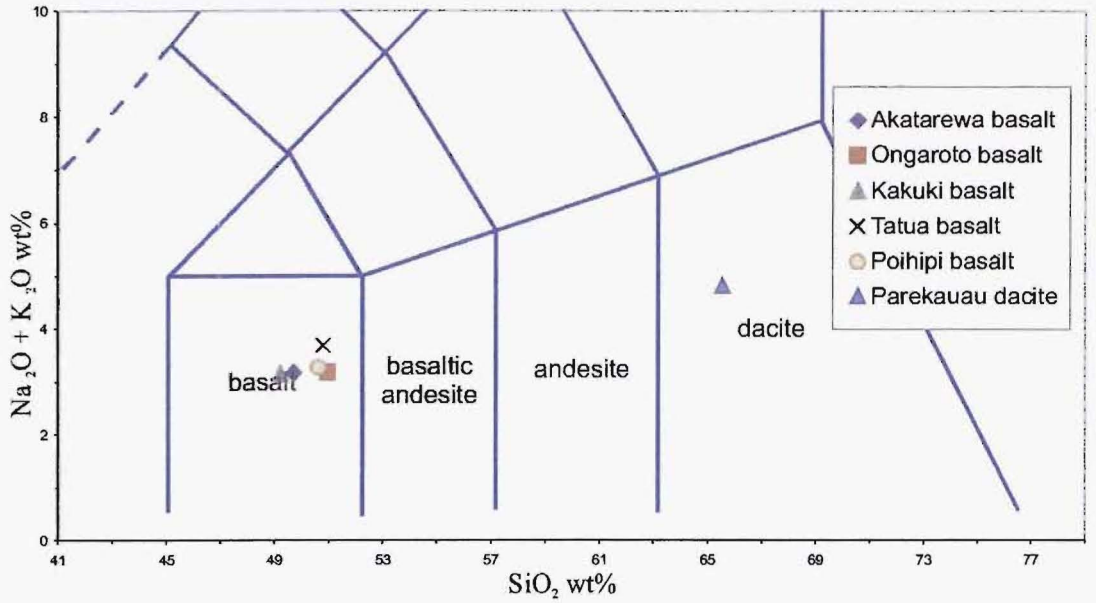

Figure 4.26 Total Alkali-Silica classification (after Le Maitre et al., 1989) of Maroa-area non-rhyolite samples.

4.8.2 Parekauau dacite

Although colloquially referred to as an 'andesite' (e.g. Lloyd, 1972), this deposit is instead classified as a dacite using the TAS classification system (Fig. 4.26). This lava contains plagioclase, augite and opaques as phenocrysts and groundmass. Some of the large opaques are the result of alteration, mostly of augite. The groundmass is dark brown and contains 5 % glass. It is slightly vesicular with dispersed vesicles. Much of the groundmass is devitrified to very fine, translucent, minerals, which are probably feldspars. These are discussed further in Section 5.3.8.

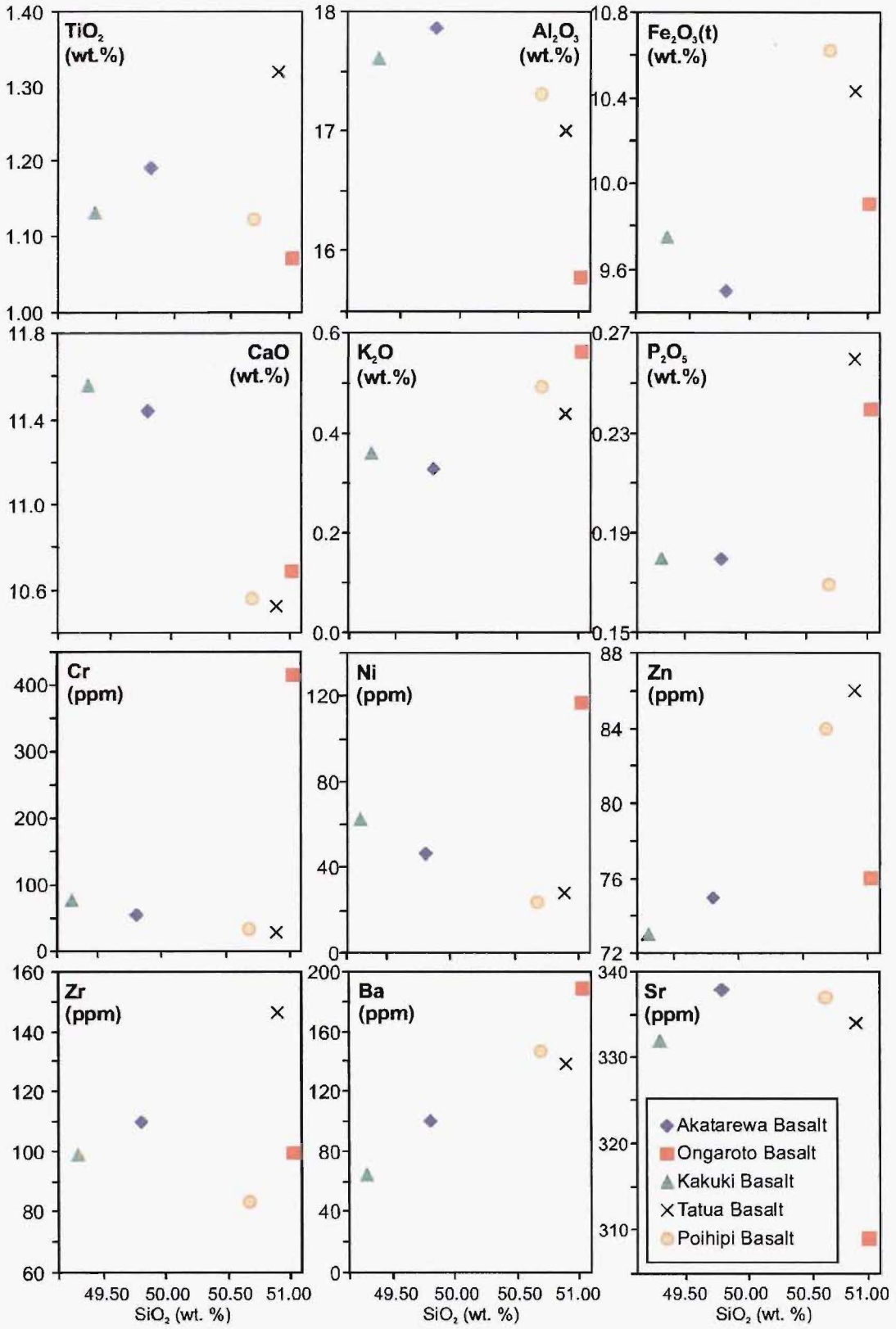

Figure 4.27 Plots of silica vs. various key major oxide and trace element concentrations for MVC-area basalt deposits.

CHAPTER 5

Discussion

5.1 Introduction

In this thesis, three suites of data have been documented. 1) a review of existing (but largely unpublished) studies by E.F. Lloyd and co-workers, together with my new data, has been presented on stratigraphical aspects of the Maroa eruptive history in Chapter 2. 2) my new $^{40}Ar/^{39}Ar$ age data have been presented in Chapter 3, and combined with existing (but, again, largely unpublished) age data obtained by B.F. Houghton and colleagues to provide a chronostratigraphic framework for the evolution of Maroa and adjacent areas. 3) my petrographic and geochemical data on the Maroa eruption products are presented in Chapter 4. The scope of this thesis research precluded large-scale collection of isotopic or mineral-compositional data, but a limited suite of $^{87}Sr/^{86}Sr$ data supplied (from my samples), analysed by B.L.A. Charlier, are also presented in Chapter 4.

In this chapter, I draw together these three main groups of information to discuss the following key elements of Maroa:

- the initiation and eruptive history of Maroa, including relationships between Maroa and adjacent contemporaneous centres (particularly Taupo) (Section 5.2),
- the evolution of Maroa magmas (Section 5.3),
- the inter-relationships between Maroa activity and faulting (Section 5.4),
- implications of the ages of surface geology to infilling rates of the underlying Whakamaru caldera (Section 5.5), and
- volcanic hazards associated with Maroa at the present day (Section 5.6).

The concept of Maroa Volcanic Centre has evolved over the last 40 years and it is important to summarise this first so the reader can place this thesis in context (aspects of this concept were also given while defining the term Maroa in Section 1.4.2). Healy's (1962) definition of Maroa Volcanic Centre as one of the two main concentrations of rhyolite lava bodies in TVZ (the other being Okataina) was the first time Maroa had been formally named and singled out as a locus of volcanic activity. His map shows domes distributed from Maroa to the northern shores of Lake Taupo, but he does not

draw a definitive southern boundary for Maroa. Healy (1964) distinguished Taupo domes as separate from those of Maroa, but introduced the term Mokai Ring Complex (described in Section 1.4.2) and suggested that all of the domes within the complex, including Maroa, were petrogenetically related. This was perpetuated by Ewart (1967; 1968) and Ewart et al. (1975). Cole (1990) referred to the entire Mokai Ring Compex as 'Maroa Volcanic Centre'. Wilson et al. (1986; 1995) clearly showed that there was no evidence to support the existence of the Mokai Ring Complex (and thus Cole's definition of 'Maroa Volcanic Centre') as a petrogenetically related feature and noted that Maroa domes overlay a strong magnetic anomaly which could be related to an old caldera. They also postulated that activity at the northern end of Whakamaru caldera appears to be distinctly older than in northern Taupo. This general age distinction between the older Maroa and younger Taupo is clear in the new chronological data presented in Chapter 3.

Sutton (1995) delineated a somewhat arbitrary (but based on predictions of the likely values of some ages determined here) boundary between Taupo and Maroa as the northing just north of Ben Lomond dome. He noted that north of this line magmas appeared petrologically distinct from the magma systems that he defined for Taupo. This is where the definition of Maroa stood prior to commencing this study, and the new data here confirms that Sutton's boundary between Maroa and Taupo is the most logical; north of that boundary most surface volcanic deposits and lavas are older than 100 ka, and vice versa. The new data presented in Chapter 4 also shows that Maroa magmas are indeed clearly distinct from most of those below Taupo (mostly M- and N-type, vs. T-type for the latter). This is explored in detail in Section 5.3.

Extensive petrological and volcanological datasets are available for many central-TVZ deposits contemporaneous with Maroa. This chapter discusses my new Maroa data in the context of these wider data sets. These include the volcanology and petrology of the Pokai (Karhunen, 1993), Mamaku (Milner, 2001) and Ohakuri (Gravley, 2003) pyroclastics north of Maroa, the Whakamaru group pyroclastics west of and beneath Maroa (Brown, 1994), the Western Dome Belt (Brown, 1994), Taupo domes and pyroclastics south and southeast of Maroa (Wilson et al., 1984; Wilson et al., 1986; Sutton, 1995) and deposits of Okataina Volcanic Centre (Nairn, 1989; Nairn, 2002a).

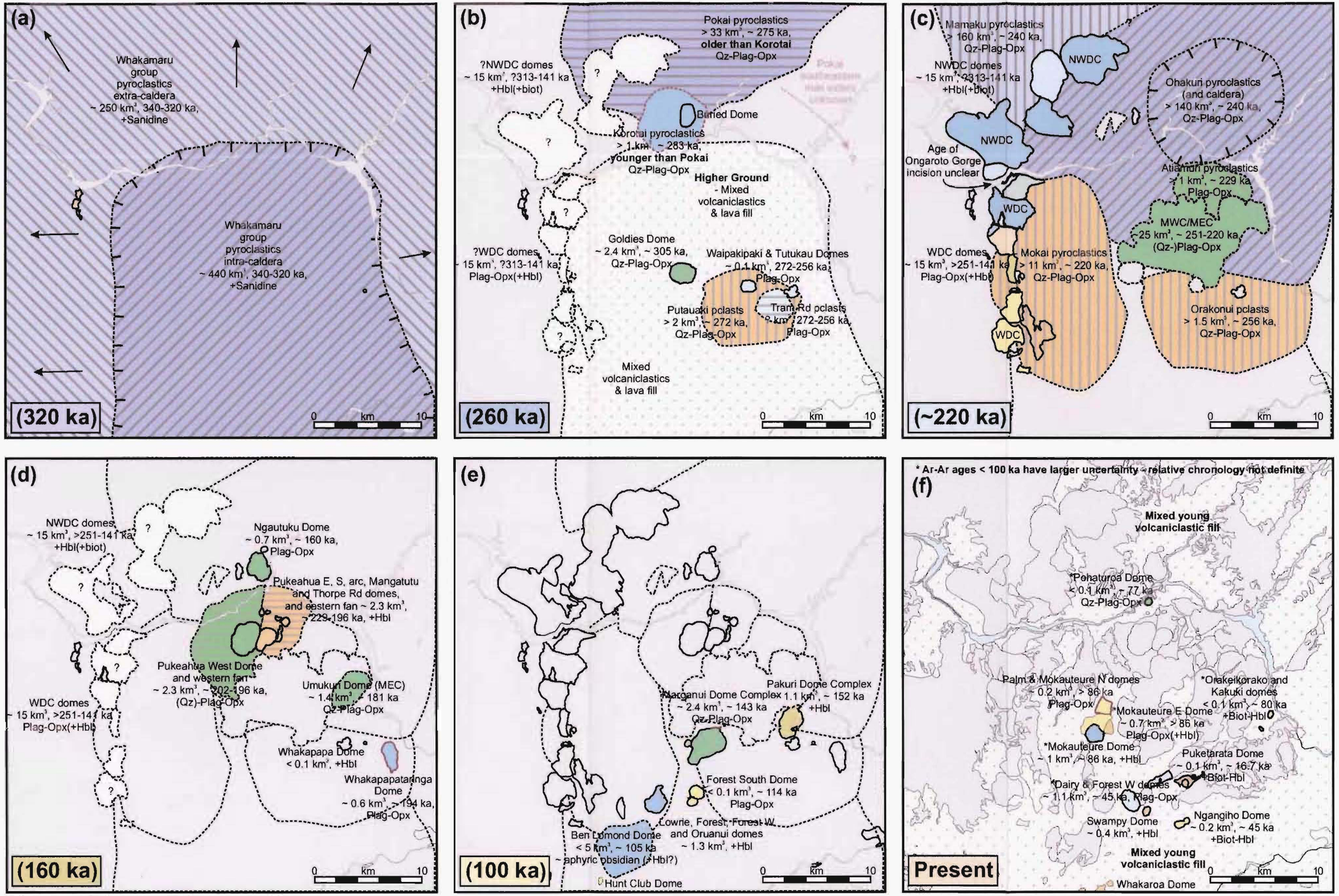

Figure 5.1 Summary of the evolution of MVC rhyolitic deposits, with colours denoting Rb-Sr based magma types as used in Figure 5.10. Hatching distinguishes pyroclastics. Only deposits which were emplaced during the time elapsed since the previous frame are coloured. Annotations detail deposit name, age (if determined by Ar-Ar experiments) and key mineralogy. Korotai pyroclastics and Whakapapataringa Dome with pink borders are from high-$^{87}Sr/^{86}Sr$ group.

Details of the work done by these people are given in Section 1.4.5, the relevant volcanology is summarised in Chapter 2 and the relevant petrology in Chapter 4.

5.2 The Initiation and Eruptive History of Maroa

Figure 5.1 presents a summary of the history of Maroa developed using the new chronology from Chapter 3 combined with relevant petrological data from Chapter 4. The evolution of Maroa is separated into 6 periods over which key events have occurred. Deposits which have not been directly dated are placed in the most likely period based on petrological and/or field associations with dated deposits. I now discuss major elements of this new history of Maroa in the context of the evolution of the wider TVZ.

5.2.1 The oldest Maroa surface deposit and the infilling of Whakamaru caldera

The new geochronology (Chapter 3) highlights the very short period between the end of deposition of Whakamaru intra-caldera ignimbrites, and the time at which the collapsed region had been infilled back to the point where domes and pyroclastics crop out at the present-day surface. The Whakamaru group pyroclastics, and thus the collapse of the Whakamaru caldera, are dated at 340-320 ka (Houghton et al., 1995) and the oldest deposit at the surface within Whakamaru caldera lies at 300 m asl., only ~ 15 - 35 kyr younger (Fig. 5.1 (a) and (b)). This suggests that in the Maroa area at least, infilling to 300 m had occurred very rapidly (see Section 5.5).

The chronology was combined in Chapter 3 with detailed estimates of the volumes of all deposits within the caldera to determine the maximum rate of infilling of the caldera after its collapse. The analysis showed clearly that infilling was very rapid (maximum rates of 17-29 km^3/kyr), from which two important points can be made:

1. A large volume of pyroclastics and lava was erupted in and around the Whakamaru caldera directly after its collapse, of which there is little or no exposure at the present day land surface.
2. The intra-caldera volcanism we see at the surface, although not much younger than the caldera collapse, is the product of magmas active after a much greater amount had already been erupted and buried.

The infilling of silicic calderas in general is discussed in the context of international caldera collapse and infilling in Section 5.5.

5.2.2 The Ongaroto Gorge, paleo-lakes and regional pyroclastic eruptions

The ages of Maroa deposits, and those of the Mokai, Mamaku and Ohakuri pyroclastics and of the WDB (distribution and volcanology given in Chapter 2, ages detailed in Chapter 3), constrain the age of the formation of the Ongaroto Gorge, and timing and location of a paleo-Lake Ohakuri that probably existed north (D. Gravley, pers. comm., 2003), and possibly west of, Maroa (Fig. 5.2).

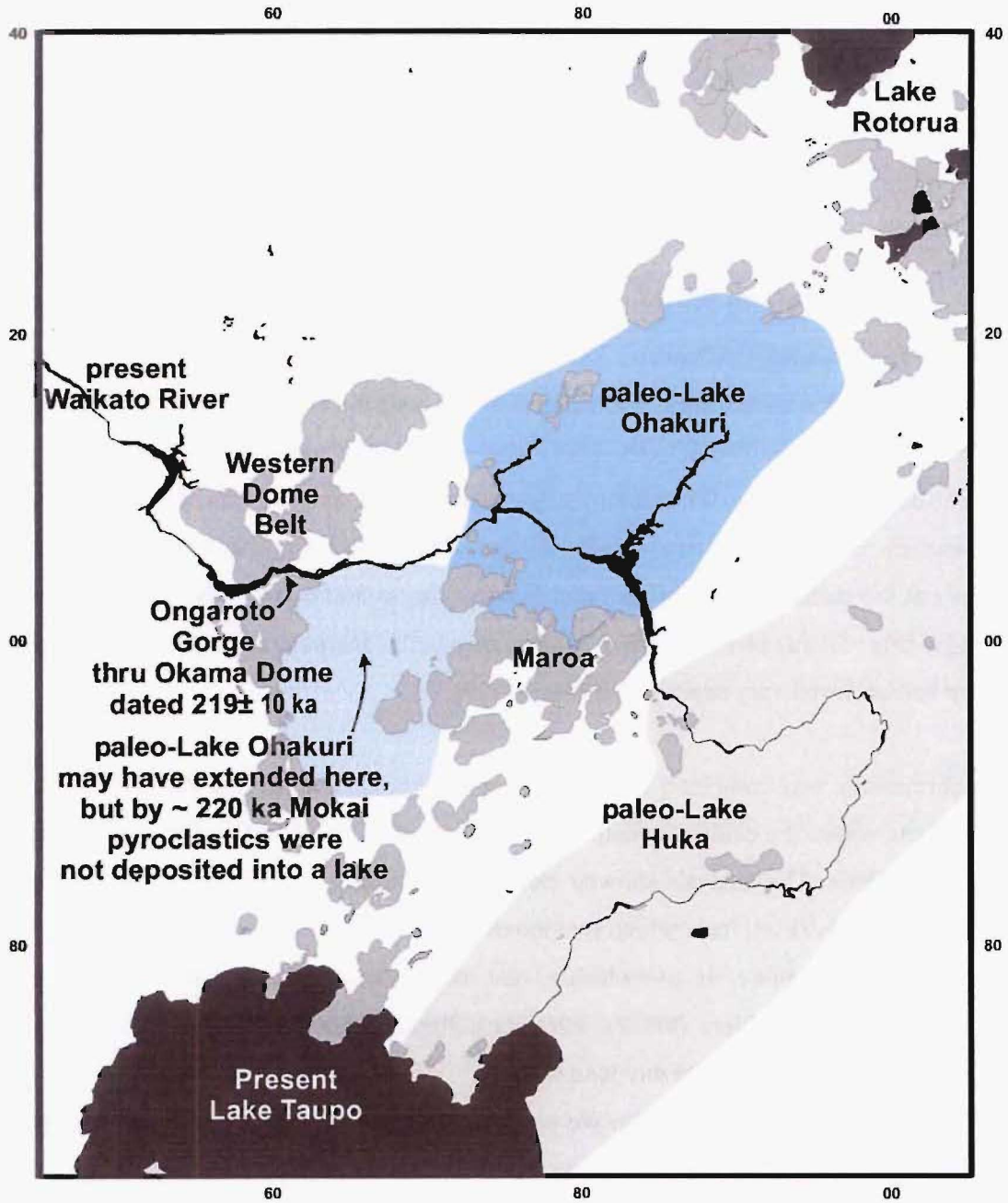

Figure 5.2 Paleo-Lakes Huka (light grey) and Ohakuri (blue) in relation to Maroa and the Ongaroto Gorge through the Western Dome Belt. The present locations of Lakes Rotorua, Taupo and the Waikato River are shown in black. Domes are mid grey.

A large, elongate lake from the present Lake Taupo through the Reporoa Basin existed from the mid-late Pleistocene (Smith et al., 1993). This probably drained west and connected to Paleo-Lake Ohakuri north of Maroa. Gravley (2004) notes that paleo-Lake Ohakuri (as evidenced by phreatomagmatic pyroclastic density current deposits within the Ohakuri pyroclastics) probably extended over a substantial area (Fig. 5.2) prior to ~ 240 ka Ohakuri eruption, based on the distribution of lacustrine interaction with the pyroclastics.

In contrast to the Ohakuri pyroclastics, the Mamaku pyroclastics do not show evidence of interaction with water during emplacement in the few exposures in the Guthrie Graben (Milner et al., 2002b) and they do not outcrop southwest of this. This gives control on the northern extent of paleo-Lake Ohakuri at ~ 240 ka (Fig. 5.2). The lake should also have extended into the Mokai area at that time because there is no evidence for high ground between the paleo-Lake Ohakuri and the area west of Maroa. The ~ 220 ka Mokai pyroclastics do not show evidence for aqueous interaction, even though they lie at a similar, or even lower, elevation to the older Ohakuri pyroclastics. This suggests that paleo-Lake Ohakuri had ceased to exist, in at least the Mokai area, before ~ 220 ka. The destruction of the lake may have been directly associated with the emplacement of the Ohakuri pyroclastics (Gravley, 2004).

Today the Guthrie-Ngakuru-Mokai area drains into the Waikato River, which in turn flows through the Ongaroto Gorge (Fig. 2.23). Okama dome in the WDB, cut by the present day Ongaroto Gorge, is dated at 219 ± 10 ka (Stipp, 1968; see Chapter 3). A lack of lacustrine deposits atop/against the Mokai pyroclastics or on WDB domes suggests that no significant lake existed after this time until the ~ 26.5 ka Oruanui eruption (which does have extensive associated lacustrine deposits). Therefore, the present day gorge is no older than ~ 219 ka and its cutting must have occurred during or directly after Okama dome's emplacement.

The age of the Mokai pyroclastics also constrains the age and timing of movement on the unusual Pokuru Fault. This is the only major north-south trending structure in Maroa and the age of displacement along it is discussed further in Section 5.4. Interestingly, the fault has major (> 100 m) Mokai pyroclastics displacement south of the Waikato River, but no displacement is seen north of the river in the nominally older Ohakuri

pyroclastics. The northern terminus of the Pokuru Fault is directly east of the Ongaroto gorge and this raises the interesting possibility that some deep east-west striking structure is controlling the location of the Ongaroto gorge and the terminus of the fault. Data are not available to explore this possibility further here.

5.2.3 Maroa dome extrusions: a period of quiescence in TVZ pyroclastic eruptions

Together Maroa and the WDB form the main locus of TVZ volcanism from ~ 230 to 64 ka (Fig. 5.1(c)-(e)), in terms of both volume and frequency of eruptions (Maroa chronology in Chapter 3 compared to Houghton et al., 1995). Significant volumes of rhyolite in this age range do exist in Okataina and Taupo (esp. north Taupo), but approximate calculations suggest that the volumes in Maroa are at least three times the volumes for this period erupted in each of these centres. This period is also distinct from the periods before and after because it apparently contains no caldera-forming ignimbrite eruptions.

Following the Whakamaru group eruptions there was a sustained period of large caldera-forming eruptions in central TVZ (each with > 30 km^3 magma erupted as mostly ignimbrites). The Pokai, Matahina, Mamaku, Ohakuri, and Kaingaroa pyroclastics were all erupted in the period ~ 283-230 ka (Houghton et al., 1995, with modifications justified in Chapter 3). The smaller Mokai pyroclastics eruption of > 11 km^3 was a last gasp of moderately large pyroclastic activity in TVZ at ~ 220 ka. The volume of the Mokai pyroclastics suggests that this may have been associated with caldera collapse, but such collapse has not been identified by previous workers, or this study (Chapter 2). There was then a distinct quiescence in large pyroclastic eruptions until the ~ 64 ka Rotoiti (Okataina) and 26.5 ka Oruanui (Taupo) eruptions. This was noted by Houghton et al. (1995) who used the quiescence to separate their TVZ caldera-forming period IIIB from IIIC.

The decrease at ~ 230 ka in TVZ eruption rates (and associated explosivity) coincides with the onset of eruption of the bulk of the Maroa deposits still present at the surface, mostly as domes. From ~ 251 ka, around 23 km^3 of lava was extruded as the MWC/MEC dome cluster in only ~ 29 kyr (Chapter 3). Extrusion of Maroa lavas is the largest volume of magma erupted within a geographically concentrated area during this

hiatus in TVZ caldera collapse events. The WDB eruptions appear to cover a similar time period (> 251 to 141 ka) to those at Maroa and are almost as voluminous.

Note that a subset of unexposed subsurface ignimbrites within Whakamaru caldera may provide evidence for caldera collapse from 230 to 64 ka. These were considered in Section 5.2.1 to be part of the initial infilling of Whakamaru caldera, but the possibility exists that they have been deposited into younger depressions. These are seen in Wairakei, Orakeikorako and Mokai drill cores (various confidential Crown Minerals drill logs, kindly provided for this study) but sources and volumes cannot be determined.

It is important to highlight that the downturn in central TVZ eruption volume and explosivity from ~ 230 – 64 ka does not necessarily represent a downturn in magma production rates below the surface. In northern Taupo a substantial magma body was building during this period, which eventually erupted the enormous Oruanui pyroclastics (Charlier et al., submitted). The distinction of volcanic versus plutonic history across TVZ is highlighted by Charlier et al. and is discussed further in Section 5.3.6.

By the time of the resumption of caldera-forming eruptions at ~ 64 ka, Maroa volcanism had all but ceased; less than 3 km^3 of magma has been erupted from Maroa since 100 ka. The following section explores the shift of volcanism away from Maroa. Section 5.4.5 discusses the processes that may be driving shifts in the loci of TVZ eruptions.

5.2.4 Smaller ignimbrites: a by-product of clustered dome eruptions in TVZ

Maroa typifies a correlation of smaller pyroclastics to dome complexes seen across the TVZ. Maroa contains the greatest volume of ignimbrite not associated with caldera-collapse erupted from ~ 283 to 196 ka (where the vent has been identified) (Fig. 5.1(b)-(d)). The relatively small ignimbrites of the Korotai, Orakonui, Atiamuri and Pukeahua pyroclastics were erupted between these times over the period of highest dome eruption rate (see above). Across TVZ ignimbrite deposits smaller (volumes usually less than 1 km^3) than those caldera-forming ones discussed above mostly occur in association with dome extrusions. At Okataina they are seen around the Haroharo (e.g. Whakatane pyroclastics fan) and Tarawera (Kaharoa and Waiohau pyroclastics) Volcanic Complexes (Nairn, 1989), at Taupo around the domes along the northern and western

shores of Lake Taupo (unpublished IGNS mapping) and in the NWDC to the west of Whakamaru Lookout and Skyline domes (Wilson et al., 1986). Some of the pyroclastic units seen in Taupo, especially pyroclastics at Kawakawa Bay and Rangatira Point, and in drill core at Wairakei geothermal field, are of substantial volume (> 1 km^3) but of unknown source and age.

5.2.5 The foci of TVZ volcanism shifting away from Maroa, 200 ka to present

From 100 ka to present, TVZ activity outside of Maroa, primarily at Okataina and Taupo, has dramatically increased in terms of volume, explosivity and frequency. In contrast, by 200 ka ~ 75 %, and by 100 ka ~ 95 %, of the total volume of Maroa surface deposits had been erupted (Fig. 5.1 (b)-(e); volumes and chronology from Chapter 3). This represents a shift of volcanism from central TVZ towards the north and south.

<table>
<tr><th>Period</th><th>Okataina</th><th>Maroa</th><th>Taupo</th></tr>
<tr><td>340-320 ka</td><td rowspan="2">Relatively small volumes of dome lavas preserved</td><td colspan="2">Whakamaru caldera-forming eruption >500 km^3</td></tr>
<tr><td>320-305 ka</td><td colspan="2">< 80 % of Whakamaru caldera infilling (see Section 5.5.1)</td></tr>
<tr><td>305-240 ka</td><td>~ 280 ka Matahina eruption</td><td rowspan="2">~ 95 % of volcanism at Maroa, > 42 km^3. Dominated by dome-building eruptions (> 35 km^3) with some pyroclastic eruptions producing ~ 5 locally-distributed ignimbrites (> 8 km^3). Up to 6 magma systems, some of which may be genetically related. One system overlaps with an eruption ~ 105 ka in northern-Taupo</td><td rowspan="3">Predominantly small-volume lava dome extrusions all around Lake Taupo from distinct small discrete magma batches</td></tr>
<tr><td>*
240-100 ka</td><td>Relatively low volume (likely <<20 km^3) of rhyolite lavas extruded as domes with minor pyroclastics in the west and southwest of the centre.</td></tr>
<tr><td>100-70/60 ka</td><td>~ 64 ka ~ 50 km^3 Rotoiti eruption (caldera-forming)</td><td>< 2.5 km^3 of small rhyolite dome-building eruptions from two magma systems.</td></tr>
<tr><td>70/60-26.5 ka</td><td rowspan="2">45 – 28 ka ~ 30 km^3 Mangaone eruptions</td><td rowspan="3">< 0.5 km^3 of small rhyolite dome-building eruptions from the same two magma sources as for the previous period. At least one source overlaps with an eruption in northern Taupo.</td><td>Onset of explosive-dominated activity, some dome building in north, onset of activity from Oruanui magma system</td></tr>
<tr><td>26.5 ka</td><td>Oruanui caldera-forming eruption ~ 530 km^3</td></tr>
<tr><td>26.5 - 2.2 ka</td><td rowspan="2">~ 80 km^3 of magma erupted predominantly as domes of the Haroharo and Tarawera Volcanic Complexes, with subordinate pyroclastics.</td><td>Dacitic dome-forming, and predominantly-pyroclastic rhyolitic eruptions from multiple non-Oruanui magma systems</td></tr>
<tr><td>2.2 ka</td><td>NO ERUPTIONS</td><td>Three eruptions, including the ~ 30 km^3 Taupo caldera-collapse, tap a new magma batch</td></tr>
</table>

Table 5.1 Summary of distribution of style and volume of volcanism across time at Maroa vs. Okataina and Taupo. All volumes are DRE. Taupo data is summarised from Sutton et al. (1995) with modifications from C. J. N. Wilson (pers comm., 2003). Okataina data is summarised from Nairn (2002a). * The Kaingaroa pyroclastics were erupted from Reporoa caldera ~ 230 ka (Beresford, 1997). Bold boxes enclose the periods of greatest activity.

Table 5.1 summarises the frequency, scale and style of eruptions at Maroa compared to Okataina (modified from Nairn, 2002b) and Taupo (modified from Sutton et al., 1995), since the collapse of Whakamaru caldera. Almost all of the Maroa eruptions occured from 305 to 100 ka, as mostly lava domes with 5 subordinate ignimbrite-forming local pyroclastic eruptions (discussed above). In contrast Taupo activity prior to 60-70 ka was mostly small dome-forming eruptions from small discrete magma bodies scattered around Lake Taupo. The large Oruanui magma system started producing eruptions 60-70 ka, culminating in the 26.5 ka eruption and caldera collapse. The period from 60 to 70 ka also marked the onset of predominantly pyroclastic eruptions from Taupo, which have continued up to the most recent (also caldera-forming) explosive eruption at ~ 1.8 ka.

5.2.6 Most likely future volcanism

Maroa volcanism appears to have waned significantly over the last 100 ka, with only 0.02 km^3 of magma erupted since 26.5 ka. In contrast Okataina and Taupo are now highly active when compared to period from 230 – 64 ka (Section 5.2.5). Both the latter volcanoes also have a much higher rate of shallow (< 20 km) earthquake events than Maroa (reviewed in Section 1.7.2, Bryan et al., 1999).

Based on the history over the last 100 ka, future eruptions at Maroa are considered most likely to be small dome-forming events of Puketarata-eruption scale (Brooker et al., 1993). The typical Maroa eruption sequence was discussed in more general terms in Section 2.8. The hazard and risk implications of a future Maroa eruption are investigated in Section 5.6 based on the rate, volume and style of Maroa eruptions in the last 100 ka. In contrast eruptions from Okataina and Taupo will probably continue to be more frequent and of larger volume than < 100 ka Maroa eruptions and, based on recent history, either or both of Taupo and Okataina may produce another caldera forming eruption in the future.

5.2.7 High heat flow and the possibility of a future increase in Maroa volcanism

Despite the waning volcanism and shallow seismicity at Maroa, the geothermal output remains high across northern Whakamaru caldera (see shallow resistivity as a proxy, in the Maroa geophysical review in Section 1.8.2). The thermal output of geothermal areas around Maroa is almost 20 % of the 4200 ± 500 MW TVZ total thermal flux (Bibby et

al., 1995). Bibby et al. (1995) summarise the combined thermal outputs of Orakeikorako, Atiamuri, Ngatamariki, Mokai and Ongaroto geothermal fields as 790 ± 160 MW. The first two fields are within Maroa proper and the last three are all within 4 km of the margin of Maroa. This compares to ~ 1230 MW from the entire Lake Taupo/Taupo area, ~ 850 MW from Okataina, ~ 420 MW from Rotorua and ~ 850 MW from the combined Horohoro, Waikite/Waiotapu, Te Kopia, Reporoa and Ohaaki geothermal fields northeast and east of Maroa. Bibby et al. (1995) suggest high heat flow in TVZ is produced by mid- to upper-crustal (5 to 10 km) magmatic intrusion. The high Maroa thermal flux suggests that there is still a significant quantity of molten magma below Maroa, comparable to that below the rest of central TVZ. Thus, although volcanism is now at a very low rate at Maroa the possibility of a future increase in volcanism cannot be wholly discounted. A possible tectonic link to the variation in the rate and volume of volcanism across TVZ is discussed later in Section 5.4.5.

5.2.8 Caldera Collapse at Maroa

Rogan (1982) and Wilson et al. (1984) had noted a negative gravity anomaly below Maroa and both suggested that this was related to caldera-collapse that post-dates the Whakamaru eruption. Wilson (1986) also highlights this geophysical data but notes that Maroa is unusual as a caldera because (1) it lacks any single large ignimbrite associated with the caldera, and (2) it has a particularly limited range (< 20 km from Maroa) of pyroclastics associated with the centre. Houghton et al. (1995) correctly linked the Korotai, Atiamuri and Orakonui pyroclastics to eruptions from Maroa. They also dashed a circular caldera margin around the northern two thirds of the centre and indicated that these three eruptive units were caldera-forming. However, they did not provide direct evidence for these assertions (they mention Wilson et al., 1984 only in general terms).

Maroa also lies over a particularly strong magnetic anomaly (Fig. 1.18). However, I do not consider this, and the presence of a gravity low below Maroa (which is in fact offset, straddling the north edge of Maroa, Fig. 1.17) to be sufficient evidence to infer a caldera below the centre, when taking into consideration the following distinct lack of geological evidence for any caldera collapse:

(a) There is a large amount of new data on Maroa pyroclastics discussed here, in which there is no field evidence (such as lithic-lag deposits) within the larger units (Putauaki, Orakonui, Atiamuri or Pukeahua, Section 2.3), or the nearby

Mokai pyroclastics (not related to a Maroa source at all, Section 2.5.2), to suggest that they have been produced by caldera collapse at Maroa.

(b) New analysis of Maroa faulting is given below in Section 5.4. Faults at the surface appears to show either volcano-tectonic single event displacements < 90 m, or tectonic single event displacements < 2 m. Both of these mechanisms are unrelated to catastrophic caldera collapse but the down faulting they represent may, conversely, help explain the gravity lows below Maroa.

The gravity low and magnetic anomaly below Maroa are most likely simply related to the rapid infilling of Whakamaru caldera.

5.3 Evolution of Maroa Magmas

5.3.1 Introduction

This section draws on the synthesis of Maroa chronology (Chapter 3) and petrology (Chapter 4) to explore the associations and possible sources of magmas feeding Maroa eruptions; I then discuss these associations in the context of petrogenesis of the wider TVZ. I address the following key issues here:

- Two case studies exploring the petrogenetic association of Maroa dome clusters.
- Magma associations for Maroa deposits with specific chronological, spatial and petrological similarities based on the results from the case studies.
- End-member models for the magma systems that feed these associations.
- Comparison of Maroa magmas to those of other contemporaneous volcanic centres within central TVZ, discussing possible reasons for correlations and differences.
- Models for the petrogenesis of TVZ magmas.
- The scarcity of basalts within Maroa compared to other TVZ centres and to international models to make inferences on the relationship of basalt to rhyolite magmas.

5.3.2 Case study 1: the MWC/MEC dome cluster

The possibility that the MWC/MEC dome cluster has been erupted from a single magma association is considered likely because these domes are closely spatially related, and they were, apart from two outliers at 305 ± 17 and 189 ± 8 ka, erupted over

a short ~ 29 kyr period from ~ 251 ka (Chapter 3). Their chemistries also show a narrow range in Sr and wider range in Rb, which defines a geochemical type (M-type, Chapter 4) unlike any compositions reported from Taupo or the WDB. The unique Rb-Sr geochemistry of these deposits is mirrored to varying extents in all other elemental contents (as shown in Figs. 4.11 and 4.13). Figure 5.3 presents the Sr content of all MWC/MEC domes plotted against Rb content. Where available from Chapter 3 the ages determined for domes are shown in black over the corresponding geochemical data point for that dome.

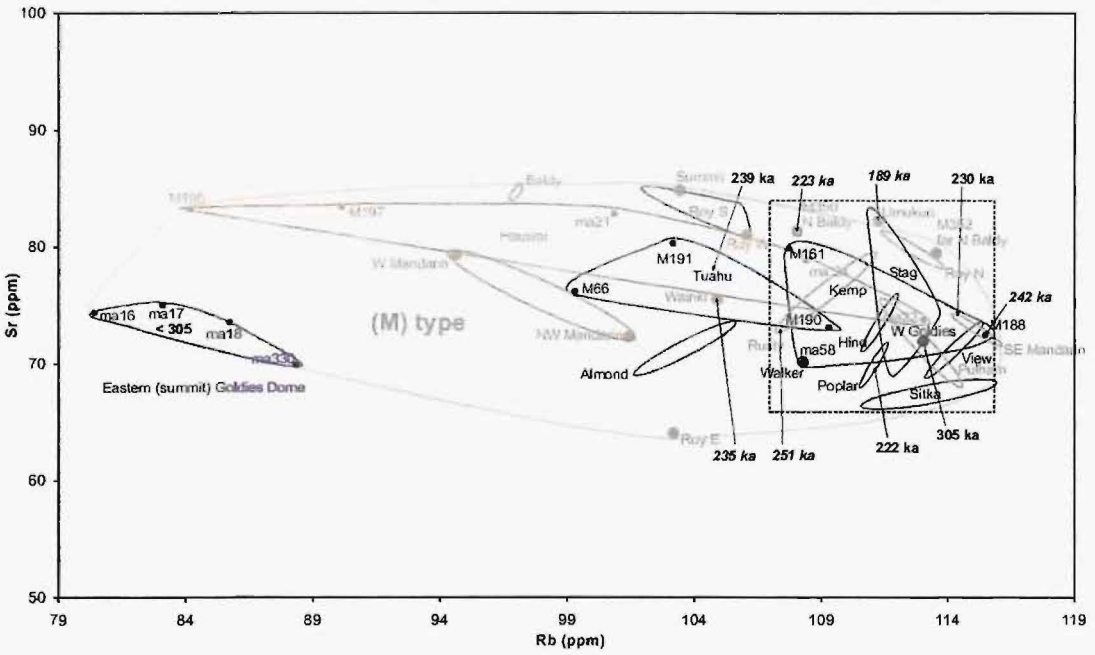

Figure 5.3 Rb-Sr variation diagram for MWC/MEC domes. The green background field is that defined based on these points in Section 4.5 for M-type magmas. Dark blue points and fields are MWC deposits and green are MEC deposits. The dashed box excloses the area of maximum concentration of points (discussed in text). Ages for individual domes are shown over their analyses in black numerals. Analytical random error (precision) for the XRF for Rb and Sr are .02 and .005 ppm, respectively; therefore, they are insignificant compared to the variation between analyses and error bars cannot be plotted at this scale.

Geochemical and chronological variation that must be accounted for

Addressing Rb-Sr variation first, any model for the association of these deposits must account for the geochemical variation seen in Figure 5.3. Five observations can be made about the variation:

(1) All points have a narrow Sr range of 66 to 84 ppm. The bulk of points have a narrow Rb range from 107 to 116 ppm (boxed area on Fig. 5.3).

(2) Hauwai and Tuahua domes have some analyses with compositions that range to lower Rb but the fields for these domes overlap with the above group.

(3) Baldy, NW and W Mandarin, Summit, Almond and the Roy S and W domes lie at slightly lower Rb concentrations than the main group.

(4) Eastern Goldies dome has a lower Rb content than all but one of the rest of the samples.

(5) Roy East dome lies at a slightly lower Sr content than the rest of the deposits.

The association model must also take into account the distribution of ages for the deposits. On Figure 5.3 no clear order to the ages can be seen, with compositions for domes aged from 305 to 189 ka apparently randomly distributed across the main group of concentrations.

Defining the term 'magma source'

For the purposes of this discussion the term 'magma source' is used to define the common magma chamber that an associated group of Maroa deposits last resided in prior to eruption. It does not necessarily refer to any upper-mantle/basal-crust 'origin', unless that was the last place an associated group of deposits commonly resided. 'Magma source' is used instead of 'magma chamber' because determining the exact nature of each 'source' is beyond the limitations of the data collected for this thesis. Instead, two end-member models for the location of, and ascent mechanisms from, such sources are given below in Section 5.3.5 and the location of each source along this spectrum is left for future research, needing further data, to define.

Models for geochemical variation in a magma source

Models for magmatic processes causing geochemical variation within an evolved (silicic) magma body fall into two main categories (both first explored at length by Bowen 1928, and revised by many workers, e.g. De Paolo, 1981):

- Assimilation of melted country/wall rock.
- Fractional crystallisation, removing crystals from the main magma body to some cumulate or marginal location not tapped by eruptions.

A full continuum between these two processes is possible, and a mix of the two is termed Assimilation-Fractional-Crystallisation (AFC). Any model must also consider the possibility of multiple injections of melt (recharge) from one or more magma origins.

The composition of a magma source may vary:

- across time (AFC +/- recharge changing a homogeneous source)

- and/or across space (AFC +/- recharge producing a heterogeneous, zoned body).

MWC/MEC from a heterogeneous vs. homogeneous source

Assuming for a moment that these deposits are petrogenetically associated, the apparently random distribution of MWC/MEC dome ages compared to their vent location and compositions suggests that, although chemically quite homogeneous, the relatively small compositional variation that did exist in the source is dominantly spatial rather than chronological (ie. AFC +/- recharge producing a heterogeneous, zoned source).

In this model, eruptions of slightly different compositions are tapping different zones in the source. Applying this concept to the MWC/MEC data 'observation (1)' above may be explained by the bulk of eruptions tapping a homogeneous zone, and the eruptions with compositions overlapping (observation (2)), and slightly offset from (observations (3), (4) and (5)), the members of this group are tapping other zones, of slightly different composition, in the source.

Testing fractionation vs. assimilation/recharge causing MWC/MEC variation

The relative involvement of assimilation vs. fractional crystallisation, and recharge, in causing the variation in MWC/MEC chemistry can only be discussed to a relatively simple level with the data available. If fractionation of the erupted mineral assemblage alone had produced the geochemical variation seen across MWC/MEC deposits then their data points on a geochemical plot would be expected to follow a fractionation vector that matched the bulk distribution coefficient of that mineral assemblage (on average 80 % plagioclase, 15 % quartz and 5 % orthopyroxene for MWC/MEC domes). The slope of such a vector is shown for Rb and Sr content in Figure 5.4 (methods for calculating the vector are detailed in Appendix 6) and it clearly does not match the spread across the entire dataset. Also, Ba and Zr content falls in a widely varied field for MWC/MEC deposits (Fig. 4.16), so a single vector could not be expected to explain variation in these elements. Therefore, if fractional crystallisation is involved in producing the spread of these data then it is either (a) not of the mineral assemblage being erupted, (b) more complex than a single fractionation vector and/or (c) complicated by assimilation or recharge.

Evaluating the involvement of assimilation of sedimentary country/wall rock in producing chemical variation is best done for TVZ rocks by looking for $^{87}Sr/^{86}Sr$ variation. This is because $^{87}Sr/^{86}Sr$ is quite distinctly higher in TVZ sedimentary basement than in primary mantle-derived melt (Ewart and Stipp, 1968). Because $^{87}Sr/^{86}Sr$ is only available for one MWC/MEC sample (Chapter 4) such interaction is difficult to determine for this case study. The $^{87}Sr/^{86}Sr$ for Mandarin dome (MEC) is within the main low $^{87}Sr/^{86}Sr$ group encompassing most WDB domes, Pukeahua East dome, and the Mamaku, Ohakuri and Mokai pyroclastics (Section 4.7.8). This suggests that sedimentary-crust interaction is not significantly varied among these spatially widely distributed deposits. Crustal assimilation in the petrogenesis of TVZ rhyolite is discussed further in Section 5.3.7. The possibility of assimilation of rhyolitic volcanic/plutonic wall rock is difficult to test because of its similar composition to the melt.

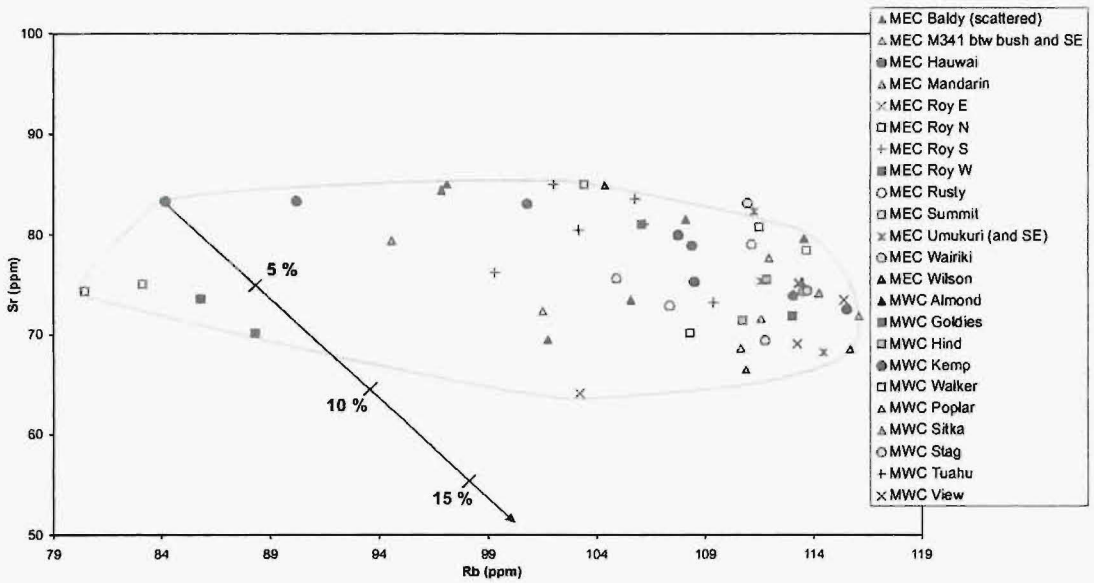

Figure 5.4 Fractionation vector for MWC/MEC average mineral assemblage plotted over the Rb and Sr data for these domes. Ticks along the vector denote percent fractionation.

It is important to take into consideration any mineralogical variation across the MWC/MEC domes. The two lowest-Rb samples from Hauwai dome (MEC) also contain the lowest crystal contents. This is roughly consistent with Hauwai dome tapping a less-crystallised zone. The crystal content does not show any other obvious variation across MWC/MEC deposits or ages. MEC deposits generally contain up to 3 % quartz, while MWC deposits are almost all free of quartz. Quartz content does not

appear to correlate to detectable geochemical variation in MEC deposits. The implications of the presence of quartz in MEC domes, and absence in MWC domes, is explored further in Section 5.3.5 as a constraint on the source configuration for this association.

In summary:

- The close proximity in time and space for the MWC/MEC domes, and overlapping closely similar chemistry, distinct from almost all other contemporaneous magmas in the vicinity, makes me consider them as probably associated in a common magma source.
- Variation within this association does not appear to be due to fractional crystallisation of the mineral assemblage seen in the deposits.
- It is difficult to evaluate the level of assimilation involved in producing the variation, but the variation in sedimentary rock assimilation is probably low.
- More complex fractional crystallisation, assimilation of rhyolite volcanics/plutonics and/or multiple recharge from one or more source magmas may be involved (i.e. this appears to be an open system).
- Further data, outlined in Section 6.2, are needed to evaluate the cause(s) of the variation in this association.

5.3.3 Case study 2: The Pukeahua dome cluster and pyroclastic fans

The Pukeahua cluster of domes, and the pyroclastics fan which surrounds it, are a tight temporal (229 – 196 ka) and spatial (< 10 km diameter) entity with vents geographically separate from those of other deposits of similar age (Chapters 2 and 3). The western and eastern parts of Pukeahua, however, have distinctly different petrology from one another (Chapter 4), and appear to have been erupted in the order eastern then western (Chapter 2). This contrasts to case study 1 in which the MWC/MEC domes appear to have a random age distribution across space but are considered (in this study) to be from a single magma source.

Figure 5.5 shows the distribution of Sr vs. Rb concentrations for Pukeahua deposits. The younger western part has the same petrological character described in case study 1 (the MWC/MEC cluster) and because it is less than 3 km offset from the nearest MWC/MEC vent the western half of Pukeahua is considered to be magmatically associated with MWC/MEC. Variation within the Pukeahua west deposits is probably

due to the tapping of the same variable source proposed for the MWC/MEC domes, discussed above.

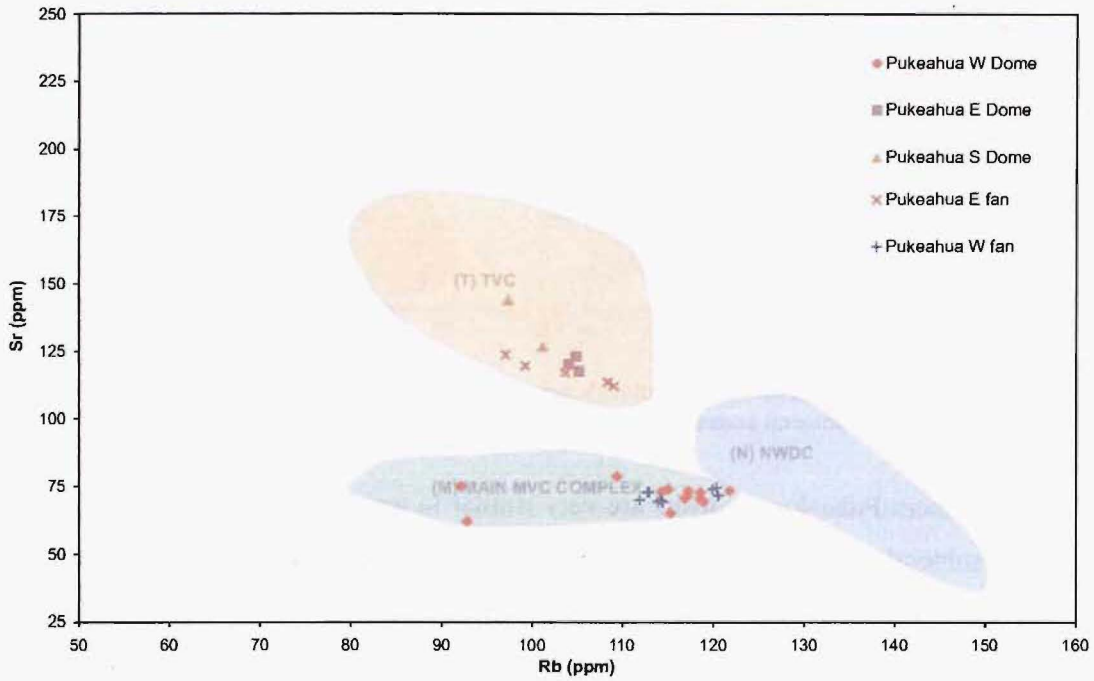

Figure 5.5 Sr versus Rb for Pukeahua deposits.

The chemical variations for the eastern Pukeahua deposits are considered in the same way as for case study 1 above and the same possible AFC +/- recharge processes are evaluated as causes for the chemical variations. Figure 5.6(a) presents the Rb-Sr vector, and 5.6(b) the Zr-Ba vector, that would be expected (methods given in Appendix 6) for fractionation of the mineral assemblage (on average 60 % plagioclase, 30 % quartz, 5 % orthopyroxene and 5 % hornblende) present in Pukeahua East deposits. Vectors on both of these plots coincide with the distribution of these deposits, although there is some scatter within each deposit that does not trend with the vector. This subordinate scatter is within the range that could be caused by variation in mineral abundance between samples analysed, and also possibly partly by analytical uncertainty ± sensitivity, and is therefore not interpreted further.

It is not possible to determine whether the fractionation has been over time in a homogeneous body, or over space in a zoned body, because I lack separate age data for individual Pukeahua eastern deposits.

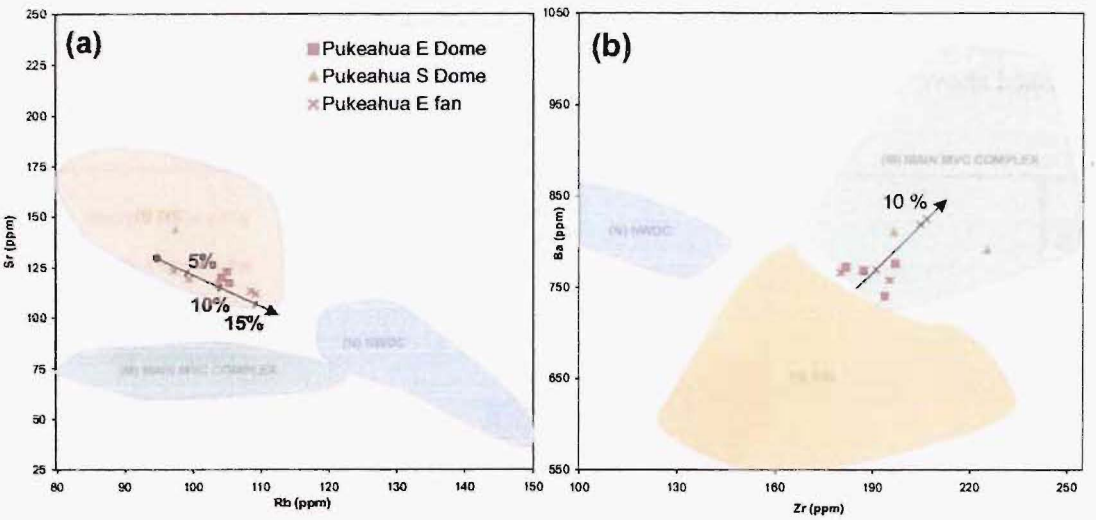

Figure 5.6 (a) Rb-Sr and (b) Ba-Zr variation plot showing fractionation vectors expected for fractionation of the mineral assemblage present in the eruption units (see text).

All of the western Pukeahua deposits are very similar in terms of relative abundance of individual minerals, and overall crystal content, to MWC/MEC deposits, strengthening the case for a common magma association linking them all. The eastern Pukeahua deposits have much higher crystal content than the western deposits, and contain hornblende. Both of these points highlight the lack of association between the western and eastern Pukeahua magmas.

5.3.4 Maroa magma associations

The two case studies above suggest that general magma associations can be postulated for Maroa deposits where spatial, temporal and petrological similarities exist. Variation within each association may be due to AFC +/- recharge processes, but the only test available with the current dataset is for fractionation of the mineral assemblage present in eruptives.

The magma association determined in case study one for the MWC/MEC dome cluster (apart from eastern Goldies dome and Roy East dome) is here termed 'association (1)'. The magma association determined in case study two for the eastern Pukeahua deposits is here termed 'association (2)'.

Based on the similarities seen is associations (1) and (2) I now link other Maroa deposits to these associations in Table 5.2 and identify the eruption units that fall into a further four magma associations, based on the same levels of spatial, chronological and

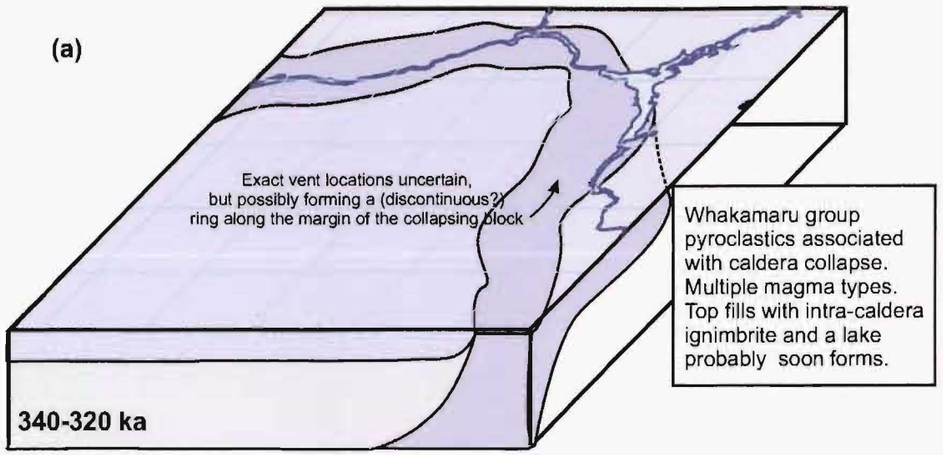

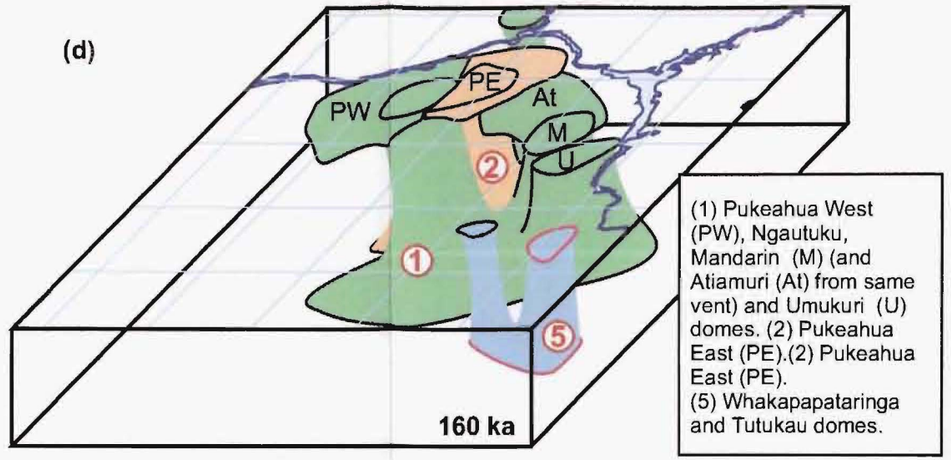

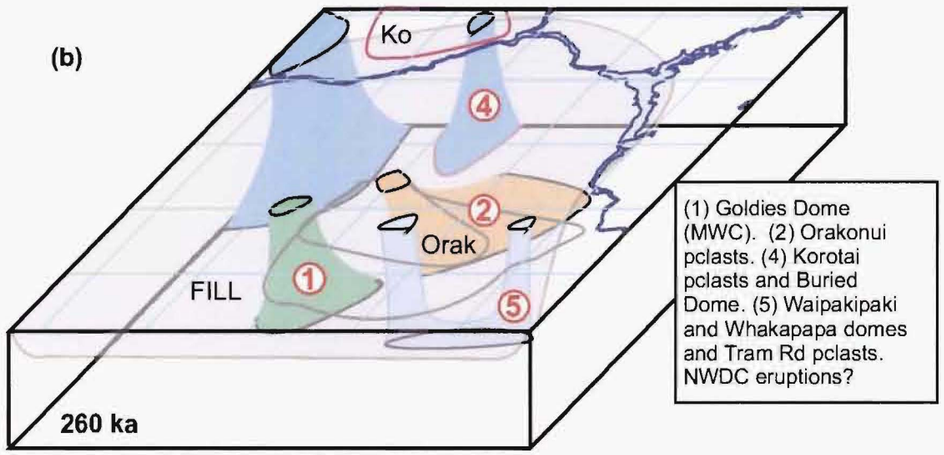

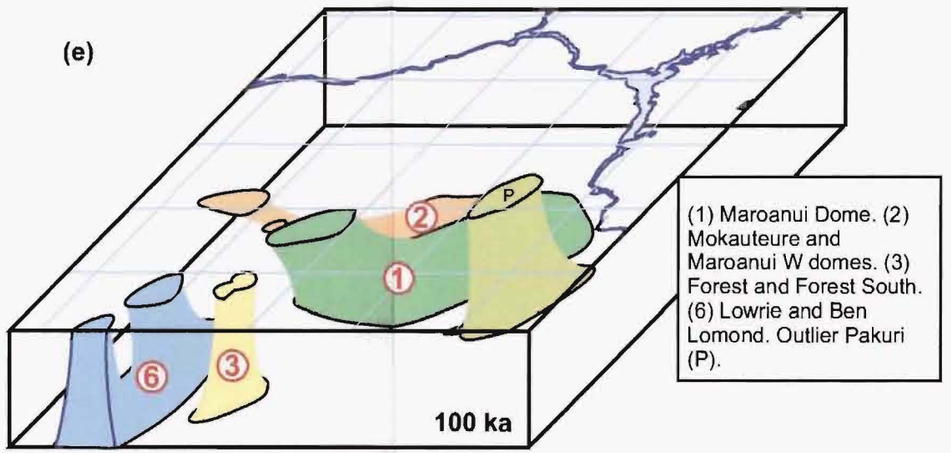

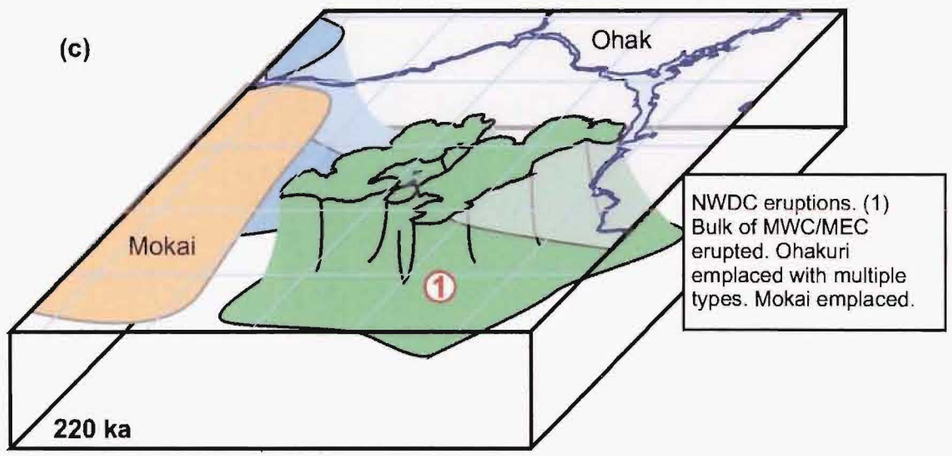

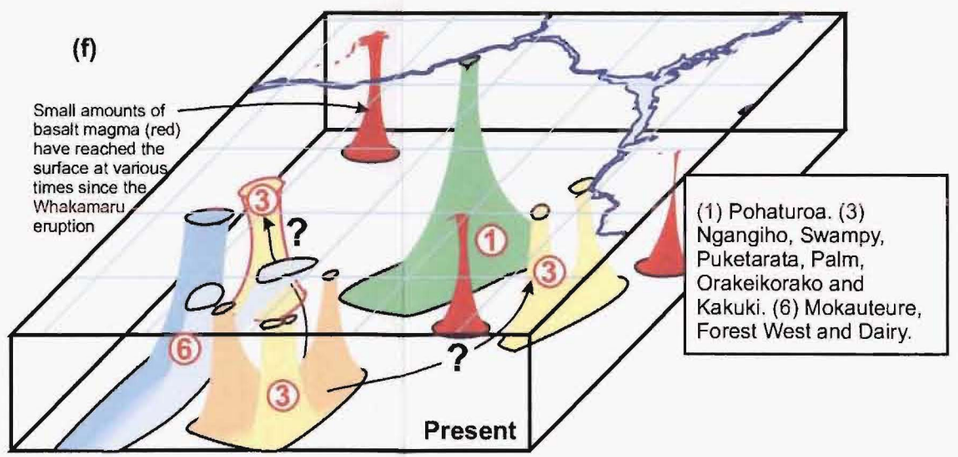

Figure 5.7 3D representation of the distribution of the six MVC magma associations (numbered in red) represented by surficial eruptives over time (340 ka to present, (a) to (f)). Colours: orange/yellow is low/high-Sr T type, Blue is N type (light is outlier) and Green is M type. Shapes and depths of connections not necessarily related to true shape of magma source. Grid line spacing is 5 km. Present river pattern shown to facilitate spatial orientation.

Depth (approx. 5 km) is proportional to horizontal scale and represents the 'upper crustal' region

petrological similarity shown above for associations (1) and (2). This total of 6 magma associations collectively accounts for nearly all of the deposits at the surface in Maroa (the few deposits not included in the associations are listed at the bottom of the table, and are considered to be from small magma sources isolated from those of the 6 associations). The next section discusses possible models for the sources of these magma associations.

Magma types T and N (defined in Chapter 4) are best split up into two and three separate associations (Table 5.2), respectively, based on spatial and chronological clustering of deposits. Almost all M-type eruptives are considered to be a single separate association, as described in case study (1) above. Note that some association (3) and (6) domes are both found together in the cluster along the end of Whangamata Fault (Fig. 5.1(f)) Implications of this clustering are discussed in Section 5.4.4.

5.3.5 Sources for Maroa magma associations

A graphical representation of the distribution of the magma associations across time (the same 6 chronological frames as in Figure 5.1) and space is given in Figure 5.7.

Deposits of each association are linked below the surface in order to aid visualisation of the relationship of all of the deposits within each association. (The links do not necessarily represent the shape, size or depth of the source chamber for the associations in any way). I propose two end-member models (Figure 5.8) for the actual configuration of the magma sources within which each association is linked:

Source Model 1: A single body at relatively shallow depth feeding multiple eruptions.

Source Model 2: A common source body at a deeper location than that for Model 1, feeding spatially scattered offshoot bodies at a relatively shallow level.

The key difference is that all of the pathways between a Model 1 source and the surface directly transport unmodified magma from the source to the surface, whereas the magmas travelling between a Model 2 source and the surface receive AFC/recharge modification along the way.

Assocn.	Deposits	Definition	Notes	Magma type
(1)	MWC/MEC dome cluster; Pukeahua W, Ngautuku, Pohaturoa and Maroanui domes, Atiamuri pyroclastics	Rb 80-123, Sr 67–88, Ba 740-1030 and Zr 170-265 ppm Opx is the only Fe/Mg mineral bulk of volume erupted from ~ 251 to 222 ka, all between ~ 305 and 77 ka.	Distinct chemistry from all other contemporaneous dome forming eruptions in the Maroa area	M
(2)	Pukeahua E and S Domes and eastern Pukeahua Fan, Orakonui and Putauaki pclasts	Rb 96-113, Sr 110-130, Ba and Zr within assn. 1 field. Emplaced between ~ 272 and 196 ka	Tight spatial and chronological entity	T
(3)	Forest S, Forest, Orakeikorako, Kakuki, Palm, Ngangiho, Swampy and Puketarata domes	Rb 93-106, Sr 118-140, , Ba and Zr mostly within Taupo field. From ~ 114 ka to 16.7 ka **Association (3) deposits are widely spatially spread and future data (discussed in Section 6.2) may show their origin to be more complex than from a single assoeiated source.**	Type 3 separate from type 2 because there is a gap between their fields on both Rb - Sr and Zr – Ba plots	T
(4)	Korotai pyroclastics and Buried dome	~ 277 ka Locally distributed at northern edge of Maroa	Distinct Zr content to otherwise similar nearby WDB domes.	N
(5)	Waipakipaki , Whakapapa , Tutukau and Whakapapataringa domes; and Tram Rd pyroclastics	Locally distributed at southeastern edge of Maroa	Spatially far removed from associations 4 and 6.	N
(6)	Ben Lomond, Lowrie, Dairy and Forest West domes.	Clustered along and near southwestern end of Whangamata Fault	Spatially far removed from associations 4 and 5	N
OUT-LIERS	Pakuri complex Pukeahua E lava arcs	Sr between association (1) and (2)/(3) Assocation (2) but low-Rb	Mix of (1) and (2)/(3)? -	M-T near T

Table 5.2 The spatial, chronological, petrographic and geochemical characteristics that distinguish the 6 associations. Magma types M, T and N as defined in Section 4.5.

Magma sources for the six associations defined above probably lie along on a continuum between these theoretical Model 1 and Model 2 end-members. A Model 1 source chamber would more likely feed eruptions over a surface area relatively close (within a few km) to that magma source. Vents from a single Model 1 source would not be expected to overlap with vents from other sources because of the conflict of space occupied at a relatively shallow level.

A Model 2 source would feed surface vents through shallower offshoot bodies. Because the source is probably deeper, these vents may sometimes be more widely separated

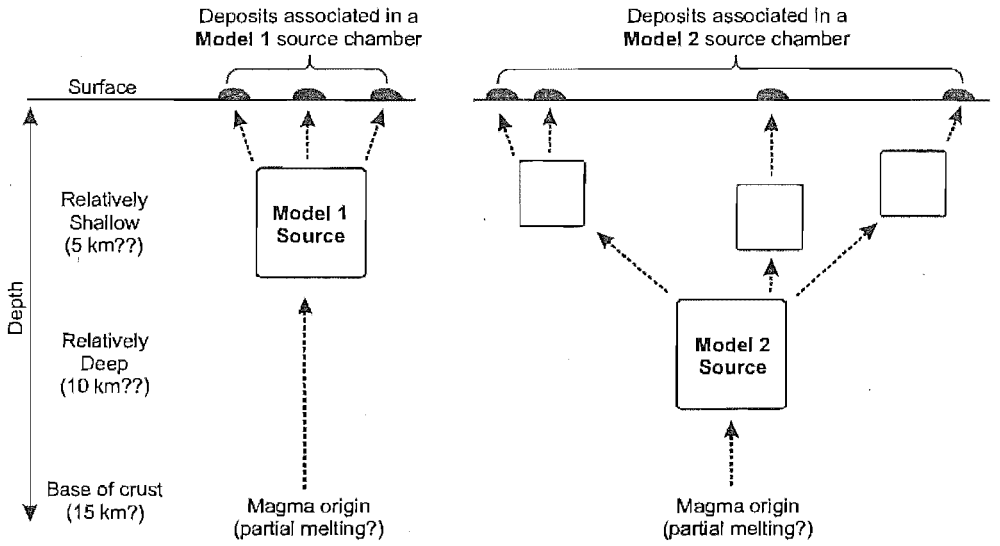

Figure 5.8 Configuration of the two end-member models for sources of each of the Maroa magma associations. Sources are magma chambers in which magmas feeding associated deposits last commonly resided. Sources differ from the magma origin, which is considered to be the basal crust location of partial melting. Crustal assimilation may occur at any or all depths in either model.

than vents of a Model 1 source. Different AFC processes in each shallow offshoot could produce complex (if only subtle) AFC ± recharge-derived variation among deposits from a common Model 2 source. Vents associated in a deeper Model 2 source could be expected to spatially overlap more easily with vents of other Model 2 source(s). For example, in case study (1) above perhaps two separate small shallow bodies existed below MWC and MEC, but connected in a common geochemically-zoned Model 2 source. This could account for the very close geochemical and mineralogical similarities of MWC to MEC, and for the fact that MWC contains quartz while MEC usually does not (i.e. a common deeper magma source but distinct late stage crystalisation histories). Note that $^{87}Sr/^{86}Sr$ variation and absolute values in the NWDC are similar to those of the Whakamaru group pyroclastics and MWC/MEC magmas, suggesting that there is a commonality in the level of crustal assimilation, at least, amongst all of these. Section 6.2 outlines extra data required to define further the sources for Maroa magma associations.

5.3.6 Maroa magmas compared to other centres/deposits

I now discuss Maroa magmas in relation to other contemporaneous magmas across the wider TVZ. Contemporaneous magmas have existed below Okataina for the period over which Maroa has been active, but detailed comparison of the two is omitted here because (1) Okataina is spatially more distant to Maroa that those centres discussed

here, and thus unlikely to have interacted with Maroa magmas, and (2) Ph.D. work being conducted by V. Smith (University of Auckland) and K. Spinks (University of Canterbury) will soon provide a more complete summary of Okataina petrology than is available for this thesis.

Whakamaru group ignimbrites

Brown et al. (1998) separate pumice from the Whakamaru-group ignimbrites into four geochemical types (A-D). Together these have a wider range of concentrations of all elements for one petrogenetically linked system than any other rhyolitic TVZ deposit erupted since. Brown et al. (1998) model their data by invoking at least two independent magma sources below Whakamaru caldera (Fig. 1.14, reviewed in Section 1.6.4). Rb-Sr fields for Whakamaru magma types A and B partly overlap with Maroa T magma type, and B also partly overlaps with Maroa N (Fig. 4.24). $^{87}Sr/^{86}Sr$ values of Whakamaru-group ignimbrites range across Maroa low- and moderate-$^{87}Sr/^{86}Sr$ groups (Fig. 4.21). The Whakamaru-group ignimbrites are mineralogically distinct from most other TVZ deposits; they almost all contain sanidine. Considering Maroa overlies the Whakamaru caldera there are at least two explanations for the overlap in petrology of Whakamaru group and Maroa deposits: (1) some remnant magma(s) from the Whakamaru system have contributed to Maroa magmas, but sanidine had been resorbed by the time Maroa eruptions occurred, or (2) Whakamaru and Maroa magmas are partly from a common source, and thus have overlapping compositions, but distinct mineralogies have since crystallised. The data to explore these possibilities further, or suggest others, are not available here.

Caldera-related magma systems 283 to 230 ka

The Pokai, Mamaku and Ohakuri pyroclastics were associated with formation of collapse features at Kapenga and Rotorua calderas, but have some intriguing similarities despite their widely disparate sources. They have geochemical compositions clustered into types that occupy two very similar fields (described in Section 4.7.11, Ohakuri has a third much higher Sr than any sample from the Mamaku or Pokai, discussed below). These two types are seemingly randomly distributed throughout each pyroclastics deposit. The $^{87}Sr/^{86}Sr$ is, in contrast, very different between the Pokai (high $^{87}Sr/^{86}Sr$ group) and the Mamaku and Ohakuri (low $^{87}Sr/^{86}Sr$ group) pyroclastics. Geochemical similarities and distinctions among these three deposits may suggest some commonality

in (a) deep source and/or (b) AFC process producing the geochemical variation in each of them. This is being explored further by Gravley (2004).

The two major Rb-Sr fields for the Pokai, Mamaku and Ohakuri pyroclastics overlap with Maroa M-, N- and T-type chemistries (Figure 4.24). Spatial separation between Maroa, and Mamaku and Pokai vents, indicates that the commonalities in deep source and/or AFC process described above may be the reason for overlap of these two deposits with Maroa chemistry, rather than in any common shallower level magma chamber source. Gravley (2004) suggests the source for the Ohakuri pyroclastics is very close to the northern boundary of Maroa, so the possibility of direct interaction between Ohakuri and Maroa magmas is possible. The Ohakuri pyroclastics have $^{87}Sr/^{86}Sr$ ratios that overlap with those of at least some M- and T-type Maroa magmas, which does not preclude a direct involvement between the magmas. The third, high-Sr, Ohakuri geochemical type is not expressed at all in Maroa magmas, so at least this part of the Ohakuri system has not interacted with Maroa magmas.

Compared to the regional pyroclastics described so far, the Kaingaroa (~ 230 ka, from Reporoa caldera) and Mokai (~ 220 ka, unknown source) pyroclastics, show relatively little geochemical variation. The Kaingaroa pyroclastics fall into four Rb-Sr types that overlap with N through T Maroa magma types, but the source is several 10s of km from Maroa so any commonality between the two must be in origin or AFC process only. The Mokai pyroclastics lie within the field for T-type Maroa magmas and a direct link in the sources of the two is possible. The T-type field is defined by 100-27 ka Taupo magmas so a link of the Mokai source to Taupo magma systems (discussed further below) is equally possible. Without a vent defined for the Mokai pyroclastics conclusions about any physical link between their magma source and that of Taupo and/or Maroa is not possible.

Taupo Volcanic Centre

Around 100 ka the majority of Maroa eruption volume began to shift from M and N-type, to T-type magmas (Figure 5.1(e)-(f)). Overall, M- and N-type deposits constitute an order of magnitude greater volume at Maroa than T-type deposits (Chapter 4). In contrast all of the eruptions at Taupo from 100 ka to 26.5 ka have been T-type. Oruanui and post-Oruanui Taupo eruptions also lie almost entirely within the field for T-type magmas. The only Maroa deposits that plausibly share connected magma source(s) with

Taupo are association 3 deposits. This is because association 3 deposits lie in the southern half of Maroa, nearest to Taupo, and the chemistry mostly lies within the Ba-Zr field (Fig. 5.9), and wholly within the Rb-Sr field (Fig. 4.10), for 100-27 ka Taupo deposits. In contrast, although association 2 is similar in Rb-Sr content to Taupo magmas, it has wholly different Ba-Zr chemistry to that of Taupo (Fig. 5.6 above). Mineral and isotopic data (see Section 6.2 'further work') for association 3 is needed to further explore the possibility of connectivity between the source for this association and any Taupo magmas.

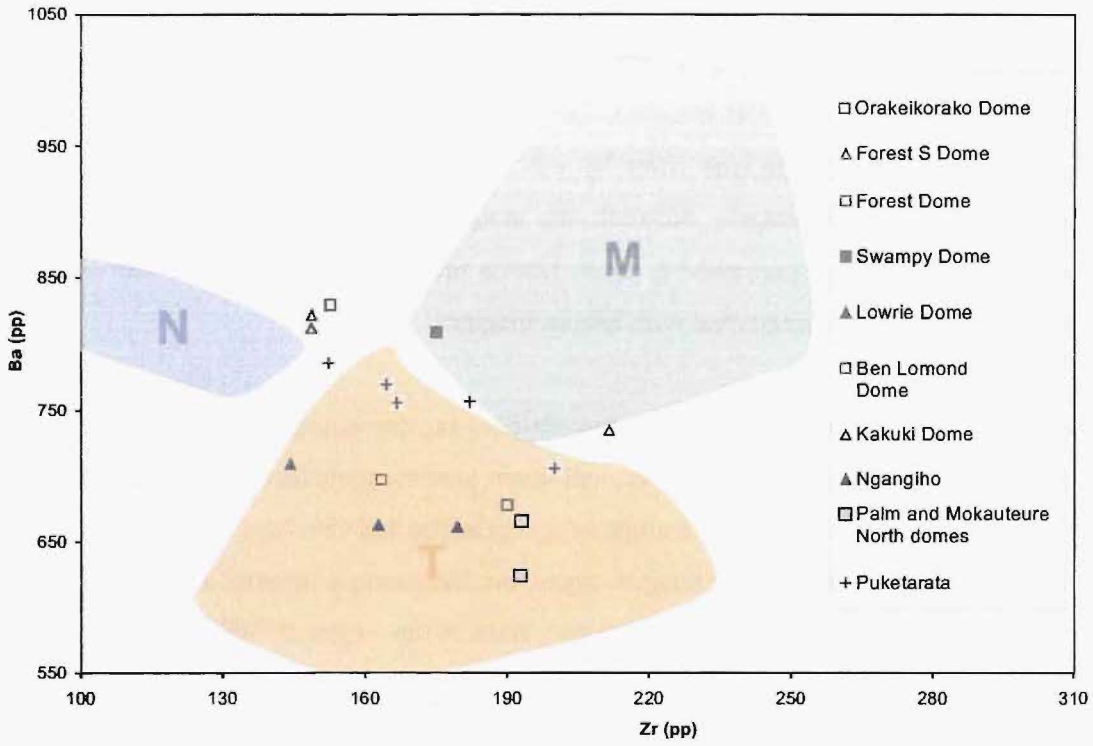

Figure 5.9 Ba plotted against Zr for Association 3 deposits. Blue, green and orange fields are those of NWDC, MWC/MEC and Taupo 100-27 ka deposits, respectively.

5.3.7 TVZ rhyolite petrogenesis

The scope of the Maroa petrological dataset obtained for this thesis research does not provide significant new insights into the petrogenesis of Maroa rhyolites, or those of the wider TVZ. A review and discussion of current theories on TVZ rhyolite petrogenesis is given here.

There has been a long-running debate over the origin of rhyolite magmas in the TVZ, and no single definitive model has so far been widely accepted. AFC of ~ 90 % fractional crystallisation of high-alumina basalts, such as those seen at the surface in

TVZ, could produce rhyolite melts (Graham et al., 1992; McCulloch et al., 1994), but these would have trace element abundances significantly greater (enrichment in Nd, Sm, Eu, Gd, Dy and Yb; Reid, 1983) than those seen in TVZ rhyolites.

An alternative model is one where crustal melting dominates. Graham et al. (1995) inferred that wholesale crustal melting is precluded by differences in Sr, Nd, Pb and particularly O isotopes between TVZ rhyolites and greywacke basement. In reality the situation is, however, not so clear-cut because the composition of the basement below TVZ has not been directly determined, but is rather inferred from analyses of greywacke exposed along the margins of the TVZ. If Graham et al.'s inference is correct, some proportion of fractional crystallisation of mantle-derived basalt is required, but the proportions are still equivocal. The predominance of crustal melting has most recently been argued by Graham et al. (1992); whereas McCulloch et al. (1994) calculate that ~ 15 to 25 % greywacke contamination of basalt, followed by fractional crystallisation is enough to explain TVZ rhyolite trace element and isotopic compositions. The debate continued, with Graham et al. (1995) maintaining that McCulloch et al.'s analysis was biased due to a limited dataset compared to that used by Graham et al. (1992). The integral problem hampering any one definitive model is that the real composition of the crustal end-member is unknown.

Recent zircon data from C. J. N. Wilson and B. Charlier (Charlier et al., submitted) shows a Mesozoic and Palaeozoic contribution to the zircon population in two eruption units at Taupo, consistent with at least some interaction with greywacke basement. Charlier et al.'s new data, however, suggests that the ages, and thus componentry, of this greywacke basement are more complex than previously thought. It appears to contain some component(s) which are not seen at the surface and are thus of unknown composition. This has wider implications to the provenance and evolution of New Zealand greywacke terranes, as well as to the petrogenesis of TVZ rhyolites.

5.3.8 Why are basalts scarce at Maroa?

The scarcity of basalts in Maroa is typical of the TVZ, where basalts make up < 1 % of the volume of magma erupted (Healy, 1962; Gamble et al., 1990). At Maroa there is, however, a lack of evidence for the interaction of basalt magmas with rhyolite magmas, compared to contemporaneous centres elsewhere in TVZ. Rhyolite eruptions at 18 ka

and ~ 1315 AD (Nairn, 1989; Nairn, 1992; Leonard et al., 2002) from Tarawera Volcanic Complex, Okataina, have included minor amounts of basalt, clearly showing mixing and mingling with the rhyolite in the most recent event (Leonard et al., 2002). Similarly, the rhyolitic Whakamaru group from Whakamaru caldera (Brown et al., 1998), Waimihia and Oruanui eruptions (Blake et al., 1992; Sutton et al., 1995) from Taupo, and Mamaku eruption from Rotorua caldera (Milner et al., 2002b) contain traces of basaltic to andesitic clasts. Maroa rhyolite deposits contain no basalt clasts, no basalt-rhyolite mixed magmas and no basalt xenoliths or xenocrysts at microscopic scale.

There is an observation that a paucity of basalt eruptives exist in areas where silicic magma has accumulated or is inferred to be present (e.g. Christiansen, 2001). These areas have been termed 'basalt shadow zones', especially in discussion of North America areas of silicic volcanism. It has been suggested that the paucity of basalt at the surface is due to the rhyolite magma bodies preventing the ascent of basalt magma from below (refer to the review in Valentine, 1993). In this theory basalt magma is ascending in greater volumes than reaches the surface. Valentine notes that most authors consider the density contrast between rhyolite and more dense basaltic magmas blocks the ascent of basalt melt through rhyolite magma bodies. He suggests, however, that instead a rheological contrast to the rhyolite chamber is what hinders the ascent of the basalt.

The lack of basalt within rhyolite deposits at Maroa suggests that the 'shadow zone' theory may be applicable here. The continued high geothermal flux at geothermal areas around Maroa suggests that there is a continued magma flux below Maroa, which must be being fed by continued basalt ascent. The paucity of < 100 ka eruptions at Maroa, relative to this continued basalt flux may be a result of the 'shadow zone' affect of rhyolite magma still present below Maroa.

Maroa basalts appear to lie along the trace of Whangamata Fault, which appears to be a much more deeply-seated, regional, feature than the other faults and lineaments across Maroa (see below). This fault may be providing the only pathway for basalts to reach the surface from deep crustal depths.

5.4 Maroa and faulting

5.4.1 Introduction

The zone of extensional faulting that coincides with the TVZ is termed the Taupo Fault Belt (TFB, as defined by Berryman and Villamor, 1999). Maroa lies in the central intensely faulted part (The 'Central Domain' of Rowland and Sibson, 2001) in terms of its location along the length of the belt. This section is considered to have the highest rate of extension (Villamor and Berryman, 2001). Maroa also lies along the central axis of the TFB, which theoretically contains the youngest faulting within the belt, created as the TVZ widens through rifting (Rowland and Sibson, 2001).

Conventional thinking on the nature of TFB faults has revolved around a model of relatively constant slip rate across the history of any one fault (e.g. Rowland and Sibson, 2001; Villamor and Berryman, 2001). A fault trenching project in Maroa that I was involved with, and application of the new geochronology dataset in Chapter 3, raise the possibility of temporal clustering of displacement during periods of volcanism.

Three elements of Maroa faulting are discussed in the context of the current neotectonic theories on TFB faulting:

- identification of fault scarps and assessment of whether they are 'active' or not;
- the role of localised (dike-related) rifting in generating fault structures;
- the use of dated domes to constrain amounts and timing of movement: steady-state or episodic?

It is important to first define the locations of Maroa faults. Previous workers (especially Lloyd, 1972) have mapped a plethora of smaller lineaments as faults within Maroa. In this study, however, it has been difficult to determine if there has been any significant offset on many of these lineaments. For others it is questionable whether they represent a tectonic structure (ie. show no apparent movement). Many may simply be small scale fissures or gravity slumps (with only 1 or 2 m of displacement, if any) associated with dome growth (e.g. those across Pukeahua dome complex), or settling in response to movement on nearby faults. Lineaments, and faults with a detectable offset and sense of motion, are distinguished from each other on Figure 5.10.

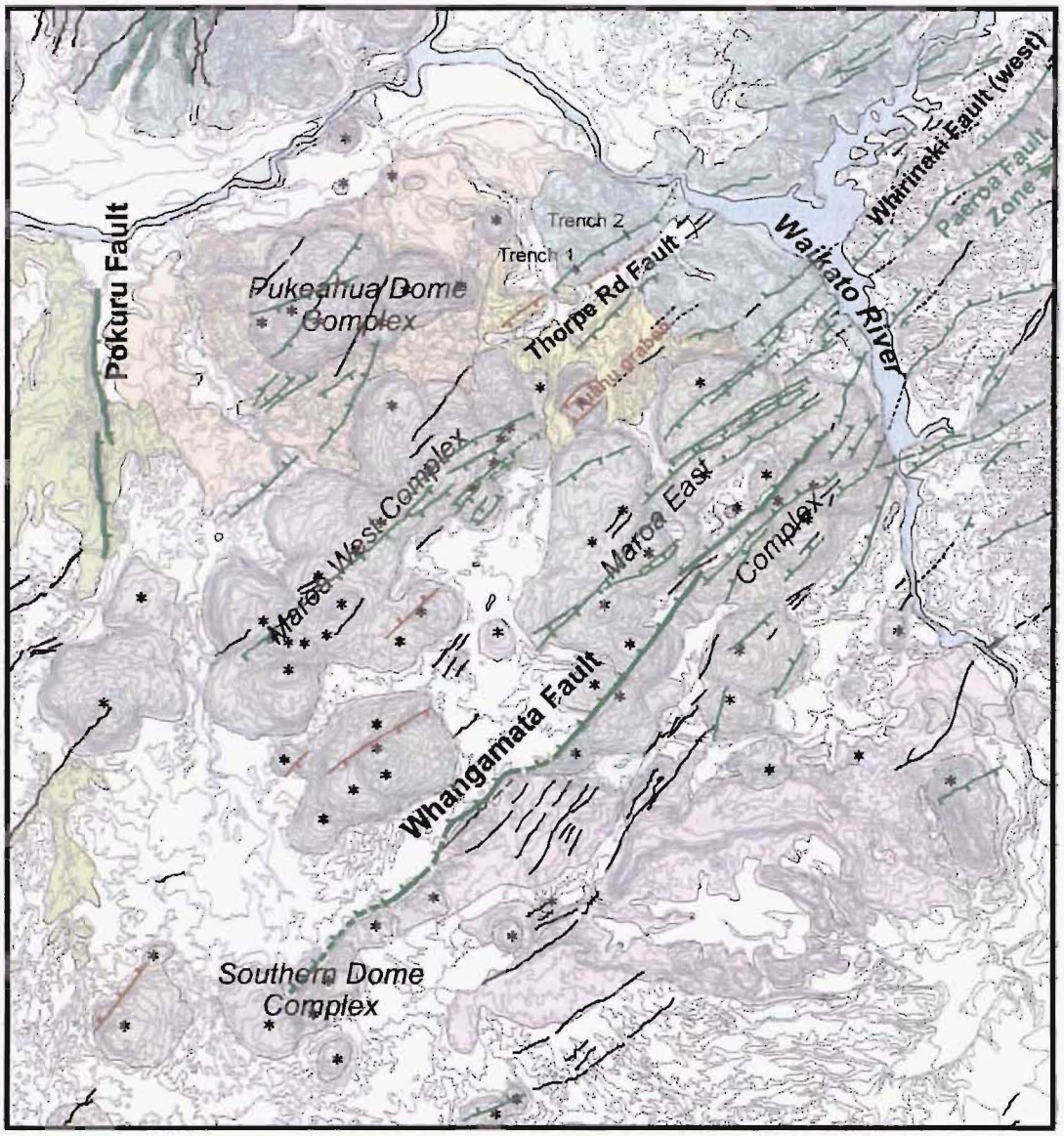

Figure 5.10 Faults, lineaments and likely vent locations across Maroa. Lineaments without notable offset are shown in black. Faults presented in green are those clearly identified as having a sense of motion by Rowland and Sibson (2001) and Villamor and Berryman (2001) based on the active faults database maintained by IGNS and kindly made available for viewing in this project. Those in Red are additional faults determined as part of this research. Rhyolite domes are shown in dark grey. Mokai pyroclastics are light yellow-green, Ohakuri are light green, Korotai are green, Pukeahua are light orange, Atiamuri are light yellow and Putauaki/Orakonui are light pink. Contour interval is 20 m.

The Pokuru and Whangamata Faults show far more displacement (> 100 m vertically) than any others in Maroa. Thorpe Road and Tuahu graben faults show up to 40 m each of vertical displacement and all of the others appear to have had 10 m or less of displacement. This section discusses the nature of displacement on Thorpe Road fault, while faulting across Tuahu dome addressed in Section 5.4.3 and Whangamata Fault is discussed in detail in Section 5.4.4. As mentioned earlier in Section 5.2.2 the rate of movement on the Pokuru Fault is constrained by the ~ 220 ka Mokai pyroclastics. A

vertical displacement of 140 ± 20 m is seen in the Mokai pyroclastics, but the southern end of the fault does not displace the 86 ± 12 ka Mokauteure dome. Therefore all of the visible displacement on this fault has occurred between ~ 220 and 86 ka.

5.4.2 Fault scarps: active or inactive?

Over the course of fieldwork for this thesis a distinct lack of faults displacing Oruanui (~ 26.5 ka) and post-Oruanui deposits, compared to that seen in the Ngakuru Graben to the northeast, became apparent. K. Spinks and V. Acocella (pers. comm. 2002) made the same observation while searching for roadside Holocene displacements across the TVZ. The model of uniform displacement rates on central TFB faults implies that the faults delineated in Figure 5.10 should have rates of movement related to the overall extension rate in the area. In this view the timing of displacement events would not be correlated to the timing of volcanic events and late-Quaternary/Holocene displacements should be as common in Maroa as they are to the northeast. A paleoseismic investigation of Thorpe Road Fault (Fig. 5.11) provides a case study of a Maroa fault that does not fit the uniform displacement-rate model.

Trenching the Thorpe Road Fault

The Thorpe Road Fault in the northern part of the Atiamuri pyroclastics creates terraces in the major northeast-trending gully north of Thorpe Road. The fault also appears to continue west into a ~ 40 m displacement in the Atiamuri pyroclastics bluffs west of SH1. Terraces, along the Thorpe Road Fault, that showed apparent vertical displacements of 1 to 10 m were trenched in October 2002 as part of an IGNS paleoseismic investigation contracted by Mighty River Power. The project aimed at determining seismic acceleration hazard posed by the fault to the Ohakuri Dam foundations (Fig. 5.11). The objectives were to (1) identify the stratigraphy, (2) identify Thorpe Road Fault ruptures in the stratigraphy, (3) estimate the frequency and timing of faulting events and (4) estimate the maximum single event displacement that could be expected. I was present at the trench sites, helped log the trench walls and was contracted by IGNS to help interpret the geology exposed. Permission has been kindly granted by Mighty River Power and IGNS to use in this thesis some of the data and images obtained during the trenching. Summary logs and descriptions of trenches are given in Appendix 7.

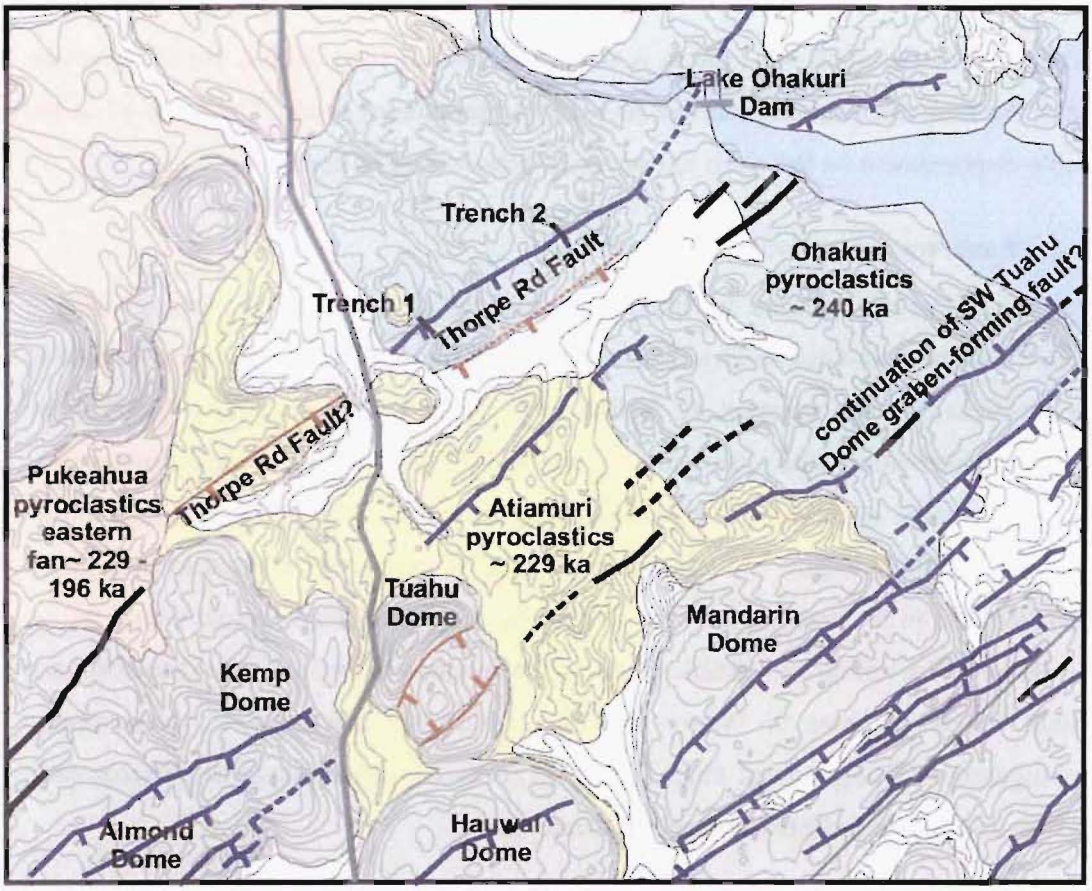

Figure 5.11 Map of contours, lithologies and faults in the northeast of Maroa. Locations of Trenches 1 and 2 are shown.

The stratigraphy within the trenches is summarised in Figure 5.12. Neither trench showed displacement in Oruanui (~ 26.5 ka) or younger deposits, but Trench 2 reached the top of underlying Ohakuri pyroclastics, which showed multiple fractures with < 200 mm of displacement. Augering above and below the 8 to 10 m scarp alongside Trench 2 showed Ohakuri pyroclastics at ~ 4 m below the surface in each. This suggests that the scarp was produced by an offset in Ohakuri pyroclastics but not the younger mantling material. Figure 5.13 is a diagrammatic cross section summarising the relationship between the faulted Ohakuri ignimbrite and mantling deposits seen in the two trenches.

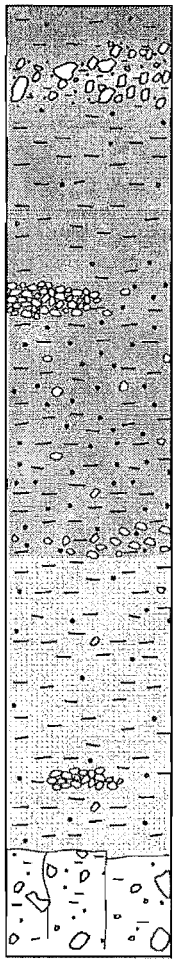

Dark brown soil horizon formed from young local sediments and reworking of the Taupo Ignimbrite

Primary Taupo ignimbrite (186 A.D.)

Thick late-Pleistocene and Holocene loess, with some interbedded, poorly-preserved, tephras. There is strong bioturbation and development of paleosols.

The c. 13.8 ka Waiohau tephra is present in Trench 2 only

Alternating moderately firm pumice rich sandy gravels and gravely sands. Sediments (pumice and whole-rock clasts) derived during cold-climate from the surrounding paleo-hills of Ohakuri and Atiamuri pyroclastics, as a result of the high rates of erosion that followed the Oruanui eruption

Variable amounts of primary Oruanui pyroclastics sequence seen at some locations in Trench 1

A siltier sequence of sediments lies below the Oruanui pyroclastics. It is probably derived from the Ohakuri and Atiamuri pyroclastics, probably deposited at a much slower rate while the landscape was relatively stable compared to the post-Oruanui period

Traces of Okaia tephra (c. 29 ka) are occasionally preserved

Trench 2 reaches local basement which is in-situ weathered Ohakuri pyroclastics (~ 240 ka) with occasional fractures

Figure 5.12 A diagrammatic summary of the stratigraphy in the trenches across the Thorpe Road Fault. Age of Waiohau Tephra (13.8 ka) from Speed et al. (2002). Age of Okaia tephra (29 ka) from Newnham et al. (2003)

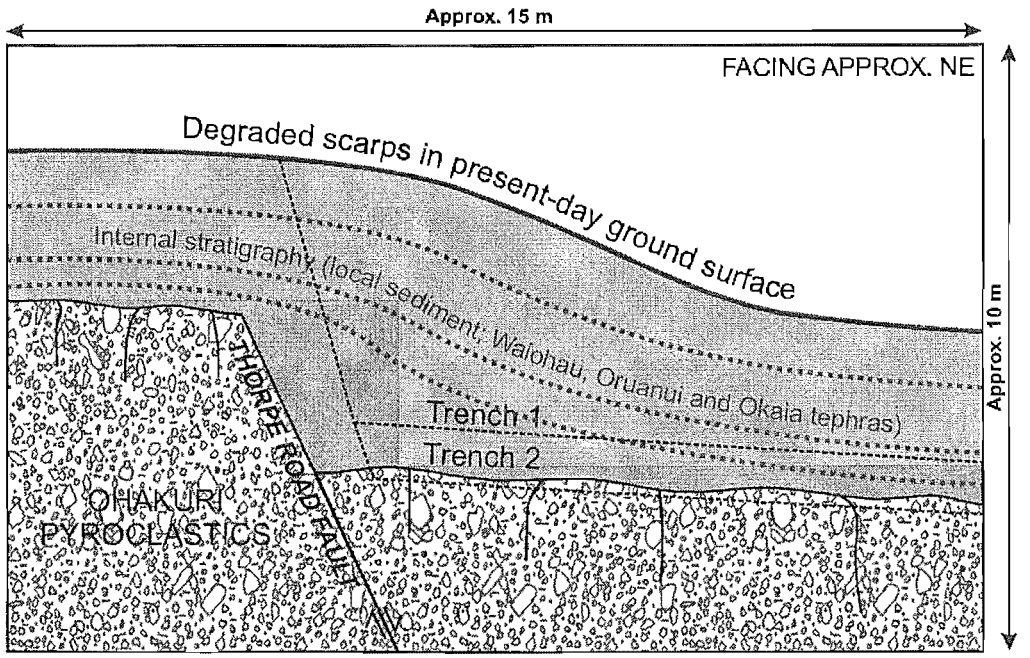

Figure 5.13 Block diagram of Thorpe Road Fault relationship to younger material and topography.

The key result of this trenching is that there has been no displacement on Thorpe Road Fault in the last 28.5 kyr, even though it creates a distinct terrace in the modern landscape. The terrace clearly continues through the ~ 240 ka Ohakuri and 229 ± 12 ka Atiamuri pyroclastics to the southwest (Fig. 5.11). However, the terrace disappears against the younger Pukeahua eastern fan that is no younger than 196 ± 8 ka. It appears that the young-looking Thorpe Road fault is in fact a inactive feature, no younger than 196 ± 12 ka. It is, therefore, quite possible that other young-looking fault displacements within Maroa, and the wider TVZ, are in fact inactive features mantled by younger material.

5.4.3 Faulting related to dike emplacement

The case study above represents an example of a Maroa fault scarp distinctly visible at the surface but which is in fact an 'inactive feature'. This puts the displacement in Maroa's earlier history (between ~ 229 and 196 ka), when volcanism in the area was at its height. The association in TVZ of faulting with volcanism has been overlooked by some workers, which is surprising given the strong fault-parallel elongation of the majority of rhyolite dome clusters across the entire central TVZ area. Haroharo and Tarawera Volcanic Complexes in Okataina, Horohoro dome and the dome complexes along the northern shores of Lake Taupo are all elongated northeast and in line with grabens bounded by faults considered presently active (Rowland and Sibson, 2001).

Berryman et al. (2002) demonstrate the intimate association of faulting events with deposits from two Holocene eruptions at Okataina in several paleoseismic investigation trenches along Ngapouri Fault. Local explosion crater deposits of the ~ 1350 AD rhyolite Kaharoa eruption directly overly deposits reworked by a faulting event independently ^{14}C dated at the same age. Displacement on this fault also accompanied the 1886 AD basalt Tarawera eruption. Berryman et al. conclude that the fault is primarily a structural feature reactivated during the two eruptions, both of which appear to have been dike-fed along the centre axis of a graben bounded by the fault itself. The ~ 10 ka multiple vent andesitic eruption sequence at Tongariro Volcanic Centre, at the southwestern end of TVZ, is also inferred to have occurred along the axis of a graben controlled by regional tectonics (Nairn et al., 1998).

These are examples of the relatively few published cases of TVZ faulting associated with dike emplacement. However, based on (1) the structure-parallel trend of many

TVZ dome complexes, (2) the cases of Tuahu dome and the domes along the southwestern end of Whangamata Fault discussed below and (3) similarities to international case studies discussed below, I consider it likely that a substantial amount of faulting occurs in association with dike emplacement in TVZ.

I highlight the Tuahu example as a case where dike intrusion has directly caused graben formation. The Ngapouri (Okataina) and Whangamata (see below) faults are, in contrast, examples where clearly tectonic features have probably controlled the location of diking and, in the case of at least the Ngapouri Fault, had displacement events activated during that diking. These are two end members of what is probably a continuum in TVZ between volcanic (dike) and tectonic-driven faulting.

Tuahu dome case study: dike intrusion causing normal faulting

Several Maroa dome complexes are cut by normal faults (Fig. 5.10). The most striking example is the graben across the summit of Tuahu dome. A pair of normal faults drop the central part of Tuahu dome by ~ 40 m. Two factors suggest that the faulting in Tuahu domes is of a very similar age to the dome itself: (1) the faults do not propagate into the ~ 9 kyr-younger Kemp dome to the southwest, or across the ~ 10 ka younger Atiamuri pyroclastics to the northeast; (2) beyond the Atiamuri pyroclastics a fault northeast along strike of the southeastern Tuahu dome fault is apparent in the Ohakuri pyroclastics, which are only ~ 1 ka older than Tuahu dome (Fig. 5.11).

Probable minimum critical dike width and graben depth

The close chronological tie of the graben faults to Tuahu dome raises the possibility that the graben in the dome was driven by blind dike intrusion below the dome possibly related to eruption at an offset distance along the fault strike. To discuss this I have calculated the range of minimum critical widths of a silicic dike required for magma ascent using the methods of Petford et al. (1993; 1994) (values and calculations used in Appendix 8). The minimum conceivable width is ~ 1 m and the maximum ~ 58 m, based on their range of realistic values for magma viscosity, depth to magma source, difference in density of magma to wallrock, melt temperature and wall-rock temperature, and modified to reflect the possible values in the TVZ. The most probable dike width for the Tuahu dome case is ~ 10 m (moderate viscosity, 10 km source depth, melt temperature ~ 850 °C and wall-rock temperature ~ 300 °C, justified in Appendix 8).

TVZ normal faults are considered to generally dip from 45° to 70° by Villamor and Berryman (2001). The apparent dip of both faults at Tuahu is close to 45°, at the least steep end of their suggested range. The distance between the fault planes at their highest elevation (550 m asl.) on top of the dome is ~ 600 m (Fig. 5.11). Assuming a dip of 45° this places the junction of the faults at about 250 m asl., ~230 m below the surface that Tuahu dome lies on.

Extension through blind propagation of dikes to within a few tens to thousands of metres of the surface has been considered a viable mechanism for graben formation by many international workers (e.g. Mastin et al., 1988; Rubin and Pollard, 1988; Chadwick and Embley, 1998). Chadwick and Embley calculated that up to 15 m of down-throw occurred across a graben ~ 50 m wide and 600 m long above a 3 m wide basalt dike intruded to ~ 20 m below the surface in the Juan de Fuca Mid-Ocean Ridge. They also report data from an Icelandic 6 km wide graben which has had 1 m of down faulting caused by a 1.5 m wide dike propagating to 1.5 km below the surface. From these two examples we can see that dikes intruded closer to the surface (100s of metres depth) produce narrower grabens (10s of metres rather than kilometres) with more down throw.

In the Tuahu dome case, a relatively shallow dike (reaching ~ 230 m below the surface as suggested above) would come closer to the Juan de Fuca rather than Iceland example. Because the width of the Tuahu dome dike is probably several times that of the Juan de Fuca basalt dike, ~ 90 m of down throw across the ~ 600 m wide graben in Tuahu dome is plausible. In a case study very similar in all parameters to Tuahu dome, Mastin and Pollard (1988) interpret 10s of metres of down-throw across a ~ 400 m wide graben to be the product of 10 or more metres of extension induced by silicic dike intrusion. They suggest that the dike was shallow (250 m below the Inyo Craters, Long Valley CA) and associated with the eruption of the Obsidian, Glass Creek and South Deadman flows (rhyolite domes) offset 2-7 km further along strike from the graben.

Southwestern Whangamata Fault: diking along a major structural fault?

This continues from discussion in Section 5.3.4 regarding the peculiar concentration of two magma associations along the southwestern end of Whangamata Fault (Fig. 5.10). Forest West, Forest South, Forest and Dairy domes all lie in a coalescing complex

elongated southwest along the end ~ 5 km of Whangamata Fault. In contrast to the Tuahu dome case study, and many other domes in Maroa, the relationship to normal faulting is not clear. Forest West dome appears in line with the end of the fault but is not displaced by it. Forest South and Forest domes (the former dated at 114 ± 11 ka in Chapter 3), have northwestern margins in line with the fault but whether these are just the natural edge of the domes or a degraded fault scarp is unclear. Dairy dome, dated at 45 ± 9 ka, has a margin that looks the most likely to be part of the Whangamata Fault scarp.

I suggest that rather than Whangamata Fault simply cutting these domes, it has instead provided a preferred dike pathway for multiple magma associations to reach the surface. This accounts for the spurious distribution of dome ages compared to offset within the complex. Note that the vents for all of these lavas appear to be offset to the southeast of the fault, a feature also seen in the vents of the K-Trig basalts west of Taupo (C. J. N. Wilson, pers comm.., 2003). The cause of this offset is unclear. The nature of movement along Whangamata Fault is discussed further in the following section.

5.4.4 Faulting: steady state or episodic?

The previous three sections have discussed the likelihood of an episodic, volcano-tectonic, rate of faulting for at least some Maroa faults. The Thorpe Road fault is clearly inactive, and probable diking associated with the southwestern Whangamata Fault, Tuahu dome faults and from other studies in the TVZ have been discussed. Is there any evidence for Maroa faults that do follow a long-term constant slip rate model?

The only Maroa fault for which I can see evidence to support this case is the Whangamata Fault. This is also the fault with the largest overall displacement seen in Maroa, and the length is much longer (~ 15 km) than those of all other Maroa faults. It is the only Maroa fault to show any late-Pleistocene/Holocene displacement; D. Fellows (pers. comm., 2003) has observed ~ 9 m of vertical offset in the ~ 26.5 ka Oruanui pyroclastics along Whangamata Fault. In comparison, the maximum offset on Whangamata Fault is seen in 204 ± 20 m vertical displacement of the 189 ± 8 ka Umukuri dome. These two values produce offset rates of 0.3 and 1.1 m/kyr over the last 26.5 and 189 ka, respectively.

This fault is quite distinct from the others in Maroa, as it appears to be the only fault that continues into any major fault or fault-zone outside of Maroa. Whangamata Fault is in line with the Paeroa Fault Zone (Fig. 5.10), and based on evidence for continual slip of similar rates over the last 189 ka it is considered to be part of a regional tectonic feature.

5.4.5 A correlation between faulting and volcanism?

It is apparent from Figure 5.10 that there is some concentration of likely vent locations amongst the more densely faulted areas in Maroa, especially across Pukeahua dome, MWC, MEC and Whakapapataringa dome. There is also a particularly strong alignment of vents along Whangamata fault. These correlations are unlikely to be due to chance and the question then arises: what is the cause of that relationship? And is the faulting controlling vent locations, are the vent locations increasing faulting, or both?

The discrepancy between (a) waning Maroa volcanism and faulting, and (b) continued high thermal flux and thus presumably ongoing magma intrusion, is highlighted in Section 5.2.7. This suggests that the shifting focus of volcanism away from Maroa might not be a direct result of reduction in magma flux below the centre. The case studies of volcano-tectonic interaction discussed in the sections above highlight an association between faulting and volcanism that has been little recognised across TVZ. Maybe this volcano-tectonic correlation represents a structural control on the release of magma to surface, where magma ascent rates and volumes remain relatively constant across TVZ but volcanism varies instead in relation to shifting zones of tectonic activity. This possibility has so far been little explored but has recently been raised by Charlier et al. (submitted). We cannot be certain that the composition of magma currently being intruded below Maroa is still dominantly rhyolitic, because only the very small amount that is reaching the surface can be observed. It is possible that a greater proportion, compared to the more active period > 100 ka, is not rhyolitic and that this is partly responsible for the relative paucity of eruptions.

5.5 Implications of surface geology for infill rates of calderas

5.5.1 Introduction

This discussion follows on from the discussion in Section 5.2.1 which highlighted the extraordinarily fast rate of infill of Whakamaru caldera apparent from the new

chronology and volume estimates (Chapter 3). Here I present the case of Whakamaru caldera infilling followed by three international case studies, and then use these to discuss the infilling of silicic calderas in general.

5.5.2 Infilling of Whakamaru caldera

Figure 5.14 summarises the relationship of different volumes of material filling the collapsed Whakamaru caldera. All volumes given here are DRE rounded to the nearest 10 km^3. During the Whakamaru eruption 440 km^3 of intra-caldera Whakamaru group ignimbrites were deposited inside the newly formed Whakamaru caldera between 340 and 320 ka (the total duration of these eruptions is equivocal from 1 to 20 kyr, C. J. N. Wilson and S. Brown, pers. comm., 2003). The top of the intra-caldera ignimbrites lies at 700 to 1100 m below the present day land surface and the fill overlying the intra-caldera ignimbrites totals 590 to 860 km^3 (calculations in Chapter 3). Variability in the volume of this fill may be due to (a) an undulating caldera floor which has collapsed asymmetrically or piecemeal, (b) rifting-induced down faulting across the caldera and/or (c) structural resurgence (see below) within the caldera. No attempt is made to attribute volume variability to any one or all of these mechanisms as there is no visible evidence for resurgence in TVZ, and there is no easy way to quantify the other two processes.

The new age data presented in Chapter 3 from my work and the unpublished data of B. F. Houghton allow estimates to be placed on the rate of infill of the Whakamaru caldera. Goldies dome lies on a surface at ~ 300 m asl. and is the oldest reliably dated surface eruption unit (~ 305 ± 17 ka) within Whakamaru caldera. Whakamaru caldera fill below 300 m asl. (and thus likely to be mostly > 305 ka, discussed at the end of this section) totals 450 to 720 km^3 (average 580 km^3) from 340-320 to 305 ka; a rate of 39-17 km^3/kyr over the first 35-15 kyr (range controlled by whether infill started 340 or 320 ka). From data in Figure 3.10 I conclude that by 200 ka, ~ 690 km^3 of material, ~ 95 % of the total caldera infill, had been deposited in the caldera, giving a rate of 5.8-4.9 km^3/kyr over the first 120-140 kyr.

These data reflect an exponential decrease in the rate of filling of Whakamaru caldera after collapse. Fill above the intra-caldera ignimbrites has been shown from drillhole records (Chapter 3) to consist of pyroclastics, lavas and sediments, decreasing in abundance in that order.

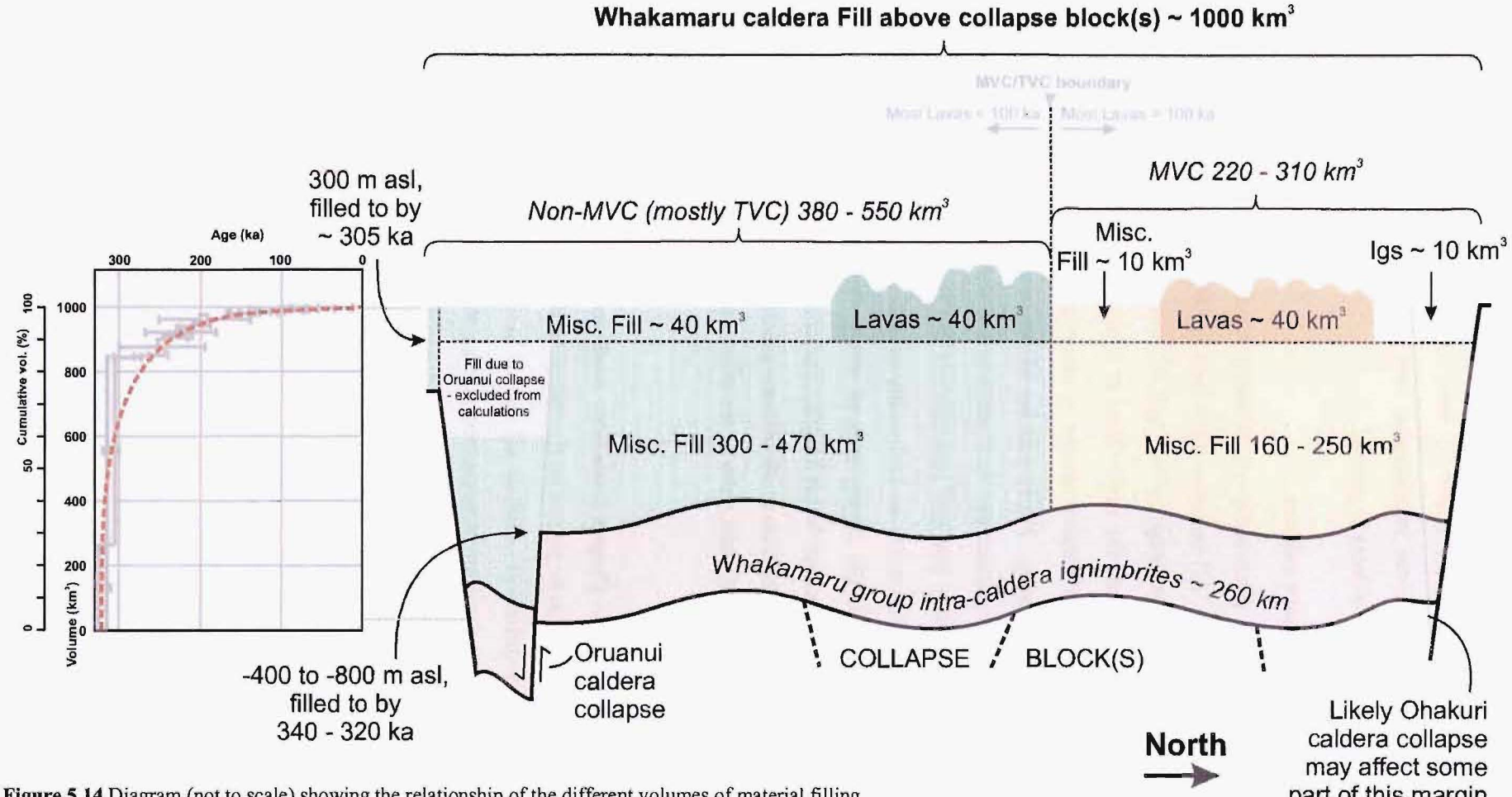

Figure 5.14 Diagram (not to scale) showing the relationship of the different volumes of material filling the Whakamaru caldera. Note the three time marker planes: (1) the undulating -400 to -800 m asl. top of the Whakamaru group intra-caldera ignimbrites, filled by 340-320 ka, (2) the 300 m asl. reference elevation considered to have been filled by ~ 305 ka and (3) the undulating present day ground surface. Cumulative volume curve at left is simplified from Figure 4.10.

The important point is that within Whakamaru caldera, although ~ 580 km^3 of material was deposited over the intra-caldera ignimbrites prior to 305 ka (about 80 % of the total fill), none of these deposits is preserved at the surface. The surface deposits within the caldera, generally considered to be a record of post-collapse caldera activity, represent only the most recent ~ 20 vol.% of the caldera fill. The only way to access the older 80 % of fill, deposited soon after caldera collapse, is via drilling. This data is now compared below to three international examples in order to discuss rates of post-caldera activity in general.

A conservative estimate of infill rates, for comparison

The rates of infill calculated in Chapter 3 and summarised above assume that the majority of the caldera had been infilled to ~ 300m asl. by 305 ka. It is important to recognise the possibility that a portion of the Whakamaru caldera outside of Maroa took longer to infill. Two lines of evidence point to this possibility: (1) the top of the ~ 220 ka Mokai pyroclastics lie at ~ 300 m asl, so infilling in that area had largely been completed by 220 ka at the latest; and (2) the base of the ~ 26.5 ka Oruanui pyroclastics in Wairakei geothermal area lie on average at 300 m asl. (drill hole logs, Steiner, 1977). A conservative estimate of the rate of infill would be that Whakamaru caldera had been infilled to ~ 300 m asl:

(a) In the Maroa area by ~ 305 ka at the same extraordinarily high rate of 17-39 km^3/kyr calculated above, over 40 % of the caldera area.

(b) In half of the remaining area by ~ 220 ka from the Mokai pyroclastics age. A rate of infill of 3.4 km^3/kyr across 30 % of the caldera area.

(c) In the other half of the remaining area by ~ 26.5 ka from the Oruanui pyroclastics age. A rate of infill of 1.2 km^3/kyr across 30 % of the caldera area.

The average of these three post collapse infill rates (which would apply over the shortest of the three time-periods – i.e. prior to 305 ka), weighted by the area each covers, is 8-17 km^3/kyr (range controlled by whether infill started 340 or 320 ka) across the entire Whakamaru caldera. This is still a very high rate of infill compared to the examples that follow.

5.5.3 Other examples of caldera infilling rates

Details of three North American calderas are compared here to the data for Whakamaru caldera presented above. These examples are chosen because they express some or all of the stages of the caldera cycle proposed by Smith and Bailey (1968): (1) regional doming and generation of a ring fracture, (2) caldera-forming eruptions, (3) caldera-collapse, (4) pre-resurgence volcanism and sedimentation, (5) Resurgent doming, (6) major ring fracture volcanism and (7) solfataric and hot-spring activity. The infilling of Whakamaru caldera coincides with stage (4) of this theoretical cycle. Eruption of the WDB could also be considered to be part of stage (6). The validity of this cycle theory is discussed in Section 5.5.4.

Yellowstone Plateau Volcanic Field

The activity of Yellowstone Plateau Volcanic Field has been divided into three volcanic 'cycles' with the following climactic caldera-forming eruptions (Christiansen, 2001): (1 – oldest) Huckleberry Ridge Tuff; (2) Mesa Falls Tuff; and (3 – youngest) the ~ 1000 km^3, ~ 639 ka (Lanphere et al., 2002), Lava Creek Tuff. The Lava Creek Tuff eruption produced a two-segment caldera collapse (related to tuff members A and B), which was followed by resurgent doming interspersed with rhyolite lava eruptions and then infilling of the caldera depression by rhyolite lavas. The caldera collapsed over an oval area of 45 by 85 km (~ 3000 km^2). Christiansen (2001) notes that some sedimentation probably occurred prior to resurgence, but no evidence is preserved because it has been buried and/or eroded off of the resurgent dome. Two domes were uplifted, one over each collapse block. Sour Creek Dome (13 x 21 km, flanks < 15°) rose soon after caldera collapse (some time prior to ~ 484 ka), but Mallard Lake Dome (similar size and shape to Sour Creek Dome) appears to have formed by ~ 160 ka. The 516 ±17 ka Biscuit Basin flow postdates the initial uprising of the Mallard Lake Dome. The uppermost fill appears to be ~ 900 km^3 Christiansen (201) of Plateau Rhyolite lava, erupted from 160 to 70 ka (Obradovich, 1992).

Long Valley caldera

At ~ 760 ka the Long Valley caldera (an oval 17 x 32 km, ~ 430 km^2) collapsed by 2 to 3 km in the eruption of the > 600 km^3 Bishop Tuff (Bailey et al., 1976). Intra-caldera Bishop Tuff, also containing > 300 m of granophyric lava intrusions, is ~ 1180 m in thickness over most of the caldera (McConnell et al., 1995). Early post-caldera surface rhyolite lavas with a volume of > 65 km^3 were erupted between 750 and 650 ka. There

was post-caldera structural resurgence ~ 500 m-high (~ 760 to 660 ka) over a 10 km diameter area (Bailey, 1989) that was accompanied by voluminous tuff and obsidian lava fill of the caldera. The caldera was also filled by Long Valley Lake, which was not drained until ~ 100 - 50 ka.

Assuming a 2.5 km deep collapse, ~ 570 km^3 of pyroclastics and lava filled the caldera above the intra-caldera Bishop Tuff from ~760 ka to 650 ka; resurgent doming uplifted this fill over the same period, uplifting ~ 210 km^3 of the caldera fill. This gives a total volume of 360 km^3 of fill deposited within 10 kyr, a rate of 36 km^3/kyr. A further ~65 km^3 of surface lavas were deposited at the surface before 650 ka, bringing the total to 425 km^3 by 650 ka; a rate of 3.9 km^3/kyr.

Creede caldera

Creede caldera formed at ~ 26.7 Ma as the youngest of 9 calderas in the central San Juan caldera cluster of the San Juan volcanic field (Lipman, 2000). The caldera collapsed by > 3.5 km (probably 4-5 km) during the eruption of the dacitic Snowshoe Mountain Tuff. The caldera ring-fault is ~ 18 km in diameter (equivalent to ~ 255 km^2) and intra-caldera tuff is > 1800 m thick. Landsliding of the caldera rim during, and immediately after, caldera collapse significantly enlarged the topographic rim and added up to 2 km of fill to the caldera. The caldera filled rapidly with sediments after collapse, pyroclastics, lava and water, the latter forming the ancient Lake Creede. Major structural resurgence then formed Snowshoe Mountain Dome.

Sediments (nearly all tuffaceous, Heiken et al., 2000) were derived from ongoing mass-wasting of the caldera topographic rim and re-sedimentation of caldera fill off of the resurging dome. The sedimentary moat fill has largely been eroded by the Rio Grande River in the last few million years. Attempts to determine the duration of sedimentation have yielded varied geochronological results. Some upper beds within the fill have yielded dates as much as 0.66 Ma younger than the caldera collapse (Lanphere, 2000). Major resurgent uplift (~ 1.5 km) may have still been underway 0.6 Ma after collapse and this delayed resurgence may have led to the long period of intra-caldera re-sedimentation (Lanphere, 2000). Eruptive activity decreased in volume after about 26 Ma in the Creede area. The > 3.5 km collapse filled in 435 km^3 with pyroclastics and lavas (above the intra-caldera Snowshoe Mountain Tuff) over < 660 kyr. Less than 255 km^3 of fill was uplifted by resurgence over the first ~ 600 kyr (assuming the base of 1.5

km of resurgence is the full width of the caldera), which leaves 180 km^3 of fill over 660 kyr, a rate of 0.3 km^3/kyr.

5.5.4 Discussion of post-collapse activity in the context of all above examples

Do calderas follow a set cycle?

TVZ calderas do not show all stages of Smith and Bailey's (1968) proposed cycle of caldera volcanism. This is in contrast to their assertion that all stages are usually present at all calderas. They identify the presence or possible presence of all stages at all of their example calderas, although they do acknowledge the possibility of the absence of some stages. The presence of all of Smith and Bailey's (1968) stages at the North American calderas reviewed here is equivocal. Stage (1) 'regional doming' is rarely seen internationally, (5) structural 'resurgent doming' is apparently absent at TVZ calderas and variable in other examples, and stage (6) major ring fracture volcanism is not present in most of the examples given above. It could be argued that Whakamaru post-collapse intra-caldera volcanism (i.e. Maroa) is magmatic resurgence, except that petrological variation within and between domes of Maroa and the WDB (described in Chapter 4 and discussed above in Section 5.3.6) preclude these volcanic features as representing direct magmatic resurgence of the caldera-forming magma body.

Smith and Bailey's 'cycle' might better be called a list of features that may occur associated with caldera volcanism, especially in the case of TVZ calderas. It is interesting to note that Smith and Bailey give up-warping within the 'Mokai Ring Complex' (Section 5.1 above) centred around Maroa as a specific example of structural resurgence based on the information in Healy (1963; 1964). Healy (1964) had suggested that the Paeroa fault scarp was a resurgent block-bounding fault. Instead the fault is inferred to be a tectonic feature which, at its northern end at least, has had most of its offset with relatively constant displacement over the last 64 ka (Berryman et al., 2002). This is much younger than, and spatially outside of, the only adjoining calderas, Whakamaru and Kapenga.

Style of post-caldera activity

The style of TVZ post-caldera activity differs significantly from the international examples above in that structural resurgence (stage 3 of Smith and Bailey, 1968) is not

seen in TVZ calderas. Structural resurgence cannot be ruled out in the TVZ, but if it is present it has not been identified.

It cannot be ruled out that Whakamaru caldera contained a lake from 340 to 305 ka (as is seen at Long Valley and Creede). However, lake sediments were not identified specifically in a description of drill-cores from geothermal fields within the Whakamaru caldera. Furthermore a lack of hydro-volcanic deposits at Maroa suggests that any paleo-lake that may have formed in the Whakamaru caldera had already been displaced by fill before the onset of Maroa eruptions at ~ 305 ka. This is consistent with the assumption, implicit within this thesis, that Maroa surface deposits have always stood on high ground relative to the caldera (as opposed to being uplifted by structural resurgence). In contrast Creede post-collapse intra-caldera eruptions generally progressed from hydro-volcanic to mixed magmatic/hydro-volcanic as sedimentation and structural resurgence elevated vent sites out of ancient Lake Creede (Lipman, 2000).

Rate of post-caldera infilling

Table 5.3 compares the rate and timing of infilling of Whakamaru caldera to the three other examples. At Long Valley and Whakamaru calderas there has been an exponential decrease in the rate of infill between 15/35 kyr and 120/140 kyr after caldera collapse. Almost all of the volume of fill is emplaced by 110/140 kyr post-collapse at these two calderas.

Caldera Name	Rate 1 (km^3/kyr)	Period (kyr post-collapse)	Control 1	Rate 2 (km^3/kyr)	Period (kyr post-collapse)	Control 2
Whakamaru	39-17	0 to 15-35 kyr	Maroa lava	5.8-4.9	0 to 120-140 kyr	Maroa lava
Yellowstone	Rate of fill reduced by delayed or prolonged resurgence			>1.0	0-122 kyr	Lava fill
Long Valley	33	0-10 kyr	Surface lava	3.9	0-110 kyr	Surface lava
Creede	Rate of fill reduced by delayed or prolonged resurgence			0.3	0-660 kyr	Lava on resurgent dome

Table 5.3 Rates of caldera infilling for Whakamaru caldera compared to three international examples.

The duration of intra-caldera infilling appears to have been much longer at Creede (up to 660 kyr.) than at Whakamaru (95 % in 140 kyr.), Yellowstone (~ 122 kyr) and Long Valley (mostly within 110 kyr) calderas. Massive delayed structural resurgence at

Creede caldera, continuing up to 600 kyr after collapse, probably significantly increased the duration of major intra-caldera re-sedimentation there.

In essence prolonged structural resurgence appears to have prolonged the duration of intra-caldera (re)sedimentation at Creede, whereas an exponential decrease in infilling, and almost all of the infill volume, occurs within 110/140 kyr of collapse at Yellowstone and Long Valley (resurgence finished < 100 kyr post-collapse), and Whakamaru (no resurgence seen) calderas.

Conclusions about the infilling of silicic calderas in general

- Rhyolite calderas infill quickly, with ~ 80 % of fill occurring within ~ 35-15 kyr of caldera collapse in the case of Whakamaru caldera.
- Structural resurgence causes caldera infill to be (re)sedimented until uplift ceases.
- TVZ calderas, which are apparently non-structurally resurgent, provide data for the analysis of the rates of caldera infilling. In contrast, infilling is distorted by structural resurgence at many other calderas worldwide.
- Intra-caldera volcanism at the surface usually continues much longer than the period of initial infill back to the elevation of the structural rim.
- Intra-caldera surface volcanic units represents a small fraction of the volume filling the caldera, and are emplaced after the bulk of the fill has already occurred.
- When structural resurgence and deep intra-caldera erosion are not present, as is the case in TVZ, drilling of intra-caldera fill is the only way to interpret and sample the material erupted and deposited directly after caldera collapse.

5.6 Volcanic hazards at Maroa

5.6.1 Maroa eruption history post 100 ka

Given the history of eruptions at Maroa over the last 100 ka the likelihood of future eruption(s) at similar recurrence intervals should be considered from a hazard perspective. Table 5.4 presents the age, volume and styles of Maroa eruptions since 100 ka. For this section the Ngangiho eruption is also included within Maroa, even though it technically lies in Taupo Volcanic Centre as defined elsewhere in this thesis, because (a) hazard and risk assessments should be conservative, and (b) it lies so close to Maroa that its hazard zones (discussed below) would have almost identical ranges to those of Maroa proper.

The last eruption from Maroa of 1 km^3 or larger was ~ 86 ka. Since then one eruption, probably around 45 ka, was ~ 0.9 km^3 and the remaining 7 eruptions were 0.2 km^3 or less. There appears to have been a burst of activity around 45 ka with up to three eruptions totalling ~ 1.3 km^3 occurring within a short period (two have analytical ages within the uncertainty ranges of each other). The most recent eruption, Puketarata, has the best preservation of pyroclastics, including both airfall and surge deposits. Two of the three eruptions prior to it also have airfall deposits preserved. It is possible that many of the remaining six older eruptions also produced pyroclastics, but if so these have since been eroded away.

Name	Age	Volume	Style
Palm	assoc. Mokauteure (~86 ka)	~ 0.2 km^3	Dome
Mokauteure	86± 12 ka	~ 1.6 km^3	Dome (and pyroclastics?)
Kakuki	assoc. Orakeikorako (~ 80 ka)	< 0.1 km^3	Dome (and pyroclastics?)
Orakeikorako	80 ± 7 ka	< 0.1 km^3	Dome (and pyroclastics?)
Pohaturoa	77 ± 9 ka	< 0.1 km^3	Dome (and pyroclastics?)
Forest West	assoc. Dairy (~ 45 ka)	~ 0.9 km^3	Dome (and pyroclastics?)
Dairy	45 ± 9 ka	~ 0.2 km^3	Dome (and pyroclastics?)
Ngangiho	~ 45 ka*	~ 0.2 km^3	Dome and airfall
Puketarata	~ 16.7 ka*	~ 0.2 km^3	Dome, airfall and surge

Table 5.4 Post 100 ka Maroa eruptions, their age, volume and style, in order of decreasing age. Ages determined by Ar-Ar experiments (Chapter 3), except *ages determined by stratigraphic position relative to ^{14}C dated non-Maroa eruptions. The three eruptions with associated ages are geochemically and spatially linked to the named eruption.

There have also been at least two basalt eruptions in and around the Maroa area in the last 100 ka; the Ongaroto Basalt, in the northwestern corner of Maroa, is K-Ar dated at 86 ± 20 ka, and the Akatarewa Basalt, a few km east of Maroa's eastern-most rhyolite, lies between the Okaia (~ 29 ka) and Mangaone (< 64 ka) tephras (Section 2.6.1, tephra ages from Newnham et al., 2003 and Smith et al., 2002, respectively). The effect of these on the risk from future Maroa eruptions is discussed in Section 5.6.5 below.

5.6.2 Magnitude of future probable eruptions

For magnitude estimates the Puketarata eruption is considered to represent the size and style of the most probable future Maroa eruption because (a) it is of a similar volume and style to the majority of eruptions in the last 100 ka and (b) it is the most recent. It also has the best preservation of pyroclastic deposits, with isopachs published for its

pyroclastic fall deposits (Brooker et al., 1993; Fig. 5.15). The probable maximum range of surges (pyroclastic density currents) is shown as a pink circle. This is conservatively determined as 150 % of the distance to the farthest point that surge deposits are distinguishable in Puketarata pyroclastic deposit outcrops (between 'medial' and 'distal' outcrops of Brooker et al., 1993).

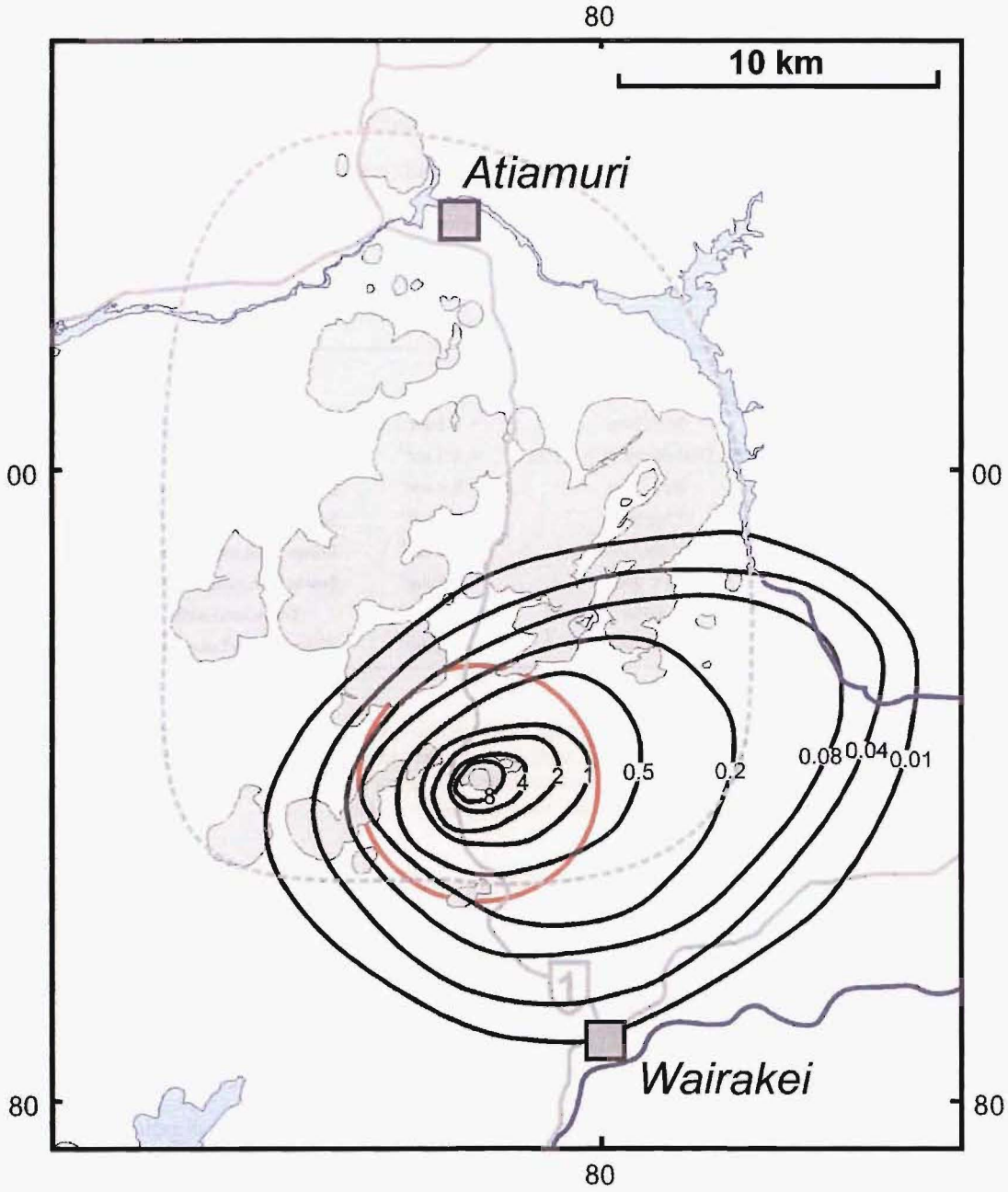

Figure 5.15 Puketarata airfall deposit isopachs after Lloyd (1972) and Brooker et al. (1993). Isopachs are in metres. Pink circle marks the likely maximum extent of surges. Dashed grey line is the Maroa boundary and Maroa rhyolite domes are shown in grey.

5.6.3 Hazards from such an eruption

Based on a Puketarata-style eruption, hazards from a future probable Maroa eruption and their impacts are:

Lava Total destruction (slow movement rate, can be outrun)

Surge Total destruction (cannot be outrun)

Ash fall Impact is thickness-dependent: slippery/impassable road surface, water/sewage systems, electrical transmission, vegetation, crops, pasture, livestock, structure (loading), vehicles and equipment (abrasion and clogging), human health (respiratory, eyesight, toxicity), air traffic (visibility, abrasion, clogging).

Zone	Control	Summary of probable Impact
A	Range of pyroclastic density currents	Likely lethal with destruction of most structures. Impossible to outrun.
B	>300 mm ash fall	Heavy destruction of vegetation and burial of soil. Livestock/aquatic life heavily distressed/killed. Major collapse of roofs. Roads unusable until cleared.
C	100-300 mm ash fall	Roofs not cleared may collapse, especially if wide span and/or wet ash. Major damage to vegetation. Loss of electrical reticulation due to direct and indirect line breakage.
D	5-100 mm ash fall	Burial of pasture and low plants. Major ash removal necessary in urban areas. Weaker roofs may collapse if ash is wet. Vehicle mobility hampered by road closure and air filter clogging.
E	1-5 mm ash fall	Possible crop damage and livestock may be stressed directly or indirectly. Minor building damage. Short circuiting of power lines and substations possible. Water supply contamination and possible failure. Dust nuisance. Blockage of sewage systems. Damage to electrical equipment and machinery.
	< 1 mm ash fall	Irritant to eyes and lungs. Halt to air traffic. Minor damage to equipment/structures from abrasion. Possible water supply contamination. Road visibility and traction reduced.

Table 5.5 Hazard zones vs. probable impact summary.

Each of the different volcanic hazards from a rhyolite eruption has a different distance range. Maroa rhyolite lava forms domes, which do not flow far from the vent (< 1 km radius for all Maroa eruptions, post-100 ka) so the total destruction hazard from pyroclastic density currents (surges in the case of Puketarata, reaching up to 4 km from vent) over-ride them as a hazard in terms of distance and lethality. Table 5.5 presents

hazard groups for such a future eruption, based on pyroclastic density current and ash-fall hazards. It is a compilation based on Neall et al.'s (1999) hazard assessment for Ruapehu andesites, with corroboration from Nairn (2002b) and Blong (2003); Nairn addresses hypothetical rhyolitic ash impacts on paved/sealed surfaces in New Zealand, and Blong deals with dacitic ash impacts to structures at Rabaul (still relatively close in composition and density to rhyolite ash).

Figure 5.16 shows an attenuation curve for ashfall thickness and surge deposition from the Puketarata eruption, based on a section down the dispersal axis of the isopachs in Figure 5.15. Boundaries and fields for hazard zones from Table 5.5 are shown. The distance from vent for the maximum range of each hazard zone is then applied as a buffer outside of the margins of Maroa in Figure 5.17, to provide a hazard map for zones of potential ranges of each hazard from a future Puketarata-sized eruption at any location within Maroa. Atiamuri lies within Zone A, Wairakei within Zone B, Taupo within Zones C and D and Tokoroa within Zone D. Rotorua and other towns off of the map may lie within the range of ash fall (Zone E) depending on wind direction.

The extents of hazard zones for ash-thickness, lava flow run-out and pyroclastic density currents for minor TVZ basalt eruptions (as seen for Kakuki and Tatua basalts within Maroa) are considered to be within those of this rhyolite-based hazard map.

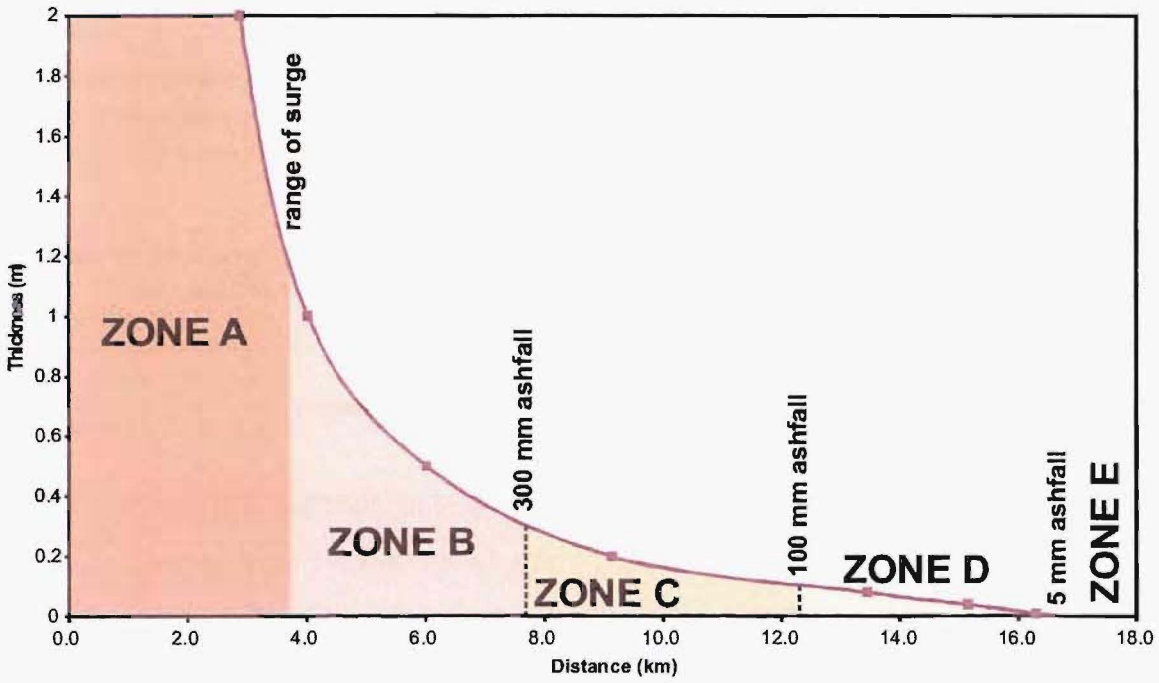

Figure 5.16 Curve for impact zones vs. distance from Puketarata vent.

5.6.4 Probability of eruption

In terms of probability, nine eruptions appear to have occurred in the last 100 ka, giving an average eruption interval of 11,000 years. However, it is clear that Maroa volcanism has been somewhat temporally clustered, and this is apparent in the last 100 ka with the burst of activity around 45 ka. If these eruptions ~ 45 ka are grouped together as a single event, separated from the other events by a much greater time period than they are separated from one another, then there are seven events in the last 100 ka. This gives an average eruption interval of ~ 14,000 years. Maroa volcanic eruptions are not regularly spaced, so an eruption cannot be expected exactly 14,000 years after the previous eruption; this eruption interval should, instead, be used only statistically to calculate the probability of eruption(s) in a given time period (see below).

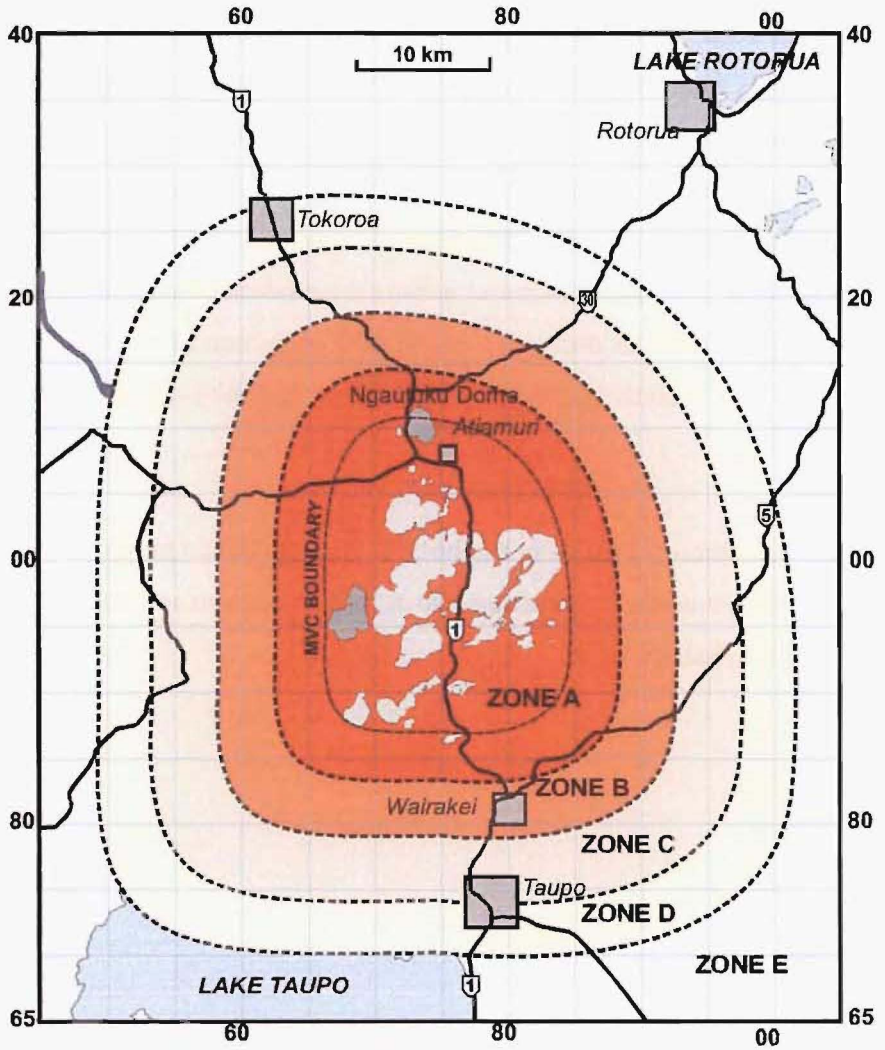

Figure 5.17 Volcanic hazard map for a probable future eruption from Maroa. Hazard zones are defined in Table 5.5. Note that Atiamuri lies within Zone A, Wairakei within Zone B, Taupo within Zones C and D and Tokoroa within Zone D. Rotorua and other towns off of the map may lie within the range of ash fall (Zone E) dependent on wind direction.

5.6.5 Risk from future Maroa eruptions

At an average rate of one eruption every 14,000 years the probability of an eruption in a person's lifetime (assumed ~ 80 years) is 0.6 %. This is a very low probability and in terms of risk even those people in the highest hazard zone on the probability map presented above (mostly forestry workers and farmers) are likely to face many other major-impact natural hazards of much higher probability of occurring over their lifetime (e.g. erosion, drought, fire, pests, earthquakes etc.). This very low eruption probability, coupled with the low population density, and relatively low per-hectare land and infrastructure value risk (probability x loss) from Maroa renders the risk from volcanic hazards relatively insignificant.

The probability of basalt eruptions is likely to be relatively constant across TVZ and lower than that for a future rhyolite eruption at Maroa. Considering that their hazard zone boundaries are likely to be within those delineated above for a future Maroa rhyolite eruption, very little additional risk is considered to be added to the total Maroa volcanic risk from basalt eruptions. However, if one is to take into account the occurrence of the Ongaroto and Akatarewa basalts the recurrence interval for all Maroa eruptions over the last 100 ka decreases to ~ 11,000 years and the probability of an eruption in an 80 year lifetime increases to 0.7 %. This is only a slight change and is still a very low risk.

The distribution of Maroa eruptions in the last 100 kyrs has been predominantly in the southern section of the centre, suggesting that a future eruption is more likely in this area than the northern half of Maroa.

CHAPTER 6

Conclusions and recommendations

The main result of this thesis is a detailed understanding of the volcanology, and the chronological and petrological evolution of the Maroa Volcanic Centre. This thesis also provides the foundation for a substantial future project (possibly another Ph.D. thesis) investigating the Maroa magma system, its evolution and relationship to TVZ magmas in detail. Such a study was beyond the scope of this thesis and would require substantial geochemical data beyond that collected here. The following section summarises the major points that arise from the thesis.

6.1 Conclusions

6.1.1 The evolution of Maroa Volcanic Centre

- Dome lavas make up the majority of volume (~ 38 km^3) erupted from Maroa, with the major Maroa West and East complexes (MWC and MEC) erupted mostly over a short 29 kyr period starting at 251 ± 17 ka.

- The ages of the Mamaku, Ohakuri and Mokai pyroclastics are equivocal. Field evidence shows that the Ohakuri overlie the Mamaku pyroclastics with very little time elapsed between. The Mamaku and Ohakuri pyroclastics appear to be older (~ 240 ka) than the age previously accepted for the Mamaku pyroclastics.

- The rate of Maroa volcanism has decreased exponentially from a maximum prior to 200 ka. In contrast, volcanism at Taupo and Okataina has increased from ~ 64 ka to present. This reflects a migration of volcanic focus from Maroa to opposite ends of the central TVZ over the last ~ 200 kyr.

- The distinction between Maroa and Taupo is somewhat arbitrary and is best considered to be the easting directly north of Ben Lomond, north of which most volcanism is older than 100 ka and M and N type, and south of which most volcanism is younger than 100 ka and T type.

- There is a lack of evidence for any 'Maroa caldera'. The gravity and aeromagnetic anomalies associated with the centre are instead more likely due to volcano-tectonic down faulting with single event displacements several orders of magnitude less than a caldera collapse.

6.1.2 The origin and nature of key Maroa pyroclastic deposits

- The Korotai pyroclastics are mostly comprised of non-welded massive ignimbrite but contain at least two horizons of high-grade welding. They are the deposit of a small (< 1 km^3) eruption in the north of Maroa dated at 283 ±11 ka, but overlying the Pokai pyroclastics dated at 275 ± 10 ka.

- The Putauaki and Orakonui pyroclastics are the largest volume (> 4 km^3) pyroclastics deposits erupted from Maroa. They are petrologically very similar and appear to have been erupted from a similar vent location within central Maroa at 272 ± 10 and 256 ± 12 ka, respectively.

- The Atiamuri pyroclastics are a small (< 1 km^3) ignimbrite-dominated unwelded to slightly welded deposit. They contain a horizon of intense welding near the vent. The vent is inferred to be now overlain by Mandarin dome.

- The Pukeahua pyroclastics (~ 1 km^3) are a fan comprised of small ignimbrites, BAF deposits and airfall layers associated with the eruption of the Pukeahua dome complex. The fan can be petrographically divided into eastern (hornblende-bearing) and western (hornblende-free) halves, associated with the eruption of the Pukeahua East and South, and Pukeahua West domes, respectively. The Pukeahua east deposits are older, deposited over the 229 ± 12 ka Atiamuri pyroclastics, but underlying the Pukeahua west deposits dated at ~ 202 to 196 ka.

- The ~ 220 ka Mokai pyroclastics (~ 11 km^3) partly crop out within Maroa but their source remains unclear. There is no conclusive evidence to petrogenetically link them to the Mamaku pyroclastics, to Taupo or to Maroa. They do not appear to have interacted with water so any paleo-lake that may have filled this area after the Whakamaru caldera collapse was gone by ~ 220 ka..

- The Ohakuri pyroclastics appear to have come from a caldera just north of Maroa and the Ohakuri magma source(s) may have interacted with those of Maroa.

6.1.3 Maroa petrology

- Maroa eruptives are all plagioclase-orthopyroxene bearing, commonly with lesser quartz. Hornblende ± biotite are present in some deposits primarily correlated with T geochemical type (see below). These Fe/Mg minerals act as a diagnostic characteristic for some magma associations (e.g. Pukeahua eastern vs. western deposits).

- All Maroa deposits are rhyolites (apart from two high-silica dacite analyses) and are peraluminous and calcic. They all have the LILE enriched, HFSE depleted, signature of arc-related rocks. Both of these classifications are typical of TVZ deposits.

- Maroa deposits fall chemically into three magma types based on Rb and Sr content: M (Rb 80-123 ppm, Sr 65-88 ppm), T (Rb 80-113 ppm, Sr 100-175 ppm) and N (Rb 120-150 ppm, Sr 35-100 ppm) (see Fig. 4.10). The geochemical distinction of these types is mirrored to varying extents in the concentrations of all other elements that were analysed.

6.1.4 Maroa magma source models

- Nearly all of the lavas of the MWC/MEC dome cluster are spatially, chronologically and petrologically associated in a common open system source.

- The Pukeahua western deposits are probably associated in the same source as the MWC/MEC deposits. In contrast, the Pukeahua eastern deposits are probably associated in a separate source. The Pukeahua eastern geochemical variation is plausibly controlled by fractionation of the mineral proportions seen in erupted deposits.

- Based on the spatial, chronological and petrological similarities of the MWC/MEC and Pukeahua eastern magma associations (termed associations (1) and (2)) a further four magma associations are determined ((3) through (6)). These six associations account for almost all Maroa deposits (Table 5.2).

- Two end-member models are proposed for the sources of the Maroa magma associations. Model 1 is a single relatively shallow magma body feeding spatially clustered eruptions that do not spatially overlap with those of other sources. Model 2 is a deeper source feeding multiple shallower offshoots which in turn can produce eruptions over a wider area than a model 1 source. Sources for the Maroa magma associations probably lie on a continuum between these two model end members.

- The ascent of basalts in regions of rhyolite volcanism is commonly considered to be inhibited by the basalt encountering rhyolite magma bodies during ascent. Evidence for this not occurring at Maroa is given in the form of minor basalt included, mixed and mingled with erupted rhyolite (seen in some other TVZ eruption products and other international examples). The absence of basalt within rhyolites at Maroa suggests that it too may be a 'basalt shadow zone' with rhyolite magma still present below the centre, shadowing ongoing basalt ascent (inferred from continued high geothermal flux around Maroa).

6.1.5 Rates of caldera infilling

- The oldest Maroa dome (305 ± 17 ka) constrains the maximum rate of infilling of Whakamaru caldera as 39-17 km^3/kyr immediately after the deposition of the intra-caldera Whakamaru group pyroclastics.

- The above is in agreement with international rates except where post-collapse structural resurgence has continued for more than 100 kyr. The majority of caldera fill, representing voluminous eruption deposits in the 10s of kyr post collapse, is therefore buried and only accessible via drilling.

- Structural resurgence is not seen at TVZ calderas and an analysis of the Whakamaru and other caldera case studies shows that calderas do not all follow the cycle proposed by Smith and Bailey (1968). Their stages may rather be considered as a set of features of which some or all are present at silicic calderas.

6.1.6 Maroa magmas in a wider context

- The WDB is almost as voluminous as Maroa and appears to have been erupted over a similar period. However, various petrological distinctions, and distinctions in some or all of Rb, Sr, Ba and Zr content, preclude a common source for the two.

- Magma sources for Maroa and the WDB may have been partly or wholly derived from the Whakamaru caldera magma system(s), but petrological distinctions among all three mean that Maroa and the WDB cannot be considered as simple magmatic resurgence of the Whakamaru caldera; these distinctions are primarily the presence of sanidine in only the Whakamaru group ignimbrites, plus distinctions in some or all of the Rb, Sr, Ba and Zr contents.

- TVZ rhyolite magma petrogenesis probably consists of a mixture of fractional crystallisation of mantle partial melts and some melting and assimilation of sedimentary continental crust (greywacke). An inability to determine the real composition of the sedimentary end-member has limited workers' ability to model this process more exactly. Groupings of similar $^{87}Sr/^{86}Sr$ ratio across widely distributed TVZ vents suggests similar trace element geochemistry in many TVZ rhyolites is due to common magma origin(s) (with common level(s) of crustal ^{87}Sr input) rather than parallel but separate AFC evolution.

- The sustained high heat flow, and thus presumably ongoing significant Maroa magmatic intrusion of basalt (see the last conclusion in Section 6.1.4), compared to low levels of volcanism and faulting raises the possibility of a causative link between faulting and volcanism. This is in contrast to traditional views of volcanism being directly related to rates and volumes of magmatic ascent.

6.1.7 Maroa faulting and regional tectonics

- Paleoseismic investigations along the Thorpe Road Fault provide a case study of a fault with a clear, apparently active surface expression that is in fact a fossil feature which may not have been active for as long as 200 kyr.

- Based on calculations of dike width and a review of international case studies, the graben across Tuahu dome is inferred to have been created by blind diking to within ~ 230 m of the surface below the dome. The dike may have been associated with eruptions offset along the strike of the dike.

- Recent studies at Okataina and Tongariro, and along the southwestern end of Whangamata Fault in Maroa, highlight examples of structural features with some associated dike intrusion/eruption. Such volcano tectonic interaction is not always highlighted in TVZ but the interrelationship may in fact be relatively common and lie on a continuum between dike-induced faulting and dikes following predominantly structural features.

6.1.8 Future volcanic activity and hazards at Maroa

- Future eruptions from Maroa are likely to be of similar scale (e.g. the Puketarata eruption 16.7 ka) and frequency (~ 14,000 year recurrence interval) to those over the last 100 ka. In contrast Taupo and Okataina appear set to continue their post ~ 64 ka high rates of eruption with each having the potential for another caldera collapse.

- As magmatic intrusion has not necessarily decreased in proportion to the volcanism at Maroa (evidence from sustained high heat flow at Maroa geothermal fields), a future increase in Maroa eruption rates and volumes is possible.

- Hazard zones for a future possible Maroa eruption place Atiamuri within the highest (total destruction) zone, Wairakei, Taupo and Tokoroa within heavy to moderate damage zones, respectively. Rotorua and other Bay of Plenty towns may lie within the range of ash fall depending on wind direction.

- The probability of a future eruption (~ 0.6 % in a 80 year lifetime) shows that most other natural hazards have orders of magnitude greater probability of occurrence and an analysis of probable loss (risk) is therefore not conducted.

6.2 Recommendations for further work

Previous work combined with my new data, presented in Chapter 2, form a reasonably comprehensive stratigraphic and volcanologic understanding of Maroa. Further detailed individual studies on the internal stratigraphy of the Maroa pyroclastics will likely elucidate interesting eruption scenarios. The controls on the highly welded zones in the Korotai and Atiamuri pyroclastics may be of particular interest.

There is scope for detailed volcanological studies on each of the Maroa pyroclastics deposits. Such studies, on the Korotai, Pukeahua, Atiamuri, Orakonui and Putauaki pyroclastics, should encompass stratigraphic logging, sampling and correlation of all outcrops, in more detail than was provided for in the scope of this thesis research. These data sets would then lend themselves to interpretation of the vent locations and emplacement mechanisms of each deposit. The interpretations could then be compared to those of younger TVZ eruptions, and international case studies, to shed new light on the styles of volcanic activity in central TVZ from ~ 300 to 200 ka.

A significant amount of further analytical work is now needed on Maroa eruptives. Further insight into Maroa requires testing of the Maroa magma associations suggested in Section 5.3, and determining the sources and their petrogenesis. Comprehensive suites of (a) mineral chemistry, (b) Sr, Nd, Pb and O isotope data, and (c) zircon age determinations are needed. These will allow (a) more detailed correlation of Maroa magmas to each other and to those of nearby magma systems, (b) interpretation of the petrogenesis of Maroa rhyolites compared to those of the wider TVZ, and (c) the residence times and level of crustal interaction in Maroa magmas, respectively.

References

Arth, J.G., 1976. Behavior of trace elements during magmatic processes; a summary of theoretical models and their applications. Journal of Research of the U. S. Geological Survey, 4: 41-47.

Bailey, R.A., 1989. Geologic map of Long Valley Caldera, Mono-Inyo Craters volcanic chain, and vicinity, eastern California, U.S. Geological Survey Miscellaneous Investigations Series Map I-1933.

Bailey, R.A., Dalrymple, G.B. and Lanphere, M.A., 1976. Volcanism, structure, and geochronology of Long Valley Caldera, Mono County, California. Journal of Geophysical Research, 81: 725-744.

Beresford, S.W., 1997. Volcanology and geochemistry of the Kaingaroa Ignimbrite, Taupo Volcanic Zone. Ph.D. Thesis, University of Canterbury, Christchurch, 311 pp.

Beresford, S.W., Cole, J.W. and Weaver, S.D., 2000. Weak chemical and mineralogical zonation in the Kaiangaroa Ignimbrite, Taupo volcanic zone, New Zealand. New Zealand Journal of Geology and Geophysics, 43: 639-650.

Berryman, K.R. and Villamor, P., 1999. Spatial and temporal zoning of faulting in the Taupo volcanic zone, New Zealand, Geological Society of New Zealand 1999 annual conference programme and abstracts. Geological Society of New Zealand miscellaneous publication 108 A, Palmerston North, New Zealand, pp. 15.

Berryman, K., Begg, J., Villamor, P., Nairn, I., Lee, J., Alloway, B., Rowland, J. and Capote, R., 2002. Volcano-tectonic interactions at the southern margin of the Okataina Volcanic Centre, Taupo Volcanic Zone, New Zealand. Eos Transactions AGU, 83(22), Western Pacific Geophysics Meeting Supplement, Abstract SE31C-06: WP70.

Bibby, H.M., Caldwell, T.G., Davey, F.J. and Webb, T.H., 1995. Geophysical evidence on the structure of the Taupo volcanic zone and its hydrothermal circulation. Journal of Volcanology and Geothermal Research, 68: 29-58.

Blake, S., Wilson, C.J.N., Smith, I.E.M. and Walker, G.P.L., 1992. Petrology and dynamics of the Waimhia mixed magma eruption, Taupo Volcano, New Zealand. Journal of the Geological Society of London, 149: 193-207.

Blong, R., 2003. Building damage in Rabaul, Papua New Guinea, 1994. Bull. Volcanol., 65: 43-54.

Bowen, N.L., 1928. The evolution of the igneous rocks. Princeton University Press, Princeton, 334 pp.

Bradshaw, J.D., 1989. Cretaceous geotectonic patterns in the New Zealand region. Tectonics, 8: 803-820.

Briggs, N.D., 1976a. Welding and crystallisation zonation in Whakamaru Ignimbrite, central North Island, New Zealand. New Zealand Journal of Geology and Geophysics, 19: 189-212.

Briggs, N.D., 1976b. Recognition and correlation of subdivisions within the Whakamaru Ignimbrite, central North Island, New Zealand. New Zealand Journal of Geology and Geophysics, 19: 463-501.

Briggs, R.M., Gifford, M.G., Moyle, A.R., Taylor, S.R., Norman, M.D., Houghton, B.F. and Wilson, C.J.N., 1993. Geochemical zoning and eruptive mixing in ignimbrites from Mangakino Volcano, Taupo volcanic zone, New Zealand. Journal of Volcanology and Geothermal Research, 56: 175-203.

Brooker, M.R., Houghton, B.F., Wilson, C.J.N. and Gamble, J.A., 1993. Pyroclastic phases of a rhyolitic dome-building eruption; Puketarata tuff ring, Taupo volcanic zone, New Zealand. Bulletin of Volcanology, 55: 395-406.

Brown, G.C., 1982. Calc-alkaline intrusive rocks; their diversity, evolution, and relation to volcanic arcs. In: R.S. Thorpe (Editor), Andesites; orogenic andesites and related rocks. John Wiley & Sons, Chichester, United Kingdom, pp. 437-461.

Brown, S.J.A., 1994. Geology and geochemistry of the Whakamaru Group ignimbrites, and associated rhyolite domes, Taupo Volcanic Zone, New Zealand. Doctoral Thesis, University of Canterbury, Christchurch, 286 pp.

Brown, S.J.A. and Fletcher, I.R., 1999. SHRIMP U-Pb dating of the preeruption growth history of zircons from the 340 ka Whakamaru Ignimbrite, New Zealand; evidence for >250 k.y. magma residence times. Geology, 27: 1035-1038.

Brown, S.J.A., Wilson, C.J.N., Cole, J.W. and Wooden, J.L., 1998. The Whakamaru Group ignimbrites, Taupo volcanic zone, New Zealand; evidence for reverse tapping of a zoned silicic magmatic system. Journal of Volcanology and Geothermal Research, 84: 1-37.

Browne, P.R.L., Graham, I.J., Parker, R.J. and Wood, C.P., 1992. Subsurface andesite lavas and plutonic rocks in the Rotokawa and Ngatamariki geothermal systems, Taupo volcanic zone, New Zealand. Journal of Volcanology and Geothermal Research, 51: 199-215.

Bryan, C.J., Sherburn, S., Bibby, H.M., Bannister, S.C. and Hurst, A.W., 1999. Shallow seismicity of the central Taupo volcanic zone, New Zealand; its distribution and nature. New Zealand Journal of Geology and Geophysics, 42: 533-542.

Cas, R.A.F. and Wright, J.V., 1988. Volcanic Successions: Modern and Ancient. Chapman & Hall, London, 528 pp.

Chadwick, W.W., Jr. and Embley, R.W., 1998. Graben formation associated with recent dike intrusions and volcanic eruptions on the mid-ocean ridge. Journal of Geophysical Research, 103: 9807-9825.

Charlier, B.L.A., 2000. U-Th isotopic constraints on the pre-eruptive dynamics of large scale silicic volcanism: Examples from New Zealand. Ph.D. Thesis, The Open University, Milton Keynes, 328 pp.

Charlier, B.L.A., Peate, D.W., Wilson, C.J.N., Lowenstern, J.B., Storey, M. and Brown, S.J.A., 2003. Crystallisation ages in coeval silicic magma bodies; ^{238}U-^{230}Th disequilibrium evidence from the Rotoiti and Earthquake Flat eruption deposits,

Taupo volcanic zone, New Zealand. Earth and Planetary Science Letters, 206: 441-457.

Charlier, B.L.A., Wilson, C.J.N., Lowenstern, J.B., Blake, S., van Calsteren, P. and Davidson, J.P., submitted. Generation of magmas at a hyperactive silicic volcano, Taupo Volcanic Zone, New Zealand. Journal of Petrology.

Chase, C.G., 1978. Plate kinematics; the Americas, East Africa, and the rest of the world. Earth and Planetary Science Letters, 37: 355-368.

Christiansen, R.L., 2001. The Quaternary and Pliocene Yellowstone Plateau Volcanic Field of Wyoming, Idaho, and Montana. U.S. Geological Survey Professional Paper 729-G.

Cole, J.W., 1970. Structure and eruptive history of the Tarawera volcanic complex. New Zealand Journal of Geology and Geophysics, 13: 879-902.

Cole, J.W., 1990. Structural control and origin of volcanism in the Taupo volcanic zone, New Zealand. Bulletin of Volcanology, 52: 445-459.

Dalrymple, G.B., 1989. The GLM continuous laser system for $^{40}Ar/^{39}Ar$ dating; description and performance characteristics. In: W.C. Shanks, III and R.E. Criss (Editors), New frontiers in stable isotopic research; laser probes, ion probes, and small-sample analysis. U.S. Geological Survey, Reston, pp. 89-96.

Dalrymple, G.B. and Lanphere, M.A., 1969. Potassium-argon dating; principles, techniques and applications to geochronology. W. H. Freeman and Co., San Fransisco, 258 pp.

Darby, D.J. and Meertens, C.M., 1995. Terrestrial and GPS measurements of deformation across the Taupo back arc and Hikurangi forearc regions in New Zealand. Journal of Geophysical Research, 100: 8221-8232.

Davey, F.J., Henrys, S.A. and Lodolo, E., 1995. Asymmetric rifting in a continental back-arc environment, North Island, New Zealand. Journal of Volcanology and Geothermal Research, 68: 209-238.

DePaolo, D.J., 1981. Trace element and isotopic effects of combined wallrock assimilation and fractional crystallization. Earth and Planetary Science Letters, 53: 189-202.

Ewart, A., 1963. Petrology and petrogenesis of the Quaternary pumice ash in the Taupo area, New Zealand. Journal of Petrology, 4: 392-431.

Ewart, A., 1965. Mineralogy and petrogenesis of the Whakamaru ignimbrite in the Maraetai area of the Taupo volcanic zone, New Zealand. New Zealand Journal of Geology and Geophysics, 8: 611-677.

Ewart, A., 1967. The petrography of the central North Island rhyolitic lavas; part I, Correlations between the phenocryst assemblages. New Zealand Journal of Geology and Geophysics, 10: 182-197.

Ewart, A., 1968. The petrography of the central North Island rhyolitic lavas; part 2, Regional petrography including notes on associated ash-flow pumice deposits. New Zealand Journal of Geology and Geophysics, 11: 478-542.

Ewart, A. and Stipp, J.J., 1968. Petrogenesis of the volcanic rocks of the central North Island, New Zealand, as indicated by a study of $^{87}Sr/^{86}Sr$ ratios, and Sr, Rb, K, U and Th abundances. Geochimica et Cosmochimica Acta, 32: 699-736.

Ewart, A., Hildreth, W. and Carmichael, I.S.E., 1975. Quaternary acid magma in New Zealand. Contributions to Mineralogy and Petrology, 51: 1-27.

Freundt, A., Wilson, C.J.N. and Carey, S.N., 2000. Ignimbrites and block-and-ash flow deposits. In: Encyclopedia of volcanoes. Academic Press, London, pp. 581-599.

Froggatt, P.C. and Lowe, D.J., 1990. A review of late Quaternary silicic and some other tephra formations from New Zealand; their stratigraphy, nomenclature, distribution, volume, and age. New Zealand Journal of Geology and Geophysics, 33: 89-109.

Gamble, J.A., Smith, I.E.M., Graham, I.J., Kokelaar, B.P., Cole, J.W., Houghton, B.F. and Wilson, C.J.N., 1990. The petrology, phase relations and tectonic setting of basalts from the Taupo volcanic zone, New Zealand and the Kermadec island arc-Havre Trough, SW Pacific. Journal of Volcanology and Geothermal Research, 43: 253-270.

Gamble, J.A., Smith, I.E.M., McCulloch, M.T., Graham, I.J. and Kokelaar, B.P., 1993. The geochemistry and petrogenesis of basalts from the Taupo volcanic zone and Kermadec island arc, S.W. Pacific. Journal of Volcanology and Geothermal Research, 54: 265-290.

Graham, I.J., Gulson, B.L., Hedenquist, J.W. and Mizon, K., 1992. Petrogenesis of late Cenozoic volcanic rocks from the Taupo volcanic zone, New Zealand, in the light of new lead isotope data. Geochimica et Cosmochimica Acta, 56: 2797-2819.

Graham, I.J., Cole, J.W., Briggs, R.M., Gamble, J.A. and Smith, I.E.M., 1995. Petrology and petrogenesis of volcanic rocks from the Taupo volcanic zone; a review. Journal of Volcanology and Geothermal Research, 68: 59-87.

Grange, L.I., 1929. A classification of soils of Rotorua County. New Zealand Journal of Science and Technology, 11: 219-228.

Grange, L.I., 1931. Volcanic-ash showers. New Zealand Journal of Science and Technology, 12: 228-240.

Grange, L.I., 1937. The Geology of the Rotorua Taupo subdivision. New Zealand Geological Survey Bulletin 37, 138 pp.

Gravley, D.M., 2004. The Ohakuri Ignimbrite. (in progress) Ph.D. Thesis, University of Canterbury, Christchurch.

Grindley, G.W., 1959. Geological map of New Zealand 1:63,360 Sheet N85 Waiotapu. Department of Scientific and Industrial Research, Wellington.

Grindley, G.W., 1960. Geological Map of New Zealand 1:250,000 Sheet 5 Taupo. Department of Scientific and Industrial Research, Wellington.

Grindley, G.W., 1961. Geological Map of New Zealand 1:63,360 Sheet N94 Taupo. Department of Scientific and Industrial Research, Wellington.

Harvey, P.K., Taylor, D.M., Hendry, R.D. and Bancroft, F., 1973. An accurate fusion method for the analysis of rocks and chemically related materials by X-ray fluorescence spectrometry. X-Ray Spectrometry, 2: 33-44.

Healy, J., 1946. Geology of the Karapiro District, Cambridge. New Zealand Journal of Science and Technology, B27: 199-217.

Healy, J., 1962. Structure and volcanism in the Taupo volcanic zone, New Zealand. American Geophysical Union, Geophysical Monograph, 6: 151-157.

Healy, J., 1963. Geology of the Rotorua district. Proceedings New Zealand Ecological Society, 10: 53-58.

Healy, J., 1964. Volcanic mechanisms in the Taupo volcanic zone, New Zealand. New Zealand Journal of Geology and Geophysics, 7: 6-23.

Healy, J., Schofield, J.C. and Thompson, B.N., 1964. Geological Map of New Zealand 1:250,000 Sheet 8 Rotorua. Department of Scientific and Industrial Research, Wellington.

Heiken, G., Krier, D., McCormick, T. and Snow, M.G., 2000. Intracaldera volcanism and sedimentation; Creede Caldera, Colorado. Ancient Lake Creede; its volcano-tectonic setting, history of sedimentation, and relation to mineralization in the Creede mining district. Geological Society of America Special Paper, 346: 127-157.

Henneberger, R.C. and Browne, P.R.L., 1988. Hydrothermal alteration and evolution of the Ohakuri hydrothermal system, Taupo volcanic zone, New Zealand. Journal of Volcanology and Geothermal Research, 34: 211-231.

Herrero-Bervera, E., Helsley, C.E., Sarna-Wojcicki, A.M., Lajoie, K.R., Meyer, C.E., McWilliams, M.O., Negrini, R.M., Turrin, B.D., Donnelly-Nolan, J.M. and Liddicoat, J.C., 1994. Age and correlation of a paleomagnetic episode in the Western United States by $^{40}Ar/^{39}Ar$ dating and tephrochronology; the Jamaica, Blake, or a new polarity episode? Journal of Geophysical Research, 99: 24,091-24,103.

Hochstein, M.P. and Ballance, P.F., 1993. Hauraki Rift; a young, active, intra-continental rift in a back-arc setting. In: P.F. Ballance (Editor), Sedimentary basins of the world 2: South pacific sedimentary basins. Elsevier, Amsterdam, pp. 295-305.

Hochstein, M.P., Smith, I.E.M., Regenauer-Lieb, K. and Ehara, S., 1993. Geochemistry and heat transfer processes in Quaternary rhyolitic systems of the Taupo volcanic zone, New Zealand. Tectonophysics, 223: 213-235.

Hochstetter, F.v., Petermann, A. and Fischer, C.F., 1864. The geology of New Zealand (English translation by C. A. Flemming, Government Printer, Wellington, 1959). T. Delattre, Auckland, 113 pp.

Houghton, B.F., Lloyd, E.F., Wilson, C.J.N. and Lanphere, M.A., 1991. K-Ar ages from the Western Dome Belt and associated rhyolitic lavas in the Maroa-Taupo area, Taupo volcanic zone, New Zealand. New Zealand Journal of Geology and Geophysics, 34: 99-101.

Houghton, B.F., Wilson, C.J.N., McWilliams, M.O., Lanphere, M.A., Weaver, S.D., Briggs, R.M. and Pringle, M.S., 1995. Chronology and dynamics of a large silicic magmatic system; central Taupo Volcanic Zone, New Zealand. Geology, 23: 13-16.

Houghton, B.F., Wilson, C.J.N., Lanphere, M.L. and Leonard, G.S., in prep. A new chronology of the central Taupo Volcanic Zone.

Jurado-Chichay, Z. and Walker, G.P.L., 2000. Stratigraphy and dispersal of the Mangaone Subgroup pyroclastic deposits, Okataina volcanic centre, New Zealand. Journal of Volcanology and Geothermal Research, 104: 319-383.

Karhunen, R.A., 1993. The Pokai and Chimp ignimbrites of NW Taupo Volcanic Zone. Ph.D. Thesis, University of Canterbury, Christchurch, 356 pp.

Kohn, B.P., 1973. Some studies of New Zealand Quaternary pyroclastic rocks. Ph.D. Thesis, Victoria University of Wellington.

Langridge, R.M., 1990. The geology of the Upper Atiamuri region, Taupo Volcanic Zone, with special reference to the existence of the Kapenga caldera volcano. M.Sc. Thesis, University of Waikato, Hamilton, 155 pp.

Lanphere, M.A., 2000. Duration of sedimentation of Creede Formation from $^{40}Ar/^{39}Ar$ ages. Geological Society of America Special Paper, 346: 71-76.

Lanphere, M.A. and Dalrymple, G.B., 2000. First-principles calibration of ^{38}Ar tracers; implications for the ages of $^{40}Ar/^{39}Ar$ fluence monitors, U. S. Geological Survey Professional Paper, pp. 10.

Lanphere, M.A., Champion, D.E., Christiansen, R.L., Izett, G.A. and Obradovich, J.D., 2002. Revised ages for tuffs of the Yellowstone Plateau volcanic field; assignment of the Huckleberry Ridge Tuff to a new geomagnetic polarity event. Geological Society of America Bulletin, 114: 559-568.

Le Maitre, R.W., Bateman, P., Dudek, A., Keller, J., Lemeyre, J., Le Bas, M.J., Sabine, P.A., Schmid, R., Sorensen, H., Streckeisen, A., Wooley, A.R. and Zanettin, B., 1989. A classification of igneous rocks and glossary of terms. Recommendations of the IUGS Subcommission on the Systematics of Igneous Rocks. Blackwell Sci. Publ., Oxford, 193pp.

Leonard, G.S., 1999. Magmatic processes associated with the c 1350 A.D. Kaharoa Eruption, Tarawera Volcanic Complex, New Zealand. B.Sc. (Hons.) Thesis, University of Canterbury, Christchurch, 98 pp.

Leonard, G.S., Cole, J.W., Nairn, I.A. and Self, S., 2002. Basalt triggering of the c. AD 1305 Kaharoa rhyolite eruption, Tarawera volcanic complex, New Zealand. Journal of Volcanology and Geothermal Research, 115: 461-486.

Leonard, G.S., Houghton, B.F., Calvert, A. and Lanphere, M.L., in prep. Chronology of the Maroa area, Taupo Volcanic Zone.

Lipman, P.W., 1997. Subsidence of ash-flow calderas; relation to caldera size and magma-chamber geometry. Bulletin of Volcanology, 59: 198-218.

Lipman, P.W., 2000. Central San Juan caldera cluster; regional volcanic framework. Geological Society of America Special Paper 346: 9-69.

Lloyd, E.F., 1972. Geology and hot springs of Orakeikorako. New Zealand Geological Survey Bulletin, 85: 142pp.

Ludwig, K.R., 1999. User's Manual for Isoplot/Ex Version 2.1a, A geochronological Toolkit for Microsoft Excel, Berkeley Geochronology Centre, Berkeley.

Maniar, P.D. and Piccoli, P.M., 1989. Tectonic discrimination of granitoids. Geological Society of America Bulletin, 101: 635-643.

Manville, V. and Wilson, C.J.N., 2004. The 26.5 ka Oruanui eruption, New Zealand: A review of the roles of volcanism and climate in the post-eruptive sedimentary response. New Zealand Journal of Geology and Geophysics: (in press).

Martin, R.C., 1961. Stratigraphy and structural outline of the Taupo volcanic zone. New Zealand Journal of Geology and Geophysics, 4: 449-478.

Martin, R.C., 1965. Lithology and eruptive history of the Whakamaru ignimbrites in the Maraetai area of the Taupo volcanic zone, New Zealand. New Zealand Journal of Geology and Geophysics, 8: 680-701.

Mastin, L.G. and Pollard, D.D., 1988. Surface deformation and shallow dike intrusion processes at Inyo Craters, Long Valley, California. Journal of Geophysical Research, 93: 13,221-13,235.

McConnell, V.S., Shearer, C.K., Eichelberger, J.C., Keskinen, M.J., Layer, P.W. and Papike, J.J., 1995. Rhyolite intrusions in the intracaldera Bishop Tuff, Long Valley Caldera, California. Journal of Volcanology and Geothermal Research, 67: 41-60.

McCulloch, M.T., Kyser, T.K., Woodhead, J.D. and Kinsley, L., 1994. Pb-Sr-Nd-O isotopic constraints on the origin of rhyolites from the Taupo volcanic zone of New Zealand; evidence for assimilation followed by fractionation from basalt. Contributions to Mineralogy and Petrology, 115: 303-312.

McDougall, I. and Harrison, T.M., 1999. Geochronology and thermochronology by the $^{40}Ar/^{39}Ar$ method. Oxford University Press, New York.

McWilliams, M., 2001. Global correlation of the 223 ka Pringle Falls Event. International Geology Review, 43: 191-195.

Milner, D.M., 2001. The structure and eruptive history of Rotorua Caldera, Taupo Volcanic Zone, New Zealand. Ph.D. Thesis, University of Canterbury, Christchurch, 434 pp.

Milner, D.M., Cole, J.W. and Wood, C.P., 2002a. Asymmetric, multiple-block collapse at Rotorua Caldera, Taupo Volcanic Zone, New Zealand. Bulletin of Volcanology, 64: 134-149.

Milner, D.M., Cole, J.W. and Wood, C.P., 2002b. Mamaku Ignimbrite: a caldera-forming ignimbrite erupted from a compositionally zoned magma chamber in Taupo Volcanic Zone, New Zealand. Journal of Volcanology and Geothermal Research, 122: 243-264.

Mortimer, N., 1994. Origin of the Torlesse Terrane and coeval rocks, North Island, New Zealand. International Geology Review, 36: 891-910.

Nairn, I.A., 1972. Rotoehu Ash and the Rotoiti Breccia Formation, Taupo volcanic zone, New Zealand. New Zealand Journal of Geology and Geophysics, 15: 251-261.

Nairn, I.A., 1989. Sheet V16AC - Tarawera. Geological Map of New Zealand 1:50,000. Department of Scientific and Industrial Research, Wellington.

Nairn, I.A., 1992. The Te Rere and Okareka eruptive episodes - Okataina Volcanic Centre, Taupo Volcanic Zone, New Zealand. N.Z. Journal of Geology and Geophysics, 35: 93-108.

Nairn, I.A., 2002a. Institute of Geological and Nuclear Sciences geological map 25: Geology of Okataina Volcanic Centre, 1:50,000, Lower Hutt.

Nairn, I.A., 2002b. The effects of volcanic ash fall (tephra) on road and airport surfaces, Institute of Geological and Nuclear Sciences Science Report 2002/13, Lower Hutt.

Nairn, I.A. and Kohn, B.P., 1973. Relation of the Earthquake Flat Breccia to the Rotoiti Breccia, central North Island, New Zealand. New Zealand Journal of Geology and Geophysics, 16: 269-279.

Nairn, I.A., Kobayashi, T. and Nakagawa, M., 1998. The approximately 10 ka multiple vent pyroclastic eruption sequence at Tongariro Volcanic Centre, Taupo Volcanic Zone, New Zealand; Part 1, Eruptive processes during regional extension. Journal of Volcanology and Geothermal Research, 86: 19-44.

Nash, W.P. and Crecraft, H.R., 1985. Partition coefficients for trace elements in silicic magmas. Geochimica et Cosmochimica Acta, 49: 2309-2322.

Neall, V.E., Houghton, B.F., Cronin, S.J., Donoghue, S.L., Hodgson, K.A., Johnston, D.M., Lecointre, J.A. and Mitchell, A.R., 1999. Volcanic Hazards at Ruapehu Volcano. Ministry of Civil Defence, Volcanic Hazards Information Series No. 8, 30 pp.

Newnham, R.M., Eden, D.N., Lowe, D.J. and Hendy, C.H., 2003. Rerewhakaaitu Tephra, a land-sea marker for the last termination in New Zealand, with

implications for global climate change. Quaternary Science Reviews, 22: 289-308.

Norrish, K. and Hutton, J.T., 1969. An accurate x-ray spectrographic method for the analysis of a wide range of geological samples. Geochimica et Cosmochimica Acta, 33: 431-453.

Norrish, K. and Chappell, B.W., 1977. X-ray fluorescence spectrometry. In: J. Zussman (Editor), Physical methods in determinative mineralogy, Academic, London, pp. 201-272.

Obradovich, J.D., 1992. Geochronology of the late Cenozoic volcanism of Yellowstone National Park and adjoining areas, Wyoming and Idaho, U. S. Geological Survey Open-File Report 92-0408.

Pearce, J.A., 1983. Role of the sub-continental lithosphere in magma genesis at active continental margins. In: C.J. Hawkesworth and M.J. Norry (Editors), Continental basalts and mantle xenoliths. Shiva Publ., Nantwich, pp. 230-249.

Petford, N., Kerr, R.C. and Lister, J.R., 1993. Dike transport of granitoid magmas. Geology, 21: 845-848.

Petford, N., Lister, J.R. and Kerr, R.C., 1994. The ascent of felsic magmas in dykes. Lithos, 32: 161-168.

Pettinga, J.R., Chamberlain, C.G., Yetton, M.D., Van Dissen, R.J. and Downes, G., 1998. Earthquake Source Identification and Characterisation, Canterbury Regional Council Report, Christchurch.

Pringle, M.S., McWilliams, M., Houghton, B.F., Lanphere, M.A. and Wilson, C.J.N., 1992. $^{40}Ar/^{39}Ar$ dating of Quaternary feldspar; examples from the Taupo volcanic zone, New Zealand. Geology, 20: 531-534.

Reid, F., 1983. Origin of the rhyolitic rocks of the Taupo Volcanic Zone, New Zealand. Journal of Volcanology and Geothermal Research, 15: 315-338.

Richnow, J., 1999. Eruptional and Post-Eruptional Processes in Rhyolite Domes. Ph.D. Thesis, Canterbury, Christchurch.

Rogan, M., 1982. A geophysical study of the Taupo volcanic zone, New Zealand. Journal of Geophysical Research, 87: 4073-4088.

Rollinson, H.R., 1993. Using geochemical data: Evaluation, presentation, interpretation. Longman, Essex, 352 pp.

Rowland, J.V. and Sibson, R.H., 2001. Extensional fault kinematics within the Taupo Volcanic Zone, New Zealand; soft-linked segmentation of a continental rift system. New Zealand Journal of Geology and Geophysics, 44: 271-283.

Rubin, A.M. and Pollard, D.D., 1988. Dike-induced faulting in rift zones of Iceland and Afar. Geology, 16: 413-417.

Schofield, J.C., 1965. The Hinuera Formation and associated Quaternary events. New Zealand Journal of Geology and Geophysics, 8: 772-791.

Self, S., 1983. Large-scale phreatomagmatic silicic volcanism; a case study from New Zealand. Journal of Volcanology and Geothermal Research, 17: 433-469.

Sherburn, S., Bannister, S. and Bibby, H., 2003. Seismic velocity structure of the central Taupo volcanic zone, New Zealand, from local earthquake tomography. Journal of Volcanology and Geothermal Research, 122: 69-88.

Smith, R.C.M., Smith, I.E.M., Browne, P.R.L. and Hochstein, M.P., 1993. Volcano-tectonic controls on sedimentation in the Taupo volcanic zone, New Zealand. In: P.F. Ballance (Editor), Sedimentary basins of the world 2: South pacific sedimentary basins. Elsevier, Amsterdam, pp. 143-156.

Smith, R.L. and Bailey, R.A., 1968. Resurgent cauldrons, Geological Society of America Memoir 116, pp. 613-662.

Smith, V. and Shane, P., 2002. Geochemical characteristics of the widespread Tahuna Tephra. New Zealand Journal of Geology and Geophysics, 45: 103-107.

Smith, V.C., Shane, P. and Smith, I.E.M., 2002. Tephrostratigraphy and geochemical fingerprinting of the Mangaone Subgroup tephra beds, Okataina Volcanic Centre, New Zealand. New Zealand Journal of Geology and Geophysics, 45: 207-219.

Soengkono, S., 1995. A magnetic model for deep plutonic bodies beneath the central Taupo volcanic zone, North Island, New Zealand. Journal of Volcanology and Geothermal Research, 68: 193-207.

Speed, J., Shane, P. and Nairn, I., 2002. Volcanic stratigraphy and phase chemistry of the 11 900 yr BP Waiohau eruptive episode, Tarawera Volcanic Complex, New Zealand. New Zealand Journal of Geology and Geophysics, 45: 395-410.

Spray, J.G., 1997. Superfaults. Geology, 25: 579-582.

Stagpoole, V.M., 2000. Residual gravity anomaly map of the Taupo Volcanic Zone, New Zealand, 1:250,000, version 1.0. Institute of Geological and Nuclear Sciences, Lower Hutt.

Steiger, R.H. and Jaeger, E., 1977. Subcommission on geochronology; convention on the use of decay constants in geo- and cosmochronology. Earth and Planetary Science Letters, 36: 359-362.

Steiner, A., 1977. The Wairakei geothermal area, North Island, New Zealand; its subsurface geology and hydrothermal rock alteration. New Zealand Geological Survey Bulletin 90, 133 pp.

Stern, T.A. and Davey, F.J., 1987. A seismic investigation of the crustal and upper mantle structure within the central volcanic region of New Zealand. New Zealand Journal of Geology and Geophysics, 30: 217-231.

Stipp, J.J., 1968. The geochronology and petrogenesis of the Cenozoic volcanics of North Island, New Zealand. PhD Thesis, Australian National University, Canberra.

Sutton, A.N., 1995. Evolution of a large silicic magma system: Taupo volcanic centre, New Zealand. Ph.D. Thesis, The Open University, Milton Keynes, 416 pp.

Sutton, A.N., Blake, S. and Wilson, C.J.N., 1995. An outline geochemistry of rhyolite eruptives from Taupo volcanic centre, New Zealand. Journal of Volcanology and Geothermal Research, 68: 153-175.

Sutton, A.N., Blake, S., Wilson, C.J.N. and Charlier, B.L.A., 2000. Late Quaternary evolution of a hyperactive rhyolite magmatic system; Taupo volcanic centre, New Zealand. Journal of the Geological Society of London, 157: 537-552.

Tanaka, H., Turner, G.M., Houghton, B.F., Tachibana, T., Kono, M. and McWilliams, M.O., 1996. Palaeomagnetism and chronology of the central Taupo volcanic zone, New Zealand. Geophysical Journal International, 124: 919-934.

Thompson, B.N., 1958. The geology of the Atiamuri dam site. New Zealand Journal of Geology and Geophysics, 1: 275-306.

Thompson, B.N., 1966. The geology of the Maroa district. M.Sc. Thesis, University of Auckland, Auckland, 189 pp.

Thompson, G.E.K., 1980. Temperature gradients within and adjacent to the Taupo Volcanic Zone. New Zealand Journal of Geology and Geophysics, 23: 407-412.

Valentine, G.A., 1993. Note on the distribution of basaltic volcanism associated with large silicic centers. Journal of Volcanology and Geothermal Research, 56: 167-170.

Vazquez, J.A. and Reid, M.R., 2002. Time scales of magma storage and differentiation of voluminous high-silica rhyolites at Yellowstone Caldera, Wyoming. Contributions to Mineralogy and Petrology, 144: 274-285.

Villamor, P. and Berryman, K.R., 2001. A late Quaternary extension rate in the Taupo volcanic zone, New Zealand, derived from fault slip data. New Zealand Journal of Geology and Geophysics, 44: 243-269.

Vucetich, C.G. and Howorth, R., 1976. Late Pleistocene tephrostratigraphy in the Taupo District, New Zealand. New Zealand Journal of Geology and Geophysics, 19: 51-69.

Walcott, R.I., 1987. Geodetic strain and the deformational history of the North Island of New Zealand during the late Cainozoic. Philosophical Transactions of the Royal Society of London, A321: 163-181.

Walker, G.P.L., 1980. The Taupo pumice; product of the most powerful known (ultraplinian) eruption? Journal of Volcanology and Geothermal Research, 8: 69-94.

Weaver, B.L. and Tarney, J., 1984. Major and trace element composition of the continental lithosphere. Physics and Chemistry of the Earth, 15: 39-68.

Webb, T.H. and Anderson, H., 1998. Focal mechanisms of large earthquakes in the North Island of New Zealand; slip partitioning at an oblique active margin. Geophysical Journal International, 134: 40-86.

Whiteford, C.M. and Lumb, J.T., 1975. A catalogue of physical properties of rocks; volume 1; listing by catalogue number. Geophysics Division Report 105.

Williams, H., 1941. Calderas and their origin. University of California Publications in Geological Sciences, 25: 239-346.

Wilson, C.J.N., 1985. The Taupo eruption, New Zealand; II, The Taupo ignimbrite. Philosophical Transactions of the Royal Society of London, A, 314: 229-310.

Wilson, C.J.N., 1993. Stratigraphy, chronology, styles and dynamics of late Quaternary eruptions from Taupo Volcano, New Zealand. Philosophical Transactions of the Royal Society of London, A, 343: 205-306.

Wilson, C.J.N., 2001. The 26.5 ka Oruanui eruption, New Zealand; an introduction and overview. Journal of Volcanology and Geothermal Research, 112: 133-174.

Wilson, C.J.N. and Walker, G.P.L., 1985. The Taupo eruption, New Zealand; I, General aspects. Philosophical Transactions of the Royal Society of London, 314 A: 199-228.

Wilson, C.J.N., Rogan, A.M., Smith, I.E.M., Northey, D.J., Nairn, I.A. and Houghton, B.F., 1984. Caldera volcanoes of the Tuapo volcanic zone, New Zealand. Journal of Geophysical Research, 89: 8463-8484.

Wilson, C.J.N., Houghton, B.F. and Lloyd, E.F., 1986. Volcanic history and evolution of the Maroa-Taupo area, central North Island. In: I.E.M. Smith (Editor), Late Cenozoic Volcanism in New Zealand. Royal Soc. New Zealand Bull. 23. pp. 194-223.

Wilson, C.J.N., Houghton, B.F., Lanphere, M.A. and Weaver, S.D., 1992. A new radiometric age estimate for the Rotoehu Ash from Mayor Island volcano, New Zealand. New Zealand Journal of Geology and Geophysics, 35: 371-374.

Wilson, C.J.N., Houghton, B.F., McWilliams, M.O., Lanphere, M.A., Weaver, S.D. and Briggs, R.M., 1995. Volcanic and structural evolution of Taupo volcanic zone, New Zealand; a review. Journal of Volcanology and Geothermal Research, 68: 1-28.

York, D., 1969. Least squares fitting of a straight line with correlated errors. Earth and Planetary Science Letters, 5: 320-324.

Acknowledgements

I would first like to thank both of my supervisors Jim Cole and Colin Wilson for the invaluable support and guidance they have given me over the course of this project. Jim has been a fantastic academic coach and Colin has repeatedly spurred me on and provided outstanding intellectual advice. Both Jim and Colin have been great friends. I would also like to thank Bruce Houghton, of the University of Hawaii, for his help and guidance.

Thank you also to my fellow University of Canterbury Ph.D. students Darren Gravley, Karl Spinks and Dave Milner. You've all been great mates. Darren has provided superb help in the field and throughout this thesis, and generated enthusiastic debate in each of our research. Karl has also helped with keen discussion and memorable times in the field. Dave gave me a lot of guidance in the early parts of my thesis and helped me focus my work. Thanks also to Greg Teen for late stage proof reading.

Cheers to Jane Guise, Rob Spiers, Stephen & Catherine Brown, John Southward and Cathy Knight for so much fast and good-natured help in the lab and office. I'd also like to express my gratitude to the whole staff of the Department of Geological Sciences and the University of Canterbury for providing such a fun study environment.

I'd like to thank the staff and management of the Institute of Geological and Nuclear Sciences both at Wairakei and Gracefield. So many of you have helped me over my time in the field and writing up. You've provided a wealth of resources and knowledge, and I've made a lot of close friends.

To Andy Calvert, James Saburomaru, Marvin Lanphere, Jennifer Adleman and many other people at the US Geological Survey, Menlo Park: Thanks for the good fun over my two seasons of work there. See you all again soon. Take a holiday James!

Thank you to Mum and Dad for nurturing a scientific mind in me from a young age. You're both always great to talk to and have supported me in everything I did for as long as I can remember. Dad, thanks for the monumental task of proof-reading this thing, and Mum, thanks for your offers to help if it got too much for Dad. Finally, thank you Lisa for making life so much fun while I've been working so hard, and especially for going camping. I love you all.

Appendix 1 - Location number and grid reference by deposit

Please note that for the purposes of this thesis 'location number' and 'sample number' are two separate, but related, attributes. 'Location number' ('Locn.' here) is a unique identifyer, beginning with an 'M', given to a specific horizontal location within Maroa (see 'Grid Ref' here in NZ map grid series 260 sheet/100-metre-coordinates). 'Sample number' is the 'location number' if only one sample was collected from that location. However, if more that one sample has been collected from a single location the 'sample numbers' are distinguised from the 'location number' by letter suffixes (e.g. M123a, M123b, etc.). Such 'sample numbers' are used in Appendices 3 and 4.

Type	Deposit	Locn.	Grid Ref	Description
Basalt	Kakuki Basalt 'bombs'	**M293**	U17/834959	forest road
Basalt	Kakuki Basalt scoria	**M291**	U17/833964	Orakeikorako Rd cutting
Basalt	Kakuki Basalt spatter	**M292**	U17/834959	Kakuki stream (vent area)
Basalt	Ongaroto Basalt	**M112**	T17/669088	Watts Quarry
Basalt	Poihipi/Ben Lomond Basalt	**M326**	U17/667871	east of turn in Poihipi Rd
Basalt	Tatua Basalt	**M028**	U17/796948	
Basalt	Tatua Basalt	**M029**	U17/805959	scoria cone through dome
Basalt	Tatua Basalt	**M303**	U17/795947	flows off access rd, TYPE SECTION
Dome	(Acacia) Maroanui	**M242**	T17/680946	road cutting
Dome	(Acacia) Maroanui	**M243**	T17/679944	back of skid site
Dome	(Acacia) Maroanui	**M245**	T17/675940	marginal breccia
Dome	(Acacia) Maroanui East	**M239**	U17/694956	slip in road cutting
Dome	(Acacia) Maroanui East	**M240**	U17/692952	skid scrapings
Dome	(Acacia) Maroanui East	**M241**	T17/689958	road cutting
Dome	(Acacia) Maroanui North	**M244**	T17/682957	boulder in road cutting
Dome	(Acacia) Palm	**M235**	T17/688987	Palm Rd boulder in cutting
Dome	(Acacia) Palm	**M236**	T17/683976	skid cutting
Dome	(Acacia) Palm	**M237**	U17/681970	boulders in road scrapings by skid site
Dome	(Acacia) Palm	**M238**	U17/691972	road surface between cuts
Dome	(MEC) Baldy	**M347**	U17/798980	~50 m up Pulham Rd
Dome	(MEC) Baldy	**M349**	U17/796984	skid cutting
Dome	(MEC) Baldy	**M362**	U17/739975	access road quarry
Dome	(MEC) Baldy	**M363**	U17/784978	ridge SE of Baldy Rd
Dome	(MEC) Baldy North	**M202**	U17/795995	dome carapace?
Dome	(MEC) Baldy North	**M203**	U17/797993	road cutting
Dome	(MEC) Baldy North	**M346**	U17/801989	east cut Roy Simmonds Rd
Dome	(MEC) Baldy North	**M348**	U17/799983	skid side boulder
Dome	(MEC) Baldy North	**M350**	U17/793993	blocks in base of skid
Dome	(MEC) Baldy North	**M351**	U17/789989	base of skid
Dome	(MEC) Baldy North	**M352**	U17/788988	boulder below elongate ridge
Dome	(MEC) Baldy North	**M353**	U17/787990	road cutting
Dome	(MEC) Hauwai	**M193**	U17/773003	road cutting
Dome	(MEC) Hauwai	**M194**	U17/780007	road cutting
Dome	(MEC) Hauwai	**M196**	U17/782993	road cutting and intersection
Dome	(MEC) Hauwai	**M197**	U17/775003	good view north and to Tuahu
Dome	(MEC) Hauwai	**M198**	U17/789999	in road cutting corner
Dome	(MEC) Hauwai obsidian	**M032**	U17/772001	
Dome	(MEC) Kemp	**M184**	U17/767019	bluffs
Dome	(MEC) Mandarin	**M199**	U17/795000	margin or carapace
Dome	(MEC) Mandarin	**M200**	U17/797017	back of skid
Dome	(MEC) Mandarin	**M201**	U17/806021	back of skid at end of road
Dome	(MEC) Mandarin	**M341**	U17/811001	roadside cutting
Dome	(MEC) Mandarin	**M343**	U17/799996	boulder in pile of skid scraps
Dome	(MEC) Mandarin	**M344**	U17/807000	road cutting
Dome	(MEC) Mandarin ?	**M345**	U17/803991	small scrape in road cut
Dome	(MEC) Mandarin Dome	**M474**	U17/792007	western toe in skid track
Dome	(MEC) Mandarin Dome	**M475**	U17/792006	western toe in skid track
Dome	(MEC) McPhersom	**M266**	U17/776973	roadside cutting
Dome	(MEC) Roy E ridge to north	**M371**	U17/796969	skid track south end

Dome	(MEC) Roy East	**M369**	U17/792964	Roy Simmonds Rd cut
Dome	(MEC) Roy East	**M370**	U17/794966	road cut
Dome	(MEC) Roy North	**M257**	U17/782962	blocks in road cutting
Dome	(MEC) Roy North	**M259**	U17/782963	blocks in PABU/carapace
Dome	(MEC) Roy North	**M260**	U17/780962	road cutting
Dome	(MEC) Roy North	**M365**	U17/784957	Roy Simmonds Rd cutting
Dome	(MEC) Roy North	**M366**	U17/784957	boulders in skid base
Dome	(MEC) Roy North	**M367**	U17/785961	boulders from base of skid
Dome	(MEC) Roy North	**M368**	U17/789959	access road to summit
Dome	(MEC) Roy South	**M373**	U17/776942	NE cutting Tram Rd
Dome	(MEC) Roy West	**M372**	U17/776950	road side cutting
Dome	(MEC) Roy West	**M374**	U17/772949	Tram Rd cutting
Dome	(MEC) Rusty	**M261**	U17/776965	culvert cutting
Dome	(MEC) Rusty	**M262**	U17/784974	culvert cutting
Dome	(MEC) Rusty	**M263**	U17/783968	road cutting
Dome	(MEC) Rusty	**M264**	U17/781969	Rusty's Rd cutting
Dome	(MEC) Rusty	**M265**	U17/782975	bluff in road cutting
Dome	(MEC) Summit	**M364**	U17/777983	skid base atop dome
Dome	(MEC) Umukuri	**M424**	U17/809986	new road cutting
Dome	(MEC) Umukuri	**M460**	U17/821992	bluffs at base of fallen tree
Dome	(MEC) Umukuri	**M461**	U17/831983	water supply headworks
Dome	(MEC) Umukuri SE	**M425**	U17/801975	blocks by road
Dome	(MEC) Umukuri SE	**M426**	U17/799977	bluffs by intersection
Dome	(MEC) Wairiki	**M342**	U17/818997	boulder on fan off SE line
Dome	(MEC) Wilson	**M204**	U17/819014	road cutting
Dome	(MEC) Wilson	**M205**	U17/818011	dirty bluff
Dome	(MEC) Wilson	**M206**	U17/819010	road cutting
Dome	(MEC) Wilson	**M207**	U17/818009	bluffs in road cut
Dome	(MEC) Wilson	**M208**	U17/819007	
Dome	(MEC) Wilson	**M209**	U17/827007	base of skid
Dome	(MEC) Wilson	**M210**	U17/835007	
Dome	(MEC) Wilson	**M211**	U17/833009	culvert cutting
Dome	(MEC) Wilson	**M212**	U17/828008	boulders next to road
Dome	(MEC) Wilson	**M213**	U17/825013	base of skid
Dome	(MEC) Wilson	**M214**	U17/819002	bluff or boulder? near skid
Dome	(MWC) Almond	**M155**	U17/753995	base of skid
Dome	(MWC) Almond	**M156**	U17/751997	
Dome	(MWC) Almond	**M157**	U17/749000	
Dome	(MWC) Almond	**M179**	U17/755990	block beside road
Dome	(MWC) Almond	**M180**	U17/752990	cutting for culvert
Dome	(MWC) Almond	**M181**	U17/759985	base and side of skid
Dome	(MWC) Almond West	**M008**	U17/743992	road cutting
Dome	(MWC) Almond West	**M158**	U17/744997	
Dome	(MWC) Almond West	**M159**	U17/745998	2 m deep cutting
Dome	(MWC) Almond West	**M172**	U17/741995	
Dome	(MWC) Almond West	**M178**	U17/748990	inside corner View and Poplar Rds
Dome	(MWC) eastern Goldies	**M330**	U17/720953	
Dome	(MWC) eastern Goldies	**M331**	U17/718949	
Dome	(MWC) eastern Goldies	**M332**	U17/712956	skid cutting boulders
Dome	(MWC) Goldies	**M234**	U17/724957	boulder upslope of skid
Dome	(MWC) Goldies	**M255**	U17/726960	road cutting
Dome	(MWC) Goldies	**M256**	U17/724959	cutting
Dome	(MWC) Goldies	**M329**	U17/722958	
Dome	(MWC) Hind	**M334**	U17/722963	
Dome	(MWC) Hind	**M359**	U17/727968	high on south side
Dome	(MWC) Kemp	**M009**	U17/756018	
Dome	(MWC) Kemp	**M102**	U17/756022	sandlewood Rd
Dome	(MWC) Kemp	**M160**	U17/757003	skid cutting
Dome	(MWC) Kemp	**M161**	U17/758008	skid cutting
Dome	(MWC) Kemp	**M162**	U17/758009	
Dome	(MWC) Kemp	**M163**	U17/759010	
Dome	(MWC) Kemp	**M164**	U17/762011	
Dome	(MWC) Kemp	**M165**	U17/764013	
Dome	(MWC) Kemp	**M188**	U17/771003	west SH1 cutting
Dome	(MWC) Kemp	**M189**	U17/771001	west SH1 cutting

Dome	(MWC) Kemp	**M335**	U17/758003	bush track
Dome	(MWC) lower Goldies	**M232**	U17/714944	boulder on slope above skid
Dome	(MWC) lower Goldies	**M246**	U17/700951	cutting
Dome	(MWC) lower Goldies	**M247**	U17/701949	cutting
Dome	(MWC) lower Goldies	**M248**	U17/708961	surface of road
Dome	(MWC) lower Goldies	**M251**	U17/702948	road cut
Dome	(MWC) Poplar	**M139**	U17/721992	bluffs east of Mulga Rd
Dome	(MWC) Poplar	**M140**	U17/720990	
Dome	(MWC) Poplar	**M141**	U17/723994	base of skid
Dome	(MWC) Poplar	**M142**	U17/726995	side of skid
Dome	(MWC) Poplar	**M144**	U17/730992	skid beside road
Dome	(MWC) Poplar	**M145**	U17/728989	road cutting
Dome	(MWC) Poplar	**M146**	U17/726998	road cutting
Dome	(MWC) Poplar	**M147**	U17/727998	
Dome	(MWC) Sitka	**M143**	U17/736990	bluffs
Dome	(MWC) Sitka	**M173**	U17/739991	
Dome	(MWC) Sitka	**M354**	U17/737976	hillside outcrop
Dome	(MWC) Sitka	**M355**	U17/737985	track cutting
Dome	(MWC) Sitka	**M356**	U17/733986	top of dome
Dome	(MWC) Sitka	**M357**	U17/731983	track cutting
Dome	(MWC) Sitka	**M358**	U17/728981	quarry
Dome	(MWC) Stag	**M360**	U17/741966	track cutting
Dome	(MWC) Stag	**M361**	U17/742968	boulders from bluffs
Dome	(MWC) Stag SW	**M254**	U17/729959	cutting
Dome	(MWC) View	**M137**	U17/730010	from block in gully below bluffs
Dome	(MWC) View	**M149**	U17/736020	knoll beside dome toe
Dome	(MWC) View	**M150**	U17/742015	southern road cutting
Dome	(MWC) View	**M151**	U17/736997	
Dome	(MWC) View	**M152**	U17/734002	side of new skid
Dome	(MWC) View	**M153**	U17/735011	
Dome	(MWC) View	**M167**	U17/754013	boulder from bluffs to west
Dome	(MWC) View	**M168**	U17/753016	long exposed bluff
Dome	(MWC) View	**M170**	U17/749008	
Dome	(MWC) View	**M171**	U17/741000	
Dome	(MWC) Walker	**M249**	U17/710967	cutting
Dome	(MWC) Walker	**M250**	U17/707962	road surface
Dome	(MWC) Walker	**M333**	U17/716965	skid cutting boulders
Dome	(Southern) Dairy	**M314**	U17/727900	Forest Rd cut downhill of cnr
Dome	(Southern) Dairy	**M315**	U17/729900	bluffs south of road
Dome	(Southern) Forest	**M319**	U17/730892	outcrops in flank
Dome	(Southern) Forest	**M320**	U17/725891	atop dome
Dome	(Southern) Forest South	**M317**	U17/723883	boulder atop dome
Dome	(Southern) Forest South	**M318**	U17/723883	cutting behind farmhouse
Dome	(Southern) Forest South	**M321**	U17/722887	track cutting
Dome	(Southern) Forest West	**M322**	U17/718883	track cutting atop dome
Dome	(Southern) Forest West	**M323**	U17/717881	loose boulder on top
Dome	Beehive	**M312**	U17/764964	SH1 cutting
Dome	Beehive	**M313**	U17/763963	SH1 cutting
Dome	Ben Lomond	**M325**	U17/674866	Poihipi Rd obsidian
Dome	Buried	**M467**	U17/719096	above Kakariki Rd
Dome	Buried	**M51**	U17/719097	Kakarihi Rd cut
Dome	Kakuki	**M299**	U17/830954	boulder off Orakeikorako Rd
Dome	Kakuki	**M300**	U17/831953	outcrop on dome
Dome	Lowrie	**M327**	U17/685884	Lowrie farm tarck
Dome	Lowrie	**M328**	U17/679884	Lowrie farm tarck
Dome	Mangatoetoe	**M305**	U17/810958	bluffs on dome top
Dome	Mangatoetoe	**M307**	U17/811958	knoll at top of dome
Dome	Mangatoetoe	**M308**	U17/805966	boulder at base of slope
Dome	Mangatoetoe	**M309**	U17/816974	hummock saddle north of Mangatoetoe Dome
Dome	Mangatoetoe	**M310**	U17/823962	back of arcuate structure
Dome	Mangatoetoe	**M311**	U17/823957	arcuate structure
Dome	Mangatutu	**M084**	U17/763053	outer facies
Dome	Mangatutu	**M85**	U17/763049	
Dome	Mangatutu	**M017**	U17/763050	Thorpe Rd

Dome	Mangatutu	M087	U17/760054	road
Dome	Mangatutu	M088	U17/759053	road
Dome	Mangatutu	M089	U17/757052	road
Dome	Mangatutu	M090	U17/758048	road
Dome	Mangatutu	M091	U17/757049	road
Dome	Mangatutu	M092	U17/756051	road
Dome	Maroanui	M222	U17/736950	road cutting
Dome	Maroanui	M223	U17/729945	base of skid
Dome	Maroanui	M224	U17/727942	base of skid site
Dome	Maroanui	M225	U17/727939	cutting at back of skid
Dome	Maroanui	M226	U17/729938	bluff in skid track cutting, second sample from track bed
Dome	Maroanui	M230	U17/728931	end of Jumbo Rd
Dome	Maroanui	M215	U17/736938	surface near Vodafone tower
Dome	Maroanui	M216	U17/735937	road cutting
Dome	Maroanui	M217	U17/739936	base of road
Dome	Maroanui	M218	U17/740939	surface of road
Dome	Maroanui	M219	U17/749947	slope boulder/bluff
Dome	Maroanui	M220	U17/742948	gully bottom in farm bush
Dome	Maroanui	M221	U17/743953	boulder likely from bluffs likely 40 m upslope
Dome	Maroanui South	M229	U17/720928	
Dome	Maroanui South	M231	U17/722928	road surface
Dome	Maroanui West	M042	U17/716943	Tram Rd cutting
Dome	Maroanui West	M228	U17/714941	Jumbo Rd
Dome	Maroanui West	M477	U17/715936	un-named Rd bluff
Dome	Mokai Quarry	M094	U17/727057-8	Mokai Quarry
Dome	Ngautuku NW	M077	U16/732113	Springbok Rd cutting
Dome	Ngautuku NW	M078	U16/731113	Springbok Rd bluffs
Dome	Ngautuku SE	M074	U17/739098	
Dome	Ngautuku SE	M075	U17/737098	
Dome	Ngautuku SE	M076	U17/736097	
Dome	Ngautuku SE	M096	U17/741088	skid by Lake
Dome	Ngautuku SE	M097	U17/744090	road cut by Lake
Dome	Orakeikorako	M301	U17/838967	base of slope inside gate
Dome	Orakeikorako	M302	U17/841968	Hill Rd corner atop dome
Dome	Oruanui	M316	U17/723878	cutting above house
Dome	Oruanui	M324	U17/724876	west side outcrop
Dome	Pakuri	M304	U17/803951	cutting just below scoria
Dome	Pakuri	M305	U17/808953	top of dome
Dome	Pohaturoa	M114	U17/731067	boulder behind skid
Dome	Puhaturoa	M419	U17/729068	block at base of sth bluffs
Dome	Pukeahua East	M011	U17/741035	summit
Dome	Pukeahua East	M082	U17/732042	bluffs N side
Dome	Pukeahua East	M110	U17/746038	e'nd of low road
Dome	Pukeahua east arc	M106	U17/738029	moat south of Pukeahua East Dome
Dome	Pukeahua east arc	M107	U17/739029	moat south of Pukeahua East Dome
Dome	Pukeahua eastern arc	M083	U17/751039	
Dome	Pukeahua South	M010	U17/735024	
Dome	Pukeahua South	M103	U17/738024	road cut
Dome	Pukeahua South	M104	U17/732025	road cut
Dome	Pukeahua South	M105	U17/731028	road cut
Dome	Pukeahua West	M111	U17/717023	lower southern dome
Dome	Pukeahua West	M115	U17/722048	northern bluffs
Dome	Pukeakua East	M108	U17/743084	access road to summit
Dome	Pukeakua East	M109	U17/745033	low road
Dome	Puketarata	M479	U17/764903	north end above track
Dome	Puketarata	M480	U17/759901	boulder at base of SSW side
Dome	Thorpe 1	M098	U17/756053	Thorpe Rd by Mangatutu
Dome	Thorpe 1	M099	U17/753052	Thorpe Rd by Mangatutu
Dome	Thorpe 2	M093	U17/739060	carapace
Dome	Tuahu	M183	U17/770015	road cutting
Dome	Tuahu carapace	M030		SH1
Dome	Tuahu carapace	M031		SH1
Dome	Tuahu carapace?	M187	U17/772015	east SH1 cutting
Dome	Tuahu Central	M191	U17/774009	base of road

Dome	Tuahu Central	M192	U17/773010	cutting in road
Dome	Tuahu North	M066	U17/774013	
Dome	Tuahu North	M195	U17/779019	boulder in skid road below bluffs
Dome	Tuahu South	M190	U17/778010	base of track to pylon
Dome	Tutukau	M283	U17/808938	south side
Dome	Tutukau	M284	U17/809938	east of M283
Dome	Tutukau	M285	U17/811936	ridge touching Orakonui bluffs
Dome	Tutukau	M286	U17/811936	boulder below M285
Dome	Tutukau	M287	U17/811938	short hill N of M285/6
Dome	Waipakipaki	M282	U17/759931	marginal dome breccia?
Dome	Waipakipaki	M34	U17/760933	
Dome	Waipakipaki?	M281	U17/772937	Tutukau Rd corner cutting
Dome	Whakapapa	M297	U17/833939	top of dome
Dome	Whakapapa	M298	U17/834939	top of dome
Dome	Whakapapataringa	M288	U17/852933	outcrop below tower
Dome	Whakapapataringa	M289	U17/853932	road cut
Dome	Whakapapataringa	M290	U17/854933	road cutting
Dome	Whakapapataringa West	M296	U17/846934	ridge crest
Dome	Whakapapataringa West	M295	U17/846934	ridge crest
Other	Atiamuri 'Crater' view	M086	U17/761036	road end
Other	Fluvial sequence	M268	U17/781051	
Other	Kaingaroa Ignimbrite	M410	U17/866024	cnr Coates & Tutukau Rds
Other	Kaingaroa Ignimbrite	M411	U17/880062	Puaiti Rd cutting
Other	Korotai access skid site	M415	T17/687079	look/access Korotai bluffs
Other	Lacustrine sediments	M060	U17/719059	
Other	Lacustrine sediments	M065	U17/792024	
Other	Loess and fluvially reworked	M019	U17/784923	Tram Rd around Tutukau Forest access Rd
Other	Parekauau dacite	M279	U17/868941	Tutukau Rd near Waikato River
Other	Reworked material	M003	T17/688075	Cutting on RHS skid site with view of Putauaki
Other	Reworked material	M118	U17/703044	massive sandy deposit
Other	Reworked material	M124	T17/698026	Pukeahua western fan
Other	Reworked material	M431	U17/789018	cutting at back of skid
Other	Reworked material	M95	U16/722101	SH1 north of river
Other	Taupo ash	M294	U17/849940	farm
Pclast	Airfall	M038	U17/735023	south side of Tatua Rd
Pclast	Airfall	M055	?	on Taranui Rd, N of Kiwi
Pclast	Airfall	M056	U17/770066	on Ohakuri Rd
Pclast	Airfall	M072	U17/741094	skid site at end of road, Springbok Hill
Pclast	Airfall	M166	U17/756017	
Pclast	Airfall	M444	U17/743096	atop Ngautuku E Dome
Pclast	Airfall	M446	U17/727097	atop Ngautuku W Dome
Pclast	Airfall	M450	U17/788010	base of Atiamuri?
Pclast	Airfall below Atiamuri lg	M405	U17/772042	below type bluffs
Pclast	Airfall beside Ohakuri lg.	M068	U17/786046	Mawsons Rd
Pclast	Airfall sequence above paleosol beneath Okaia	M079	U17/732052	
Pclast	Airfall sequence to base of Rotoehu over thick paleosol	M269	U17/773061	back of skid
Pclast	Airfall sequence with possible interbedded flows	M117	U17/702044	top of plateau north of Pukeahua West Dome
Pclast	Airfall to base of Okaia	M445	U17/741095	el. 519 m
Pclast	Airfall to base of Rotoehu	M073	U17/742098	cutting at entrance to skid
Pclast	Airfall west of Maroanui West	M233	U17/716943	above M42 (dips to west)
Pclast	Atiamuri	M101	U17/763031	
Pclast	Atiamuri	M451	U17/785012	track cutting E of Tuahu Dome
Pclast	Atiamuri	M452	U17/785015	back of skid E of Tuahu Dome
Pclast	Atiamuri lg welded top	M404	U17/772044	old Lloyd type section bluffs
Pclast	Atiamuri lg welded top	M406	U17/769034	below skid W of SH1
Pclast	Atiamuri lg welded top	M407	U17/768035	above skid W of SH1
Pclast	Atiamuri Ignimbrite	M012	U17/772035	type section. Terraced SH1 cutting
Pclast	Atiamuri Ignimbrite	M013	U17/787025 to U17/784030	two outcrops, one on Olive Rd, and one in bluffs off Olive Rd
Pclast	Atiamuri Ignimbrite	M014	U17/792028	Olive Rd cutting
Pclast	Atiamuri Ignimbrite	M058	U17/792019	Thorpe Rd

Pclast	Atiamuri Ignimbrite	M185	U17/769022	unwelded
Pclast	Atiamuri Ignimbrite	M186	U17/770021	unwelded
Pclast	Atiamuri Ignimbrite	M271	U17/777025	road corner cutting
Pclast	Atiamuri Ignimbrite	M416	U17/771020	at end of logging Rd
Pclast	Atiamuri Ignimbrite	M417	U17/770029	Tatua Rd inside gate off SH1
Pclast	Atiamuri Ignimbrite	M418	U17/765033	inside corner of Rd
Pclast	Atiamuri Ignimbrite	M422	U17/773044	below welded top
Pclast	Atiamuri Ignimbrite	M423	U17/773043	type section upper bluffs
Pclast	Atiamuri Ignimbrite	M430	U17/773042	type bluffs south facing
Pclast	Atiamuri Ignimbrite	M432	U17/788014	bottom 1m of skid cutting
Pclast	Atiamuri Ignimbrite + airfall	M270	U17/776023	back of skid site
Pclast	Atiamuri Ignimbrite + airfall	M272	U17/772028	SH1 cutting. Includes basal paleosol
Pclast	Atiamuri Ignimbrite + lenticulite	M339	U17/795024-U17/798024	high forestry road cut
Pclast	Atiamuri welded + overlying	M182	U17/765023	road cutting
Pclast	BAF off Mandarin Dome	M059	U17/791012	Thorpe Rd
Pclast	BAF off Walker Dome	M253	U17/706984	road cutting north of Walker Dome
Pclast	Korotai	M004	T17/696096	in Owens Rd
Pclast	Korotai	M005	T17/697098	cutting in north side of skid site at end of Owens Rd
Pclast	Korotai	M176	T17/696095	
Pclast	Korotai	M473	T17/	between welded zones
Pclast	Korotai	M48	T17/695087	Owens Rd
Pclast	Korotai (non-welded)	M414	T17/688078	above lenticulte in elevation
Pclast	Korotai lenticulite	M001	T17/689091	E of Korotai Rd
Pclast	Korotai lenticulite	M002	T17/688084 T17/689083-4	E of Korotai Rd
Pclast	Korotai lenticulite	M413	T17/687075	off edge of Korotai w ridge
Pclast	Korotai lenticulite boulder	M175	T17/695087	in culvert cutting with PABU above
Pclast	Korotai?	M070		
Pclast	Korotia lenticulite	M53	U17/701092	Weka Rd
Pclast	Kototai lenticulite	M470	?	bluffs below Pakaha Rd
Pclast	Kototal lenticulite	M471	?	bluffs below Pakaha Rd
Pclast	Kototal lenticulite	M472	?	above Korotai Rd
Pclast	Mamaku	M448	U16/714156	Tar Hill
Pclast	Mokai	M007	T17/638035 - T17/634040	Okama Stream TYPE SECTION
Pclast	Mokai	M420	T17/671043	Tirohanga Rd cutting
Pclast	Mokai	M421	T17/664000	road cutting, near hill crest
Pclast	Mokai	M427	T17/676036	boulder below stream bluffs
Pclast	Mokai	M428	T17/635993	Tirohanga Rd, near school
Pclast	Mokai	M429	T17/621990	Pokuru Rd cutting
Pclast	Ohakuri	M015	U17/779039	bluffs south of Thorpe Rd
Pclast	Ohakuri	M016	U17791052	west of Mawsons Rd
Pclast	Ohakuri	M057	U17/772041	back of Skid
Pclast	Ohakuri	M069		
Pclast	Ohakuri	M449	U16/713157	base over vapour phase altered unit
Pclast	Ohakuri	M462	U17/837984	track cutting below MEC ridge
Pclast	Ohakuri	M482	U17/791053	bluffs beside Mawsons Rd
Pclast	Ohakuri	M067	U17/735083	skid site
Pclast	Ohakuri	M267	U17/780046	road cutting
Pclast	Ohakuri	M408	T17/692087	skid track cutting in Korotai area
Pclast	Ohakuri or reworked	M442	U17/842001	Lake Ohakuri (kayaked)
Pclast	Ohakuri?	M049	T17/696086	cutting north side of road off Owens Rd
Pclast	Ohakuri?	M050	T17/680083	Pakaha Rd
Pclast	Ohakuri?	M054	U17/703092	off Weka Rd
Pclast	Ohakuri?	M071	T17/690087	
Pclast	Ohakuri?	M177	T16/697115	Kereru Rd
Pclast	Ohakuri?	M337	U17/800032	boulders in Orange Rd
Pclast	Ohakuri?	M338	U17/795027	bluffs
Pclast	Ohakuri?	M340	U17/814027	Pouapu Rd
Pclast	Ohakuri?	M400	U17/773063	skid off Ohakuri Rd
Pclast	Ohakuri?	M401	U17/745099	beside Ngautuku Dome
Pclast	Ohakuri?	M402	U17/743089	beside Ngautuku Dome
Pclast	Ohakuri?	M403	U17/736081	near Ngautuku Dome??

Pclast	Ohakuri?	M412	T17/686075	Korotai area
Pclast	Ohakuri?	M468	T17/685082	road cutting below Kor ridge
Pclast	Ohakuri?	M469	T17/692075	new skid Pakaha Rd
Pclast	Ohakuri? lg. (Whak. Lithic)	M409	T17/691087	atop Korotai ridge
Pclast	Ongarahu ignimbrite	M336	U17/706008	Ongarahu stream
Pclast	orakonui	M275	U17/775896	gully track back of dairy farm SW of Tram Rd
Pclast	Orakonui	M026	U17/809933	road on Ron Clark's farm
Pclast	Orakonui	M027	U17/831939	Mouth of type gully, lower sheet?
Pclast	Orakonui	M047	U17/832925	Upper cutting on Whakapapa Rd
Pclast	Orakonui	M276	U17/788907	Tram Rd cutting
Pclast	Orakonui	M277	U17/832937	cutting both sides of Whakapapa Rd
Pclast	Orakonui	M278	U17/838929	Whakapapa Rd cutting
Pclast	Orakonui	M280	U17/839926	curved Whakapapa Rd cutting
Pclast	Orakonui	M433	U17/787920	high slope east of Tram Rd
Pclast	Orakonui	M434	U17/788920	high slope east of Tram Rd
Pclast	Orakonui	M435	U17/788922	high slope east of Tram Rd
Pclast	Orakonui	M436	U17/791922	shallow valley wall
Pclast	Orakonui	M437	U17/793937	nose SE of Tram Tutukau x
Pclast	Orakonui	M438	U17/793937	high slope east of Tram Rd
Pclast	Orakonui	M439	U17/791936	bluffs south of Tutukau Rd
Pclast	Orakonui	M440	U17/793934	east facing slope
Pclast	Orakonui	M441	U17/791930	cow race cutting
Pclast	Orakonui	M453	U17/791928	cow race cutting
Pclast	Orakonui	M454	U17/793928	case hardened
Pclast	Orakonui	M455	U17/796928	cliffs near cow shed
Pclast	Orakonui	M456	U17/799927	case hardened
Pclast	Orakonui	M457	U17/800928	
Pclast	Orakonui	M458	U17/802930	bluffs S of Tutukau Rd
Pclast	Orakonui	M459	U17804932	bluffs S of Tutukau Rd
Pclast	Orakonui	M463	U17/821934	bluffs W of tree farm
Pclast	Orakonui	M464	U17/825933	
Pclast	Orakonui	M465	U17/826932	
Pclast	Orakonui	M466	U17/829930	case hardened
Pclast	Oruanui	M273	U17/784918	Tram Rd cutting
Pclast	Oruanui & Roto Tephra	M443	?	south of Oruanui Rd new skid
Pclast	Oruanui unit 8 or 9	M040	T17/693991	
Pclast	Oruanui units 1 to 6	M037		
Pclast	Pokai	M447	U16/714155	under VPA unit Tar Hill
Pclast	Pokai and cream ignimbrites + lentiCulite	M006	~U16/736164	corner of Bob and Len Rds
Pclast	Pokai?	M052	U16/706103	bluffs above Taiko Rd
Pclast	Pukeahua fan NE	M022	U17/766057	SH1 cuts
Pclast	Pukeahua fan NE	M023	U17/766056	SH1 tiered cutting
Pclast	Pukeahua fan NE	M024	U17/766056	SH1 cut
Pclast	Pukeahua fan NE	M081	U17/735055	Conifer Rd
Pclast	Pukeahua fan NW	M061		
Pclast	Pukeahua fan NW	M113	T17/695042	
Pclast	Pukeahua fan NW	M116	U17/707044	road cut
Pclast	Pukeahua fan NW	M119	U17/704043	
Pclast	Pukeahua fan NW	M120	U17/706044	and possible airfall
Pclast	Pukeahua fan NW	M121	T17/696036-7	~100m long
Pclast	Pukeahua fan NW	M122	T17/697034	road cutting
Pclast	Pukeahua fan NW	M123	T17/697029	
Pclast	Pukeahua fan SE	M100	U17/751030	Skid site, closest access to arcuate structure
Pclast	Pukeahua fan SE	M154	U17/751022	Tatua Rd cutting
Pclast	Pukeahua fan SW	M063	U17/728021	Tatua Rd
Pclast	Pukeahua fan SW	M064	U17/722016	Tatua Rd type section. Layered PABU and Tephra
Pclast	Pukeahua fan SW	M125	U17/711018	
Pclast	Pukeahua fan SW	M126	U17/712017	face at back of skid below M125
Pclast	Pukeahua fan SW	M127	U17/714016	back of Skid
Pclast	Pukeahua fan SW	M128	U17/719018	west cutting of road
Pclast	Pukeahua fan SW	M129	U17/726019	skid south of road, with clay layer

Pclast	Pukeahua fan SW	**M130**	U17/713015	dirty outcrop
Pclast	Pukeahua fan SW	**M131**	U17/712014	
Pclast	Pukeahua fan SW	**M132**	U17/729021	Tatua Rd south cutting
Pclast	Pukeahua fan SW	**M133**	U17/727020	outcrop in south cutting.
Pclast	Pukeahua fan SW	**M134**	U17/731015	back of skid above end of Rosewood Rd
Pclast	Pukeahua fan SW	**M135**	U17/730015	lower elevation than M134
Pclast	Pukeahua fan SW	**M136**	U17/725004	
Pclast	Pukeahua fan SW	**M138**	U17/717006	road cut
Pclast	Pukeahua fan SW	**M148**	U17/724999	return with ladder, airfall interbedded with flows
Pclast	Pukeahua fan SW	**M476**	U17/711017	SW of Puk W D in road cut
Pclast	Pukehua fan SW airfall	**M062**	T17/699037	road cutting
Pclast	Puketarata Tuff Ring	**M478**	U17/765901	track cutting SE side
Pclast	Puketarata Tuff Ring	**M481**	U17/759901	track cutting SW side
Pclast	Putauaki	**M021**	U17/786929	Tram Rd corner cutting - debris flow at top
Pclast	Putauaki	**M033**	U17/752922	off end of airstrip, proximal
Pclast	Putauaki	**M035**	U17/764928	medial airstrip access Rd
Pclast	Putauaki	**M036**	U17/766934	medial airstrip
Pclast	Putauaki	**M046**	U17/782930	north side of CHH road cut
Pclast	Putauaki	**M045**	U17/785927	high Tram Rd cuts, overlain by lacustrine and debris flow
Pclast	regional airfall sequence	**M043**	U17/861989	Te Kopia Rd
Pclast	Taupo Ignimbrite	**M018**	U17/767050	SH1
Pclast	Taupo Pumice	**M025**		cut beside SH1
Pclast	Tram Rd	**M044**	U17/782912	cuts in west and east sides of tram Rd (was U17/783913)
Pclast	Tram Rd	**M274**	U17/783909	roadside cutting
Pclast	Unknown BAF over airfall	**M258**	U17/785965	culvert cutting
Pclast	Unknown lg north of Pukeahua	**M080**	U17/733052	Conifer Rd
Pclast	Unknown, above Maroanui W	**M041**	U17/720945	southwest Tram Rd, south side
Pclast	Unknown, above Maroanui W	**M227**	U17/721940	skid cut at back of hill. Same as M41?
Pclast	Unknown, off Poplar Dome	**M252**	U17/710984	too far to be carapace
	Bedded deposits (tephra?)	**M169**	U17/755023	Tatua Rd cutting opposite Sandalwood turn

APPENDIX 2

Ar-Ar age dating

2.1 Methodology

Standard Ar-Ar analytical techniques were used, as explained by McDougall and Harrison (1999). The K-Ar age dating theory that the Ar-Ar technique is based on is clearly explained by Dalrymple and Lanphere (1969) and decay constants used have been revised by Steiger and Jaeger (1977).

2.1.1 Sample preparation

Samples were crushed and then sized by sieving to remove particles significantly larger or smaller than the modal plagioclase crystal short axis. Where coarse enough, plagioclase phenocrysts were hand picked. For samples with feldspar too fine to hand pick, felsic minerals were separated from glass and mafic minerals using the Sodium Polytungstate and washed repeatedly in deionised water. Two batches of experiments were run, the first in 2001 and the second in 2002. For the second batch of experiments the density separates were refined further than the first batch using a Frantz Barrier Separator to remove quartz. All separates were immersed in 5 to 40 vol. % hydrofluoric acid in a warm ultrasonic bath for 1 to 10 minutes (as required) to remove adhering glass. For the second batch only an ultrasonic probe was used to more intensely agitate clasts and remove any glass remaining after having used the ultrasonic bath.

2.1.2 Laboratory procedures

The purified plagioclase separates were wrapped in pure copper foil, encapsulated in quartz tubing and irradiated in the central thimble of the USGS TRIGA reactor in Denver, Colorado. Batch one (IRR177 and IRR178) was irradiated for 2 hours, whereas batch two (IRR187) was irradiated for 1.5 hours. The *J* neutron-flux parameter (which quantifies the exact amount of irradiation received) for each sample packet was determined from Taylor Creek sanidine (TCR-2) monitors bracketing the unknowns at four points along the irradiation tube placed 2 – 8 mm above the peak of the neutron flux. TCR-2 sanidine is a secondary mineral standard calibrated at 27.87 Ma against the primary standard, SB-3 biotite, a 162.9±0.9 Ma mineral whose age was determined using first-principles calibrations (Lanphere and Dalrymple, 2000). Monitors were run

using the continuous argon-ion laser system attached to the MAP 216 mass spectrometer (Dalrymple, 1989) and the calculated *J* at each monitor location was then graphed against height in the sample tube. A second-order polynomial fit of flux monitor data was applied to the height of each sample packet to determine its individual *J* value.

The irradiated plagioclase separates were step heated using a low-blank resistance furnace with a molybdenum crucible controlled by an infrared pyrometer. Reactive gases were removed by two SAES AP-10 getters, and argon isotopes were measured with the MAP spectrometer. Measured ratios were corrected for instrumental blanks, mass discrimination, abundance sensitivity, decay and reactor-derived interfering isotopes. Plateau ages are reported for samples with > 50 % of the ^{39}Ar released for which samples are within error at the 95% confidence level and atmospheric intercepts are within 1 σ of the present-day atmospheric concentration. For samples that don't meet these criteria, isochron ages are reported, with statistics calculated using the methods of York (1969). The Isoplot package (Ludwig, 1999) was used to calculate these statistics.

2.2 Ar-Ar results

The following sub-sections present the plateau and isochron diagram for each samples analysed by the Ar-Ar method. Both diagrams were plotted using Isoplot with extra data added from USGS proprietary

Appendix 2.2.1 - Ar-Ar data for D40, Ohakuri pyroclastics

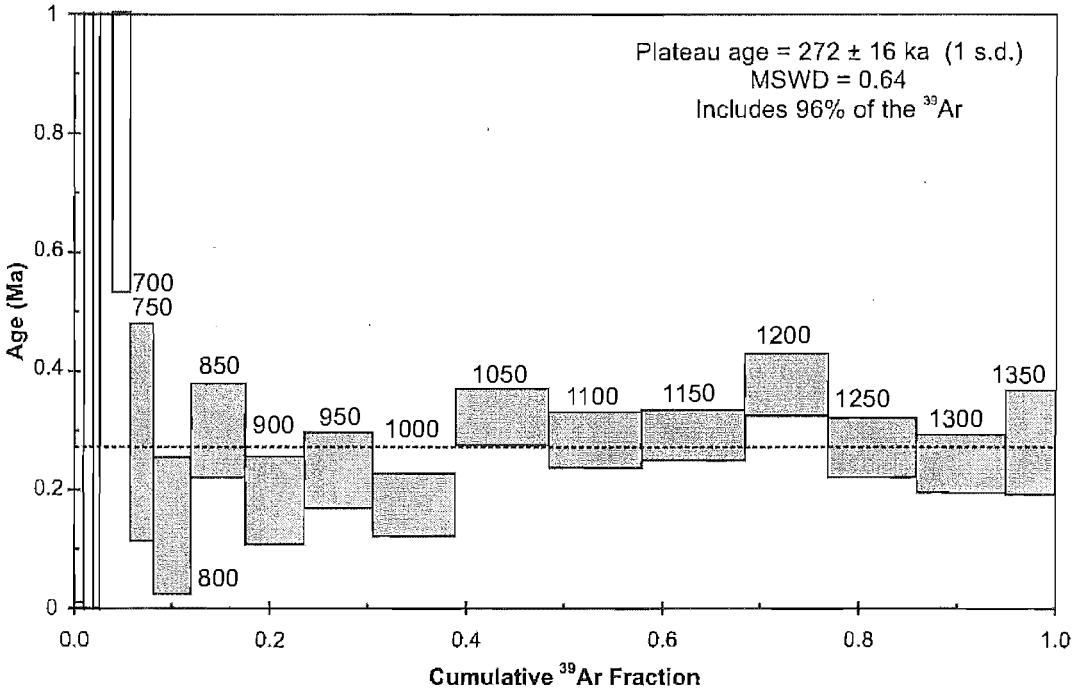

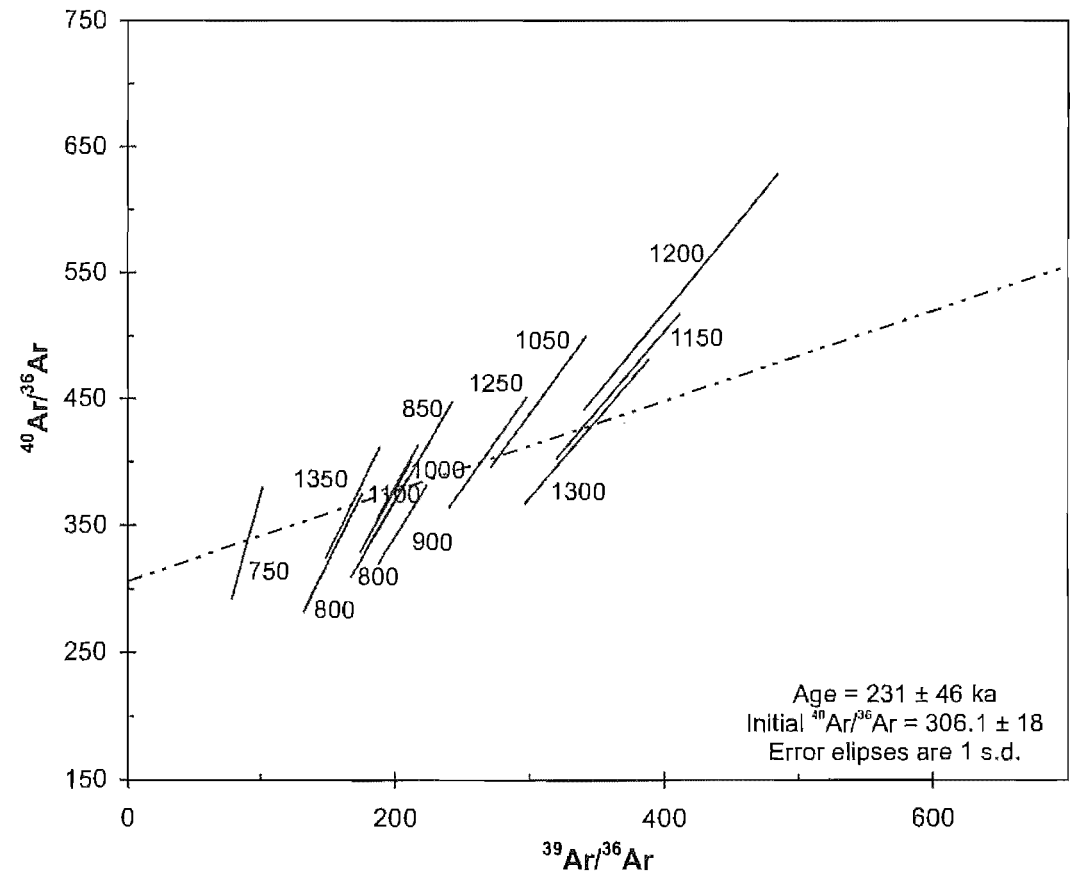

(Above) Plateau diagram showing heating steps used (filled boxes) in the WPMA (dashed line). **(Below)** Inverse isochron plot showing error elipses for heating steps used in calculating the isochron age. Details of the methodology are given in Appendix 3.1. Step temperatures are given in °C.

Appendix 2.2.2 - Ar-Ar data for D64, Ohakuri pyroclastics

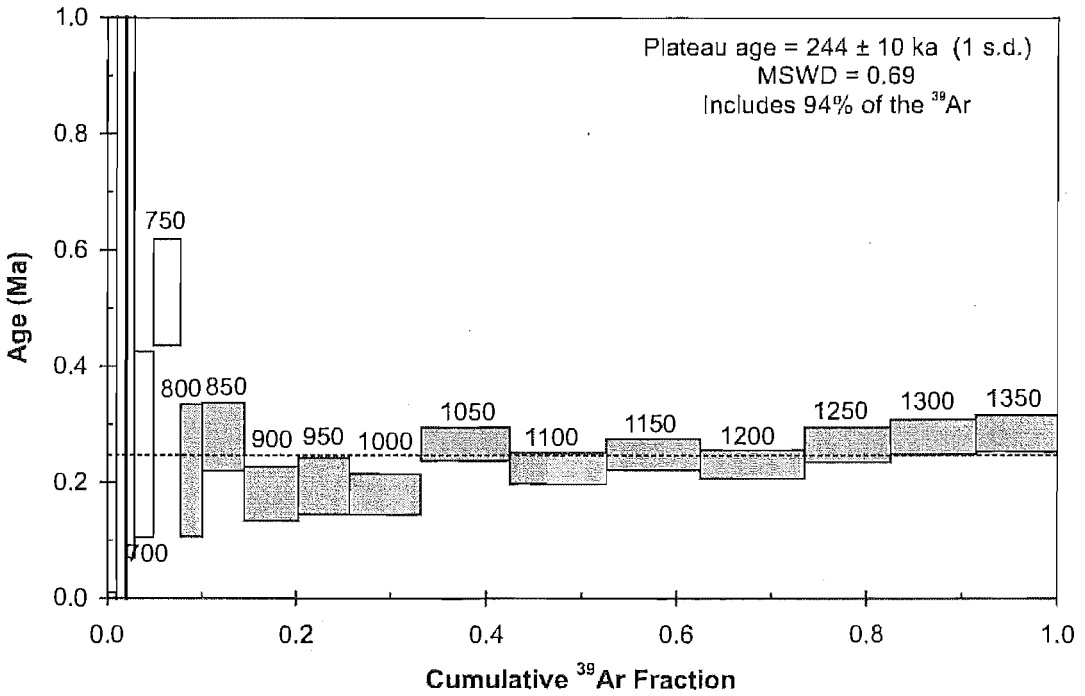

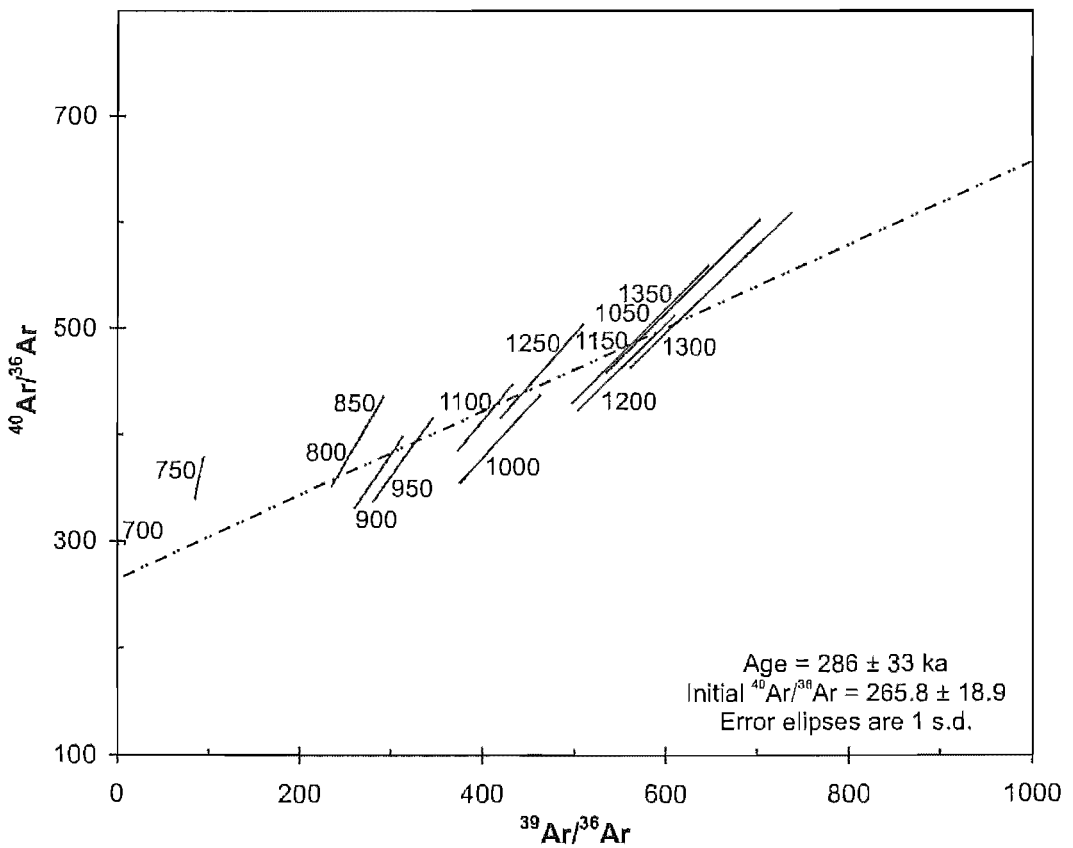

Appendix 2.2.3 - Ar-Ar data for M12, Atiamuri pyroclastics

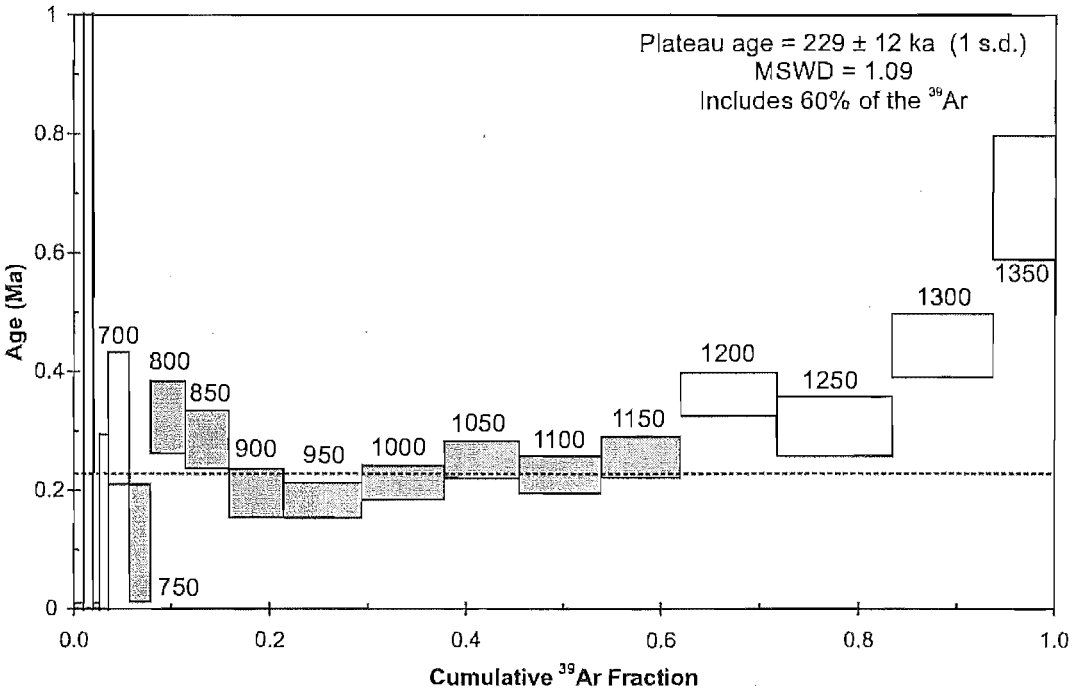

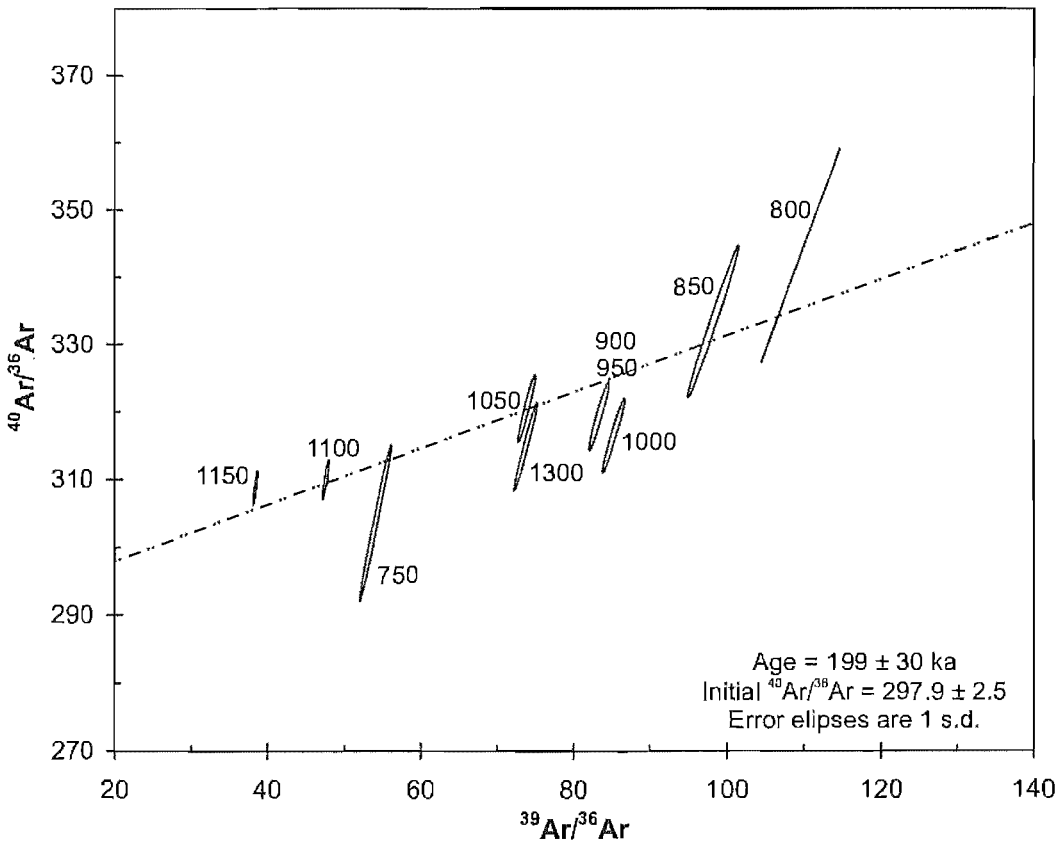

Appendix 2.2.4 - Ar-Ar data for M46, Putauaki pyroclastics

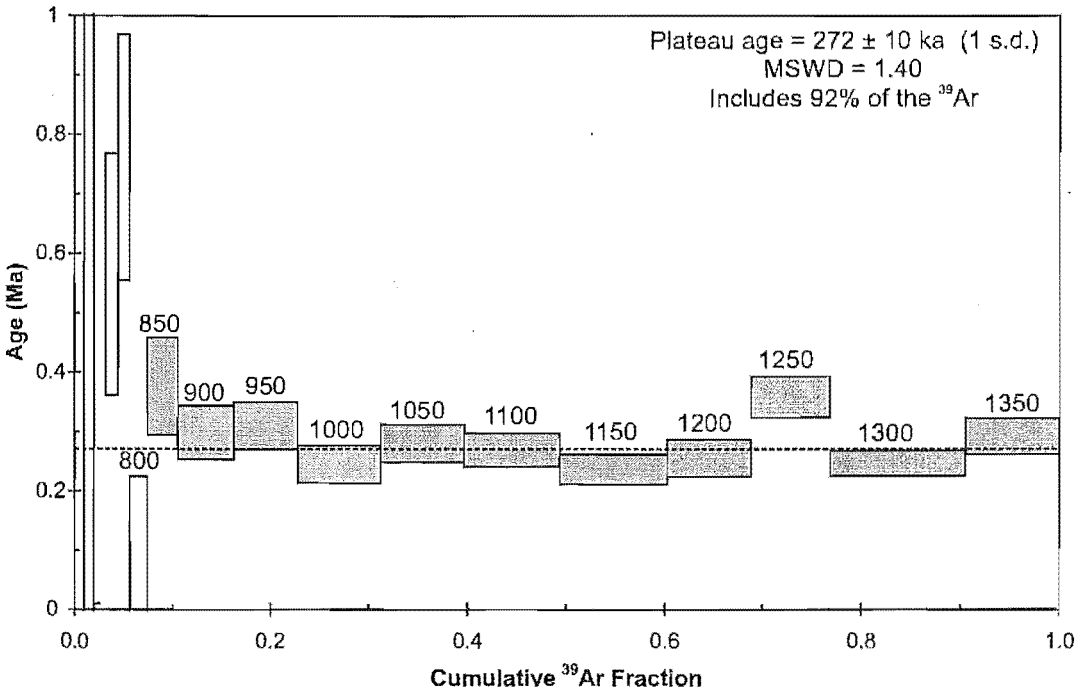

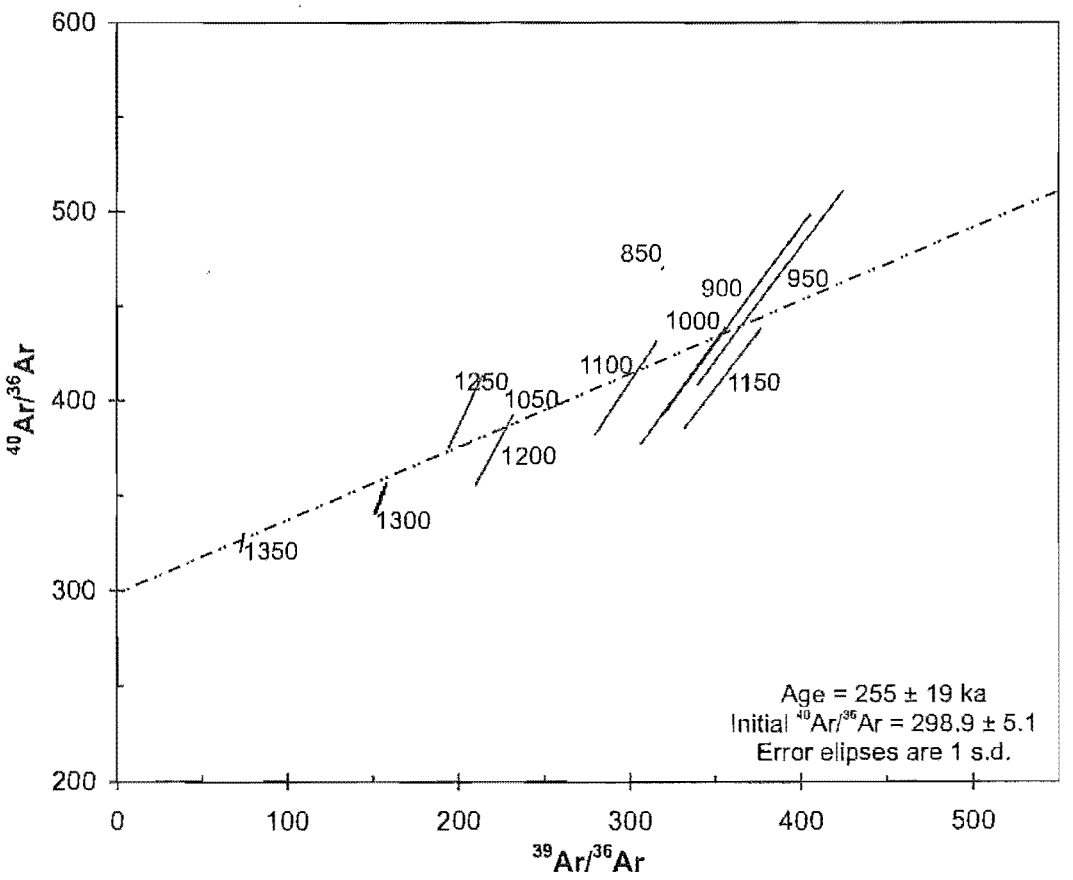

Appendix 2.2.5 - Ar-Ar data for M47, Orakonui pyroclastics

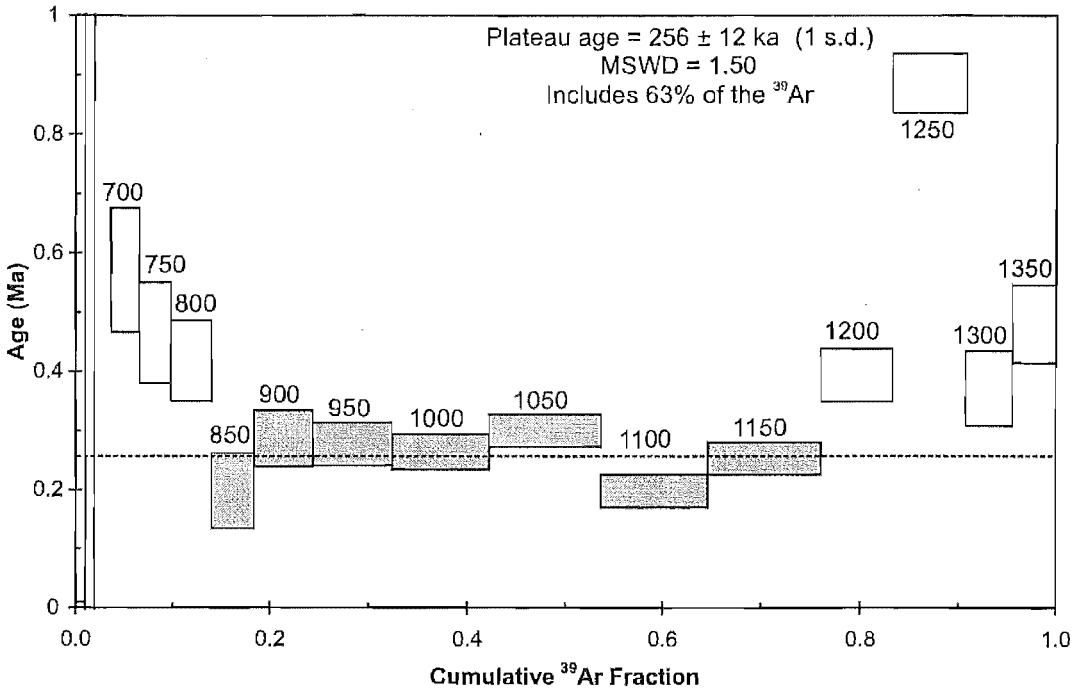

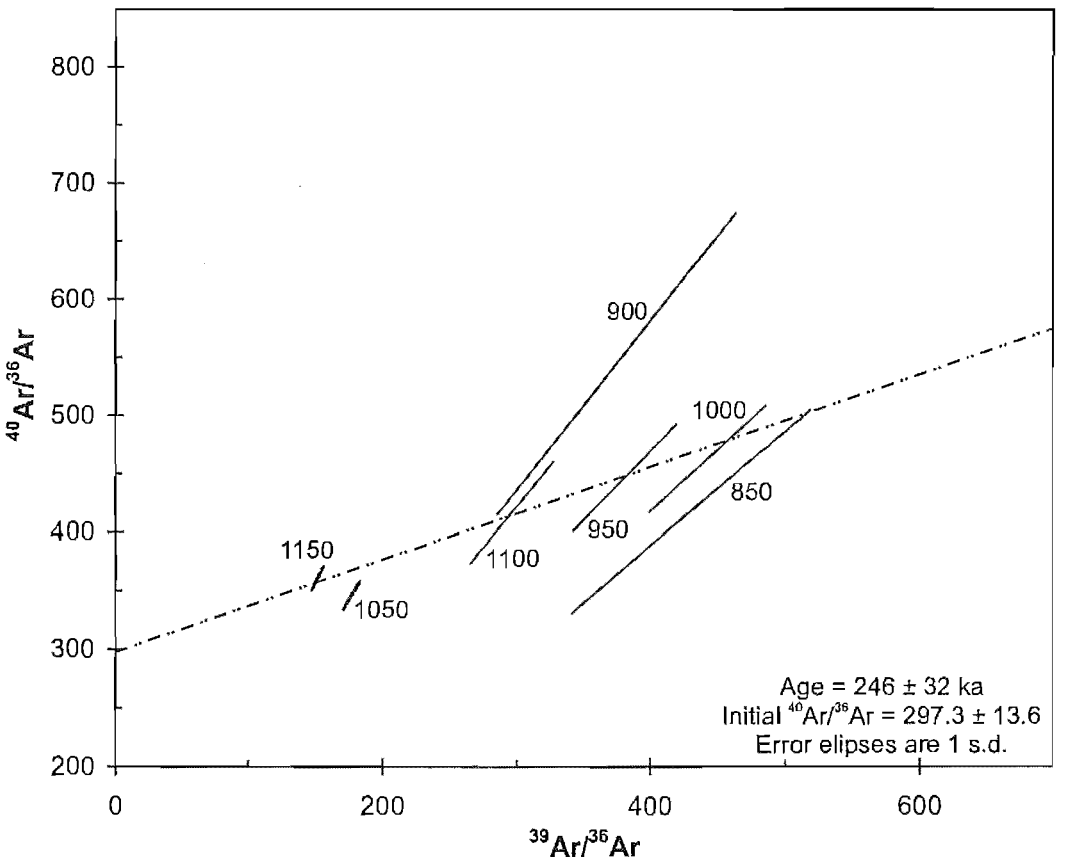

Appendix 2.2.6 - Ar-Ar data for M63, Pukeahua western pyroclastics fan

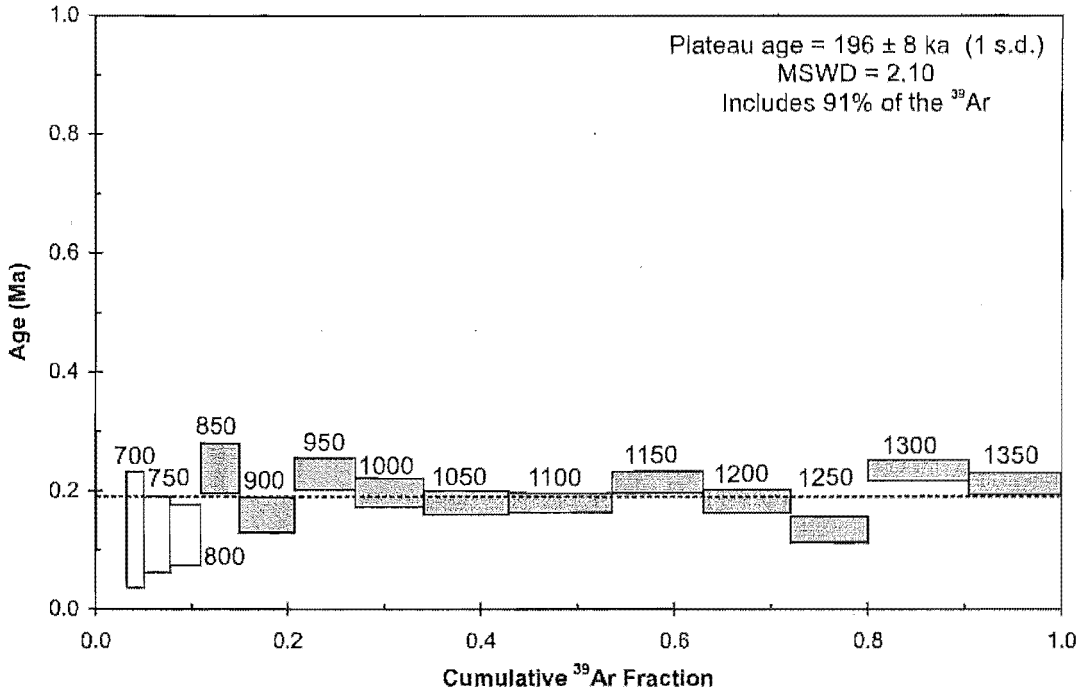

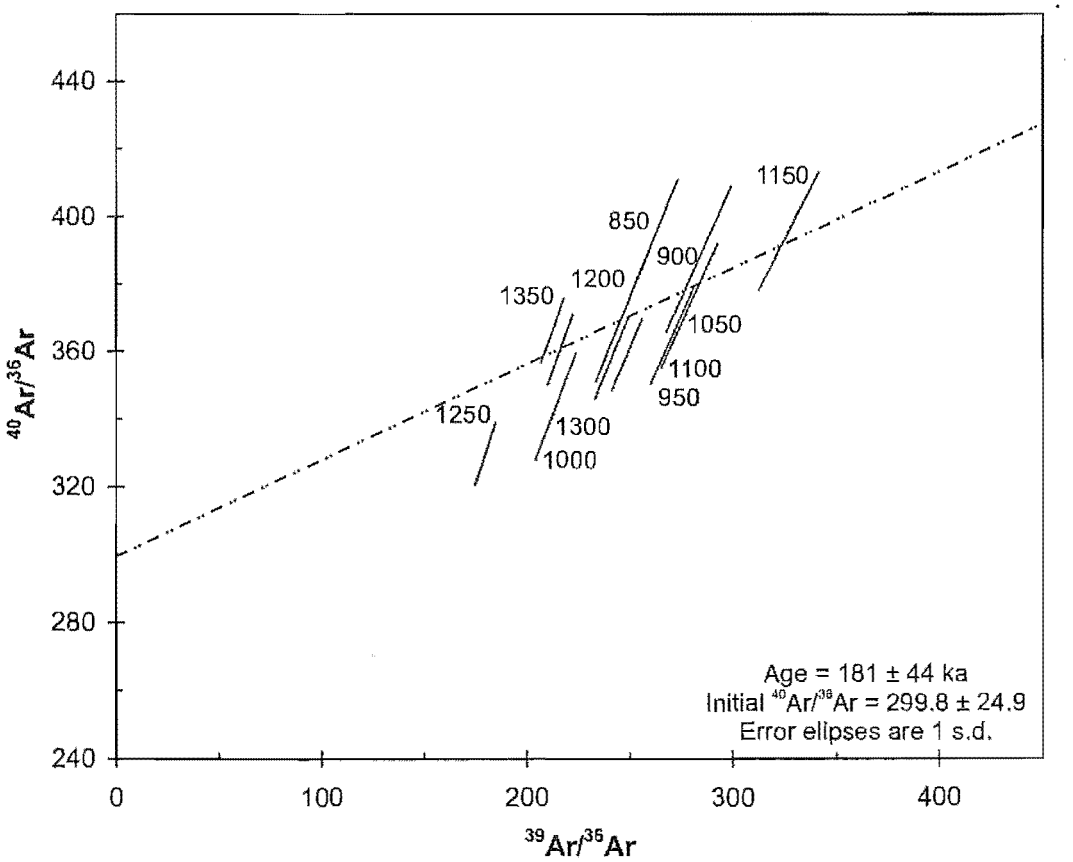

Appendix 2.2.7 - Ar-Ar data for M111, Pukeahua West Dome

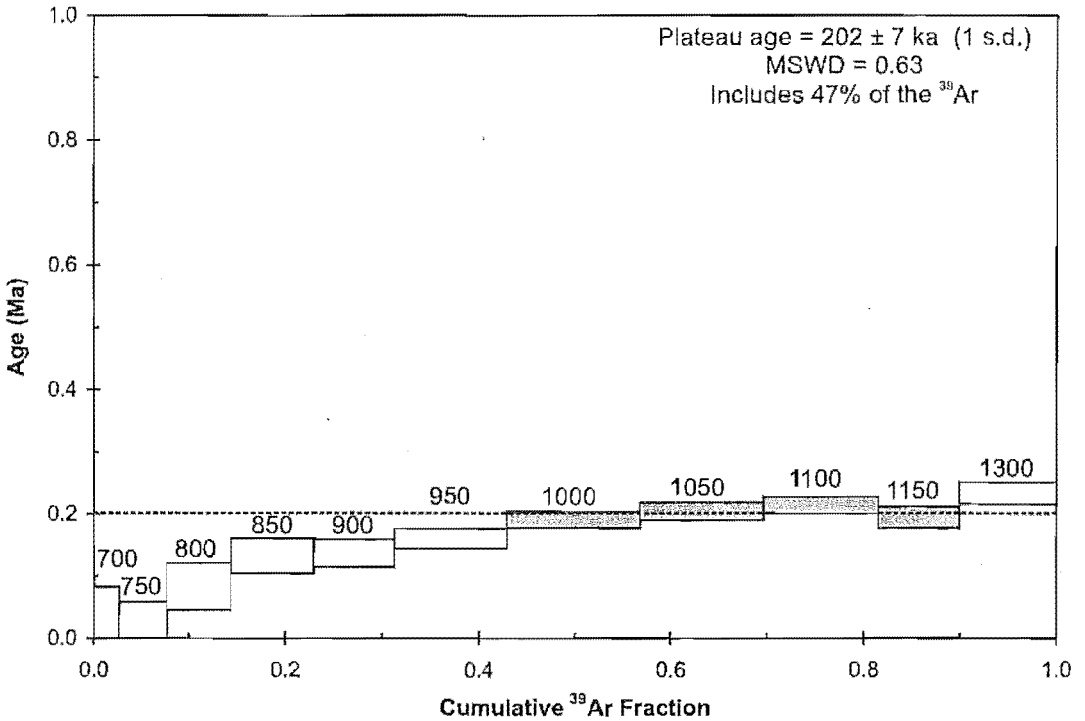

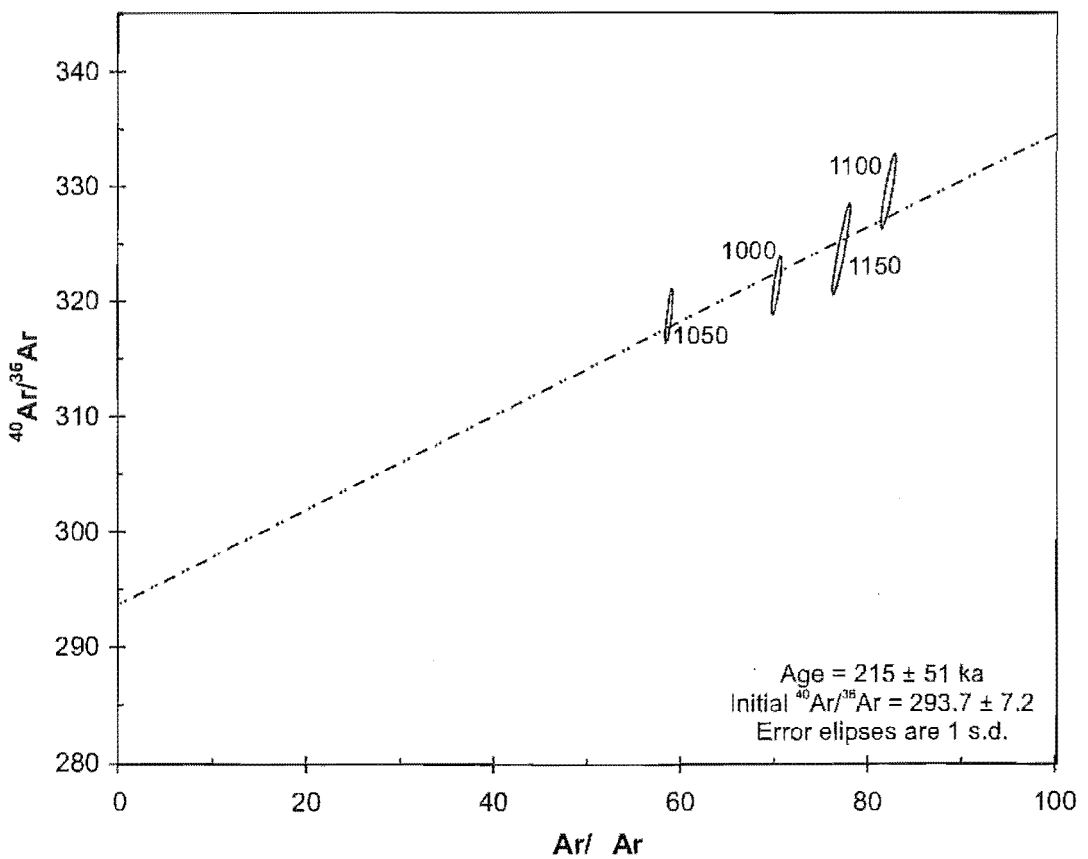

Appendix 2.2.8 - Ar-Ar data for M145, Poplar Dome (MWC)

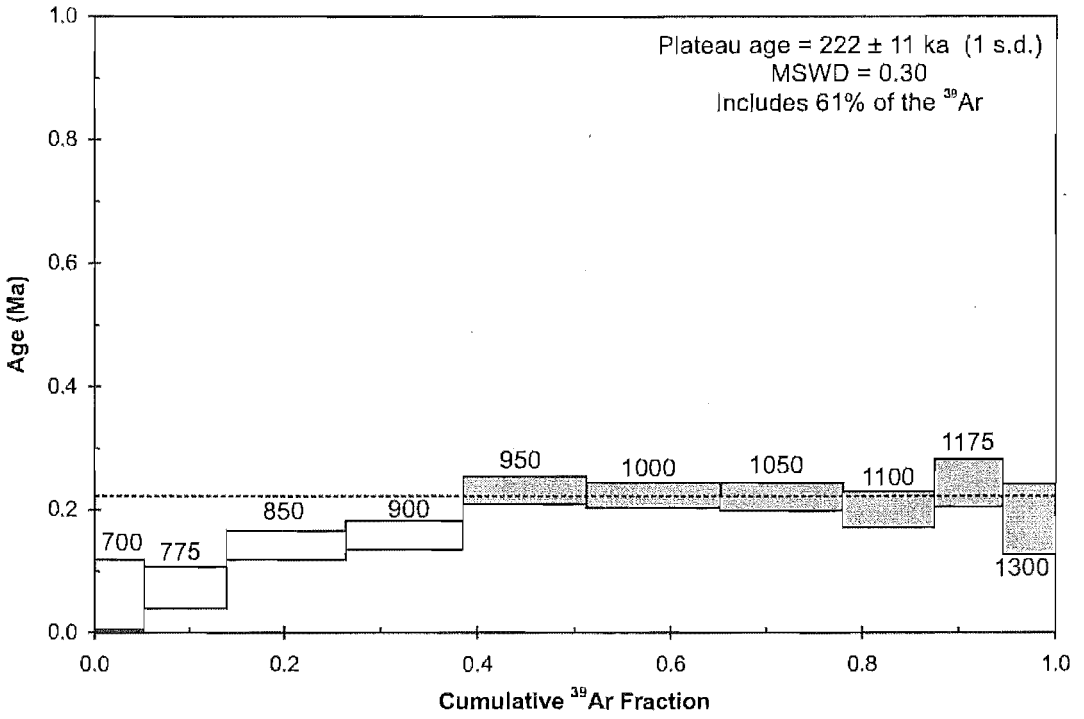

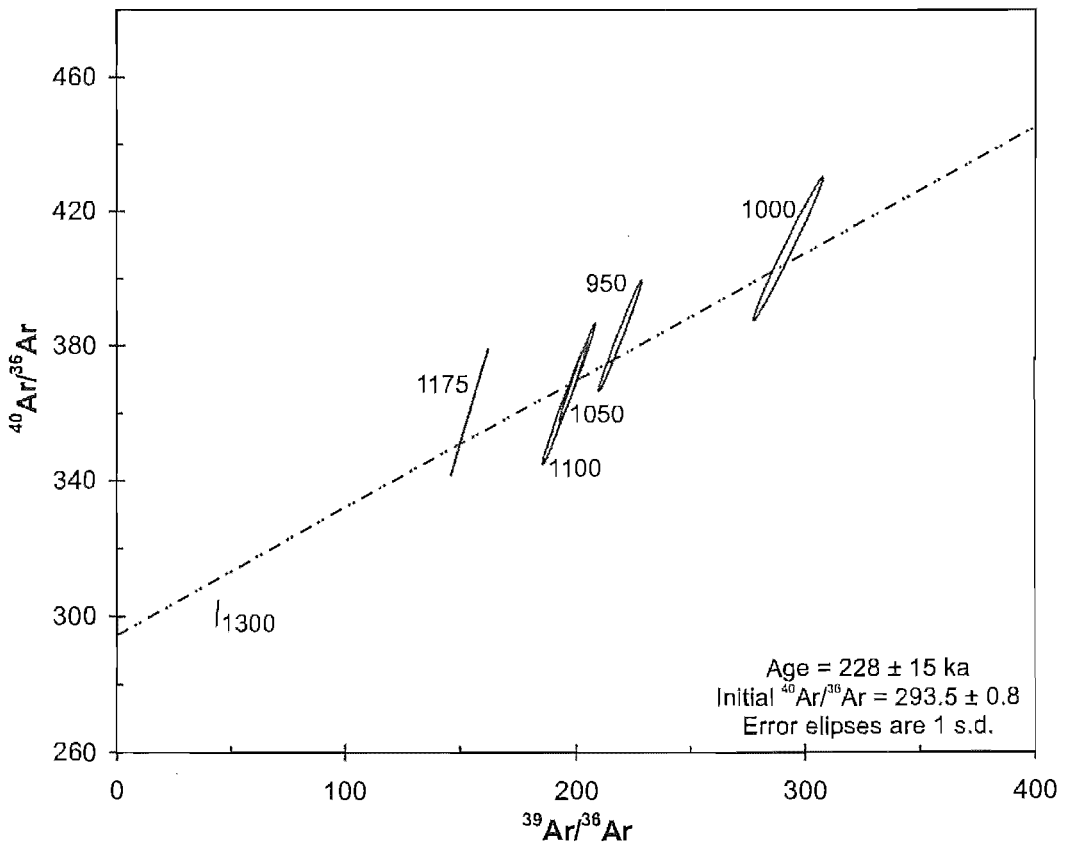

Appendix 2.2.9 - Ar-Ar data for M188, Kemp Dome (MWC)

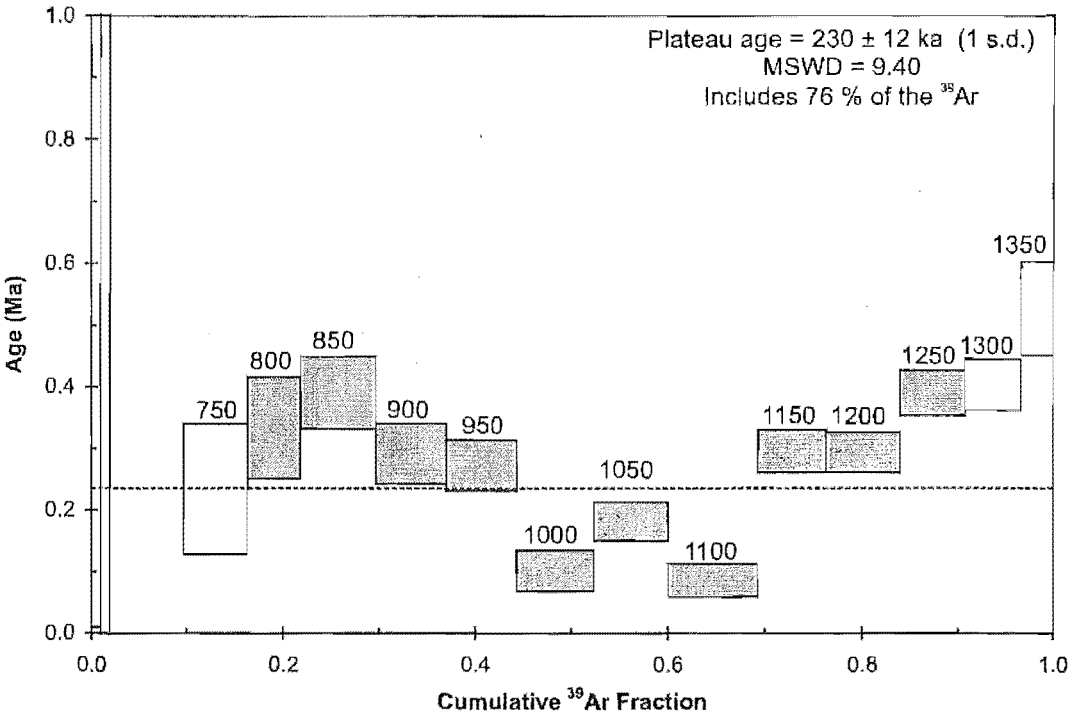

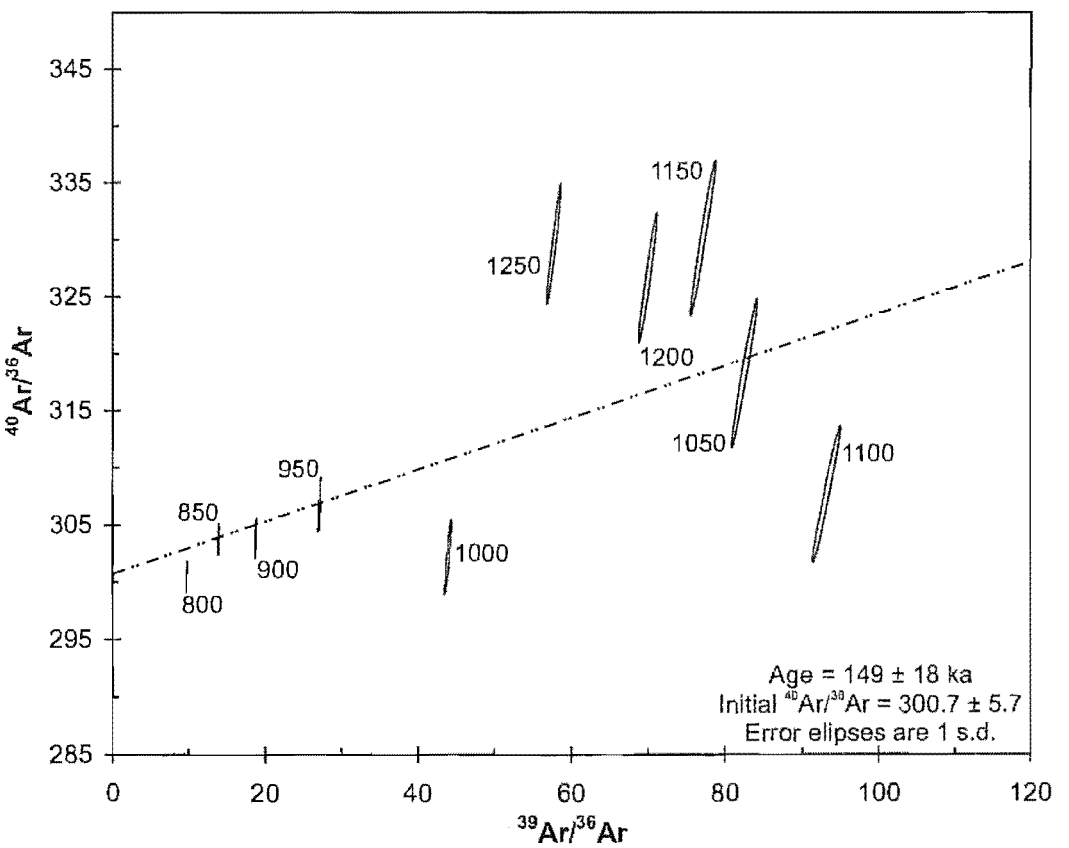

Appendix 2.2.10 - Ar-Ar data for M211, Wairiki Dome (MEC)

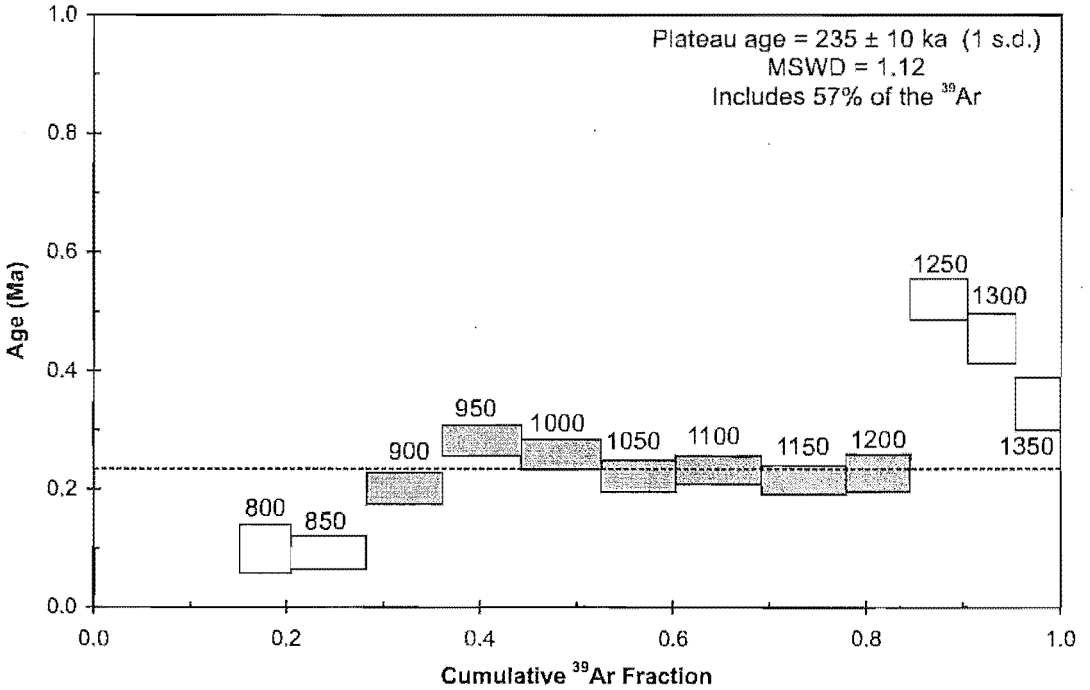

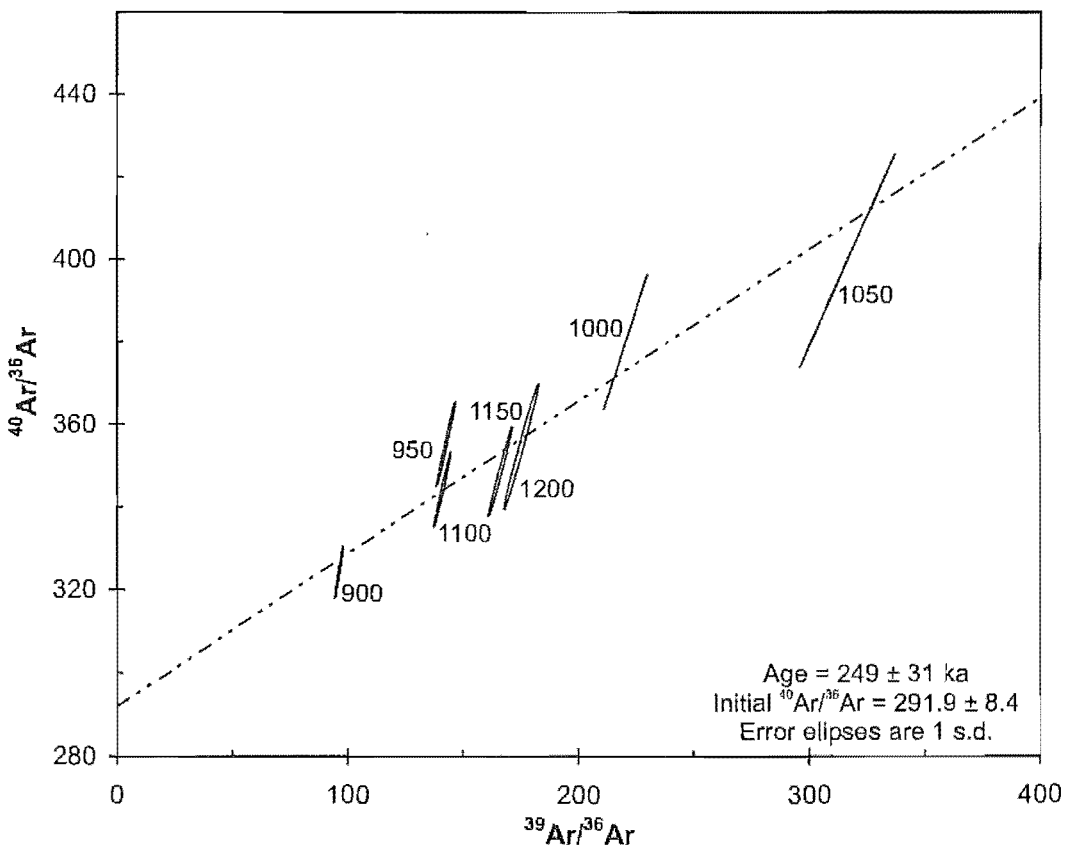

Appendix 2.2.11 - Ar-Ar data for M223, Maroanui East Dome

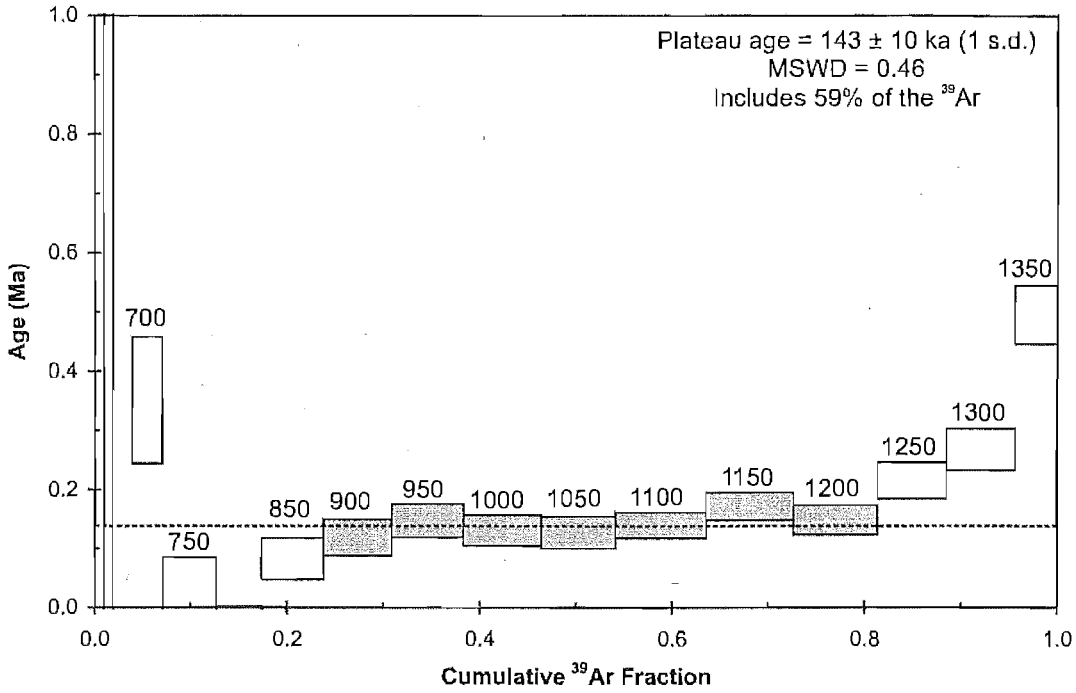

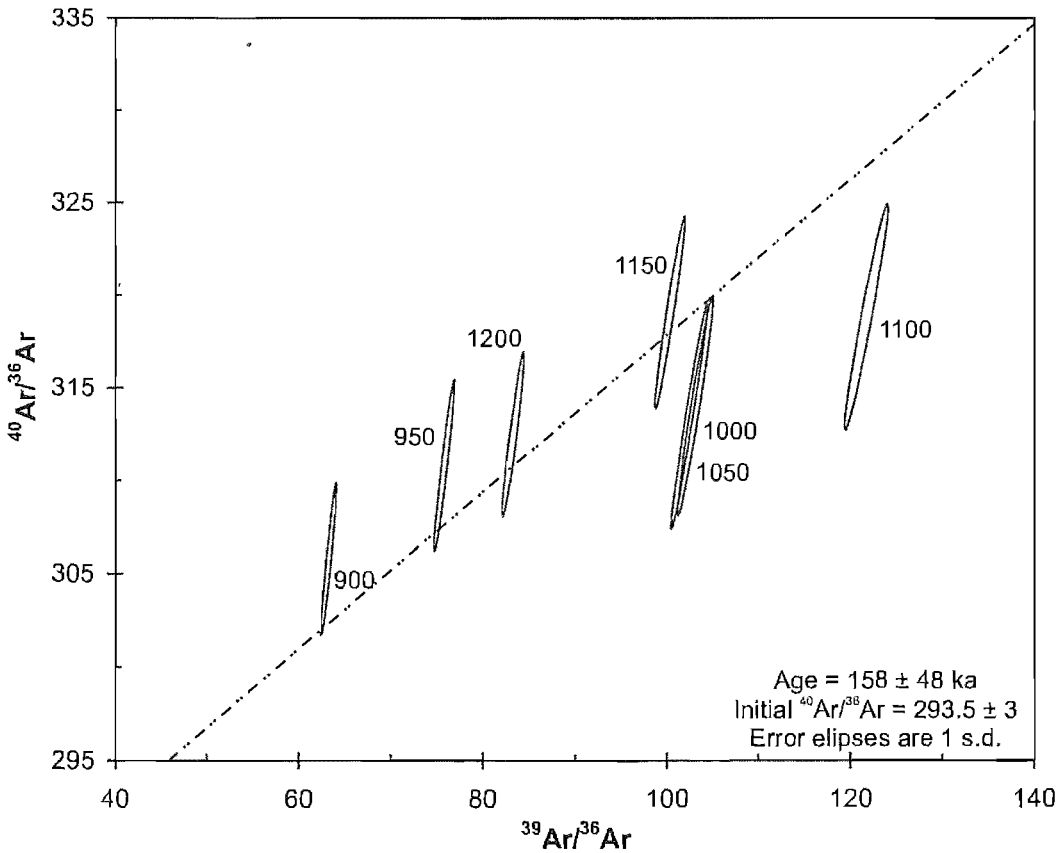

Appendix 2.2.12 - Ar-Ar data for M243, Mokauteure Dome

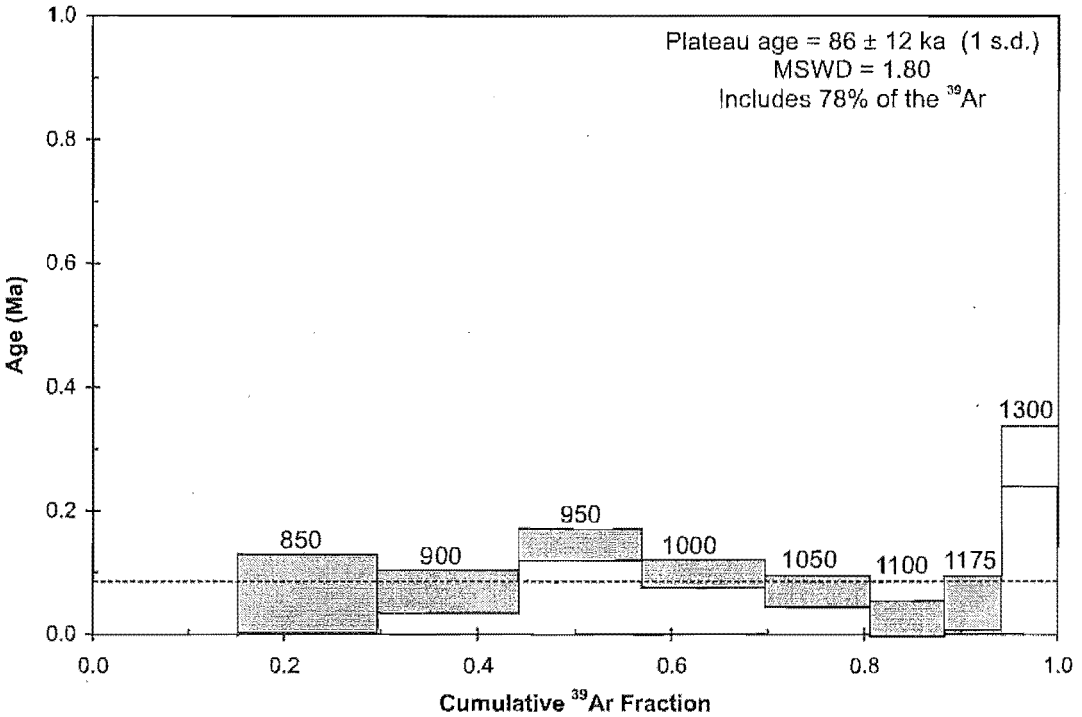

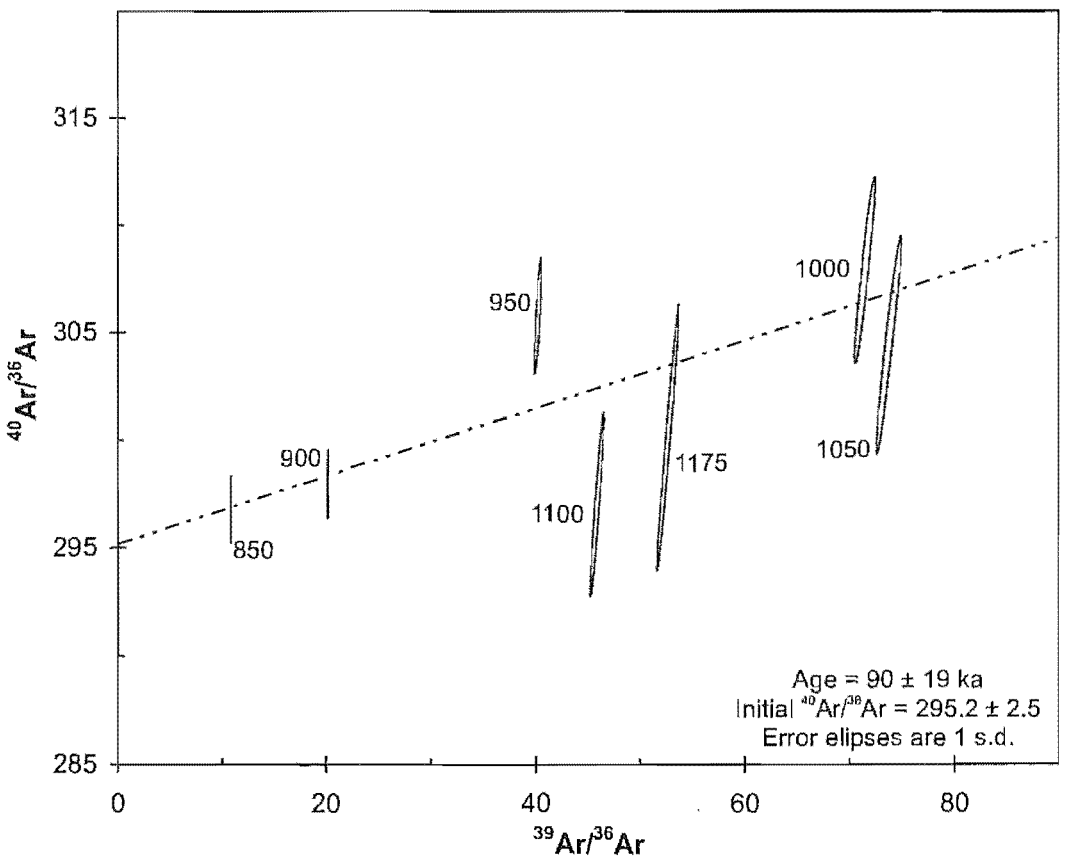

Appendix 2.2.13 - Ar-Ar data for M247, Goldies Dome (MWC)

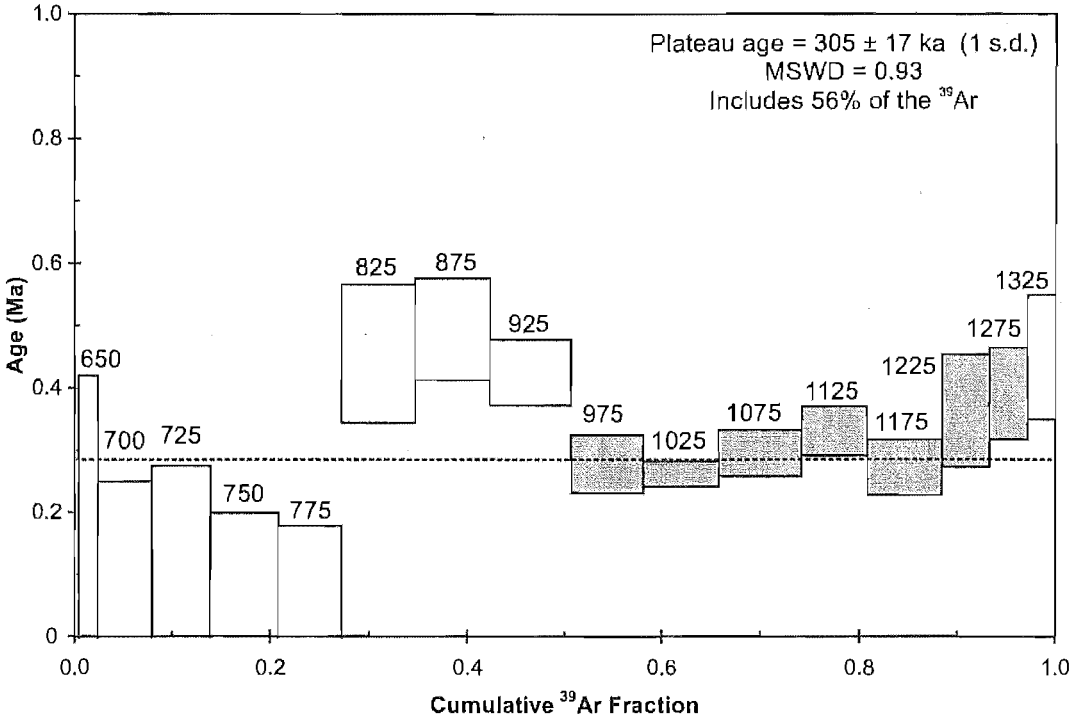

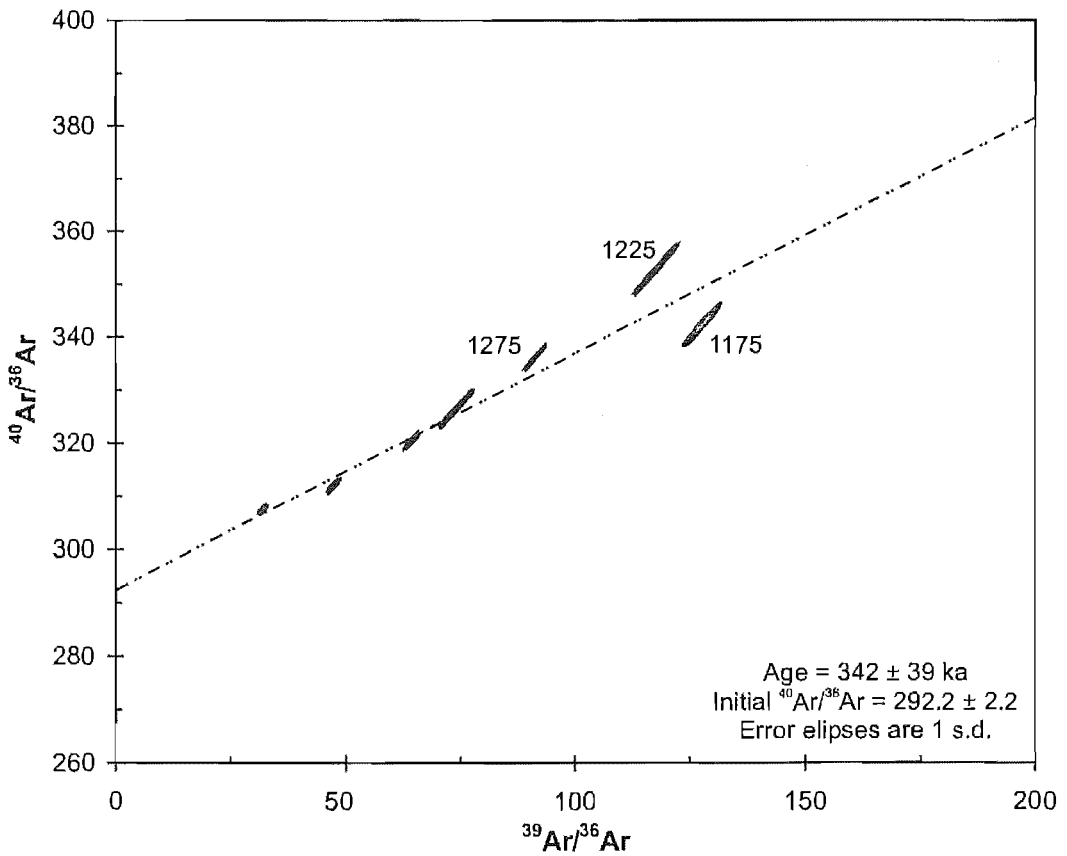

Appendix 2.2.14 - Ar-Ar data for M260, McPherson Dome (MEC)

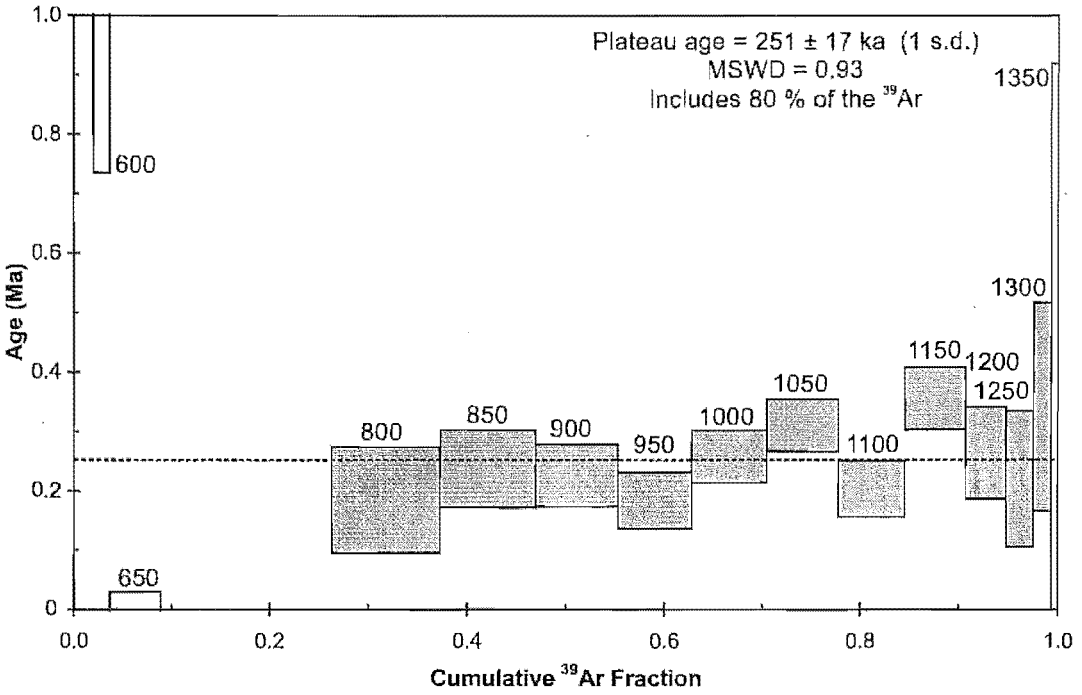

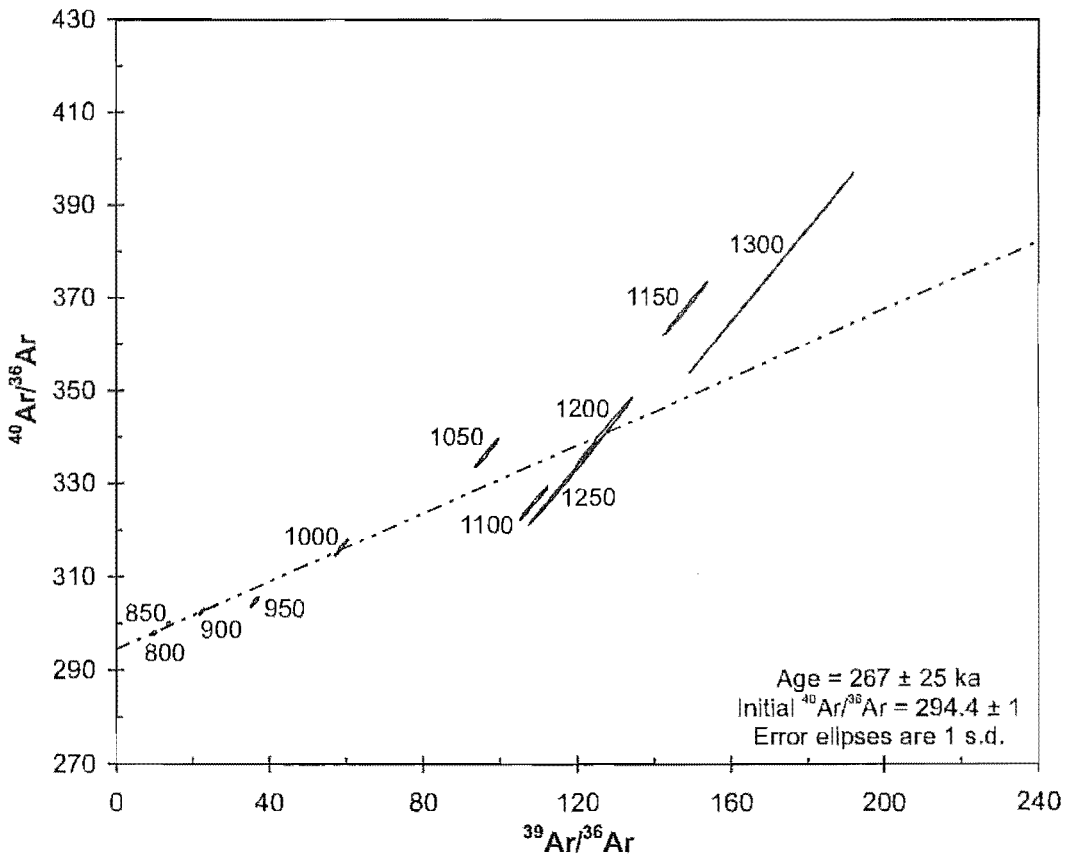

Appendix 2.2.15 - Ar-Ar data for M301, Orakeikorako Dome

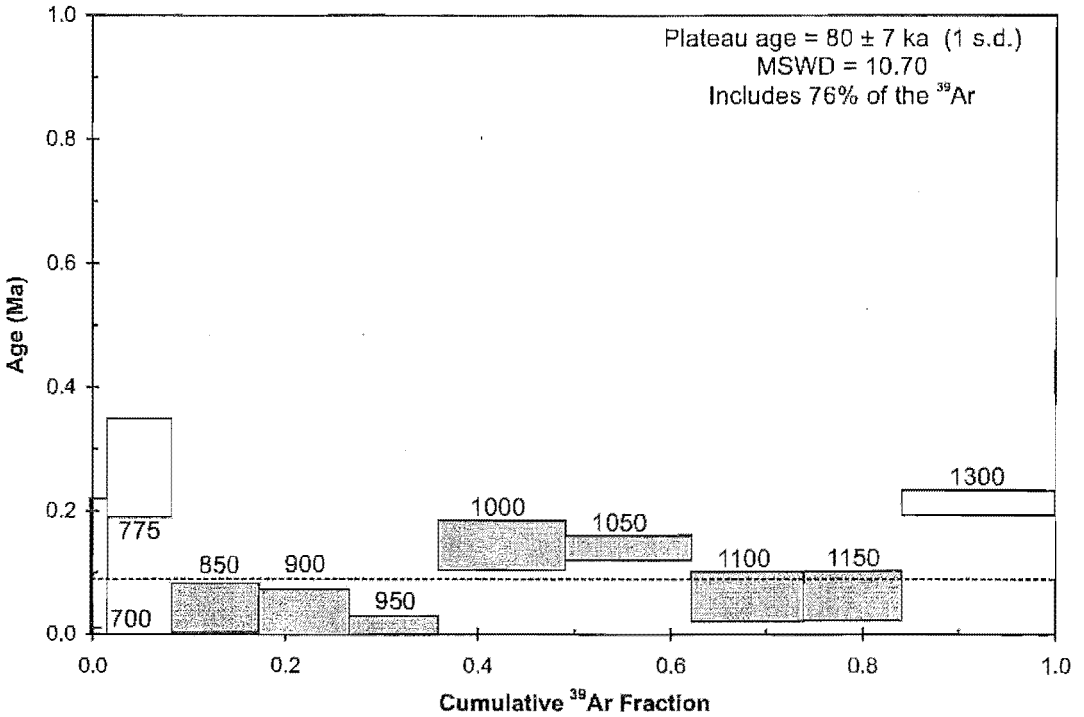

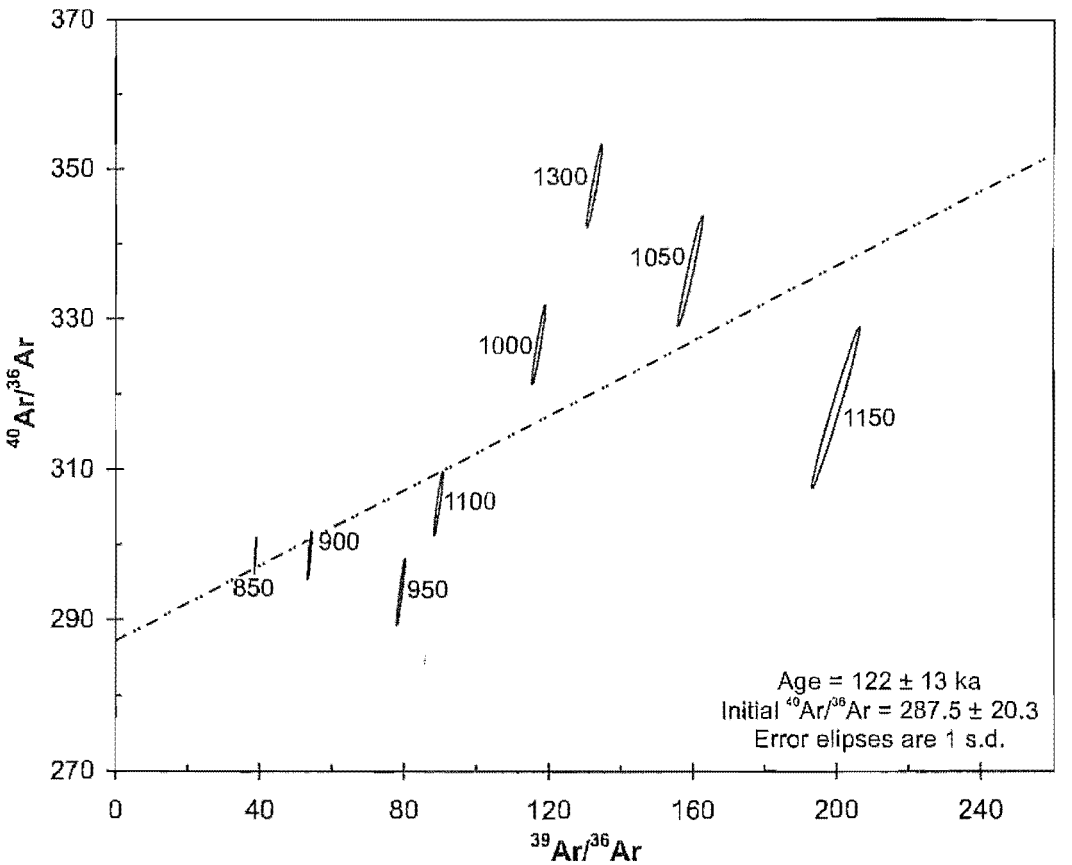

Appendix 2.2.16 - Ar-Ar data for M304, Pakuri Dome

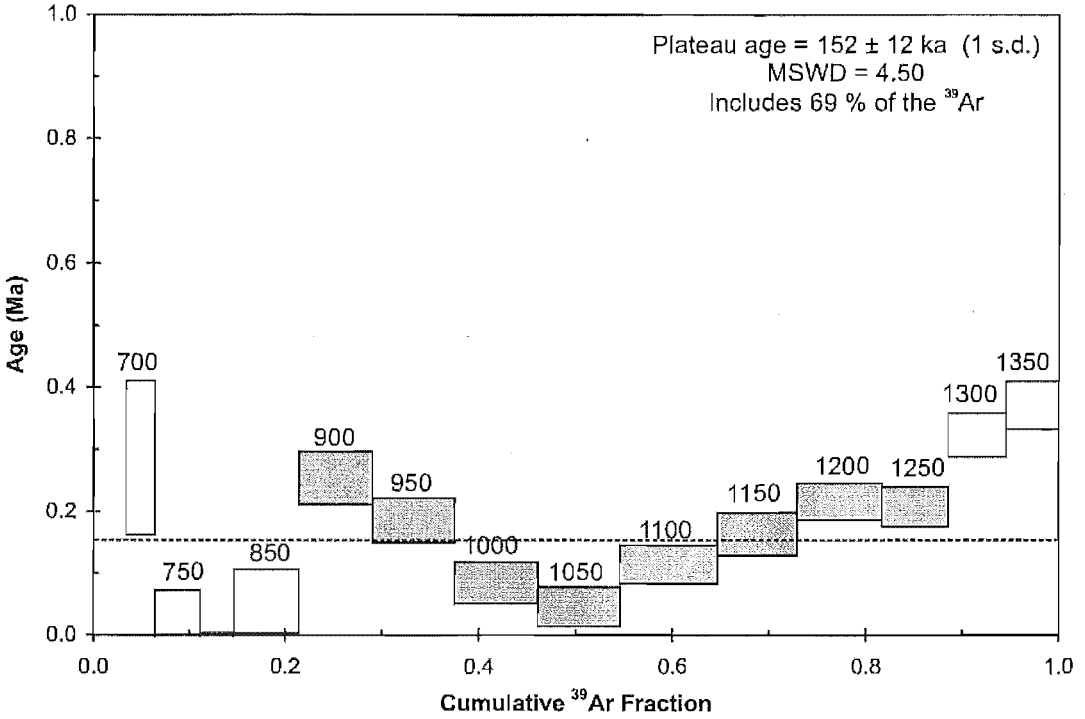

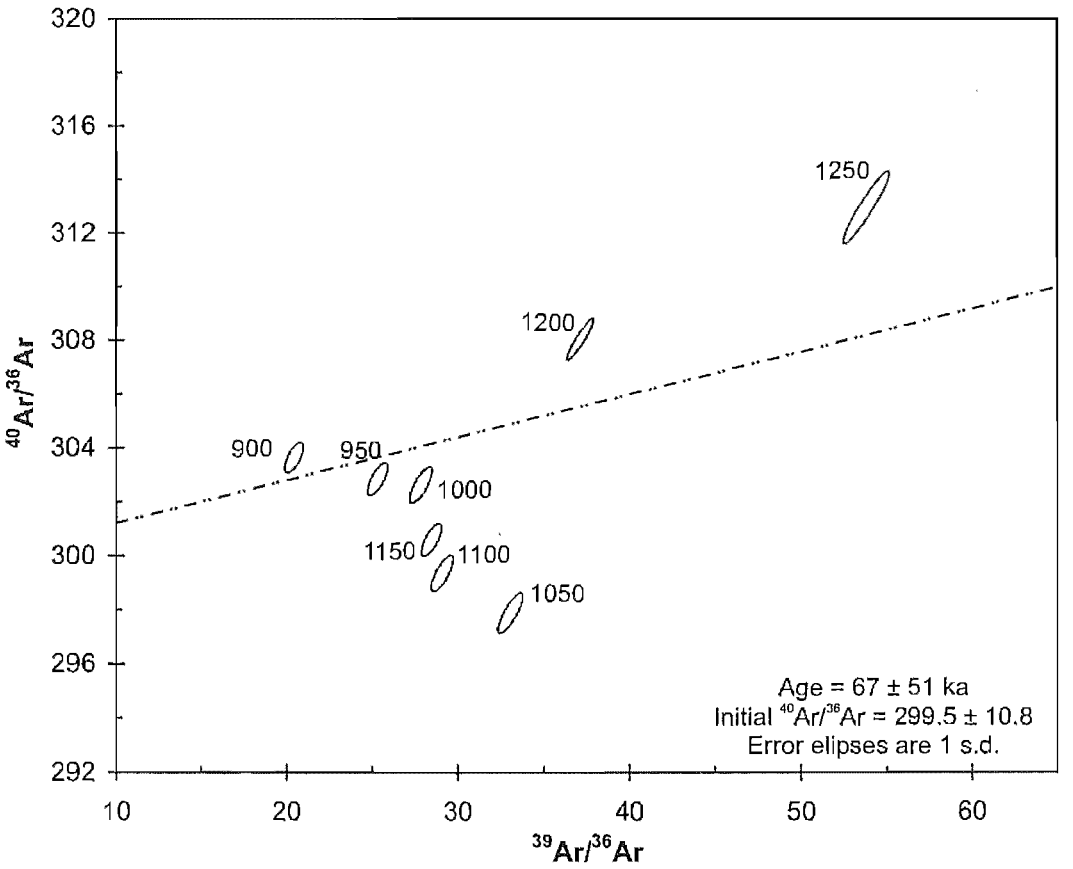

Appendix 2.2.17 - Ar-Ar data for M321, Forest South Dome

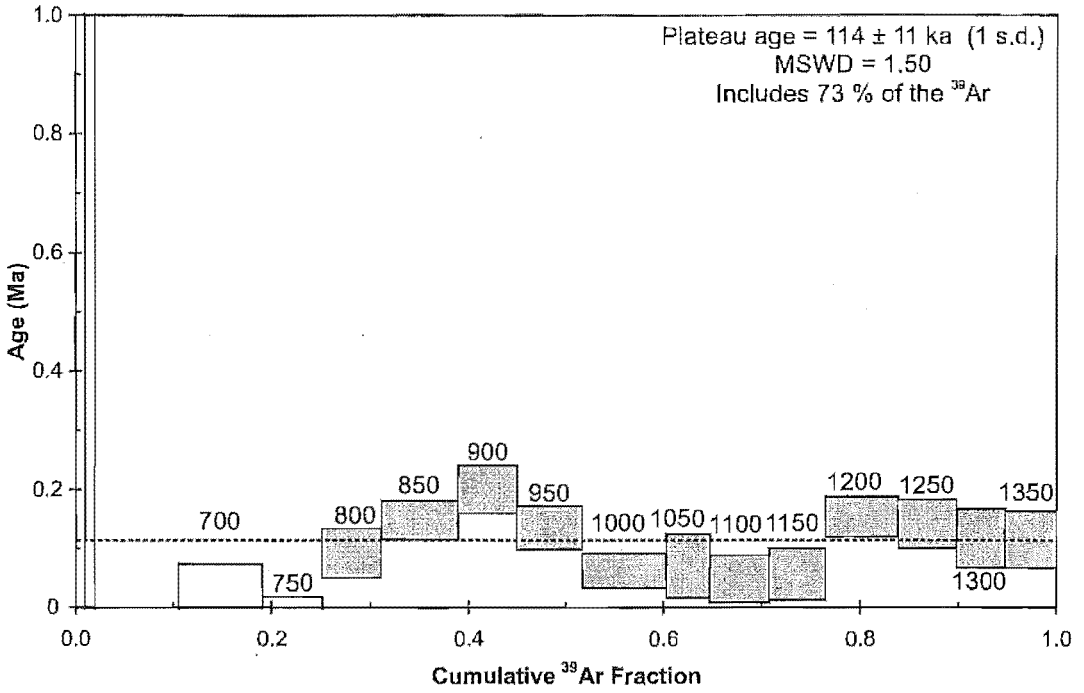

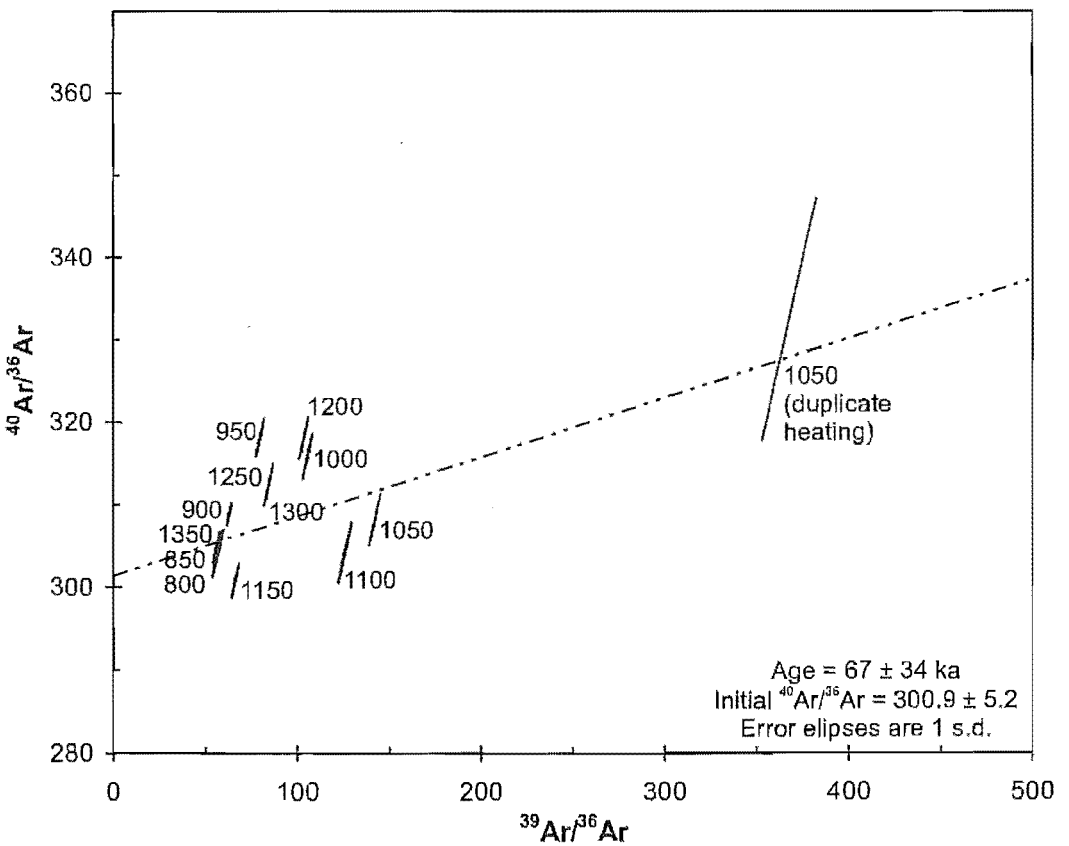

Appendix 2.2.18 - Ar-Ar data for M344, Mandarin Dome (MEC)

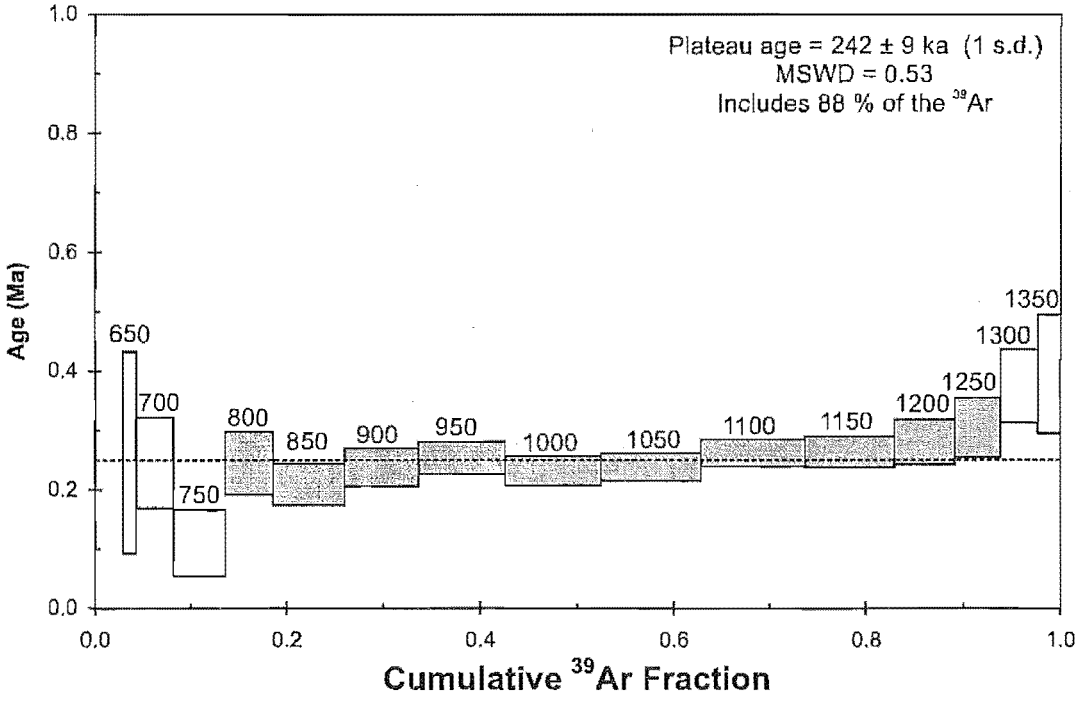

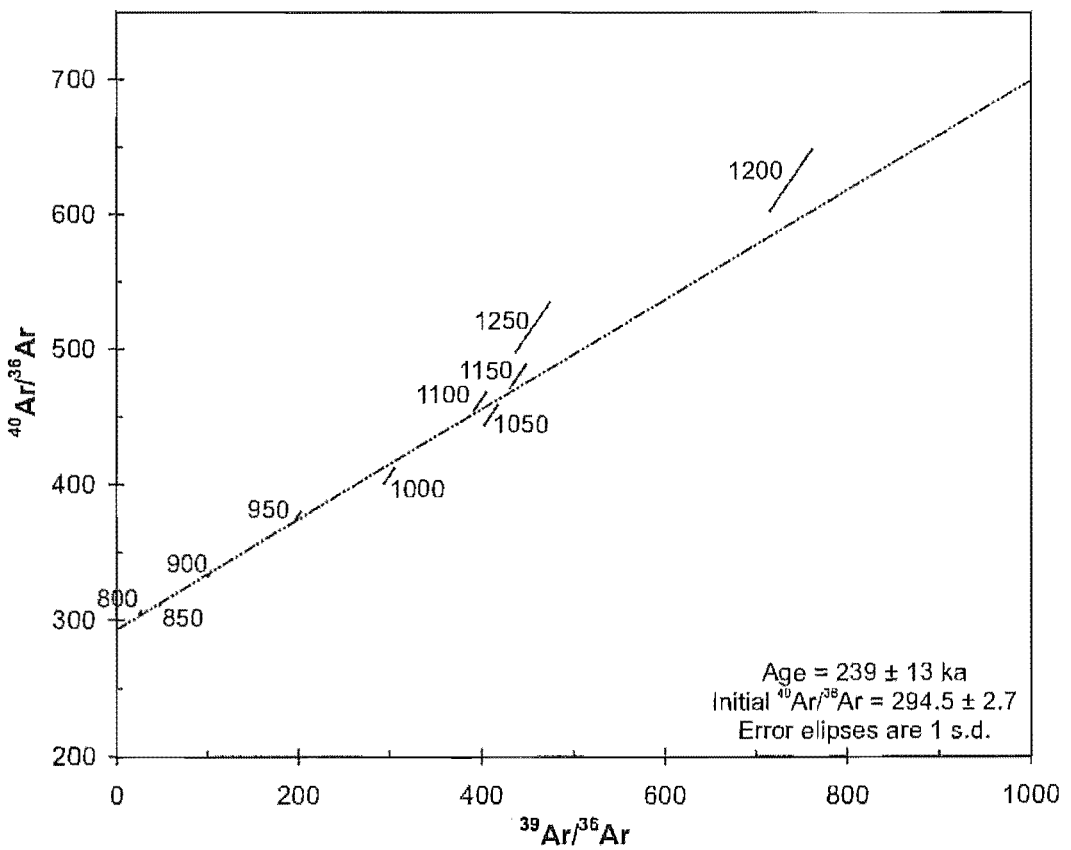

Appendix 2.2.19 - Ar-Ar data for M352, Baldy Dome (MEC)

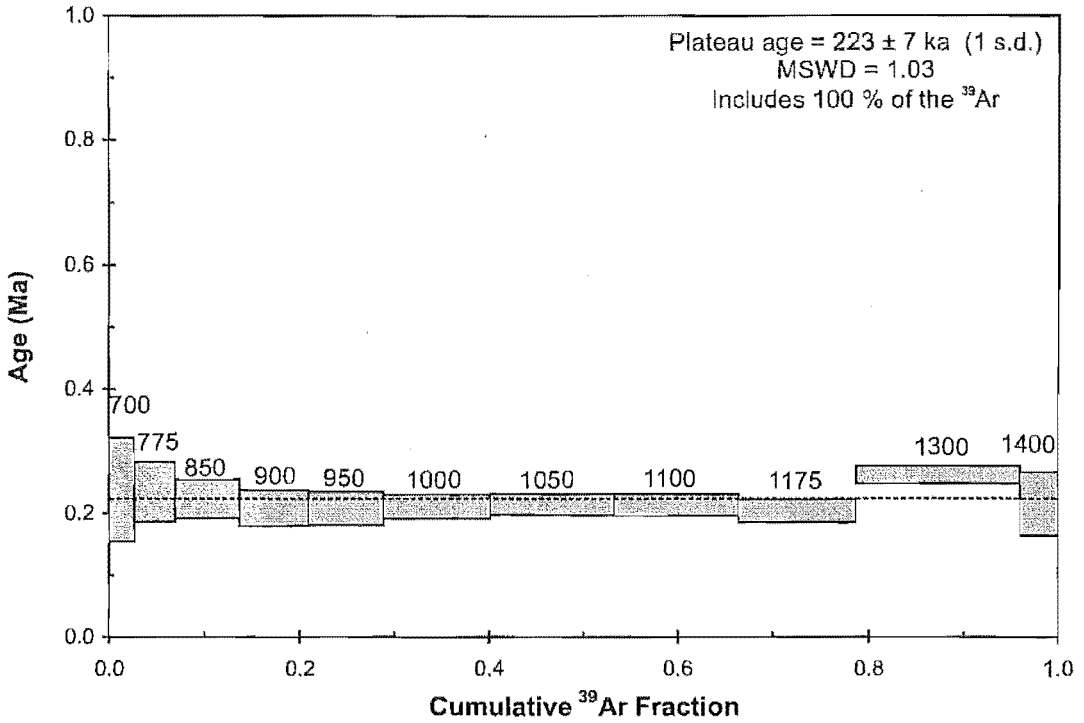

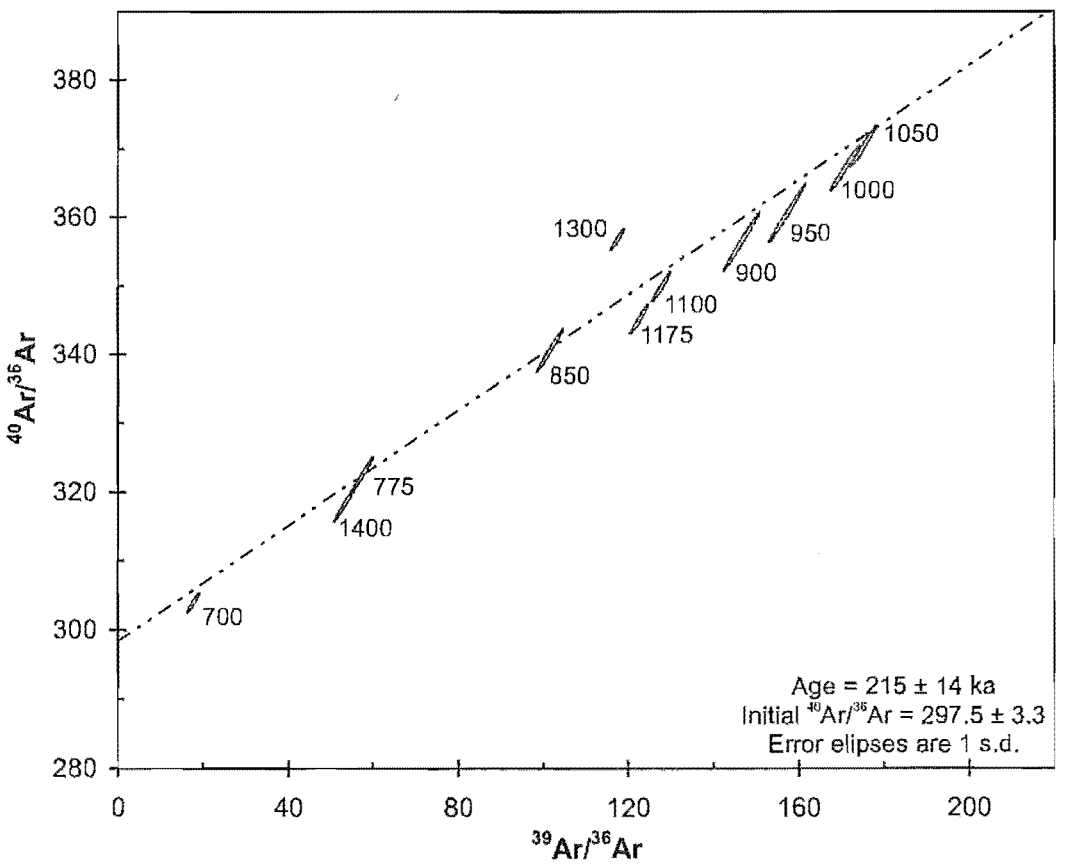

Appendix 2.2.20 - Ar-Ar data for M460, Umukuri Dome (MEC)

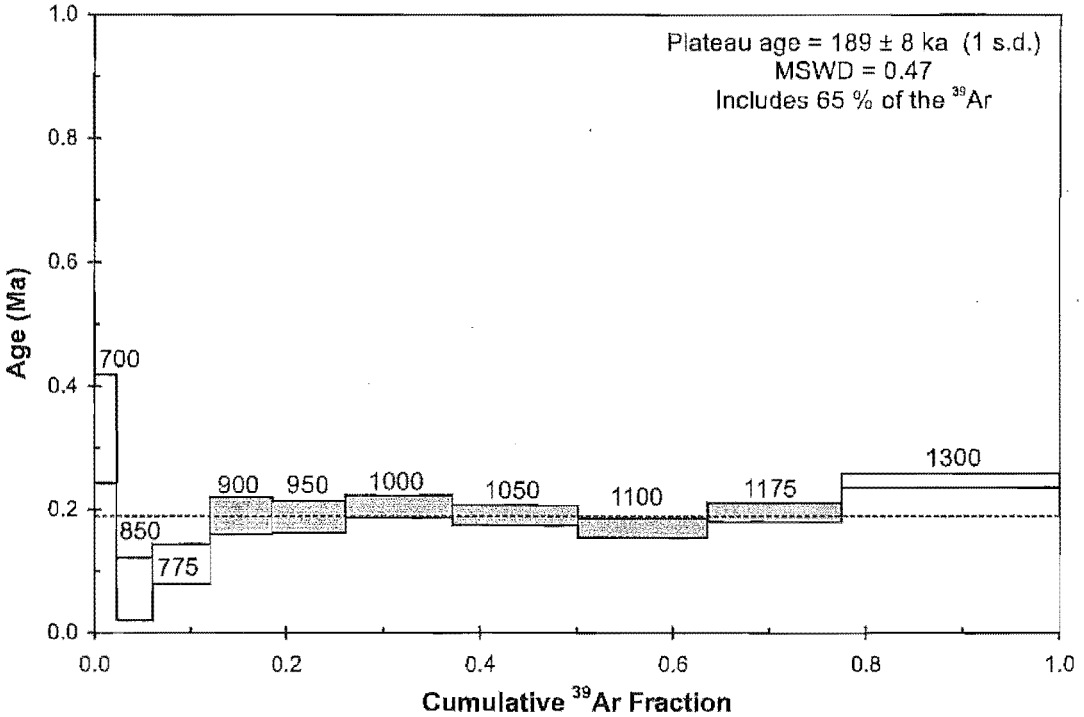

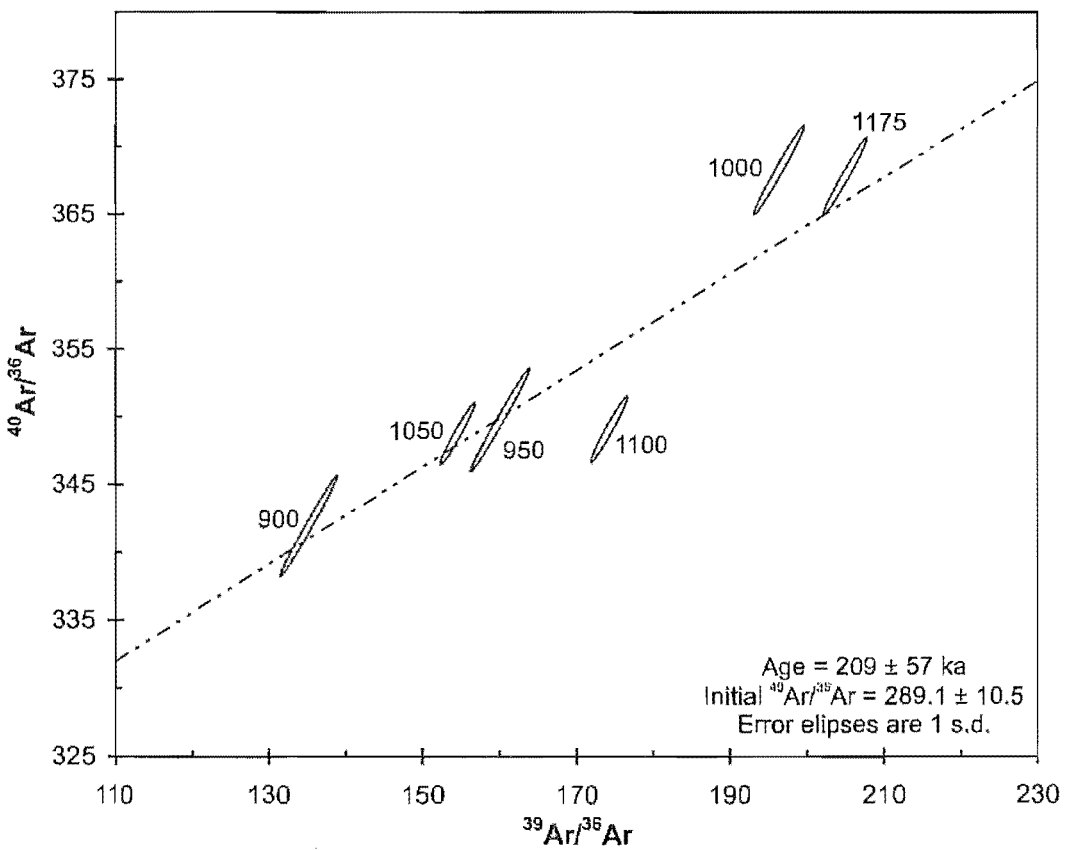

Appendix 2.2.21 - Ar-Ar data for M470, Korotai pyroclastics

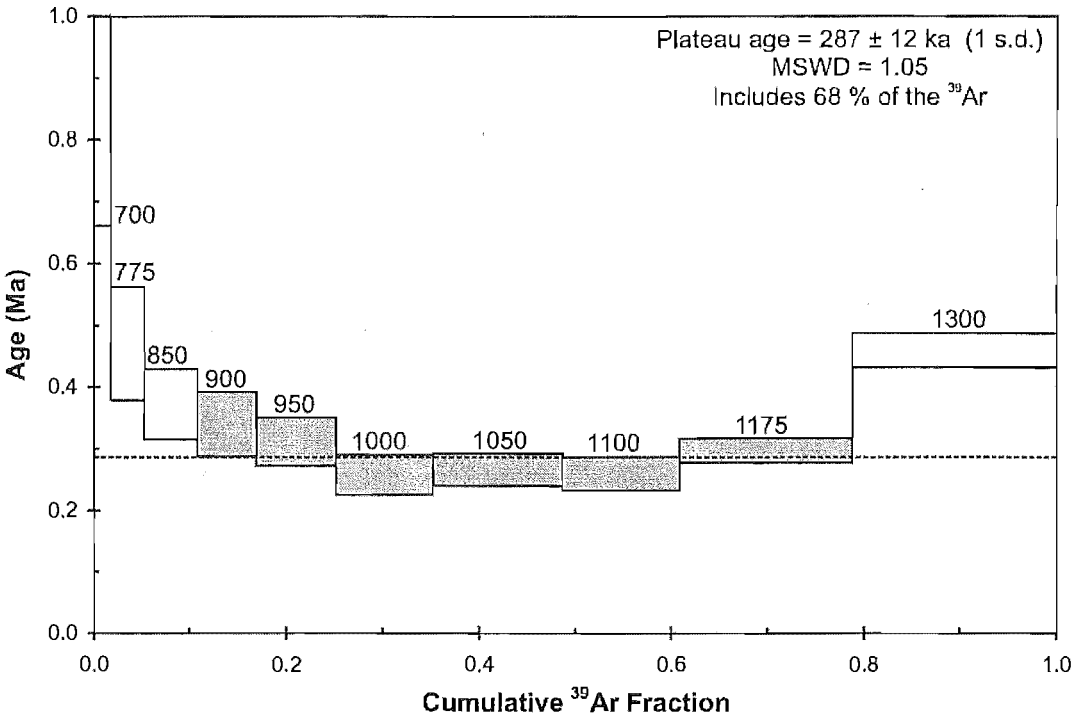

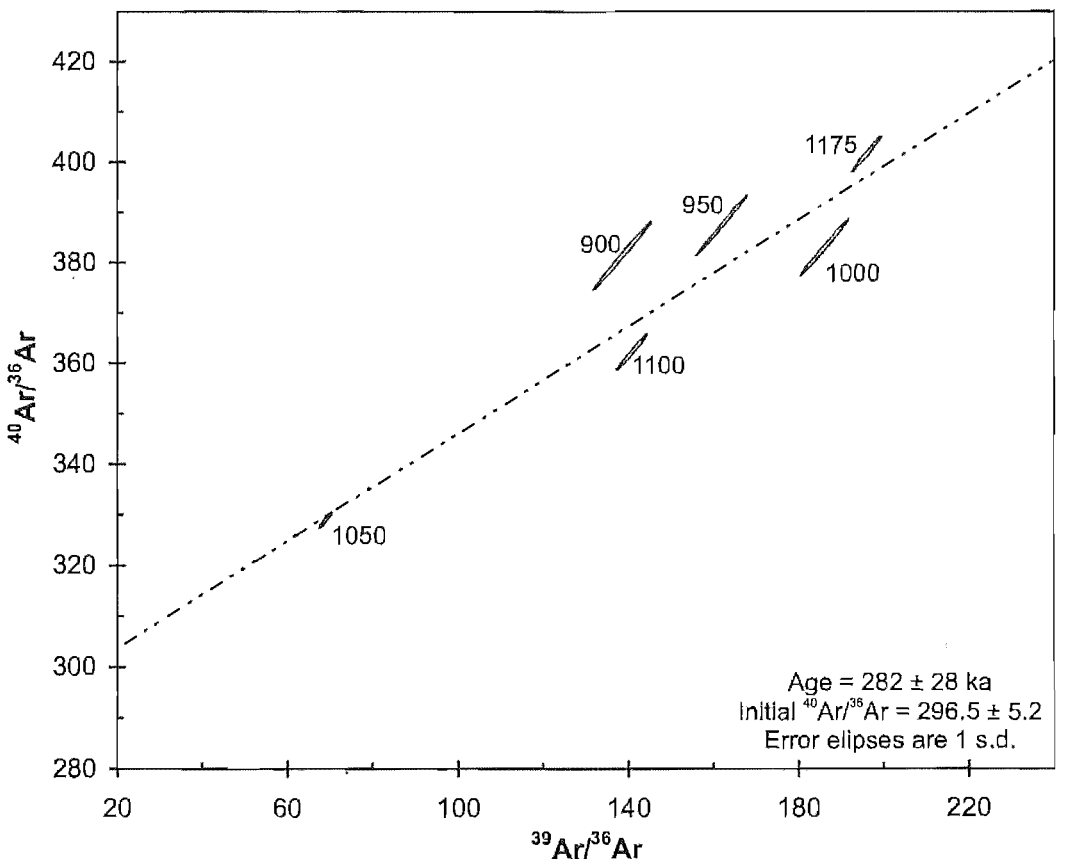

Appendix 2.2.22 - Ar-Ar data for MK, Mamaku pyroclastics

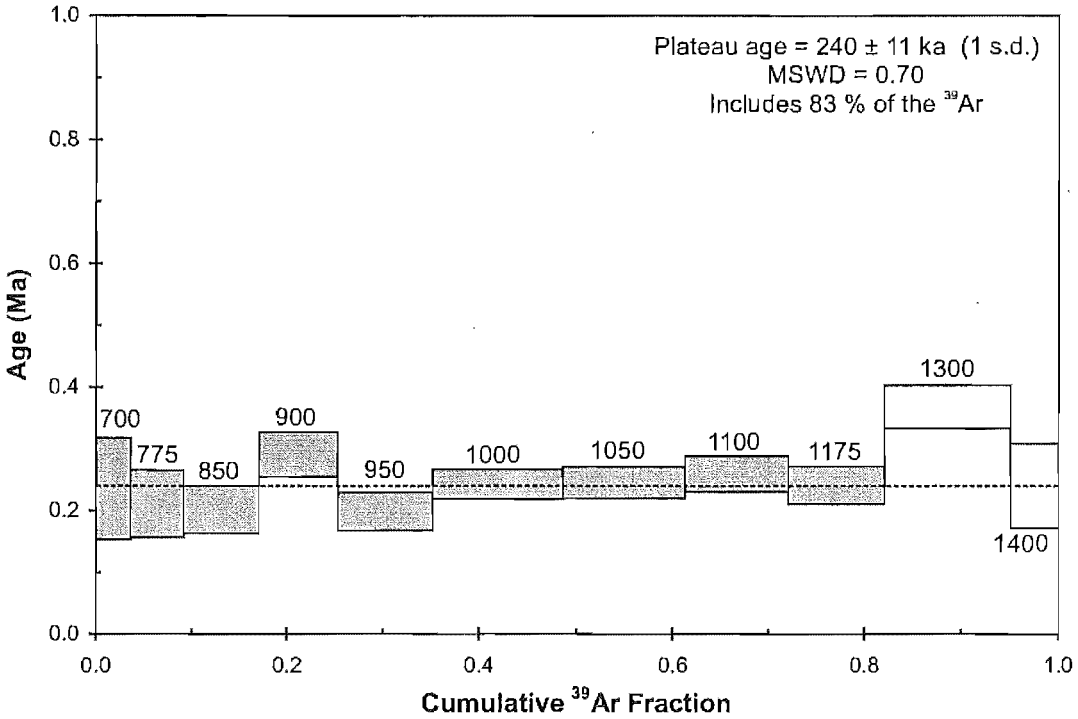

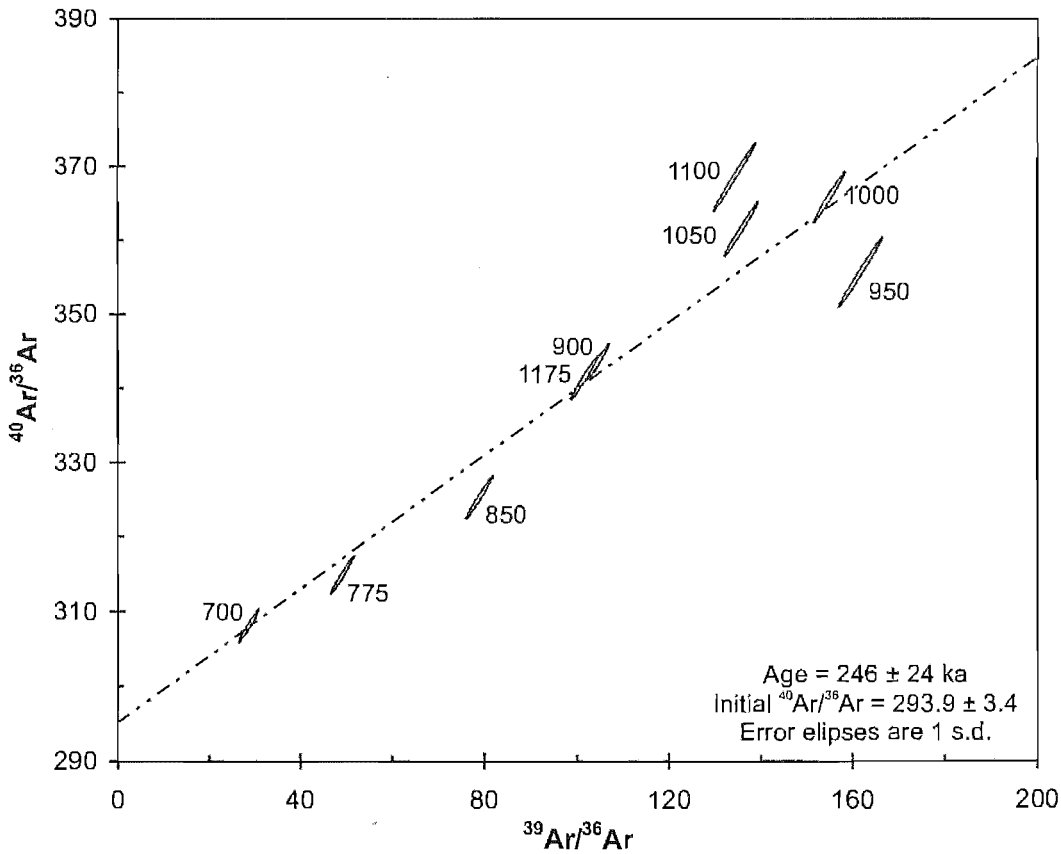

Appendix 2.2.23 - Ar-Ar data for OH3, Ohakuri pyroclastics

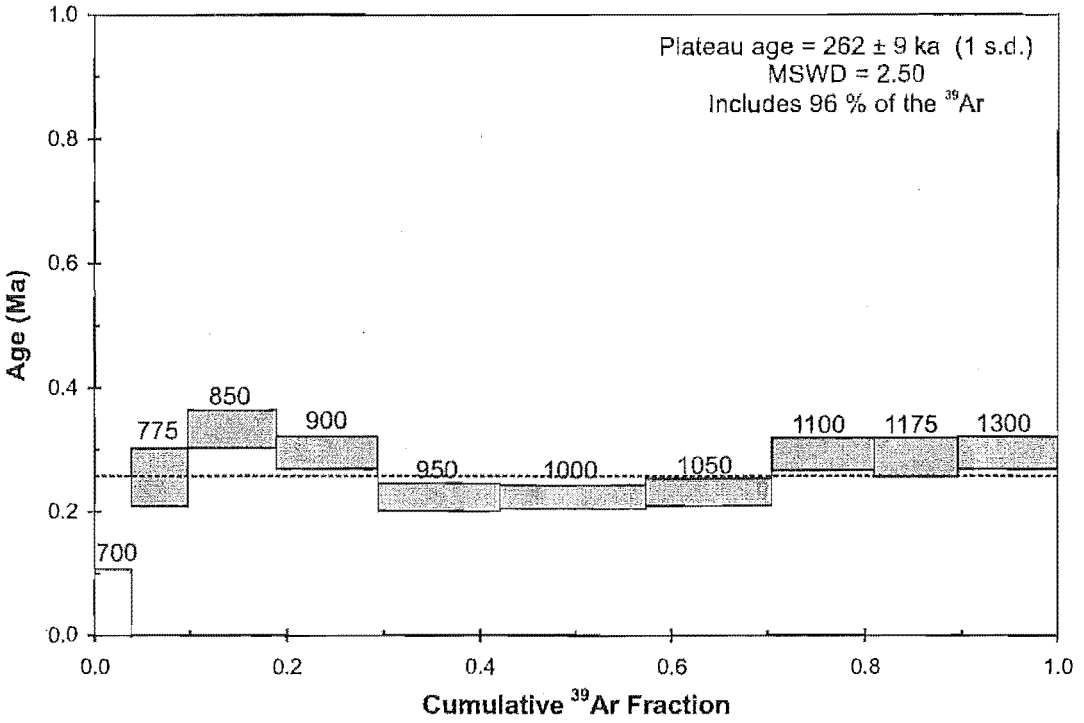

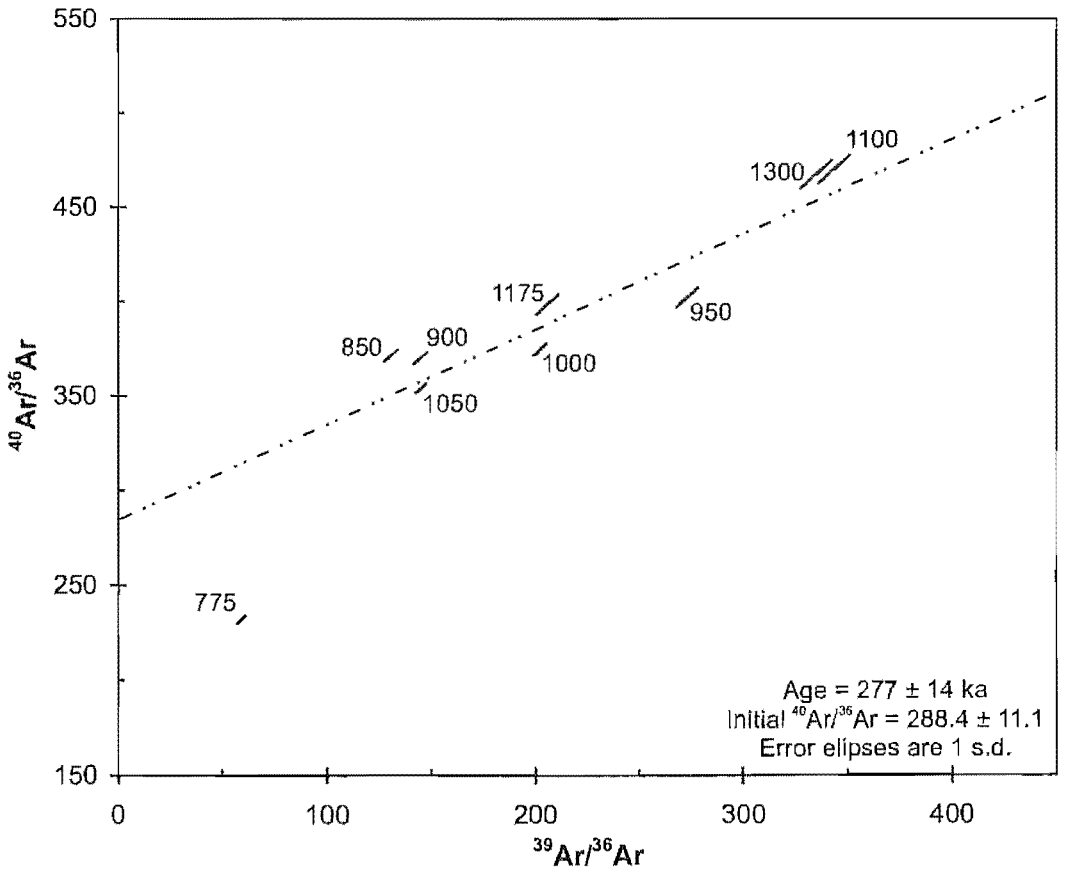

Appendix 2.2.24 - Ar-Ar data for PK, Pokai pyroclastics

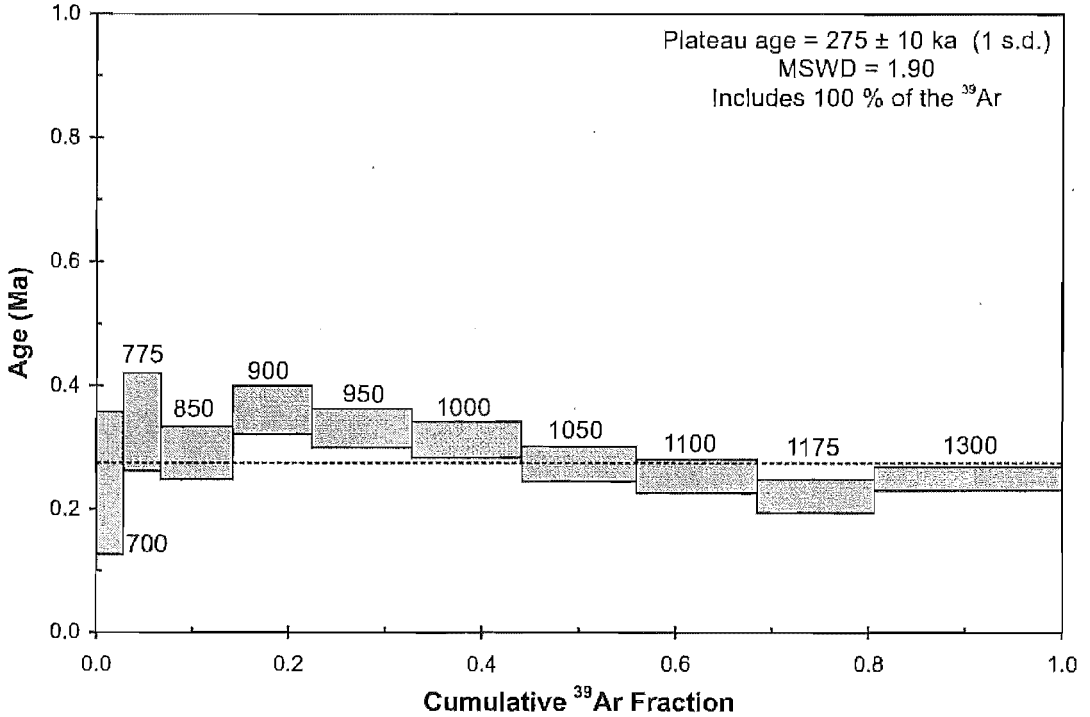

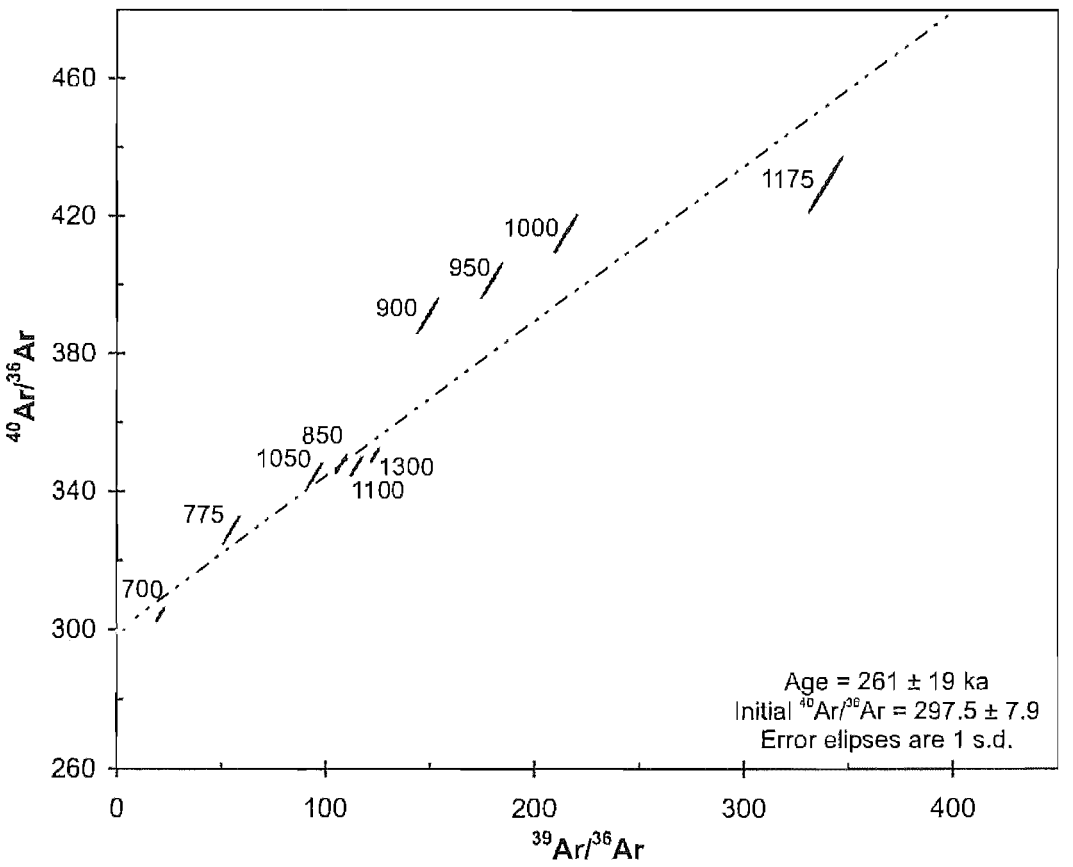

APPENDIX 3

Petrographic Descriptions

3.1 Introduction

This appendix presents the petrographic description data for all of the new thin sections analysed for this thesis. All mineral percentages are recalculated to vesicle free and are of volume. Under maximum crystal length a '?' indicates that small ambiguous crystal(s) may be of a particular phase, but the mineral has not been positively identified as such in this thin section.

3.2 Legend

Heading	*Description*
Samp	Sample number
Pl %	Plagioclase vol.% (recalculated vesicle free)
Max Pl size (mm)	Long axis length of the longest plagioclase crystal
Pl sieve	Plagioclase sieve texture
Pl gloms	Plagioclase glomeroporphyritic aggregates
Pl n, r, o zone	Plagioclase normal, reverse, and/or oscillatory zoning
Pl incl	Plagioclase glass inclusions
Pl ptch xtn	Plagioclase patchy extinction (other than zoning)
Pl rou/emb	Plagioclase resorption - rounding/embayment
Qtz %	Quartz vol.% (recalculated vesicle free)
Max Qtz size (mm)	Long axis length of the longest quartz crystal
Qtz rou/emb	Quartz resorption - rounding/embayment
Amph %	Amphibole vol.% (recalculated vesicle free)
Max Amph size (mm)	Long axis length of the longest amphibole crystal
Opx %	Orthopyroxene vol.% (recalculated vesicle free)
Max Opx size (mm)	Long axis length of the longest orthopyroxene crystal
Biot %	Biotite vol.% (recalculated vesicle free)
Max Biot size (mm)	Long axis length of the longest biotite crystal
Opq %	Opaque minerals vol.% (recalculated vesicle free)
Opq el m st	Elongate, moderate, stubby (maximum in section, helps locating ilmenite)
Opq e s a	Euhedral, subhedral or anhedral opaque minerals
Max Opq size (mm)	Long axis length of the longest opaque mineral
Gmass %	Groundmass vol.% (recalculated vesicle free)
Gmass Cl	Clear groundmass
Gmass Cless	Colourless or colour abbreviation(s)
Gm sph %	Spherulites (granoph = granophyric intergrowths)
Max sph size (mm)	Long axis length of the largest groundmass spherulite
Porph	Porphyritic

Hypo	Hypocrystalline, s = spherulitic, d=devitrified
Vesic %	Vesicles vol.%
Max Vesic size (mm)	Short axis length of the widest vesicle
Fl Bnd s m l	Flow banding slight, moderate, lots, n = none
V:	Comments on the vesicularity
P:	Comments on the phenocrysts
G:	Comments of the groundmass
R:	Comments on the whole-rock
	Additional for mafic samples:
Olivine %	Olivine vol.% (recalculated vesicle free)
Max Ol size (mm)	Long axis length of the longest olivine crystal
Clinopyroxene %	Clinopyroxene vol.% (recalculated vesicle free)
Max Cpx size (mm)	Long axis length of the longest clinopyroxene crystal
Gmass %	Groundmass vol.% (recalculated vesicle free)
Gmass cl m op	clear, medium, opaque
Gmass Col	colour abbreviation (see 'G:' notes)
ig, so, o, is, hy	intergranular, subophitic, ophitic, intersertal, and/or hyalopilitic texture
Max gmass size (mm)	Long axis length of the longest groundmass crystal
Gmass Gl %	Groundmass glass vol.% (recalculated vesicle free)
Gmass Pl %	Groundmass plagioclase vol.% (recalculated vesicle free)
Gmass Cpx/Ol %	Groundmass Clinopyroxene/Olivine vol.% (recalculated vesicle free)
Gmass Opq %	Groundmass Opaque minerals vol.% (recalculated vesicle free)

Miscellaneous Abbreviations	***Definition***
Xtal(s)	Crystal(s)
Defm	Deformation
Conc(s)	Concentration(s)
Ves	Vesicle(s)/vesicularity
Recrystn	Re-crystallisation
Granoph	Granophyric intergrowth(s)
Agg(s)	Aggregate(s)
XRF	X-Ray Fluorescence (see Appendix XX)
Fract(s)	Fracture(s)(d)
Igrowth(s)	Intergrowth(s)
Cless	Colourless
Popn	Population
Phen(s)	Phenocrysts
Feld(s)	Feldspar(s)
Incl	Inclusion/include(d)
Ogrow	Overgrow(s)(th)
Altrn	Alteration
Devit	Devitrify(ied)/devitrification
Hspec	Hand specimen
Pptn	Precipitation
Esp	Especially
Crystn	Crystallisation

3.3 Sample petrography

Samples are listed according to their 'sample number' (with rhyolitic samples first, then basaltic and dacitic samples). 'Sample number' is the 'location number' (Appendix 1, Map 1, back pocket) for locations where only one sample was collected. If more than one sample was collected from a single location the 'sample number' is the 'location number' suffixed with letter(s) (e.g. M123a, M123b, etc.).

Sample Number	Plagioclase %	Max Pl size (mm)	Pl sieve	Pl glom aggregates	Pl n, r, o zone	Pl inclusions	Pl patchy extinction	Pl rounded/embayed	Quartz %	Max Qtz size (mm)	Qtz rounded/embayed	Amphibole %	Max Amph size (mm)	Orthopyroxene %	Max Opx size (mm)	Biotite %	Max Biot size (mm)	Opaques %	Opq el, m, st,	Opq e, s, a,	Max Opq size (mm)	Groundmass %	Gmass Clear	Gmass Colourless	Gm spherulites %	Max sph size (mm)	Porphyritic	Hypocrystalline	Vesicularity %	Max vesic size (mm)	Flow banding s, m, l	
M010	20.0	3.1		y	y	y		r	6.7	2.7	re	2.0	2.3	0.7	0.9			0.1			0.5	71	y	y			y	y	25	0.8	m	V: width & banding vary
	P: some euhedral ilmenite, Amph grubby												G: no devitrification														R:					
M012b	1.2	2.3			nr	y	y							0.1	0.3			0.1	el	s	0.2	99	y	y			y	y	15	1	n	V: irregular, some plucked xtals?
	P: nearly aphyric, pl defm twins, altered opx												G: dusty														R: very low crystal content					
M012c	8.0	2.0			y	y		re							0.8				el	s	0.2	92	y	y			y	y	40	0.2	m	V: most elongated
	P:												G:														R:					
M012e	2.5	1.5			nr	y	y	r						0.1	1.7			0.1	st	e	0.2	97	y	br			y	y	20	0.9	m	V: fine & sinuous
	P: nearly aphyric, some broken, opx resorbed												G: 40% clear, 60% slightly brown														R: low crystal content, some plucked					
M013	1.3	1.4		y	nro	y	y	re						0.1	0.4			0.1	m	a	0.2	98	y	lbr			y	y	25	2.5	l	V: openness varies across
	P: nearly aphyric												G: glass darker brown in patches														R: very low crystal content					
M022l	13.3	1.1		y	nro	y	y	r	6.7	2.2	re	0.6	4.1	0.7	1.4			0.7	st	s	0.4	78	y	y			y	y	25	0.9	ml	V: varies with banding
	P: many broken												G: dispersed patches of brown glass														R:					
M022u	18.5	3.6		y	nro	y		r	8.7	2.6	re	0.5	1.8	0.1	1.4			0.1	st	s	0.3	72	y	y			y	y	8	0.3	s	V: equant to elongate
	P: aggregate of 0.3mm Amph & pl - xenolith?												G: occasional <0.3mm slightly brown patches														R: dense					
M023	18.8	3.7	y	y	nro	y	0	r	4.7	2.2	re	0.6	2.7	0.6	1.3			0.1	st	e	0.3	75	y	y			y	y	15	0.3	s	V: concentration & banding vary
	P: most phases euhedral												G: fibrous in places														R: moderate to high crystal content					
M026	8.9	3.0		y	nro		y	r	0.6	1.1	re			0.1	1.2			0.1	st	s	0.5	90	y	y			y	y	10	0.4	m	V: flow bands & ves size vary
	P: Many pl and occasional Qtz broken, opx dirty												G: some areas slightly brown														R: fragmented crystals tend to group					
M033	7.0	3.9	y	y	nro	y		re	1.0	1.8	re			0.1	0.8			0.1	m	s	0.3	92	n	lbr	60	0.8	y	d			n	V: overprinted by recrystn
	P: many pl embayed & altered, opx to opqs often												G: spherulites grade into granoph														R: some Fe staining					
M036	6.3	1.8		y	nro	y	y	r						0.1	0.7			0.1	st	e	0.4	93	y	y			y	y	5	3.5	n	V: open ves in few patches
	P: some broken												G: dispersed brn glass, dusty														R: very dense, few iron stain patches					
M042	8.2	3.0		y	nro	y		re						0.6	1.0			0.1	st	e	0.4	91	y	y			y	y	15	0.4	s	V: varies
	P: many pl fractured, finer aggs of opx and pl, opx roun												G: small occasional lbr patches														R: fracturing from polishing?					
M044	12.9	2.7		y	nro	y	y	r	0.1	0.8	r	0.1	0.5	1.1	1.2			0.1	m	s	0.5	86	y	y			y	y	7	0.5	s	V: open and patchy
	P: some broken, fine agg of pl, opx & Amph - xenolith?												G: dusty														R: DACITE XRF					
M046	7.1	1.7			nro	y	y	re						0.1	0.6							93	y	y			y	y	15	0.1	n	V: jagged, irregular, varied conc.
	P: pl with or rim, pl, opx fract on cleavage, many broker												G: some slightly tan glass														R: fragmented crystals					
M047	14.3	2.5			nro	y	y	re						0.1	0.5							86	y	br			y	y	30	0.1	m	V: fine, partly collapsed
	P: pl <An14deg												G: slightly brown to colourless																			

Sample Number	Plagioclase %	Max Pl size (mm)	Pl sieve	Pl glom aggregates	Pl n, r, o zone	Pl inclusions	Pl patchy extinction	Pl rounded/embayed	Quartz %	Max Qtz size (mm)	Qtz rou/emb	Amphibole %	Max Amph size (mm)	Orthopyroxene %	Max Opx size (mm)	Biotite %	Max Biot size (mm)	Opaques %	Opq el, m, st,	Opq e, s, a,	Max Opq size (mm)	Groundmass %	Gmass Clear	Gmass Colourless	Gm spherulites %	Max sph size (mm)	Porphyritic	Hypocrystalline	Vesicularity %	Max vesic size (mm)	Flow banding s, m, l	
M049	3.3	2.0		nr		y	y	re						0.2	0.9			0.2	m	a	0.2	96	y	y			y	y	40	2	n	V: polishing damage?
	P: all crystals damaged, pl resorption may be damage												G: dusty																R: BAD THINSECTION, few crystals present				
M051	6.3	2.3		nro		y	y	re										0.1	st	s	0.2	94	y	br			y	y	5	0.3	n	V: dispersed
	P: all plagioclase and minor opaques												G: dusty																R: HIGH Si RHYOLITE XRF				
M053	4.3	1.5		y	nro	y	y	r				0.1	0.3	1.1				0.5	st	s	0.7	94	y	2			y	y	7	0.2	l	V: long collapsed
	G: gloms of fine pl & Amph with br glass around - xenol												G: Bands l brown & clear glass, patches more brn, twinkle																R: Banded, mixed?, reasonably dense				
M056	7.8	1.8		nro		y		r	0.6	0.9	re			0.1	1.5			0.1	st	s	0.3	91	y	y			y	y	10	0.7	sm	
													G: slightly brown in places																R: low crystal content				
M058	6.7	2.1		y	nro	y	y	r						0.8	0.6			0.2	st	e	0.2	92	y	br			y	y	40	0.7	l	V: sinuous & open
	P: some pl broken, opx dirty												G: brown hue varies																			
M063	15.3	4.0		nro		y	y	r	4.7	6.0	e	0.1	1.5	0.1	1.0			0.6	m	sa	2.0	79	y	2	40	1	y	y	15	4	s	V: large + popn of <0.3mm fine
	P: some larger vesicles may be plucked phens												G: colourless glass and slightly brown spherulites																R: partially devitrified/recrystallised				
M063b	4.6	2.3		y	nro	y	y	re						0.2	0.5			0.2	el	e	0.3	95	y	y			y	y	35	1.3	m	V: sinuous
	P: aggs of opx & pl												0																R: low crystal content				
M063c	5.0	2.1		y	nro	y	y	re						0.5	1.1			0.1	st	e	0.3	94	y	y			y	y			n	
	P: some plucked, pl grows around some opx												G: perlitically fractured glass																R: OBSIDIAN				
M064	3.7	1.0		nro		y	y	r						0.1	1.0			0.1	m	s	0.4	96	y	y			y	y	18	3.5	ml	V: varies highly
	P: some open vesicles may be plucked phens												G: patches of br glass																R: low crystal content				
M066	7.1	2.1	?	y	nro	y	y							0.1	0.6			0.1	m	e	0.3	93	y	br	13	0.4	y	y	2	0.3	n	V: virtually none
	P: slight sieve one pl, opx resorbed and dirty												G: spherulite concentration varies, br shade varies																R: dense				
M075	14.1	2.2		y	nro	y	y	r	3.5	1.7	re			0.1	0.5			0.1	m	s	0.3	82	y	y	0.5	0.3	y	y	15	0.7	m	V: width varies
													G: dispersed brown spherulites																			
M078a	15.2	3.2		y	nro	y	y	r	5.1	1.6	re			0.1	0.8			0.1	st	a	0.4	80	n	br	100	0.9	y	s	1	0.1	n	V: lava
	P: opx dirty, some Fe staining, patchwork in pl - igrowth												G: dusty spherulites																R: devitrified lava				
M078b	14.0	2.3		y	nro	y		r	4.0	1.0	r			0.5	1.2			0.1	st	s	0.3	81	n	br	100	1.7	y	s			n	V: lava
	P: opx resorbing, dirty, most phens fragmented												G: dark brown large spherulites																R: pervasively fractured highly devitrified lava				
M080	8.8	2.4		y	nro	y	y	re	1.3	1.7	re			0.1	0.8			0.6	m	a	0.5	89	n	lbr	80	0.4	y	d	20	2.1	n	V: size varies, recryst overprints
	P: some opqs altered opx, some pl fractured												G: dusty, br spherulites going to granoph at edges																R: some Fe staining				
M083	21.1	4.1		y	nro	y	y	re	4.2	1.8	re	0.5	0.8	0.1	0.7			0.1	st	s	0.3	74	n	br	100	0.4	y	s	5	1	n	V: recrystn overprints, plucks?
	P: some opx to opqs, some plucking												G: dusty mosaic of spherulites																R: partly altered, moderate crystal content				

Sample Number	Plagioclase %	Max Pl size (mm)	Pl sieve	Pl glom aggregates	Pl n, r, o zone	Pl inclusions	Pl patchy extinction	Pl rounded/embayed	Quartz %	Max Qtz size (mm)	Qtz rou/emb	Amphibole %	Max Amph size (mm)	Orthopyroxene %	Max Opx size (mm)	Biotite %	Max Biot size (mm)	Opaques %	Opq el, m, st,	Opq e, s, a,	Max Opq size (mm)	Groundmass %	Gmass Clear	Gmass Colourless	Gm spherulites %	Max sph size (mm)	Porphorytic	Hypocrystalline	Vesicularity %	Max vesic size (mm)	Flow banding s, m, l	
M085	18.3	3.2		y	nro	y	y	r	5.0	2.8	re	0.2	1.1	0.8	1.2			0.2	st	e	0.2	76	y	y			y	y	40	1.3	s	V: irregular, open & jagged
	P: aggs of pl, opx &/or Amph, plucking?												G: dusty																R: high vesicularity & moderate crystal content			
M089	9.5	3.8			nro	y	y	r	2.3	1.0	e	0.5	1.5	0.1	0.5			0.1	m	se	0.3	88	y	y	15	0.2	y	y	5	0.2	m	V: sinuous collapsed
													G: spherulites up to 30%																			
M093	18.1	2.5	y	y	nro	y	y	r	7.2	1.7	re	1.2	3.0	0.1	1.2			0.1	m	s	0.3	73	y	y			y	y	17	0.4	m	V: some may be plucked crystals
	P: grubby opx, euhedral Amph, Qtz fract, aggs fine pl &																															
M094	14.4	2.7		y	nro	y	y	r						1.0	1.8			0.1	m	s	0.3	84	n	br	20	0.3	y	d	3	0.3	n	
	P: note fine feld popn under gmass (not incl in % phen)												G: 80% devitrified brown, some to spherulites, some granoph <10%														R: dense					
M096	6.7	2.1		y	nro	y	y	r	2.2	1.2	re			0.6	1.7			0.1	st	e	0.3	90	y	y			y	y	10	1	s	V: overprinted by fracturing
	P: opx tends to ogrow grouped opqs												G: fractured glass														R: some Fe staining					
M098	18.8	3.8		y	nro	y	y	r	12.5	2.3	re	1.3	1.3	1.3	0.5			0.6	st	s	0.4	66	y	y			y	y	20	0.7	sm	V: jagged walls
	P: Qtz fractured, fine aggs of pl & opx - xenolithic?												G: small patches of l br glass														R: crystal rich					
M104	20.0	6.5		y	nro	y		r	3.8	3.1	re	0.6	2.5	0.6	2.9			0.1	st	e	0.3	75	y	y			y	y	20	1	n	V: mostly fracture voids
	P: many phens broken up, some plucking												G: mostly open patches of uninterrupted glass, pervasively fractured														R: partly fractured in thin sectioning					
M106	23.2	4.1		y	nro	y			8.4	2.9	re	0.5	2.3	0.1	0.8			0.1	m	s	0.3	68	n	lbr	90	0.5	y	d	5	2	n	V: recryst masks, big = plucks?
	P: opx going to opqs												G: mostly lbr spherulites going to granoph at edges														R: high crystal content					
M109	20.5	2.8		y	nro	y	y	r	8.0	2.1	re	0.6	1.1	1.1	1.4			0.6	st	a	0.5	69	y	y	5	0.3	y	y	12	0.4	m	V: some jagged
	P: opx often with opq inclns, finer aggs of opx & pl												G: patches of l br glass becoming spherulites														R: slightly spherulitic					
M110	17.8	3.4	y	y	nro	y			4.4	2.2	re	0.6	1.6	0.6	0.9			0.1	st	e	0.3	77	y	y	0.5	0.8	y	y	10	0.3	s	V: elongation varies
	P: aggs of all phases, some broken crystals												G: some fracturing, occasional br spherulites																			
M111	4.1	4.2		y	nro	y	y	r	0.5	1.2	e			0.1	0.3			0.1	m	se	0.5	95	y	y			y	y	2	0.2	s	V: sinuous collapsed
																											R: dense					
M113	10.0	1.9			nro	y	y	re	3.3	1.1	re			0.1	0.7			0.1	m	s	0.3	86	y	y			y	y	10	1	m	V: most collapsed and fine
	P: some pl broken and corroded																										R: finely vesicular					
M114	8.0	3.6			nro	y	y	r	6.0	1.8	e			0.1	0.8			0.1	m	a	1.0	86	n	lbr	70	0.3	y	y			n	V: overprinted by silicification?
	P: some pl rounded intergrowth rim <0.2mm, few broke												G: opaques likely alteration, spherulite conc varies, dusty														R: silicified?					
M115	8.6	2.8		y	nro	y	y	r	3.2	1.8	re			0.1	1.3			0.5	m	e	0.5	88	n	br	100	0.3	y	d	7	0.3	n	V: overprinted by recrystn
	P: some opqs were opx												G: edges of spherulites going to granoph														R: partly devitrified					
M116	4.5	3.0		y	nro	y	y	re	2.3	2.2	re			0.1	1.0			0.1	st	s	0.2	93	y	y			y	y	12	0.3	m	V: varies across
													G: some lbr patches														R: relatively low crystal content					

Sample Number	Plagioclase %	Max Pl size (mm)	Pl sieve	Pl glom aggregates	Pl n, r, o zone	Pl inclusions	Pl patchy extinction	Pl rounded/embayed	Quartz %	Max Qtz size (mm)	Qtz rou/emb	Amphibole %	Max Amph size (mm)	Orthopyroxene %	Max Opx size (mm)	Biotite %	Max Biot size (mm)	Opaques %	Opq el, m, st,	Opq e, s, a,	Max Opq size (mm)	Groundmass %	Gmass Clear	Gmass Colourless	Gm spherulites %	Max sph size (mm)	Porphorytic	Hypocrystalline	Vesicularity %	Max vesic size (mm)	Flow banding s, m, l	
M121	3.5	2.3		nro	y	y	r		0.6	1.3	re		0	0.1	1.3			0.1	st	e	0.3	96	y	y			y	y	15	0.5	l	V: varies collapsed to open
																												R: low crystal content				
M134	8.2	2.3		nro	y		re							0.1	1.0			0.1	st	e	0.2	92	y	y			y	y	15	0.5	l	V: sinuous collapsed
	P: one brown patch may be Amph <0.4mm, few plucks												G: occasion areas of l br glass														R: low crystal content				
M138	7.1	1.9		nro	y	y								0.1	0.4			0.1	st	s	0.2	93	y	y			y	y	30	0.3	sm	V: fine, stubby
	P: occasional plucking												G: dusty																			
M140	10.0	2.0		nro	y	y	r		0.1	0.4	e			0.1	2.1			0.1	st	se	0.3	90	y	y			y	y	20	0.2	s	V: high aspect ratio
	P: opx sub - eu and stubby												G: fibrous glass														moderate to low crystal content				
M145	3.8	2.7		y	nro	y	y	r						0.1	0.6			0.1	st	se	0.2	96	y	y			y	y	20	1	m	V: varies collapsed to open
	P: crystals highly cracked - polishing? Opx altering												G: some brown patches - Fe staining?														R: low crystal content				
M148a	4.7	2.5		y	nro	y		re						0.1	1.3			0.1	st	s	0.2	95	y	y			y	y	15	0.6	m	V: banding varies
	P: aggs of pl & opx																										R: low crystal content				
M148b	4.0	2.1		nro	y	0	r							0.1	0.4			0.1	st	s	0.2	96	y	y			y	y	25	1.5	l	V: anastomosing banding
	P: many likely plucked												G: dispersed l br patches														R: low crystal content - due to plucking?				
M148c	6.2	2.3		y	nro	y		r				0.2	0.4	0.2	0.4			0.2	st	e	0.2	93	y	y			y	y	35	0.4	l	V: elongate and fibrous
	P: pl overgrows opqs & opx sometimes												G:														R: low crystal content				
M152	7.6	2.6		y	nro	y		re						0.1	0.7			0.1	st	se	0.4	92	y	y			y	y	8	0.3	s	V: width & banding vary
	P: pl fractured, opq usually inclusions												G: fine fractured or regrown feld in patches,														R: low crystal content				
M153	3.0	3.9		nro	y	y	r							0.1	1.0			1.0	st	e	0.2	96	y	y	3	2.2	y	y			n	
	P: some opx resorbed & often ogrows opqs												G: clumped dk br spherulites - along cracks?, perlitic fractures														R: OBSIDIAN				
M154	17.8	2.1		y	nro	y	y	r	4.4	2.1	re	0.6	0.8	0.6	0.7			0.1	st	e	0.3	77	y	y	0.5	0.2	y	y	10	0.2	s	V: narrow vesicles
	P: various phases in aggs												G: dusty																			
M157	8.4	2.8	y	y	nro	y								0.5	1.0			0.5	m	s	0.3	91	n	br	40	1	y	d	5	0.2	n	V: overprinted by recrystn
	P: opx dirty & going to opqs												G: dusty recrystallised gmass to spherulites & granoph														R: some Fe staining				
M161	4.2	2.5		y	nro	y	y	r						0.1	1.8			0.1	st	e	0.3	96	y	y			y	y	5	0.1	m	V: overprinted by cracking
	0												G: regular cracking < 0.3 mm, brown patches in places														R: low crystal content				
M172	10.3	2.5		y	nro	y	y							0.1	0.9			0.5	st	s	0.3	89	y	lbr	25	0.4	y	d	3	0.2	n	V: overprinted by recrystn
	P: opx altering to opq, pl damaged												G: dusty, thin at edges - spherulites may be higher %, some granoph																			
M176a	2.4	1.8	?		nr	y		r	0.1	0.5	r			0.1	0.3			0.1	st	e	0.2	97	y	y			y	y	18	0.4	s	V: most rounded & equant
	P: nearly aphyric												G: patches of l br glass														R: very low crystal content				

Sample Number	Plagioclase %	Max Pl size (mm)	Pl sieve	Pl glom aggregates	Pl n, r, o zone	Pl inclusions	Pl patchy extinction	Pl rounded/embayed	Quartz %	Max Qtz size (mm)	Qtz rou/emb	Amphibole %	Max Amph size (mm)	Orthopyroxene %	Max Opx size (mm)	Biotite %	Max Biot size (mm)	Opaques %	Opq el, m, st,	Opq e, s, a,	Max Opq size (mm)	Groundmass %	Gmass Clear	Gmass Colourless	Gm spherulites %	Max sph size (mm)	Porphorytic	Hypocrystalline	Vesicularity %	Max vesic size (mm)	Flow banding s, m, l	
	0.5	1.0			nro	y	y	y						0.1	0.3							99	y	lbr							n	V: non vesicular
M176b	P: not "phenocrysts"												G: l br mud grains														R: LAYERED CLAY					
	13.3	3.3		y	nro	y		r	0.0	?				0.7	1.6			0.1	m	s	0.3	86	y	y			y	y	25	0.3	m	V: elongation varies
M179													G: some brown Fe staining																			
	12.5	3.0			nro	y	y	r						0.1	1.2							87	y	y			y	y	20	0.2	m	V: elongate
M188	P: no opaques?																															
	12.1	4.6	0	y	nro	y		re	0.1	0.8	r			0.5	1.2			0.1	m	s	0.3	87	n	br	40	0.3	y	d	1	0.1	n	V: almost none
M190	P: some fine plag recryst from glass												G: devitrified glass is forming some spherulites, dusty														R: dense					
	5.4	2.3		y	nro	y		re						0.1	0.9			0.1	el	e	0.2	94	y	y			y	y	8	0.4	s	V: overprinted by fracturing
M191	P: some pl fractured, some grubby												G: pervasively fractured, som e recryst to felds														R: low crystal content					
	14.3	3.3		y	nro	y		r	0.1	0.8	r			0.1	1.0			0.1	m	s	0.2	85	n	br	100	4.3	y	s	30		n	V: voids - ves destroyed by sph
M197	P: difficult to estimate %												G: large spherulites with air voids between, dusty														R: strongly devitrified					
	14.0	1.6		y	nro	y	y		2.0	0.8	re			0.2	0.7			1.0	st	e	0.3	83	y	lbr	70	1.8	y	d	50	2.5	n	V: rounded - rotten spherulites?
M198	P: opx going to opqs												G: dusty														R: large voids					
	8.3	3.7		y	nro	y	y	r	2.1	0.8				0.1	1.3			0.5	m	sa	0.8	89	n	br	70		y	d	4	0.4	n	V: equant
M200	P: fine feld recryst glass some opqs are altrn, opx shot												G: brown devitrified glass, most to spherulites														R: devitrified lava, some Fe staining					
	11.1	3.3		y	nro	y		r	2.2	1.3	re			0.1	0.7			0.6	el	a	0.8	86	n	lbr	100	1.7	y	d	10	0.5	n	V: overprinted by recrystn
M207	P: most opqs are alteration, most opx gone												G: brown spherulites grade out into coarse granoph rays														R: partly altered					
	11.1	1.9			nro	y	y	r	1.1	0.4	e			0.1	1.2			0.1	st	sa	0.5	88	y	y	2	0.4	y	y	10		n	V: voids along fracts not vesicles
M211	P: many phens appear fractured												G: spherulites dispersed														R: bread crusted?					
	13.0	2.8		y	nro	y	y	r										0.5	m	a	0.9	87	y	y	40	0.5	y	d			n	V: recrystallised
M212	P: opx likely mostly shot to opq,												G: 30% recryst to granoph, some dusty l brn spherulite, conc varies														R: some Fe staining					
	8.2	2.1		y	nro	y	y	r	2.1	1.6	re			0.1	0.9			0.5	m	e	0.4	89	n	br	100	1.3	y	d	3	0.2	n	V: overprinted by recrystn
M218	P: most opx to opqs, broken crystals												G: dusty, outer spherulites going to granoph														R: partly altered					
	16.7	2.3			nro	y	y	r	2.2	1.5	e			1.1	0.4			0.1	m	sa	0.3	80	y	y			y	y	10	0.4	s	V: irregular & jagged
M223													G: one .3mm l br spherulite																			
	11.6	3.6		y	nro	y		r	2.1	1.5				0.1	0.6			0.5	m	e	0.4	86	y	y	0.1	0.2	y	y	5	0.1	s	V: fracturing overprints ves
M231	P: pl & Qtz some fractured												G: pervasively fractured, occasional spherulites																			
	8.3	2.6		y	nro	y	y	r	1.7	1.0	re			0.2	0.8			0.2	m	s	0.3	90	y	y			y	y	40	2	l	V: vary to open & jagged
M233b	P: most crystals cracked or fractured												0														R: highly vesicular					

Sample Number	Plagioclase %	Max Pl size (mm)	Pl sieve	Pl glom aggregates	Pl n, r, o zone	Pl inclusions	Pl patchy extinction	Pl rounded/embayed	Quartz %	Max Qtz size (mm)	Qtz rou/emb	Amphibole %	Max Amph size (mm)	Orthopyroxene %	Max Opx size (mm)	Biotite %	Max Biot size (mm)	Opaques %	Opq el, m, st,	Opq e, s, a,	Max Opq size (mm)	Groundmass %	Gmass Clear	Gmass Colourless	Gm spherulites %	Max sph size (mm)	Porphorytic	Hypocrystalline	Vesicularity %	Max vesic size (mm)	Flow banding s, m, l	
M236	17.6	3.3	y	y	nro	y	y	r						0.6	1.5			0.1	m	s	0.4	82	y	y			y	y	15	0.3	l	
	P: fine aggs of pl & opx - xenoliths?												G: slight Fe staining, few patches of l br glass																			
M240	11.4	2.3		y	nro	y		r	2.9	2.8	re	0.7	1.5	0.7	1.7			0.1	m	s	0.3	84	y	y			y	y	30	0.9	m	V: vary collapsed to open
	P many opqs in large opx, aggs of all phases																															
M243	9.5	1.3			nro	y	y	r	7.4	1.3	e	0.5	1.0	0.1	1.1			0.1	st	s	0.3	82	y	y			y	y	5	0.4	s	
	P: check for biotite																															
M244	27.5	3.6		y	nro	y								2.0	2.1			1.3	st	s	0.3	69	y	y			y	y	60	0.4	l	V: coarse, fibrous
	P: aggs of all phases, some fine												G: very fresh-looking														R: coarse and very highly vesicular					
M247	5.9	2.3			nro	y	y	r						0.1	0.7			0.1	m	a	0.3	94	y	y			y	y	15	0.8	s	
M254	5.1	2.8	y	y	nro	y	y	r						0.5	1.2			0.1	m	e	0.5	94	y	y			y	y	2	0.1	n	V: almost devoid
	P: some pl broken												R: perlitically fractured obsidian														R: mostly OBSIDIAN					
M258	10.0	2.8			nro	y	y	r	2.9	1.5	e			0.1	0.7			0.1	m	a	0.4	87	y	y			y	y	30	0.2	s	
	P: some crystals are broken												G: open patches of glass slightly br														0					
M260	10.7	3.2			nro	y	y	r	2.7	0.8	e			0.1	1.3			0.1	el	se	0.2	86	y	y			y	y	25	2	s	
M264	7.5	2.5		y	nro	y	y	r	1.1	1.0	re							1.1	m	a	1.0	90	n	br	40	0.6	y	d	7	0.3	n	V: recrystallised
	P: some opq is altrn, possibly rotten opx												G: glass devit brown dusty to spherulites & granoph														R: some Fe staining					
M265	13.0	2.7		y	nro	y	y	r						0.1	0.6			0.5	m	a	0.7	86	n	br	70	2	y	s			n	V: recrystallised
	P: some opq is altrn, opx mostly rotten, some plucking												G: strongly devit to granoph & spherulites														R: some Fe staining					
M267																																
M272	8.3	2.2		y	nro	y	y	r	1.7	1.3	re			0.8	1.1			0.2	el	s	0.3	89	y	y			y	y	40	0.5	ml	V: elongate, some jagged
	P: some fractured, opx in aggs with pl																															
M272a	5.7	0.2		y	nro	y		r	0.7	1.3	re	0.1	0.4	0.7	1.0			0.1	st	e	0.3	93	y	y			y	y	30	3	m	V: fine to huge, some plucks?
	P: some plucking												G: mostly v l br														R: some Fe staining, low crystal content					
M272g	0.7	2.0			nro	y	y	r						0.1	0.3			0.1	m	a	0.4	99	y	y			y	y	30	4	m	V: fine to huge, some plucks?
	P: nearly aphyric - many plucked?												G: mostly v l br, some dust/alteration														R: very low crystal content - plucking?					
M272i	4.3	1.8		y	nro	y	0	r						0.7	1.6			0.1	st	e	0.2	95	n	gy			y	y	30	1.7	m	V: fine to open
	P: aggs of opx & pl												G: gy colour from bubbles in epoxy?														R: high vesicularity & low crystal content					

Sample Number	Plagioclase %	Max Pl size (mm)	Pl sieve	Pl glom aggregates	Pl n, r, o zone	Pl inclusions	Pl patchy extinction	Pl rounded/embayed	Quartz %	Max Qtz size (mm)	Qtz rou/emb	Amphibole %	Max Amph size (mm)	Orthopyroxene %	Max Opx size (mm)	Biotite %	Max Biot size (mm)	Opaques %	Opq el, m, st,	Opq e, s, a,	Max Opq size (mm)	Groundmass %	Gmass Clear	Gmass Colourless	Gm spherulites %	Max sph size (mm)	Porphorytic	Hypocrystalline	Vesicularity %	Max vesic size (mm)	Flow banding s, m, l	
M272j	7.5	4.2	y	nro	y			r						0.3	0.5			0.3	st	e	0.2	92	y	y			y	y	60	1.1	m	V: open & jagged
	P: some probably plucked												G: light brown patches														R: very high vesicularity					
M274																																
M276	2.7	1.7	t	nro	y			re						0.1	0.9			0.1	st	a	0.2	97	n	gy			y	y	25	0.9	l	V: elongate to fibrous
	P: lots of plucking probably												G: gy colour from bubbles in epoxy, l br glass														R: apparent low crystal content					
M281	7.2	1.8	y	nro	y									0.1	0.4			0.1	st	s	0.2	93	y	y	0.1	2.4	y	y	3	0.1	n	V: fracturing overprints
	P: some phens broken												G: pervasively fractured, occasional br spherulites														R: low crystal content					
M282	5.6	1.9		nro	y	y	r		0.5	0.6	e			0.1	0.9			0.1	st	s	0.3	94	y	y			y	y	10	0.1	s	V: collapsed & sinuous
																											R: appears fractured in places - bread crusting?					
M283	4.0	2.1	y	nro	y	y	r							0.1	1.1			0.1	m	s	0.2	96	n	br	35	2.1	y	d			n	V: recrystallised
													G: dusty devitrified to felds & some spherulites														R: dense, low crystal content					
M288	2.7	2.3		nr	y	y								0.1	0.3			0.1	m	s	0.4	97	n	br	100	2.5	y	s	27	3.5	n	V: most dissolved spherulites
	P: most opx gone to opqs, some pl weathered out?												G: dusty br														R: altered and weathered, low crystal content					
M290	5.1	3.7	y	nro	y	y	r							0.1	0.4			0.5	el	a	0.4	94	n	lbr	3	0.4	y	d	1		n	V: recrystallised
	P: some opqs altrn, opx rotting, pl often fractured												G: devitrified to granoph, dusty														R: some Fe staining					
M296	7.8	1.6	y	nro	y	y	r		0.1	0.6	r			0.1	0.7			0.1	st	s	0.3	92	n	br			y	d	10	1	m	V: hard to determine - recryst
	P: sparse fine feld - recrystn product												G: varied darkness and dust in bands of recrystn														R: banded in hspec, areas of Fe pptn					
M297	9.2	1.7	y	nro	y	y	r		2.0	0.8	e	0.5	0.6	1.0	0.9							87	n	br	80	0.6	y	y	2	0.5	n	V: voids may be plucking
	P: Amph & opx euhedral laths												G: some < 0.1 mm recrystn, dusty														R: dense & devitrified					
M299	21.3	5.3		nro	y	y	r		3.8	4.2	e	0.6	0.5	0.6	0.5	1.3	1.3	0.1	st	s	0.4	74	y	y			y	y	20	0.6	m	V: varied, sinuous and wide some
	P: bi has inclusions, some bi partly replaced by pl & opq																										R: high crystal content					
M301	21.3	2.5	y	nro	y	y	r		6.7	3.0	e	1.3	4.1	0.1	0.6	0.1	0.5	0.1	m	s	0.3	70	y	y			y	y	25	0.7	m	
	P: pl in aggs with Amph, many crystals fractured, esp C												G: dispersed l br streaks and patches														R: high crystal content					
M304	18.5	3.1	y	nro	y	y	r		3.3	2.3	e	1.1	2.1	1.1	1.3			0.5	st	sa	0.3	76	y	y	0.1	0.4	y	y	8	0.3	s	V: fine vesicles
	P: Amph & opx euhedral elongate laths												G: dispersed br spherules																			
M308	12.2	2.3	y	nro	y		r		0.6	1.1	re	0.6	0.6	1.1	1.6			0.1	m	se	0.5	85	y	y	1	0.5	y	y	10	0.3	s	V: overprinted by fracturing
	P: aggs of opx & pl												G: dispersed br spherulites														R: fractured					
M309	12.0	3.2		nro	y				3.0	1.8	re	0.1	0.7	0.1	1.3			0.1	m	s	0.3	85	n	lbr	30	0.4	y	d			n	V: recrystallised
	P: some pl grubby												G: dusty recryst to granoph & spherulites														R: devitrified					

Sample Number	Plagioclase %	Max Pl size (mm)	Pl sieve	Pl glom aggregates	Pl n, r, o zone	Pl inclusions	Pl patchy extinction	Pl rounded/embayed	Quartz %	Max Qtz size (mm)	Qtz rou/emb	Amphibole %	Max Amph size (mm)	Orthopyroxene %	Max Opx size (mm)	Biotite %	Max Biot size (mm)	Opaques %	Opq el, m, st,	Opq e, s, a,	Max Opq size (mm)	Groundmass %	Gmass Clear	Gmass Colourless	Gm spherulites %	Max sph size (mm)	Porphorytic	Hypocrystalline	Vesicularity %	Max vesic size (mm)	Flow banding s, m, l	
M313	7.4	3.4		nro	y	y	r		2.1	1.0	e			0.1	1.3	0.0	0.0	0.1	st	se	0.2	90	y	y			y	y	5	0.1	s	
																											R: reasonably dense					
M315	2.9	1.0		nro	y	y	re							0.1	0.4			0.1	st	e	0.2	97	y	y			y	y	30	0.5	s	V: mostly open & jagged
	P: nearly aphyric, many pl resorbed																										R: low crystal content					
M316	7.4	2.2		y	nro	y	y	r	4.2	1.5	e	0.1	2.1	0.1	1.4			0.1	st	e	0.6	88	y	y			y	y	5	0.2	s	
	P: some Qtz highly fractured, Amph & opx elongate												G: some fine crystal fragments or recrystallisation																			
M320	16.3	3.3		y	nro	y	y	r	2.5	2.1	re	1.3	1.0	1.3	1.2			0.1	el	e	0.3	79	y	y			y	y	20	1	m	V: varies
	P: some pl in aggs with opx																															
M321																																
M322	5.2	1.5		nr	y	y	r					0.1	0.3	0.1	0.3			0.1	st	s	0.4	95	y	y	10	0.3	y	y	3	0.1	s	V: overprinted by recrystn
	P: dispersed phens												G: devitrifying to ~20% granoph & to l br spherulites														R: low crystal content					
M325																						100	y	y	0.5	1.5	n	n	0.5	1.5	n	V: rotten spherulites likely
	P: Aphyric												G: flow banded holocrystalline, perlitically fractured														R: OBSIDIAN					
M327	12.0	2.7		y	nro	y	y	r	10.7	2.2	re	0.7	0.8	0.7	0.7			0.1	st	e	0.3	76	y	y	10	0.4	y	y	25	1	n	V: open vesicles
	P: occasional graphic intergrowths												G: dusty, partly devitrifying to br spherulites																			
M330	6.1	2.8	y	t	nro	y								0.5	1.2			0.1	st	s	0.4	93	n	br	80	1.7	y	d	1	0.2	n	V: overprinted by recrystn
	P: grubby opx going to opqs												G: dusty														R: partly altered, Fe staining					
M333	8.2	2.3		y	nro	y	y	r						0.1	0.8			0.1	m	sa	0.7	92	y	lbr	80	1.3	y	d	3	0.3	n	V: overprinted by recrystn
	P: opx highly altered to opq												G: glass recrystallised to granoph and spherulites, banded														R: some Fe staining, low crystal content					
M336	5.0	2.5	0	0	nro	y	y	r										0.2	st	e	0.3	95	y	y			y	y	40	1.1	m	V: flattening varies
													G: some areas slightly brown														R: low crystal content					
M336b	3.5	2.3	y		nro	y								0.1	0.7			0.1	el	e	0.3	96	y	lbr			y	y	15	0.9	m	V: relatively even
	G: plucking, some pl broken												G: br hue varies														R: low crystal content					
M339a	2.9	2.2		nro	y		r							0.1	0.3			0.1	st	s	0.2	97	y	y			y	y	30	1.4	m	V: large vesicles
	P: nearly aphyric												G: dusty														R: very low crystal content					
M339b	0.5	1.5		nr	y																	99	y	y			y	y	8	0.5	n	V: round
	P: nearly aphyric												G: dusty														R: very low crystal content					
M339c	7.2	2.7		y	nro	y	y	r	1.0	1.0	re			0.1	1.1			0.1	st	e	0.2	92	y	y	0.1	0.4	y	y	3	0.2	s	V: elongate
	P: some broken												G: glass perlitically fractured, occasional brown spherulites														R: fractured					

Sample Number	Plagioclase %	Max Pl size (mm)	Pl sieve	Pl glom aggregates	Pl n, r, o zone	Pl inclusions	Pl patchy extinction	Pl rounded/embayed	Quartz %	Max Qtz size (mm)	Qtz rou/emb	Amphibole %	Max Amph size (mm)	Orthopyroxene %	Max Opx size (mm)	Biotite %	Max Biot size (mm)	Opaques %	Opq el, m, st,	Opq e, s, a,	Max Opq size (mm)	Groundmass %	Gmass Clear	Gmass Colourless	Gm spherulites %	Max sph size (mm)	Porphorytic	Hypocrystalline	Vesicularity %	Max vesic size (mm)	Flow banding s, m, l	
M339d	3.2	2.4	y	nro	y	y	r							0.1	0.7			0.1	m	e	0.3	97	y	y			y	y	5	0.5	m	V: size and concentration varies
	P: some pl broken, opx dirty												G: dusty															R: very low crystal content				
M341	5.9	2.3	y	y	nro	y	y	r	1.2	1.2	re			0.1	1.3			0.1	m	s	0.3	93	y	y	0.1	0.5	y	y	15	1	l	V: collapsed to open
	P: some opx rotting to opqs												g: irregular fracturing																		
M342	12.6	2.5	y	nro	y	y	r		1.6	0.9	re							0.5	el	e	<.8	85	n	br	60	<.9	y	d	5	1	s	V: recrystallised, varies
	P: some plucked?, some opqs rotten opx												G: dusty recrystallised to granoph and brown spherulites															R: some Fe staining				
M344	12.9	2.1	y	nro	y	y	r		2.9	1.0	e			0.1	1.0			0.1	st	se	0.3	84	y	y			y	y	30	0.8	s	
M347	10.8	2.3	y	nro	y	y	r		0.5	0.9	re			0.1	0.6			0.5	m	e	0.6	88	y	y	3	1.3	y	y	7	0.2	s	V: fracturing overprints
	P: some opqs altrn (of opx?), opx messy												G: pervasively fractured, dispersed br spherulites																		
M350	7.4	1.8		nro	y	y	r		2.1	1.0	e			0.5	0.9			0.1	st	se	0.3	90	y	y			y	y	5	0.1	s	
																												R: fractured - bread crusted?				
M352	9.1	2.9	y	nro	y		r		0.5	1.2	re			0.5	1.0			0.1	m	s	0.3	90	n	br	95	3	y	s	1	0.2	n	V: overprinted by recrystn
	P: opx dirty & going to opqs												G: br spherulites going to granoph at edges															R: partly altered, some Fe staining				
M357	6.3	4.1	y	nro	y	y	r		0.1	0.7	r							0.5	m	s	1.2	93	n	br	50	0.8	y	d	5	0.3	n	V: recrystallisation overprints
	P: some opqs may be altered opx												G: recrystallised to br spherulites & granoph, some Fe staining															R: partly altered, low crystal content				
M359	8.2	2.6	y	nro	y	y	re							0.1	0.8			0.5	m	s	0.8	91	n	br	50	1.7	y	d	3	0.3	n	V: overprinted by recrystn
	P: some opqs may be altered opx, opx shot												G: recrystallised to br spherulites & granoph, some Fe staining															R: partly altered, some Fe staining				
M360	5.3	2.2		nro	y	y	r		0.5	0.7	e			0.1	2.0			0.1	st	se	0.2	94	y	y			y	y	6	0.1	s	
																												R: finely fractured - bread crusting?				
M362	3.8	3.7	y	y	nro	y		re						0.1	1.6			0.1	m	s	0.2	96	y	y			y	y	20	1.1	m	V: varies
	P: aggs of opx & pl																															
M363	11.4	3.8	y	y	nro	y		r	0.7	1.5	re			0.7	1.0			0.1	m	e	0.5	87	n	br	100	3	y	s	30	2	n	V: voids are eroded spherulites
	P: some opx totally gone to opqs												G: dusty															R: weathering out, some Fe staining				
M364	10.9	2.5	y	nro	y	y	r		0.1	1.1	re			0.5	1.3			0.1	m	s	0.4	88	y	br	3	0.2	y	y	8	0.4	s	V: two domains, one fractured
	P: good euhedral opx												G: one section colourless flow banded glass, rest br fractured															0				
M367	7.3	3.4	y	nro	y	y	re		0.1	1.3	r			0.1	0.7			0.5	el	e	0.7	92	y	y	40	0.4	y	d	4	0.3	n	V: overprinted by recrystn
	P: some opqs alt opx, opx shot, some pl altered, fractur												G: recrystallised to granoph & br spherulites															R: partly altered, some Fe staining				
M370	4.4	2.9		nro	y	y			0.6	1.1	re			0.1	0.4			0.1	st	s	0.4	95	n	br	80	1.1	y	s	10	0.3	s	V: overprinted by recrystn
	P: some pl fractured												G: spherulites & granoph															R: partly altered, some Fe staining				

Sample Number	Plagioclase %	Max Pl size (mm)	Pl sieve	Pl glom aggregates	Pl n, r, o zone	Pl inclusions	Pl patchy extinction	Pl rounded/embayed	Quartz %	Max Qtz size (mm)	Qtz rou/emb	Amphibole %	Max Amph size (mm)	Orthopyroxene %	Max Opx size (mm)	Biotite %	Max Biot size (mm)	Opaques %	Opq el, m, st,	Opq e, s, a,	Max Opq size (mm)	Groundmass %	Gmass Clear	Gmass Colourless	Gm spherulites %	Max sph size (mm)	Porphorytic	Hypocrystalline	Vesicularity %	Max vesic size (mm)	Flow banding s, m, l	
M372	10.1	2.2	y	nro	y				2.0	1.5	re			0.1	1.4			0.1	m	e	0.7	88	n	br	70	2.2	y	d	1	0.1	n	V: overprinted by recrystn
	P: opx altering to opq												G: br spherulites going to granoph at edges = total 100%, dusty to opaque															R: partly altered, some Fe staining				
M373	6.0	3.4	y	nro	y	y	re		3.0	1.4	re			0.5	1.5			0.5	st	a	0.4	90	n	br	95	0.2	y	d			n	V: overprinted by recryst?
	P: some opx altering to opq												G: mostly fine br spherulites with some crystn of plags and granoph														R: partly altered, some Fe staining				
M416	5.0	1.7	y	nro	y	y								0.1	0.9			0.1	st	e	0.2	95	y	lbr			y	y	20	1	m	V: mostly fine & fibrous
	P: some plucking												G: mix of cless & l br glass																			
M418	5.5	2.1	y	nro	y	y	re							0.2	0.4			0.2	st	s	0.2	94	y	y			y	y	45	1.1	m	V: rounded & relatively. even
	P: some plucking																										R: high vesicularity					
M419	8.2	3.2	y	nro	y		r		2.0	1.7	re			0.1	1.2			0.1	m	a	0.4	90	n	br	100	0.3	y	s	2	0.2	n	V: overprinted by recrystn
	P: opx going to opqs												G: dusty														R: partly altered					
M423	6.7	2.1	0	y	nro	y		r						0.2	0.7			0.2	st	s	0.2	93	y	lbr			y	y	40	0.7	m	V: relatively even, open
	P: some pl broken, aggs of pl & opx												G: varies cless to br																			
M424	9.0	2.2	y	nro	y	y	r		1.0	1.0	re			0.1	0.5			0.5	m	a	0.6	89	n	lbr	30	0.4	y	d			n	V: overprinted by recrystn
	P: opx going to opqs												G: recrystallised to br spherulites & granoph, some Fe staining														R: partly altered					
M425	8.2	2.3	y	nro			r		1.0	1.3	re	0.1	0.4	0.1	0.7			0.1	m	e	0.5	91	n	br	70	1.5	y	d	2	0.2	n	V: overprinted by recrystn
	P: aggs of pl & opx												G: recryst to br spherulites & granoph																			
M429	25.0	2.5	y	nro	y				0.5	0.8	re			0.5	0.8			0.5	st	a	0.2	74	y	y			y	y	80	0.8	s	V: round & open, jagged
	P: some pl broken, aggs of pl & opx												G: some brown patches														R: very high vesicularity					
M432a	6.7	2.3		nro	y		r		1.3	1.3	re			0.1	0.9			0.1	st	s	0.2	92	y	y			y	y	25	0.7	m	V: mostly collapsed
	P: some broken																										R: some Fe staining					
M432b	8.2	2.4		nro	y		r		1.0	1.2	re			1.0	1.5			0.1	st	s	0.4	90	y	y			y	y	2	0.2	n	V: round
													G: perlitic fracturing														R: OBSIDIAN					
M433	10.5	2.9	y	nro	y		r		2.1	1.8	re			0.5	0.6			0.1	st	e	0.3	87	n	lbr	40	2	y	d	5	0.8	n	V: weathered spherulites?
	P: aggs of pl & opx, opx going to opqs												G: brown spherulites going to granoph														R: weathering out, some Fe staining					
M439	11.1	2.3	y	nro	y	y	r		0.1	0.8	re			0.5	1.3			0.5	m	s	0.6	88	n	br	40	1.5	y	d	1	0.3	n	V: overprinted by recrystn
	P: aggs of pl & opx, opx going to opqs												G: brown spherulites going to granoph														R: partly altered					
M460	7.0	4.0	y	nro	y	y	r		0.5	1.8	re			0.1	0.5			0.5	m	s	0.7	92	n	br	80	1.8	y	d			n	V: recrystallised
	P: some opqs were opx, some plucks												G: dusty, br spherulites going to granoph at edges, coarse altered cracks														R: partly altered					
M461	5.4	3.9	y	y	nro	y	y	r	0.5	1.1	re			0.1	1.3			0.1	st	e	0.3	94	y	y			y	y	7	0.1	m	V: collapsed & fine
	P: few aggs of pl & opx												G: br patches														R: relatively low crystal content					

Sample Number	Plagioclase %	Max Pl size (mm)	Pl sieve	Pl glom aggregates	Pl n, r, o zone	Pl inclusions	Pl patchy extinction	Pl rounded/embayed	Quartz %	Max Qtz size (mm)	Qtz rou/emb	Amphibole %	Max Amph size (mm)	Orthopyroxene %	Max Opx size (mm)	Biotite %	Max Biot size (mm)	Opaques %	Opq el, m, st	Opq e, s, a,	Max Opq size (mm)	Groundmass %	Gmass Clear	Gmass Colourless	Gm spherulites %	Max sph size (mm)	Porphorytic	Hypocrystalline	Vesicularity %	Max vesic size (mm)	Flow banding s, m, l	
	3.0	2.3			nro	y		r	0.1	0.5	r			0.1	1.4			0.1	el	e	0.3	97	n	lbr			y	d			n	V: recrystallised
M467	P: some broken crystals												G: recrystallised to br granoph, dusty														R: low crystal content					
	2.9	1.8		y	nro	y	y							0.1	0.3			0.1	st	s	0.2	97	y	tbr			y	y	30	0.9	m	V: mostly elongate, sinuous
M470	P: few 2 grain aggs												G: dusty with some br glass														R: low crystal content					
	6.7	2.7		y	nro	y		r	0.1	0.6	r			0.1	1.4			0.1	m	s	0.4	93	y	y	50	1	y	n	10	1	n	V: some = weathering?
M474	0												G: spherulites of coarser granoph, occasional br spherulites																			
	7.3	2.3		y	nro	y		r	1.8	1.8	re			0.2	0.8			0.2	st	e	0.2	91	y	y			y	y	45	0.5	l	V: even, open, elongate
M476	P: opx often ogrows opqs																															
	4.0	2.5		y	nro	y	y	re	0.1	0.9	r			0.1	1.3			0.1	m	s	0.3	96	y	br	90	4	y	d			n	V: recrystallised
M477	P: lots of plucking probably												G: large br spherulites with granoph between														R: partly altered, some Fe staining					
	11.3	3.0	y	y	nro	y	y	r	12.5	3.9	re	0.1	0.8			2.5	1.7	0.1	m	e	0.3	76	y	y			y	y	20	0.7	m	V: most collapsed and fine
M479	P: large phens, lots Qtz																										R: BIOTITE-bearing					
	13.3	2.0	y	y	nro	y	y	re	8.3	1.8	re	0.2	1.3			3.3	1.3	0.2	st	e	0.2	78	y	y			y	y	40	2	m	V: highly varied - damaged?
M481	P: many broken phens												G: polished thin, damaged?														R: high vesicularity, BIOTITE-bearing					

Sample Number	Plagioclase %	Max Pl size (mm)	Pl sieve	Pl glom aggregates	Pl n, r, o zone	Pl inclusions	Pl patchy extinction	Pl rounded/embayed	Olivine %	Max Ol size (mm)	Amphibole %	Max Amph size (mm)	Orthopyroxene %	Max Opx size (mm)	Clinopyroxene %	Max Cpx size (mm)	Opaques %	Opq ei, m, sl,	Opq e, s, a,	Max Opq size (mm)	Groundmass %	Gmass cl, med, opq	Gmass Colour	ig, so, o, is, hy	Max gmass size (mm)	Gmass glass %	Gmass Pl %	Gmass Cpx/Ol %	Gmass Opq %	Porphyritic	Hypocrystalline	Vesicularity %	Max vesic size (mm)	
	25	1.3			nr	y									10	0.5				?	65	op	bk	ig	25u	0	50	20	30	y	y	0		V: dense
M43	P: most < 0.5 mm - could also call gmass, opaques disguised													G: black, some Fe-stained bands																R: basalt lava				
					nr	y			2.1	0.9					3.3	1.4					95	m	dbr	ig	0.6	3	70	20	7	y	y	7	1.5	V: dispersed
M112	P: cpx sub-anhedral, broken													G: plag character above for groundmas crystals																R: basalt lava				
	10	3.3	y	y	nro	y	y	re							5	1	1	m	e	0.4	83	m	dbr	ig	0.2	5	80	10	10	y	y	5	3	V: dispersed
M279	P: some opq is alteratn (some of cpx)													G: lots devitrified to translucent semi birefringent likely felds																R: slightly weathered basalt lava				
	15	1.4			nr		y		2.9	0.2					2.5	0.3				?	79	op	bk	ig	0.1	0	40	30	30	y	y	7	0.4	V: irregular, rounded
M291	P: some vesicles may be plucked phens													G: black																R: basalt lava				
	27	1.8			nr	y	y	re	2.1	0.2					6.1	1.4					58.6	op	bk	ig	0.1	0	30	20	50	y	y	15	1.8	V: large, dispersed
M303	P: some vesicles may be plucked phens, cpx cruddy													G: black																R: basalt scoria				
	3	1.8			nro	y	y	r							0.8	0.4				?	96	op	bk	ig	0.2	0	40	10	40			35	1.8	V: highly vesicular
M326	P: opaques disguised,													G: black, most crystals < 0.2 mm so called gmass here																R: basalt scoria				

APPENDIX 4

XRF Analyses

4.1 Methodology

X-Ray Fluorescence (XRF) analyses were conducted at the University of Canterbury. Samples were crushed and a portion was milled to a fine silt in a tungsten carbide ring mill. Glass fusion beads and compressed powder pellets of this powder were prepared for major and trace element analysis, respectively.

Samples were analysed on a Philips PW2400 x-ray fluorescence spectrometer (sequential sample analysis, wavelength dispersive) using a 3kW Rhodium x-ray tube (end window), operated at 50kV-55mA for major elements and 60kV-46mA for trace elements. The software used was Philips SuperQ Quantitative program. The spectrometer was calibrated using standard reference materials sourced form ANRT(GIT/IWG), CCRMP, GSJ, NIST, SABS, USGS. The analytical methods used are based on Norrish & Hutton (1969), modified by Harvey et. al. (1973) for major elements, and Norrish & Chappell (1977) for trace elements.

4.2 XRF Data

The following table presents the whole-rock XRF data obtained at the University of Canterbury (with an M prefix). Samples with an 'ma' prefix are from G. Corlette's unpublished work and are kindly provided by I. E M. Smith (University of Auckland).

Sample is the location number (Appendix 1), suffixed with a letter code if more than one sample was taken at that location.

Quality Is the sample quality code, as defined in Table 3.1.

Type is the type of sample 'Dome' lava.
'Pumice' or 'Obsidian' from a pyroclastic deposit.
'Lithic (type)' within a pyroclastic deposit.

Location is a description (if any) of the sampling location.

'**Eruptive**' and '**Unit**' are the name of the sample's source eruptive unit, and broader combined unit (if applicable).

Grid is the grid reference ('sheet number'/'easting''northing') in New Zealand map series 260 (1:50,000) map grid coordinates, to the nearest 100 m.

Major elements are expressed as weight percent of their oxide (Fe_2O_3(t) is the sum of FeO_2, recalculated as Fe_2O_3, combined with Fe_2O_3) and recalculated to 'volatile-free' (i.e. with Loss on Ignition (LOI) removed).

Trace element concentrations are given in ppm and any elements below XRF detection limit are marked as 'n.d.' (not detected).

Note that all original totals were in the range 99.5 to 100.5 % to save inclusion of the original totals.

Sample	M010	M012b	M012c	M012e	M022L	M022u	M023	M026	M033	M036	M042	M046	M047	M049	M051
Type	Dome	Pumice	Pumice	Pumice	Pumice	Pumice	Pumice	Pumice	Lithic lava	Pumice	Dome	Pumice	Pumice	Pumice	Dome
Quality	1	1	1	1	1	1	1	1	2	3	1	2	2	1	3
Location	Pukeahua Rd	SH1	SH1	SH1	SH1	SH1	SH1	central north cliffs	lithic W of SH1	airstrip Rd E of SH1	Tram Rd	off Tutukau Rd	top Whakapapa Rd	off Owens Rd	Kakarihi Rd
Deposit	Pukeahua S Dome	Atiamuri lg 2nd from base	Atiamuri lg lower airfall	Atiamuri lg upper airfall	Pukeahua Fan NE	Pukeahua Fan NE	Pukeahua Fan NE	Orakonui pclast	Putauaki pclast	Putauaki pclast	Maroanui W Dome	Putauaki pclast	Orakonui pclast	Cream-coloured lg	Buried Dome
Unit	Pukeahua	Atiamuri	Atiamuri	Atiamuri	Pukeahua	Pukeahua	Pukeahua	Orakonui	Putauaki	Putauaki		Putauaki	Orakonui	Korotai	
Grid	U17/735024	U17/772035	U17/772035	U17/772035	U17/766057	U17/766057	U17/766056	U17/809933	U17/752522	U17/766934	U17/716943	U17/782930	U17/832925	T17/696086	U17/719097
SiO2	72.24	76.03	76.01	74.55	74.00	73.83	74.01	73.92	76.04	73.56	73.81	73.59	72.44	77.40	76.68
TiO2	0.29	0.16	0.16	0.19	0.25	0.27	0.25	0.28	0.21	0.27	0.30	0.28	0.31	0.14	0.19
Al2O3	15.12	13.09	13.05	14.64	14.27	14.34	14.12	14.13	13.65	14.74	14.09	14.18	15.46	12.38	13.03
Fe2O3T	2.38	1.68	1.67	1.89	2.10	2.21	2.12	2.27	1.39	2.17	2.30	2.52	2.53	1.42	1.29
MnO	0.08	0.06	0.06	0.07	0.07	0.06	0.06	0.06	0.07	0.07	0.07	0.07	0.12	0.05	0.02
MgO	0.41	0.12	0.12	0.13	0.33	0.33	0.35	0.24	0.08	0.18	0.32	0.28	0.30	0.10	0.06
CaO	1.88	1.00	0.96	0.98	1.55	1.56	1.55	1.34	1.03	1.24	1.52	1.32	1.47	0.83	1.02
Na2O	4.75	4.23	4.42	4.25	4.42	4.38	4.39	4.53	4.26	4.52	4.38	4.61	4.30	3.68	4.23
K2O	2.81	3.62	3.52	3.28	2.98	2.99	3.12	3.20	3.26	3.18	3.20	3.13	3.01	3.98	3.45
P2O5	0.04	0.01	0.02	0.02	0.02	0.02	0.03	0.02	0.02	0.06	0.02	0.01	0.05	0.01	0.02
(LOI)	1.48	3.13	2.80	3.20	1.88	1.68	2.54	2.07	1.10	1.95	3.21	0.76	2.61	3.49	0.53
(Total)	100.00	100.00	100.00	100.00	100.00	100.00	100.00	100.00	100.00	100.00	100.00	100.00	100.00	100.00	100.00
V	15	6	6	5	15	14	13	11	7	13	12	12	11	7	7
Cr	n.d.	n.d.	n.d.	n.d.	n.d.	n.d.	n.d.	n.d.	n.d.	n.d.	n.d.	n.d.	n.d.	n.d.	n.d.
Ni	4	n.d.	n.d.	n.d.	n.d.	n.d.	n.d.	n.d.	n.d.	n.d.	n.d.	n.d.	n.d.	n.d.	n.d.
Zn	50	51	48	54	48	52	47	51	41	56	54	80	54	44	34
Zr	225	192	188	219	195	205	191	249	246	235	233	251	268	144	199
Nb	10	9	9	11	9	9	9	10	11	9	9	9	10	8	9
Ba	792	815	801	833	759	820	770	733	784	735	740	755	749	793	777
La	18	27	25	22	16	18	21	21	13	8	24	16	31	28	30
Ce	76	63	59	73	52	47	61	55	100	55	66	68	95	73	70
Nd	19	37	35	33	36	22	32	37	21	15	37	38	51	35	30
Ga	16	14	14	16	14	16	15	15	15	15	15	16	16	14	14
Pb	21	21	17	23	18	16	14	17	11	14	15	21	17	18	29
Rb	97	119	117	110	104	99	108	105	120	111	108	111	101	135	122
Sr	144	72	69	70	117	119	113	122	93	113	126	117	130	54	87
Th	11	10	11	14	12	11	12	12	12	6	13	10	12	11	15
Y	29	36	37	37	28	26	31	33	19	12	35	29	47	38	37

Sample	M053	M056	M058	M063a	M063b	M063c	M064	M066	M075	M078a	M078b	M080	M083	M085	M089
Type	Obsidian	Pumice	Pumice	Pumice	Pumice	Pumice	Pumice	Dome	Dome	Dome	Dome	Pumice	Dome	Dome	Dome
Quality	2	2	2	2	1	1	2	3	3	3	5	3	3	3	2
Location	Weka Rd	Atiamuri Rd	Thorpe Rd	Tatua Rd	Tatua Rd	Tatua Rd	Tatua Rd	Tuahu Rd	off Springbok Rd	Springbok Rd	Springbok Rd	Conifer Rd	Plum Rd	Deodar Rd	Deodar Rd
Deposit	Korotai lg obs flamme	Reworked!	Atiamuri lg	Pukeahua Fan SE	Pukeahua Fan SW	Pukeahua Fan SW	Pukeahua Fan SW	Tuahu N Dome	Ngautuku SE Dome	Ngautuku NW Dome	Ngautuku NW Dome	Pukeahua Fan NE	Pukeahua Arc E	Magatutu Dome	Magatutu Dome
Unit	Korotai		Atiamuri	Pukeahua	Pukeahua	Pukeahua	Pukeahua					Pukeahua	Pukeahua		
Grid	U17/701092	U17/770068	U17/792019	U17/728021	U17/728021	U17/728021	U17/722016	U17/774013	U17/737098	U16/731113	U16/731113	U17/733052	U17/751039	U17/763049	U17/757052
SiO2	76.33	76.01	75.07	74.70	75.66	75.95	75.49	76.01	76.36	75.97	76.09	75.91	74.39	74.51	74.39
TiO2	0.17	0.18	0.16	0.24	0.16	0.17	0.17	0.18	0.17	0.18	0.17	0.17	0.25	0.23	0.25
Al2O3	12.83	13.36	14.19	13.71	13.52	12.94	13.64	13.13	13.28	12.89	12.89	13.63	14.00	13.53	13.79
Fe2O3T	1.60	1.75	1.79	1.96	1.74	1.73	1.73	1.73	1.31	1.69	1.67	1.74	2.11	2.01	2.15
MnO	0.05	0.07	0.06	0.06	0.07	0.07	0.06	0.05	0.05	0.06	0.05	0.04	0.06	0.06	0.07
MgO	0.11	0.17	0.12	0.24	0.13	0.15	0.12	0.12	0.11	0.15	0.13	0.05	0.27	0.33	0.31
CaO	1.00	1.01	0.95	1.44	0.98	1.01	0.98	0.96	0.97	1.04	0.94	0.75	1.42	1.58	1.46
Na2O	4.13	3.54	4.31	4.45	4.29	4.57	4.25	4.60	4.25	4.62	4.61	4.05	4.34	4.32	4.41
K2O	3.75	3.90	3.33	3.16	3.43	3.37	3.55	3.20	3.46	3.37	3.44	3.65	3.13	3.38	3.15
P2O5	0.02	0.02	0.01	0.04	0.01	0.02	0.01	0.02	0.02	0.03	0.01	0.02	0.02	0.04	0.02
(LOI)	2.45	3.49	3.24	0.39	3.36	2.87	2.96	0.58	2.82	0.19	0.38	1.07	0.62	1.83	1.16
(Total)	100.00	100.00	100.00	100.00	100.00	100.00	100.00	100.00	100.00	100.00	100.00	100.00	100.00	100.00	100.00
V	7	12	7	16	8	7	4	5	5	7	9	15	15	15	16
Cr	n.d.	n.d.	n.d.	n.d.	n.d.	n.d.	n.d.	n.d.	n.d.	n.d.	n.d.	n.d.	n.d.	n.d.	n.d.
Ni	n.d.	4	n.d.	n.d.	n.d.	n.d.	n.d.	n.d.	n.d.	n.d.	n.d.	n.d.	n.d.	n.d.	n.d.
Zn	46	55	52	31	52	48	52	39	44	45	34	26	43	43	45
Zr	188	199	199	180	198	196	199	174	184	182	179	178	191	179	210
Nb	9	10	10	9	9	9	10	10	10	10	10	10	9	8	9
Ba	792	780	759	767	808	760	817	811	776	778	774	712	771	752	760
La	23	24	24	23	27	26	23	20	22	24	21	13	26	21	21
Ce	73	69	81	53	67	70	76	54	74	64	52	61	63	63	66
Nd	21	15	32	37	37	37	31	25	25	39	22	20	46	18	20
Ga	13	15	16	16	15	15	15	15	15	15	15	16	15	14	14
Pb	24	21	20	80	16	16	20	18	19	19	19	12	13	15	17
Rb	133	121	112	109	114	113	114	99	118	109	121	130	88	113	108
Sr	81	74	67	112	69	73	70	76	74	76	73	65	110	115	109
Th	13	12	9	12	8	9	12	11	12	12	13	9	10	7	13
Y	31	37	36	21	40	36	37	24	37	35	24	12	30	31	29

Sample	M093	M094	M096	M098	M104	M106	M109	M110	M111	M113	M114	M115	M116	M121	M134b
Type	Dome	Dome	Dome	Dome	Dome	Dome	Dome	Dome	Dome	Pumice	Dome	Dome	Pumice	Pumice	Pumice
Quality	3	3	2	1	1	2	1	2	2	1	3	3	3	3	2
Location	Thorpe Rd	Mokai Quarry	Whangapoa Rd	Thorpe Rd	Pukeahua Rd	Arcuate structure	East side	East side	Mahogany Rd	Manawa Rd	off Tirohanga Rd	North bluffs	Pepper Rd	Manawa Rd	Rosewood Rd
Deposit	Thorpe 1 Dome	Mokai Quarry Dome	Ngautuku SE Dome	Thorpe 2 Dome	Pukeahua S Dome	Pukeahua Arc SE	Pukeahua E Dome	Pukeahua E Dome	Pukeahua W Dome	Pukeahua Fan NW	Pohaturoa Dome	Pukeahua W Dome	Pukeahua Fan NW	Pukeahua Fan NW	Airfall
Unit					Pukeahua	Pukeahua	Pukeahua	Pukeahua	Pukeahua	Pukeahua		Pukeahua	Pukeahua	Pukeahua	
Grid	U17/739060	U17/727057	U17/741088	U17/755053	U17/732025	U17/738029	U17/745033	U17/746038	U17/717023	T17/695042	U17/731067	U17/722048	U17/707044	T17/696037	U17/731015
SiO2	73.96	73.21	75.38	73.87	73.12	74.79	73.97	74.24	75.41	75.98	76.08	76.08	76.40	75.99	75.08
TiO2	0.26	0.31	0.18	0.25	0.25	0.24	0.26	0.24	0.19	0.17	0.18	0.17	0.16	0.17	0.17
Al2O3	14.06	13.86	13.67	14.14	14.87	13.66	13.87	13.87	13.57	12.91	12.93	12.92	12.72	12.92	14.06
Fe2O3T	2.18	2.62	1.83	2.12	2.15	2.01	2.15	2.07	1.81	1.71	1.67	1.68	1.66	1.70	1.82
MnO	0.07	0.07	0.06	0.07	0.07	0.06	0.07	0.07	0.06	0.06	0.04	0.05	0.06	0.06	0.07
MgO	0.38	0.45	0.17	0.34	0.35	0.29	0.35	0.33	0.15	0.16	0.11	0.13	0.15	0.17	0.12
CaO	1.55	2.11	1.02	1.58	1.68	1.45	1.64	1.58	1.02	1.05	0.92	0.93	1.01	1.02	0.98
Na2O	4.43	4.51	4.34	4.47	4.54	4.36	4.64	4.47	4.33	4.30	4.57	4.56	4.15	4.20	4.37
K2O	3.09	2.77	3.33	3.11	2.91	3.12	3.00	3.09	3.42	3.62	3.44	3.44	3.65	3.77	3.31
P2O5	0.02	0.08	0.01	0.04	0.05	0.02	0.05	0.03	0.03	0.02	0.07	0.03	0.02 *		0.02
(LOI)	2.11	0.48	2.48	1.94	1.52	0.56	1.34	1.49	2.27	2.39	0.36	0.35	2.17	2.50	2.92
(Total)	100.00	100.00	100.00	100.00	100.00	100.00	100.00	100.00	100.00	100.00	100.00	100.00	100.00 *		100.00
V	15	14	7	14	14	12	17	13	7	8	6	7	8	10	6
Cr	n.d.	n.d.	n.d.	n.d.	n.d.	n.d.	n.d.	n.d.	n.d.	n.d.	n.d.	n.d.	n.d.	n.d.	n.d.
Ni	5	n.d.	n.d.	n.d.	4	n.d.	n.d.	n.d.	5	n.d.	n.d.	n.d.	n.d.	3	n.d.
Zn	49	49	53	46	45	31	45	45	52	48	42	38	68	46	54
Zr	199	191	194	196	196	168	197	187	192	180	177	176	178	174	206
Nb	9	7	9	9	9	9	9	9	9	9	9	9	9	9	10
Ba	792	633	835	772	811	758	777	769	845	776	757	746	750	760	918
La	20	16	26	22	19	16	27	19	22	29	25	26	26	24	28
Ce	62	52	75	65	69	52	63	69	63	66	73	66	70	76	72
Nd	33	22	27	23	26	18	19	31	40	32	34	29	33	32	27
Ga	14	15	15	15	16	15	15	15	15	14	14	15	14	13	15
Pb	19	16	20	19	19	12	18	15	20	19	16	36	16	18	21
Rb	107	102	115	108	101	91	104	105	117	120	120	115	120	121	113
Sr	115	159	75	115	126	110	120	117	73	74	72	74	74	72	70
Th	12	10	10	12	8	9	12	10	12	13	13	11	9	10	14
Y	28	26	37	34	29	23	32	29	39	37	34	31	40	38	37

Sample	M138	M140	M145	M148a	M148b	M148c	M152	M153	M154	M157	M161	M172	M176a	M176b	M179
Type	Pumice	Dome	Dome	Pumice	Pumice	Pumice	Dome	Dome	Pumice	Dome	Dome	Dome	Obsidian	Pumice	Dome
Quality	3	3	3	2	2	2	3	4	3	5	3	5	2	2	3
Location	off Poplar Rd	Poplar Rd	Poplar Rd	Poplar Rd	Poplar Rd	Poplar Rd	Sitka Rd	Sitka Rd	Tatua Rd	View Rd	Cedar Rd	View Rd	Owens Rd	Owens Rd	Almond Rd
Deposit	Pukeahua Fan SW	Poplar Dome	Poplar Dome	Poplar Rd Basal lg	Poplar Rd Airfall	Poplar Rd Lithic obsidian	View Dome	View Dome	Pukeahua Fan SE	Almond Dome NW	Kemp Dome W	View Dome S	Obsidian-rich lg	Obsidian-rich lg	Almond Dome
Unit	Pukeahua	MWC	MWC				MWC	MWC	Pukeahua	MWC	MWC	MWC	Korotai	Korotai	MWC
Grid	U17/717006	U17/720990	U17/728989	U17/724999	U17/724999	U17/724999	U17/734002	U17/735011	U17/751022	U17/749000	U17/758008	U17/741995	T17/696095	T17/696095	U17/755990
SiO2	75.68	74.52	75.49	75.87	74.66	74.55	75.22	76.03	72.77	75.79	74.56	75.95	76.30	76.06	73.18
TiO2	0.16	0.18	0.15	0.17	0.20	0.19	0.18	0.16	0.28	0.17	0.19	0.17	0.18	0.18	0.22
Al2O3	13.42	14.65	14.08	13.52	14.84	15.04	13.83	13.00	15.29	13.41	14.32	13.13	12.90	12.84	15.98
Fe2O3T	1.67	1.83	1.39	1.51	1.82	1.72	1.80	1.68	2.34	1.76	1.94	1.78	1.66	1.65	2.12
MnO	0.06	0.06	0.05	0.06	0.06	0.06	0.07	0.06	0.07	0.06	0.08	0.06	0.05	0.06	0.07
MgO	0.15	0.15	0.13	0.12	0.16	0.16	0.12	0.07	0.39	0.12	0.15	0.14	0.10	0.15	0.17
CaO	1.03	0.97	0.94	1.01	1.03	1.05	0.99	1.02	1.62	0.89	1.05	0.87	1.05	1.12	0.97
Na2O	4.38	4.39	4.51	4.26	3.85	4.21	4.48	4.64	4.36	4.44	4.51	4.47	4.34	4.34	4.26
K2O	3.42	3.21	3.23	3.46	3.37	3.02	3.28	3.31	2.84	3.34	3.18	3.40	3.40	3.56	3.01
P2O5	0.02	0.02	0.02	0.02	0.02	0.01	0.02	0.02	0.04	0.02	0.01	0.02	0.02	0.03	0.02
(LOI)	2.94	2.74	2.75	3.35	4.10	3.67	2.44	0.55	2.57	1.11	2.87	0.52	1.76	0.54	3.76
(Total)	100.00	100.00	100.00	100.00	100.00	100.00	100.00	100.00	100.00	100.00	100.00	100.00	100.00	100.00	100.00
V	8	4	5	4	8	6	6	5	15	9	6	10	9	8	5
Cr	n.d.	n.d.	n.d.	n.d.	n.d.	n.d.	n.d.	n.d.	n.d.	n.d.	n.d.	n.d.	n.d.	n.d.	n.d.
Ni	n.d.	4	n.d.	n.d.	n.d.	n.d.	n.d.	n.d.	n.d.	n.d.	n.d.	n.d.	n.d.	n.d.	n.d.
Zn	54	55	46	47	50	53	52	48	46	39	53	38	45	45	61
Zr	200	208	225	192	223	215	205	191	206	199	220	197	187	188	240
Nb	10	10	11	10	10	10	10	9	9	10	10	10	8	9	12
Ba	791	864	810	778	762	783	794	775	826	769	827	747	792	772	989
La	23	25	23	25	34	26	24	26	21	16	22	20	23	23	21
Ce	69	55	74	64	67	68	73	70	65	62	88	61	63	67	72
Nd	34	52	30	37	49	32	28	32	36	27	30	23	19	25	29
Ga	14	16	15	15	18	17	15	15	16	15	16	15	14	14	18
Pb	18	20	19	17	19	20	20	18	14	15	21	38	17	22	23
Rb	112	112	111	109	107	102	115	113	97	102	108	113	134	131	106
Sr	70	72	69	73	76	80	73	75	124	69	80	69	83	85	73
Th	12	12	10	11	12	10	15	10	10	8	10	9	14	14	14
Y	37	38	35	37	45	35	37	37	36	28	37	26	30	31	35

Sample	M188	M190	M191	M197	M198	M200	M207	M211	M212	M218	M223	M231	M233b	M236	M240
Type	Dome	Dome	Dome	Dome	Dome	Dome	Dome	Dome	Dome	Dome	Dome	Dome	Pumice	Dome	Dome
Quality	2	5	3	4	5	5	5	3	3	3	1	2	3	2	2
Location	SH1	Tuahu Rd	Tuahu Rd	Fletchers Rd	off Lemon Rd	Mandarin Rd	Pouaru Rd	Pouaru Rd	Pouaru Rd	E Maroanui Dome	W Maroanui Dome	Maroanui S Dome	Tram Rd	Palm Rd	Matthews Rd
Deposit	Kemp Dome SE	Tuahu S Dome	Tuahu C Dome	Hauwai Dome NW	Hauwai Dome E	Mandarin Dome NW	Mandarin Dome E	Wilson Dome E	Wilson Dome	Maroanui Domes	Maroanui Domes	Maroanui Domes	Airfall	Palm Dome	Mokauteure Dome E
Unit	MWC			MEC	MEC	MEC	MEC	MEC	MEC					Acacia	Acacia
Grid	U17/771003	U17/778010	U17/774009	U17/775003	U17/789999	U17/797017	U17/818009	U17/833009	U17/828008	U17/740939	U17/729945	U17/722928	U17/716943	T17/683976	U17/892952
SiO2	75.58	76.00	73.09	75.48	75.32	75.81	76.04	73.96	75.66	76.14	74.59	74.60	74.10	72.91	74.70
TiO2	0.17	0.17	0.22	0.20	0.19	0.18	0.18	0.20	0.19	0.17	0.20	0.21	0.27	0.32	0.24
Al2O3	13.32	13.14	16.04	13.40	13.63	13.49	13.08	14.95	13.25	12.82	14.01	14.02	13.74	14.20	13.58
Fe2O3T	1.74	1.71	2.13	1.83	1.83	1.78	1.88	2.03	1.80	1.71	1.90	1.93	2.25	2.80	2.21
MnO	0.06	0.06	0.08	0.07	0.07	0.06	0.03	0.07	0.06	0.06	0.07	0.07	0.08	0.08	0.06
MgO	0.13	0.11	0.15	0.15	0.15	0.05	0.08	0.17	0.09	0.14	0.20	0.20	0.32	0.45	0.32
CaO	1.00	0.91	1.00	1.06	1.06	0.87	0.90	1.10	0.94	0.99	1.24	1.21	1.50	2.03	1.67
Na2O	4.39	4.54	4.25	4.69	4.61	4.45	4.43	4.46	4.63	4.51	4.60	4.56	4.25	4.40	4.20
K2O	3.57	3.33	3.02	3.09	3.10	3.29	3.35	3.03	3.36	3.43	3.15	3.18	3.45	2.78	3.00
P2O5	0.03	0.02	0.02	0.02	0.03	0.02	0.02	0.02	0.02	0.03	0.03	0.02	0.05	0.03	0.02
(LOI)	2.40	0.58	3.52	0.49	0.50	0.77	0.54	2.66	0.63	0.38	1.99	1.58	2.61	1.83	2.15
(Total)	100.00	100.00	100.00	100.00	100.00	100.00	100.00	100.00	100.00	100.00	100.00	100.00	100.00	100.00	100.00
V	7	8	8	7	8	9	8	7	9	8	9	9	10	18	12
Cr	n.d.	n.d.	n.d.	n.d.	n.d.	n.d.	n.d.	n.d.	n.d.	n.d.	n.d.	n.d.	n.d.	n.d.	n.d.
Ni	n.d.	3	n.d.	n.d.	4	n.d.	4	n.d.	n.d.	3	n.d.	n.d.	n.d.	n.d.	n.d.
Zn	51	38	61	46	46	34	61	72	28	39	50	51	56	53	45
Zr	197	194	242	211	203	196	191	223	195	176	198	206	236	194	172
Nb	9	10	12	10	10	11	8	11	10	10	10	10	9	7	6
Ba	801	797	996	821	819	789	732	921	773	749	823	842	729	665	679
La	22	20	19	23	21	22	31	26	12	25	24	20	25	17	20
Ce	71	54	83	68	70	54	85	76	54	68	70	68	76	51	48
Nd	24	23	24	22	28	19	53	31	20	27	22	28	23	24	14
Ga	15	14	18	15	16	15	14	17	15	14	16	15	15	14	14
Pb	18	16	22	19	19	18	13	21	17	16	18	19	14	17	14
Rb	115	109	103	90	84	101	114	104	113	109	108	109	112	98	104
Sr	73	73	80	83	83	72	74	85	75	71	94	91	120	159	128
Th	11	11	15	13	12	14	12	13	13	12	12	11	9	11	9
Y	40	24	33	34	29	21	64	37	22	33	38	35	37	25	25

Sample	M243	M244	M247	M254	M258	M260	M264	M265	M267	M272	M272a	M272g	M272i	M272j	M274
Type	Dome	Dome	Dome	Dome	Pumice	Dome	Dome	Dome	Pumice	Pumice	Pumice	Pumice	Pumice	Pumice	Pumice
Quality	1	5	3	4	2	3	5	5	2	3	3	3	3	3	2
Location	off Aspen Rd	Aspen Rd	Monterey Rd	Goldies Rd	off Saddle Rd	off Saddle Rd	off Saddle Rd	Baldy Rd	S Ohakuri Ignimbrites	SH1	SH1	SH1	SH1	SH1	SW on Tram Rd
Deposit	Mokauteure Dome	Mokautere Dome N	Goldies Dome SW	Hind Dome S	Airfall	Roy N Dome W	Rusty Dome	Rusty Dome N	Souther Ohakuri	Atiamuri Ig	Atiamuri Ig basal airfall	Atiamuri Ig coarse airfall	Atiamuri Ig airfall	Atiamuri Ig	Orakonui pclast
Unit	Acacia	Acacia	MWC	MWC		MEC	MEC	MEC	Ohakuri	Atiamuri	Atiamuri	Atiamuri	Atiamuri	Atiamuri	Orakonui
Grid	T17/679944	T17/682957	U17/701949	U17/729959	U17/785965	U17/780962	U17/781969	U17/781969	U17/780046	U17/772028	U17/772028	U17/772028	U17/772028	U17/772028	U17/783909
SiO2	76.59	72.87	74.83	75.77	73.51	75.28	74.95	75.78	73.32	76.01	75.68	75.80	75.90	75.74	75.85
TiO2	0.17	0.31	0.18	0.17	0.23	0.19	0.21	0.19	0.27	0.17	0.18	0.17	0.16	0.17	0.17
Al2O3	12.90	13.97	14.28	13.13	15.32	13.51	14.88	13.50	14.54	13.00	13.46	13.28	13.29	13.42	13.75
Fe2O3T	1.55	2.74	1.86	1.73	2.09	1.83	1.94	1.70	2.32	1.68	1.76	1.93	1.76	1.81	1.58
MnO	0.05	0.08	0.06	0.06	0.07	0.06	0.07	0.05	0.08	0.06	0.06	0.06	0.06	0.07	0.05
MgO	0.17	0.47	0.15	0.15	0.19	0.16 *		0.05	0.29	0.14	0.17	0.14	0.14	0.13	0.13
CaO	1.10	2.11	0.97	1.04	1.13	1.06	0.80	0.91	1.64	1.05	1.06	0.97	0.99	0.95	1.02
Na2O	4.05	4.62	4.31	4.61	4.41	4.61	3.90	4.49	3.72	4.26	4.11	3.93	3.99	4.14	3.79
K2O	3.41	2.76	3.33	3.32	3.03	3.26	3.22	3.29	3.77	3.60	3.50	3.70	3.68	3.54	3.63
P2O5	0.02	0.06	0.02	0.01	0.03	0.02	0.02	0.03	0.05	0.02	0.02	0.02	0.02	0.01	0.02
(LOI)	2.05	1.10	2.93	0.97	3.65	2.60	1.54	0.58	3.96	2.24	3.37	3.58	3.13	2.80	2.66
(Total)	100.00	100.00	100.00	100.00	100.00	100.00 *		100.00	100.00	100.00	100.00	100.00	100.00	100.00	100.00
V	8	15	8	4	8	6	11	8	14	7	8	6	6	7	7
Cr	n.d.	n.d.	n.d.	n.d.	n.d.	n.d.	n.d.	n.d.	n.d.	n.d.	n.d.	n.d.	n.d.	n.d.	n.d.
Ni	n.d.	n.d.	n.d.	3	4	n.d.	n.d.	n.d.	n.d.	n.d.	n.d.	n.d.	n.d.	n.d.	n.d.
Zn	36	49	66	48	60	49	85	30	59	48	51	54	55	56	46
Zr	140	193	212	191	235	204	215	197	244	175	188	194	200	203	172
Nb	7	7	10	9	11	10	11	10	9	9	9	9	9	10	8
Ba	721	623	838	768	933	778	1016	835	823	794	824	775	786	798	816
La	22	22	22	27	26	18	17	21	23	26	24	23	27	29	22
Ce	56	54	76	59	71	69	65	52	71	64	61	74	68	75	60
Nd	28	21	37	28	32	33	n.d.	37	33	37	26	28	32	39	26
Ga	13	15	15	15	17	15	15	15	16	14	14	14	15	15	14
Pb	17	13	25	17	22	19	46	17	19	21	19	20	19	17	19
Rb	122	97	113	112	104	111	107	111	111	119	117	118	118	116	130
Sr	80	159	72	76	88	81	73	79	134	75	76	67	70	68	82
Th	11	7	13	9	12	12	14	11	12	13	12	11	9	10	13
Y	26	26	37	36	35	36	24	18	34	37	39	38	40	39	28

Sample	M276	M281	M282	M283	M288	M290	M296	M297	M299	M301	M304	M308	M309	M313	M315
Type	Pumice	Dome	Dome	Dome	Dome	Dome	Dome	Dome	Dome	Dome	Dome	Dome	Dome	Dome	Dome
Quality	2	4	3	5	5	5	5	5	1	2	2	3	3	2	3
Location	SW on Tram Rd	Tutukau Rd	Under Putauaki lg	Farm track	Summit track	Summit track	Western ridge	off Whakapapa Rd	off Orakeikorako Rd	off Orakeikorako Rd	Pakuri Dome	Mangatoetoe Dome	Farm track	SH1	Forest Rd
Deposit	Orakonui pclast	Waipakipaki Dome S	Goose Dome	Tutukau Dome	Whakapapaaringa Dome	Whakapapaaringa Dome	Whakapapaaringa Dome	Whakapapa Dome	Kakuki Dome	Orakeikorako Dome	Pakuri Domes	Pakuri Domes	Vicki Dome SE	Bee Hive Dome	Forest NE Ridge
Unit	Orakonui	MEC	MEC	Indep SE				Indep SE	Indep SE	Indep SE	Pakuri	Pakuri	Pakuri		Southern
Grid	U17/788907	U17/772937	U17/759931	U17/808938	U17/852933	U17/854933	U17/846934	U17/833939	U17/830954	U17/838957	U17/803951	U17/805965	U17/816974	U17/753953	U17/729900
SiO2	75.86	75.64	74.37	75.86	75.95	75.89	75.48	74.82	73.34	73.71	73.28	74.64	75.04	75.53	76.83
TiO2	0.19	0.21	0.23	0.17	0.17	0.17	0.18	0.28	0.27	0.28	0.23	0.22	0.22	0.18	0.13
Al2O3	13.17	13.20	14.74	13.23	13.32	13.02	13.51	13.51	14.20	13.89	15.26	13.76	13.58	13.33	12.67
Fe2O3T	1.80	1.71	1.86	1.83	1.68	1.74	1.84	2.03	2.16	2.28	2.12	1.96	1.96	1.80	1.49
MnO	0.06	0.06	0.06	0.04	0.05	0.06	0.04	0.05	0.06	0.07	0.07	0.07	0.06	0.07	0.05
MgO	0.18	0.18	0.21	0.06	0.09	0.10	0.09	0.25	0.45	0.48	0.27	0.25	0.23	0.14	0.07
CaO	1.25	1.27	1.22	0.99	1.03	1.08	1.07	1.33	2.14	2.04	1.31	1.34	1.21	1.00	0.86
Na2O	3.70	4.22	3.99	4.19	4.14	4.36	4.06	4.18	4.31	4.16	4.42	4.59	4.49	4.58	3.95
K2O	3.75	3.49	3.31	3.61	3.55	3.56	3.71	3.51	2.99	3.01	3.02	3.14	3.18	3.33	3.92
P2O5	0.02	0.02	0.02	0.02	0.02	0.02	0.02	0.04	0.07	0.07	0.02	0.03	0.02	0.02	0.01
(LOI)	2.37	1.15	3.84	1.12	-0.17	0.23	2.37	0.45	1.06	1.06	2.16	1.66	0.54	2.15	3.03
(Total)	100.00	100.00	100.00	100.00	100.00	100.00	100.00	100.00	100.00	100.00	100.00	100.00	100.00	100.00	100.00
V	7	9	5	7	5	5	6	16	20	24	10	11	10	7	4
Cr	n.d.	n.d.	n.d.	n.d.	n.d.	n.d.	n.d.	n.d.	n.d.	n.d.	n.d.	n.d.	n.d.	n.d.	n.d.
Ni	n.d.	n.d.	n.d.	n.d.	n.d.	n.d.	n.d.	n.d.	3	n.d.	n.d.	n.d.	n.d.	n.d.	n.d.
Zn	46	41	49	66	41	43	46	39	36	37	53	48	37	51	45
Zr	196	190	211	198	196	194	200	209	149	153	213	197	189	203	152
Nb	7	7	8	9	8	9	9	9	7	7	10	9	10	10	8
Ba	759	771	776	783	774	783	763	727	821	829	892	730	754	798	814
La	29	22	20	20	31	23	21	19	16	19	23	19	16	26	24
Ce	64	47	61	47	59	52	68	55	53	66	65	63	43	79	55
Nd	35	36	22	30	33	31	34	28	13	15	39	27	15	33	31
Ga	13	13	16	14	14	13	14	15	14	13	16	14	15	15	13
Pb	17	20	19	29	20	19	24	18	15	13	19	18	14	21	22
Rb	128	127	120	128	125	130	127	130	105	106	104	109	100	115	135
Sr	106	108	103	88	90	95	96	105	159	151	100	101	94	73	65
Th	11	14	13	13	11	13	13	14	11	9	13	10	11	12	14
Y	28	26	31	25	26	28	30	22	19	18	32	31	23	38	34

Sample	M316	M320	M321	M322	M325	M327	M330	M333	M336	M336	M339a	M339b	M339c	M339d	M341
Type	Dome	Dome	Dome	Dome	Obsidian	Dome	Dome	Dome	Pumice	Pumice	Pumice	Pumice	Obsidian	Pumice	Dome
Quality	2	3	2	3	2	3	5	5	2	2	2	2	1	2	2
Location	Farm track	Farm track	Farm track	Summit track	Poihipi Rd	Summit track	Goldies Rd	Goldies Rd	Manawa Rd	Manawa Rd	off Thorpe Rd	off Thorpe Rd	off Thorpe Rd	off Thorpe Rd	Pouaru Rd
Deposit	Oruanui dome	Forest Dome	Forest S Dome	Forest W Dome	Ben Lomond Dome	Lowrie Dome	Goldies Dome E	Milner Dome SE	Manawa Ig	Manawa Ig	Atiamuri Ig unwelded	Atiamuri Ig airfall	Atiamuri Ig fiamme	Unknown Ig near At Ig	Btwn Bush & MECs
Unit	Southern	Southern	Southern	Southern	Southern	Southern	MWC	MWC	Pukeahua	Pukeahua	Atiamuri	Atiamuri	Atiamuri	Atiamuri	Bush/SE
Grid	U17/723878	U17/725891	U17/722887	U17/718883	U17/674866	U17/685884	U17/720953	U17/716965	U17/706008	U17/706008	U17/795024	U17/796025	U17/795026	U17/798027	U17/811001
SiO2	74.64	73.78	71.72	76.57	76.75	76.17	75.79	76.02	76.14	75.33	75.01	75.24	75.87	76.42	75.66
TiO2	0.24	0.28	0.31	0.13	0.18	0.17	0.17	0.18	0.17	0.18	0.18	0.18	0.18	0.18	0.18
Al2O3	14.21	14.20	16.36	13.38	12.57	13.11	13.61	13.30	13.21	14.38	12.72	13.16	12.99	12.79	13.63
Fe2O3T	1.91	2.28	2.55	1.32	1.42	1.56	1.74	1.74	1.76	1.75	1.66	1.74	1.72	1.68	1.79
MnO	0.06	0.07	0.08	0.05	0.05	0.05	0.06	0.06	0.05	0.04	0.07	0.06	0.06	0.06	0.06
MgO	0.30	0.37	0.40	0.07	0.17	0.16	0.11	n.d.	0.11	0.09	0.21	0.15	0.14	0.13	0.15
CaO	1.43	1.77	1.81	0.78	1.14	1.17	0.86	0.85	0.90	0.86	0.99	1.03	1.03	0.99	1.05
Na2O	4.10	4.34	4.15	3.96	4.23	4.24	4.38	4.46	4.17	3.91	5.37	4.78	4.66	4.25	4.18
K2O	3.08	2.88	2.59	3.72	3.45	3.33	3.26	3.36	3.46	3.45	3.77	3.62	3.32	3.47	3.31
P2O5	0.02	0.03	0.03	0.02	0.03	0.03	0.02	0.02	0.02	0.02	0.03	0.03	0.03	0.02	0.01
(LOI)	1.55	2.00	2.93	2.26	0.47	1.28	0.70	0.53	2.76	3.68	2.67	2.62	1.29	3.29	3.83
(Total)	100.00	100.00	100.00	100.00	100.00	100.00	100.00	100.00	100.00	100.00	100.00	100.00	100.00	100.00	100.00
V	12	13	14	6	8	7	6	8	5	8	5	5	7	7	6
Cr	n.d.	n.d.	n.d.	n.d.	n.d.	n.d.	n.d.	n.d.	n.d.	n.d.	n.d.	n.d.	n.d.	n.d.	n.d.
Ni	5	n.d.	n.d.	n.d.	n.d.	n.d.	n.d.	n.d.	4	n.d.	n.d.	n.d.	n.d.	3	n.d.
Zn	42	48	51	47	35	43	35	36	45	42	51	51	49	50	53
Zr	175	190	212	129	163	144	195	199	201	212	177	186	194	192	200
Nb	8	7	9	7	7	6	11	10	10	n.d.	9	9	9	9	9
Ba	808	677	733	927	697	709	844	831	779	740	596	655	768	774	746
La	18	17	19	27	22	23	26	16	29	26	13	18	23	27	23
Ce	54	45	59	65	43	52	57	48	73	68	61	56	65	75	67
Nd	32	n.d.	14	29	26	27	15	13	42	41	25	24	28	33	34
Ga	14	14	16	14	13	13	16	15	14	17	12	13	14	14	16
Pb	17	15	19	22	16	18	14	17	24	25	20	23	20	20	20
Rb	112	105	95	131	124	121	88	108	116	113	131	126	115	117	112
Sr	112	137	141	55	86	90	70	70	71	69	70	74	77	71	78
Th	12	11	14	15	13	14	10	12	11	11	9	11	13	12	10
Y	23	24	24	29	23	25	21	21	40	35	33	35	35	36	36

Sample	M342	M344	M347	M350	M352	M357	M359	M360	M362	M363	M364	M367	M370	M372	M373
Type	Dome	Dome	Dome	Dome	Dome	Dome	Dome	Dome	Dome	Dome	Dome	Dome	Dome	Dome	Dome
Quality	5	3	3	3	3	5	5	2	3	4	5	5	3	5	5
Location	Slope boulder	Pouaru Rd	Roy Sim. Rd	Hauwai Rd	Hauwai Rd	off Poplar Rd	Farm track	Farm track	Farm track	Baldy Rd	Hauwai Rd	off Saddle Rd	Roy Sim. Rd	off Tram Rd	Tram Rd
Deposit	Wairiki Dome W	Mandarin Dome S	Baldy Dome E	Baldy Dome far-N	Baldy Dome N	Spinks Dome W	Hind Dome	Stag Dome	Spinks Dome SE	Baldy Dome SW	Summit Dome	Roy N Dome	Roy E Dome	Roy W Dome	Waipakipaki Dome N
Unit	MEC	MEC	MEC	MEC	MEC	MWC	MWC	MWC	MWC	MEC	MEC	MEC	MEC	MEC	MEC
Grid	U17/818997	U17/807000	U17/798980	U17/793993	U17/788988	U17/731983	U17/727988	U17/741966	U17/739975	U17/784978	U17/777983	U17/785961	U17/794966	U17/776950	U17/776942
SiO2	76.54	76.32	72.64	74.48	75.92	75.76	75.65	74.72	76.02	75.64	74.06	75.22	76.70	75.66	75.64
TiO2	0.18	0.17	0.24	0.20	0.18	0.17	0.18	0.18	0.16	0.19	0.22	0.20	0.16	0.20	0.19
Al2O3	12.93	12.80	16.43	14.29	13.09	13.83	13.30	14.32	13.05	13.28	14.84	13.94	12.93	13.44	13.26
Fe2O3T	1.72	1.70	2.23	1.96	1.74	1.98	1.79	1.88	1.71	1.79	2.02	1.92	1.31	1.84	1.95
MnO	0.02	0.07	0.07	0.07	0.05	0.04	0.07	0.07	0.06	0.07	0.07	0.06	0.04	0.06	0.06
MgO	n.d.	0.14	0.20	0.17	0.11	0.13	0.10	0.13	0.12	0.16	0.18	0.08	0.08	0.11	0.13
CaO	0.90	0.98	1.08	1.08	0.99	0.76	0.94	0.98	0.96	1.03	1.10	0.91	0.82	0.96	0.97
Na2O	4.39	4.35	4.32	4.55	4.58	4.08	4.59	4.48	4.47	4.60	4.44	4.33	4.54	4.47	4.49
K2O	3.30	3.44	2.77	3.16	3.33	3.23	3.36	3.22	3.42	3.21	3.05	3.32	3.40	3.24	3.30
P2O5	0.02	0.02	0.03	0.03	0.02	0.02	0.02	0.02	0.02	0.02	0.03	0.02	0.02	0.02	0.01
(LOI)	0.64	3.04	3.17	2.22	-0.05	1.09	0.85	3.01	2.66	0.30	2.75	0.97	0.49	0.38	0.57
(Total)	100.00	100.00	100.00	100.00	100.00	100.00	100.00	100.00	100.00	100.00	100.00	100.00	100.00	100.00	100.00
V	7	7	8	7	7	9	10	n.d.	7	10	9	12	6	7	9
Cr	n.d.	n.d.	n.d.	n.d.	n.d.	n.d.	n.d.	n.d.	n.d.	n.d.	n.d.	n.d.	n.d.	n.d.	n.d.
Ni	n.d.	n.d.	n.d.	n.d.	n.d.	n.d.	n.d.	n.d.	4	3	n.d.	n.d.	n.d.	n.d.	n.d.
Zn	60	67	54	54	39	31	35	67	49	44	71	39	47	33	39
Zr	188	198	253	218	192	193	197	216	190	205	230	207	170	201	198
Nb	9	9	11	10	10	10	10	10	9	10	11	11	10	10	10
Ba	749	786	794	821	750	730	770	885	797	799	981	790	818	769	792
La	18	23	22	25	21	29	18	22	25	28	22	16	24	28	19
Ce	47	69	66	73	59	51	58	73	64	68	75	62	76	65	50
Nd	22	30	33	37	40	30	32	34	27	36	32	19	26	21	13
Ga	14	14	16	15	15	15	15	16	14	15	15	16	15	16	14
Pb	17	18	25	21	16	17	18	98	19	18	44	16	17	15	16
Rb	113	116	97	108	114	111	111	111	116	97	103	114	103	106	106
Sr	74	72	84	82	80	67	71	83	69	85	85	78	64	81	81
Th	10	11	15	14	12	12	11	12	9	10	13	13	13	12	12
Y	28	37	43	39	23	24	29	38	38	27	34	18	35	24	28

Sample	M416	M418	M419	M423	M424	M425	M429	M432a	M432b	M433	M439	M460	M461	M467	M470
Type	Pumice	Pumice	Dome	Pumice	Dome	Dome	Pumice	Pumice	Lithic obsid	Lithic lava	Lithic lava	Dome	Dome	Dome	Pumice
Quality	2	2	5	2	3	5	2	2	2	3	3	3	5	3	2
Location	Hill Rd	off Sycamore Rd	off Tirohanga Rd	off Thorpe Rd	off Roy Sim. Rd	off Roy Sim. Rd	Waipapa Stream bluffs	off Fletchers Rd	off Fletchers Rd	lithic E of Tram Rd	lithic nth by Tram Rd	Summit track	Stream head	off Kakarihi Rd	off Korotai Rd
Deposit	Atiamuri Ig	Atiamuri Ig	Pohaturoa Dome	Atiamuri Ig bluffs	Vicki Dome NE	Vicki Dome SW	Massive Mokai Ig	Atiamuri Ig	Atiamuri Ig lithic obsidian	Orakonui pclast	Orakonui pclast	Wairiki Dome S	Umukuri Dome E	Buried Dome	Korotai Rd bluffs
Unit	Atiamuri	Atiamuri		Atiamuri	MEC	Pakuri	Mokai	Atiamuri	Atiamuri	Orakonui	Orakonui	MEC	MEC		Korotai
Grid	U17/771020	U17/765033	U17/729068	U17/773043	U17/809986	U17/801975	T17/621990	U17/788014	U17/788014	U17/787920	U17/791936	U17/821992	U17/831984	U17/719096	T17/689083
SiO2	74.37	74.82	76.36	75.92	76.06	76.01	72.23	73.30	75.72	74.07	73.91	75.76	75.03	76.09	75.12
TiO2	0.18	0.17	0.17	0.15	0.17	0.18	0.30	0.22	0.18	0.27	0.26	0.20	0.20	0.19	0.19
Al2O3	15.20	14.50	12.72	13.16	13.34	13.33	15.97	15.82	13.20	13.91	14.28	14.01	13.76	13.10	13.53
Fe2O3T	1.89	1.88	1.60	1.65	1.74	1.66	2.42	2.12	1.76	2.36	2.23	1.57	1.87	1.78	2.05
MnO	0.06	0.05	0.06	0.06	0.05	0.03	0.07	0.07	0.06	0.06	0.07	0.01	0.07	0.02	0.06
MgO	0.11	0.13	0.14	0.11	0.07	0.11	0.30	0.17	0.16	0.22	0.21	0.06	0.18	0.08	0.13
CaO	0.86	0.94	0.95	0.97	0.84	0.90	1.42	1.07	1.02	1.29	1.30	0.88	1.09	1.01	1.15
Na2O	4.07	4.27	4.50	4.37	4.35	4.41	4.34	4.26	4.59	4.54	4.57	4.24	4.36	4.12	4.17
K2O	3.24	3.22	3.48	3.58	3.36	3.34	2.93	2.96	3.29	3.22	3.13	3.27	3.42	3.59	3.58
P2O5	0.01	0.01	0.02	0.02	0.02	0.02	0.02	0.01	0.02	0.05	0.03	0.01	0.03	0.02	0.02
(LOI)	2.85	2.73	0.06	2.46	0.67	0.84	3.04	3.09	0.63	0.84	1.11	1.15	3.20	0.61	2.69
(Total)	100.00	100.00	100.00	100.00	100.00	100.00	100.00	100.00	100.00	100.00	100.00	100.00	100.00	100.00	100.00
V	4	5	8	5	7	8	12	8	8	13	11	9	7	9	7
Cr	n.d.	n.d.	n.d.	n.d.	n.d.	n.d.	n.d.	n.d.	n.d.	n.d.	n.d.	n.d.	n.d.	n.d.	n.d.
Ni	n.d.	n.d.	3	4	n.d.	n.d.	n.d.	n.d.	n.d.	n.d.	n.d.	n.d.	n.d.	n.d.	n.d.
Zn	58	54	39	47	47	33	62	69	49	43	54	33	50	37	49
Zr	230	210	169	188	197	190	272	232	200	232	235	209	205	197	223
Nb	11	11	9	9	10	10	10	12	9	9	10	10	10	9	9
Ba	785	774	772	776	744	742	704	831	784	704	752	792	784	765	752
La	29	24	23	25	21	14	27	24	27	14	13	23	29	25	19
Ce	82	77	58	65	57	48	73	73	75	46	38	43	56	44	63
Nd	31	29	29	28	32	27	47	24	37	16	22	14	33	24	33
Ga	16	16	14	13	16	14	19	17	15	15	15	16	15	15	15
Pb	22	18	17	19	28	12	19	22	19	14	12	16	18	16	18
Rb	108	110	118	115	114	112	95	101	112	132	106	105	111	126	124
Sr	71	70	69	70	68	75	122	83	76	120	118	76	82	87	96
Th	13	11	11	12	12	9	10	12	11	8	8	12	12	11	11
Y	40	36	32	37	27	24	44	34	36	17	18	25	35	27	32

Sample	M474	M476	M477	M479	M481	ma01	ma02	ma03	ma04	ma05	ma06	ma07	ma08	ma09	ma10
Type	Dome	Pumice	Dome	Dome	Pumice	Dome	Dome	Dome	Dome	Dome	Dome	Dome	Dome	Dome	Dome
Quality	4	3	5	2	2	(G. Corlette)	(G. Corlette)	(G. Corlette)	(G. Corlette)	(G. Corlette)	(G. Corlette)	(G. Corlette)	(G. Corlette)	(G. Corlette)	(G. Corlette)
Location	off Thorpe Rd	Near Puk W D	off Bracey Rd	NE side	SE side of tuff ring										
Deposit	Mandarin Dome W	Pukeahua Fan SW	Maroanui W Dome	Puketarata Dome	Puketarata Tuff	Pukeahua W Dome	Pohaturoa Dome	Pukeahua W Dome	Pukeahua W Dome	Pukeahua W Dome	Pukeahua W Dome	Pukeahua W Dome	Pukeahua W Dome	Pukeahua W Dome	Pukeahua W Dome
Unit	MEC	Pukeahua				Pukeahua		Pukeahua	Pukeahua	Pukeahua	Pukeahua	Pukeahua	Pukeahua	Pukeahua	Pukeahua
Grid	U17/792007	U17/711017	U17/715936	U17/765904	U17/759901	U17/708035	U17/729072	U17/708034	U17/713035	U17/714340	U17/714034	U17/716028	U17/718029	U17/723035	U17/724030
SiO2	75.61	74.85	74.02	74.90	74.39	76.22	78.05	76.22	74.84	75.66	75.65	74.21	76.34	76.12	70.53
TiO2	0.18	0.18	0.28	0.23	0.24	0.17	0.19	0.20	0.18	0.17	0.16	0.20	0.17	0.18	0.16
Al2O3	13.36	14.44	13.88	13.43	13.80	12.79	13.13	13.03	13.83	13.21	13.04	14.32	12.72	13.16	11.93
Fe2O3T	1.79	1.87	2.37	1.97	2.02	1.55	0.93	1.35	1.69	1.58	1.58	1.76	1.60	1.68	1.55
MnO	0.06	0.05	0.05	0.06	0.06	0.05	0.01	0.04	0.05	0.05	0.05	0.05	0.04	0.05	0.05
MgO	0.15	0.17	0.24	0.36	0.40	0.16	0.03	0.14	0.16	0.14	0.15	0.16	0.13	0.06	0.56
CaO	1.04	1.03	1.42	1.60	1.60	0.98	0.37	0.90	0.99	0.96	0.97	0.98	0.93	0.80	7.80
Na2O	4.68	4.12	4.60	4.14	4.23	4.40	3.66	4.20	4.37	4.31	4.32	4.29	4.44	4.21	4.00
K2O	3.13	3.27	3.10	3.27	3.23	3.45	3.24	3.46	3.32	3.55	3.53	3.27	3.47	3.52	3.21
P2O5	0.01	0.01	0.03	0.04	0.03	0.21	0.39	0.46	0.57	0.36	0.55	0.75	0.16	0.22	0.20
(LOI)	0.92	3.06	0.62	1.58	1.74	1.85	1.90	2.41	2.60	2.22	2.14	2.40	0.10	0.41	0.39
(Total)	100.00	100.00	100.00	100.00	100.00	100.00	100.00	100.00	100.00	100.00	100.00	100.00	100.00	100.00	100.00
V	8	8	15	16	19	3	3	1	n.d.	3	1	4	4	6	3
Cr	n.d.	n.d.	n.d.	n.d.	n.d.	n.d.	n.d.	n.d.	n.d.	n.d.	n.d.	n.d.	n.d.	n.d.	
Ni	n.d.	n.d.	n.d.	n.d.	n.d.	2	n.d.	2	n.d.	2	n.d.	n.d.	n.d.	2	n.d.
Zn	36	125	43	35	38	46	44	46	52	50	51	50	42	37	33
Zr	189	199	226	153	183	183	181	187	195	185	185	192	176	182	168
Nb	9	10	9	8	9	9	10	10	11	10	10	10	9	9	9
Ba	804	749	704	785	756	746	670	766	815	780	775	890	750	796	715
La	18	26	24	22	24	26	22	29	27	28	28	30	27	28	28
Ce	55	78	53	49	55	63	47	69	70	68	65	71	63	67	50
Nd	25	28	25	23	27	9	10	10	11	10	10	10	9	9	9
Ga	15	16	16	14	14	n.d.	n.d.	n.d.	n.d.	n.d.	n.d.	n.d.	n.d.	n.d.	
Pb	11	36	17	13	13	18	14	20	21	40	36	20	16	13	32
Rb	95	113	97	108	107	119	119	115	114	117	117	109	122	119	93
Sr	79	73	124	120	118	73	33	65	73	71	71	79	74	70	62
Th	9	13	11	11	11	15	16	16	16	16	15	16	14	15	15
Y	26	37	25	22	23	33	33	35	34	34	33	34	35	31	24

Sample	ma11	ma12	ma13	ma14	ma15	ma16	ma17	ma18	ma19	ma20	ma21	ma22	ma23	ma24	ma25
Type	Dome	Dome	Dome	Dome	Dome	Dome	Dome	Dome	Dome	Dome	Dome	Dome	Dome	Dome	Dome
Quality	(G. Corlette)	(G. Corlette)	(G. Corlette)	(G. Corlette)	(G. Corlette)	(G. Corlette)	(G. Corlette)	(G. Corlette)	(G. Corlette)	(G. Corlette)	(G. Corlette)	(G. Corlette)	(G. Corlette)	(G. Corlette)	(G. Corlette)
Location						SE side	SE side						Off Mandarin Dome		
Deposit	Pukeahua W Dome	Pukeahua W Dome	Pukeahua E Dome	Pukeahua E Dome	Maroanui West	Walker Dome	Walker Dome	Goldies Dome	Stag Dome	Stag Dome	Hauwai Dome	Hauwai Dome	BaF	Hauwai Dome	Maroanui Dome
Unit	Pukeahua	Pukeahua	Pukeahua	Pukeahua	Maroanui	MWC	MWC	MWC	MWC	MWC	MEC	MEC	Maroa P	MEC	Maroanui
Grid	U17/732032	U17/732043	U17/736030	U17/737038	U17/715942	U17/723959	U17/723959	U17/715953	U17/742967	U17/742967	U17/773003	U17/773003	U17/792018	U17/783992	U17/735937
SiO2	75.85	76.15	74.18	74.17	73.84	76.14	75.88	75.94	76.40	76.16	75.76	76.07	76.27	74.93	75.72
TiO2	0.17	0.16	0.26	0.26	0.30	0.16	0.18	0.17	0.15	0.16	0.18	0.16	0.16	0.19	0.19
Al2O3	13.10	12.74	13.75	13.71	13.65	13.10	13.13	12.99	12.91	12.90	13.12	12.95	12.76	13.83	13.13
Fe2O3T	1.61	1.52	2.01	1.95	2.15	1.43	1.60	1.78	1.58	1.62	1.68	1.68	1.56	1.76	1.74
MnO	0.05	0.04	0.05	0.06	0.06	0.04	0.05	0.05	0.02	0.05	0.05	0.04	0.05	0.06	0.04
MgO	0.13	0.15	0.31	0.35	0.34	0.13	0.14	0.13	0.08	0.08	0.17	0.14	0.15	0.15	0.17
CaO	0.93	0.95	1.49	1.64	1.58	0.93	0.94	0.90	0.87	0.92	1.04	0.93	0.95	0.98	1.07
Na2O	4.61	4.29	4.39	4.49	4.39	4.55	4.61	4.59	4.45	4.61	4.59	4.55	4.55	4.34	4.47
K2O	3.36	3.52	3.05	3.13	3.28	3.25	3.21	3.24	3.42	3.43	3.30	3.41	3.41	3.22	3.32
P2O5	0.19	0.47	0.51	0.23	0.41	0.28	0.26	0.20	0.12	0.08	0.11	0.07	0.14	0.52	0.15
(LOI)	0.45	2.04	0.42	0.77	2.64	0.36	0.37	0.47	0.29	0.17	0.33	0.21	0.50	2.23	0.26
(Total)	100.00	100.00	100.00	100.00	100.00	100.00	100.00	100.00	100.00	100.00	100.00	100.00	100.00	100.00	100.00
V	1	3	7	10	9	2	3	2	2	n.d.	1	n.d.	1	2	3
Cr	n.d.	n.d.	n.d.	n.d.	n.d.	n.d.	n.d.	n.d.	n.d.	n.d.	n.d.	n.d.	n.d.	n.d.	n.d.
Ni	n.d.	4	2	n.d.	2	n.d.	n.d.	n.d.	2	n.d.	n.d.	2	2	2	2
Zn	37	46	29	44	52	30	33	41	38	30	44	32	48	54	46
Zr	179	179	182	194	219	197	200	215	191	193	207	200	198	216	194
Nb	10	10	8	9	9	9	10	11	10	10	10	10	10	10	10
Ba	786	752	773	742	710	765	756	792	735	749	776	747	754	798	753
La	32	28	21	24	26	21	21	29	26	27	27	30	27	30	29
Ce	65	63	49	59	60	46	49	60	52	57	59	64	60	62	66
Nd	10	10	8	9	9	9	10	11	10	10	10	10	10	10	10
Ga	n.d.	n.d.	n.d.	n.d.	n.d.	n.d.	n.d.	n.d.	n.d.	n.d.	n.d.	n.d.	n.d.	n.d.	n.d.
Pb	19	18	14	15	17	14	14	48	14	14	15	17	18	19	34
Rb	92	119	84	105	106	80	83	86	112	114	101	113	114	108	107
Sr	75	71	117	123	129	74	75	74	69	74	83	74	70	79	88
Th	16	15	12	13	13	15	14	15	13	13	14	15	14	15	13
Y	26	35	18	28	33	24	24	27	33	32	31	36	33	36	34

Sample	ma26	ma27	ma28	ma29	ma30	ma31	ma32	ma33	ma34	ma35	ma36	ma37	ma38	ma40	ma42
Type	Dome	Dome	Dome	Dome	Dome	Dome	Dome	Dome	Dome	Dome	Dome	Dome	Dome	Dome	Dome
Quality	(G. Corlette)	(G. Corlette)	(G. Corlette)	(G. Corlette)	(G. Corlette)	(G. Corlette)	(G. Corlette)	(G. Corlette)	(G. Corlette)	(G. Corlette)	(G. Corlette)	(G. Corlette)	(G. Corlette)	(G. Corlette)	(G. Corlette)
Location	Mokai Quarry														
Deposit	Mokai Quarry Dome	NWDC	NWDC	NWDC	NWDC	NWDC	NWDC	NWDC	NWDC	NWDC	NWDC	NWDC	NWDC	NWDC	NWDC
Unit		WDB	WDB	WDB	WDB	WDB	WDB	WDB	WDB	WDB	WDB	WDB	WDB	WDB	WDB
Grid	U17/727058	T17\542088	T17\542084	T17\567097	T17\557075	T17\567072	T17\571071	T17\573069	T17\580075	T17\580075	T17\581090	T17\574088	T17\576082	T17\570085	T17\638080
SiO2	73.54	77.16	77.32	77.30	77.43	77.09	77.15	77.29	77.04	77.12	77.23	77.29	77.22	77.33	76.54
TiO2	0.31	0.14	0.14	0.14	0.15	0.15	0.14	0.15	0.14	0.15	0.14	0.14	0.14	0.15	0.12
Al2O3	13.77	12.46	12.47	12.45	12.44	12.49	12.48	12.38	12.64	12.46	12.48	12.49	12.42	12.43	12.26
Fe2O3T	2.52	1.14	1.13	1.13	1.13	1.12	1.14	1.15	1.19	1.14	1.20	1.14	1.14	1.13	1.05
MnO	0.07	0.03	0.03	0.03	0.03	0.03	0.04	0.03	0.03	0.03	0.03	0.03	0.03	0.03	0.03
MgO	0.43	0.16	0.14	0.13	0.15	0.14	0.14	0.15	0.14	0.15	0.10	0.14	0.13	0.13	0.11
CaO	2.11	1.03	1.02	1.03	1.03	1.02	1.03	1.05	1.01	1.04	1.01	1.03	1.02	1.01	0.87
Na2O	4.36	3.77	3.83	3.84	3.72	3.97	3.93	3.92	3.51	3.96	3.88	3.79	3.88	3.87	4.03
K2O	2.78	3.98	3.82	3.82	3.80	3.82	3.81	3.77	3.87	3.81	3.84	3.79	3.80	3.81	3.81
P2O5	0.11	0.13	0.11	0.12	0.11	0.16	0.14	0.11	0.43	0.14	0.10	0.15	0.21	0.10	1.20
(LOI)	0.31	0.45	0.40	0.12	0.39	0.30	0.46	0.41	2.76	0.31	0.13	0.57	0.52	0.50	50.00
(Total)	100.00	100.00	100.00	100.00	100.00	100.00	100.00	100.00	100.00	100.00	100.00	100.00	100.00	100.00	100.00
V	7	1	3	3	3	2	2	1	3	3	2	3	3	2	n.d.
Cr	n.d.	n.d.	n.d.	n.d.	n.d.	n.d.	n.d.	n.d.	n.d.	n.d.	n.d.	n.d.	n.d.	n.d.	n.d.
Ni	n.d.	n.d.	2	n.d.	2	n.d.	n.d.	n.d.	n.d.	n.d.	n.d.	4	n.d.	2	n.d.
Zn	48	31	29	30	28	29	29	30	31	29	23	30	30	30	31
Zr	201	129	128	129	127	127	127	131	132	127	127	127	128	124	111
Nb	7	7	7	7	6	7	7	6	7	7	7	7	7	7	7
Ba	630	808	803	802	805	808	800	799	815	800	811	802	802	807	797
La	21	23	22	21	21	22	23	23	23	22	28	22	23	24	23
Ce	45	44	46	47	49	48	49	48	47	47	49	50	474	49	49
Nd	7	7	7	7	6	7	7	6	7	7	7	7	7	7	7
Ga	n.d.	n.d.	n.d.	n.d.	n.d.	n.d.	n.d.	n.d.	n.d.	n.d.	n.d.	n.d.	n.d.	n.d.	n.d.
Pb	13	16	15	15	15	15	15	15	15	15	14	15	15	15	16
Rb	93	134	134	134	135	134	133	131	135	135	133	135	134	135	135
Sr	162	85	86	86	85	84	84	86	84	85	85	85	84	84	73
Th	13	16	17	16	16	16	15	16	16	15	16	15	15	16	16
Y	24	18	19	18	18	18	18	18	19	19	21	19	18	18	19

Sample	ma43	ma44	ma45	ma46	ma47	ma48	ma49	ma51	ma52	ma53	ma54	ma55	ma56	ma60	ma61
Type	Dome	Dome	Dome	Dome	Dome	Dome	Dome	Dome	Dome	Dome	Dome	Dome	Dome		
Quality	(G. Corlette)	(G. Corlette)	(G. Corlette)	(G. Corlette)	(G. Corlette)	(G. Corlette)	(G. Corlette)	(G. Corlette)	(G. Corlette)	(G. Corlette)	(G. Corlette)	(G. Corlette)	(G. Corlette)	(G. Corlette)	(G. Corlette)
Location															
Deposit	NWDC	NWDC	NWDC	NWDC	NWDC	NWDC	NWDC	NWDC	NWDC	NWDC	NWDC	WDC	WDC	Puketarata	Puketarata
Unit	WDB	WDB	WDB	WDB	WDB	WDB	WDB	WDB	WDB	WDB	WDB	WDB	WDB		
Grid	T17\637083	T17\642086	T17\653090	T17\655070	T16\644103	T17\644093	T17\586096	T17\588076	T17\588069	T17\588064	T17\591065	T17\607022	T17\598020	U17\762903	U17\762903
SiO2	77.36	77.45	77.38	77.52	77.41	77.44	77.01	77.22	77.46	77.09	77.18	77.05	77.53	74.76	74.74
TiO2	0.11	0.12	0.11	0.12	0.11	0.12	0.15	0.18	0.15	0.17	0.15	0.15	0.12	0.23	0.24
Al2O3	12.42	12.40	12.45	12.48	12.41	12.43	12.57	12.51	12.49	12.57	12.48	12.51	12.34	13.35	13.42
Fe2O3T	1.07	1.06	1.06	1.08	1.07	1.08	1.15	1.31	1.14	1.26	1.14	1.14	1.08	1.82	1.78
MnO	0.03	0.03	0.03	0.03	0.03	0.03	0.03	0.04	0.03	0.04	0.04	0.03	0.03	0.05	0.05
MgO	0.11	0.11	0.11	0.11	0.11	0.11	0.16	0.15	0.14	0.19	0.15	0.15	0.10	0.34	0.35
CaO	0.87	0.86	0.88	0.88	0.88	0.88	1.03	1.07	1.07	1.17	1.02	1.03	0.87	1.62	1.64
Na2O	4.06	4.00	3.99	3.82	4.00	3.98	3.93	3.69	3.63	3.71	3.88	3.99	3.89	4.14	4.14
K2O	3.87	3.87	3.86	3.85	3.86	3.83	3.80	3.70	3.75	3.65	3.79	3.81	3.87	3.31	3.27
P2O5	0.10	0.10	0.12	0.11	0.12	0.10	0.18	0.12	0.14	0.14	0.16	0.14	0.17	0.38	0.35
(LOI)	0.42	0.52	0.46	0.40	0.02	0.53	0.44	0.35	0.45	0.40	0.51	0.31	0.55	1.20	1.07
(Total)	100.00	100.00	100.00	100.00	100.00	100.00	100.00	100.00	100.00	100.00	100.00	100.00	100.00	100.00	100.00
V	n.d.	n.d.	n.d.	n.d.	1	n.d.	3	2	2	3	2	4	n.d.	11	10
Cr	n.d.	n.d.	n.d.	n.d.	n.d.	n.d.	n.d.	n.d.	n.d.	n.d.	n.d.	n.d.	n.d.	n.d.	n.d.
Ni	n.d.	n.d.	n.d.	n.d.	n.d.	2	2	1	n.d.	2	2	n.d.	1	4	1
Zn	31	31	32	31	32	31	30	29	29	30	29	29	32	37	36
Zr	113	113	111	112	114	117	128	131	132	142	126	127	113	167	165
Nb	7	7	7	8	7	7	7	7	7	6	7	7	6	8	8
Ba	809	814	813	823	816	799	806	794	798	787	808	810	801	756	769
La	23	23	23	23	22	24	23	23	23	21	22	21	23	24	23
Ce	48	49	49	45	49	51	50	51	46	48	49	47	52	50	53
Nd	7	7	7	8	7	7	7	7	7	6	7	7	6	8	8
Ga	n.d.	n.d.	n.d.	n.d.	n.d.	n.d.	n.d.	n.d.	n.d.	n.d.	n.d.	n.d.	n.d.	n.d.	n.d.
Pb	16	16	16	16	16	15	15	16	15	15	15	14	16	13	15
Rb	135	135	136	136	136	135	133	130	130	126	132	133	134	107	107
Sr	71	72	75	74	74	73	85	89	87	96	83	84	71	120	124
Th	14	16	15	15	16	16	18	15	16	16	15	16	16	14	13
Y	20	20	19	19	20	19	18	18	18	18	19	18	20	22	21

Sample	ma62	ma63	ma64	ma65	ma66	ma67	ma70	ma71	ma72	ma73	ma74	ma77	ma78	ma79	ma80
Type		Dome	Dome	Dome	Dome	Dome	Dome	Dome	Dome	Dome	Dome	Dome	Dome	Dome	Dome
Quality	(G. Corlette)	(G. Corlette)	(G. Corlette)	(G. Corlette)	(G. Corlette)	(G. Corlette)	(G. Corlette)	(G. Corlette)	(G. Corlette)	(G. Corlette)	(G. Corlette)	(G. Corlette)	(G. Corlette)	(G. Corlette)	(G. Corlette)
Location															
Deposit	Puketarata	Forest Gorge	Forest Gorge	Forest Gorge	North Taupo	WDC	Whakapapaaringa Dome	Whakapapaaringa Dome	Waipakipaki S	Roy S Dome	Roy S Dome	Near Ben Lomond	Near Ben Lomond	Near Ben Lomond	Taupo Hunt Club
Unit		Southern	Southern	Southern	Taupo D	WDB	Maroa D	Maroa D		MEC	MEC				Taupo D
Grid	U17\762903	U17\730898	U17\730898	U17\727899	T17\587819	T17\610863	U17\852933	U17\857934	U17\778940	U17\777943	U17\776945	T17\664826	T17\664826	T17\632834	T17\634812
SiO2	74.75	76.96	76.78	78.35	71.29	74.22	76.12	76.10	76.07	75.87	75.56	76.96	76.89	76.24	72.46
TiO2	0.25	0.12	0.12	0.12	0.54	0.32	0.16	0.17	0.16	0.20	0.19	0.18	0.19	0.19	0.29
Al2O3	13.45	12.62	12.47	12.62	15.27	13.93	13.09	12.92	13.03	13.05	13.12	12.58	12.48	13.08	14.36
Fe2O3T	1.85	1.39	1.33	1.37	2.89	1.84	1.70	1.66	1.71	1.72	1.74	1.39	1.39	1.49	2.36
MnO	0.05	0.03	0.04	0.04	0.07	0.06	0.04	0.04	0.03	0.05	0.04	0.02	0.04	0.02	0.05
MgO	0.36	0.08	0.09	0.09	0.63	0.33	0.07	0.13	0.08	0.18	1.03	0.10	0.17	0.08	0.53
CaO	1.68	0.82	0.86	0.03	2.39	1.58	1.01	1.09	1.02	1.07	4.68	1.09	1.14	1.08	2.33
Na2O	4.24	4.26	4.08	3.14	4.03	3.98	3.94	4.14	4.16	4.42	3.29	4.04	4.04	4.08	4.09
K2O	3.26	3.53	3.87	3.86	2.43	3.21	3.69	3.58	3.59	3.27	0.09	3.51	3.48	3.60	3.02
P2O5	0.11	0.20	0.36	0.37	0.46	0.52	0.17	0.17	0.15	0.16	0.25	0.13	0.18	0.12	0.53
(LOI)	0.81	0.61	1.34	2.08	1.02	2.93	0.32	0.20	0.26	0.31	0.02	0.30	0.45	0.39	2.00
(Total)	100.00	100.00	100.00	100.00	100.00	100.00	100.00	100.00	100.00	100.00	100.00	100.00	100.00	100.00	100.00
V	11	n.d.	n.d.	n.d.	14	4	2	2	n.d.	3	3	2	3	4	16
Cr	n.d.	n.d.	n.d.	n.d.	n.d.	n.d.	n.d.	n.d.	n.d.	n.d.	n.d.	n.d.	n.d.	n.d.	n.d.
Ni	2	n.d.	1	n.d.	2	n.d.	n.d.	1	n.d.	n.d.	n.d.	2	n.d.	4	2
Zn	39	40	46	47	50	52	35	49	31	46	37	32	35	27	40
Zr	201	156	151	154	213	217	197	196	210	204	201	167	163	189	150
Nb	9	9	9	9	7	7	9	9	9	10	10	7	8	8	6
Ba	706	797	775	789	707	710	766	760	759	751	745	674	675	752	622
La	24	27	27	28	23	24	30	26	27	27	27	21	22	23	22
Ce	51	58	60	63	42	55	58	62	51	61	60	42	47	49	51
Nd	9	9	9	9	7	7	9	9	9	10	10	7	8	8	6
Ga	n.d.	n.d.	n.d.	n.d.	n.d.	n.d.	n.d.	n.d.	n.d.	n.d.	n.d.	n.d.	n.d.	n.d.	n.d.
Pb	13	22	21	22	13	16	19	20	19	16	15	14	15	15	14
Rb	104	110	133	135	54	111	129	127	127	106	102	122	122	124	110
Sr	122	67	67	66	196	143	92	98	93	84	85	89	87	100	162
Th	13	16	16	17	11	13	14	16	16	14	13	14	14	16	14
Y	22	26	30	30	17	26	29	27	26	32	36	18	21	17	21

Sample	ma81	ma82	ma102
Type	Dome	Dome	Dome
Quality	(G. Corlette)	(G. Corlette)	(G. Corlette)
Location			
Deposit	Ngangiho	Ngangiho	Puketarata
Unit	Taupo D	Taupo D	
Grid	U17\764868	U17\759867	not supplied
SiO2	73.95	74.96	75.51
TiO2	0.26	0.22	0.21
Al2O3	13.56	13.32	13.77
Fe2O3T	2.18	1.92	1.68
MnO	0.06	0.05	0.04
MgO	0.39	0.33	0.18
CaO	1.80	1.64	1.15
Na2O	4.40	3.94	3.76
K2O	2.92	3.07	3.72
P2O5	0.46	0.55	0.00
(LOI)	1.20	1.48	0.00
(Total)	100.00	100.00	100.00
V	9	7	3
Cr	n.d.	n.d.	n.d.
Ni	n.d.	3	n.d.
Zn	44	40	53
Zr	180	163	197
Nb	7	7	8
Ba	662	663	683
La	21	21	25
Ce	45	49	57
Nd	7	7	8
Ga	n.d.	n.d.	14
Pb	14	14	26
Rb	99	105	128
Sr	135	120	98
Th	12	14	n.d.
Y	22	23	27

APPENDIX 5

Sr isotope analyses

5.1 Methodology

5.1.1 Laboratory techniques

All Sr isotope analytical work was carried out by Dr B. L. A. Charlier in the Arthur Holmes Isotope Geology Laboratory, University of Durham, UK.

5.1.2 Dissolution procedure for Sr analysis

The samples were run unspiked for $^{87}Sr/^{86}Sr$ isotope composition only, the aim being to obtain approximately 500 ng of Sr on the filament for TIMS analysis. This is the ideal amount for a whole rock analysis as there is enough Sr loaded on the filament to give a long-lasting stable beam, but not too much as to impair the ionisation efficiency. Between 6 and 21 mg of the sample powders were weighed out into clean PTFE Savilex™ beakers.

The samples had~100µl triple distilled (TD) 6M HCl added to which ~ 3 ml of TD Hf were added. The HCl was added to minimise the risk of a violent reaction on addition of the Hf and to inhibit the formation of fluorides. The samples were allowed to stand on a hotplate to digest overnight and then dried down under evaporating hoods. The evaporations between each of the following steps were carried out under Teflon drying hoods with a supply of compressed air being passed over them. The hoods were cleaned before the drying down of each sample at each stage with a wipe over with 6M HCl.

The residue was then taken up in 3-4 ml TD 6M HCl and then the beakers were sealed and placed on a hotplate overnight. The samples were then dried down and the addition of HCl repeated. After drying the samples down again, the samples were then taken up in ~ 5 ml TD 14M HNO_3 and left on the hotplate again. These were then taken to dryness and taken up again in ~ 200 µl TD 3M HNO_3. At the end of the dissolution procedure, a light yellow clear solution was obtained which was centrifuged at 4000

rpm for 5 minutes to obtain a clear solution free of any fluoride residue. These solutions were then ready for separation using Sr-spec resin.

5.1.3 Column chemistry

In all the dissolutions carried out in this work, 1 ml polypropylene columns were used. These were stored in 6M HCl prior to use and flushed through with several passes of 6M HCl prior to the loading of the resin. The columns were set up by the addition of ~70 μl of cleaned (repeated H_2O, 6M HCl, 0.1M HNO_3, 0.05M H_2SO_4 rinses) Eichrom Sr-spec (100-200 mesh) extraction chromatography resin. The columns were then washed twice with alternate rinses of 6M HCl and RO H_2O. Prior to the addition of the sample, the columns were pre-conditioned with two column volumes of 3M HNO_3. Whilst taking great care not to disturb the resin, the sample solutions were loaded onto the resin bed and washed on with 2 rinses of 50 μl TD 3M HNO_3 which was followed by eluting 800 μl TD 3M HNO_3, then by 200 μl 0.05M HNO_3. Cleaned 3.5 ml PTFE Savilex™ beakers were placed under the columns and the Sr fraction was collected in the 0.05M HNO_3. Each of these fractions was dried down ready for loading onto filaments and analysis in the mass-spectrometer.

Total procedural blanks using this technique are routinely monitored in the Durham lab and are usually in the range 20-50 pg, which is negligible when compared with the >>500 ng of sample used for dissolution.

5.1.4 Mass spectrometry

Samples were taken up in 1μl 16M HNO_3 and loaded onto out-gassed single Re filaments with ~1μl 1M H_3PO_4. $^{87}Sr/^{86}Sr$ measurements were performed using a Finnigan Triton thermal ionisation mass spectrometer in static collection mode. All analyses were corrected online for mass-fractionation following an exponential law based on $^{86}Sr/^{88}Sr = 0.1194$. ^{85}Rb was monitored in the axial Faraday cup, and $^{87}Rb/^{85}Rb = 0.386$ was used to correct for ^{87}Rb interference on ^{87}Sr. During the course of the analyses, the long-term NBS 987 average for 596 ng loads on Re filaments was NBS 987 = 0.710263 (n=35), with an external precision of 12 ppm 2σ.

5.2 Results

Sample	D154b	D153a	D59	D139	D95	MKP35	MKP38	MKP29	D213a	D175b	D175a	R2/1
Source	Gravley	Gravley	Gravley	Gravley	Gravley	Milner	Milner	Milner	Gravley	Gravley	Gravley	Karhunen
Description	Main Ohakuri pyroclastics type 1	Main Ohakuri pyroclastics type 2	Main Ohakuri pyroclastics type 3	Tar Hill Ohakuri pyroclastics type 1	Tar Hill Ohakuri pyroclastics type 2	Mamaku pyroclastics type 1	Sutcliffe Rd Mamaku pyroclastics type 2	Sutcliffe Rd Mamaku pyroclastics type 3	Tar Hill Mamaku pyroclastics type 1	Tar Hill Mamaku pyroclastics type 2	Tar Hill Mamaku pyroclastics type 3	Pokai Rd Pokai pyroclastics type 1
Rb	120	110	84	131	105	119	98	91	118	105	95	121
Sr	57	114	231	57	138	62	125	150	54	122	181	68
Rb/Sr	2.11	0.96	0.36	2.30	0.76	1.92	0.78	0.61	2.19	0.86	0.52	1.78
Sample wt. (g)	9.11	5.75	21.88	13.46	8.27	10.13	12.1	9.22	10.4	11.5	13.06	9.26
ng Sr	519	656	5054	767	1141	628	1513	1383	562	1403	2364	630
87Sr/86Sr	0.705329	0.705291	0.705287	0.705296	0.705239	0.705279	0.705286	0.705287	0.705301	0.705277	0.705215	0.70584
1 std. error	0.000009	0.000012	0.000014	0.000008	0.000007	0.000004	0.000004	0.000008	0.000005	0.000007	0.000003	0.000006

Sample	R5/1	R10/1	M110	M236	M344	M470	MoP1	MP87	M5055	M5060	M5054	MP86
Source	Karhunen	Karhunen	Leonard	Leonard	Leonard	Leonard	Milner	Brown	Brown	Brown	Brown	Brown
Description	Pokai Rd Pokai pyroclastics type 2	Pokai pyroclastics type 3	Pukeahua E Dome	Palm Dome	Mandarin Dome (MEC)	Korotai pyroclastics	Mokai pyroclastics	WDC	WDC	WDC	WDC	WDC
Rb	119	129	105	98	116	127	100	136	116	118	128	62
Sr	87	84	117	159	72	96	126	69	144	134	94	96
Rb/Sr	1.37	1.54	0.90	0.62	1.61	1.32	0.79	1.97	0.81	0.88	1.36	0.65
Sample wt. (g)	6.1	6.5	7.22	8.6	7.71	9.95	5.76	17.89	17.06	10.32	8.56	10.52
ng Sr	531	546	845	1367	555	955	726	1234	2457	1383	805	1010
87Sr/86Sr	0.705823	0.705815	0.705304	0.705555	0.705259	0.705806	0.705306	0.705284	0.705589	0.705618	0.705607	0.705274
1 std. error	0.000007	0.000005	0.000007	0.000007	0.000012	0.000004	0.000007	0.000011	0.000007	0.000005	0.000006	0.000004

Sources: Samples from the theses of Leonard (this study), Gravley (2003), Milner (2001), Brown (1994) and Karhunen (1993)

APPENDIX 6

Fractionation vector modelling

Fractionation trajectory modelling for Rb, Sr, Ba and Zr concentrations was carried out to determine if geochemical associations apparently present in MWC/MEC and Pukeahua eastern eruptive units could be explained by fractionation of minerals present in the same units. Partition coefficients for each mineral are summarised in Table A6.1(a) and the bulk partition coefficient for each case, based on the real abundance of each mineral seen in thin section (see Chapter 4), is calculated in Table A6.1(b).

(a)	Opx (1)	Hbl (1)	Biot (2)	Plag (2)	Qz (1)
Rb	0.003	0.014	3.200	0.041	0.041
Sr	0.009	0.022	0.447	4.400	0.000
Zr	0.200	0.310	1.197	0.100	0.000
Ba	0.003	0.044	6.360	0.360	0.022

(b)

	Opx	Hbl	Biot	Plag	Qz	D (Rb)	D (Sr)	D (Zr)	D (Ba)
MWC/MEC	5%	0%	0%	85%	15%	*0.039*	*1.320*	*0.090*	*0.291*
Pukeahua E	5%	5%	0%	60%	30%	*0.038*	*2.642*	*0.086*	*0.225*

Table A6.1 (a) Rb, Sr, Zr and Ba mineral partition coefficients (for dacitic to rhyolitic melts) used in the calculation of bulk partition coefficients for MWC/MEC domes, and for Pukeahua eastern deposits. Source publications (in brackets): (1) Arth (1976) and (2) Nash and Crecraft (1985). (b) Bulk partition coefficient for each case is calculated as the mean of the individual mineral partition coefficients from (a) weighted by the relative abundance (percentage shown) of that mineral in that case.

The model concentration of Rb, Sr, Zr and Ba in a given fraction of fractionated liquid is calculated according to the following Rayleigh fractionation equation (describing the extreme case where crystals are effectively removed from the melt the instant they have formed, ie. non-equilibrium crystallisation, Rollinson, 1993):

$$\frac{C_L}{C_0} = F^{(D-1)}$$

Where C_L is the weight concentration of a trace element in the liquid produced, C_0 is the weight concentration in the parental liquid, F is the weight fraction of melt remaining

and D is the bulk distribution coefficient of the fractionating assemblage. Model fractionation trajectories are then plotted across data points for each case in figures in Chapter 5. Percentage of fractionation is marked on each calculated trajectory at 5 or 10 % intervals.

APPENDIX 7

Details of Thorpe Road Fault trenches

7.1 Trench 1: undisturbed active-TVZ stratigraphy

Trench 1 was opened at a site 300 m east of SH1 and 100 m north of Thorpe Road, just off of Sequoia Rd. The trench crossed a ~ 1 m high Thorpe Road Fault degraded scarp trending ~ 055°. It was excavated 22 m long and 4 m deep, parallel to the ground surface, with a long axis trending ~ 325°. Figure A7.1 presents a photo-mosaic with annotations of the stratigraphy in the southwestern wall of Trench 1. None of the stratigraphy present in Trench 1 is disturbed by faulting.

The top 100 to 200 mm is a dark brown soil horizon formed from sediments and reworking of the Taupo ignimbrite. Below this lies 50 to 300 mm of primary Taupo ignimbrite. Below the Taupo ignimbrite is thick late-Pleistocene and Holocene loess, with some interbedded, poorly-preserved, tephras. There is strong bioturbation and development of palaeosols.

Below the loessic material lie alternating moderately firm, pumice-rich sandy gravels and gravelly sands, with Oruanui pyroclastics at their base. This sandy material above the Oruanui pyroclastics appears to be material (pumice and whole-rock clasts) derived during cold-climate conditions from the surrounding hills of Ohakuri and Atiamuri pyroclastics, as a result of the high rates of erosion that followed the Oruanui eruption (Wilson, 2001).

Below the Oruanui pyroclastics is a siltier sequence of sediments also derived from the Ohakuri and Atiamuri pyroclastics, probably deposited at a much slower rate while the landscape was relatively stable compared to the post-Oruanui period. Okaia tephra from Taupo (age c. 29 ka) is occasionally preserved within this siltier sediment (C. J. N. Wilson, pers comm.. 2003). In Trench 2 (see below) this sequence is shown to lie conformably on local basement, which is in-situ Ohakuri pyroclastics.

7.2 Trench 2: fractures in Ohakuri pyroclastics

Trench 2 was opened at a site further northeast along Thorpe Road Fault from Trench 1, on Mawsons Rd. The trench crossed a 3.4 m high Thorpe Road Fault scarp trending ~ 055°. It was excavated 52 m long and 4 m deep, parallel to the ground surface, with a long axis trending ~ 340°. The trench sits next to an 8 to 10 m scarp in line with the one trenched. Figure A7.2 presents a photo-mosaic with annotations of the stratigraphy in Trench 2. None of the stratigraphy present in Trench 1 is disturbed by faulting in Trench 2 either.

Trench 2 contains similar stratigraphy to Trench 1. In the northern section of the trench a few-metresdeep gully has been eroded into a substantial portion of the sequence and subsequently filled with silty sand. In the southern section of the trench (Fig. A7.2) the 13.8 ka Waiohau Tephra from Okataina Volcanic Centre (Speed et al., 2002) is well-preserved within the pre-Taupo loessic sediments. At the base of the loessic sediments the Oruanui pyroclastics are present in some places, but generally poorly preserved. Below the Oruanui pyroclastics lie Okaia-bearing silty sediments, and below these lie weathered Ohakuri pyroclastics. A few fractures with variable displacement in the order of 100 mm are present in the top of the Ohakuri pyroclastics, but do not propagate into the sediments above.

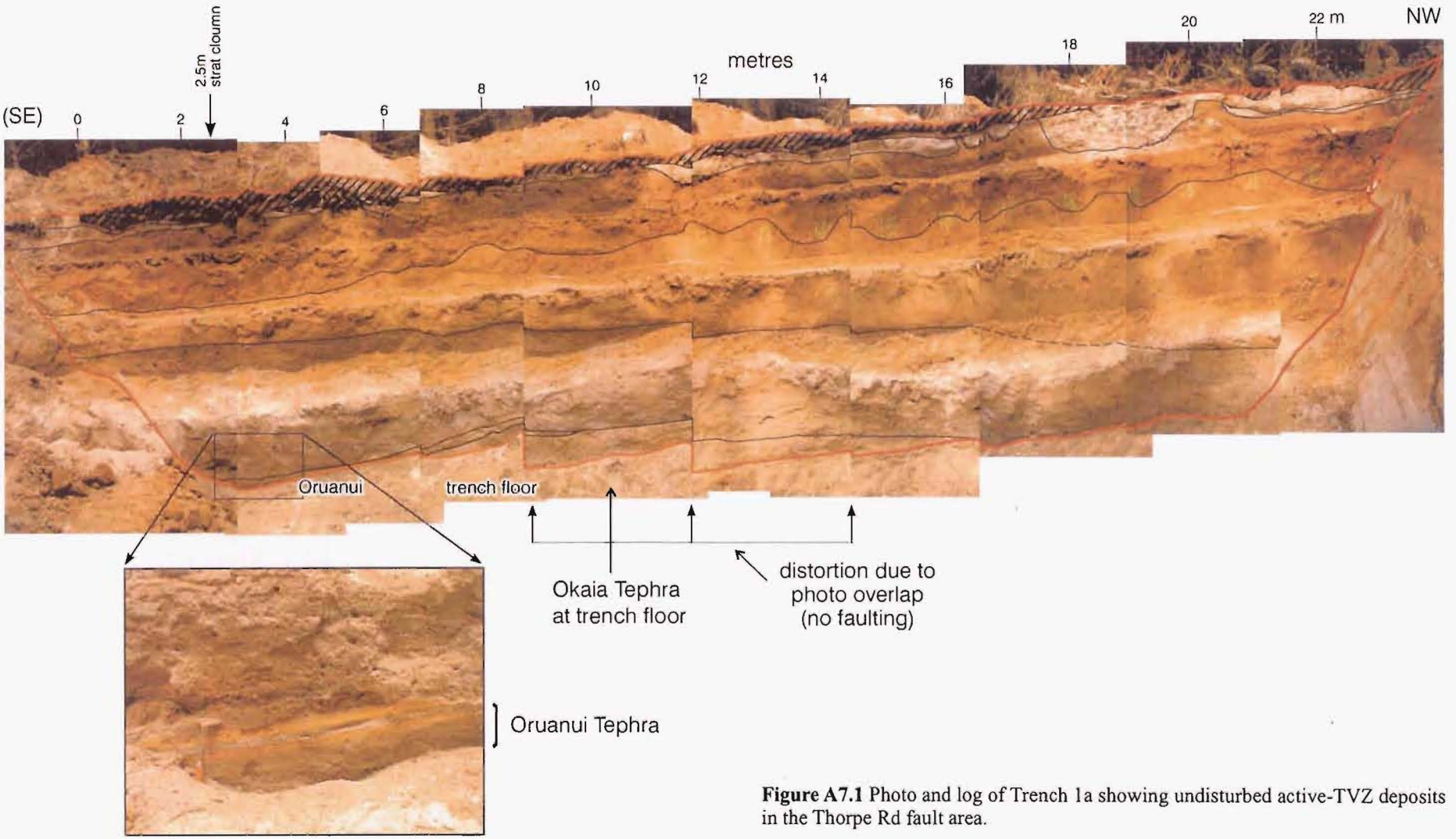

Figure A7.1 Photo and log of Trench 1a showing undisturbed active-TVZ deposits in the Thorpe Rd fault area.

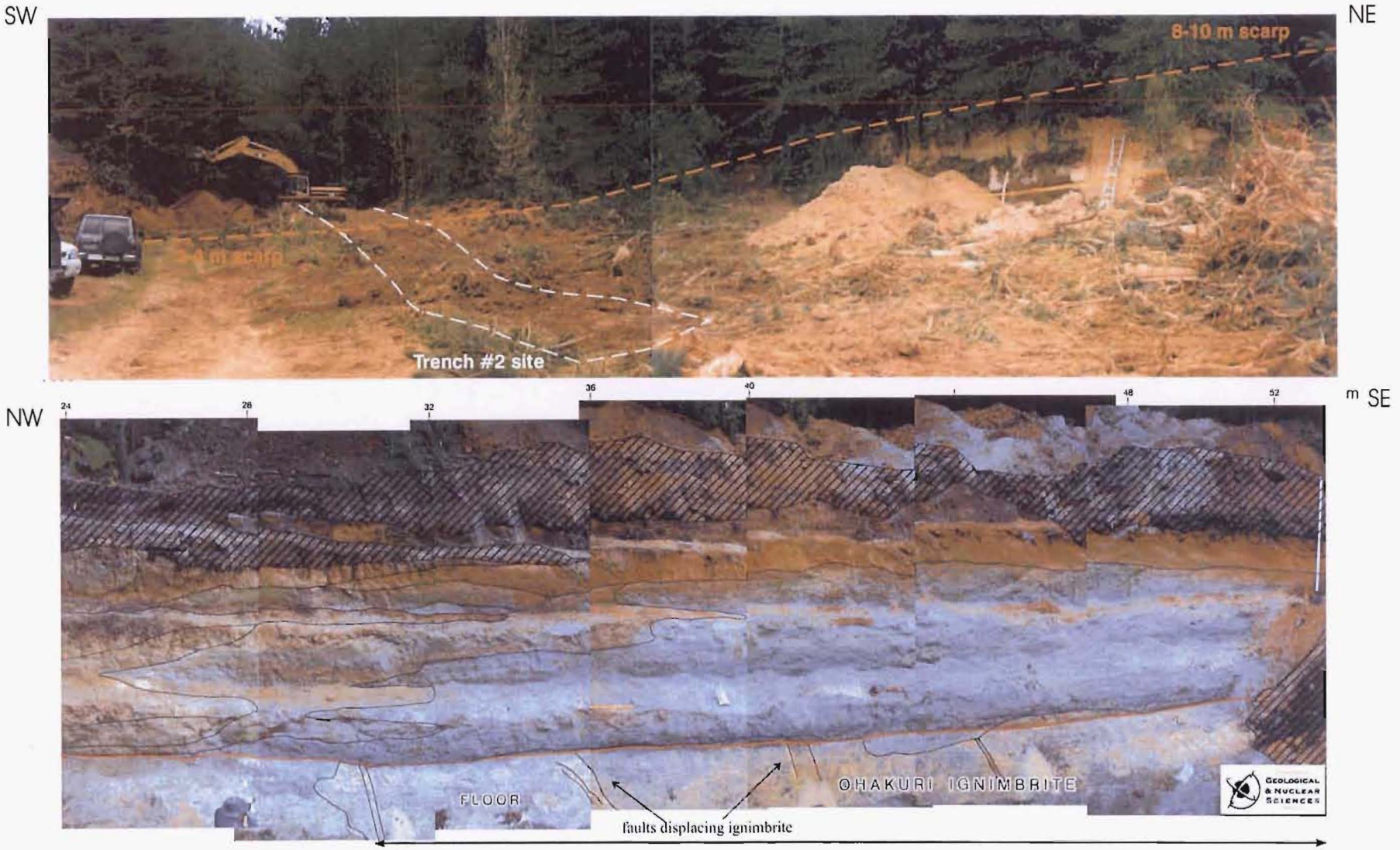

Figure A7.2 (a) Location of trench 2 and (b) Poto mosaic and log of trench 2 showing fractured Ohakuri ignimbrite overlain by undisturbed active-TVZ deposits

APPENDIX 8

Critical Dike Width Calculations

The critical width below which the magma within a granitic dike will freeze is calculated using the equation of Petford et al. (1993; 1994):

$$w_c = 1.5\left(\frac{S_m}{S_\infty{}^2}\right)^{3/4}\left(\frac{\mu\kappa H}{g\Delta\rho}\right)^{1/4}$$

Where:

$$S_m = \frac{L}{c(T_i - T_f)}$$

$$S_\infty = \frac{L}{c(T_f - T_\infty)}$$

L = 300 = Latent heat of solidification (J/g)

c = 1.2 = specific heat (J/g/°C)

T_i = Initial magmatic temperature (°C)

T_f = 750 = Freezing temperature of the magma (°C)

T_∞ = Far-field crustal temperature (°C)

μ = magmatic viscosity (Pa.s)

κ = 8 x 10^{-7} = thermal diffusivity (m^2/s)

H = dike length (km)

g = 9.8 = gravitational acceleration (m/s^2)

$\Delta\rho$ = difference in density between the magma and crust (kg/m^3)

There are a range of conceivable TVZ values for the 5 unconstrained variables above. Initial magmatic temperature inversely controls critical dike width and is expected to be in the range of 800 to 900 °C for TVZ rhyolites (based on estimates from deposits at Mangakino caldera, Briggs et al., 1993). The far-field crustal temperature inversely affects critical dike width and is more difficult to determine; the TVZ geothermal gradient is locally up to 100 times greater at shallow depths in geothermal fields, but generally only a little higher than the assumed background gradient of 30 °C/km (Thompson, 1980). Therefore a range of gradients from 20 to 40 °C/km is considered plausible. In the central Maroa area high shallow resistivity suggests the presence of shallow down-going groundwater (Section 1.9.2), supporting a relatively low shallow

geothermal gradient, close to that of the assumed background. The magmatic viscosity for silicic melts positively affects critical dike width and is considered by Petford et al. (1993) to fall in the range of 10^4 to 10^8 Pa.s. They also consider the difference in density between the magma and crust to inversely affect dike width and be between 50 and 500 kg/m^3, varying in response to temperature and crystal and volatile content in the magma.

Dike length is the depth to the top of the magma source. It positively affects critical dike width and at TVZ cannot exceed the base of the crust at depth 15 km and probably does not lie at < 5 km. The latter figure is from geophysical evidence which suggests a lack of large quantities of molten magma < 5 km depth from (a) a basement to earthquake swarms at 6 – 8 km (Bryan et al., 1999) and (b) the jump in seismic velocity at ~ 5 km depth modelled by many workers, most recently modelled from earthquake tomography by Sherburn et al. (2003).

A minimum and maximum plausible dike width for TVZ is calculated in Table A8.1. The most probable dike width for the Tuahu Dome case study is calculated by equations above and given in Chapter 5.4.3.

		M	H	$\Delta\rho$	T_i	T_∞
Minimum plausible critical width	1 m	10000	5	500	900	500
Maximum plausible critical width	58 m	100000000	15	50	800	400
Moderate (probable)	10 m	1000000	10	200	850	300

Table A8.1 Critical widths calculated as described in text for plausible and probable TVZ dikes.

APPENDIX 9

Methodology

Most of the methods used in the preparation of data for this thesis are common knowledge within geology. They are briefly summarised here for the benefit of readers without a geological background.

9.1 Field mapping and sampling

Mapping is necessary to provide a framework for geological interpretation. The maps produced also have their own intrinsic value as an information resource. Mapping involves comprehensive coverage of the field area on foot and by vehicle to discover and record relevant geomorphology and outcrops of rock. For this thesis almost all of the mapping had previously been completed (see above) and coverage of the field area on foot and vehicle was made only to check and make some corrections to this. Air photo interpretation provides more geomorphologic information and identifies structures such as faulting that are not apparent on the ground. Field sampling is undertaken concurrently with field mapping. A comprehensive suite of rock samples is necessary for petrographic, geochemical and age comparison between outcrops, and between eruptives.

9.2 Physical volcanology and paleoseismology

Detailed study at the individual outcrop scale identifies the rock type(s) and structure present, and allows these to be correlated or contrasted across the field area. This involves a spectrum from relatively simple description of the rock type to detailed descriptive and graphic logging (Chapter 2) of the deposit centimetre by centimetre.

Maximum pumice and lithic sizes are recorded at outcrop for Maroa pyroclastic density current deposits for later contouring across the entire deposit. The five largest pumice/lithic clasts are each measured in their longest and shortest axes. The five long axis measurements are averaged and contoured for a maximum length plot. Data points for a maximum volume plot are the average of each of the five volumes. Volumes are calculated based on long axis length L and short axis length S, as a prolate ellipsoid of formula:

$$\frac{3}{4}\pi \times \left[(\frac{L}{2}) \times (\frac{S}{2}) \times (\frac{(L+S)}{4}) \right]$$

Paleoseismology is the science of modelling fault characteristics and earthquake events from geological evidence (as opposed to direct seismological data). It is usually applied to faulting events that predate modern seismological records. Analysis of the previous events along key faults within Maroa is made in Chapter 5 and the methods are detailed there.

9.3 Petrology

Petrology includes petrography and geochemistry. Petrographic description is made on thin-sections (0.03 mm thick) cut from some selected samples. Descriptions of thin-sections using a polarised microscope provide information on micro-structure and mineralogy (petrography). Geochemical analysis is conducted on samples that are representative of key eruptives. X-Ray Fluorescence (XRF) analysis provides the average chemical composition and is used for correlation of eruptives and modelling of the magma system from which they were erupted. Details of sample preparation and XRF experiments are given in Appendix 4. Thermal Ionisation Mass Spectrometry (TIMS) analysis of $^{87}Sr/^{86}Sr$ for selected samples allows interpretation of the influence of crustal melting on the evolution of a magma. The methods of obtaining these data are detailed in Appendix 5.

9.4 Radiometric age dating and volume estimates

$^{40}Ar/^{39}Ar$ age dating is a specialised geochemical analysis that uses a mass-spectrometer to determine relative quantities of argon isotopes within a rock or mineral. The ratios of these elements can be calculated (with some correction and calibration) to give the time elapsed since the material was cooled (usually coincident with the time of eruption). Detailed description of this technique is given in Appendix 2.

Volume estimates are made on polyhedrons modelled after individual eruptives in Maroa. The method is detailed within Chapter 3.